8603510

Earlywine, Arthur Dale

THE STEREOCHEMISTRY AND MECHANISM OF THE IRON PENTACARBONYL-PROMOTED COUPLING OF STRAINED OLEFINS TO CARBON MONOXIDE, A NMR-FACILITATED STUDY OF THE EQUILIBRIUM CONSTANTS BETWEEN AND COLLISION COMPLEX OF A 10,11-DIPHENYL-1,4:5,8-DIMETHANO-1,4,4A,4B,5,8,8A,8B-OCTAHYDROFLUORENE-9-ONE STEREOISOMER AND THE LANTHANIDE SHIFT REAGENT EU(FOD)(,3), THE ELECTROPHILIC AROMATIC THALLATION OF SOME SELECTED BIOMOLECULES, AND THE SYNTHESIS AND HIGH RESOLUTION NMR STUDY OF THE TWO SERIES OF 1,4,4A,8A-TETRAHYDRO-ENDO-1,4-METHANONAPHTHALENE-5,8-DIONES AND PENTACYCLO(5.4.0.0('2,6).0('3,10).0('5,9))UNDECANE-8,11-DIONES

The University of Oklahoma PH.D. 1985

University
Microfilms
International 300 N. Zeeb Road, Ann Arbor, MI 48106

PLEASE NOTE:

In all cases this material has been filmed in the best possible way from the available copy. Problems encountered with this document have been identified here with a check mark __✓__.

1. Glossy photographs or pages _____
2. Colored illustrations, paper or print _____
3. Photographs with dark background _____
4. Illustrations are poor copy _____
5. Pages with black marks, not original copy _____
6. Print shows through as there is text on both sides of page _____
7. Indistinct, broken or small print on several pages ✓
8. Print exceeds margin requirements _____
9. Tightly bound copy with print lost in spine _____
10. Computer printout pages with indistinct print _____
11. Page(s) _____ lacking when material received, and not available from school or author.
12. Page(s) _____ seem to be missing in numbering only as text follows.
13. Two pages numbered _____. Text follows.
14. Curling and wrinkled pages _____
15. Dissertation contains pages with print at a slant, filmed as received _____
16. Other _____

THE UNIVERSITY OF OKLAHOMA

GRADUATE COLLEGE

THE STEREOCHEMISTRY AND MECHANISM OF THE IRON PENTACARBONYL-PROMOTED COUPLING OF STRAINED OLEFINS TO CARBON MONOXIDE, A NMR-FACILITATED STUDY OF THE EQUILIBRIUM CONSTANTS BETWEEN AND COLLISION COMPLEX OF A 10,11-DIPHENYL-1,4:5,8-DIMETHANO-1,4,4A,4B,5,8,8A,BB-OCTAHYDROFLUORENE -9-ONE STEREOISOMER AND THE LANTHANIDE SHIFT REAGENT EU(FOD)$_3$, THE ELECTROPHILIC AROMATIC THALLATION OF SOME SELECTED BIOMOLECULES, AND THE SYNTHESIS AND HIGH RESOLUTION NMR STUDY OF THE TWO SERIES OF 1,4,4A,8A-TETRAHYDRO-<u>ENDO</u>-1,4-METHANONAPHTHALENE-5,8-DIONES AND PENTACYCLO[5.4.0.0^{2,6}.0^{3,10}.0^{5,9}]UNDECANE-8,11-DIONES

A DISSERTATION

SUBMITTED TO THE GRADUATE FACULTY

in partial fulfillment of the requirements for the

degree of

DOCTOR OF PHILOSOPHY

By

ARTHUR DALE EARLYWINE

Norman, Oklahoma

1985

THE STEREOCHEMISTRY AND MECHANISM OF THE IRON PENTACARBONYL-PROMOTED COUPLING OF STRAINED OLEFINS TO CARBON MONOXIDE, A NMR-FACILITATED STUDY OF THE EQUILIBRIUM CONSTANTS BETWEEN AND COLLISION COMPLEX OF A 10,11-DIPHENYL-1,4:5,8-DIMETHANO-1,4,4A,4B,5,8,8A,8B-OCTAHYDROFLUORENE -9-ONE STEREOISOMER AND THE LANTHANIDE SHIFT REAGENT $EU(FOD)_3$, THE ELECTROPHILIC AROMATIC THALLATION OF SOME SELECTED BIOMOLECULES, AND THE SYNTHESIS AND HIGH RESOLUTION NMR STUDY OF THE TWO SERIES OF 1,4,4A,8A-TETRAHYDRO-ENDO-1,4-METHANONAPHTHALENE-5,8-DIONES AND PENTACYCLO[5.4.0.0^{2,6}.0^{3,10}.0^{5,9}]UNDECANE-8,11-DIONES

A DISSERTATION

APPROVED FOR THE DEPARTMENT OF CHEMISTRY

By

Alan P. Marchand

Wayne Nelson

Robert S. Ruh

Eddie Carol Smith

Lars A. Thiesler

ACKNOWLEDGEMENTS

The author wishes to express his appreciation to Dr. A. P. Marchand for his guidance and support in this research and writing of this dissertation.

Further thanks is offered to: Dr. Eric Enwal for assistance in adapting a least squares computer program for use in the lanthanide shift reagent "collision-complex" study, Dr. M. J. Heeg for her solving of several X-ray stuctures, Dr. M. D. Johnston for his providing of the LISA4 computer program used in the lanthanide shift reagent NMR and equilibrium studies and for the helpful suggestions concerning its use, Dr. D. J. Nelson for the theoretical MNDO calculations on trans-1,2-dimethylcyclopropanone, and Dr. D. F. Marten for clarification of certain aspects of the organometallic chemistry involved in the iron pentacarbonyl-promoted coupling of strained olefins to carbon monoxide.

Special gratitude is extended to the Gigers, Rileys, Sarah, and Mr. C".

Most importantly, the support of my wife and friend Janet is gratefully acknowledged.

TABLE OF CONTENTS

LIST OF TABLES

LIST OF FIGURES

LIST OF SCHEMES

SCHEMES

ABSTRACT

The stereochemistry and mechanism of the iron pentacarbonyl-induced coupling of strained olefins (e.g., 7-phenylnorbornadiene) to carbon monoxide is discussed. Emphasis is placed on determination of the structure of one dimeric ketone coupling product with the aid of the lanthanide shift reagent $Eu(fod)_3$ in nuclear magnetic resonance decoupling experiments. The use of a computer program which calculates the equilibrium constants (K_1 and K_2) and bound chemical shifts ($\Delta 1$ and $\Delta 2$) for the one step ($L + S \rightleftharpoons LS$) and the two step ($LS + S \rightleftharpoons LS_2$) lanthanide shift reagent-dimeric ketone interactions (L_mS_n) is also demonstrated. The position of the europium atom in the L_1S_1 "collision-complex" is determined with the aid of another computer program. Other new iron carbonyl coupling products and two unique cage compounds synthesized from them are also discussed.

Introduction of the easily replaceable thallium ditrifluoroacetate substituent into several biologically active compounds and its eventual substitution by radioactive iodine (for use as an imaging agent in tracer studies) is investigated.

Finally, the synthesis of as interesting series of highly strained pentacyclo[5.4.0.0^{2,6}.0^{3,10}.0^{5,9}]undecane-8,11-diones is demonstrated, comprehensive ^{1}H and ^{13}C NMR signal assignments are made using high resolution conventional and 2-dimensional nuclear magnetic resonance techniques, and the X-ray crystal structure of the 3-methylpentacyclo[5.4.0.0^{2,6}.0^{3,10}.0^{5,9}]undecane-8,11-dione isomer is demonstrated.

THE STEREOCHEMISTRY AND MECHANISM OF THE IRON PENTACARBONYL-PROMOTED COUPLING OF STRAINED OLEFINS TO CARBON MONOXIDE, A NMR-FACILITATED STUDY OF THE EQUILIBRIUM CONSTANTS BETWEEN AND COLLISION COMPLEX OF A 10,11-DIPHENYL-1,4:5,8-DIMETHANO-1,4,4A,4B,5,8,8A,8B-OCTAHYDROFLUORENE -9-ONE STEREOISOMER AND THE LANTHANIDE SHIFT REAGENT $EU(FOD)_3$, THE ELECTROPHILIC AROMATIC THALLATION OF SOME SELECTED BIOMOLECULES, AND THE SYNTHESIS AND HIGH RESOLUTION NMR STUDY OF THE TWO SERIES OF 1,4,4A,8A-TETRAHYDRO-ENDO-1,4-METHANONAPHTHALENE-5,8-DIONES AND PENTACYCLO[$5.4.0.0^{2,6}.0^{3,10}.0^{5,9}$]UNDECANE-8,11-DIONES

PART I

THE STEREOCHEMISTRY AND MECHANISM OF THE IRON PENTACARBONYL-PROMOTED COUPLING OF STRAINED OLEFINS TO CARBON MONOXIDE, WITH EMPHASIS ON THE NUCLEAR MAGNETIC RESONANCE LANTHANIDE SHIFT REAGENT STUDY OF A 10,11-DIPHENYL-1,4:5,8-DIMETHANO-1,4,4A,4B,5,8,8A,8B-OCTAHYDROFLUORENE -9-ONE STEREOISOMER

Introduction

Previous investigations[1,2] concerning the stereochemistry and mechanism of iron carbonyl-promoted coupling of strained olefins to carbon monoxide have provided interesting results. Examples of several such reactions are shown in Table I-1. As illustrated, anti-7-t-butoxynorbornadiene is inert under the normal reaction conditions, whereas syn-7-t-butoxynorbornadiene affords dimeric ketones IV and V. Since 7-t-butoxynorbornadiene affords only one dimeric ketone, the double bond anti to the t-butoxy group must be involved in the transition state and participate in the reaction.

Conventions regarding configurational nomenclature are illustrated in Fig I-1. The central cyclopentanone ring contains four

TABLE I-1

Examples of Iron Pentacarbonyl-Promoted Coupling Reactions.

Reaction		Reference
1	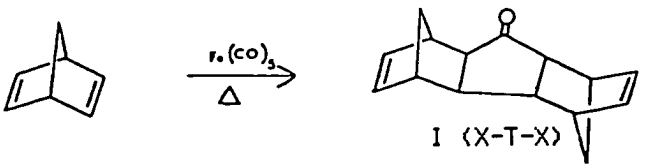	1
2	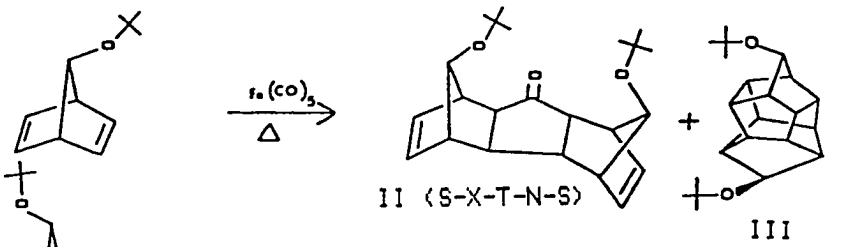	2
3	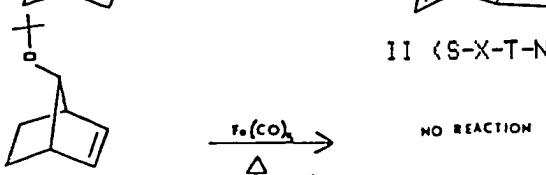	2
4	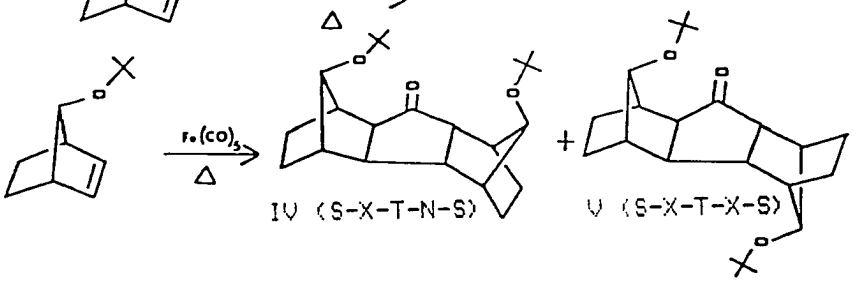	2

trated in Fig I-1. The central cyclopentanone ring contains four hydrogens (two from each of the two norbornadiene moieties). In formation of these dimeric ketones, hydrogens A and B from the precursor olefin must be cis, whereas hydrogens A and A′ may be either cis (C) or trans (T) with respect to the cyclopentanone ring. The latter cis or trans stereochemistry also applies to hydrogens B and B′. Also, during ring formation the norbornadiene moiety may become substituted at either its endo (N) or its exo (X) face. Finally, the position of a substituent on the 7-bridge carbon may be conveniently specified as being syn (S) or anti (A) with respect to the cyclopentanone ring. For example, the product (II) of Reaction 2 is unambiguously described as syn-exo-trans-endo-syn (SXTNS).

FIGURE I-1

Conventions Regrding Configurational Nomenclature Pertinent to Iron Pentacarbonyl Coupling Products.

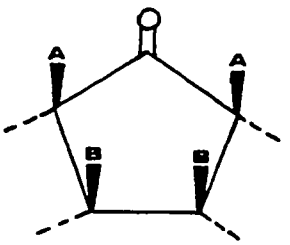

Cis (C)

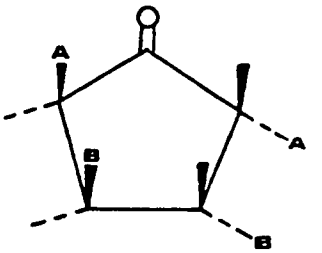

Trans (T)

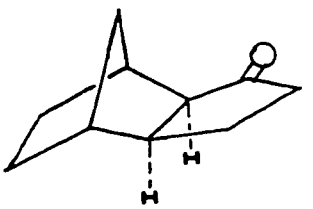

Exo (X)

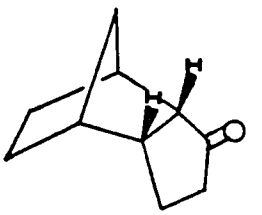

Endo (N)

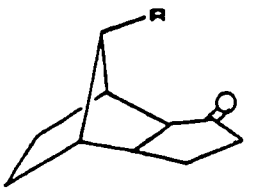

Syn (S)

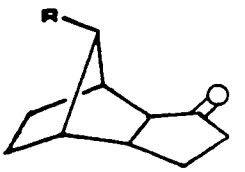

Anti (A)

The question of mechanism naturally arises. Mantzaris and Weisberger[3] have suggested that production of dimeric ketones results from $Fe(CO)_4$-olefin complex formation followed by: (i) substitution of a CO ligand by another olefin, (ii) rearrangement, and (iii) loss of the iron moiety (Scheme I-1). The S-X-T-N-S

SCHEME I-1

Mechanism of the Iron Pentacarbonyl Promoted Coupling of Olefins to Carbon Monoxide Suggested by Mantzaris and Weisberger.

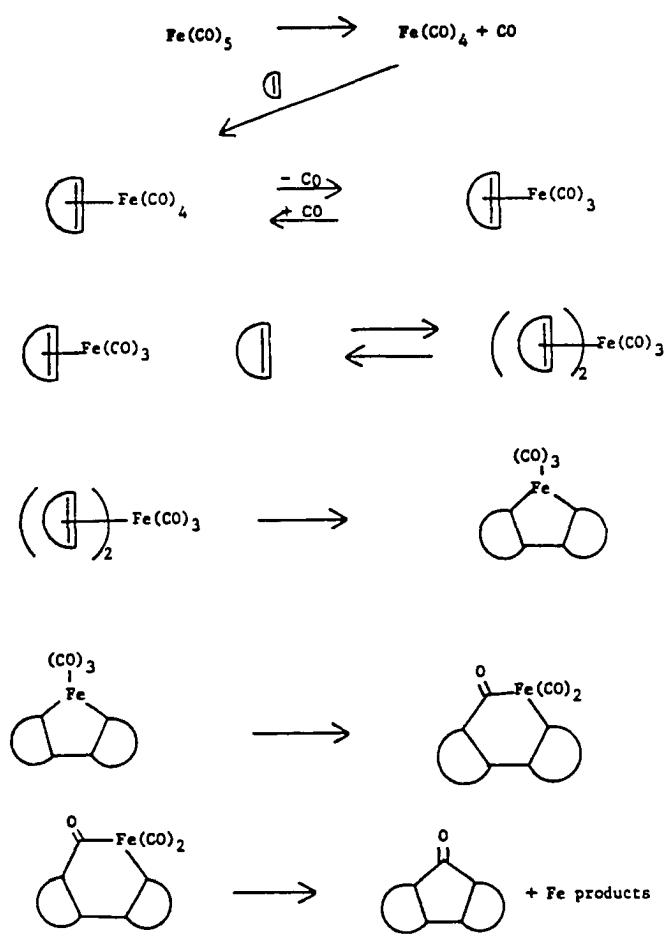

preference has been noted[2] and has been attributed to the presence of a Lewis base substituent at the 7-bridge position[4-6] which might displace CO as shown in Fig I-2.

FIGURE I-2

Effect of 7-Lewis Base Substituents on Product Stereochemistry.

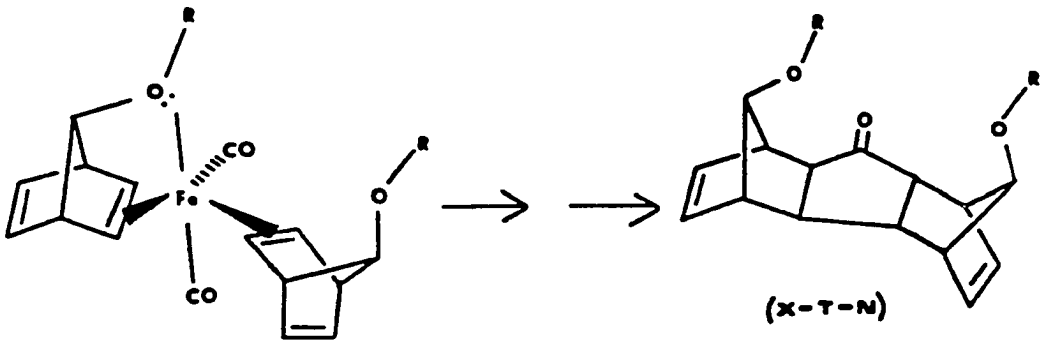

Results and Discussion

To further elucidate the mechanism of involvement of 7-Lewis base substituents, a study was undertaken of the reactions of 7-phenylnorbornadiene (VI) and 7-o-anisylnorbornadiene (VIII) with iron pentacarbonyl (Fig I-3).[7] Based upon consideration of the interactions depicted in Fig I-2, compound VIII might be expected to yield dimer ketone IX possessing the SXTNS configuration. Such stereochemistry might be a direct result of methoxy oxygen participation in CO displacement during the coupling reaction.

Specific nuclear magnetic resonance decoupling experiments have proven useful in the structural determinations of similar ketones. Two types of long range coupling have been observed. Figure I-4a demonstrates the 'vinyl' long range coupling caused by interaction of the vinyl π cloud and the back lobe of the sp^3 hybridized bridge hydrogen.[8] The second type of long range coupling is illustrated in Fig I-4b and is called 'W-letter' coupling.[9,10]

FIGURE I-3

Proposed Reactions

Reaction

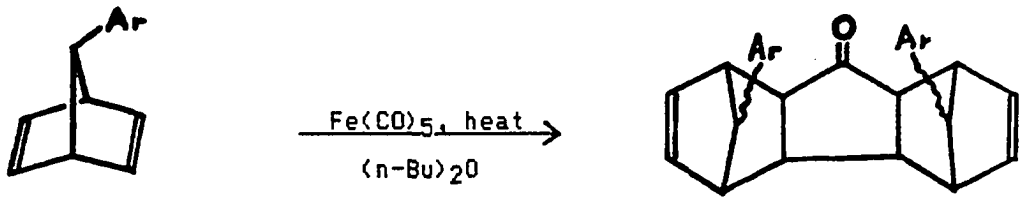

4. VI: Ar = Phenyl VII: Ar = Phenyl

5. VIII: Ar = o-Anisyl IX: Ar = o-Anisyl

Normal 60 MHz proton NMR spectra[11] of VII (Fig I-5) and IX (Fig I-8) exhibit striking similarities which are easily compared in Fig I-9. A sharp AB pattern (corresponding to the protons so labeled in Fig I-1 for the trans configuration about the cyclopentanone ring) is seen for both VII and IX in the 2.2-2.8 ppm region. Similar results have been observed for other dimer ketones of this type.[2,12] This simple AB pattern arises because $^{J}H_a-H_{a'}$ = 0.0 Hz and $^{J}H_b-H_{b'}$ = 0.0 Hz as a result of the trans configuration of the cyclopentanone ring (see Fig I-11 for a labeling scheme).[2,4,12] The similarity and simplicity of the proton spectra suggests symmetrical products. Also, the ^{13}C spectra of VII (cf. Fig I-22,

FIGURE I-4

Two Types of Long-Range $^{1}H-^{1}H$ Coupling.

Vinyl

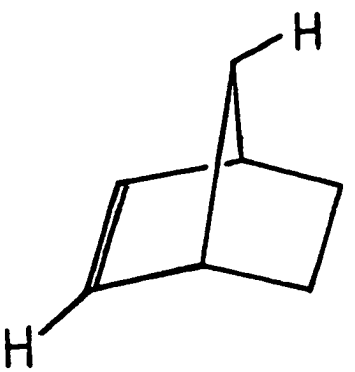

(a)

$J_{H-H} \approx 0.5$ Hz

reference 8

Meinwald's 'W-Letter'

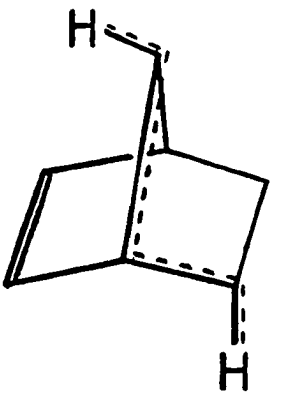

(b)

$J_{H-H} \approx 2.0$ Hz

references 9, 10

containing only twelve ^{13}C signals as would be expected for a symmetrical dimer ketone instead of a maximum of twenty three signals expected for an unsymmetrical dimer ketone) and of IX (cf. Fig I-26, containing only fifteen ^{13}C signals as would be expected for a symmetrical dimer ketone instead of a maximum of twenty nine signals expected for an unsymmetrical dimer ketone) supports this contention. Therefore, it was tentatively assumed that magnetically $H_a = H_{a'}$, $H_b = H_{b'}$, $H_c = H_{c'}$, $\cdots$ $H_g = H_{g'}$. This assumption, disregarding for the moment the aromatic and methoxy protons, implies that the proton spectrum of each compound should consist of resonances corresponding to seven pairs of protons, the members of a pair being equivalent with respect to their magnetic environments. The infrared spectra[11] of VII and of IX also exhibit

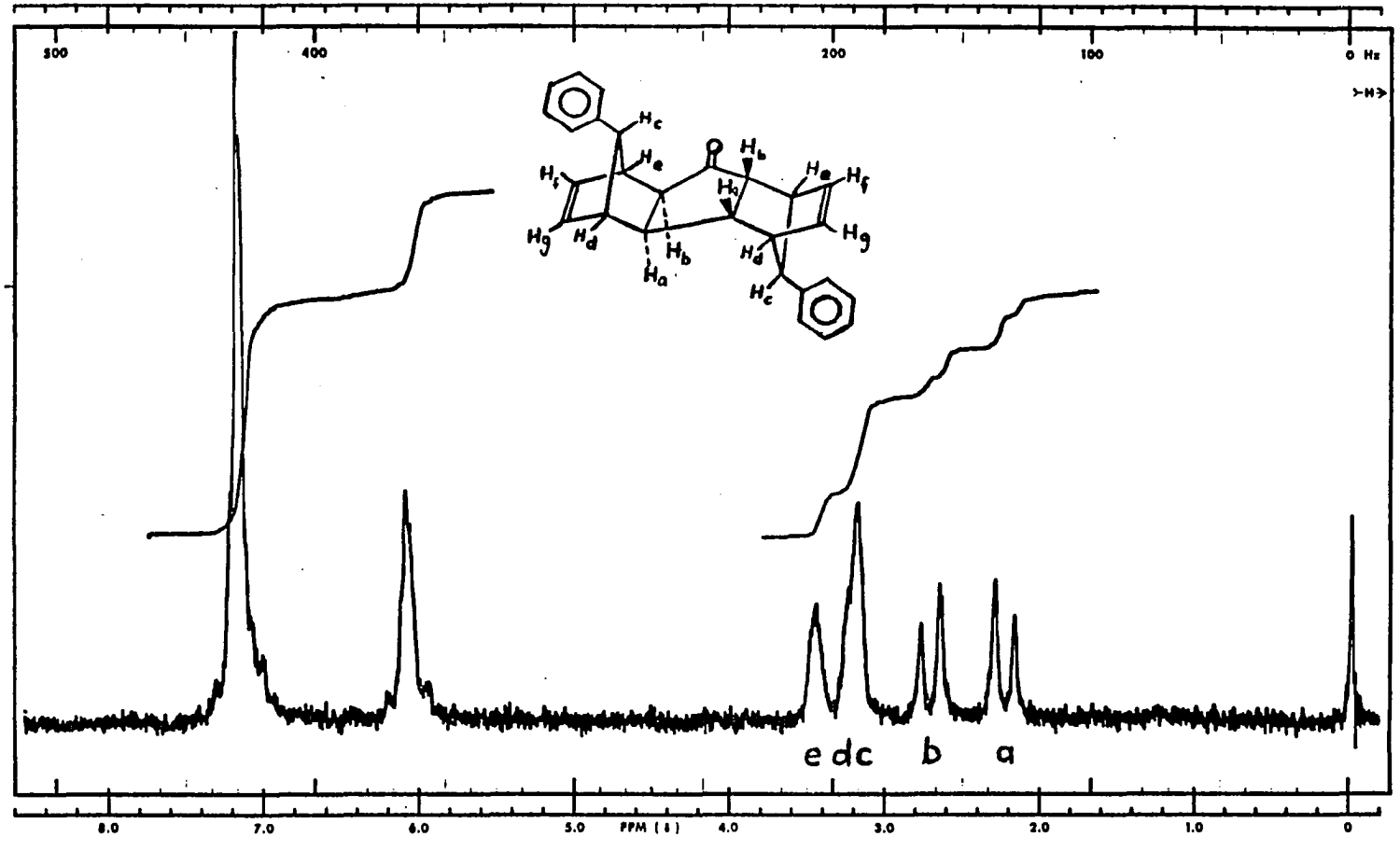

Figure I-5. 60 MHz ^{1}H NMR Spectrum of 7-Phenyl Dimer Ketone VII ($CDCl_3$/TMS).

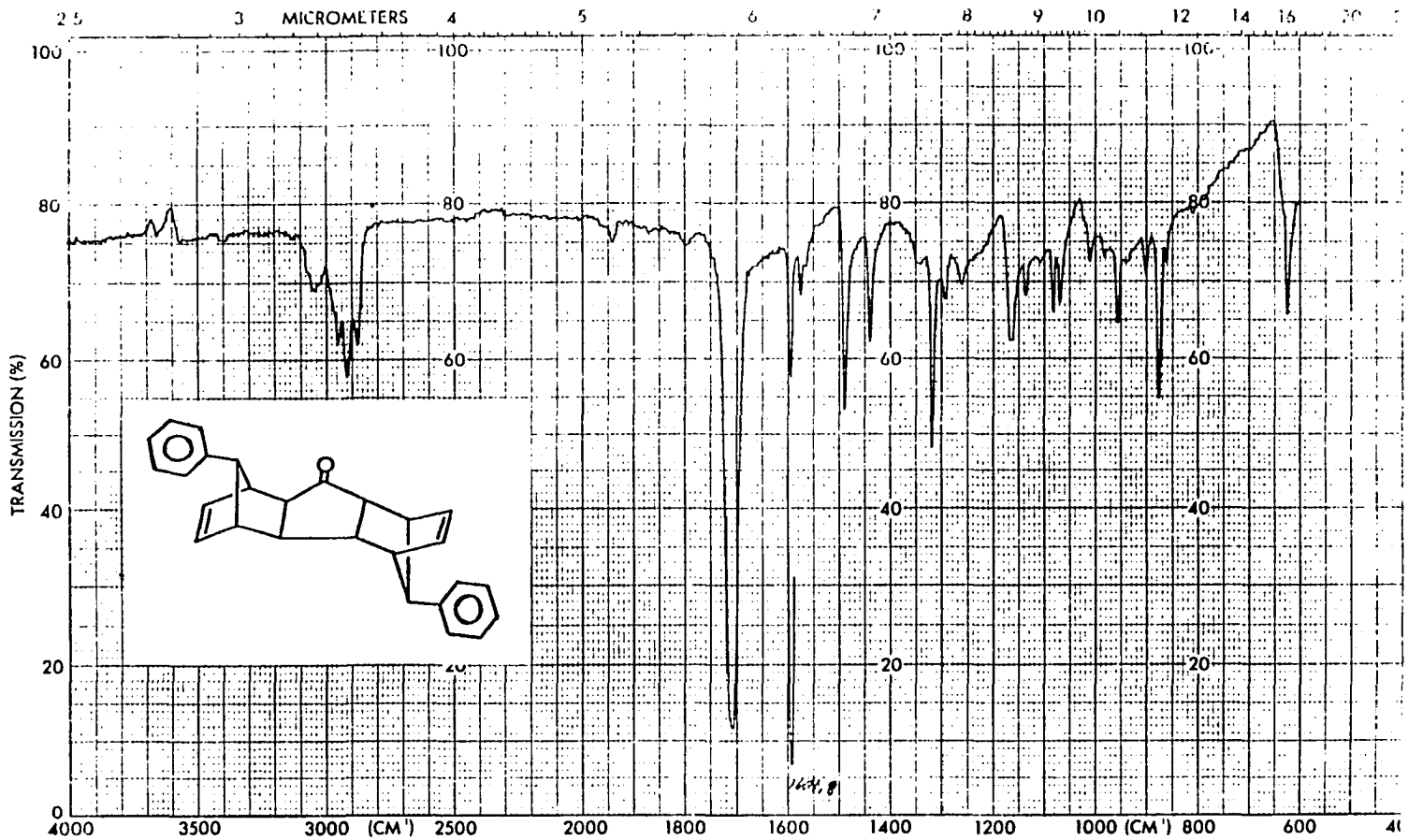

Figure I-6. IR Spectrum of 7-Phenyl Dimer Ketone VII (CCl_4 film).

FIGURE I-7

Mass Spectrum of 7-Phenyl Dimer Ketone VII.

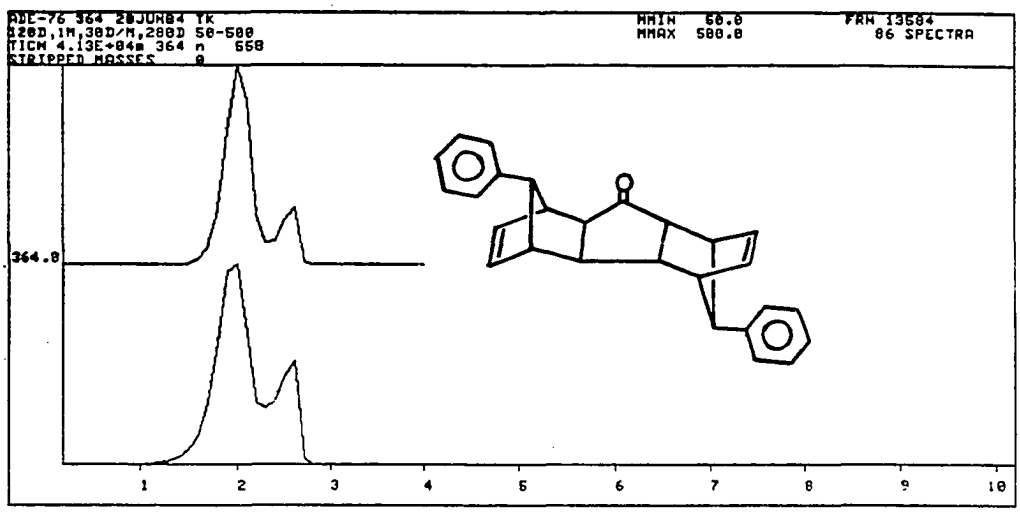

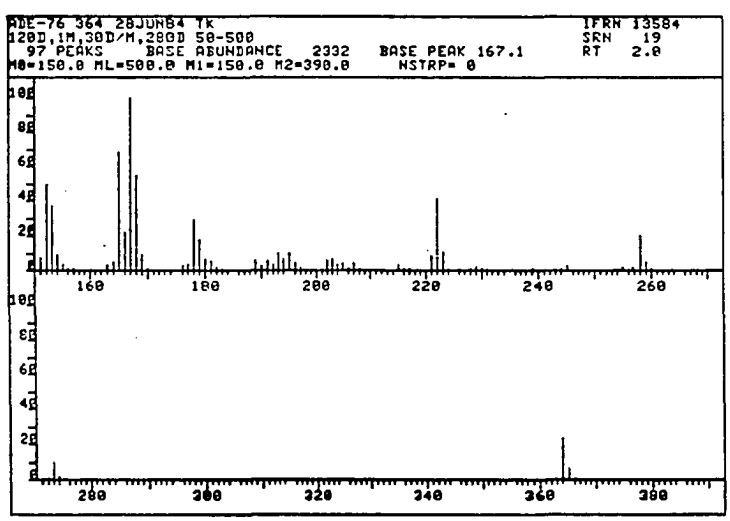

MASS	%	MASS	%
BIG 60		205.1	4.1
150.0	1.5	206.0	1.4
151.0	7.0	207.0	4.6
152.0	48.9	208.0	1.2
153.0	36.9	215.1	3.3
154.0	8.0	216.0	1.4
155.0	3.7	217.0	1.5
157.0	1.2	221.0	8.5
163.0	3.2	222.0	41.6
164.0	5.3	223.1	10.7
165.0	68.4	224.1	1.5
166.0	22.0	228.0	1.5
167.1	100.0	229.0	1.0
168.1	55.1	231.0	1.2
169.0	9.2	239.0	1.2
176.0	2.5	245.0	2.5
177.0	3.7	255.1	1.6
178.0	29.4	256.9	1.7
179.1	10.1	258.1	20.1
180.1	6.9	259.1	4.8
181.0	5.7	260.1	1.2
182.0	1.6	272.0	1.5
189.0	6.2	273.0	9.0
190.0	3.2	274.1	2.1
191.0	5.7	364.1	23.9
192.1	3.5	365.1	6.4
193.0	9.0	366.1	1.0
194.0	6.6		
195.0	10.2		
196.0	4.8	LAST 4	
197.0	1.8	346.1	.6
202.0	6.3	364.1	23.9
203.0	6.7	365.1	6.4
204.1	3.9	366.1	1.0

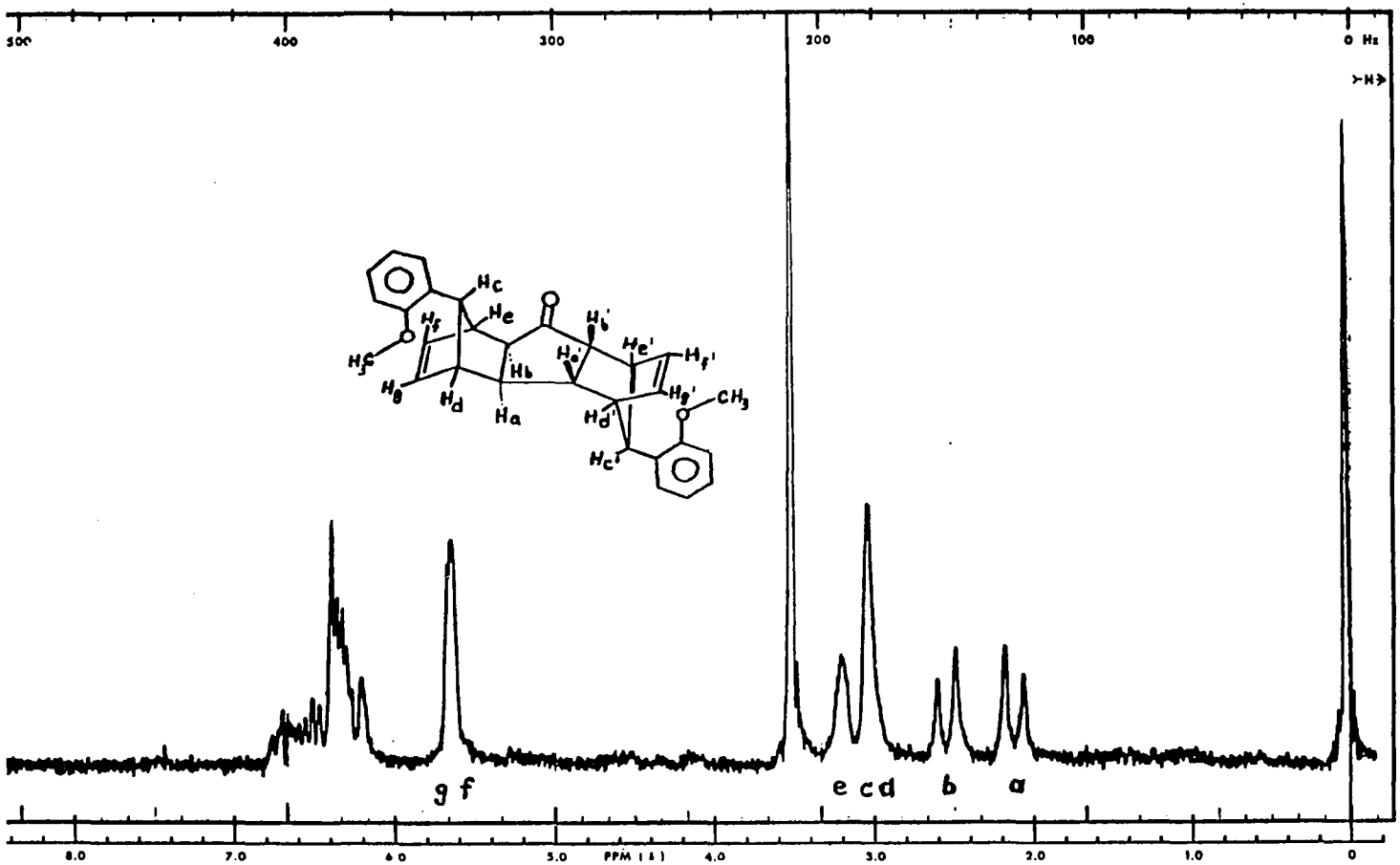

Figure I-8. 60 MHz ^{1}H NMR Spectrum of 7-o-Anisyl Dimer Ketone IX ($CDCl_3$/TMS).

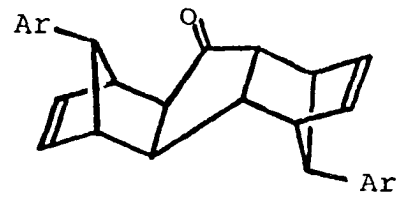

top trace: X = o- anisyl

bottom trace: X = phenyl

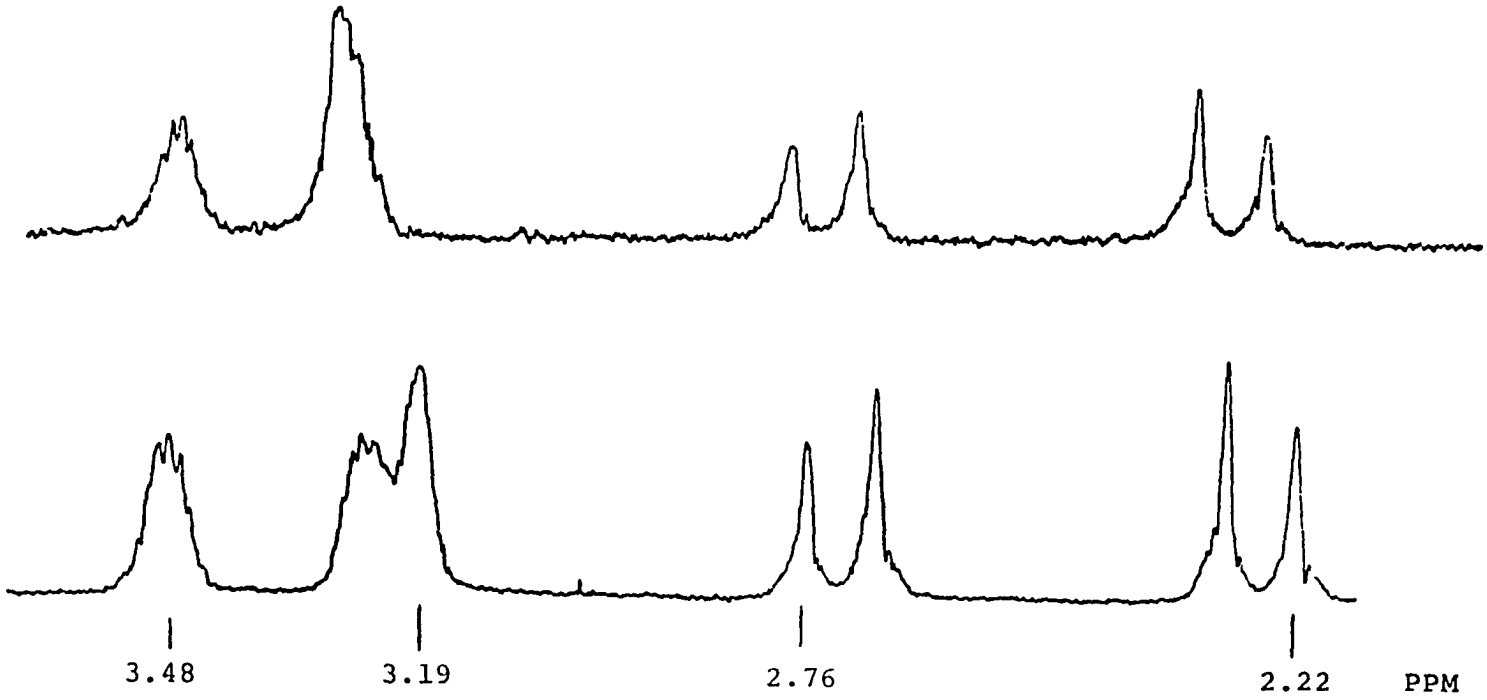

Figure I-9. Comparison of the 60 MHz ^1H NMR Spectra of 7-Phenyl (VII) and 7-o-Anisyl (IX) Dimer Ketones ($CDCl_3$/TMS).

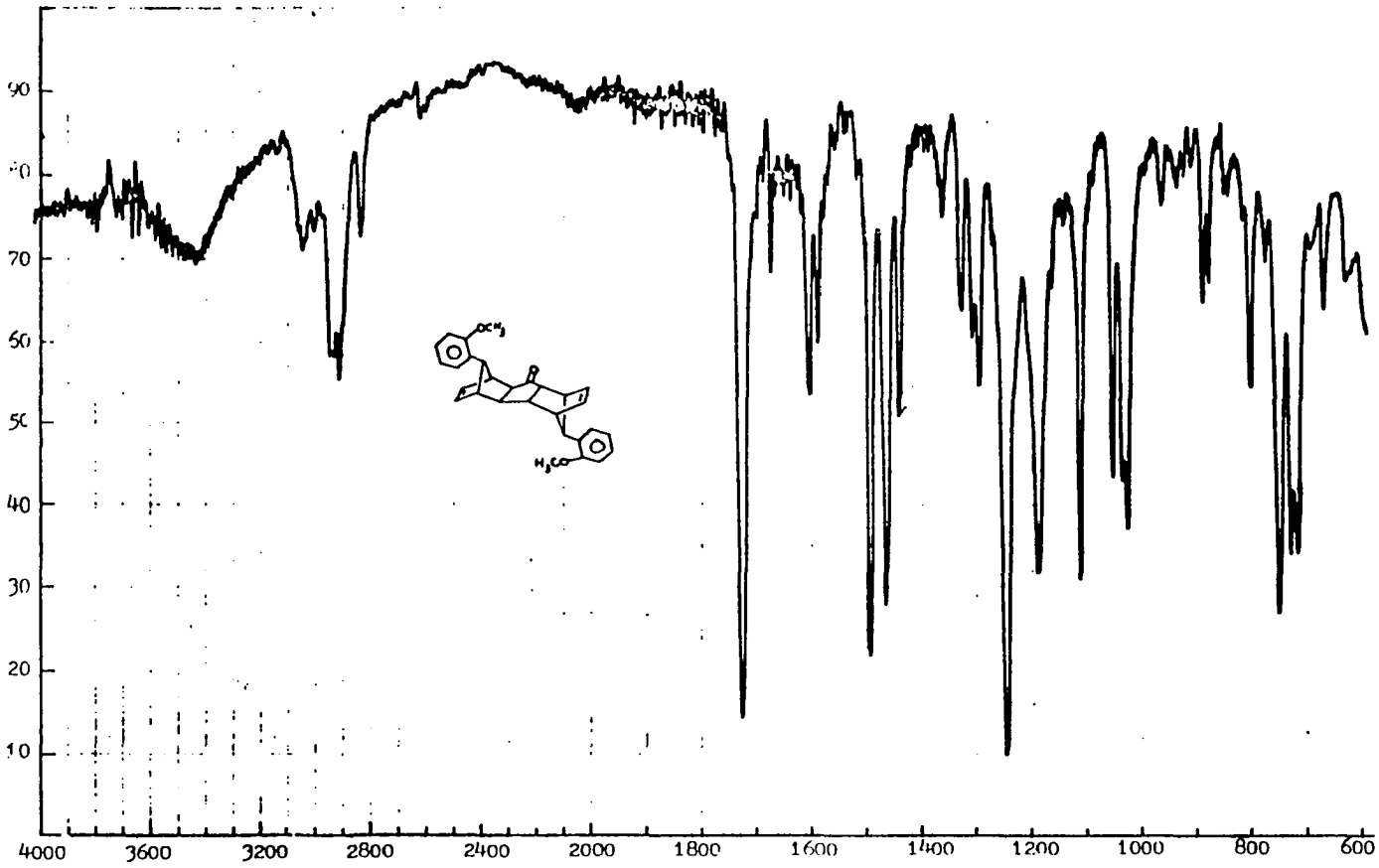

Figure 1-10. IR Spectrum of 7-o-Anisyl Dimer Ketone IX (KBr).

FIGURE I-11

Proton, Carbon, Oxygen, and C_i-C_j-C_k Bond Angle Labeling Scheme for Phenyl Ketone VII. Bond distances are shown in Å, as determined from X-ray study.

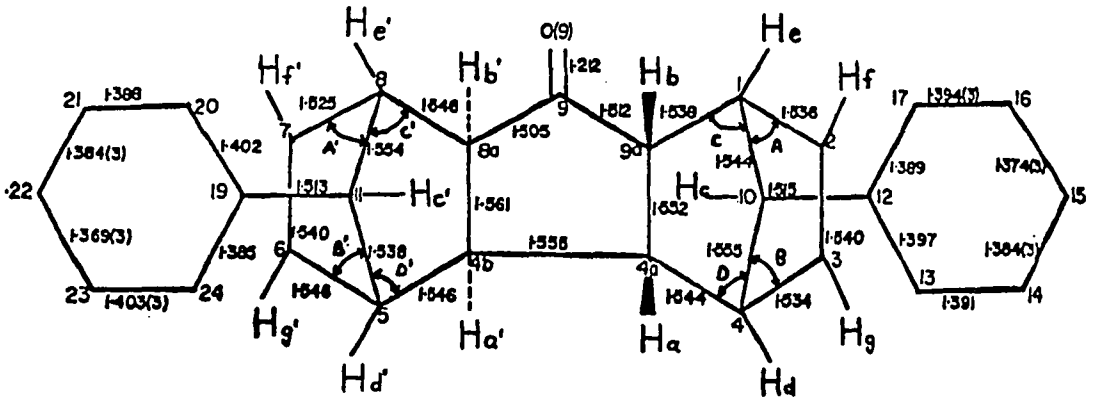

similar features: C=C and C=O stretching for VII (Fig I-6) at 1600 and 1720 cm^{-1}, respectively, and for IX (Fig I-10) at 1600 and 1725 cm^{-1}, respectively. The mass spectrum[11] of VII is shown in Fig I-7.

The $H_c(H_{c'})$ stereochemistry at the bridge carbons remains to be determined. Inspection of Figs I-5 and I-8 reveals certain complications regarding the ability to selectively irradiate and observe specific proton resonances which is a necessary condition for NMR decouplings. Figure I-9 illustrates the overlap of resonances (especially for VII) of two different protons in the 3.0-3.3 ppm region for both compounds. This precludes NMDR investigation which requires first order clarity in this region of each spectrum.

Lanthanide shift reagents (LSR's) have often been used to make NMR spectra amenable to first order analysis.[13-15] The remainder of PART I is devoted to just such an analysis, with the immediate need being to resolve these spectra so that specific resonances may be individually decoupled and observed.

In lanthanide shift reagent-substrate complexes (L_mS_n, where m is usually 1 and n is usually 1 or 2), interaction between the paramagnetic metal ion and nuclei of the substrate causes changes in the chemical shift of the substrate nuclei. Two types of interactions have been described: contact (Fermi) and pseudocontact.

The pseudocontact shift[16] acts through space, describes all magnetic-dipolar types of interactions between the nucleus and the electron spin magnetization of the paramagnetic metal ion, and can be formulated as a dipolar magnetic field. Two theories have been developed giving expressions for the magnitude of the pseudocontact shift and both theories may be expressed by Eq I-1.

$$\begin{aligned} LIS = \Delta\delta_i &= \delta_i - \delta_{oi} \\ &= K(3\cos^2\theta_i - 1)/(RI_i)^3 \end{aligned} \qquad \text{Eq I-1}$$

$\Delta\delta_i$ is the lanthanide-induced (LIS) shift which is strictly defined as the difference between the resonance frequency (δ_{oi}) of the 'i-th' proton in the uncomplexed substrate (S) and the resonance frequency (δ_i) of the same proton in the lanthanide shift reagent-substrate complex (LS_n). The actual observed δ_i for a given nucleus is a weighted time-averaged chemical shift resulting from all species (i.e., S, LS, LS_2, etc.) in the NMR solution. θ_i is the angle between the distance vector (RI_i) joining the metal cation to the particular nucleus (H_i) in the complexed substrate and the crystal field axis of the complexed substrate, often assumed to be the line joining the metal atom to a lone pair-bearing Lewis base atom (e.g., N, O, S, P, etc.) in the substrate (cf. Fig I-12). In this study, the Lewis base is carbonyl

FIGURE I-12

Geometrical relationships in a complex in which conformational flexibility exists for europium (ω_E) and hydrogen (ω_E).

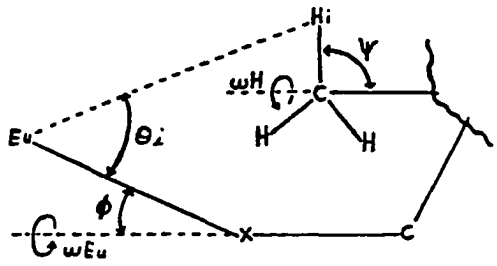

oxygen. The constant, K, is a measure of the induced magnetic dipole of the lanthanide nucleus and has a unique value for each LSR.[17,18]

The contact shift accounts for possible spin delocalization within a complex which arises from direct through-bond electron-nucleus magnetic interaction. This results in a shift of unpaired electron spin density from the metal cation to the substrate ligand by partial covalent bond formation.

It is generally accepted that lanthanides interact primarily by the pseudocontact mechanism because of their high electropositive character and shielding of unpaired electrons of the 'f' orbitals.[19] However, even with lanthanides a small degree of contact interaction is possible,[20] especially for protons attached to the carbons nearest the lone pair-bearing atom.[21] The occurrence of such contact interactions results in deviations from the behavior described by Eq I-1.

Of the several shift reagents commercially available, tris(1,1,1,2,2,3,3-heptafluoro-7,7-dimethyloctane-4,6-dionato)europium (III) [Eu(fod)$_3$][22] was chosen (Fig I-13) because of its minimal broadening of NMR resonances and its increased Lewis acidity (relative to the unfluorinated parent compound and desired in complexation with weakly basic carbonyl oxygen) and its increased

FIGURE I-13

Tris(1,1,1,2,2,3,3-heptafluoro-7,7-dimethyloctane-4,6-dionato)-Europium (III)

$Eu(fod)_3$

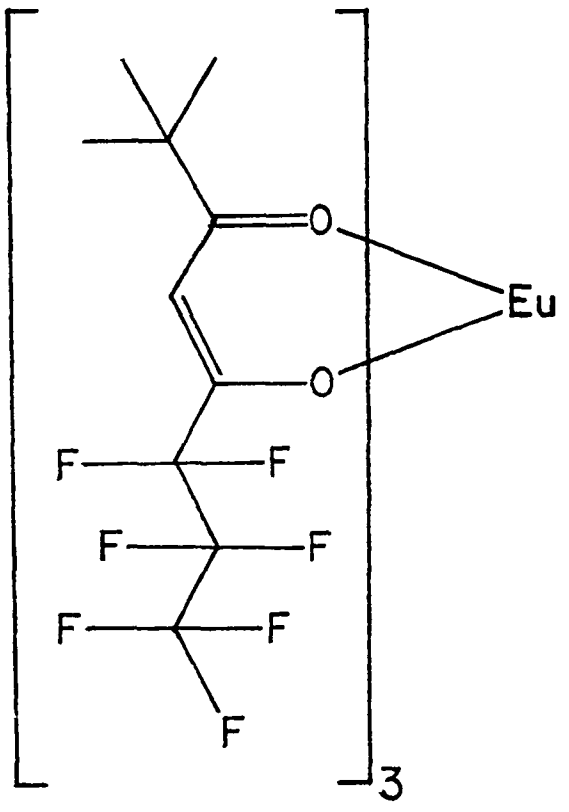

solubility (also due to the presence of the fluorines). In addition, the tert-butyl resonance of $Eu(fod)_3$ in the 1-2 ppm region of the NMR spectrum does not interfere with subsequent spectral analyses.

Returning to the problem of decoupling, weighed amounts of substrate VII and shift reagent were added to an NMR tube. Dilution to a specified volume with deuteriochloroform/1%TMS produced a solution whose calculated molar concentration ratio was defined as RHO

with RHO = $[L_0]/[S_0]$ ($[L_0]$ is the total molar concentration of $Eu(fod)_3$, complexed and uncomplexed, and $[S_0]$ is the total molar concentration of substrate VII, complexed and uncomplexed). A 60 MHz NMR spectrum was obtained and chemical shifts (δ_i) were recorded relative to TMS. Subsequent spectra were obtained (see Figs I-14 through I-17), and shifts were recorded following each incremental dilution[23] of the sample in the NMR tube with a stock solution of VII. This process began with RHO = 3.011 and was continued to RHO = 0.013 (cf. Table I-2). During this sequence, RHO = 0.25 (Fig I-18) was found to give optimum spectral clarity and the four 100 MHz decoupling experiments which are normally necessary to elucidate the stereochemistry at the bridge carbon (cf. Fig I-4) were performed at that RHO (Fig I-19). A more accurate determination of the induced chemical shifts was made at 100 MHz in a second incremental dilution experiment (the decoupling experiments were omitted. Chemical shifts and dilution volumes of this experiment are listed in Table I-2.

In the first experiment, the vinyl protons (centered at δ 6.5) were irradiated while the signal corresponding to $H_c(H_{c'})$ (δ 5.0) was observed. Next, $H_c(H_{c'})$ was irradiated and the vinyl, $H_a(H_{a'})$, and $H_b(H_{b'})$ protons were observed. No significant changes were evident (i.e., no long range vinyl coupling was seen). The third and fourth experiments involved irradiation of $H_b(H_{b'})$ and $H_a(H_{a'})$, respectively, while monitoring $H_c(H_{c'})$. Again, no significant changes in the observed resonances were detected (i.e., the 'W-letter' long range coupling was not evident)!

These experiments provided no information about the syn or anti bridge proton stereochemistries. Either one of these experiments should have confirmed the position of $H_c(H_{c'})$ by a positive result. The first pair of experiments indicate by negative evidence that the $H_c(H_{c'})$ proton(s) are anti while the second pair indicate by negative evidence that $H_c(H_{c'})$ proton(s) are syn. These contradictory, and in fact mutually exclusive, observations are the only failures we have encountered in syn vs. anti stereochemistry

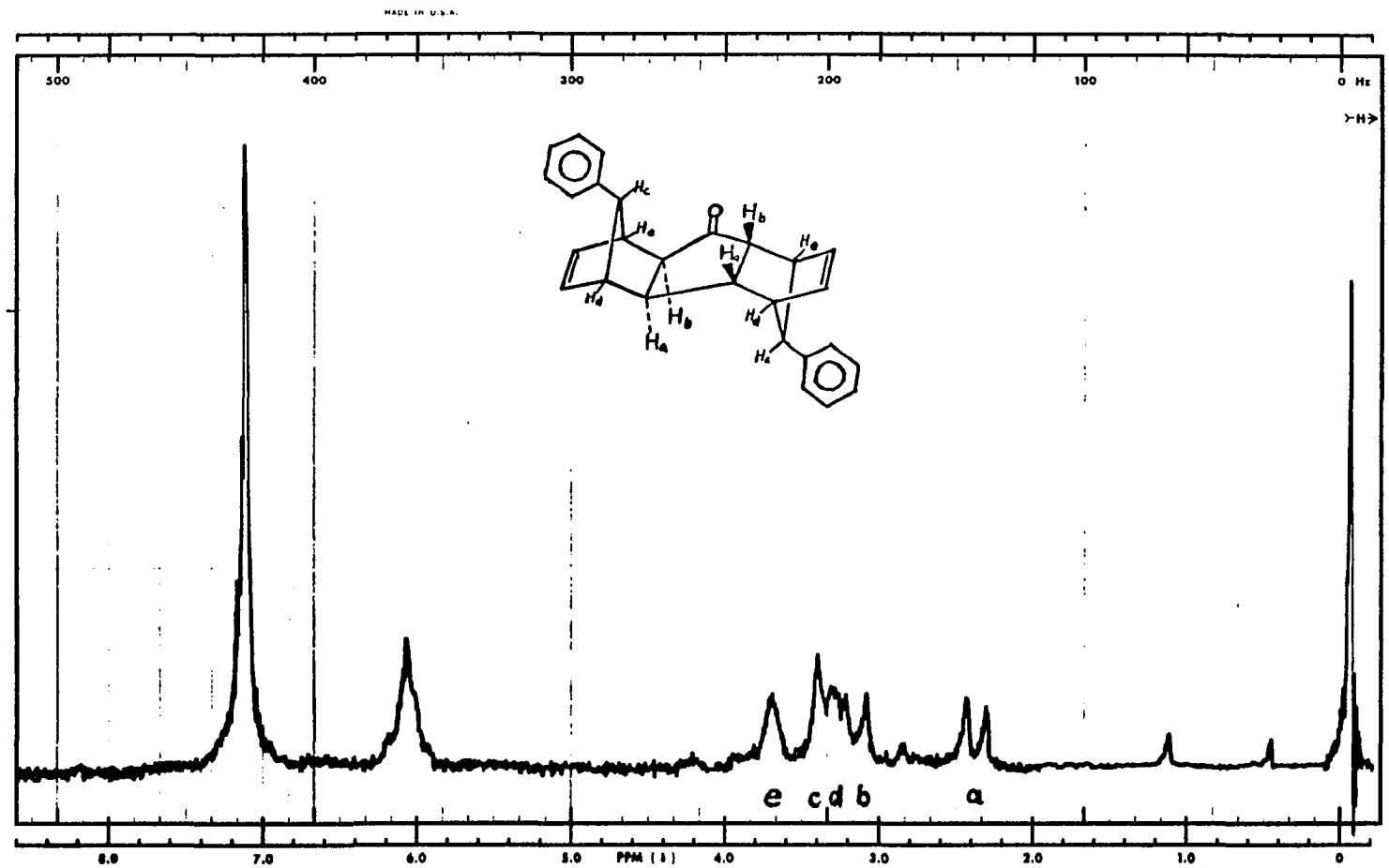

Figure I-14. 60 MHz ^1H NMR Spectrum of 7-Phenyl Dimer Ketone VII, $[S_o]$ = 0.192M and $[Eu(Fod)_3]$ = 0.009M; RHO = $[L_o]/[S_o]$ = 0.050 ($CDCl_3$/TMS).

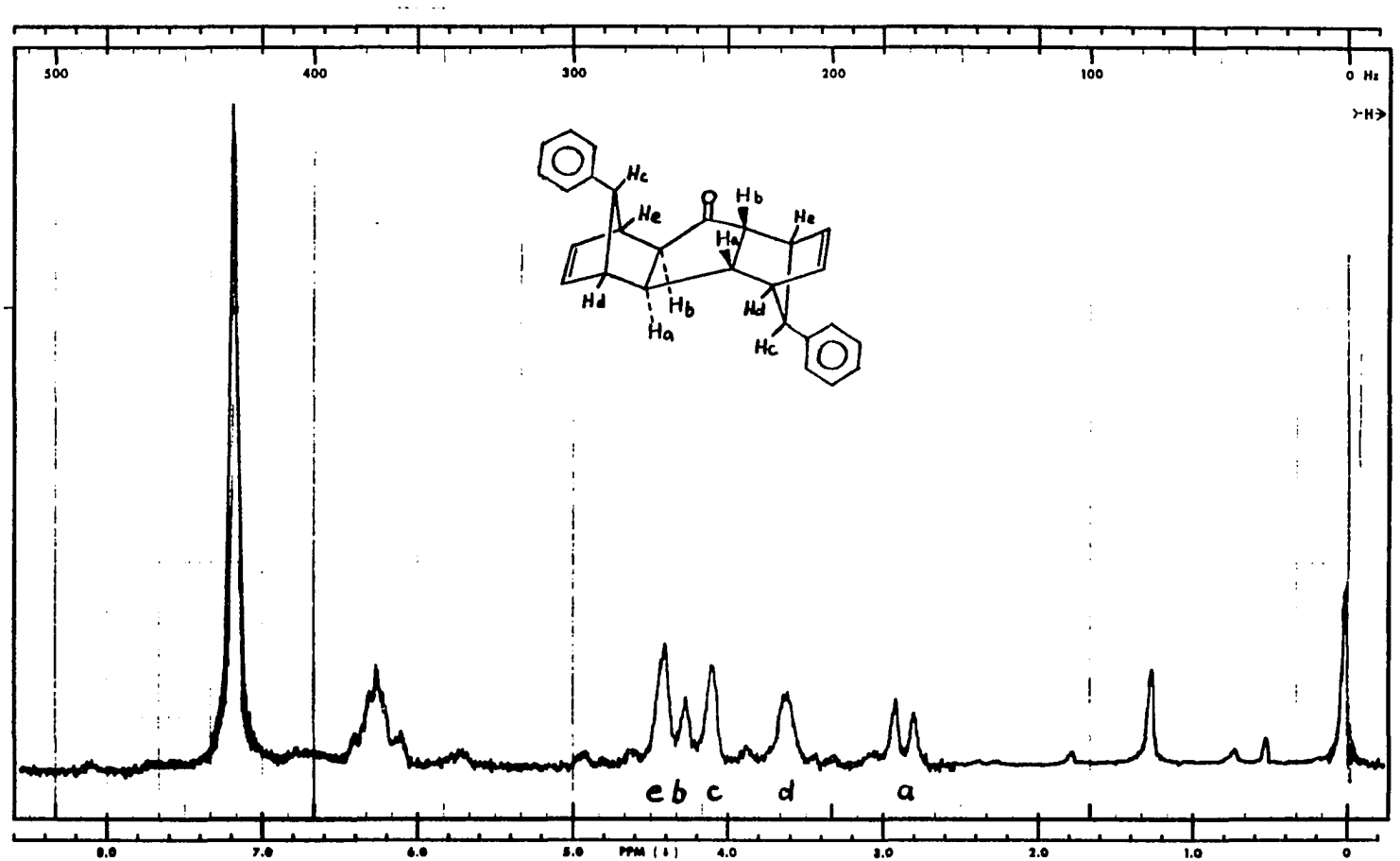

Figure I-15. 60 MHz ^{1}H NMR Spectrum of 7-Phenyl Dimer Ketone VII, RHO = 0.150 ($CDCl_3$/TMS).

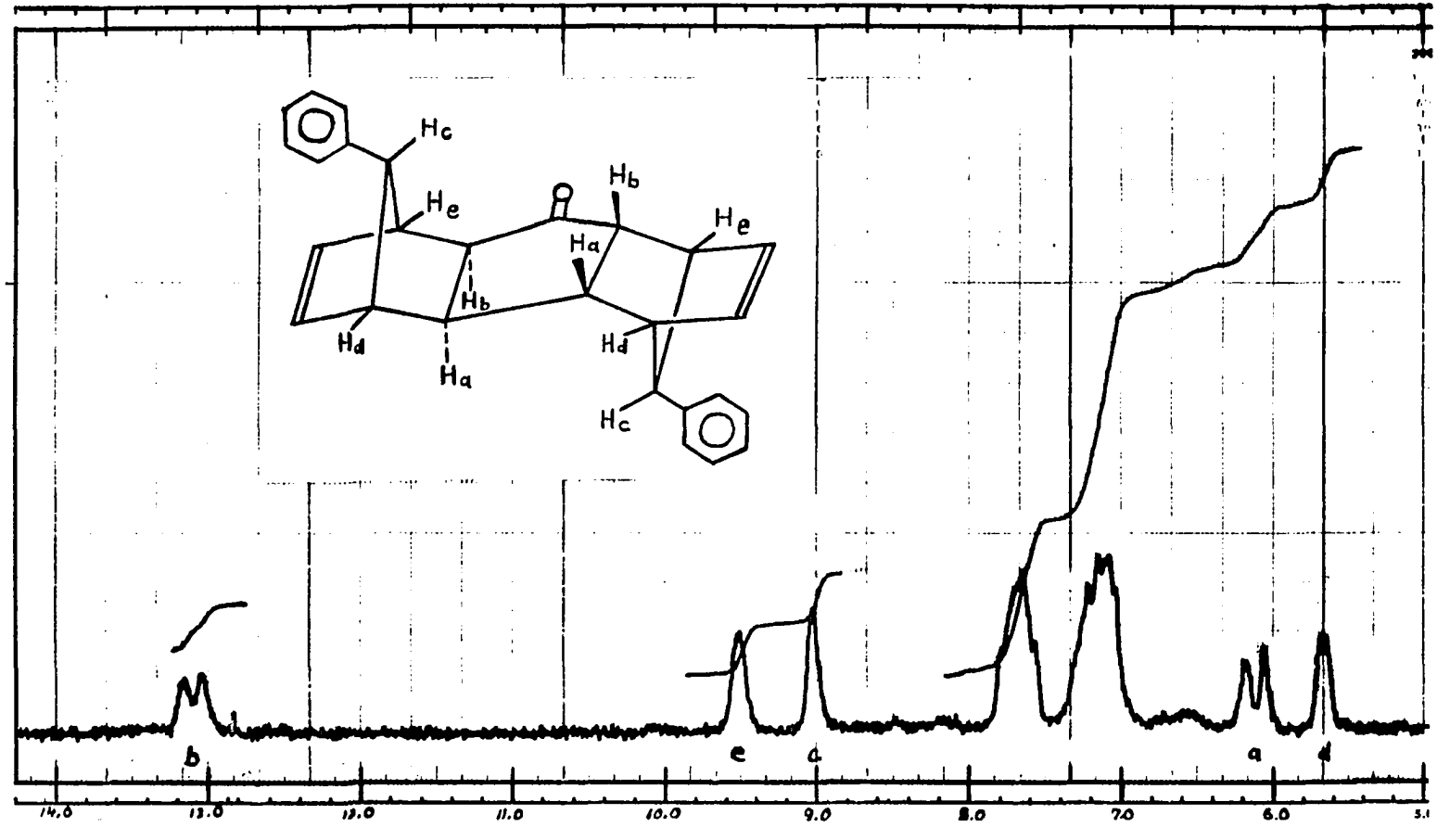

Figure I-16. 60 MHz ^{1}H NMR Spectrum of 7-Phenyl Dimer Ketone VII, RHO = 1.599 ($CDCl_3$/TMS).

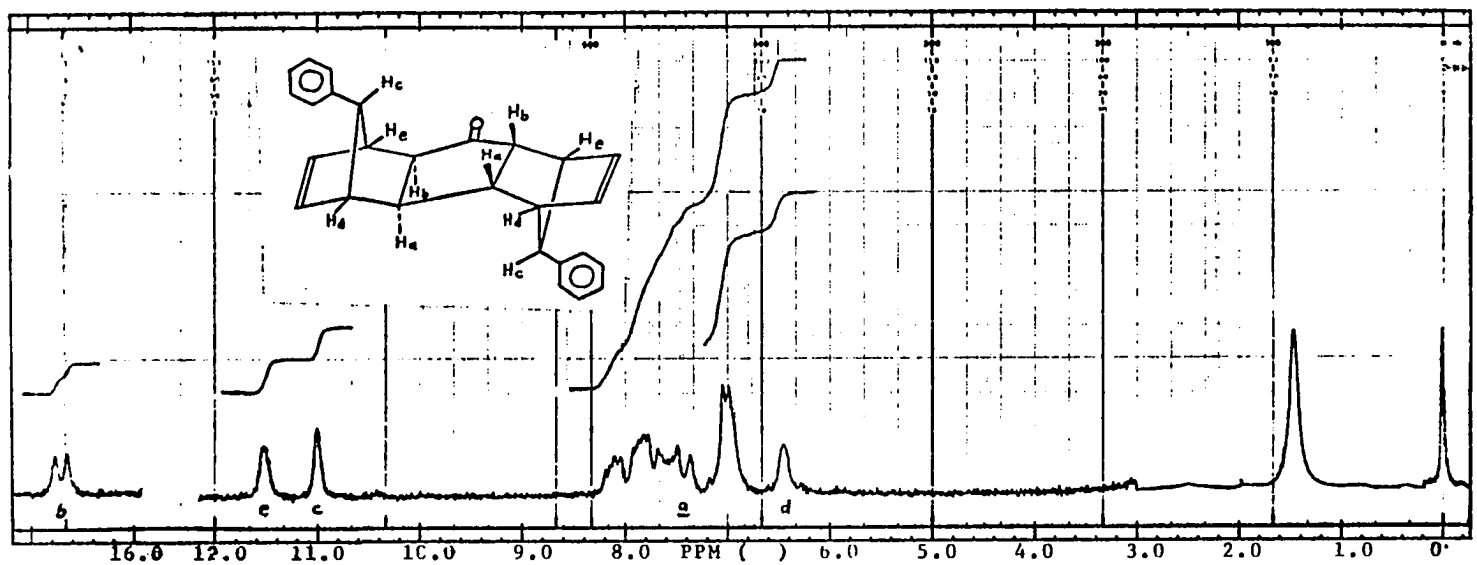

Figure I-17. 60 MHz ^{1}H NMR Spectrum of 7-Phenyl Dimer Ketone VII, RHO = 3.011 ($CDCl_3$/TMS).

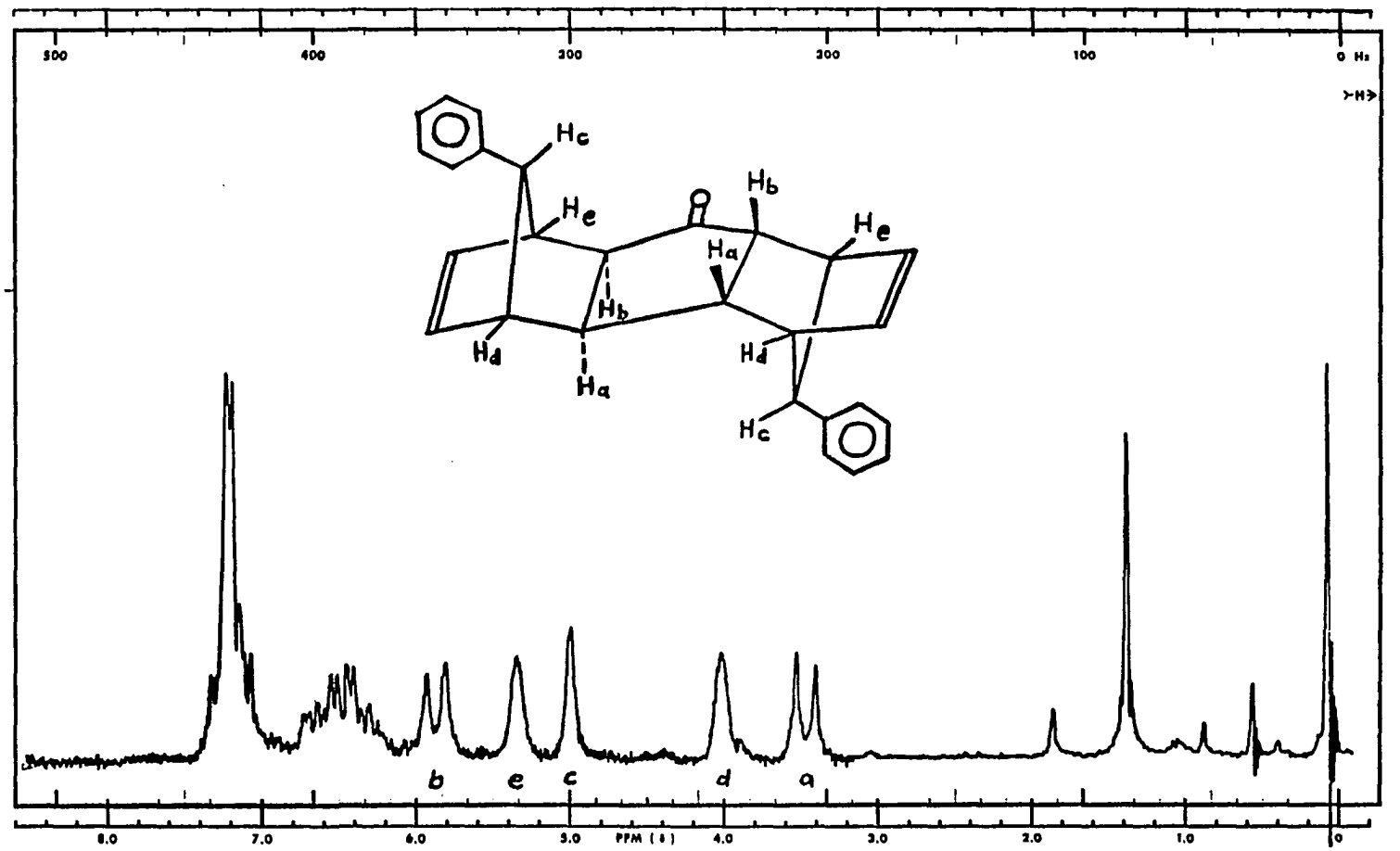

Figure I-18. 60 MHz ^{1}H NMR Spectrum of 7-Phenyl Dimer Ketone VII upon which the decoupling experiments were performed, RHO = 0.250 ($CDCl_3$/TMS).

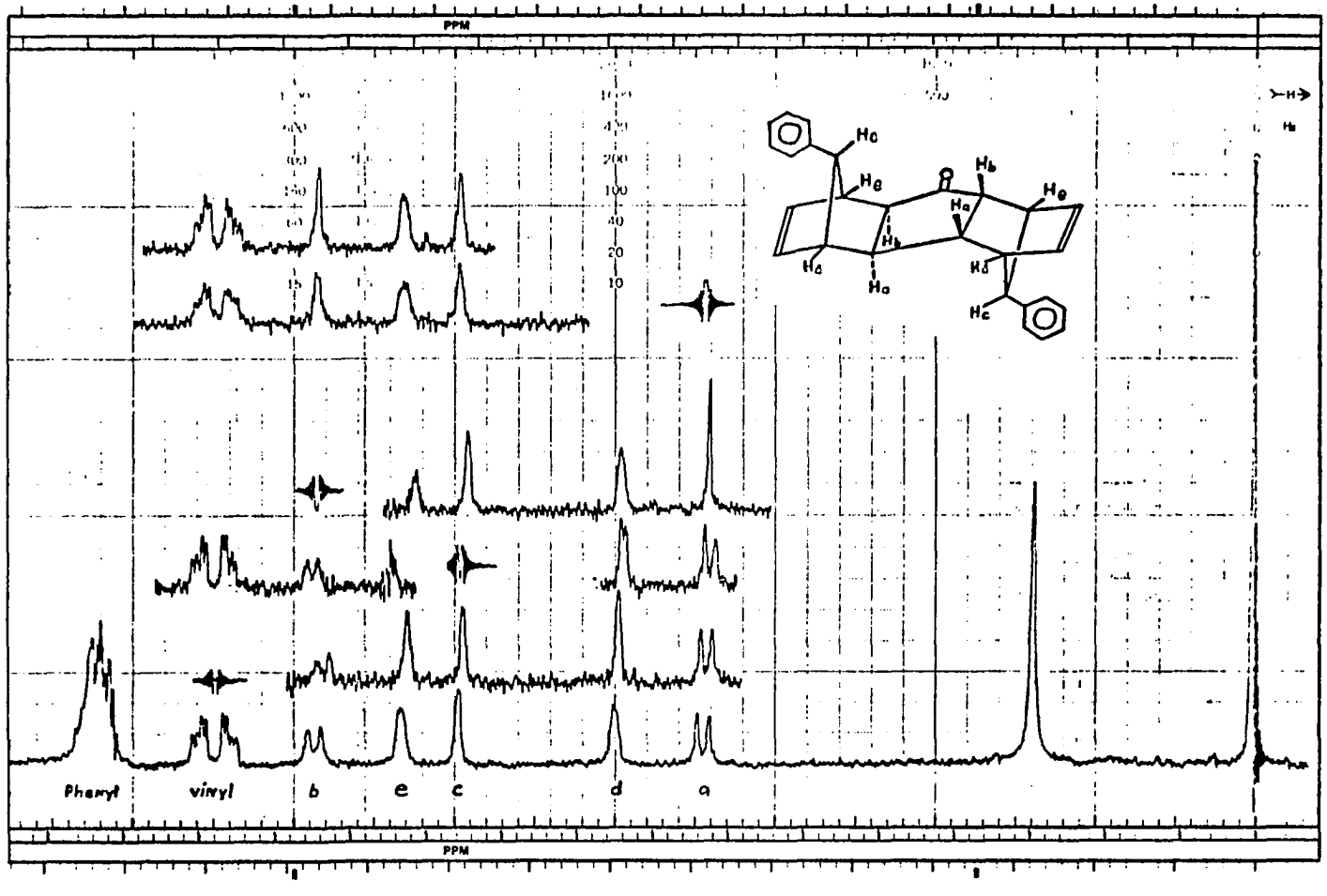

Figure I-19. 100 MHz ^{1}H NMDR Spectra of Phenyl Ketone VII at $[S_o]$ = 0.192M and $[Eu(fod)_3]$ = 0.048 M, $[L_o]/[S_o]$ = RHO = 0.25 ($CDCl_3$/TMS).

TABLE I-2

Matrix of Observed Shifts (δ_i) Read In[a] and Incremental Dilution Volumes[b] for Each RHO_j.

#	RHO	H_a	H_b	H_c	H_d	H_e	Volumes
0	0.000	2.247	2.712	3.178	3.246	3.453	-
1	0.013	2.281	2.803	3.233	3.265	3.510	250
2	0.025	2.319	2.902	3.285	3.285	3.573	250
3	0.050	2.388	3.085	3.338	3.324	3.680	250
4	0.100	2.537	3.482	3.618	3.443	3.930	167
5	0.150	2.690	3.894	3.854	3.517	4.180	125
6	0.200	2.825	4.249	4.056	3.608	4.398	100
7	0.250	2.969	4.636	4.277	3.696	4.615	83
8	0.300	3.100	4.985	4.477	3.783	4.842	72
9	0.350	3.235	5.330	4.675	3.865	5.055	62
10	0.400	3.360	5.640	4.855	3.940	5.240	100
11	0.500	3.580	6.230	5.210	4.080	5.600	83
12	0.600	3.764	6.764	5.492	4.194	5.913	72
13	0.700	3.941	7.243	5.761	4.306	6.200	62
14	0.800	4.107	7.681	6.011	4.404	6.464	56
15	0.900	4.250	8.079	6.235	4.494	6.639	50
16	1.000	4.392	8.457	6.451	4.591	6.927	83
17	1.200	4.651	9.156	6.845	4.751	7.339	72
18	1.401	4.864	9.728	7.157	4.900	7.680	62
19	1.600	5.046	10.226	7.456	5.009	7.978	43
20	1.752	5.177	10.579	7.611	5.081	8.187	63
21	2.000	5.380	11.110	7.962	5.108	8.503	55
22	2.251	5.584	11.641	8.287	5.328	8.839	50
23	2.500	5.744	12.125	8.530	5.428	9.100	46
24	2.752	5.862	12.465	8.726	5.502	9.306	43
25	3.011	5.999	12.850	8.939	5.579	9.526	0

(a) Instrumentally recorded at 100 MHz and listed in ppm for comparison with subsequent spectra obtained at 300 MHz.
(b) Incremental dilution volumes are in microliters (μL).

determinations using decoupling techniques on symmetrical dimer ketone substrates. Why the decouplings, which have proven so useful in the past, have failed for VII is not immediately apparent. Johnston and Shapiro[23] and others[14] have noted the effect of added $Eu(fod)_3$ on the magnitude of proton-proton coupling constants and indicate that erroneous deductions of molecular structure can be made using them. It must be remembered that the spectrum which is actually observed is the average of the spectra of the several species in solution (both complexed and uncomplexed) and that each resulting individual 'averaged' coupling constant is not necessarily the same as it is in the uncomplexed species.

Since the decoupling experiments failed to confirm the position of $H_c(H_{c'})$, a more direct approach was pursued. A single-crystal X-ray structural determination of X (the olefinic double bonds of IX were saturated with H_2 over Pd/C)[7] was made as a more suitable crystal was obtained from X than from either VII or IX.[7,11,24] The cell parameters are; a = 9.466(1) Å, b = 19.413(2) Å, c = 13.095(1) Å, α = 90.0°, β = 106.82(1)°, γ = 90.0°. A numbering scheme and computer drawn representation of X are found in Fig I-20. Atomic positional parameters for carbon and oxygen are listed in Table I-3, and anisotropic thermal parameters are listed in Table I-4. Atomic positional and isotropic thermal parameters for hydrogen are listed in Table I-5. Bond distances involving the non-hydrogen atoms listed in Table I-6 are illustrated in Fig I-11. Bond angles involving non-hydrogen atoms are listed in Table I-7. Carbon-hydrogen bond lengths range from 0.97-1.04 Å with an average length of 1.00 Å. The AXTXA configuration is evident.

The data obtained from the crystal structure provide further information which might be used to account for the inability to determine the syn or anti bridge configuration by decoupling of VII. Figure IV-21 illustrates that an important consideration regarding decoupling failure must be the proximate geometry of the vinyl π cloud relative to the back lobe of the bridge proton (here, H_c) on

FIGURE I-20

Numbering Scheme and Computer Drawn Representation of Compound X.

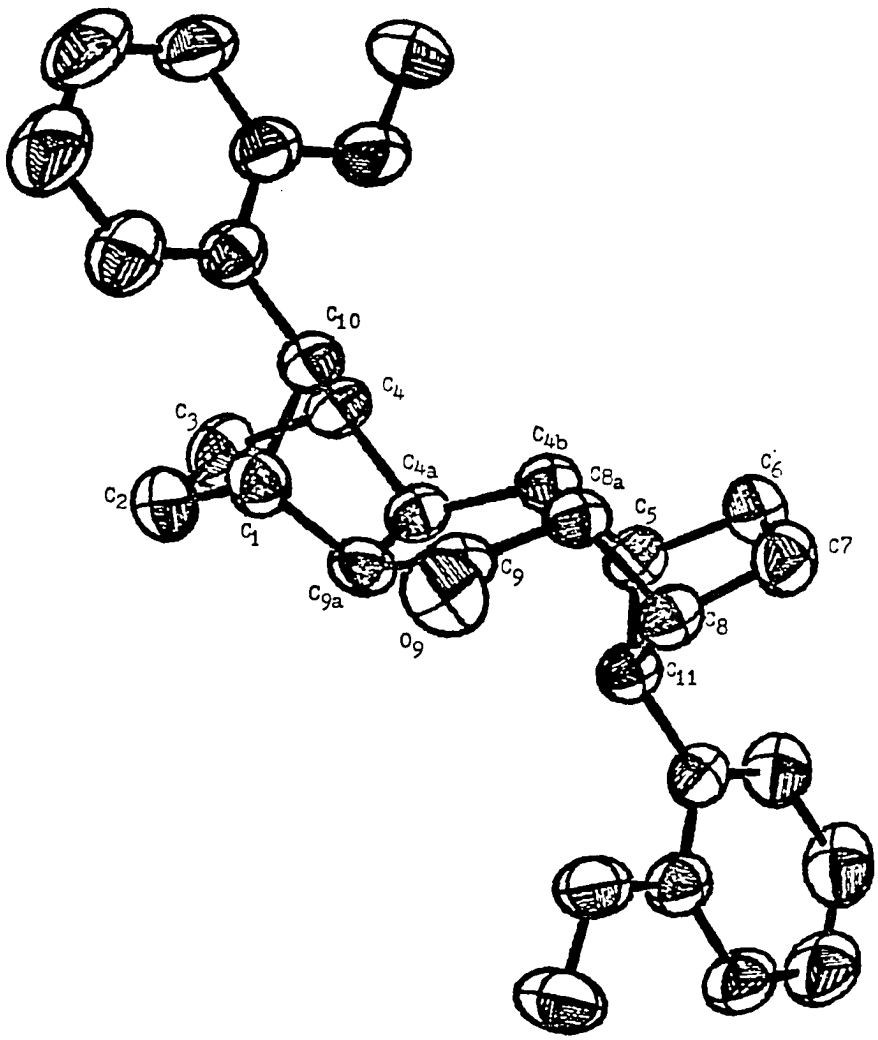

ORTEP (Johnson, 1965) drawing of a single molecule.

TABLE I-3

Atomic Positional Parameters for Carbon and Oxygen.

Standard deviations for the last digit are in parenthesis.

All parameters are multiplied by 10^4.

Atom	x/a	y/b	z/c
C_1	9239(2)	7098(1)	4760(1)
C_2	9440(2)	6398(1)	4276(1)
C_3	8718(2)	6509(1)	3073(1)
C_4	8209(2)	7262(1)	2996(1)
C_{4a}	9587(1)	7729(1)	3245(1)
C_{4b}	9248(1)	8512(1)	3080(1)
C_5	10196(2)	8900(1)	2483(1)
C_6	9620(2)	9650(1)	2337(1)
C_7	10287(2)	9969(1)	3449(1)
C_8	20993(2)	8354(1)	4133(1)
C_{8a}	9740(1)	8861(1)	4201(1)
C_9	10293(2)	8295(1)	5004(1)
C_{9a}	10285(1)	7608(1)	4458(1)
C_{10}	7726(1)	7344(1)	4028(1)
C_{11}	11671(2)	8947(1)	3369(1)
C_{12}	6373(2)	6952(1)	4098(1)
C_{13}	5009(2)	7065(1)	3345(1)
C_{14}	3754(2)	6705(1)	3382(2)
C_{15}	3858(2)	6241(1)	4204(2)
C_{16}	5169(2)	6142(1)	4985(2)
C_{17}	6422(2)	6499(1)	4929(1)
C_{18}	3659(2)	7692(1)	1795(2)
C_{19}	13002(2)	9282(1)	3158(1)
C_{20}	14357(2)	9228(1)	3953(1)
C_{21}	15623(2)	9538(1)	3836(2)
C_{22}	15550(2)	9901(1)	2913(2)
C_{23}	14254(2)	9944(1)	2108(2)
C_{24}	12978(2)	9630(1)	2230(1)
C_{25}	15688(2)	8745(1)	5645(2)
O_9	10675(1)	8376(1)	5963(1)
O_{13}	5006(1)	7550(1)	2586(1)
O_{20}	14327(1)	8859(1)	4835(1)

TABLE I-4

Anisotropic Thermal Parameters for Carbon and Oxygen.

The anisotropic temperature factors are expressed in the form:

$$T = \exp[-2\pi^2(U_{11}h^2a^{*2} + U_{22}k^2b^{*2} + U_{33}l^2c^{*2} + 2U_{12}hka^*b^* + 2U_{13}hla^*c^* + 2U_{23}klb^*c^*)].$$

Atom	U11	U22	U33	U12	U13	U23
C_1	519(8)	479(8)	450(8)	9(7)	70(6)	29(6)
C_2	615(10)	458(8)	810(11)	20(8)	176(9)	-5(8)
C_3	681(10)	504(8)	696(10)	-141(8)	294(8)	-165(8)
C_4	438(7)	506(8)	421(7)	-106(6)	120(6)	-71(6)
C_{4a}	399(7)	464(8)	441(7)	-65(6)	127(6)	-79(6)
C_{4b}	382(7)	470(8)	420(7)	-32(6)	78(5)	-43(6)
C_5	491(8)	489(8)	419(7)	-68(6)	125(6)	-63(6)
C_6	574(10)	535(10)	632(10)	33(7)	164(8)	83(7)
C_7	658(10)	449(8)	737(10)	10(7)	302(9)	-69(7)
C_8	456(8)	473(8)	482(8)	-73(6)	168(6)	-125(6)
C_{8a}	379(7)	458(8)	456(7)	-7(6)	131(6)	-90(6)
C_9	382(7)	531(8)	443(7)	-23(6)	87(6)	-64(6)
C_{9a}	373(7)	468(8)	482(8)	16(6)	38(6)	-51(6)
C_{10}	426(7)	462(8)	416(7)	-35(6)	120(6)	-17(6)
C_{11}	421(7)	443(8)	448(7)	-44(6)	146(6)	-82(6)
C_{12}	508(8)	525(8)	529(8)	-50(7)	230(7)	-37(7)
C_{13}	473(8)	563(10)	665(10)	-53(7)	222(7)	53(7)
C_{14}	508(10)	745(11)	1005(14)	-87(8)	348(9)	-125(10)
C_{15}	803(13)	815(13)	1232(17)	-220(11)	673(12)	-99(12)
C_{16}	998(15)	857(13)	929(14)	-119(12)	613(12)	102(11)
C_{17}	782(12)	727(11)	633(10)	-90(9)	358(9)	45(9)
C_{18}	527(10)	941(15)	1007(15)	90(10)	-17(10)	147(12)
C_{19}	498(8)	433(8)	562(9)	-38(6)	253(7)	-101(6)
C_{20}	465(8)	498(8)	708(10)	-43(7)	239(7)	-96(7)
C_{21}	489(9)	672(11)	1010(14)	-68(8)	343(9)	-65(10)
C_{22}	656(11)	720(11)	1202(16)	-68(9)	567(12)	-30(11)
C_{23}	925(13)	636(11)	916(13)	18(10)	616(12)	47(10)
C_{24}	694(10)	599(10)	654(10)	4(8)	348(8)	-23(8)
C_{25}	476(10)	930(13)	869(14)	89(9)	47(9)	29(10)
O_9	797(8)	720(8)	427(6)	44(6)	83(5)	-98(5)
O_{13}	446(6)	769(8)	762(7)	-39(5)	54(5)	160(6)
O_{20}	431(6)	771(8)	680(7)	-62(5)	104(5)	67(6)

TABLE I-5

Atomic Positional and Isotropic Thermal Parameters for Hydrogen.
Standard deviations for last digit are in parenthesis.
All parameters are multiplied by 10^3.

Atom	x/a	y/b	z/c	U
H_1	935(1)	710(1)	555(1)	1.8(0)
H_{2a}	893(2)	602(1)	455(1)	2.7(0)
H_{2b}	1050(2)	628(1)	447(1)	4.4(0)
H_{3a}	787(2)	620(1)	280(1)	3.1(0)
H_{3b}	937(2)	642(1)	261(1)	3.7(0)
H_4	747(1)	740(1)	231(1)	1.8(0)
H_{4a}	1028(1)	758(1)	281(1)	1.9(0)
H_{4b}	817(1)	857(1)	273(1)	1.4(0)
H_5	1022(1)	867(1)	181(1)	1.6(0)
H_{6a}	992(2)	991(1)	176(1)	3.2(0)
H_{6b}	849(2)	964(1)	209(1)	3.4(0)
H_{7a}	953(2)	1019(1)	372(1)	3.1(0)
H_{7b}	1107(2)	1031(1)	345(1)	3.6(0)
H_8	1168(2)	947(1)	186(1)	2.0(0)
H_{8a}	896(2)	912(1)	440(1)	1.8(0)
H_{9a}	1130(2)	744(1)	465(1)	2.1(0)
H_{10}	758(1)	784(1)	414(1)	1.5(0)
H_{11}	1199(1)	847(1)	366(1)	1.2(0)
H_{14}	281(2)	677(1)	277(1)	4.6(0)
H_{15}	298(2)	598(1)	423(1)	5.7(0)
H_{16}	529(2)	581(1)	561(1)	5.5(0)
H_{17}	740(2)	642(1)	552(2)	6.2(0)
H_{18a}	326(2)	726(1)	134(2)	6.7(0)
H_{18b}	285(2)	786(1)	212(2)	8.6(0)
H_{18c}	391(2)	805(1)	130(2)	6.7(0)
H_{21}	1660(2)	948(1)	443(1)	5.3(0)
H_{22}	1648(2)	1013(1)	286(1)	6.3(0)
H_{23}	1412(2)	1021(1)	145(1)	4.6(0)
H_{24}	1208(2)	965(1)	163(1)	2.3(0)
H_{25a}	1612(2)	920(1)	598(2)	7.4(0)
H_{25b}	1540(2)	844(1)	619(2)	8.1(0)
H_{25c}	1640(2)	849(1)	533(1)	6.0(0)

TABLE I-6

Bond Distances (Å) Involving Non-Hydrogen Atoms.

Atoms	Distance	Atoms	Distance
C_1-C_{10}	1.544(2)	C_{12}-C_{13}	1.397(2)
C_1-C_{9a}	1.538(2)	C_{12}-C_{17}	1.389(2)
C_1-C_2	1.536(2)	C_{13}-C_{14}	1.391(2)
C_2-C_3	1.540(2)	C_{14}-C_{15}	1.384(2)
C_3-C_4	1.534(2)	C_{15}-C_{10}	1.374(2)
C_4-C_{4a}	1.544(2)	C_{16}-C_{17}	1.394(2)
C_4-C_{4b}	1.555(2)	C_{19}-C_{24}	1.385(2)
C_{4a}-C_{9a}	1.552(2)	C_{20}-C_{21}	1.388(2)
C_{4b}-C_{8a}	1.561(2)	C_{21}-C_{22}	1.384(2)
C_{4b}-C_5	1.546(2)	C_{22}-C_{23}	1.369(2)
C_5-C_{11}	1.538(2)	C_{23}-C_{24}	1.403(2)
C_5-C_6	1.546(2)	C_9-O_9	1.212(2)
C_6-C_7	1.540(2)	C_{13}-O_{13}	1.369(2)
C_7-C_8	1.525(2)	C_{18}-O_{13}	1.419(2)
C_8-C_{11}	1.544(2)	C_{20}-O_{20}	1.366(2)
C_8-C_{8a}	1.546(2)		
C_{8a}-C_9	1.505(2)		
C_9-C_{9a}	1.512(2)		
C_{10}-C_{12}	1.515(2)		
C_{11}-C_{19}	1.513(2)		

TABLE I-7

Bond Angles (Deg) Involving Non-Hydrogen Atoms.

Standard deviations are between 0.1 and 0.2 deg.

Atoms	Angle	Atoms	Angle
$C_9-C_{8a}-C_8$	112.0	$C_9-C_{9a}-C_1$	111.2
$C_9-C_{8a}-C_{4b}$	106.8	$C_{4a}-C_{9a}-C_1$	104.2
$C_8-C_{8a}-C_{4b}$	103.9	$C_{20}-C_{21}-C_{22}$	119.4
$C_{20}-C_{19}-C_{11}$	117.6	$C_{19}-C_{11}-C_5$	120.7
$C_{20}-C_{19}-C_{24}$	117.9	$C_{19}-C_{11}-C_8$	114.8
$C_{11}-C_{19}-C_{24}$	124.5	$C_5-C_{11}-C_8$	93.5
$C_{10}-C_{12}-C_{13}$	120.3	$C_{13}-O_{13}-C_{18}$	118.4
$C_{10}-C_{12}-C_{17}$	121.9	$C_{19}-C_{24}-C_{23}$	121.1
$C_{13}-C_{12}-C_{17}$	117.8	$C_{15}-C_{16}-C_{17}$	119.4
$C_{12}-C_{10}-C_4$	117.9	$C_{24}-C_{23}-C_{22}$	119.7
$C_{12}-C_{10}-C_1$	116.8	$C_4-C_{4a}-C_{9a}$	102.2
$C_4-C_{10}-C_1$	93.3	$C_4-C_{4a}-C_{4b}$	114.6
$C_{20}-O_{20}-C_{25}$	118.4	$C_{9a}-C_{4a}-C_{4b}$	107.4
$C_{11}-C_5-C_{4b}$	100.4	$C_{14}-C_{15}-C_{16}$	121.0
$C_{11}-C_5-C_6$	104.4	$C_{8a}-C_8-C_{11}$	100.9
$C_{4b}-C_5-C_6$	106.7	$C_{8a}-C_8-C_7$	107.9
$C_{8a}-C_9-O_9$	124.6	$C_{11}-C_8-C_7$	102.3
$C_{8a}-C_9-C_{9a}$	111.1	$C_{21}-C_{22}-C_{23}$	120.7
$O_9-C_9-C_{9a}$	124.3	$C_{8a}-C_{4b}-C_5$	101.8
$C_{19}-C_{20}-O_{20}$	115.4	$C_{8a}-C_{4b}-C_{4a}$	107.5
$C_{19}-C_{20}-C_{21}$	121.3	$C_5-C_{4b}-C_{4a}$	114.8
$O_{20}-C_{20}-C_{21}$	123.4	$C_3-C_2-C_1$	103.1
$C_{12}-C_{13}-C_{14}$	121.4	$C_8-C_7-C_6$	103.3
$C_{12}-C_{13}-O_{13}$	115.3	$C_{12}-C_{17}-C_{16}$	121.3
$C_{14}-C_{13}-O_{13}$	123.3	$C_5-C_6-C_7$	103.2
$C_{13}-C_{14}-C_{15}$	119.0	$C_4-C_3-C_2$	103.8
$C_{10}-C_4-C_{4a}$	101.5	$C_{10}-C_1-C_{9a}$	101.1
$C_{10}-C_4-C_3$	101.9	$C_{10}-C_1-C_2$	102.9
$C_{4a}-C_4-C_3$	108.4	$C_{9a}-C_1-C_2$	107.0
$C_9-C_{9a}-C_{4a}$	107.0		

FIGURE I-21

Proximate Geometry of the Vinyl π Cloud Relative to the Back Lobe of the Bridge Proton (here H_c) on C_7.[25]

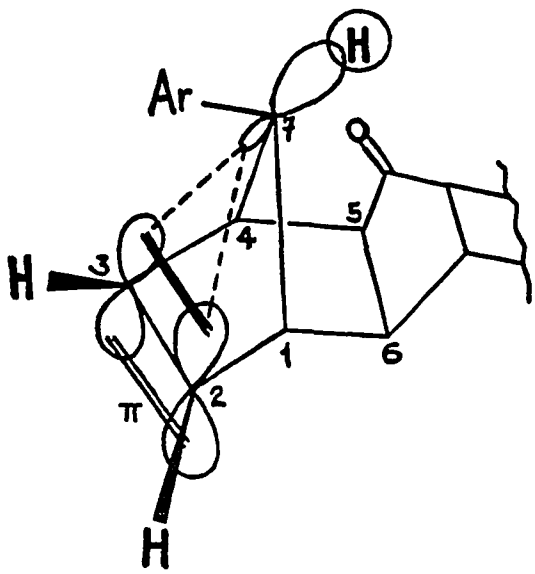

C_7.[25] One implication is that the Pauli repulsion between aromatic and vinyl electrons is sufficient to increase the four anti bond angles (i.e., C_2-C_1-C_{10}, C_3-C_4-C_{10}, C_7-C_8-C_{11}, and C_6-C_5-C_{11}, labeled A, B, C, and D, respectively) relative to the corresponding syn bond angles (C_{9a}-C_1-C_{10}, C_{4a}-C_4-C_{10}, C_{8a}-C_8-C_{11}, and C_{4b}-C_5-C_{11}, labeled A′, B′, C′, and D′, respectively) which are illustrated in Fig I-11. Table I-8 indicates this along with the corresponding non-bonded

TABLE I-8

Selected Bond Angles (Deg) and Bond Distances (Å).[a]
Errors for the last digit are in parenthesis.

Anti Bond Angles		Syn Bond Angles		Δ(deg)
Atoms	Angle	Atoms	Angle	Anti-Syn
C_2-C_1-C_{10}	102.9(.15)	C_{9a}-C_1-C_{10}	101.1(.15)	1.8
C_7-C_8-C_{11}	102.3(.15)	C_{8a}-C_8-C_{11}	100.9(.15)	1.4
C_3-C_4-C_{10}	101.9(.15)	C_{4a}-C_4-C_{10}	101.5(.15)	0.4
C_6-C_5-C_{11}	104.4(.15)	C_{4b}-C_5-C_{11}	100.4(.15)	4.0

Anti Non-bonded Distance		Syn Non-Bonded Distance		Δ(Å)
Atoms	Distance	Atoms	Distance	Anti-Syn
C_2-C_{10}	2.409(3)	C_{9a}-C_{10}	2.380(3)	0.029
C_7-C_{11}	2.390(3)	C_{8a}-C_{11}	2.383(3)	0.007
C_3-C_{10}	2.399(3)	C_{4a}-C_{10}	2.340(3)	0.029
C_6-C_{11}	2.437(3)	C_{4b}-C_{11}	2.369(3)	0.068

(a) Figure I-11 is a labeling scheme and Fig I-20 is a computer drawn representation. The bond angle errors indicated are from Table I-7. Non-bonded distances were calculated using the formula:

$a^2 = b^2 + c^2 - 2bc\cos\theta$

(where θ is the C_i-C_j-C_k angle, a = C_i-C_k non-bonded distance, b = C_i-C_j bond distance, and c = C_j-C_k bond distance). The bond distances and bond angles listed in Tables I-6 and I-7, respectively, were used as needed. Delta is the difference between the anti and syn values of the particular parameter.

atomic distances. The anti separations are all larger than their syn counterparts! Given the above 'anti > syn' bond angles and non-bonded distances, it may be that this distortion removes the requisite orbital alignment and increases the distance between the vinyl π lobes and the back side of the bridge proton sp^3 lobe to the extent that optimum transferal of spin information via this through-space mechanism is not possible.[25] Admittedly, the differences are small. Steric repulsion between the phenyl substituent and olefinic moiety and line broadening may also contribute to the lack of observable coupling.

The important role played by the rear-lobe proximity on the proton coupling constants has been demonstrated.[26,27] The coupling constants between the protons attached to the bridgehead carbon atoms of the bicycloalkane series bicyclo[1,1,1]pentane, bicyclo[2,1,1]hexane, and bicyclo[2,2,1]heptane were considered. It was assumed that these long-range proton couplings decrease substantially more than would be expected for coupling over essentially equivalent four-bond paths.[28] This assumption led to the conclusion that non-bonded interactions between the bridgehead carbon atoms should originate this behavior. It was found that the magnitude of the proton coupling constants [18 > 8 > 1.4 Hz] and the angle defined by the bridgehead C-H bonds [180 > 174.7 > 151.5°] decreased through the bicycloalkane series as the distance between the bridgehead carbon atoms [1.844 < 2.172 < 2.317 Å] increased.

Based upon the considerable similarity of the NMR and IR spectra of VII and IX, it was concluded that both VII and IX possess the same AXTXA structure as X. Mechanistically, formation of VII (Scheme I-2) is believed to parallel that shown in Scheme I-1, with the added feature that the syn double bond is effectively prevented from coupling via its exo face by the steric bulk of the phenyl ring.

Shortly after the structural confirmations of dimer ketones VII and IX, the University obtained a high resolution Varian XL-300 NMR spectrometer. Since the 100 MHz decouplings had failed to predict

SCHEME I-2

Mechanism of Formation of 7-Phenyl Dimer Ketone VII Suggested by Marchand and Goodin.

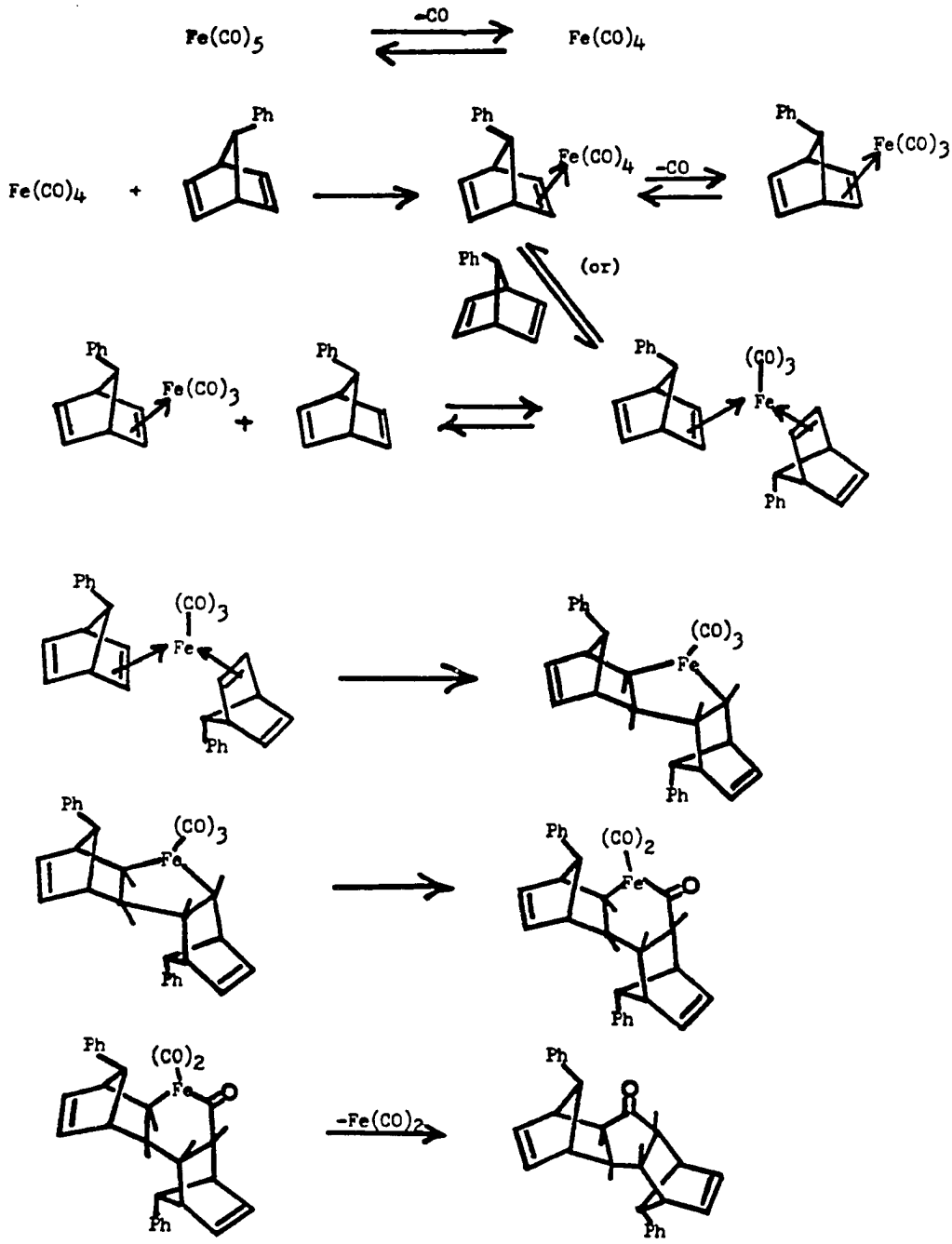

their stereochemistry, it was felt that the higher resolution of the 300 MHz instrument would confirm the presence of the undetected vinyl and 'W-letter' couplings. Accordingly, the 300 MHz ^{1}H NMR of VII was obtained. The spectrum (Fig I-22) clearly separates the protons in the critical 3.0-3.3 ppm region. However, decouplings again failed to confirm the AXTXA stereochemistry, but do support the identity and chemical shift assignments of each aliphatic and olefinic proton, as labeled on the spectrum.

A useful feature available in the spectrometer's software is the spin-echo pulse sequence whereby carbon atoms bearing an even number (0 or 2) of directly attached protons appear with opposite phase relative to carbons bearing odd (1 or 3) numbers of directly attached protons.[29] This results from an amplitude modulation of the noise-decoupled ^{13}C NMR spectrum by heteronuclear J couplings which are converted into sign and intensity information.[30] Throughout this discussion all spin-echo spectra with carbons bearing odd numbers of directly attached protons will appear as upright (i.e., positive) absorption signals, while carbons bearing even numbers of directly attached protons will appear as inverted (dispersion) signals. For phenyl ketone VII, the result of this technique and the conventional broadband decoupled ^{13}C spectra are shown in Fig I-23. The carbonyl and quaternary aromatic carbon signals appear inverted.

Another important program supplied with the spectrometer is the Homonuclear Correlated 2-D (two dimensional) NMR pulse sequence,[31] which makes it possible to correlate the chemical shifts of protons whose spins are coupled. Figures I-24 and I-25 illustrate the "HOMCOR" experiment for ketone VII. The chemical shift axis lies on the lower-left to upper-right diagonal. Symmetrically disposed off-diagonal signals denote coupling between the two protons represented by the signals at the corresponding positions on the diagonal. Figure I-24 shows that the vinyl protons are indeed coupled to $H_c(H_{c'})$, while Fig I-25 shows that $H_a(H_{a'})$ and $H_b(H_{b'})$

FIGURE I-22

300 MHz ^{1}H NMR Spectrum of 7-Phenyl Dimer Ketone VII ($CDCl_3$/TMS).

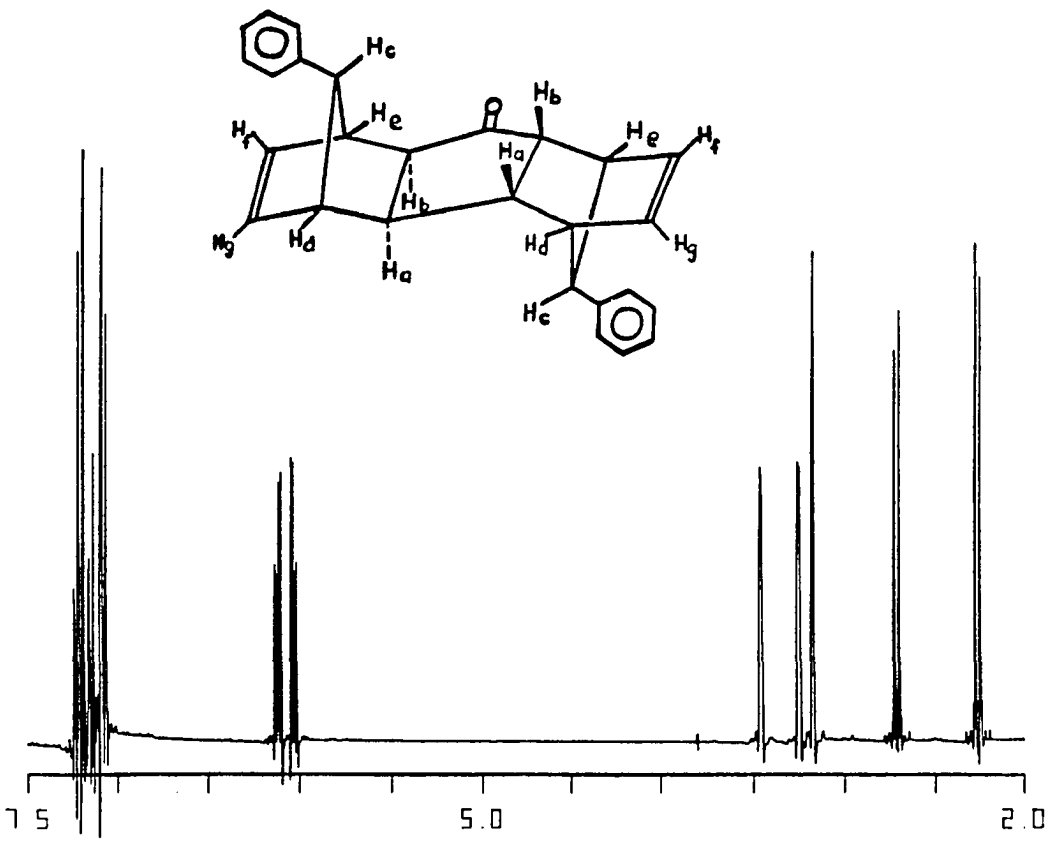

FIGURE I-23

75 MHz ^{13}C (lower) and Spin Echo (upper) NMR Spectra of 7-Phenyl Dimer Ketone VII ($CDCl_3$).

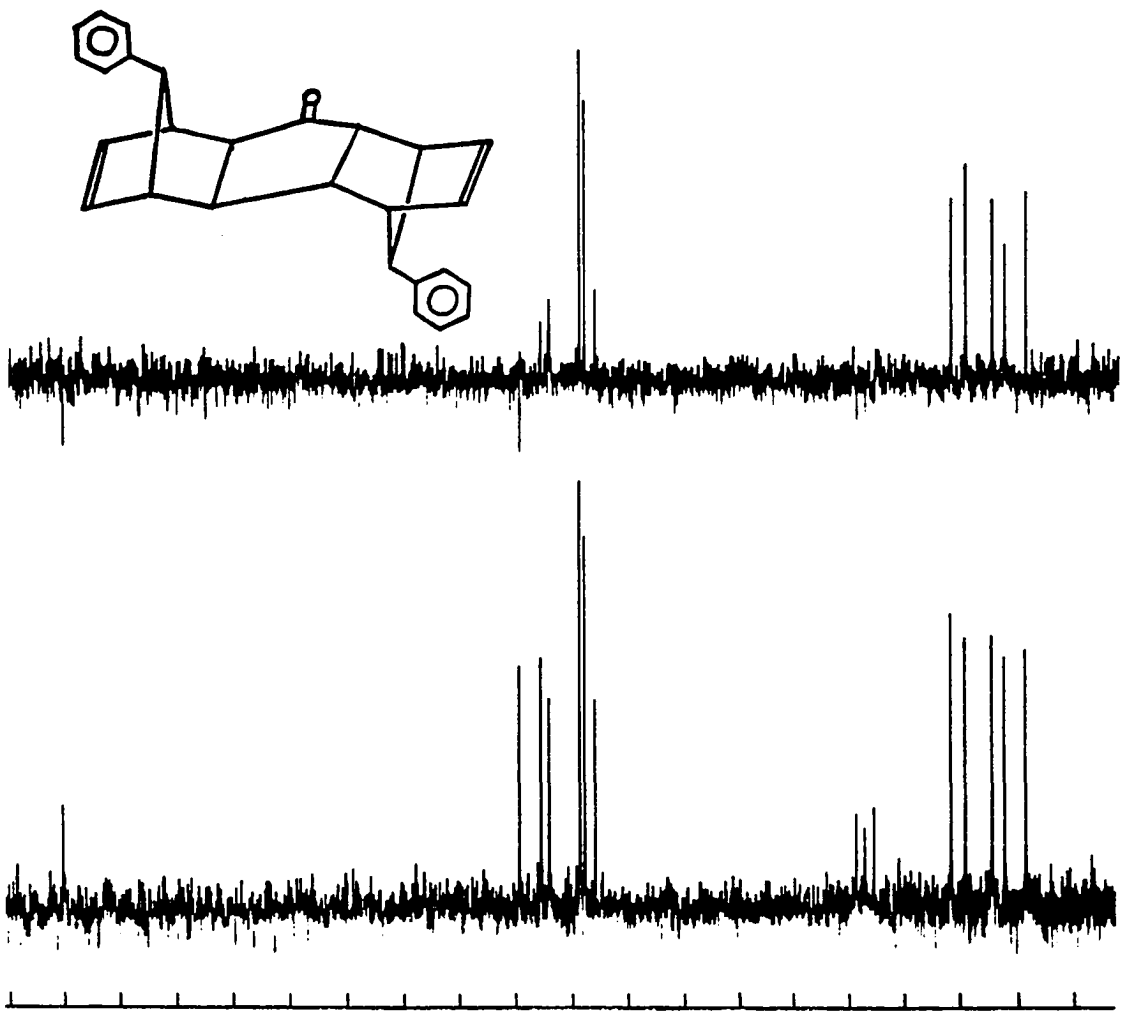

FIGURE I-24

Homonuclear Correlated 2-D NMR Spectrum of 7-Phenyl Ketone VII.

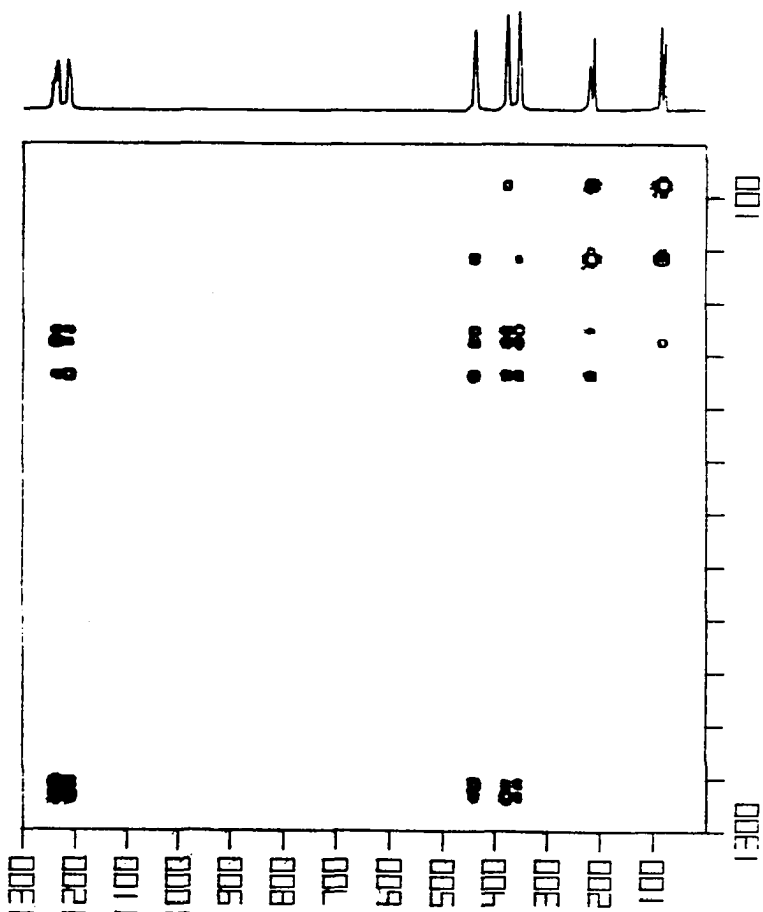

FIGURE I-25

Expanded Upfield Region of the HOMCOR Spectrum (Fig I-24) of 7-Phenyl Dimer Ketone VII.

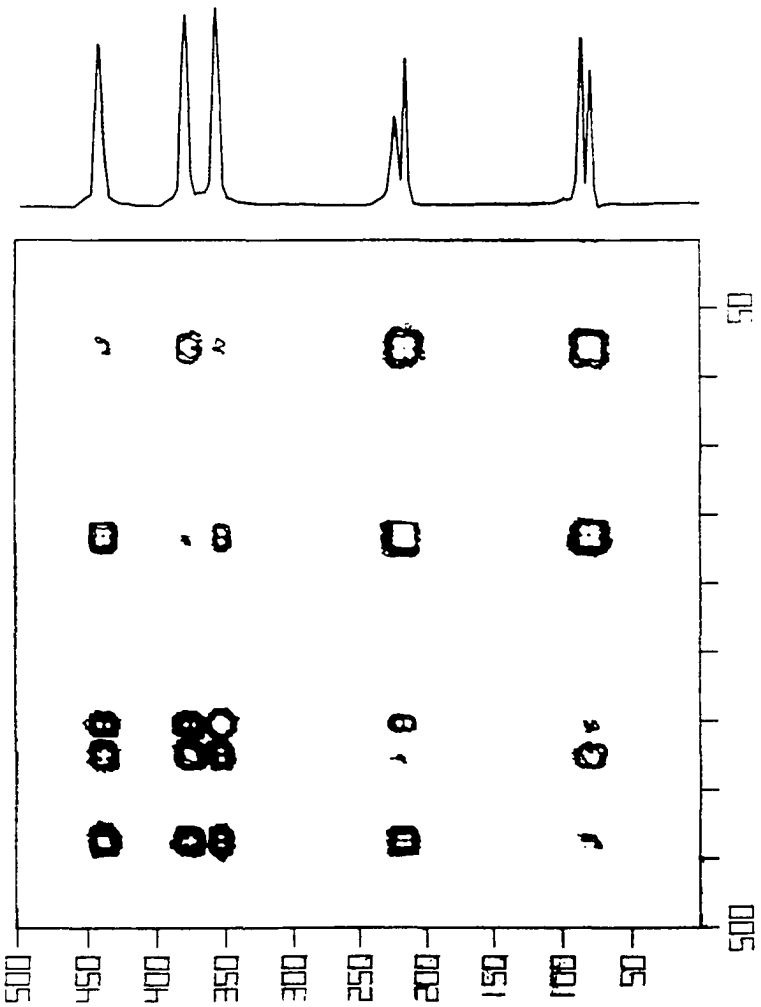

are coupled to $H_c(H_{c'})$ which is syn to them. These seemingly contradictory observations indicate the need for care in interpreting the results of decouplings since $H_c(H_{c'})$ would be coupled to $H_a(H_{a'})$ and $H_b(H_{b'})$ from both the syn and anti positions. The magnitude of coupling is smaller in the syn geometry. Figure I-25 also shows that each of the five protons is coupled to each of the other four protons!

The 300 MHz ^1H NMR spectrum of o-anisyl ketone IX (Fig I-26) shows the very small separation of the $H_d(H_{d'})$ and $H_c(H_{c'})$ signals at 3.24 and 3.26 ppm, respectively. Decouplings again fail to support the AXTXA stereochemistry but do allow identity and chemical shift assignments of the olefinic and aliphatic protons as seen on the figure. The 75 MHz ^{13}C broadband and spin-echo spectra are shown on Fig I-27, and Figs I-28 and I-29 illustrate the HOMCOR spectrum. The lack of resolution does not allow observation of $^JH_a(H_{a'})-H_d(H_{d'})$ and $^JH_b(H_{b'})-H_e(H_{e'})$, but the coupling patterns for ketones VII and IX are identical.

Experimental

ALL weights were determined on a Sargent balance. Proton NMR spectra were recorded on Varian Model T60, XL-100, and XL-300 spectrometers. Infrared spectra were recorded on Perkin-Elmer Model IR-8, IR-298, and 710-B spectrophotometers, while the mass spectrum of VII was recorded on a Hitachi Perkin-Elmer Model RMU-6E spectrometer (70 eV). The X-ray structure data was obtained on a Nonius CAD-4 automatic diffractometer using Ni-filtered $CuK\alpha_1$ radiation (λ = 2.5418 Å).[7,24] All melting points were determined on a Thomas-Hoover capillary melting point apparatus. Elemental analyses were performed by Chemalytics, Inc., Tempe, Az.

7-o-Anisylnorbornadiene (VIII) was prepared in this laboratory.[7] 7-Phenylnorbornadiene (VI) was obtained from Frinton

FIGURE I-26

300 MHz ^{1}H NMR Spectrum of 7-o-Anisyl Dimer Ketone IX ($CDCl_3$).

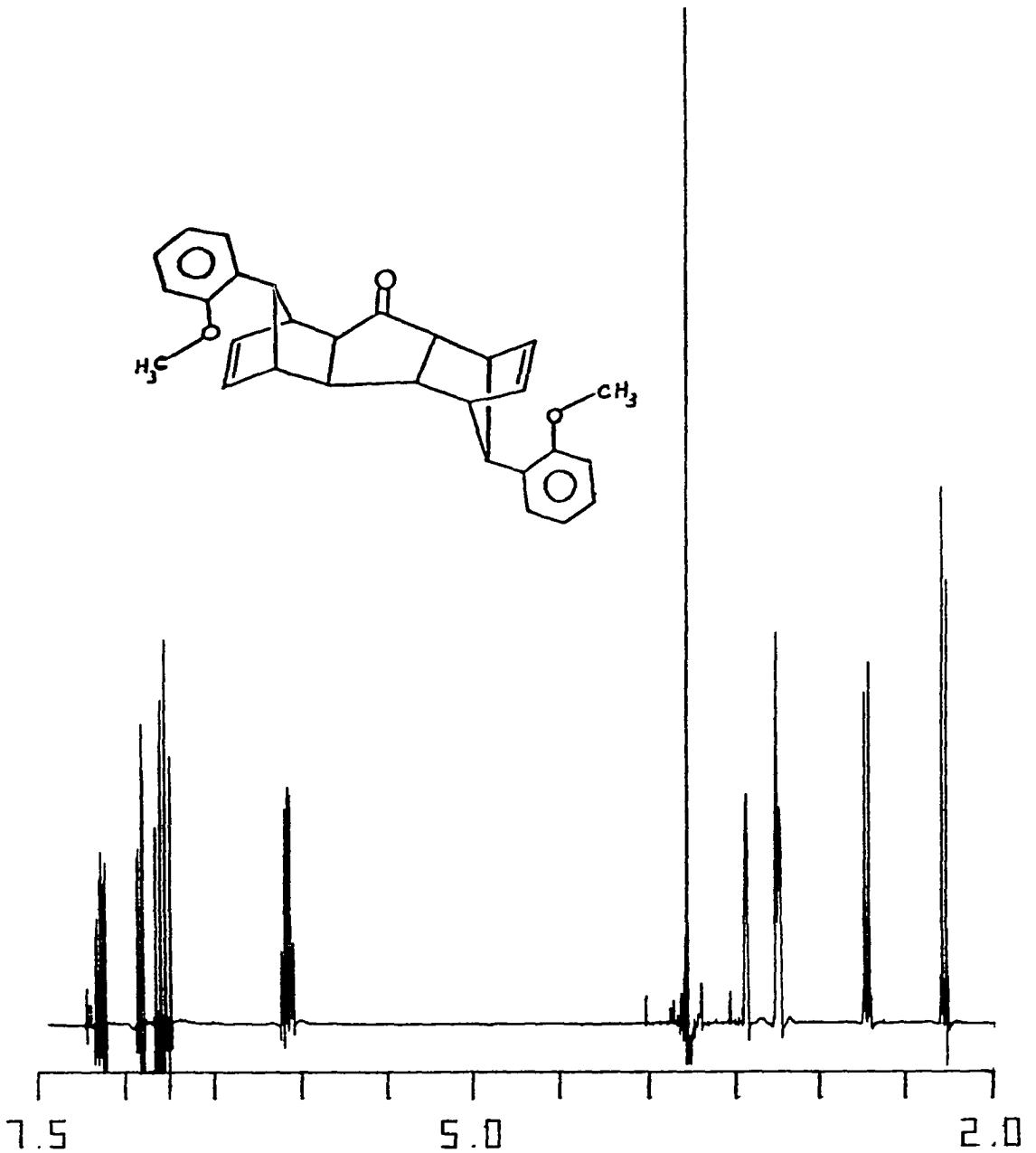

FIGURE I-27

75 MHz ^{13}C (lower) and Spin Echo (upper) Spectra of 7-o-Anisyl Dimer Ketone IX ($CDCl_3$).

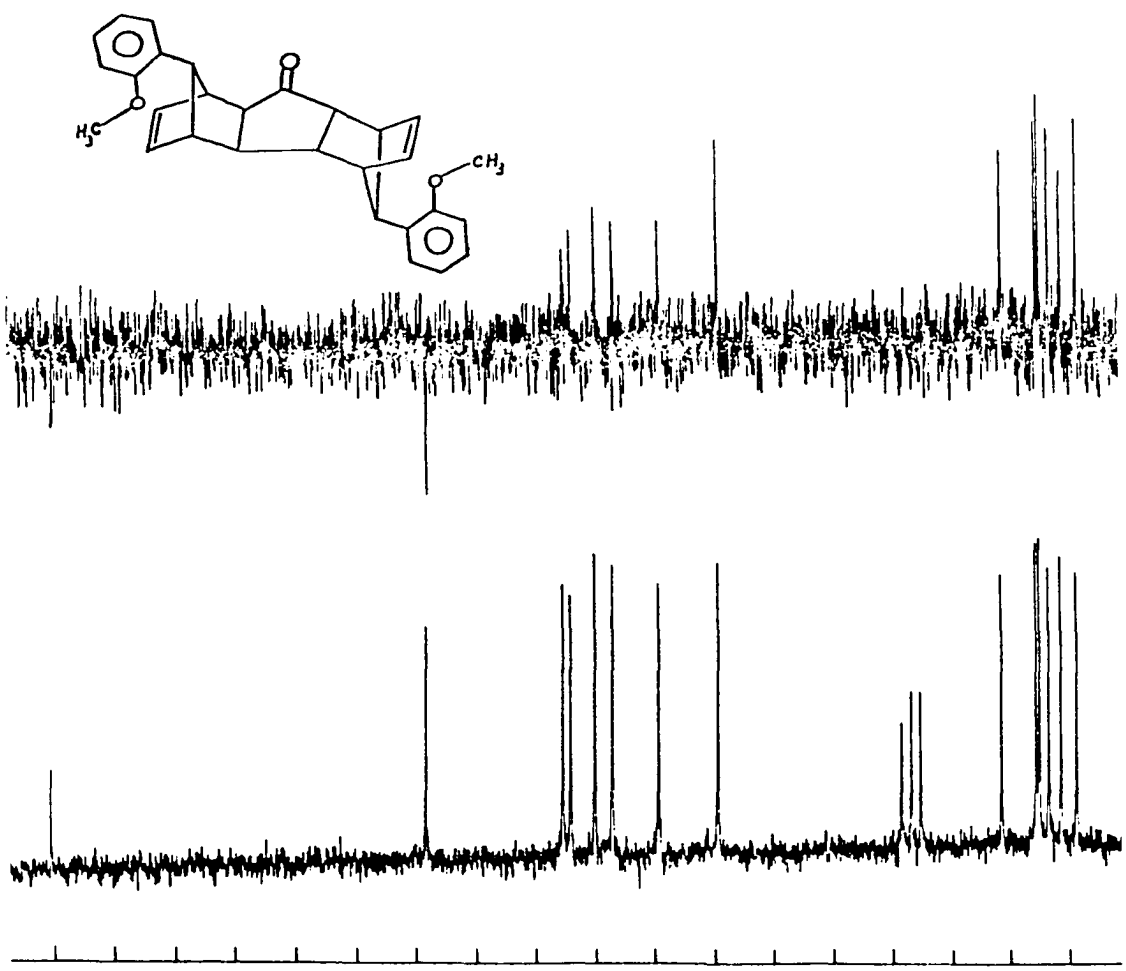

FIGURE I-28

Homonuclear Correlated 2-D NMR Spectrum of 7-o-Anisyl Ketone IX ($CDCl_3$).

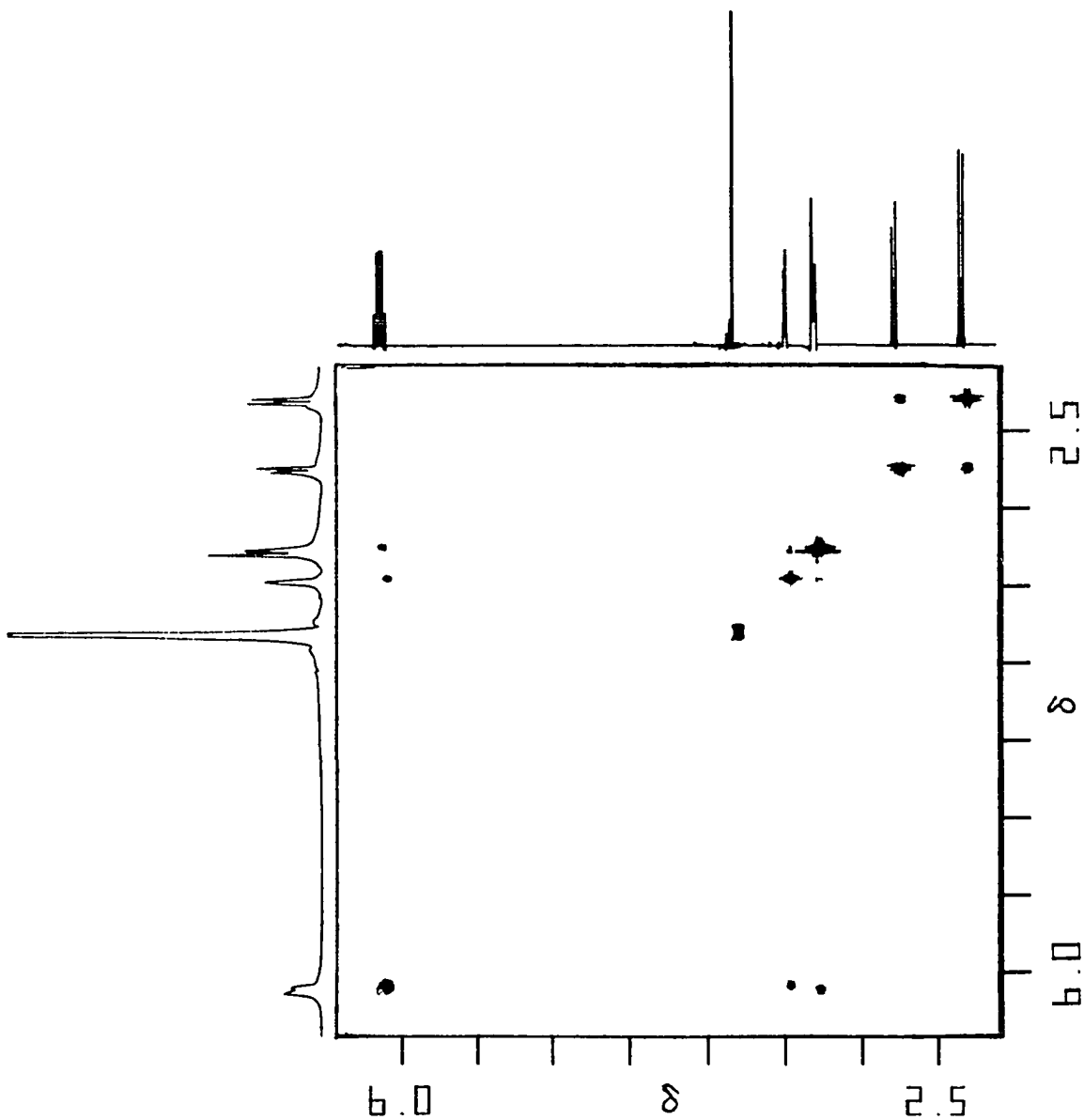

FIGURE I-29

Expanded Upfield Region of the HOMCOR Spectrum (Fig I-28) of 7-o-Anisyl Dimer Ketone IX ($CDCl_3$).

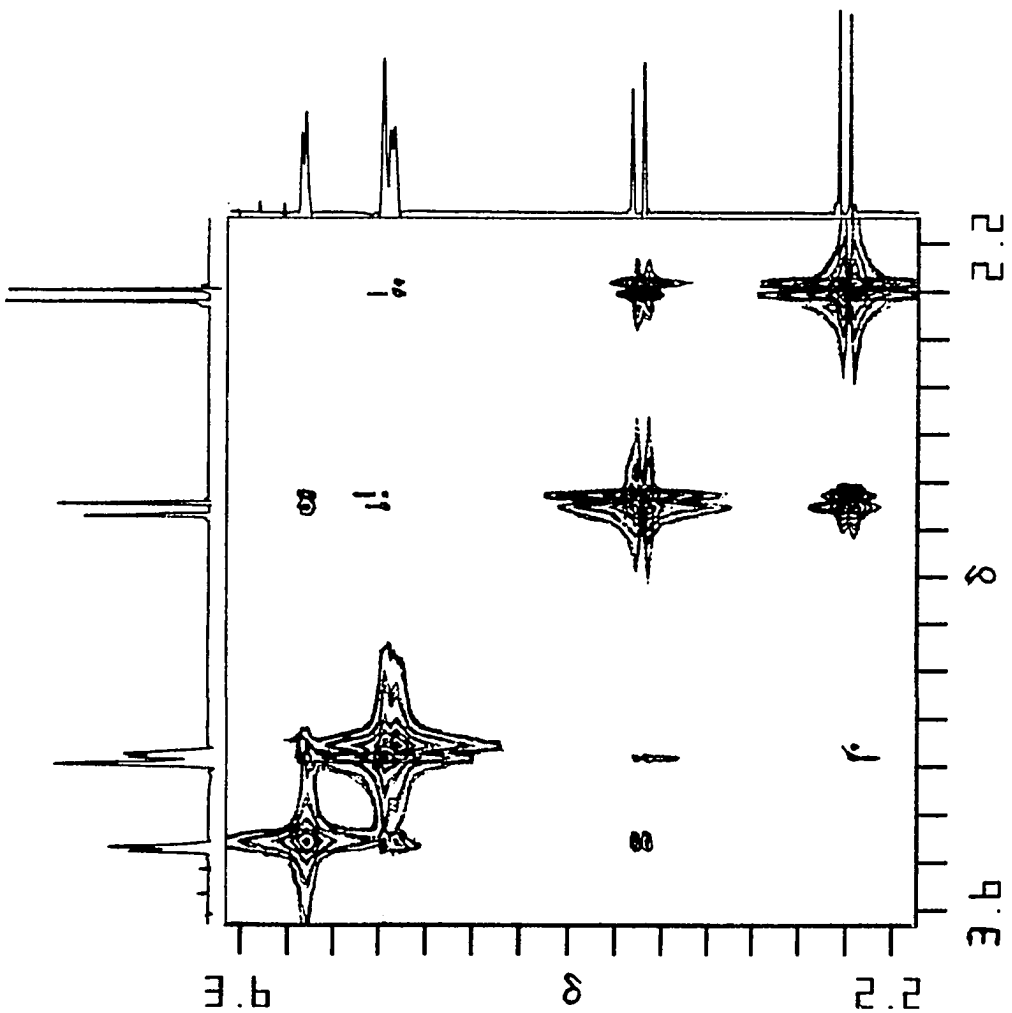

Laboratories, Vineland, NJ.; Iron pentacarbonyl from Alpha-Ventron, Andover, Ma.; $Eu(fod)_3$ from Aldrich Chemical Co., Inc., Milwaukee, Wi.; and $CDCL_3$/1%TMS from Norell Chemical Co., Inc., Landisville, NJ..

The reactions of 7-o-anisylnorbornadiene and 7-phenylnorbornadiene (VI) with iron pentacarbonyl to produce AXTXA dimer ketones IX and VII, respectively, were carried out using literature methods.[7]

High Resolution Proton NMR Spectra of Phenyl Ketone VII.

^{1}H NMR spectrum (300 MHz, $CDCl_3$, Fig I-22): δ 7.5-7.07 (m, 5 H, Ar-H), 6.11 (dd, J = 5.7 Hz, J′ = 2.9 Hz, 2 H, anti vinyl protons), 6.03 (dd, J = 5.7 Hz, J′ = 2.9 Hz, 2 H, syn vinyl protons), 3.45 (dd, J = 2.9 Hz, J′ = 1.3 Hz, 2 H, syn bridgehead protons), 3.24 (dd, J = 2.9 Hz, J′ = 1.3 Hz, 2 H, anti bridgehead protons), 3.17 (m, 2 H, bridge protons), AB pattern (J_{AB} = 7.5 Hz) δ_B 2.71 (2 H, syn cyclopentanone protons), and δ_A 2.25 (2 H, anti cyclopentanone protons);

HOMCOR NMR spectra (300 MHz, $CDCL_3$, Figs I-24 and I-25);

IR spectrum (film, Fig I-6);

Mass spectrum (70 eV, Fig I-7);

^{13}C and Spin Echo NMR spectra (20 MHz, $CDCL_3$, Fig I-23): δ 220.36, 139.22, 135.50, 134.03, 128.63, 127.75 125.94, 61.47, 59.05, 54.27, 22.17, 48.68;

High Resolution Proton NMR Spectra of o-Anisyl Ketone IX.

^{1}H NMR spectrum (300 MHz, $CDCL_3$, Fig I-26): δ 6.74-7.14 (m, 4 H, Ar-H), 6.10 (dd, J = 5.5 Hz, J′ = 2.9 Hz, 2 H, anti vinyl protons), 6.06 (dd, J = 5.5 Hz, J′ = 2.9 Hz, 2 H, syn vinyl protons), 3.77 (s, 3 H, OCH_3), 3.44 (dd, J = 2.9 Hz, J′ = 1.3 Hz, 2 H, syn bridgehead protons), 3.26 (dd, m, 2 H, bridge protons), 3.24 (dd, J = 2.9 Hz, J′ = 1.3 Hz, 2 H, anti bridgehead protons), AB pattern (J_{AB} = 7.5 Hz) δ_B 2.72 (2 H, syn cyclopentanone protons), δ_A 2.27 (2 H, anti cyclopentanone protons);

HOMCOR NMR spectra (300 MHz, $CDCL_3$, Figs I-28 and I-29).

IR spectrum (KBr pellet, Fig I-10);

^{13}C and Spin Echo NMR spectra (75 MHz, $CDCl_3$, Fig I-27): δ 220.76, 158.52, 135.63, 134.41, 130.34, 127.48, 127.30, 119.55, 109.71, 61.47, 55.63, 55.10, 53.47, 51.42, 48.77;

Lanthanide Shift Reagent Proton NMR Study of Phenyl Ketone VII

The nuclear magnetic resonance lanthanide shift reagent tris(1,1,1,2,2,3,3-heptafluoro-7,7-dimethyloctane-4,6-dionato)europium (III) [$Eu(fod)_3$, molecular weight 1037.49 g/mol] was obtained as a yellow microcrystalline solid. Since $Eu(fod)_3$ is hygroscopic and decomposes upon prolonged exposure to air,[22] it was purified via sublimation under reduced pressure (160-170 °C, 0.03 torr) prior to use and stored in a drying pistol over P_2O_5 for 24 hours to exclude moisture.

A particular molar concentration of substrate ($[S_0]$ = 0.192 M) was chosen which gave a good signal-to-noise ratio (S/N) in a 60 MHz proton NMR spectrum. Good S/N is important since subsequent addition of shift reagent decreases resolution.[13-15] This optimum molar concentration was prepared by addition of a carefully weighed amount of pure solid VII (0.035 g, 9.603×10^{-5} mol) to an NMR tube followed by dilution to 0.5 mL with $CDCL_3$/1%TMS. The deuterated solvent was purified prior to use by distillation and was stored over molecular sieves to remove traces of scavengers which can interfere with shift reagent studies by competing with the substrate for complexation with $Eu(fod)_3$.[23,29]

After selection of an appropriate $[S_0]$, a carefully weighed amount of $Eu(fod)_3$ (0.3 g, 2.892×10^{-4} mol, chosen such that RHO_{25} = 3.011) was then added to a clean dry NMR tube. A sufficient volume of a stock solution of VII (prepared by diluting 0.126 g, 3.457×10^{-4} mol, of VII to 1.3 mL with $CDCL_3$/1%TMS, giving a concentration of 0.192 M) was added until the precalibrated

tube contained 0.5 mL of LSR-VII-$CDCL_3$/1%TMS solution. Alternatively, $CDCL_3$/1%TMS may be added to an NMR tube already containing 0.3 g of $Eu(fod)_3$ and 0.035 g of VII. All initial solutions were prepared in a glove bag under a nitrogen atmosphere. A 60 MHz NMR spectrum was obtained and chemical shifts were recorded relative to internal TMS. By use of a modification of the incremental dilution technique,[23] the sample in the tube was diluted with the stock substrate solution to predetermined RHO values by: (i) removal of slightly more than a calculated amount of solution using a microliter syringe equipped with a long needle, (ii) addition of a calculated amount of the stock solution, and (iii) addition of the solution from part (i) above until the total tube contents was again 0.5 mL. This procedure was continued, 60 MHz spectra obtained, and shifts and RHO's recorded with each step, until RHO = 0.013 was reached. RHO = 0.25 was chosen during this sequence and the 100 MHz decoupling experiments were performed on that sample. The incremental dilution experiment (omitting the decouplings) was also performed at 100 MHz (Table I-2) using identical concentrations and volumes.

Appendix: Sample Calculations

The $[S_0]$ of 0.192 M was found to give an adequate signal to noise ratio. This concentration was arrived at by diluting 0.035 g of substrate VII (molecular weight 364.488 g/mol) with 0.5 mL of $CDCL_3$/1%TMS in a clean dry NMR tube (Eq I-2).

$$[(0.035\ g)/(364.488\ g/mol)]/0.5\times10^{-3}\ L = 0.19205\ M\ VII \qquad \text{Eq I-2}$$

The substrate stock solution was prepared by diluting 0.126 g of VII to 1.8×10^{-3} L with $CDCL_3$/1%TMS (Eq I-3).

$$[(0.126.g)/(364.488\ g/mol)]/1.8\times10^{-3}\ L = 0.192\ M\ of\ VII \qquad \text{Eq I-3}$$

For preparation of the initial RHO value of about 3.0, 0.035 g of substrate VII was added to a clean dry NMR tube followed by addition of 0.3 g of $Eu(fod)_3$, molecular weight 1037.49 g/mol. This was diluted to 0.5×10^{-3} L with $CDCL_3$/1%TMS. The RHO value is calculated as in Eq I-4.

$$RHO_{initial} = RHO_{25} \qquad \text{Eq I-4}$$

$$RHO_{25} = [(0.3\ g)/(1037.49\ g/mol)]/[(0.035\ g)/(364.488\ g/mol)]$$
$$= [L_o]/[S_o] = 3.011$$

The twenty-five RHO values listed in Table I-2 were arrived at using calculations similar to those shown below. First, it is necessary to approximate the succeeding RHO value by removal of part of the contents of the NMR tube and replacement of the removed fraction with a like volume of stock substrate solution. Equation I-5 illustrates the calculation of the volume which must be removed from and added to the NMR tube to achieve a RHO_{24} value near 2.75.

$$2[(RHO_{25} - RHO_{24})/RHO_{25}](0.5 \times 10^{-3}\ L) = \text{vol. replaced} \qquad \text{Eq I-5}$$
$$[(3.011 - 2.75)/3.011](0.5 \times 10^{-3}\ L) = 43.38 \times 10^{-6}\ L$$

After rearranging the equation and choosing a whole number near 43.38×10^{-6} L, Eq I-6 gives:

$$RHO_{24} = RHO_{25} - (43.0 \times 10^{-6}\ L)(RHO_{25})/0.5 \times 10^{-3}\ L \qquad \text{Eq I-6}$$
$$= 3.011 - (43.0 \times 10^{-6}\ L)(3.011)/0.5 \times 10^{-3}\ L = 2.752$$

Therefore, $RHO_{24} = 2.752$ following removal of 43×10^{-6} L from RHO_{25} and addition of 43.0×10^{-6} L of the stock solution.

Non-bonded atomic distances in Table I-8 were computed using the trigonometric formula shown in Eq I-7.

$$a^2 = b^2 + c^2 - 2bc\cos\theta \qquad \text{Eq I-7}$$

With $a = C_2\text{-}C_{10}$, $b = C_1\text{-}C_2 = 1.536(2)$ Å, $c = C_1\text{-}C_{10} = 1.544(2)$ Å (from Table I-6), and $\theta = C_2\text{-}C_1\text{-}C_{10} = 102.9^{\circ}$ (Table I-7), substitution into Eq I-7 gives:

$$a^2 = (C_2\text{-}C_{10})^2 = (1.536\ \text{Å})^2 + (1.544\ \text{Å})^2 - 2(1.536\ \text{Å})(1.544\ \text{Å})\cos(102.9^{\circ}) \qquad \text{Eq I-8}$$

and

$$a^2 = (5.802\ \text{Å})^2 \qquad \text{Eq I-9}$$

so that

$$a = C_2\text{-}C_{10} = 2.409\ \text{Å} \qquad \text{Eq I-10}$$

The yield of ketone VII may be calculated as in Eq I-11.

$$[2(\text{mol of VII})/(\text{mol of VI not recovered})](100) = \%\ \text{yield} \qquad \text{Eq I-11}$$

$$\{[2(2.33\ \text{g})/(364.488\ \text{g/mol})]/[(6.5\ \text{g})/(168.239\ \text{g/mol})]\}(100) = 33.3\%$$

The factor of 2 is necessary because two molecules of 7-phenylnorbornadiene (VI) are required for every one molecule of VII produced.

Error Analysis

Weights were recorded to an accuracy of ±0.0001 g. Calibration of the NMR tube was accomplished using a 1 mL syringe which could be read to an accuracy of $\pm 5\times10^{-6}$ L. The error in reading the microliter syringe used in the incremental dilution was 0.25×10^{-6} L. Molecular weights were estimated as accurate to ±0.001 g/mol. NMR spectra were obtained at 100 MHz and chemical shifts in hertz and ppm were instrumentally recorded to an estimated accuracy of ±0.01 ppm.

Propagation of errors was used to compute the following error

values: (i) molarity of $Eu(fod)_3$ (0.006 M, 1.04%), (ii) concentration of substrate (±0.002 M, 1.04%), (iii) largest error in calculation of RHO_i (±0.009, 0.3%), and (iv) largest error in calculating the non-bonded distances of Table I-8 (0.003 Å, 0.12%).

BIBLIOGRAPHY

1. Bird, C. W.; Cookson, R. C.; Hudec, J. Chem. Ind. (London) 1960, 20.

2. Marchand, A. P., Hayes, B. R. Tetrahedron Lett. 1977, 1027.

3. Mantzaris, J.; Weissberger, E. W. J. Am. Chem. Soc. 1974, 96, 1880.

4. Speert, A.; Gelan, J.; Anteunis, M.; Marchand, A. P.; Lazlo, P. Tetrahedron Lett. 1973, 2271.

5. Weissberger, E. W.; Laszlo, P. Acc. Chem. Res. 1976, 9, 209.

6. Laszlo, P.; Stockis, A. J. Organometal. Chem. 1976, 117, C41.

7. Marchand, A. P.; Goodin, D. B.; Hossain, M. B.; van der Helm, D. J. Org. Chem. 1984, 49, 2897.

8. Marchand, A. P.; Rose, J. E. J. Am. Chem. Soc. 1968, 90, 3724.

9. Snyder, E. I.; Franzus, B. J. Am. Chem. Soc. 1964, 86, 1166.

10. (a) Meinwald, J.; Lewis, A. J. Am. Chem. Soc. 1961, 83, 2769. (b) Meinwald, J.; Meinwald, Y. C.; Baker, T. N. J. Am. Chem. Soc. 1963, 85, 2513.

11. Goodin, D. B.; B.S. Thesis, University of Oklahoma, 1977.

12. Baird, W. C.; Surridge, H. J. Org. Chem. 1972, 37, 304.

13. Mayo, B. C. Chem. Soc. Rev. 1973, 2, 49.

14. (a) Cockerill, A. F.; Davies, G. L. O.; Harden, R. C.; Rackham, D. M. Chem. Rev. 1973, 73, 533. (b) Serve, P.; Rondeau, R. E.; Rosenberg, H. M. J. Heterocycl. Chem. 1972, 9, 721. (c) Floyd, F.; Ho, L. J. Polymer Sci., Part B, Polymers Letters 1971, 9, 491. (d) Marchand, A. P "Stereochemical Applications of NMR Studies in Rigid Bicyclic Systems"; Marchand, A. P., Ed.; Verlag Chemie International: Deerfield Beach, Fla., 1982; pp 3-9.

15. Kime, K. A.; Sievers, R. E. Aldrichimica Acta 1977, 10, 54.

16. McCarthy, P. J. "Spectroscopy and Structure of Metal Chelate Compounds"; Nakamoto, K. and McCarthy, P. J., Eds., Wiley: New York, 1968; p 346.

17. McConnell, H. M.; Robertson, R. E. J. Chem. Phys. 1958, 29, 1361.

18. (a) Bleaney, B. J. Magn. Reson. submitted for publication. (b) Richardson, M. F.; Rothstein, S. M.; Li, Wai-Kee J. Magn. Reson. 1979, 36, 69.

19. Cotton, F. A.; Wilkinson, G. "Advanced Inorganic Chemistry"; Wiley: New York, 2nd. ed.

20. Burnbaum, E. R.; Moeller, T. J. Am. Chem. Soc. 1969, 91, 7274.

21. (a) Caple, R.; Kuo, S.C. Tetrahedron Lett. 1971, 4413. (b) Hinckley, C. C.; Klotz, M. R.; Patil, F. J. Am. Chem. Soc. 1971, 93, 2417.

22. Rondeau, R. E.; Sievers, R. E. J. Am. Chem. Soc. 1971, 93, 1522.

23. (a) Shapiro, B. L.; Johnston, M. D. J. Am. Chem. Soc. 1972, 94, 8185. (b) Johnston, M. D.; Shapiro, B. L.; Proulx, T. W.; Godwin, A. D.; Pearce, H. L. J. Am. Chem. Soc. 1975, 97, 542.

24. Germain, G.; Main, P.; Woolfson, M. Acta Crystallogr., Sect. A 1971, A27, 368.

25. Contreras, R. H.; Natiello, M. A.; Scuseria, G. E. Mag. Res. Rev. 1985, 9, 239-321, especially pp 255-267.

26. Barfield, M.; Della, E. W.; Pigou, P. E.; Walter, S. R. J. Am. Chem. Soc. 1982, 104, 3549.

27. Scuseria, G. E.; Facelli, J. C.; Contreras, R. H.; Englemann, A. R. Chem. Phys. Lett. 1983, 96, 560.

28. Barfield, M.; Brown, S. E.; Canada, E. D.; Ledford, N. D.; Marshall, J. L.; Walter, S. R.; Yakali, E. J. Am. Chem. Soc. 1980, 102, 3355.

29. Shoolery, J. N.; Patt, S. L. J. Magn. Reson. 1982, 46, 535, and references therein.

30. Le Cocq, C.; Lallemand, J. Y. Chem. Commun. 1981, 150.

31. Shoolery, J. N. J. Nat. Prod. 1984, 47, 226.

32. Armitage, I.; Dunsmore, G.; Hall, L. D.; Marshall, A. G. Can. J. Chem. 1972, 50, 2119.

PART II

EVALUATION OF THE EQUILIBRIUM CONSTANTS, K_1 AND K_2, AND THE BOUND CHEMICAL SHIFTS, $\Delta 1$ AND $\Delta 2$, FOR THE ONE AND TWO STEP (L + S $\rightleftharpoons$ LS) AND (LS + S $\rightleftharpoons$ LS_2), LANTHANIDE SHIFT REAGENT-SUBSTRATE INTERACTIONS

Introduction

One important problem facing workers using lanthanide shift reagent studies for molecular structure clarification has been the determination of the equilibria taking place in solution between the lanthanide shift reagent (L) and the substrate molecule (S).[1] The problem is that multiple complexes can conceivably exist (the lanthanide ion can readily increase its coordination[2] to 7, 8, or 9 by self-association and/or by binding to substrate ligands) which, for the purpose of discussion, will be designated as L_mS_n (where m and n are integers denoting the stoichiometry). These interactions are known to obey the fast-exchange limit[3] (i.e., are rapid on the NMR time scale), and so the lanthanide-induced shift (LIS) should conform to Equation II-1.

$$LIS = \Delta\delta_i = [\Sigma (n_l C_l \Delta_i)](1/[S_o]) \qquad \text{Eq II-1}$$

$\Delta\delta_i$ is the lanthanide-induced incremental shift of the 'i-th' proton, $[S_o]$ is the <u>total</u> molar concentration of substrate in solution (both free and complexed), n_l is the number of substrate molecules in a given complex, C_l is the total molar concentration of that complex, the 'species' bound chemical shift of proton H_i

(i.e., the LIS of H_i which would be found for 100% formation of a particular complex) is Δ_i, and N is the number of different types of complexes present.

Most attempts to fit LIS data to Eq II-1 have assumed only 1:1 complex formation at low RHO (i.e., at low shift reagent to substrate ratio RHO, with RHO = $[L_0/[S_0]$), where L_mS_n [with $m \geq 1$ and $n > 1$] species predominate instead of the desired 1:1 LS complex. Shapiro and Johnston[4] have developed the LISA4 (Lanthanide Induced Shift Analysis, version 4) computer program which utilizes both a linear and a nonlinear regression analysis of the three equilibria described by Eqs II-2, II-3, and II-4.

$$[L] + [S] \rightleftharpoons [LS]_j \qquad \text{Eq II-2}$$

$$[LS]_j + [S] \rightleftharpoons [LS_2]_j \qquad \text{Eq II-3}$$

$$2[L] \rightleftharpoons [L_2]_j \qquad \text{Eq II-4}$$

The subscript '$_j$' indicates the RHO value at which the concentration of the particular species is determined. Similar methods of data analysis have been developed by Reuben[3] and Inagaki.[6] It has previously been shown that the accuracy with which such equilibrium parameters can be determined is highly dependent on the extent of complexation.[7,8] The reliability of the fitting procedure is optimal when the data points include measurements encompassing the range of molar fractions from approximately 0.2-0.8 for each complex that is formed. This requires that data points be obtained for a large number of RHO ratios.

The two step mechanism (Eqs II-2 and II-3) can be related to Eq II-5 which is another form of the fast-exchange equation.

$$\Delta\delta_i = (1/[S_0])([LS]_j\Delta 1_i + 2[LS_2]_j\Delta 2_i) \qquad \text{Eq II-5}$$

Here, $\Delta 1_i$ is the bound (fully complexed) chemical shift of H_i in the LS complex, $\Delta 2_i$ is the bound (fully complexed) chemical shift of H_i in the LS_2 complex, and $[LS]_j$ and $[LS_2]_j$ are the molar concentrations of the LS and LS_2 species, respectively, at $(RHO)_j$. Equation II-5 can be simplified by making the following variable changes:

$$x = [LS]_j; \qquad y = [LS_2]_j; \qquad z = [L_2]_j; \qquad \text{Eq II-6}$$

$$\alpha = x/[S_0]; \qquad \beta = 2y/[S_0]. \qquad \text{Eq II-7}$$

Equation II-5 can be rewritten as

$$\Delta\delta_i = (\alpha)(\Delta 1_i) + (\beta)(\Delta 2_i) \qquad \text{Eq II-8}$$

α and β are the bound fractions (reduced concentration variables) for the LS and LS_2 complexes, respectively.

The best-fit <u>calculated</u> <u>LIS</u>, $\Delta\delta_i$calc, are found by linear regression analysis upon minimizing the sum of the squares between them and the <u>experimentally</u> <u>measured</u> <u>LIS</u>, $\Delta\delta_i$obs. This quantity, denoted as Q, may be written as

$$Q = \Sigma\ (\Delta\delta_i\text{obs} - \Delta\ \delta_i\text{calc})^2 \qquad \text{Eq II-9}$$

The number of data points for a given proton is denoted by N, and the equilibrium constants and bound shifts (Δ's) are the parameters of the equation.

Fits are performed[2] by choosing a set of K's, evaluating the α_i and β_i, and then getting Δ_1 and/or Δ_2. The best K's are found iteratively (nonlinear regression analysis) whereas the Δ's for a given set of K's may be found exactly and analytically (via linear regression). The iteration in the

equilibrium constants is repeated until the best agreement, in the least squares sense, is obtained between the calculated and observed LIS.

As shown by Shapiro and Johnston[2], the parameters Δ_1 and Δ_2 may be obtained by solving the system of linear equations resulting from Eq II-10:

$$(\delta Q)/[(\delta)(\Delta 1_i)] = 0 = (\delta Q)/[(\delta)(\Delta 2_i)] \qquad \text{Eq II-10}$$

In order to evaluate x, y, and z (i.e., $[LS]_j$, $[LS_2]_j$, and $[L_2]_j$ of Eq II-6) it is convenient first to write the equilibrium constants for Eq II-2 through II-4 as shown in Eq II-11 through II-13 with ρ = RHO.

$$K_1 = x/[(\rho S_o - x - y - 2z)(S_o - x - 2y)] \qquad \text{Eq II-11}$$

$$K_2 = y/[(x(S_o - x - 2y)] \qquad \text{Eq II-12}$$

$$K_L = z/(\rho S_o - x - y - 2z)^2 \qquad \text{Eq II-13}$$

Equations II-12 and II-13 may be written in terms of x:

$$y=(K_2)(x)(S_o - x)/[1 + 2(K_2)x] \qquad \text{Eq II-14}$$

$$z=1+(4K_L(\rho S_o-x-y)-[1+8K_L(\rho S_o-x-y)]^{1/2})/8K_L \qquad \text{Eq II-15}$$

Equations II-14 and II-15 can now be used to provide the values of y and z to be used in a rearranged form of Eq II-10:

$$f(x) = K_1(\rho S_o - x - y - 2z)(S_o - x - 2y) - x \qquad \text{Eq II-16}$$

The solution for x, y, and z results when that value of x is found which gives f(x) = 0. The method chosen to solve the polynomial of Eq II-16 is the Newton-Raphson[3b] method since it gives solutions accurate to one part in 10^{10} in six iterations or less (per

point). Computer fits are performed by first selecting a trial set of equilibrium constants, evaluating the α and β, and calculating bound chemical shifts, $\Delta 1_i$ and $\Delta 2_i$. It should be noted that the degree of accuracy of the bound shifts obtained in no way depends upon the precision with which the equilibrium constants are determined. Most important for calculation of reliable bound shifts, however, is the need for exacting measurement of δ_{oi} (the undoped chemical shift) values. The mathematical rigor[4] of the two-step method means that an exact solution can also be obtained in cases where LS_2 is absent, since no problem is encountered when the appropriate expressions follow by manually setting K_2 and β equal to zero. For $Eu(fod)_3$, and possibly for lanthanides in general, consideration of K_L does not improve LISA4 fits (Eqs II-13 and II-15 are disregarded since $z = K_L = 0$) and it is generally assumed that LSR self-association is negligible.[4,9]

The purpose of this study was to evaluate the lanthanide shift reagent-substrate (i.e., $Eu(fod)_3$-phenyl ketone VII, from PART I) equilibria and to determine the bound chemical shifts of specific substrate protons in the LSR-ketone complex(es).

Results and Discussion

Input to the computer for calculation of equilibrium constants K_1 and K_2 and bound shifts $\Delta 1_i$ and $\Delta 2_i$ included: (i) the constant substrate concentration $[S_0]$, (ii) the observed (100 MHz) chemical shift for each proton of the five pairs of equivalent protons of phenyl ketone VII [labeled $H_a(H_{a'})$, $H_b(H_{b'})$, $H_c(H_{c'})$, $H_d(H_{d'})$, and $H_e(H_{e'})$ in Fig I-11, PART I], and (iii) the twenty five different RHO values [$0 \leq RHO \leq 3.0$] at which the δ_i were recorded. Table II-1 lists the δ_i values obtained at each RHO for each pair of protons after incremental

TABLE II-1

Matrix of Observed Shifts (δ_i) Read In[a] and Incremental Dilution Volumes[b] for Each $(RHO)_j$.

#	RHO	H_a	H_b	H_c	H_d	H_e	Volumes
0	0.000	2.247	2.712	3.178	3.246	3.453	-
1	0.013	2.281	2.803	3.233	3.265	3.510	250
2	0.025	2.319	2.902	3.285	3.285	3.573	250
3	0.050	2.388	3.085	3.338	3.324	3.680	250
4	0.100	2.537	3.482	3.618	3.443	3.930	167
5	0.150	2.690	3.894	3.854	3.517	4.180	125
6	0.200	2.825	4.249	4.056	3.608	4.398	100
7	0.250	2.969	4.636	4.277	3.696	4.615	83
8	0.300	3.100	4.985	4.477	3.783	4.842	72
9	0.350	3.235	5.330	4.675	3.865	5.055	62
10	0.400	3.360	5.640	4.855	3.940	5.240	100
11	0.500	3.580	6.230	5.210	4.080	5.600	83
12	0.600	3.764	6.764	5.492	4.194	5.913	72
13	0.700	3.941	7.243	5.761	4.306	6.200	62
14	0.800	4.107	7.681	6.011	4.404	6.464	56
15	0.900	4.250	8.079	6.235	4.494	6.639	50
16	1.000	4.392	8.457	6.451	4.591	6.927	83
17	1.200	4.651	9.156	6.845	4.751	7.339	72
18	1.401	4.864	9.728	7.157	4.900	7.680	62
19	1.600	5.046	10.226	7.456	5.009	7.978	43
20	1.752	5.177	10.579	7.611	5.081	8.187	63
21	2.000	5.380	11.110	7.962	5.108	8.503	55
22	2.251	5.584	11.641	8.287	5.328	8.839	50
23	2.500	5.744	12.125	8.530	5.428	9.100	46
24	2.752	5.862	12.465	8.726	5.502	9.306	43
25	3.011	5.999	12.850	8.939	5.579	9.526	0

(a) Data was instrumentally recorded in Hz on a Varian XL 100 NMR spectrometer but was converted to ppm for comparison with subsequent spectra taken at 300 MHz.
(b) The incremental volumes are in microliters (μL).

dilution with $[S_o] = 0.19205$ M.

Table II-2 contains the values of the observed incremental shifts ($\Delta_i$obs). Each of these values represents the difference between the experimentally measured LIS (δ_i) and the undoped shift (δ_{oi}) for each pair of protons at each $(RHO)_j$ (Eq II-17).

$$\Delta\delta_i obs = \delta_i - \delta_{oi} \qquad \text{Eq II-17}$$

Table II-3 lists the computer calculated theoretical incremental shifts ($\Delta\delta_i$calc) found by Eq II-5, while Table II-4 lists the deviations (σ_i's) between the experimentally measured incremental shifts and the theoretically calculated incremental shifts calculated using Eq II-18.

$$\sigma_i = [(\delta_i - \delta_{oi}) - \Delta\delta_i calc] \qquad \text{Eq II-18}$$
$$= \Delta\delta_i obs - \Delta\delta_i calc$$

Figure II-1 is the computer plot of the deviations listed in Table II-4. From the table it may be seen that proton $H_b(H_b')$ deviates most from the mean at 50% of the RHO values. In a similar 300 MHz study, the deviations for $H_b(H_b')$ are larger, occurring in 75% of the RHO values. Larger shifts for $H_b(H_b')$ are predicted from the pseudocontact theory due to the proximity of the metal ion, but the observed number and magnitudes of the deviations are not. As mentioned earlier,[10,11] this is probable evidence for contact shift interaction since $H_b(H_b')$ are alpha to the carbonyl group where complexation of the lanthanide occurs. What may be indicated for $H_b(H_b')$ is a summing of both contact and pseudocontact interactions as applicable to Eq II-5. This summing would be less pronounced for the other protons since contact interactions fall off rapidly (proportional to r^{-3}) with increasing number of intervening carbon-carbon bonds. There is evidence that the contact shift contribution for ^1H resonances is rather small and can usually be

TABLE II-2

Experimentally Measured LIS ($\Delta\delta_i$obs)
Less the Undoped Shift (δ_{oi}).[a]

#	RHO	H_a	H_b	H_c	H_d	H_e
1	0.013	.034	.091	.055	.019	.057
2	0.025	.072	.190	.107	.039	.120
3	0.050	.141	.373	.210	.078	.227
4	0.100	.373	.770	.440	.197	.477
5	0.150	.443	1.182	.676	.271	.727
6	0.200	.578	1.537	.878	.362	.945
7	0.250	.722	1.924	1.099	.450	1.162
8	0.300	.853	2.273	1.299	.537	1.389
9	0.350	.988	2.618	1.497	.619	1.602
10	0.400	1.113	2.928	1.677	.694	1.787
11	0.500	1.333	3.518	2.032	.834	2.147
12	0.600	1.577	4.052	2.314	.948	2.460
13	0.700	1.649	4.531	2.583	1.060	2.747
14	0.800	1.860	4.969	2.833	1.158	3.011
15	0.900	2.003	5.367	3.057	1.248	3.237
16	1.000	2.145	5.745	3.227	1.345	3.474
17	1.200	2.404	6.444	3.667	1.505	3.886
18	1.401	2.617	7.016	3.979	1.654	4.227
19	1.600	2.799	7.514	4.278	1.763	4.525
20	1.752	2.930	7.867	4.433	1.835	4.734
21	2.000	3.133	8.398	4.784	1.962	5.050
22	2.251	3.337	8.929	5.109	2.082	5.386
23	2.500	3.497	9.413	5.352	2.182	5.647
24	2.752	3.615	9.753	5.548	2.256	5.853
25	3.011	3.752	10.138	5.761	2.333	6.073

(a) All shifts are in ppm.

TABLE II-3

Matrix of Theoretically Calculated Incremental Shifts ($\Delta\delta_i$calc).

#	RHO	H_a	H_b	H_c	H_d	H_e
1	0.013	.038	.096	.057	.024	.061
2	0.025	.075	.199	.114	.047	.122
3	0.050	.151	.398	.228	.948	.244
4	0.100	.299	.789	.452	.188	.484
5	0.150	.445	1.175	.673	.279	.720
6	0.200	.586	1.550	.887	.368	.949
7	0.250	.723	1.916	1.096	.454	1.171
8	0.300	.855	2.267	1.296	.537	1.384
9	0.350	.981	2.602	1.487	.615	1.587
10	0.400	1.100	2.921	1.669	.690	1.780
11	0.500	1.321	3.515	2.007	.828	2.138
12	0.600	1.521	4.053	2.313	.953	2.461
13	0.700	1.701	4.536	2.587	1.605	2.751
14	0.800	1.865	4.978	2.839	1.168	3.016
15	0.900	2.013	5.380	3.066	1.260	3.255
16	1.000	2.151	5.754	3.279	11.34	3.479
17	1.200	2.396	6.418	3.655	1.499	3.874
18	1.401	2.613	7.007	3.989	1.634	4.224
19	1.600	2.803	7.523	4.281	1.753	4.531
20	1.752	2.936	7.884	4.486	1.835	4.744
21	2.000	3.133	8.422	4.790	1.958	5.064
22	2.251	3.314	8.914	5.069	2.071	5.356
23	2.500	3.476	9.355	5.319	2.172	5.617
24	2.752	3.628	9.769	5.553	2.266	5.862
25	3.011	3.771	10.160	5.774	2.355	6.094

All shifts are in ppm.

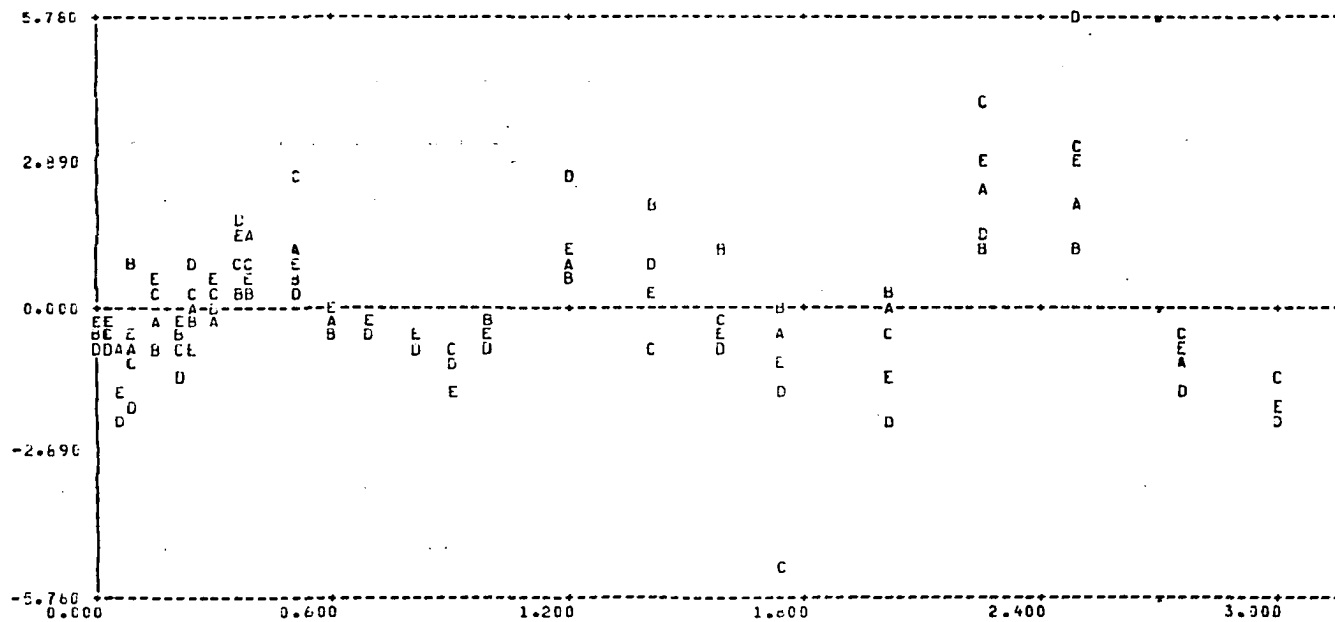

Figure II-1. LISA4 computer plot of the 100 MHz matrix of deviations between the observed (δ_i) and theoretically calculated ($\delta_i$calc) chemical shifts listed in Table II-4.

TABLE II-4

Matrix of Deviations (σ_i's) Between Experimentally Observed Incremental Shifts ($\Delta\delta_i$obs) and the Theoretically Calculated Incremental Shifts ($\Delta\delta_i$calc).[a]

#	RHO	H_a	H_b	H_c	H_d	H_e
1	0.013	-.004	-.009	-.002	-.005	-.004
2	0.025	-.003	-.009	-.007	-.008	-.002
3	0.050	-.010	-.025	-.018	-.017	-.017
4	0.100	-.009	-.019	.012	.009	-.007
5	0.150	-.002	.007	.003	-.008	.007
6	0.200	-.008	-.013	-.009	-.006	-.004
7	0.250	-.001	.008	.004	-.004	-.009
8	0.300	-.002	.007	.003	.001	.005
9	0.350	.007	.016	.010	.004	.015
10	0.400	.013	.007	.008	.004	.007
11	0.500	.012	.003	.025	.006	.009
12	0.600	-.004	-.001	.001	-.005	-.001
13	0.700	-.007	-.005	-.004	-.005	-.004
14	0.800	-.005	-.009	-.005	-.010	-.005
15	0.900	-.010	-.013	-.009	-.012	-.018
16	1.000	-.006	-.009	-.006	-.002	-.005
17	1.200	.008	.026	.012	.006	.012
18	1.401	.004	.010	.010	.020	.003
19	1.600	-.004	-.009	-.003	.010	-.006
20	1.752	-.006	-.017	-.053	-.001	-.011
21	2.000	-.001	-.024	-.006	.004	-.014
22	2.251	.023	.015	.040	.011	.030
23	2.500	.021	.058	.033	.010	.030
24	2.752	-.013	-.016	-.005	-.010	-.009
25	3.011	-.019	-.022	-.013	-.022	-.021

(a) All deviations are in ppm.

neglected.[12] However, some have found ^1H contact shifts up to about 10% of the still dominant pseudocontact contribution for some of the lanthanides.[13]

An interesting set of computer generated data is seen in Table II-5. The values of [LS], [LS_2], α, β, and $\alpha + \beta$ at each $(RHO)_j$ are listed. Two 100 MHz data sets were input to the computer. The first data set corresponds to that of each of the five pairs of equivalent protons, while the second corresponds to that of each of the four pairs of protons with the alpha proton pair [$H_b(H_{b'})$] omitted. This comparison was made in order to ascertain the effect of the contact shift contribution to the LIS. As the table indicates, there is no significant difference between the output data resulting from either data set.

As predicted from consideration of the two step equilibria, [LS_2] is larger at low RHO where there is an abundance of substrate, while [LS] is larger at high RHO with $Eu(fod)_3$ in excess (Fig II-2). The individual values of α and β, plotted against RHO in Fig II-3, graphically illustrate this with β maximum at RHO $\approx$ 1.75 (middle line) while alpha (lower line) continues to increase. The upper line is a plot of the sum of $\alpha + \beta$. The data does not account for 100% of the lanthanide ($\alpha + \beta = 0.83$ at maximum RHO). This may be an indication of the purity of the contents of the NMR tube. A value of $\alpha + \beta = 1$ would indicate that all of the $Eu(fod)_3$ added was involved in the induction of chemical shift via [LS] and/or [LS_2]. It may be that: (i) certain scavengers are present which have complexed with the LSR; (ii) some LSR self-association has occurred such that [L_m] $\leq (1 - 0.83) = 0.17$; (iii) the $Eu(fod)_3$ used was itself impure; (iv) the equilibria in the solution are such that only part of the $Eu(fod)_3$ is involved in complexation (i.e., the equilibria do not go to completion because the solutions are too dilute). The small equilibrium constants calculated for this system (<u>vide infra</u>) suggest that (iv) is the most likely explanation for the less than 100%

TABLE II-5

Concentrations and Bound Fractions from the 100 MHz Input Data.[a]

#	RHO	[LS][b]	[LS]′	[LS_2]	[LS_2]′	α[c]	β[c]	(α+β)[d]	(α+β)′
1	0.013	0.033	0.033	0.163	0.163	0.002	0.017	0.019	0.019
2	0.025	0.067	0.067	0.322	0.321	0.003	0.034	0.037	0.037
3	0.050	0.137	0.138	0.633	0.631	0.007	0.066	0.073	0.073
4	0.100	0.282	0.283	1.209	1.205	0.015	0.125	0.141	0.141
5	0.150	0.435	0.438	1.733	1.727	0.023	0.180	0.203	0.203
6	0.200	0.594	0.597	2.197	2.190	0.031	0.229	0.260	0.259
7	0.250	0.758	0.762	2.608	2.599	0.039	0.272	0.311	0.311
8	0.300	0.924	0.928	2.967	2.956	0.048	0.309	0.357	0.356
9	0.350	1.090	0.095	3.276	3.265	0.057	0.341	0.398	0.397
10	0.400	1.254	1.259	3.543	3.530	0.065	0.369	0.434	0.433
11	0.500	1.575	1.582	3.969	3.955	0.082	0.413	0.495	0.494
12	0.600	1.881	1.888	4.283	4.269	0.098	0.446	0.544	0.543
13	0.700	2.168	2.176	4.515	4.500	0.113	0.470	0.583	0.582
14	0.800	2.440	2.449	4.688	4.673	0.127	0.488	0.615	0.614
15	0.900	2.693	2.702	4.816	4.802	0.140	0.502	0.642	0.641
16	1.000	2.933	2.944	4.914	4.900	0.153	0.512	0.665	0.664
17	1.200	3.371	3.382	5.041	5.026	0.176	0.525	0.700	0.700
18	1.401	3.768	3.780	5.110	5.096	0.196	0.532	0.728	0.728
19	1.600	4.123	4.136	5.142	5.128	0.215	0.536	0.750	0.749
20	1.752	4.374	4.389	5.151	5.136	0.228	0.536	0.764	0.763
21	2.000	4.753	4.768	5.145	5.130	0.247	0.536	0.783	0.783
22	2.251	5.103	5.120	5.121	5.106	0.266	0.533	0.799	0.798
23	2.500	5.421	5.438	5.087	5.073	0.282	0.530	0.812	0.811
24	2.752	5.720	5.738	5.046	5.031	0.298	0.525	0.823	0.823
25	3.011	6.005	6.024	4.999	4.984	0.313	0.521	0.833	0.833

(a) All concentrations in square brackets are in moles/liter and have been multiplied by 100.
(b) Superscript primes (′) indicate four proton-pair data while unprimed values correspond to five proton-pair data.
(c) The α and β values from both data sets were virtually identical.
(d) The value of $(\alpha + \beta) = [LS]_j/[S_0] + 2[LS_2]_j/[S_0]$ and is the total LSR in LS and LS_2 complexes at that $(RHO)_j$.

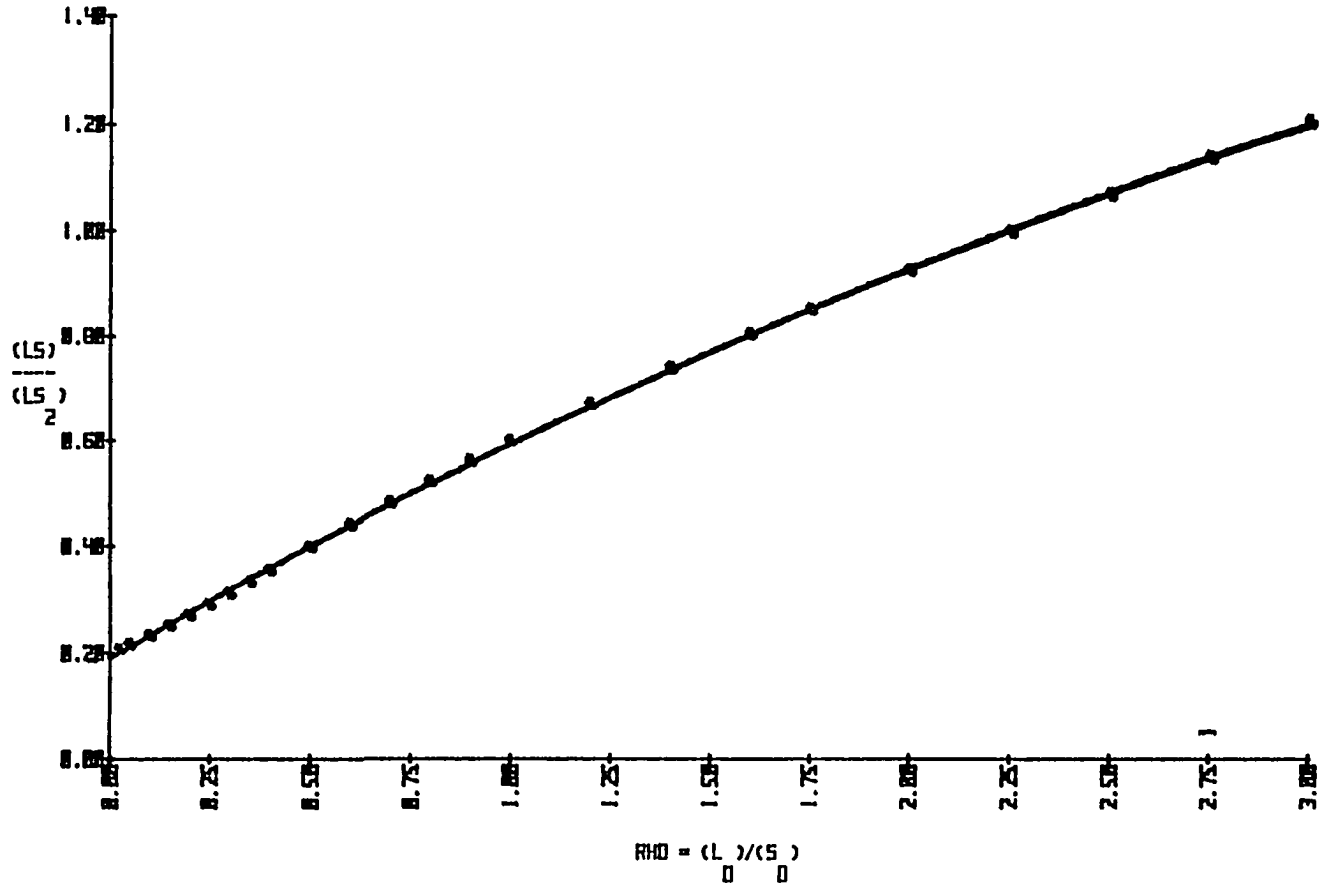

Figure II-2. Plot of RHO vs. $[LS]/[LS_2]$ from the data in Table II-5.

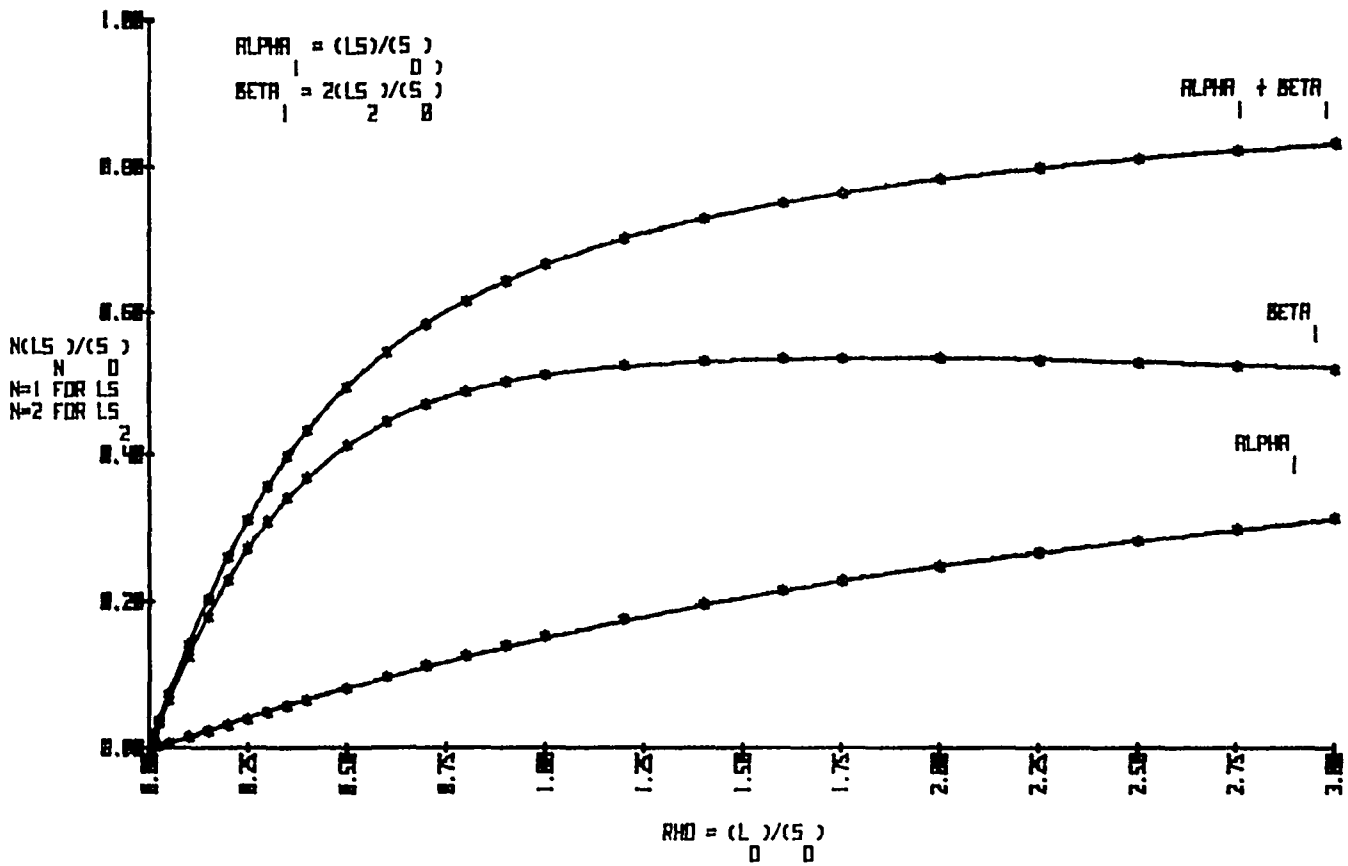

Figure II-3. Plot of α, β, and α + β from the data in Table II-5.

involvement of lanthanide in the equilibria and in the induction of chemical shift. Since the data are completely reproducible suggesting a very good fit, explanations (i)-(iii) are very unlikely.

Figure II-4 is a plot of the experimentally obtained shift (δ_i) versus RHO from the data in Table II-1, while Fig II-5 is the computer calculated LIS (δ_{calc}) plotted against RHO for the same pairs of protons. The calculated shifts listed in Table II-6 were calculated using Eq II-19.

$$\delta_i calc = \Delta\delta_i calc + \delta_{oi} \qquad \text{Eq II-19}$$
$$= \alpha(\Delta 1_i) + \beta(\Delta 2_i) + \delta_{oi}$$

$\delta_i calc$ is the calculated position of the NMR resonance in ppm, δ_{oi} is the undoped chemical shift of H_i, and α and β are the bound fractions which were discussed for Eqs II-7 and II-8.

The comparison between Figs II-4 and II-5 is excellent. Theoretically, plots for each pair of protons from a RHO value of 0.0 to 0.6 should be linear, with maximum curvature occurring between 0.6 and 2.0 RHO. At high RHO values, each graph should approach its maximum shift value asymptotically. Curvature is a problem that may occur at low LSR concentrations [attributed to competition between substrate and traces of water and/or acidic impurities (scavengers) for the LSR][14] and at high LSR concentrations (attributed to incomplete solution of the LSR[15] and to medium and association effects).[16,17] None of these problems are apparent from the data in the figures.

Table II-7 lists the equilibrium constants, Q, and the weighted standard shift deviations (calculated using using Eq II-20).

$$\sigma_s = [Q/(mN-1)]^{1/2} \qquad \text{Eq II-20}$$

The letter m designates the number of protons whose chemical shifts were measured in the particular experiment and N is the number of RHO

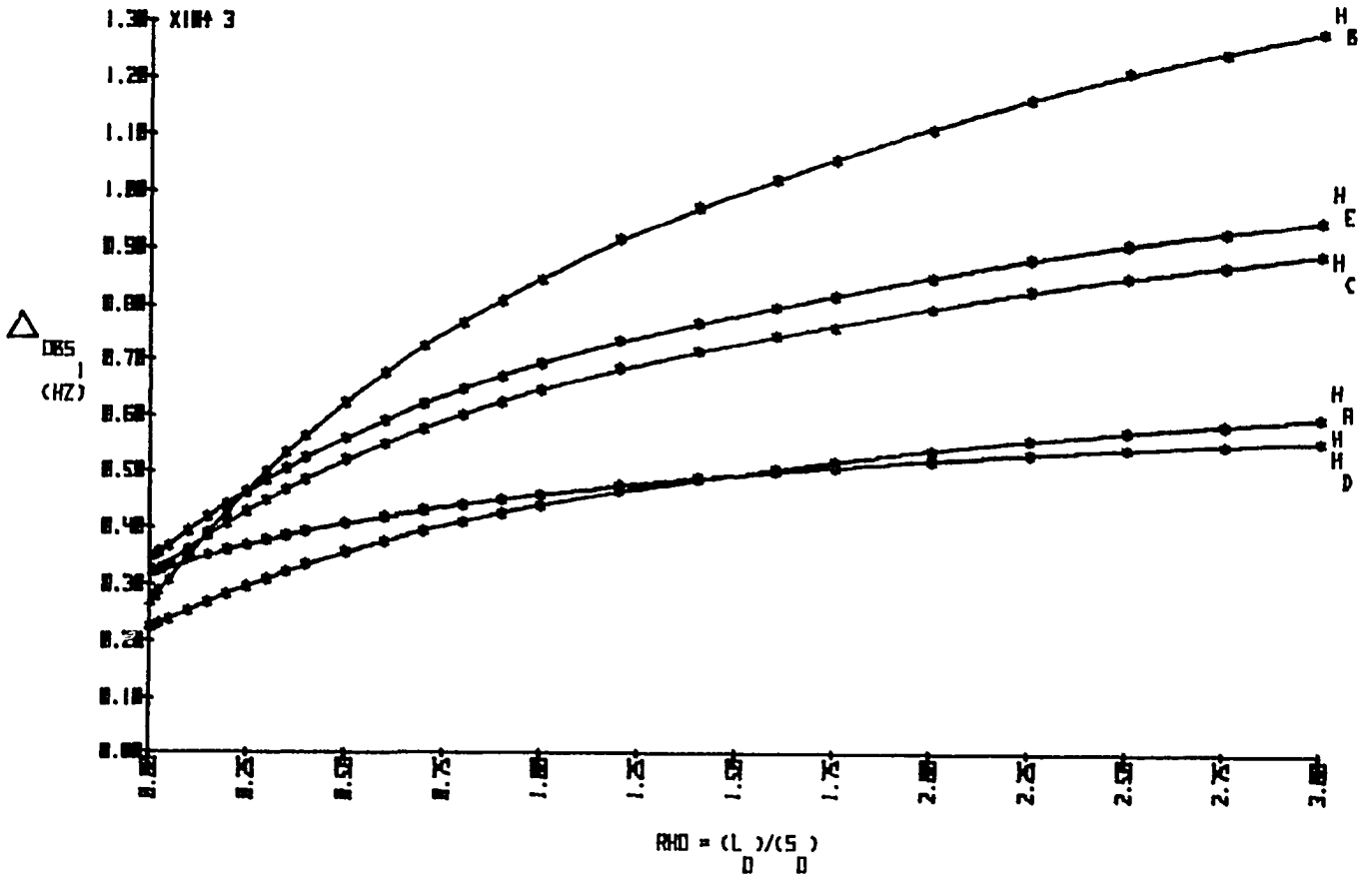

Figure II-4. Plot of the experimentally observed 100 MHz lanthanide-induced chemical shifts (δ_i) of the five pairs of protons vs. RHO from the data in Table II-1.

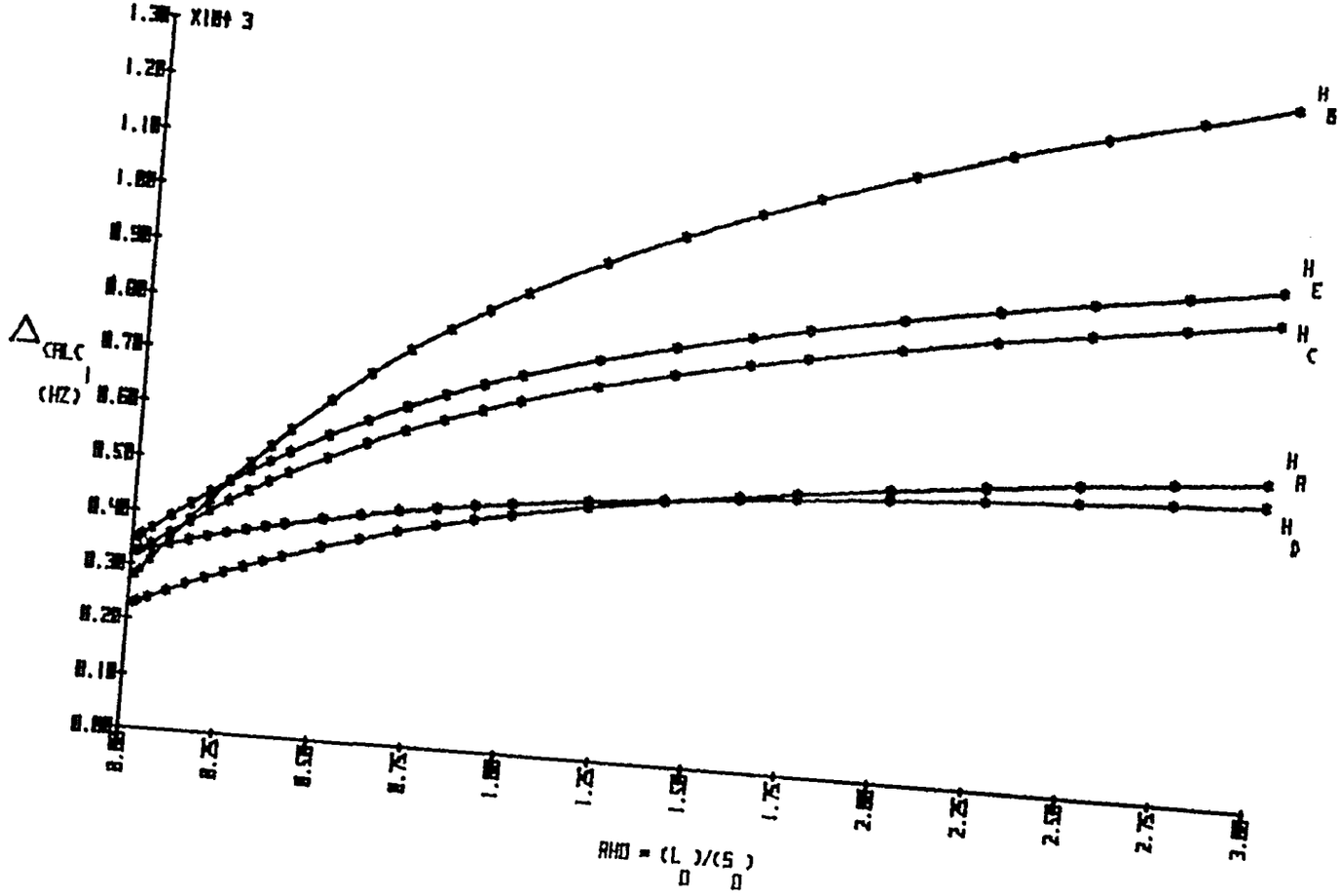

Figure II-5. Plot of the LISA4 calculated 100 MHz LIS ($\delta_i$calc) of the five pairs of protons vs. RHO from the data in Table II-6.

TABLE II-6

Computer Calculated $\delta_i$calc from

Matrix of Calculated Incremental Shifts (TABLE II-3).[a]

#	RHO	H_a	H_b	H_c	H_d	H_e
1	0.013	2.285	2.812	3.235	3.270	3.514
2	0.025	2.322	2.911	3.292	3.293	3.575
3	0.050	2.398	3.110	3.406	3.341	3.697
4	0.100	2.546	3.501	3.630	3.434	3.937
5	0.150	2.692	3.887	3.851	3.525	4.173
6	0.200	2.833	4.262	4.065	3.614	4.402
7	0.250	2.970	4.628	4.274	3.700	4.624
8	0.300	3.102	4.979	4.474	3.783	4.837
9	0.350	3.228	5.314	4.665	3.861	5.040
10	0.400	3.347	5.633	4.847	3.936	5.233
11	0.500	3.568	6.227	5.185	4.074	5.591
12	0.600	3.768	6.765	5.491	4.199	5.914
13	0.700	3.948	7.248	5.765	4.311	6.204
14	0.800	4.112	7.690	6.017	4.414	6.469
15	0.900	4.260	8.092	6.244	4.506	6.708
16	1.000	4.398	8.466	6.457	4.593	6.932
17	1.200	4.643	9.130	6.833	4.745	7.327
18	1.401	4.860	9.719	7.167	4.880	7.677
19	1.600	5.050	10.235	7.459	4.999	7.984
20	1.752	5.183	10.596	7.664	5.081	8.198
21	2.000	5.380	11.134	7.968	5.204	8.517
22	2.251	5.561	11.626	8.247	5.317	8.809
23	2.500	5.723	12.067	8.497	5.418	9.070
24	2.752	5.875	12.481	8.731	5.512	9.315
25	3.011	6.018	12.872	8.952	5.601	9.547

(a) All shifts are in ppm.

TABLE II-7

Equilibrium Constant, Q, and Weighted Standard Shift Deviation Values from the 100 MHz and 300 MHz $Eu(fod)_3$-Ketone LSR Studies.[a]

Expt	$K_1(M^{-1})$	% Error[c]	$K_2(M^{-1})$	% Error	Q[d]	σ_s[e]
A_4	4.01	1.93	25.76	21.08	0.016	0.0129
B_5	4.01	1.93	26.03	20.88	0.025	0.0141
C_5	7.63	-	0.0	-	0.670	0.0250
D_4	3.62	2.13	48.16	10.02	0.031	0.0158
E_5	3.72	2.08	54.20	11.27	0.047	0.0177
F_6	3.62	2.13	46.26	11.73	0.027	0.0124
G_7	3.62	2.13	54.69	9.93	0.053	0.0160
H_7	4.29	-	0.0	-	1.254	0.0775
Standard error[b]		0.08		5.43		
Ave Rel % error[c]		2.05		14.15		

Note: Maximum difference in complexation energy for K_1 and K_2 is 0.12 and 0.22 kcal/mol, respectively, while the difference between the average K_1 and K_2 values is 1.16 kcal/mol.[f]

(a) Values in the table were calculated by LISA4 from the experiments as listed below:
- A_4: 100 MHz four proton-pair input data set NLLSQ-calculated output values with input data from α protons $H_b(H_{b'})$ and vinyl protons $H_f(H_{f'})$ and $H_g(H_{g'})$ omitted from the calculations.
- B_5: Same as Exp A_4 except that input data for $H_b(H_{b'})$ protons were included, giving a five proton-pair data set.
- C_5: Same as Exp B_5 except that K_2 was set equal to zero.
- D_4: Same as Exp A_4 except that the 300 MHz data were used.
- E_5: Same as Exp B_5 except that the 300 MHz data were used.
- F_6: Same as Exp D_4 except that input data from vinyl protons $H_f(H_{f'})$ and $H_g(H_{g'})$ were included, forming a six proton-pair data set.
- G_7: Same as Exp F_6 except that input data for $H_b(H_{b'})$ were included, forming a seven proton-pair data set.
- H_7: Same as Exp G_7 except that K_2 was set equal to zero.

(b) Standard error = $([\Sigma(x_i-x)^2]/[n(n-1)])^{1/2}$, where n is the number of independent determinations, x_i is the value of K for a particular determination, and x is the mean value of K for all determinations. Data from Exps C_5 and H_7 were excluded.

(c) Relative per cent error = (standard error/equilibrium constant) multiplied by 100. Exp C_5 and H_7 data were excluded.

(d) Values of Q (in ppm^2) are given by Eq II-9.

(e) Values of σ_s (in ppm) are given by Eq II-20.

(f) A hundredfold variation in association constants (corresponding to about 1 kcal/mol difference in complexation energy) has been suggested for ketones.[1] However, based on a more recent study,[11f] the values shown here correspond to 1 kcal/mol difference in complexation energy for each tenfold increase in equilibrium constant.

values at which those shifts were measured. The value of Q is very significant since it is the term minimized in Eq II-9.

Equilibrium constants for the five-proton pair data set (Exp B_5) are 4.01 M^{-1} and 26.00 M^{-1} for K_1 and K_2, respectively. The fact that K_1 is smaller than K_2 seems unreasonable because it means that binding of the first substrate to form the 1:1 LS complex increases the likelihood that a second substrate will bind to LS and form the 1:2 LS_2 complex. The size and steric bulk of the 'fod' ligand and substrate molecule and also the weak Lewis basicity of the ketone carbonyl of the substrate should inhibit this <u>very</u> <u>rare</u> 'cooperative binding'.[18] Since our initial discovery of this '$K_2 > K_1$' result, others have found a similar phenomenon for the two step equilibrium between 2-Adamantanol and $Eu(fod)_3$ in $CDCl_3$.[19] This process has been tentatively attributed to ligand rearrangement around the central metal atom of the shift reagent because of the initial substrate binding. The new arrangement may enhance the affinity of the 1:1 adduct toward a second substrate molecule.[8]

In order to test for the presence of the cooperative process, another experiment was suggested:[20] run the experiment at a lower substrate concentration (e.g., 0.1 M) and run RHO higher (in this case up to about RHO = 6.0). The present data may be inconclusive in that the alpha bound fraction (Table II-5) has not exceeded 50% (it only goes up to 0.31). Generally it is necessary to go to much higher values to obtain good results.[8]

Accordingly, the experiment was performed (this time at 300 MHz) with $[S_0]$ = 0.09987 M and $0.01336 \leq RHO \leq 6.001$, instead of $0.01252 \leq RHO \leq 3.01129$ (as in the 100 MHz experiment). The number of RHO values was increased to thirty. While not possible at 100 MHz, spectral resolution at 300 MHz was sufficient to permit measurement of the chemical shifts of the two sets of vinyl protons [$H_f(H_{f'})$ and $H_g(H_{g'})$] which were included in the new experiment. The results are listed in Table II-8 and plotted in Fig II-6. A plot of

TABLE II-8

Matrix of Observed Shifts (δ_i) Read In and Incremental Dilution Volumes for Each $(RHO)_j$.[a]

#	RHO	H_a	H_b	H_c	H_d	H_e	H_f	H_g	Volumes
0	0.000	2.25	2.71	3.17	3.24	3.45	6.02	6.11	-
1	0.013	2.30	2.80	3.23	3.29	3.52	6.06	6.14	250
2	0.027	2.33	2.86	3.27	3.30	3.56	6.07	6.15	250
3	0.053	2.38	2.99	3.34	3.34	3.64	6.08	6.17	250
4	0.107	2.48	3.27	3.50	3.40	3.81	6.12	6.22	150
5	0.153	2.57	3.52	3.65	3.46	3.97	6.15	6.25	125
6	0.204	2.68	3.80	3.81	3.52	4.14	6.18	6.29	100
7	0.254	2.78	4.07	3.97	3.59	4.30	6.21	6.33	75
8	0.299	2.87	4.32	4.11	3.55	4.45	6.24	6.37	75
9	0.352	2.97	4.58	4.26	3.71	4.60	69.28	6.41	75
10	0.414	3.08	4.88	4.43	3.78	4.78	6.30	6.45	100
11	0.518	3.26	5.36	4.70	3.89	5.06	6.36	6.52	75
12	0.609	3.40	5.73	4.91	3.98	5.09	6.40	6.58	75
13	0.717	3.56	6.16	5.15	4.08	5.53	6.45	6.64	50
14	0.796	3.67	6.45	5.32	4.15	5.70	6.48	6.68	75
15	0.937	3.85	6.94	5.59	4.26	5.98	6.54	6.75	120
16	1.225	4.24	7.96	6.17	4.50	6.57	6.65	6.90	75
17	1.441	4.45	8.53	6.49	4.64	6.90	6.72	6.98	50
18	1.601	4.61	8.95	6.73	4.74	7.15	6.77	7.05	50
19	1.779	4.78	9.40	6.99	4.84	7.40	6.82	7.11	75
20	2.093	5.02	10.02	7.33	5.00	7.76	6.89	7.20	50
21	2.325	5.19	10.49	7.60	5.10	8.03	6.95	7.27	50
22	2.583	5.37	10.98	7.86	5.21	8.29	7.00	7.34	50
23	2.870	5.56	11.47	8.15	5.33	8.57	7.07	7.42	50
24	3.189	5.77	12.04	8.46	5.46	8.89	7.14	7.50	50
25	3.534	5.97	12.58	8.76	5.59	9.19	7.19	7.58	50
26	3.937	6.20	13.19	9.09	5.72	9.52	7.26	7.67	50
27	4.375	6.41	13.75	9.41	5.86	9.85	7.33	7.75	50
28	4.861	6.49	14.29	9.71	5.99	10.15	7.40	7.83	50
29	5.401	6.83	14.87	10.03	6.12	10.47	7.46	7.92	50
30	6.001	7.07	15.54	10.41	6.27	10.85	7.53	8.01	0

(a) δ_i (ppm) were recorded at 300 MHz and volumes are listed in µL.

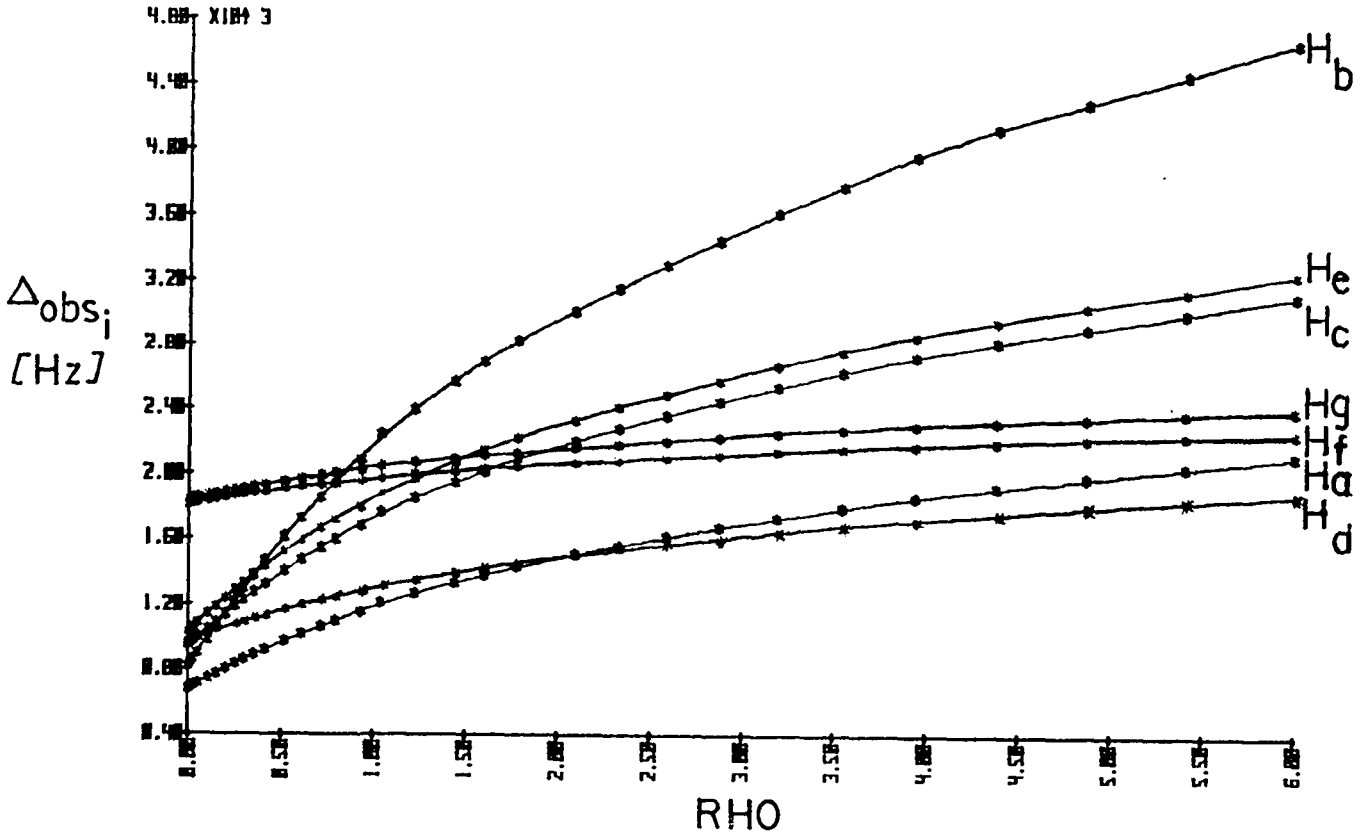

Figure II-6. Plot of the experimentally observed 300 MHz LIS (δ_i) of the seven pairs of protons vs. RHO from the data in Table II-8.

the deviations between the observed and theoretically calculated shifts is seen Fig II-7. Concentrations and bound fractions are listed in Table II-9. Beta is maximum at RHO ≈ 3.25, while alpha continues to increase. As in the 100 MHz experiment, the data does not account for 100% of the lanthanide ($\alpha + \beta = 0.84$ at maximum RHO), probably for the same reason as mentioned above during the discussion of Table II-5. Apparently, the equilibria have not gone to completion because the solutions are too dilute.

Equilibrium constants, Q, and weighted standard shift deviations are included in Table II-7 with those of the 100 MHz data set. Again, $K_1 < K_2$! Other values of K_1, K_2, Q, and the weighted standard shift deviation from experiments A_4, D_4, E_5, and F_6 were calculated for comparison. The value of K_1 varies only slightly among experiments (3.62-4.01 M^{-1}), while K_2 ranges from 25.76-54.69 M^{-1}. Further similarity between experiments is observed upon setting K_2 equal to zero (experiments C_5 and H_7). K_1, Q, and σ_s all increase which indicates that K_2 <u>must</u> be greater than zero (i.e., K_2 exists and therefore LS_2 is definitely present!).

Table II-10 lists the bound chemical shifts for the 100 MHz (A_4 and B_5) and 300 MHz (D_4, E_5, F_6, and G_7) experiments as calculated by LISA4. There is a large difference in the magnitude of the bound shifts for individual protons between the two general experiments, but good correlation of the bound shifts within each. The reproducibility of the experiments is demonstrated by the ratios in the table. The 100 MHz G_7:B_5 and E_5:B_5 ratios are equivalent and contain bound chemical shift contributions from alpha protons H_b and H_b'. The 300 MHz F_6:A_4 and D_4:A_4 ratios are equivalent and do not include contributions from H_b(H_b'). All four ratios are quite similar which suggests a relative error (rather than a random error) whose value is approximately 1.42 for $\Delta 1$ values and 0.37 for $\Delta 2$ values. Further confirmation of the comparability of these experiments is seen in Table II-11.

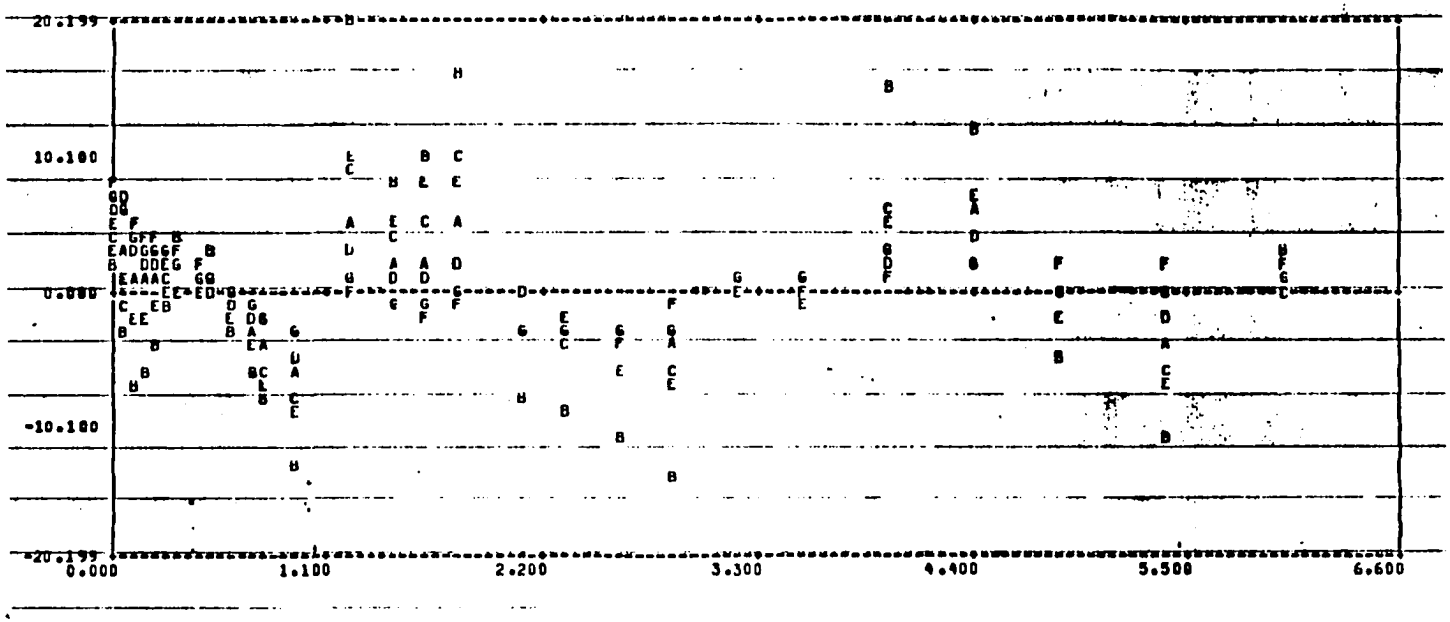

Figure II-7. LISA4 computer plot of the deviations between the oberved (δ_i) and theoretically calculated ($\delta_i$calc) chemical shifts from the 300 MHz experiment.

TABLE II-9

Concentrations and Bound Fractions from the 300 MHz Input Data.[a]

#	RHO	[LS][b]	[LS]′	[LS_2]	[LS_2]′	α[c]	α′	β	β′	(α+β)[d]	(α+β)′
1	0.013	0.015	0.016	0.078	0.073	0.001	0.002	0.016	0.015	0.017	0.016
2	0.027	0.029	0.032	0.154	0.143	0.003	0.003	0.031	0.029	0.034	0.032
3	0.053	0.059	0.064	0.300	0.279	0.006	0.006	0.060	0.056	0.066	0.062
4	0.107	0.119	0.130	0.570	0.529	0.012	0.013	0.114	0.106	0.126	0.119
5	0.153	0.172	0.187	0.777	0.722	0.017	0.019	0.156	0.145	0.173	0.163
6	0.204	0.231	0.249	0.984	0.913	0.023	0.025	0.197	0.183	0.220	0.208
7	0.254	0.290	0.312	1.166	1.083	0.029	0.031	0.234	0.217	0.263	0.248
8	0.299	0.341	0.366	1.310	1.217	0.034	0.037	0.262	0.244	0.296	0.280
9	0.352	0.400	0.429	1.460	1.358	0.040	0.043	0.292	0.272	0.332	0.315
10	0.414	0.469	0.501	1.613	1.502	0.047	0.050	0.323	0.301	0.370	0.351
11	0.518	0.578	0.617	1.823	1.702	0.058	0.062	0.365	0.341	0.423	0.403
12	0.609	0.671	0.714	1.971	1.844	0.067	0.071	0.395	0.369	0.462	0.441
13	0.717	0.773	0.822	2.111	1.980	0.077	0.082	0.423	0.396	0.500	0.479
14	0.796	0.845	0.898	2.196	2.062	0.085	0.090	0.440	0.413	0.524	0.503
15	0.937	0.966	1.025	2.317	2.181	0.097	0.103	0.464	0.437	0.561	0.539
16	1.224	1.187	1.259	2.486	2.348	0.119	0.126	0.498	0.470	0.617	0.596
17	1.441	1.336	1.417	2.568	2.431	0.134	0.142	0.514	0.487	0.648	0.629
18	1.600	1.438	1.525	2.613	2.476	0.144	0.153	0.523	0.496	0.667	0.649
19	1.779	1.544	1.637	2.651	2.515	0.155	0.164	0.531	0.504	0.686	0.668
20	2.093	1.717	1.921	2.698	2.562	0.172	0.182	0.540	0.513	0.712	0.695
21	2.325	1.834	1.945	2.720	2.585	0.184	0.195	0.545	0.518	0.728	0.712
22	2.583	1.956	2.075	2.736	2.601	0.196	0.208	0.548	0.521	0.744	0.729
23	2.870	2.083	2.209	2.746	2.611	0.209	0.221	0.550	0.523	0.759	0.744
24	3.189	2.214	2.347	2.751	2.616	0.222	0.235	0.551	0.524	0.773	0.759
25	3.554	2.349	2.490	2.749	2.614	0.235	0.249	0.551	0.523	0.786	0.773
26	3.937	2.489	2.638	2.742	2.607	0.249	0.264	0.549	0.522	0.798	0.786
27	4.375	2.633	2.790	2.729	2.594	0.264	0.279	0.547	0.519	0.810	0.799
28	4.861	2.781	2.946	2.711	2.576	0.279	0.295	0.543	0.516	0.822	0.811
29	5.401	2.934	3.107	2.689	2.552	0.294	0.311	0.538	0.511	0.832	0.822
30	6.001	3.091	3.272	2.661	2.524	0.310	0.328	0.533	0.505	0.842	0.833

(a) All concentrations (in square brackets) are in moles/liter and have been multiplied by 100.

(b) Superscript primes (′) indicate six proton-pair data while unprimed values correspond to seven proton-pair data.

(c) Values of α and β are quite similar to those in Table II-5.

(d) Values of (α + β) are also similar to those in Table II-5.

TABLE II-10

300 MHz Undoped (δ_{0i}) and Bound Chemical Shifts (Δ_i's).[a]

		Bound Chemical Shifts (ppm)[b]						Ratios[c]			
Proton	δ_{0i}	A_4	B_5	D_4	E_5	F_6	G_7	G_7/B_5	E_5/B_5	F_6/A_4	D_4/A_4
$H_a(H_{a'})$	2.25	10.03 (1.20)	10.06 (1.20)	14.79 (0.39)	14.69 (0.38)	14.08 (0.40)	14.89 (0.39)	1.48 (0.33)	1.46 (0.32)	1.40 (0.33)	1.42 (0.33)
$H_b(H_{b'})$	2.71		27.38 (3.07)		39.34 (0.87)		39.88 (0.89)	1.46 (0.29)	1.44 (0.28)		
$H_c(H_{c'})$	3.17	15.46 (1.78)	15.50 (1.70)	22.11 (0.64)	21.96 (0.63)	21.05 (0.66)	22.26 (0.65)	1.44 (0.37)	1.42 (0.35)	1.36 (0.37)	1.38 (0.36)
$H_d(H_{d'})$	3.24	6.24 (0.76)	6.27 (0.76)	9.19 (0.30)	9.13 (0.30)	8.75 (0.31)	9.25 (0.31)	1.48 (0.41)	1.46 (0.39)	1.40 (0.41)	1.42 (0.39)
$H_e(H_{e'})$	3.45	16.19 (1.95)	16.24 (1.95)	22.26 (0.85)	22.11 (0.83)	21.19 (0.88)	22.41 (0.85)	1.38 (0.44)	1.36 (0.43)	1.31 (0.45)	1.33 (0.44)
$H_f(H_{f'})$	6.02					4.31 (0.18)	1.56 (0.17)				
$H_g(H_{g'})$	6.11					5.45 (0.22)	5.76 (0.21)				
σ_s[d]		.0129	.0141	.0158	.0177	.0124	.0160				
$\Delta 1$ ratio averages[e]								1.45	1.43	1.37	1.39
$\Delta 2$ ratio averages								(0.37)	(0.35)	(0.39)	(0.38)

(a) Bound chemical shifts were determined by LISA4 in the corresponding experiments listed in Table II-7.

(b) Values in parenthesis correspond to $\Delta 2$ bound chemical shifts, while those not in parenthesis are $\Delta 1$ bound chemical shifts.

(c) Bound chemical shift ratios are for inter-experiment comparison.

(d) Weighted standard shift deviations are as listed in Table II-7.

(e) The overall normalized $\Delta 1$ ratio average is 1.42, while that for $\Delta 2$ is 0.37.

TABLE II-11

Normalized 300 MHz Bound Chemical Shifts.[a]

Proton	δ_o	A_4[b]	B_5	D_4	E_5	F_6	G_7
$H_a(H_{a'})$	2.25 2.25	1.61 (1.58)	1.61 (1.58)	1.61 (1.27)	1.61 (1.28)	1.61 (1.27)	1.61 (1.28)
$H_b(H_{b'})$	2.71 2.71		4.37 (4.04)		4.31 (2.89)		4.31 (2.91)
$H_c(H_{c'})$	3.17 3.17	2.47 (2.34)	2.47 (2.34)	2.40 (2.09)	2.41 (2.10)	2.41 (2.09)	2.41 (2.10)
$H_d(H_{d'})$	3.24 3.24	1.00 (1.00)	1.00 (1.00)	1.00 (1.00)	1.00 (1.00)	1.00 (1.00)	1.00 (1.00)
$H_e(H_{e'})$	3.45 3.45	2.59 (2.56)	2.59 (2.56)	2.42 (2.79)	2.42 (2.78)	2.42 (2.79)	2.42 (2.78)
$H_f(H_{f'})$	6.02 6.02					0.49 (0.57)	0.49 (0.57)
$H_g(H_{g'})$	6.11 6.11					0.62 (0.68)	0.62 (0.68)

(a) Values (in ppm) within each experiment were normalized to proton $H_d(H_{d'})$ in that same experiment using the appropriate bound chemical shifts listed in Table II-10.

(b) Values in parenthesis correspond to $\Delta 2$ bound chemical shifts, while those not in parenthesis correspond to $\Delta 1$ bound chemical shifts.

Normalization of the bound shifts of all protons in an experiment to proton $H_d(H_{d'})$ in that <u>same</u> experiment provides a method for comparison of the bound chemical shifts of an individual proton among experiments. Again, 100 MHz experiments A_4 and B_5 compare well as do 300 MHz experiments D_4, E_5, F_6, and G_7. The largest differences between 100 MHz and 300 MHz experiments are the values of $\Delta 2$. The 100 MHz $\Delta 2$ values are larger than the $\Delta 2$ values of the 300 MHz experiments, while the $\Delta 1$ values follow the opposite trend. The $\Delta 2$ values are reasonable in that they indicate small downfield shifts for protons in the LS_2 complex (due to the fact that two Lewis bases are complexed to one Lewis acid). Fortunately, $\Delta 1$ is the more easily determined and more accurate bound chemical shift of the two since it depends on the fewest degrees of molecular freedom of any LIS parameter.

Some investigators have used best-fit linear least squares plots similar to the nonlinear least squares plot shown in Fig II-8 (derived from the data in Table II-1, from RHO = 0.013 to 0.600) for the purpose of (i) molecular structure determination, (ii) evaluation of the equilibrium constants, (iii) calculation of bound chemical shifts, and (iv) locating the position of particular resonances in unresolved signals of undoped spectra (by extrapolation to RHO = 0). Although the relative magnitudes of the shifts, δ_{oi} values of complicated spectra, and identification of individual resonances that enter and emerge from a 'lanthanide-induced' overlap of signals can be estimated for specific protons using this method, evaluation of Δ's, K's, and molecular structure is less certain.[21] Aside from the error inherent in a linear least squares fitting procedure, the greatest uncertainty arises because a one-step equilibrium has been assumed. The structure(s) being evaluated at low RHO must in general be LS_2 or a combination of LS_2, LS, and S, and not the LS complex which predominates at high RHO (cf. the discussion concerning Figs II-2 and II-3 and Table II-5). $\Delta 2$ and K_2 and their contribution to the LIS are usually disregarded in structural interpretations.

FIGURE II-8

Plot of RHO vs. the Experimentally Measured Lanthanide Induced Shift from the Data Listed in Table II-1 for RHO from 0.0 to 0.6.

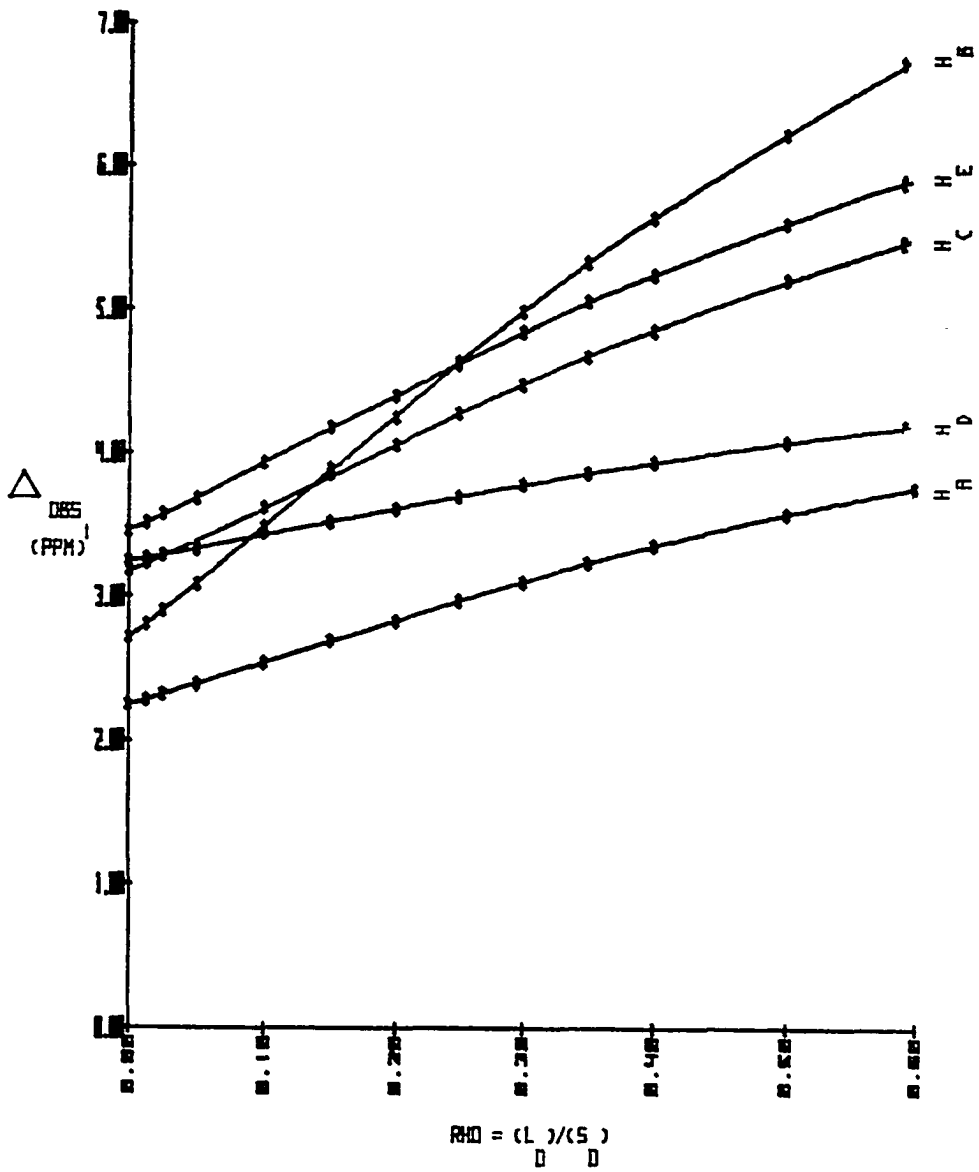

The present study takes into account the observed multi-step equilibria involved in LSR-substrate interactions and thus allows a much more accurate evaluation of the quantities derivable from them. That the present study is an example of 'cooperative binding' is supported by the excellent internal consistency of the data which is evidenced by the high precisions and standard deviations. The values of K_1 (4.01 M^{-1}) and of K_2 (25.76-26.0 M^{-1}) in the 100 MHz [0 $\leq$ RHO $\leq$ 3.0] experiments and K_1 (3.62 M^{-1}) and K_2 (46.26-48.16 M^{-1}) in the 300 MHz [0 $\leq$ RHO $\leq$ 6.0] experiments demonstrate the reproducibility of the 'K_2 > K_1' results. Further support for this conclusion will be revealed during the discussion of the 'collision complex' in PART III.

Experimental

Proton NMR spectra were obtained on Varian Model T-60, XL-100, and XL-300 spectrometers. All weights were determined on a Sartorius analytical balance (precision 000.1 mg) in a nitrogen-filled glove bag, and initial solutions were also prepared under nitrogen in a glove bag. All NMR tubes were rigorously cleaned and were dried at 110 °C for 24 hours prior to use.

Two general experiments were performed with phenyl ketone VII (from PART I). The first experiment utilized the same LSR, substrate, and stock solution concentrations and volumes as used in PART I. The 100 MHz proton NMR spectra were taken instead of the 60 MHz spectra, and chemical shifts were recorded after each of the twenty five incremental dilutions (Table II-1).

In the second experiment 0.31 g (2.997×10^{-4} mol) of $Eu(fod)_3$ and 0.0182 g (4.99×10^{-5} mol) of phenyl ketone VII in an NMR tube were diluted to 0.5 mL with $CDCL_3$/1%TMS, giving an initial RHO_{30} value of 6.001. A 300 MHz proton NMR spectrum was taken and chemical shifts were recorded. A 9.987×10^{-2} M stock solution of V (0.1092 g of VII diluted to 3.0 mL with $CDCL_3$/1%TMS) was used to increment

ally dilute RHO_{30} down to $RHO_1 = 0.0134$, and a 300 MHz proton NMR spectrum was taken after each dilution (Table II-8).

The chemical shifts recorded during these experiments were input to the LISA4 computer program and executed as discussed below.

The <u>100 MHz</u> input data sets were the observed chemical shifts (δ_i) of specific protons from $0 \leq RHO \leq 3.0$ (discussed under Table II-7) and comprise experiments A_4, B_5, and C_5 as shown below in Eqs II-21 through II-23.

<u>Experiment A_4</u>: Eq II-21

δ $H_a(H_{a'})$, $H_c(H_{c'})$, $H_d(H_{d'})$, $H_e(H_{e'})$;

<u>Experiment B_5</u>: Eq II-22

same as Exp A_4, but δ $H_b(H_{b'})$ was included;

<u>Experiment C_5</u>: Eq II-23

same as Exp B_5, but K_2 was restricted to zero.

The <u>300 MHz</u> input data sets were the observed chemical shifts (δ_i) of specific protons from $0 \leq RHO \leq 6.0$ (also discussed under Table II-7) and comprise experiments D_4, E_5, F_6, G_7, and H_7 as shown below in Eqs II-24 through II-28.

<u>Experiment D_4</u>: Eq II-24

δ $H_a(H_{a'})$, $H_c(H_{c'})$, $H_d(H_{d'})$, $H_e(H_{e'})$;

<u>Experiment E_5</u>: Eq II-25

same as Exp D_4, but $H_b(H_{b'})$ was included;

<u>Experiment F_6</u>: Eq II-26

same as Exp D_4, but $H_f(H_{f'})$ and $H_g(H_{g'})$ were included;

<u>Experiment G_7</u>: Eq II-27

same as Exp E_5, but $H_f(H_{f'})$ and $H_g(H_{g'})$ were included;

<u>Experiment H_7</u>: Eq II-28

same as Exp G_7, but K_2 was restricted to zero.

Error Analysis

Error analysis on the data contained in Tables II-3, II-5, II-6, and II-9 is not mathematically straightforward since $\Delta\delta_i$calc, [LS], α, [LS_2], β, $\Delta 1$, $\Delta 2$, and Q are calculated by iterative linear regression analysis of Eq II-5 and II-9, and K_1 and K_2 are computed by iterative non linear regression analysis of Eq II-16. The originators of the LISA4 computer program used to determine the above parameters have reported $\Delta 1$ values as accurate to ±0.02 ppm, $\Delta 2$ errors of less than 1% when K_2 lies between 5.0 and 500.0, and K_1 and K_2 to an accuracy of from less than ±2.0% to ±20.0%.[4]

The value of Q (calculated via Eq II-9 and listed in Table II-7) may be used as a guide to error estimation (statistically, Q/N = variance!) in the Table II-4 matrix of deviations. The standard deviation (σ_s) was defined in Eq II-20. The largest values of Q and σ_s found in Table II-7 are for Exp H_7 where K_2 was arbitrarily set equal to zero. More realistic maximum values are found for Exp E_5, where Q = 0.047 ppm^2 and σ_s = 0.018 ppm.

Least squares analysis of the Table II-8 data and the associated plot of Fig II-8 were performed with the error in RHO $\leq$ 0.002 (calculated as in PART I) and with the error in $\delta_i \approx$ 0.01 ppm. The average errors in the slope and y-intercept were 0.02 ppm and 0.01 ppm, respectively, while the standard deviations for the five lines were between 0.03 ppm and 0.10 ppm. It is interesting to note that the largest errors in slope, y-intercept, and standard deviation all correspond to proton $H_b(H_{b'})$. This may be a result of the fact that $H_b(H_{b'})$ is close enough to the lanthanide binding site to suffer from contact as well as pseudocontact LIS. This would yield erroneous values of the pseudocontact shift as calculated using Eq II-5.

BIBLIOGRAPHY

1. Raber, D. J.; Johnston, M. D.; Campbell, C. M.; Guida, A.; Jackson III, G. F.; Yanks, C. M.; Perry, J. W.; Propeck, G. J.; Raber, N. K.; Schwalke, M. A.; Sutton, P. M. Monatsh. Chem. 1980, 111, 43.

2. (a) Charles, R. G.; Ohlmann, R. C. J. Inorg. Chem. 1965, 27, 119. (b) Schwartzberg, J. E.; Gere, D. R.; Sievers, R. E.; Eisentraut, K. J. Inorg. Chem. 1969, 6, 1933.

3. (a) Hart, F. A.; Newbery, J. E.; Shaw, D. Nature, 1967, 216, 261. (b) Horrocks, W. De W.; Sipe, I. P. J. Am. Chem. Soc. 1971, 93, 6800.

4. (a) Shapiro, B. L.; Johnston, M. D. J. Am. Chem. Soc. 1972, 94, 8185. (b) Johnston, M. D.; Shapiro, B. L.; Proulx, T. W.; Godwin, A. D.; Pearce, H. L. J. Am. Chem. Soc. 1975, 97, 542. The helpful suggestions and kind assistance of M. D. J in furnishing a copy of the LISA4 computer program is gratefully acknowledged.

5. (a) Reuben, J. Prog. Nucl. Magn. Reson. Spectrosc. 1973, 9, 1. (b) Reuben, J. J. Am. Chem. Soc. 1973, 95, 3534.

6. (a) Inagaki, F.; Takahashi, S.; Tasumi, M.; Miyazawa, T. Bull. Chem. Soc. Jpn. 1975, 48, 853. (b) Inagaki, F.; Tasumi, M.; Miyazawa, T. Bull. Chem. Soc. Jpn. 1975, 48, 1427.

7. Deranleau, D. A. J. Am. Chem. Soc. 1969, 91, 4044, 4050.

8. Lenkinski, R. E.; Elgavish, G. A.; Reuben, J. J. Magn. Reson. 1978, 32, 367.

9. Erasmus, C. S., Boeyens, J. C. A. Acta Crystallogr. Sect. B 1970, B26, 1843.

10. Burnbaum, E. R.; Moeller, T. D. Am. Chem. Soc. 1969, 91, 7274.

11. (a) Caple, R.; Kuo, S. C. Tetrahedron Lett. 1971, 4413. (b) Hinckley, C. C.; Klotz, M. R.; Patil, F. J. Am. Chem. Soc. 1971, 93, 2417.

12. (a) Hofer, O. Top. Stereochem. 1976, 9, 111. (b) Cramer, R. E.; Dubois, R.; Seff, K. J. Am. Chem. Soc. 1974, 96, 4125. (c) Horrocks Jr., W.; Sipe III, J. P. Science 1972, 177, 994.

13. (a) Davis, R. E.; Willcott III, M. R. "Nuclear Magnetic Resonance Shift Reagents"; Sievers, R. A., Ed.; Academic: New York, 1973; p 143. (b) Johnson, B. F. G.; Lewis, J.; McArdle, P.; Norton, J. R. Chem. Commun. 1972, 535. (c) Tori, K.; Yoshimura, Y.; Kainosho,,M.; Ajisaka, K. Tetrahedron Lett. 1973, 3127. (d) Hirayama, M.; Edagawa, E.; Hanyu, Y. Chem. Commun. 1972, 1343. (e) Chalmers, A. A.; Pachler, K. G. R. Tetrahedron Lett. 1972, 4033. (f) Raber, D. J.; Johnston, M. D. Spectrosc. Lett. 1982, 15, 287. (g) Raber, D. J.; Johnston, M. D.; Campbell, C. M.; Yanks, C. M.; Sutton, P. M. Org. Magn. Reson. 1978, 11, 323.

14. (a) Shapiro, B. L.; Hulbeck, J. R.; Sullivan, G. R.; Johnson, L. F. J. Am. Chem. Soc. 1971, 93, 3281. (b) Armitage, I.; Hall, L. D. Can. J. Chem. 1971, 49, 2770. (c) Sanders, J. K.; Williams, D. H. J. Am. Chem. Soc. 1972, 94, 5325. (d) Demarko, P. V.; Elzey, T. K.; Lewis, R. B.; Wenkert, E. J. Am. Chem. Soc. 1970, 92, 5734.

15. Goldberg, L.; Ritchey, W. M. Spectrosc. Lett. 1972, 5, 201.

16. Rondeau, R. E,; Sievers, R. E. J. Am. Chem. Soc. 1971, 93, 1522.

17. (a) Cockerill, A. F.; Rackham, D. M. Tetrahedron Lett. 1970, 5149. (b) Raber, D .J.; Johnston, M. D.; Yanks, C. M.; Perry, J. W.; Jackson III, G. F. Org. Magn. Reson. 1980, 14, 32.

18. Maier, T. O.; Drago, R. S. Inorg. Chem. 1972, 11, 1861.

19. M. D. Johnston private communication.

20. M. D. Johnston private communication.

21. Raber, D. J.; Hardee, L. E. Org. Magn. Reson. 1982, 20, 125.

PART III

A DETERMINATION OF THE POSITION OF THE LANTHANIDE METAL ION IN THE LANTHANIDE SHIFT REAGENT-SUBSTRATE 'COLLISION COMPLEX'

Introduction

Within the last few years, much effort has been directed toward the elucidation of molecular structure using lanthanide shift reagents in nuclear magnetic resonance spectroscopy.[1-4] Most such studies have been performed at low lanthanide shift-reagent:substrate ratios (RHO) where the 1:2 LS_2 complex predominates rather than the 1:1 LS complex. Therefore, rigorous structural analysis of the 1:1 'collision complex' must of necessity be conducted at high RHO where LS should be the predominant species. Analysis of the 1:1 'collision' complex is the subject of this chapter.

Results and Discussion

From the simplified (dipolar) form of the pseudocontact equation (PART I, Eq I-1),

$$LIS=\Delta\delta_i = K(3\cos^2\theta_i-1)/(RI_i)^3 \qquad \text{Eq III-1}$$

The magnitude of the induced incremental shift ($\Delta\delta_i$) for proton H_i depends on the distance vectors RI_i and R_{EO}, θ_i, and the constant K, as illustrated in Fig III-1 for a europium complex. Many have used computerized procedures in which the angle θ_i and distances R_{EO} and RI_i are varied simultaneously until

FIGURE III-1

Representation of the geometrical relationship between europium and hydrogen atom 'i' in terms of distance and angle from the magnetic axis for a complex in which 'X' is the binding site.

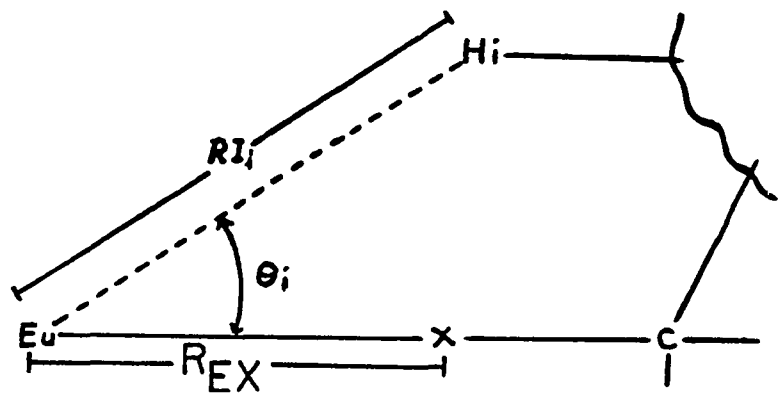

FIGURE III-2

Representation of the geometrical relationships in a complex in which conformational flexibility exists for both europium (ω_E) and hydrogen (ω_H).

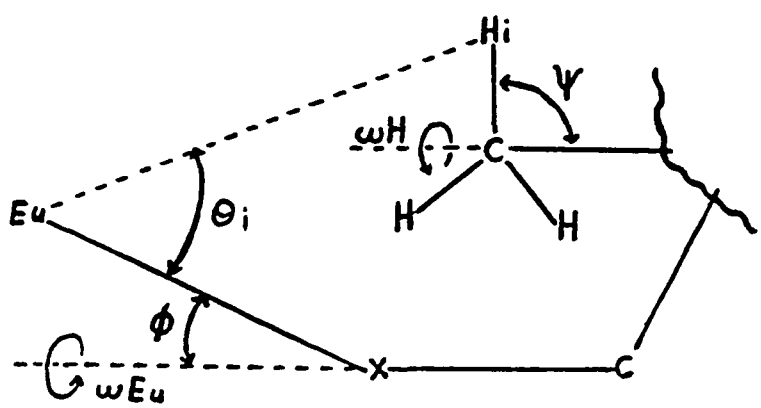

the correlation between the induced incremental shift and the geometric factor $(3\cos^2\theta_i - 1)$ for certain protons in the substrate is minimized.[5] A similar NLLSQ (Non Linear Least Squares) computer program, adapted for solution of Eq III-1, was utilized here.[6]

In order to solve Eq III-1, the variables within it must be defined in mathematical terms which can be adapted to NLLSQ. These variables are expressed in Figs III-1 and III-2. Bond angles H_i-Eu-X and Eu-X-C (i.e., θ_i and θ_o, respectively), and RI_i, ω_H, Ψ, Φ, and ω_{Eu} are all unknowns. In order to obtain reliable values of the parameters θ_i and RI_i, it is necessary to specify the geometric coordinates of the europium ion and hydrogen nuclei of interest relative to the heteroatom X. Choice of substrate eliminates Ψ and ω_H as variables and solution of Eq III-1 in terms of Cartesian coordinates eliminates Φ and ω_{Eu}. In the application of Eq III-1, it must be emphasized that the $\Delta\delta_i$ are best represented by the <u>bound</u> chemical shifts (i.e., as determined by the LISA4 linear regression analysis in PART II) of protons in the molecule instead of the relative incremental induced chemical shifts.[7,8] The results of such a study allow determination of the position of the metal ion in the LSR-substrate complex. The final lanthanide ion position, as determined in iterative programs, may depend on the choice of the initial position, since local minima in the error function often occur. A global search (complete search of all possibilities) avoids this danger, but large amounts of computer time are required.

A solution to the problem begins by making the following mathematical statements with reference to Fig III-1 (for a labeling scheme) and to Fig III-3 (for a numbering scheme):

$$R_{EO} = R_{OE} = \text{Eu to O9 bond distance} \qquad \text{Eq III-2}$$
$$= [(xO9 - xE)^2 + (yO9 - yE)^2 + (zO9 - zE)^2]^{1/2}$$

$$k = \text{constant} \qquad \text{Eq III-3}$$

FIGURE III-3

Computer Drawn Representation and Numbering Scheme for 7-Phenyl Dimer Ketone VII.

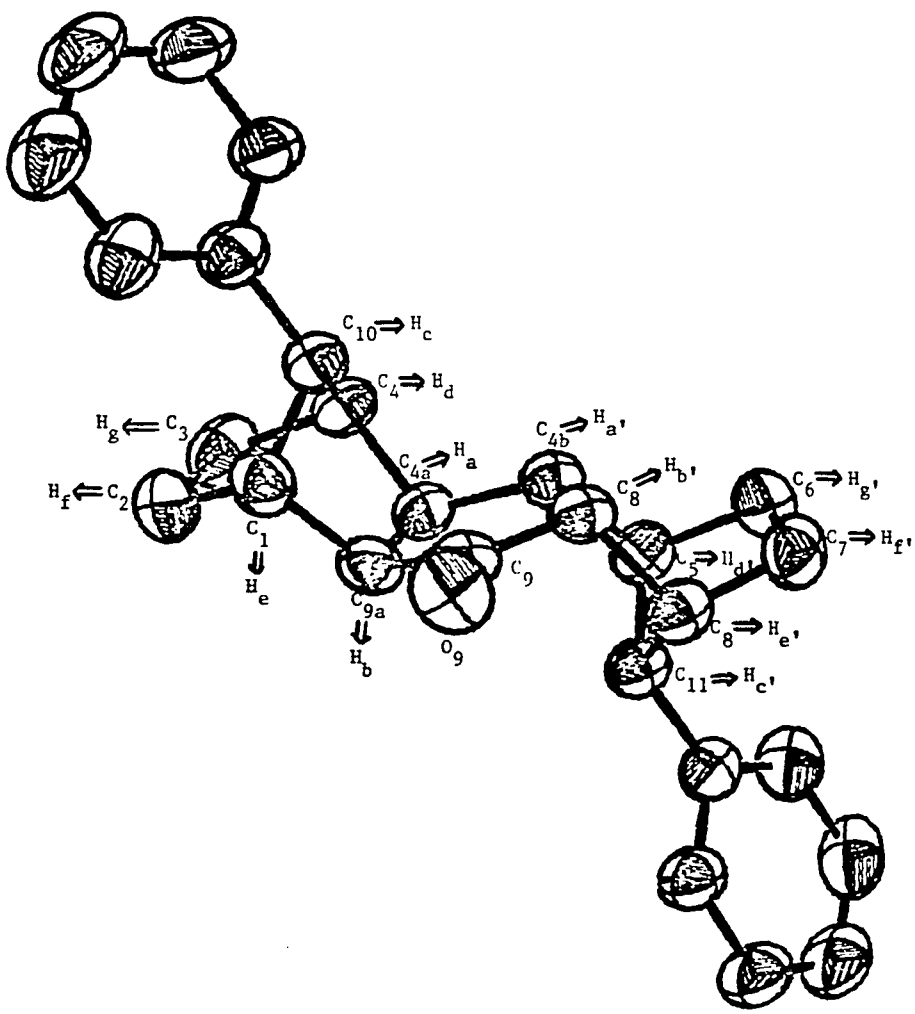

ORTEP (Johnson, 1965) drawing of a single molecule.

R_{CO} = C9 to O9 bond distance (X-ray of VI, PART I) Eq III-4

$= [(xC9-xO9)^2+(yC9-yO9)^2+(zC9-zO9)^2]^{1/2} = 1.212(2)$ Å

$R = (R_{EO} + R_{CO})/R_{CO}$ Eq III-5

xO9 = x coordinate of O9 (X-ray structure of VI, PART I) Eq III-6a

yO9 = y " " O9 " " " " " " Eq III-6b

zO9 = z " " O9 " " " " " " Eq III-6c

xC9 = x " " C9 " " " " " " Eq III-7a

yC9 = y " " C9 " " " " " " Eq III-7b

zC9 = z " " C9 " " " " " " Eq III-7c

xE = x " of europium = (xO9 - xC9)(R) + xC9 Eq III-8a

yE = y " " " = (yO9 - yC9)(R) + yC9 Eq III-8b

zE = z " " " = (zO9 - zC9)(R) + zC9 Eq III-8c

R_{EC} = europium to C9 distance Eq III-9

$= [(xC9-xEu)^2 + (yC9-yEu)^2 + (zC9-zEu)^2]^{1/2}$

RI_i = europium to H_i distance Eq III-10

Having written R_{EO}, the europium position, R_{EC}, and RI_i in terms of Cartesian coordinates x, y, and z, only θ_i and θ_o remain to be defined. Equations III-11 and III-12 express θ_i and θ_o in terms of vectors.[9]

$\cos\theta_i$ = Cos(H_i-Eu-C9 angle) Eq III-11

$= aR_{OE} \cdot aRI_i / \|aR_{OE}\| \cdot \|aRI_i\|$

$\cos\theta_o$ = Cos(Eu-O9-C9 angle) Eq III-12

$= aR_{EO} \cdot aR_{CO} / \|aR_{EO}\| \cdot \|aR_{CO}\|$

These two equations represent the scalar, dot, or inner product of vectors aR_{OE} (equivalent to $-aR_{EO}$) and aRI_i, and of vectors aR_{EO} and aR_{CO}, respectively (cf. Fig III-1). In terms of Cartesian coordinates,

aR_{OE} = (xO9 - xE),(yO9 - yE),(zO9 - zE) Eq III-13

$$aRI_i = (xH_i - xE),(yH_i - yE),(zH_i - zE) \qquad \text{Eq III-14}$$

$$||aR_{OE}||=[(xO9-xE)^2+(yO9-yE)^2+(zO9-zE)^2]^{1/2} \qquad \text{Eq III-15}$$

$$||aRI_i||=[(xH_i-xE)^2+(yH_i-yE)^2+(zH_i-zE)^2]^{1/2} \qquad \text{Eq III-16}$$

$$aR_{EO}=(xE-xO9),(yE-yO9),(zE-zO9) \qquad \text{Eq III-17}$$

$$aR_{CO}=(xC9-xO9),(yC9-yO9),(zC9-zO9) \qquad \text{Eq III-18}$$

$$||aR_{EO}||=[(xE-xO9)^2+(yE-yO9)^2+(zE-zO9)^2]^{1/2} \qquad \text{Eq III-19}$$

$$||aR_{CO}||=[(xC9-xO9)^2+(yC9-yO9)^2+(zC9-zO9)^2]^{1/2} \qquad \text{Eq III-20}$$

$$\begin{aligned} aR_{OE}\cdot aRI_i=&(xO9-xE)(xH_i-xE) \\ &+(yO9-yE)(yH_i-yE) \\ &+(zO9-zE)(zH_i-zE) \end{aligned} \qquad \text{Eq III-21}$$

$$\begin{aligned} ||aR_{OE}||\cdot||aRI_i||= \\ = \{[(xO9-xE)^2+(yO9-yE)^2+(zO9-zE)^2]^{1/2}\} \\ \{[xH_i-xE)^2+(yH_i-yE)^2+(zH_i-zE)^2]^{1/2}\} \end{aligned} \qquad \text{Eq III-22}$$

$$\begin{aligned} aR_{EO}\cdot aR_{CO}=&(xE-xO9)(xC9-xO9) \\ &+(yE-yO9)(yC9-yO9) \\ &+(zE-zO9)(zC9-zO9) \end{aligned} \qquad \text{Eq III-23}$$

$$\begin{aligned} ||aR_{EO}||\cdot||aR_{CO}||= \\ =\{[(xE-xO9)^2(yE-yO9)^2(zE-zO9)^2]^{1/2}\}(1.212\ \text{Å}) \end{aligned} \qquad \text{Eq III-24}$$

After substitution of Eqs III-21 and III-22 into Eq III-11, and substitution of Eqs III-23 and III-24 into Eq III-12, the following expressions are obtained:

$$\begin{aligned} \cos\theta_i &= \cos(H_i\text{-Eu-C9 angle}) \\ &= [(xO9-xE)(xH_i-xE)+(yO9-yE)(yH_i-yE)+(zO9-zE)(zH_i-zE)]/ \\ &\quad \{[(xO9-xE)^2+(yO9-yE)^2+(zO9-zE)^2]^{1/2} \\ &\quad [(xH_i-xE)^2+(yH_i-yE)^2+(zH_i-zE)^2]^{1/2}\} \end{aligned} \qquad \text{Eq III-25}$$

$$\begin{aligned} \cos\theta_O &= \cos(\text{Eu-O9-C9 angle}) \\ &= [(xC9-xO9)(xE-xO9)+(yC9-yO9)(yE-yO9)+(zC9-zO9)(zE-zO9)]/ \\ &\quad \{[(xE-xO9)^2+9yE-yO9)^2+(zE-zO9)^2]^{1/2}(1.212\ \text{Å})\} \end{aligned} \qquad \text{Eq III-26}$$

The expression for Eq III-1 becomes:

$\Delta\delta_i$ = lanthanide-induced shift Eq III-27

$$= k[3(aR_{OE}\cdot aRI_i/\|aR_{OE}\|\cdot\|aRI_i\|)^2-1]/\|aRI_i\|^3$$

After substituting the cartesian coordinate expressions for the corresponding vector expressions, Eq III-27 becomes

$\Delta\delta_i$ = lanthanide-induced shift Eq III-28

$$= k\{3([(xO9-xE)(xH_i-xE)+(yO9-yE)(yH_i-yE)+(zO9-zE)(zH_i-zE)]/$$
$$[(xO9-XE)^2+(yO9-yE)^2+(zO9-zE)^2]^{1/2}$$
$$[(xH_i-xE)^2+(yH_i-yE)^2+(zH_i-zE)^2]^{1/2})^2-1\}/$$
$$\{[(xH_i-xE)^2+(yH_i-yE)^2(zH_i-zE)^2]^{1/2}\}^3$$

Eq III-28 is the lanthanide-induced shift written in terms of the Cartesian coordinates of O9 and H_i, and also of k, xE, yE, and zE (a four-parameter 'free' fit, which allows europium to assume a position away from the carbonyl axis). Substitution of Eqs III-8a, b, and c for xE, yE, and zE, respectively, into Eq III-28 gives

$\Delta\delta_i$ = lanthanide-induced shift Eq III-29

$$= k\{3([(xO9-[(xO9-xC9)(R)+xC9])(xH_i-[(xO9-xC9)(R)+xC9])$$
$$+(yO9-[(yO9-yC9)(R)+yC9])(yH_i-[(yO9-yC9)(R)+yC9])$$
$$+(zO9-[(zO9-zC9)(R)+zC9])(zH_i-[(zO9-zC9)(R)+zC9])]/$$
$$[(xO9-[(xO9-xC9)(R)+xC9])^2$$
$$+(yO9-[(yO9-yC9)(R)+yC9])^2$$
$$+(zO9-[(zO9-zC9)(R)+zC9])^2]^{1/2}$$
$$[(xH_i-[(xO9-xC9)(R)+xC9])^2$$
$$+(yH_i-[(yO9-yC9)(R)+yC9])^2$$
$$+(zH_i-[(zO9-zC9)(R)+zC9])^2]^{1/2})^2-1\}/$$
$$\{[(xH_i-[(xO9-xC9)(R)+xC9])^2$$
$$+(yH_i-[(yO9-yC9)(R)+yC9])^2$$
$$+(zH_i-[(zO9-zC9)(R)+zC9])^2]^{1/2}\}^3$$

Eq III-29 is the lanthanide-induced shift written in terms of k,

R_{EO} (a two-parameter 'fixed' fit of Eq III-1, with the europium atom restricted to the carbonyl axis), the cartesian coordinates of O9, C9, H_i, and the X-ray determined value of the C9-O9 bond length R_{CO} (1.212 Å). Results of these fits will be discussed below. θ_i may be determined via Eq III-25, θ_o via Eq III-26 (cf. Fig III-1), or both may be determined as shown in Eqs III-30 through III-39.

X_A: $X_a = xH_i - xE$ Eq III-30a

$X_b = xO9 - xE$ 30b

$X_c = xE - xO9$ 30c

$X_d = xC9 - xO9$ 30d

Y_A: $Y_a = yH_i - yE$ Eq III-31a

$Y_b = yO9 - yE$ 31b

$Y_c = yE - yO9$ 31c

$Y_d = yC9 - yO9$ 31d

Z_A: $Z_a = zH_i - zE$ Eq III-32a

$Z_b = zO9 - zE$ 32b

$Z_c = zE - zO9$ 32c

$Z_d = zC9 - zO9$ 32d

$X_A = [(X_a)^2+(Y_a)^2+(Z_a)^2]^{1/2} = RI_i$ Eq III-33a

$X_B = [(X_b)^2+(Y_b)^2+(Z_b)^2]^{1/2} = R_{OE}$ 33b

$X_C = [(X_c)^2+(Y_c)^2+(Z_c)^2]^{1/2} = R_{EO}$ 33c

$X_D = [(X_d)^2+(Y_d)^2+(Z_d)^2]^{1/2} = R_{CO}$ 33d

$X_\alpha = X_a/X_A$ Eq III-34a

$Y_\alpha = Y_a/X_A$ 34b

$Z_\alpha = Z_a/X_A$ 34c

$$X_\beta = X_b/X_B \qquad \text{Eq III-35a}$$
$$Y_\beta = Y_b/X_B \qquad 35b$$
$$Z_\beta = Z_b/X_B \qquad 35c$$

$$X_\gamma = X_c/X_C \qquad \text{Eq III-36a}$$
$$Y_\gamma = Y_c/X_C \qquad 36b$$
$$Z_\gamma = Z_c/X_C \qquad 36c$$

$$X_\delta = X_d/X_D \qquad \text{Eq III-37a}$$
$$Y_\delta = Y_d/X_D \qquad 37b$$
$$Z_\delta = Z_d/X_D \qquad 37c$$

$$\text{Cos}\theta_i = \text{Cos}(H_i\text{-Eu-C9 angle}) = X_\alpha \cdot X_\beta + Y_\alpha \cdot Y_\beta + Z_\alpha \cdot Z_\beta \qquad \text{Eq III-38}$$

$$\text{Cos}\theta_o = \text{Cos}(\text{Eu-O9-C9 angle}) = X_\gamma \cdot X_\delta + Y_\gamma \cdot Y_\delta + Z_\gamma \cdot Z_\delta \qquad \text{Eq III-39}$$

Hinckley[10] has shown that errors in the assumed coordinates can have a dramatic effect on the structure evaluation process. Workers in the field almost invariably have resorted to the approximation that the structure of the substrate moiety in the complex is unchanged from that of the free substrate, and, given that basic assumption, a variety of procedures have been used. Some have used coordinates derived from X-ray crystal structures (from either the same or of a related compound),[11,12] while others have used standard geometry parameters,[13] or even such crude methods as measurement from Dreiding models.[14] Others have calculated the structure of the substrate molecule by methods such as empirical force field calculations[15] with full geometry optimization using Allinger's MMI and MMII programs.[16] The latter approach has been particularly successful.[15d]

However, recall that a single crystal X-ray structure of dimer

ketone X has been done (PART I) and that the NMR and IR spectra of VII and IX are very similar (both possess AXTXA stereochemistry). Since both compounds are identical except for the two o-methoxy groups of VI, the assumption was made that the carbon, hydrogen, and oxygen skeletons (excluding the aromatic substituents) were geometrically identical. The atomic coordinates (from PART I) of the atoms used in calculating the necessary Cartesian coordinates (determined by the Mean Plane Program)[6] were readily available for use in the above equations, and both are listed in Table III-1. Some slight error in the proton Cartesian coordinates is expected since X-ray structures are known to afford short C-H bond lengths.[17]

Having eliminated all variables except the constant (K) and the europium-oxygen bond distance (R_{EO}), the correlation between the lanthanide-induced shift [i.e., the bound chemical shifts ($\Delta 1_i$) as determined by LISA 4 in PART III] and the $\Delta\delta_i$ of Eq III-1 can now be maximized for each pair of equivalent protons using the NLLSQ program.

The two general data sets discussed in PART II (i.e., from the 100 MHz and 300 MHz experiments) provided the bound chemical shifts (Table II-10). Experiments C_5 and H_7 were omitted from the current discussion because of the artificial nature of their output data which resulted from setting K_2 equal to zero. The remaining experiments were handled in two ways: first is the 'free' (four-parameter) fit where europium is not restricted to the carbonyl axis and where K, xE, yE, and zE are allowed to vary within Eq III-28. Second is the 'fixed' (two-parameter) fit where europium is restricted to the carbonyl axis and where R_{EO} and K are allowed to vary within Eq III-29. The former method allows a solution which is independent of prior knowledge of the position of europium and the europium-oxygen bond distance, and therefore should probably afford a more realistic solution.

Input to the NLLSQ program was the X-ray determined value of R_{CO} (1.212±.002 Å), and the Cartesian coordinates and bound

TABLE III-1

Atomic (x/a, y/b, z/c) and Cartesian (x, y, z) Coordinates for Carbon, Hydrogen, and Oxygen Atoms. Cell: a=9.466 Å, b=19.413 Å, c=13.095 Å; α=90.0°, β=106.82°, and γ=90.0°. The standard deviation is (±1) unless otherwise specified in parenthesis.

Nucleus	x/a	x	y/b	y	z/c	z
C_9	1.0293(2)	7.847	.8295	16.103	.5004	6.272
O_9	1.0675	7.845	.8376	16.260	.5963	7.474
C_{9a}	1.0285	8.047	.7608	14.769	.4458	5.588
C_{8a}	0.9740	7.628	.8661	17.202	.4201	5.266
C_1	0.9239(2)	6.942	.7098	13.779	.4760	5.967
C_2	0.9440(2)	7.316	.6398	12.420	.4276	5.360
C_3	0.8718(2)	7.088	.6509	12.636	.3073	3.852
C_4	0.8209(2)	6.635	.7262	14.098	.2996	3.755
C_{4a}	0.9587	7.845	.7729	15.004	.3245	4.068
C_{4b}	0.9248	7.587	.8512	16.524	.3080	3.861
C_5	1.0196(2)	8.711	.8900	17.278	.2483	3.112
C_6	0.9620(2)	8.221	.9650	18.734	.2337	2.929
C_7	1.0287(2)	8.431	.9969	19.353	.3449	4.323
C_8	2.0993(2)	18.306	.8354	16.218	.4133	5.181
C_{10}	0.7726	5.787	.7344	14.257	.4028	5.049
C_{11}	1.1671(2)	9.771	.8947	17.369	.3369	4.223
C_{12}	0.6373(2)	4.480	.6592	13.496	.4098	5.137
C_{19}	1.3002(2)	1.111	.9282	18.019	.3158	3.958
$H_{4a}=H_a$	1.0280	8.666	.7580	14.715	.2810	3.522
$H_{4b}=H_{a'}$	0.8170	6.699	.8570	16.637	.2730	3.422
$H_{9a}=H_b$	1.1302(2)	8.935	.7440	14.443	.4650	5.829
$H_{8a}=H_{b'}$	0.8960(2)	6.814	.9120	17.705	.4400	5.515
$H_{10}=H_c$	0.7580	5.606	.7840	15.220	.4140	5.189
$H_{11}=H_{c'}$	1.1990	9.963	.8470	16.443	.3660	4.588
$H_4=H_d$	0.7470	6.196	.7400	14.366	.2310	2.896
$H_5=H_{d'}$	1.0220	8.988	.8670	16.831	.1810	2.269
$H_1=H_e$	0.9350	6.748	.7100	13.783	.5550	6.957
$H_8=H_{e'}$	1.1680(2)	9.215	.9470	18.384	.4860	6.092

shifts of the pairs of equivalent protons to be considered in the particular experiment. The computer was also provided with initial estimates of R_{EO} and K in the 'fixed' case, and estimates of K, xE, yE, and zE in the 'free' case, and allowed to iterate them until maximum agreement between the observed bound shifts and the corresponding $\Delta\delta_i$ values is obtained. The results of the 'free' and 'fixed' fits for calculation of the best fit $\Delta\delta_i$'s (listed in Table III-2) and the corresponding values of K, europium coordinates, R_{EO}, θ_O, and error parameters are listed in Table III-3. Values for protons $H_f(H_{f'})$ and $H_g(H_{g'})$ are omitted because the X-ray study, which was done on the saturated analog of IV, did not provide their atomic coordinates.

There is no universal agreement on the position of europium in complexes with ketones. Several investigators have suggested that lanthanides complex with ketones via the lone pairs of electrons on the oxygen atom in a two-site model (Eu-O-C angle ≈ 120°).[18] Chadwick has used the computer program LIRAS to determine a ytterbium-oxygen distance of 2.80-3.00 Å and a Eu-O-C angle near 159° in a $Yb(fod)_3$-adamantanone complex in which the lanthanide was allowed to occupy four sites of equal population (i.e., reflection in the two mirror planes passing through the carbonyl group).[19] Others are convinced that europium complexes along the carbonyl axis (Eu-O-C angle ≈ 180.0°).[1,2,20] Calculations for a number of oxygenated hydrocarbons gave a reasonable position of the lanthanide and a range of lanthanide-oxygen distances of 2.5 to 3.5 Å.[20] Others suggest the most accurate europium-oxygen distance in ketone complexes to be 2.5 Å based on a search of the crystallographic literature on tris(β-diketonate)lanthanide (III) complexes.[22,23] Another report lists a europium-oxygen distance of 2.8 Å and a Eu-O-C bond angle of 109° for a series of homologous cyclic ketones by analogy with R_2CO-$HgCl_2$.[5a] For the lanthanide ytterbium with the symmetrical compounds 2-indanone and fluorenone, a Yb-O bond distance and Yb-O-C angle of 1.5 Å and 120°,

TABLE III-2

NLLSQ Calculated 'Best-fit' Bound Chemical Shifts (Δl_i's) from the 100 MHz and 300 MHz 'Collision-Complex' LSR Studies of the 'Free'[a] and 'Fixed'[b] Data Sets.

		Experiments											
		A_4[c,d]		B_5		D_4		E_5		F_6		G_7	
H_i	δ_0	free	fixed	free	fixed	free	fixed	free	fixed	free	fixed	free	fixed
H_a	2.25	10.87	10.65	11.61	11.48	15.81	15.48	16.69	16.51	15.05	14.74	16.92	16.74
$H_{a'}$	2.25	10.82	11.02	11.71	11.87	15.73	16.01	16.88	17.08	14.98	15.25	17.11	17.31
H_b	2.71			26.64	26.57			38.29	38.14			38.81	38.66
$H_{b'}$	2.71			26.14	26.20			37.55	37.68			38.06	38.20
H_c	3.17	14.60	15.13	15.71	16.12	21.10	21.81	22.54	23.01	20.09	20.77	22.85	23.32
$H_{c'}$	3.17	14.47	14.00	15.33	15.00	20.92	20.26	21.88	21.48	19.92	19.29	22.17	21.78
H_d	3.24	6.75	6.87	7.26	7.32	9.77	9.90	10.37	10.46	9.30	9.43	10.51	10.60
$H_{d'}$	3.24	6.79	6.71	7.22	7.17	9.78	9.69	10.30	10.25	9.31	9.23	10.44	10.39
H_e	3.45	16.27	16.38	16.10	16.17	22.36	22.37	21.90	21.89	21.20	21.29	22.20	22.10
$H_{e'}$	3.45	16.24	16.03	16.39	16.18	22.34	22.23	22.36	22.26	21.26	21.16	22.66	22.55
RMSD[e]		.9457	.8436	1.136	1.113	1.122	1.020	1.658	1.486	1.060	.9714	1.682	1.587
σ_s[f]		0.0129		0.0141		0.0158		0.0177		0.0124		0.0160	

(a) 'Free' Δl_i values (in ppm) were calculated from the four-parameter best-fit to Eq III-28 by NLLSQ.

(b) 'Fixed' Δl_i values (in ppm) were calculated from the two-parameter best-fit to Eq III-29 by NLLSQ.

(c) As in Table II-7 PART II, A_4 and B_5 are 100 MHz experiments, and D_4, E_5, F_6, G_7 are 300 MHz experiments.

(d) All Δl_i values (in ppm) which served as input to NLLSQ for calculation of the best-fit 'free' and 'fixed' bound chemical shifts listed here are from Table II-10, PART II.

(e) RMSD values were computed by NLLSQ.

(f) Weighted standard shift deviations (in ppm) are repeated here from Table II-7 for comparison.

TABLE III-3

Parameters Calculated Using the 'Free' and 'Fixed' Δ_i Values of Table III-2.

	Experiments[a]											
	A_4		B_5		D_4		E_5		F_6		G_7	
Parameter	free	fixed	free	fixed	free	fixed	free	fixed	free	fixed	free	fixed
k[b]	1496.8	1495.8	1520.6	1518.6	2080.3	2081.5	2107.5	2107.4	1980.1	1981.2	2135.9	2135.8
xEu[c]	7.671	7.841	7.744	7.842	7.699	7.842	7.770	7.842	7.700	7.842	7.770	7.842
yEu	16.610	16.539	16.561	16.522	16.596	16.526	16.547	16.511	16.596	16.526	16.547	16.511
zEu	9.582	9.611	9.469	9.477	9.483	9.514	9.389	9.398	9.482	9.513	9.388	9.398
RMSD[d]	0.946	0.844	1.236	1.113	1.122	1.020	1.658	1.486	1.068	0.971	1.682	1.507
R_{E0}[e]	2.144	2.155	2.020	2.020	2.042	2.057	1.938	1.940	2.041	2.056	1.937	1.940
θ_0[f]	175.0	180.0	177.0	180.0	175.5	180.0	177.6	180.0	175.5	180.0	177.6	180.0
R-factor[g]	0.053	0.058	0.057	0.060	0.044	0.049	0.054	0.056	0.044	0.049	0.054	0.056
σ_s[h]	0.0129		0.0141		0.0158		0.0177		0.0124		0.0160	

(a) As discussed under Table III-2, A_4 and B_5 are 100 MHz experiments and D_4, E_5, F_6, and G_7 are 300 MHz experiments.

(b) Both 'free' and 'fixed' values of k were calculated by NLLSQ.

(c) 'Free" values of the europium coordinates were calculated by NLLSQ, while 'fixed' values were calculated using Eqs III-8a, b, and c.

(d) The RMSD values were calculated by NLLSQ.

(e) 'Free' R_{E0} values (in Å) were calculated using the 'free' europium coordinates and Eq II-2, while 'fixed' values were NLLSQ calculated.

(f) 'Free' values of θ_0 (in ppm) were calculated using Eq III-39.

(g) The agreement factor (R) is given by
$R=[\Sigma(\Delta_i obs - \Delta_i calc)^2/\Sigma(\Delta_i obs)^2]^{\frac{1}{2}}$, where $\Delta_i obs$ is the LISA 4 determined bound chemical shift of proton H_i, and $\Delta_i calc$ is the NLLSQ calculated best-fit bound chemical shift of proton H_i.

(h) The values of σ_s (in ppm) are given by Eq II-19, and are repeated here (from Table III-2) for comparison with the RMSD and R-factor error values.

respectively, have been reported.[24] The latter 'fixed' complexation (cf. Eq III-29) with the symmetrical dimer ketone V (from PART I) was initially assumed (Fig III-1), but a 'free' complexation was also considered (cf. Fig III-2 and Eq III-28). Two values of K have been reported for $Eu(fod)_3$ in 1:1 complexes with nitriles (760 and 976.6)[13,15c], and the value of ca. 10^3 has been calculated in work with the symmetrical compound adamantanone.[25] A recent report on the similar symmetrical compound 1-adamantanecarbonitrile in a 1:1 complex with $Eu(fod)_3$ suggests a value of ca. 10^3 for K, 2.10 Å for the europium-nitrogen bond distance, and a linear C-N-Eu angle.[11]

There are several error functions to be found in the relevant literature which have been used to assess the correspondence between bound chemical shifts and calculated bound chemical shifts. The most often used error function is the one chosen by Willcott, Lenkinski and Davis.[26] Their agreement factor 'R' is defined by Eq III-40.

$$R=[\Sigma(\Delta_i obs-\Delta_i calc)^2/\Sigma(\Delta_i obs)^2]^{1/2} \qquad \text{Eq III-40}$$

$\Delta_i$obs is the LISA 4 calculated bound shift ($\Delta\delta_i$) of proton H_i, and $\Delta_i$calc is the NLLSQ calculated 'best-fit' bound chemical shift of proton H_i in the LSR-substrate complex. Other expressions expressions for R in the literature include crystallographic disagreement factor, reliability factor, Hamilton agreement factor, or simply R-factor. In Eq III-40, weighting factors (w_i) may be introduced. For every signal yielding a LIS value w_i=1. Use of weighting factors is advantageous for symmetrical molecules, or more generally for any molecule where one observed NMR resonance signal corresponds to two or more nuclei placed at different sites in the coordinate system. The application of the agreement factor (corresponding to the least squares fit of a model) in assessment of hypothesis reliability has been studied extensively by Hamilton.[27] Values of R up to 0.10 have been

considered to represent a good fit,[3] while the 0.04 to 0.06 range for R has been considered to be acceptable for europium LSR's.[28] An R value of 0.03 has been considered by some to be a convenient upper limit for acceptability of a proposed structure.[16] However, structure fits which rely only on a minimization of the agreement factor do not necessarily afford an acceptable method for evaluation of the bond length between a donor atom and a lanthanide nucleus.[19] Three questions must now be answered: (i) Should data sets which include contributions from the α-hydrogens (which may be undergoing contact shift) be considered in determining the best-fit structure?; (ii) Are the 'free' or 'fixed' data sets most accurate?; (iii) Which data set best represents the collision complex?

Since the possibility of contact shift contribution to the bound chemical shift of proton $H_b(H_b')$ is very real [recall the discussion of the influence of the contact shift on the deviations between the observed and calculated chemical shifts for $H_b(H_b')$ in PART III], experiments B_5, E_5, and G_7 may not be as accurate as are the related experiments A_4, D_4, and F_6. The larger values of the weighted standard shift deviations for B_5, E_5, and G_7 (0.014, 0.018, and 0.016 ppm, respectively) as opposed to those for A_4, D_4, and F_6 (0.013, 0.016, and 0.012 ppm, respectively) support this conclusion. Admittedly, the differences are small and may be due in part to the fact that the extra data points introduce error. However, experiment F_6 has more data points and also has a smaller standard deviation than either A_4 or D_4.

The question of which data set ('free' or 'fixed') is most accurate cannot be determined using the weighted standard shift deviation which was previously calculated by LISA4, because the LISA4-calculated $\Delta_i$obs chemical shifts input to NLLSQ are the same for both 'free' and 'fixed' calculations within an experiment. Instead, one might rely on the results of the NLLSQ fitting procedure. In particular, the RMSD and R-factor values may provide the basis for judge-

ment. However, the trends in Table III-3 are contradictory in that, within each experiment, the 'free' fit gives larger RMSD and smaller R-factor values. Therefore, recalling the discussion of the use of Eq III-28 in which no a priori knowledge of or restriction on the position of europium in the collision complex was necessary, it was felt that the position of europium would most accurately be determined by a 'free' experiment which utilized the most accurate NLLSQ input data (i.e., the 'observed' bound chemical shifts determined by the LISA4 experiment which gave the smallest weighted standard shift deviation) and which yielded the smallest R-factor. 'Free' experiment F_6 most closely fits these qualifications.

Close inspection of Table III-3 shows remarkable experimental consistency for all values except k. The value of k does remain constant within the 100 MHz experiments and also within the 300 MHz experiments. The value of the O9-Eu distance in 'free' experiments A_4, D_4, and F_6 ranges from 2.041 to 2.144 Å (ave = 2.076 Å), while θ_O ranges from 175.0 to 175.5° (ave = 175.3°). In 'fixed' experiments A_4, D_4, and F_6, R_{EO} ranges from 2.056 to 2.155 Å (ave = 2.089 Å). The overall 'free' values of R_{EO} and θ_O are 2.020 Å and 176.4°, respectively (only 3.6° off the carbonyl axis!). The overall 'fixed' value of R_{EO} is 2.028 Å.

The conventional representation of the lone pairs of electrons bound to europium in a europium-ketone complex, shown in Eq III-41, usually assumes a Eu-O-C angle near 120°. However, the σ bond between carbon and oxygen requires a hybrid of only the 2s and a single 2p orbital on oxygen, and a second p orbital is needed for the corresponding π bond.[29] This leaves an sp hybrid available for interaction with europium via a <u>linear</u> σ bond (Eq III-42).[30] Also, the empty 5d orbitals on europium have the appropriate symmetry and size for interaction with the remaining p orbital on oxygen in a π fashion.[31] The presence of two nonequivalent lone pairs of electrons on symmetrical carbonyl groups is borne out by theory[32] and experiment.[33]

While the evidence for coordination with H^+ indicates a geometry corresponding to Eq III-41 (H-O-C = 115°),[34] calculations indicate that Li^+ prefers a linear geometry (cf. Eq III-42).[35] Extensive calculations at the STO-3G and STO-3/21G levels for the interaction of formaldehyde with various first and second row Lewis acids indicate that a linear geometry is preferred when the cation can act as both σ and π acceptors.[36] Recent MNDO calculations[37] on the interaction of trans-1,2-dimethylcyclopropanone (DMCP) with several beryllium compounds have been performed. These calculations indicate essentially linear Be-O-C bond angles of 179.98 and 179.94° for $[DMCP\text{-}Be\text{-}H]^+$ and $[DMCP\text{-}Be\text{-}CH_3]^+$ cationic complexes, respectively, and a Be-O bond length of 1.62 Å in both. Neutral $DMCP\text{-}BeH_2$ and $DMCP\text{-}Be(CH_3)_2$ complexes possessed calculated Be-O-C bond angles of 150.98 and 151.80°, and Be-O bond lengths of 1.78 and 1.80 Å, respectively.

Conclusion

Considering the considerable number of incremental dilutions steps (25 and 30), the large number of chemical shift observations (δ_i) made (125 and 210), the obtention of X-ray data from a similar but different compound, and iteration of the data through three successive computer programs, the agreement between the calculated values of the constant 'K' (1980.1), the europium-oxygen distance R_{EO} (ave = 2.076 Å), and the Eu-C9-O9 bond angle θ_o (175.3°) and their independently reported values (<u>vide supra</u>) is very encouraging. The structure of the 1:1 $Eu(fod)_3$- substrate 'collision complex' appears to be such that the europium atom binds along the carbonyl axis (actually ca. 4.7° off the C9-O9 axis) and occupies a position ca. 2.10 Å from the carbonyl carbon (Fig III-4). However, this conclusion does not rule out the fact that a similar position can be accounted for by an averaging of equilibrium positions one of which lies above and the other below the plane formed by the cyclopentanone ring and which are symmetrically disposed about the extended C_2 carbonyl axis.

Experimental

Input to the 'General NLLSQ' computer program consisted of the $\Delta_i$obs chemical shifts obtained in PART II (Table II-10) and the cartesian coordinates (Table III-1) of the five pairs of magnetically equivalent protons [$H_a(H_{a'})\cdots H_e(H_{e'})$]. The coordinates of C8a, C9, C9a, and O9 were also input as was the C9-O9 bond distance (R_{CO}). The atomic coordinates (Table III-1) and the C9-O9 bond distance (Table I-5) were obtained as discussed in the experimental section of PART I. Cartesian coordinates were calculated from the atomic coordinates by the Mean Plane program.[6]

Error Analysis

Errors in calculation of the observed bound shifts as determined by LISA4 were discussed in PART II. Errors in the Cartesian coordinates input to NLLSQ were discussed in PART I. The average error in the NLLSQ-calculated values of k, R_{EO}, and the europium coordinates are, respectively, 58.13 (ca. 3%), 0.039 Å (ca. 4%), and 0.099 Å (ca. 1%).

BIBLIOGRAPHY

1. Mayo, B. C. Chem. Soc. Rev. 1973, 2, 49.

2. Cockerill, A. F.; Davies, G. L. O.; Harden, R. C.; Rackham, D. M. Chem. Rev. 1973, 73, 533.

3. Hofer, O. Top. Stereochem. 1976, 9, 111.

4. Willcott, M. R.; Davis, R. E. Science 1975, 190, 850.

5. (a) Kristiansen, P.; Ledaal, T. Tetrahedron Lett. 1971, 2817. (b) Rondeau, R. L.; Berwick, M. A. Air Force Materials Laboratory Technical Report, AFML-TR-71-282(1972). (c) ApSimon, J. W.; Bierbeck, H. Tetrahedron Lett. 1973, 581. (d) Farid, S.; Ateya, A.; Maggis, M. Chem. Commun. 1971, 1285. (e) Briggs, J.; Hart, F. A.; Moss, G. P. Chem. Commun. 1970, 1506. (f) Roberts, J. D.; Hawkes, G. E.; Hussar, J.; Roberts, A. W.; Roberts, D. W. Tetrahedron 1974, 30, 1833. (g) Trifunac, A. D.; Katz, J. J. J. Am. Chem. Soc. 1974, 96, 5233. (h) Lavalee, D. K.; Zeltman, A. H. J. Am. Chem. Soc. 1974, 96, 5552.

6. The 'General NLLSQ' and 'Mean Plane' computer programs were provided by Dr. Eric Enwall, University of Oklahoma.

7. (a) Shapiro, B. L.; Johnston, M. D. J. Am. Chem. Soc. 1972, 94, 8185. (b) Johnston, M. D.; Shapiro, B. L.; Proulx, T. W.; Godwin, A. D.; Pearce,n H. L. J. Am. Chem. Soc. 1975, 97, 542.

8. Johnson, B. F. G.; Lewis, J.; McArdle, P.; Norton, J. R. Chem. Commun. 1972, 535

9. (a) Salas, S. L.; Hille, E. "Calculus: One and Several Variables"; 2nd ed., McCorkle, M., Ed.; Xerox College Publishing: Lexington, Mass., 1974; chp 12. (b) "CRC Handbook of Chemistry and Physics"; 59th ed., Weast, R. C. Ed.; CRC Press Inc.: West Palm Beach, Fla., 1979; p F-124.

10. (a) Hinckley, C. C.; Brumley, W. C. J. Magn. Reson. 1976, 24, 239. (b) Hinckley, C. C. Brumley, W. C. J. Am. Chem. Soc. 1976, 98, 1331.

11. Raber, D. J.; Yanks, L. M.; Johnston, M. D.; Raber, N. K. Org. Magn. Reson. 1981, 15, 57.

12. (a) Ammon, H. L.; Mazzochi, P. H.; Colicelli, E. J. Org. Magn. Reson. 1978, 11, 1. (b) Abraham, R. J.; Chadwick, D. J. Sancassan, R. Tetrahedron Lett. 1979, 265. (c) Ammon, H. L.; Mazzochi, P. H.; Liu, L. Chem. Lett. 1980, 879.

13. (a) Raber, D. J.; Johnston, M. D.; Perry, J. W.; Jackson III, G. F. J. Org. Chem. 1978, 43, 229. (b) Raber, D. J.; Johnston, M. D.; Schwalke, M. A. J. Am. Chem. Soc. 1977, 99, 7671. (c) Johnston M. D.; Raber, D. J.; De Gennaro, N. K.; D'Angelo, A.; Perry, J. W. J. Am. Chem. Soc. 1976, 98, 6042. (d) Hajek, M.; Trska, P.; Vodicka, L.; Hlavaty, J. Org. Magn. Reson. 1977, 10, 52. (e) Hofer, O. Monatsh. Chem. 1979, 110, 979.

(f) Allinger, N. J. Am. Chem. Soc. 1969, 91, 337.

14. (a) Sikirica, M.; Vikovic, I.; Caplar, V.; Sega, A.; Lisini, A.; Kajfez, F.; Sunjic, V. J. Org. Chem. 1979, 44, 4423. (b) Gray, A. I.; Waigh, R. D.; Waterman, P. G. J. Chem. Soc. Perkin Trans. 1978, 2, 391., (c) Bearden, W. H.; Davis, R.; Willcott, M. R.; Snyder, J. P. J. Org. Chem. 1979, 44, 1974.

15. (a) Raber, D. J.; Yanks, C. M.; Johnston, M. D.; Raber, N. K. Tetrahedron Lett. 1980, 21, 677. (b) Abraham, R. J.; Bovill, M. J.; Chadwick, D. J.; Griffiths, L.; Sancassan, F. Tetrahedron 1980, 36, 279. (c) De Tar, D. F.; Luthra, N. P. J. Org. Chem. 1979, 44, 3299. (d) Raber, D. J.; Yanks, C. M.; Johnston, M. D.; Schwalke, M. A. J. Org. Chem. 1981, 46, 2528.

16. (a) Allinger, N. L. QCPE 1976, 11, 318. (b) Allinger, N. L.; Yuh, Y. K. QCPE 1980, 12, 395.

17. Allinger, N. L. Adv. Phys. Org. Chem. 1972, 13, 29.

18. (a) Newman, R. H. Tetrahedron 1974, 30, 969. (b) Lienard, B. H. S.; Thomson, A. J. J. Chem. Soc., Perkin Trans. 1977, 2, 1390. (c) Lenkinski, R. E.; Reuben, J. J. Am. Chem. Soc. 1976, 98, 276, 4065.

19. Abraham, R. J.; Chadwick. D. J.; Griffiths, L. Tetrahedron Lett. 1979, 48, 4691.

20. Kime, K. A.; Sievers, R. E. Aldrichimica Acta 1977, 10, 54.

21. Erasmus, C. S.; Boyens, J. C. A. Acta Crystallogr., Sect. B 1970, B26, 1843.

23. Raber, D. J.; Yanks, C. M.; Johnston, M. D.; Raber, N. K. J. Am. Chem. Soc. 1980, 102, 6594.

24. (a) Wolkowsky, Z. W. Tetrahedron Lett. 1971, 821. (b) Dahl, S.; Groth, P. Acta Chem. Scand. in press.

25. (a) Cunningham, J. A.; Sievers, R. E. J. Am. Chem. Soc. 1975, 97, 1586. (b) Boyens, J. C. A.; de Villiers, J. P. R. Acta Crystallogr., Sect. B 1970, B26, 1843.

26. Willcott, M. R.; Lenkinski, R. E.; Davis, R. E. J. Am. Chem. Soc. 1972, 94, 1742, 1744.

27. (a) Hamilton, W. C. Acta Crystallogr. 1965, 18, 502. (b) Hamilton, W. C. "Statistics in Physical Science"; Ronald: New York, 1964; pp 157-162.

28. Davis, R.E.; Wilcott, M. R.; Lenkinski, R. E.; von Doering, W.; Birladeanu, L. J. Am. Chem. Soc. 1973, 95, 6846.

29. Cf.: Jorgensen, W. L.; Salem, L. "The Organic Chemist's Book of Orbitals"; Academic Press: New York, 1973; pp 42-43.

30. Hofer, O. Monatsh. Chem. 1979, 110, 745. (b) Foldesi, P.; Hofer, O. Tetrahedron Lett. 1980, 2137.

31. (a) Moeller, T. MTP Int. Rev. Sci.: Inorg. Chem. Ser. One, 1971, 7, 275. (b) Marks, T. J. Prog. Inorg. Chem. 1978, 24, 51.

32. Reference 29. The drawings on pp 84, 141-142, 147-148, and 213-215 illustrate the nonequivalent nonbonding orbitals for formaldehyde, acetaldehyde, formyl fluoride, and acetone, respectively.

33. (a) Hernandez, R.; Masclet, P.; Mouvier, G. J. Electron. Spectrosc. Relat. Phenom. 1977, 10, 333. (b) Cederbaum, L. S.; Domcke, W.; v. Niessin, W. Chem. Phys. Lett. 1975, 34, 60.

34. Lathan, W. A.; Curtis, L. A.; Hehre, W. J.; Liste, J. B; Pople, J. A. Prog. Phys. Org. Chem. 1974, 11, 175.

35. (a) Del Bene, J. E. Chem. Phys. 1979, 40, 329. (b) Ha, T. K.; Wild, U. P.; Kuhne, R. O. ; Loesch, C.; Schaffhauser, T.; Stachel, J.; Wokaun, A. Helv. Chim. Acta 1978, 61, 1193.

36. Raber, D. J.; Raber, N. K.; v. R. Schleyer, P., unpublished results.

37. Nelson, D. J.; Earlywine, A. D., unpublished results.

PART IV

A CONTINUATION OF THE STUDY OF THE STEREOCHEMISTRY AND MECHANISM OF THE IRON PENTACARBONYL-PROMOTED COUPLING OF STRAINED OLEFINS TO CARBON MONOXIDE

Introduction

The observation has recently been reported[1] that 7-tert-butoxynorbornadiene (I) reacts with $Fe(CO)_5$ to afford the syn-exo-trans-endo-syn (SXTNS) dimer ketone II (Table IV-1) along with at least four other products. This result was interpreted as providing evidence for the direct mechanistic involvement of the 7-Lewis base substituent in the iron carbonyl promoted coupling of I with carbon monoxide. In order to further delineate the role of syn-7-Lewis base substituents in directing the stereochemical outcome of this reaction a corresponding study of the thermal reactions of 7-phenylnorbornadiene (VIII) and 7-o-anisylnorbornadiene (X) with $Fe(CO)_5$ was undertaken (Table IV-1).[2]

The rationale for choosing VIII and X as substrates in that study were as follows: unlike lone pair substituents (such as O-t-Bu), a phenyl group lacks sufficient Lewis basicity to coordinate with $Fe(CO)_5$.[4] Hence, the 7-phenyl group should function only to block the exo face of the double bond syn to that substituent in VIII. Coupling of VIII with carbon monoxide, accordingly, should occur through the corresponding anti double bond. Prior experience with the results of the thermal reaction of norbornadiene itself with $Fe(CO)_5$ suggests that coupling through the anti double bond in VIII should probably occur through the exo face, and thereby afford the

Table IV-1

Representative Reactions of Some Substituted Norbornadiene Compounds with Iron Pentacarbonyl.

Reaction		Reference
1.	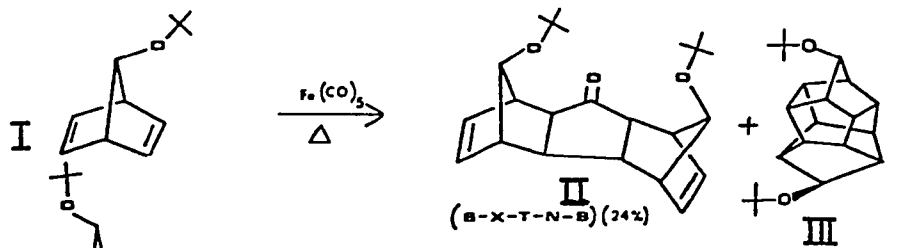	1
2.		1
3.	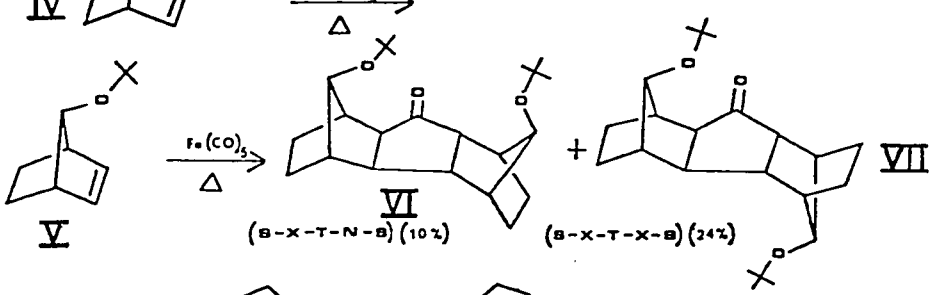	1
4.	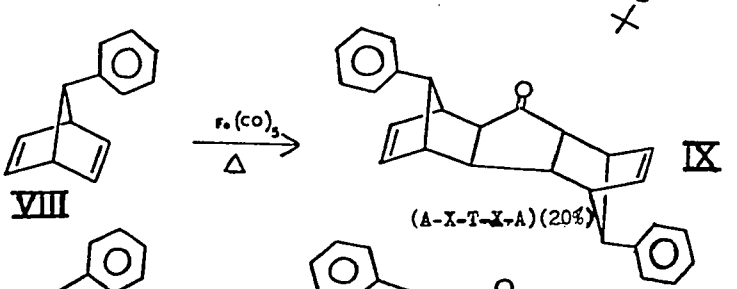	2
5.	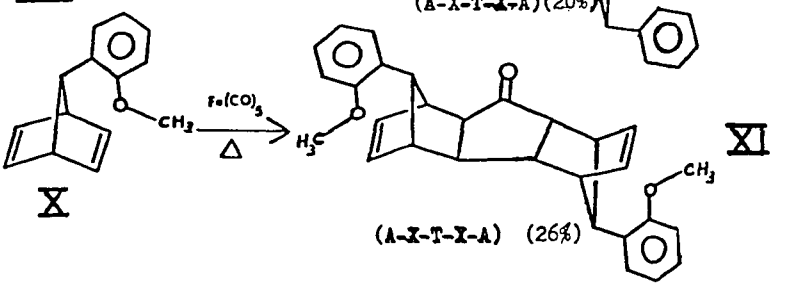	2
6.	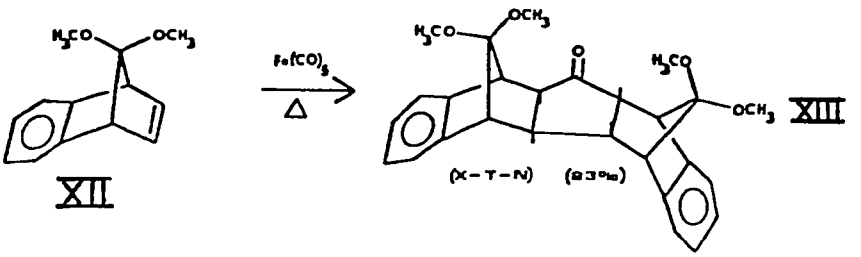	3

anti-exo-trans-exo-anti (AXTXA) dimer ketone IX.[4]

The situation could conceivably be different for the corresponding thermal reaction of X with $Fe(CO)_5$. Here, the o-methoxy group potentially can enter into complexation with Fe(0) and thereby direct coupling through the double bond syn to the 7-o-anisyl substituent. Indeed, such direct involvement of the syn-7-Lewis base substituent was suggested previously to account for the observed SXTNS stereochemistry of the dimer ketone formed via $Fe(CO)_5$-promoted coupling of I[1] and of XII[3] to carbon monoxide. Thus, it was hoped that the study might provide further evidence for the mechanistic involvement of a Lewis base substituent in additional $Fe(CO)_5$-promoted coupling reaction of this type (cf. Table IV-1).[6]

The observation that XI possesses the AXTXA configuration is noteworthy, as X is the first example of a norbornadiene bearing a Lewis base substituent which does not couple through the double bond syn to that substituent. This observation may have significant bearing on the mechanism of the coupling reaction. An important step in the Fe(0)-promoted olefin-CO coupling reaction suggested by Mantzaris and Weisberger[7] involves the reversible reaction of an (olefin)$Fe(CO)_3$ complex with a molecule of noncomplexed olefin to afford an $(olefin)_2Fe(CO)_3$ complex. This complex is believed to be trigonal bipyramidal (Fig IV-1) with the alkenes located in equatorial positions and complexed to iron via the less hindered exo side.[8] There is considerable evidence which suggests that norbornenes and norbornadienes bearing 7-oxygen-containing substituents undergo complexation with Fe(0) in syn-exo fashion (Fig IV-2).[6,9] Support for this suggestion came with the isolation of the complex shown in Fig IV-3 which was prepared by Laszlo and Stockis.[10] However, the distance between the o-anisyl oxygen atom and the syn double bond in X appears to be too small to permit incorporation of an Fe(0) moiety between these two groups; accordingly, coupling through the exo face of the syn double bond in

FIGURE IV-1

Trigonal Bipyramidal Orientation of the Organometallic (olefin)$_2$Fe(CO)$_3$ Complex Which Leads to Formation of the X-T-X Dimeric Ketone as Suggested by Mantzaris and Weisberger.

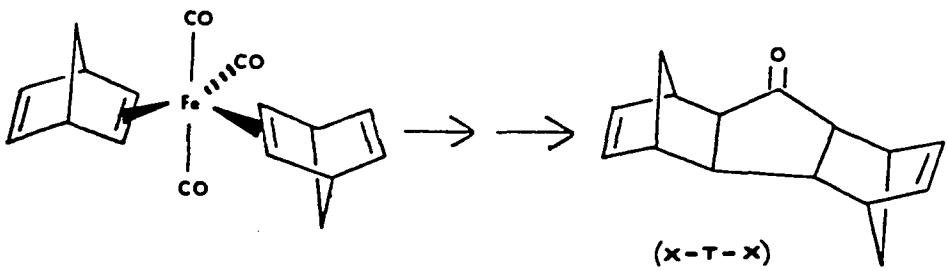

FIGURE IV-2

Syn-Exo Fe(0) Complexation in a 7-Oxygen-Substituted Norbornene or Norbornadiene Which Leads to the X-T-N Stereochemistry.

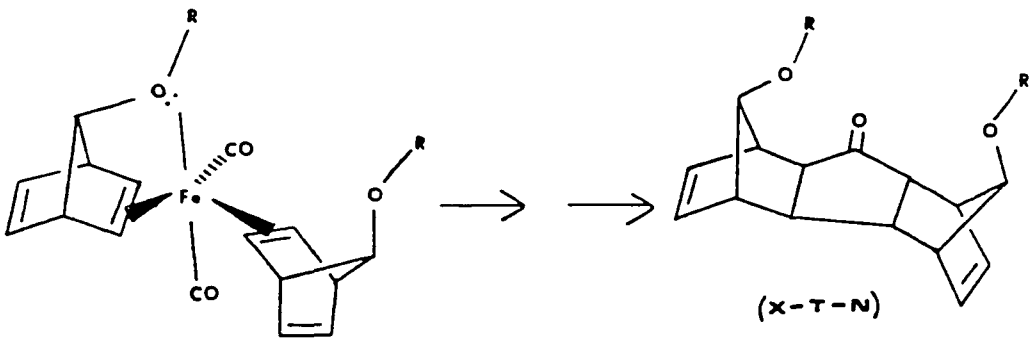

FIGURE IV-3

The Complex Prepared by Laszlo Which Supports the Possibility of Syn-Exo Complexation as Suggested in Fig IV-2.

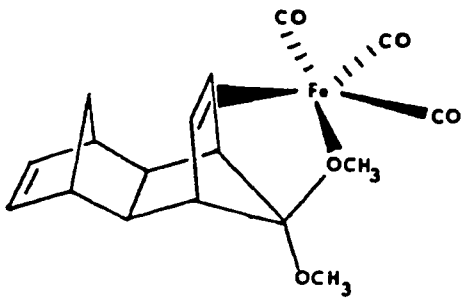

X is unlikely on steric grounds.

In contrast to this result, inspection of molecular models suggests that there is ample room for the unshared electrons on the o-anisyl oxygen atom to interact with the exo π-lobes of the syn double bond in noncomplexed X (Fig IV-4). This interaction should

FIGURE IV-4

Configurational Interconvertability of the Antiaromatic and Steric Interactions Via Rotation About the C_7-Aryl Bond.

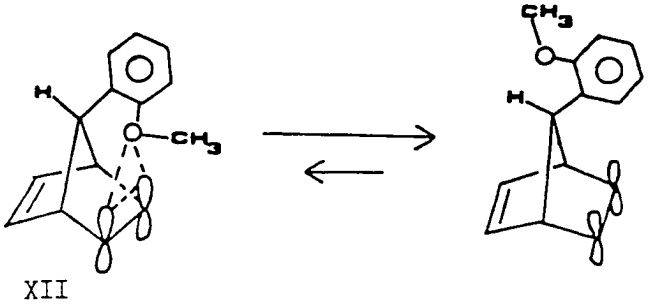

XII

result in bishomoconjugative, anti-aromatic electronic activation of the syn double bond by the o-anisyl oxygen atom. The net result of this interaction should be to raise the energy of the HOMO of the syn double bond relative to that of the anti double bond in X.[11,12] This electronic interaction in the noncomplexed olefin might explain the occurrence of coupling in e.g., I and XII, through the endo face of one of the two norbornadienyl moieties which results in the formation of an exo-trans-endo dimer ketone in the respective thermal reactions of these substrates with $Fe(CO)_5$. However, an option which is open to the methoxy group in X which is not available to any

other 7-Lewis base substituent in a norbornene or norbornadiene thus far studied is its ability to avoid the (unfavorable) antiaromatic bishomoconjugated orbital interaction discussed above simply by rotating about the C7-aryl bond (Fig IV-4). Once this occurs, the methoxy oxygen atom is removed from the reaction site, and the 7-o-anisyl group in X becomes operationally indistinguishable from 7-phenyl in the coupling reaction with $Fe(CO)_5$. For this reason, X reacts with $Fe(CO)_5$ in the same manner as does VIII, both substrates affording only the corresponding AXTXA dimer ketones (IX and XI, respectively).[12]

Based upon these considerations, Marchand and Hayes[13] proposed the following mechanism (Scheme IV-1) to explain the observed steric and electronic effects of 7-lone pair-bearing substituents and the anti double bond as they relate to product stereochemistry. Equation IV-2 is the mechanism proposed by Laszlo and Weisberger[6] for formation of the syn-exo-(olefin)$Fe(CO)_3$ complex which is in equilibrium with the $(olefin)_2Fe(CO)_3$ complex (Eq IV-5). Kinetically, endo-syn formation (Eqs IV-4 and IV-5) is thought to be favored since it allows both 7-Lewis base and anti double bond assistance in the cyclization-insertion process. Also, since the 7-alkoxy substituent is incapable of rotation away from the syn double bond and thereby removing the antiaromatic effect (cf. the discussion of Fig IV-4), the resulting more reactive syn double bond may overcome the unfavorable steric effect of endo addition and thus drive the equilibrium toward the SXTNS product (Scheme IV-2).

Results and Discussion

In an effort to further elucidate the participation and directing effect of the 7-Lewis base and the anti double bond of norbornadiene-derivative coupling to carbon monoxide, the reactions in Table IV-2 were performed.

7-Benzoyloxynorbornadiene (XIV) was thought to possess electronic

SCHEME IV-1

Mechanism of the Iron Pentacarbonyl-Promoted Coupling of Strained Olefins to Carbon Monoxide as Suggested by Marchand and Hayes.[3]

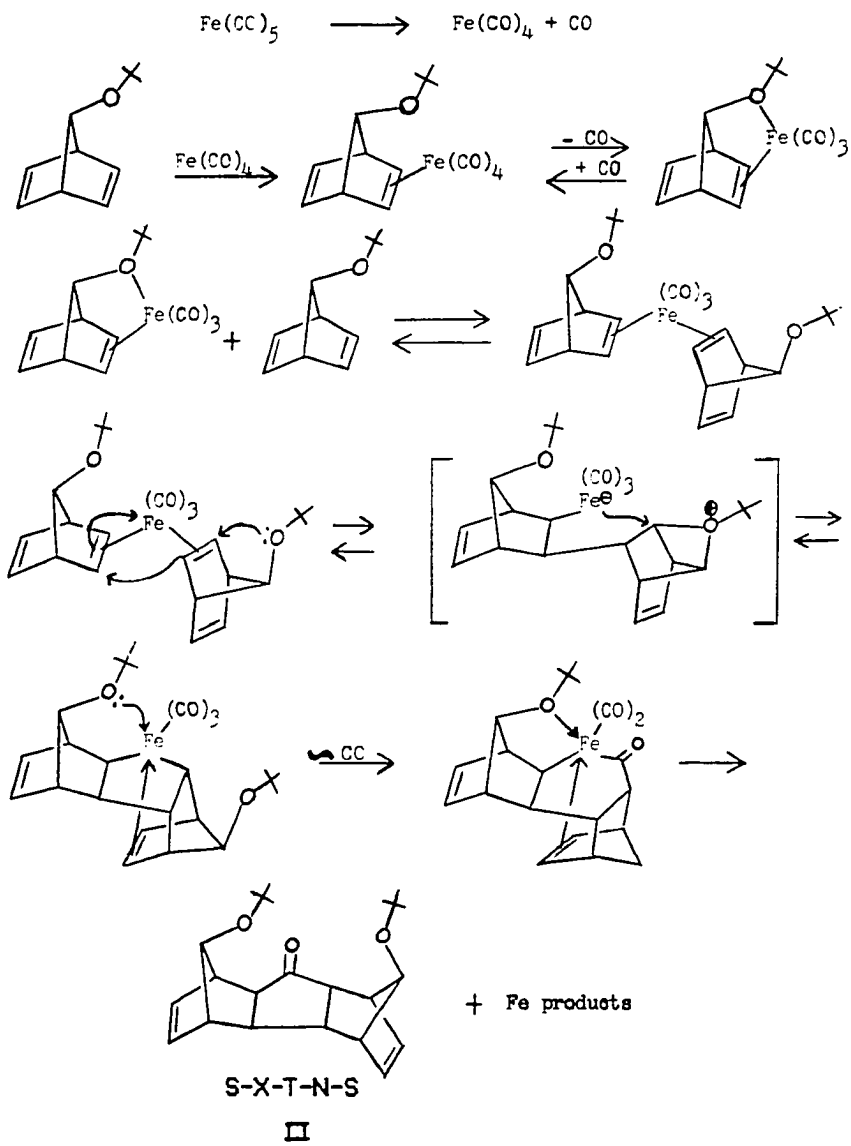

SCHEME IV-2

Suggested Mechanism for Formation of S-X-T-N-S
7-t-Butoxy Dimer Ketone II.

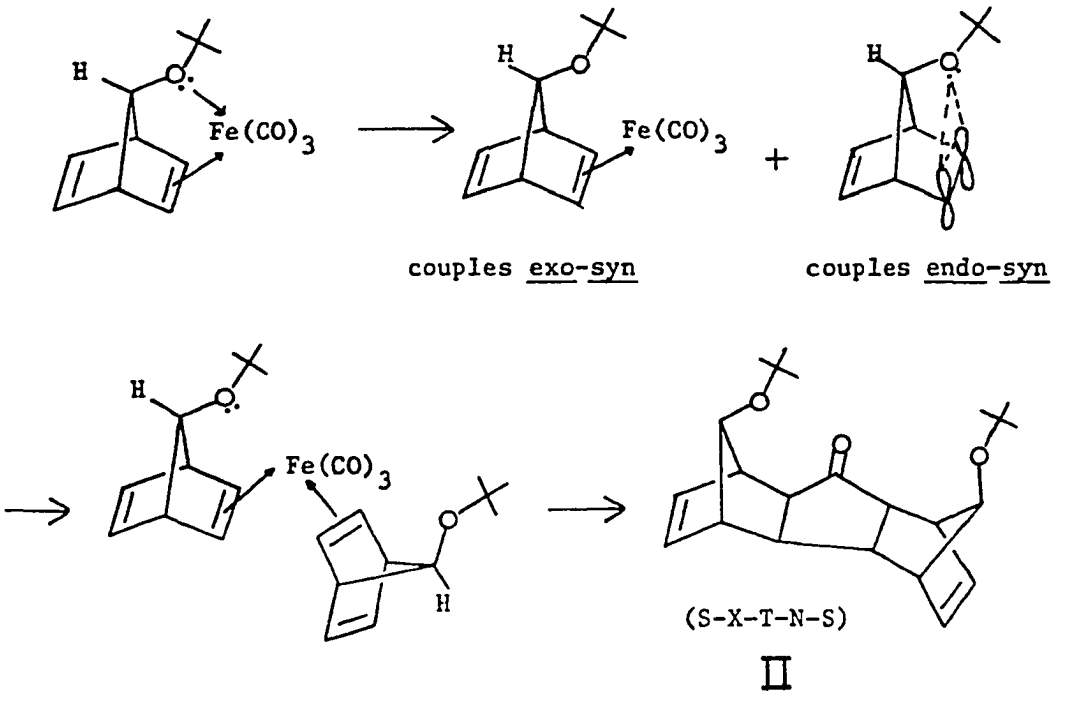

properties comparable enough to I and steric properties comparable enough to VIII and X so that a distinction could be made as to which effect (steric, electronic, or a combination of both) predominates in product structure determination. Provided that the steric factors responsible for the formation of IX and XI do not predominate, it was believed that an oxygen in XIV was capable of functioning as in compound I (Eq IV-5) to give the SXTNS product. It might then be possible to choose between SXTNS or AXTXA products by substitution of the appropriate alkoxy (or acyloxy) or alkyl (or aryl) group at the

TABLE IV-2

Proposed Reactions of Some Substituted Norbornadiene Compounds with Iron Pentacarbonyl.

Reaction

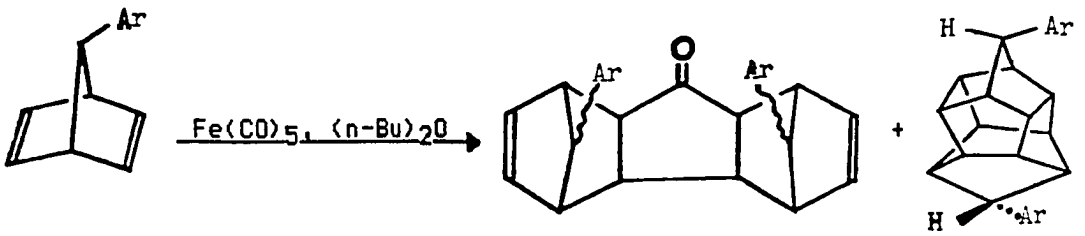

7. XIV: Ar = Benzoyloxy XV XVI

8. XVII: Ar = p-Anisoyloxy XVII XIX

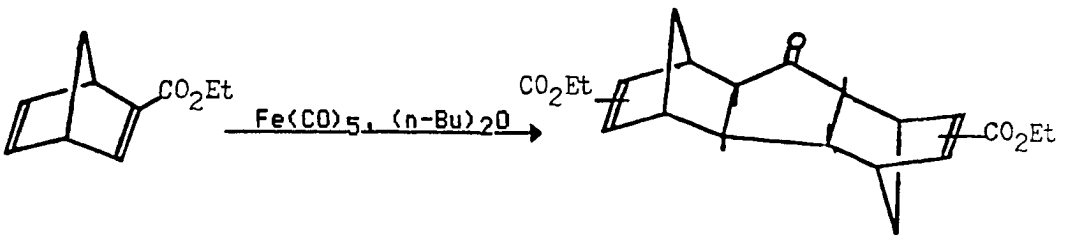

9. XX XXI

7-position.

Reaction 9 of Table IV-2 is of particular interest. Table IV-3 summarizes the possible dimeric ketone products which could result from such a reaction because of the fact that one double bond possesses an electron withdrawing group capable of altering the

TABLE IV-3

X-T-X Dimeric Ketones Which Could Result from the Reaction of 2-Carboethoxynorbornadiene with Iron Pentacarbonyl.

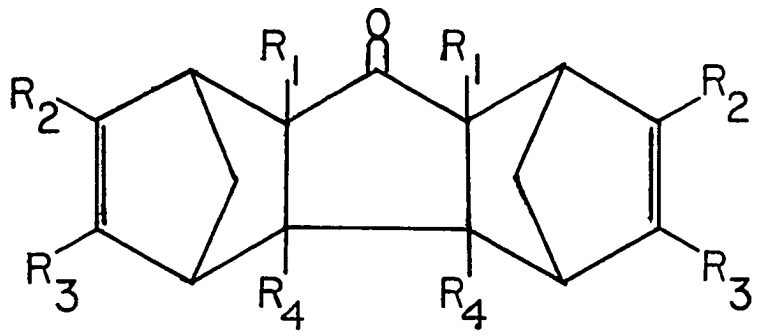

Substituents

Cmpd	R_1	R_1'	R_2	R_2'	R_3	R_3'	R_4	R_4'	CO_2Et
XXII			x	x					R_2,R_2'
XXIII			x			x			R_2,R_3'
XXIV					x	x			R_3,R_3'
XXV	x	x							R_1,R_1'
XXVI							x	x	R_4,R_4'
XXVII	x							x	R_1,R_4'
XXVIII	x			x					R_1,R_2'
XXIX			x					x	R_2,R_4'
XXX	x					x			R_1,R_3'
XXXI					x			x	R_3,R_4'

Based upon the evidence as discussed in the text, the most likely products are XXII, XXIII, and XXIV.

coupling reaction in several ways. First, in the cyclization reaction (cf. Scheme IV-I, Eq IV-4) in which the nucleophilic iron intramolecularly attacks electron deficient carbon, carboethoxy substitution of that carbon would tend to destabilize the positive charge generated there upon σ bond formation, but would at the same time tend to increase nucleophilic attack at that position. Second, displacement of CO (cf. Eq IV-5) by a double bond which is a weaker nucleophile (because of carboethoxy substitution) would be expected to be less facile than in the case of an unsubstituted double bond. Third, it is known that the presence of electron withdrawing groups such as that in methyl acrylate improves reactivity of an olefin with $Fe(CO)_5$ relative to an unsubstituted double bond.[14] If this occurs, the double bond which is carboethoxy substituted should preferentially bind the $Fe(CO)_4$ moiety (cf. Scheme IV-I, Eq IV-2), forming a stable complex which is not as likely to undergo further reaction. Fourth, formation of the new σ bond of the ketone would be unfavorable if $Fe(CO)_3$ insertion had occurred through double bonds which were carboethoxy-substituted, again due to the electron withdrawing effect. Fifth, since the present study was initiated, it has been reported[15] that 2,3-dicarboethoxynorbornadiene reacts with $Fe(CO)_5$ to form an XTX dimer ketone with no carboethoxy groups on the central cyclopentanone ring. The steric effect of having the central cyclopentanone ring tetra-substituted with CO_2Et would appear to be unfavorable due to the resulting endo substitution of groups considerably more bulky than hydrogen. The latter is believed to be the most important consideration in predicting the outcome of the reaction of $Fe(CO)_5$ with 2-carboethoxynorbornadiene. Therefore, the bulk of the available evidence suggests that any dimer ketone product(s) of reaction 9 would be expected to possess an XTX configuration and a central cyclopentanone ring which is not carboethoxy disubstituted (cf. Table IV-3 compounds XXII, XXIII, and/or XXIV).

Returning to reaction 7 of Table IV-2, 7-benzoyloxynorbornadiene

(Figs IV-5 and IV-6 for NMR and IR, respectively) was reacted with $Fe(CO)_5$ and the products isolated via column chromatography. The first compound recovered was unchanged 7-benzoyloxynorbornadiene followed by cage diester XVI (Figs IV-7 through IV-11 for NMR, IR, mass, spin echo, and HOMCOR[16] spectra, respectively, and Fig IV-12 for an expanded view of the upfield region of the HOMCOR spectrum of Fig IV-11). Next to be eluted were dimer ketones XV (AXTXA, Figs IV-13 through IV-16 for NMR, IR, mass, and spin echo spectra, respectively), XXXII (SNTNS, Figs IV-17 through IV-20 for NMR, IR, mass, and spin echo spectra, respectively), and XXXIII (AXTNA, Figs IV-21 through IV-25 for NMR, IR, mass, spin echo, and HOMCOR spectra, respectively). Next eluted was cage dimer ketone XXXIV (Figs IV-26 through IV-29 for NMR, IR, mass, and spin echo spectra, respectively). Last to be eluted were small amounts of uncharacterized oily residues.

Compound XVI was assigned its structure based on the following: (i) comparison of its NMR and IR spectra with those of compound V; (ii) accurate molecular weight determination by mass spectrometry; (iii) elemental analysis of its carbon and hydrogen content; (iv) IR, ^{13}C, spin echo, and HOMCOR spectra which contain the appropriate absorptions. That 7 pairs of enantiomeric carbon atoms [containing enantiomeric protons $H_a(H_{a'})$ through $H_g(H_{g'})$] are present in cage compounds of this type is indicated by their ^{13}C and spin echo NMR spectra (cf. Figs IV-10 and IV-46). Figure IV-12 illustrates the expanded upfield region of the HOMCOR spectrum and allows identification of the two different bridgehead protons [i.e., enantiomeric protons $H_d(H_{d'})$ and $H_e(H_{e'})$] by their coupling to proton $H_c(H_{c'})$. However, it does not indicate which specific resonance (δ 2.62 or 2.75) was produced by each bridgehead. Disregarding the bottom half of the molecule, the upfield region (δ 2.5-3.0, Fig IV-12) shows the bridgehead at δ 2.75 is coupled to a non-bridgehead proton at δ 2.94 and one or two protons at δ 2.62 (the latter signal is given by one bridgehead

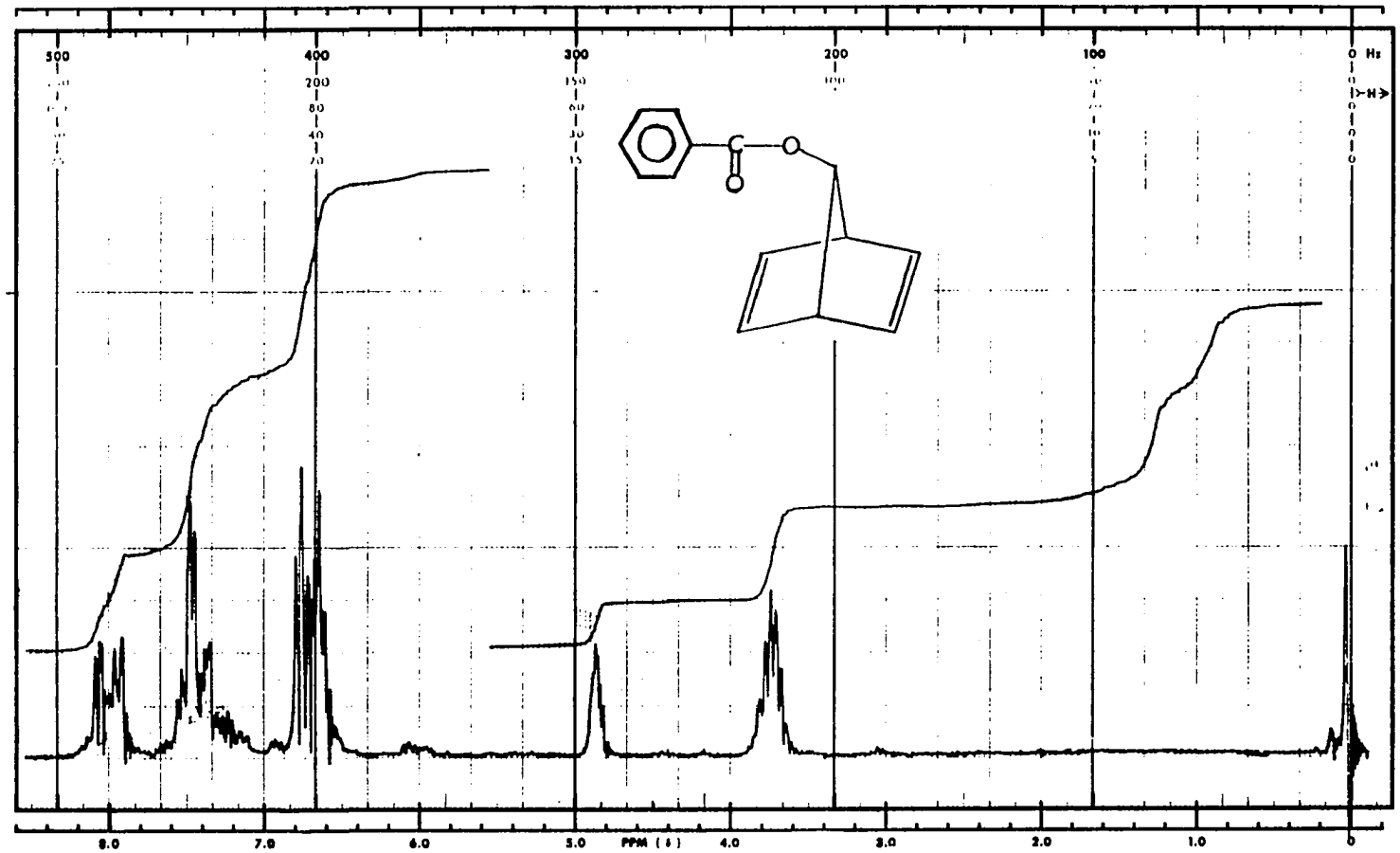

Figure IV-5. 60 MHz ^{1}H NMR Spectrum of 7-Benzoyloxynorbornadiene XIV ($CDCl_3$/TMS).

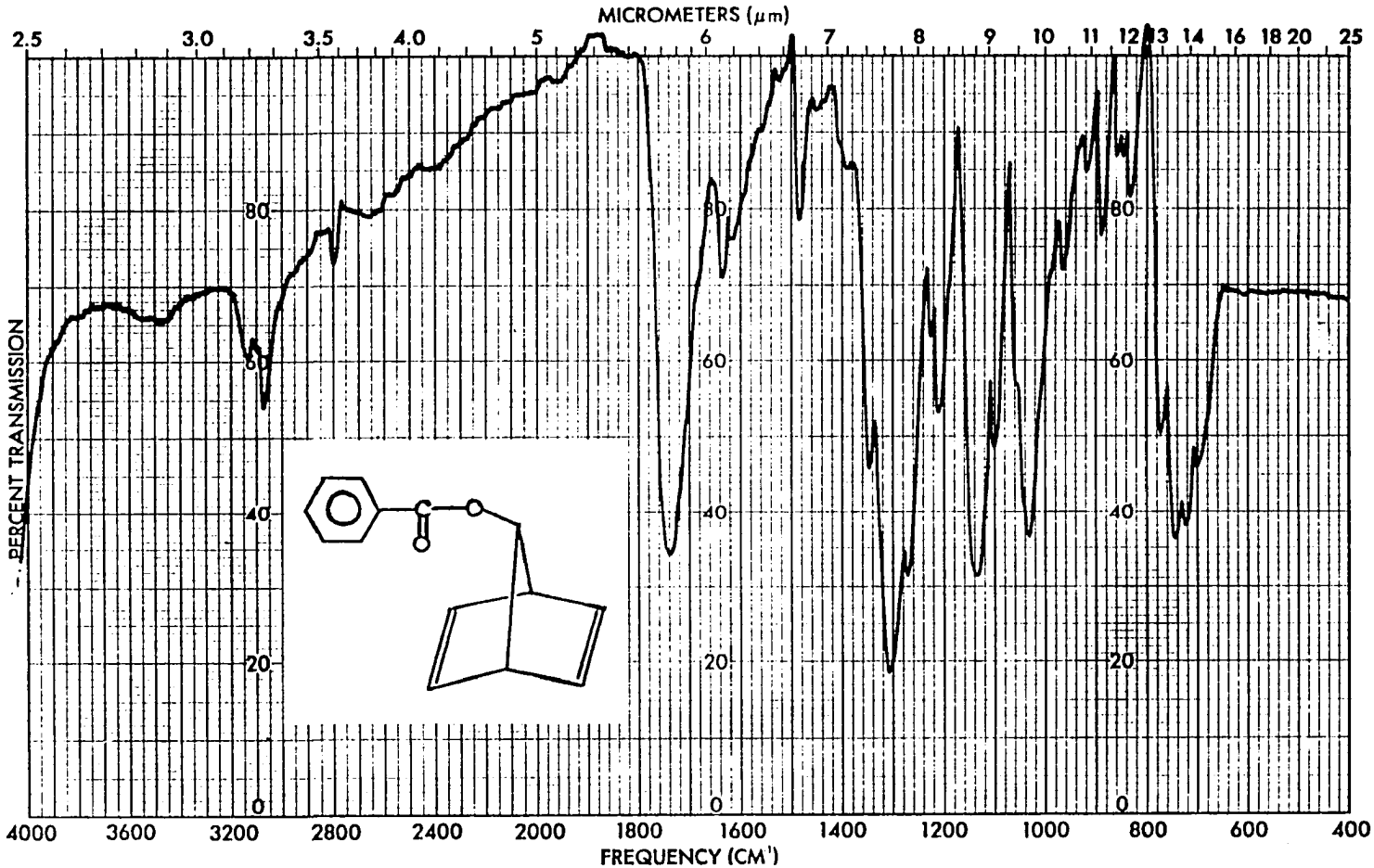

Figure IV-6. IR Spectrum of 7-Benzoyloxynorbornadiene XIV (KBr).

FIGURE IV-7

300 MHz ^{1}H NMR Spectrum of Benzoyloxy Cage Compound XVI ($CDCl_3$/TMS).

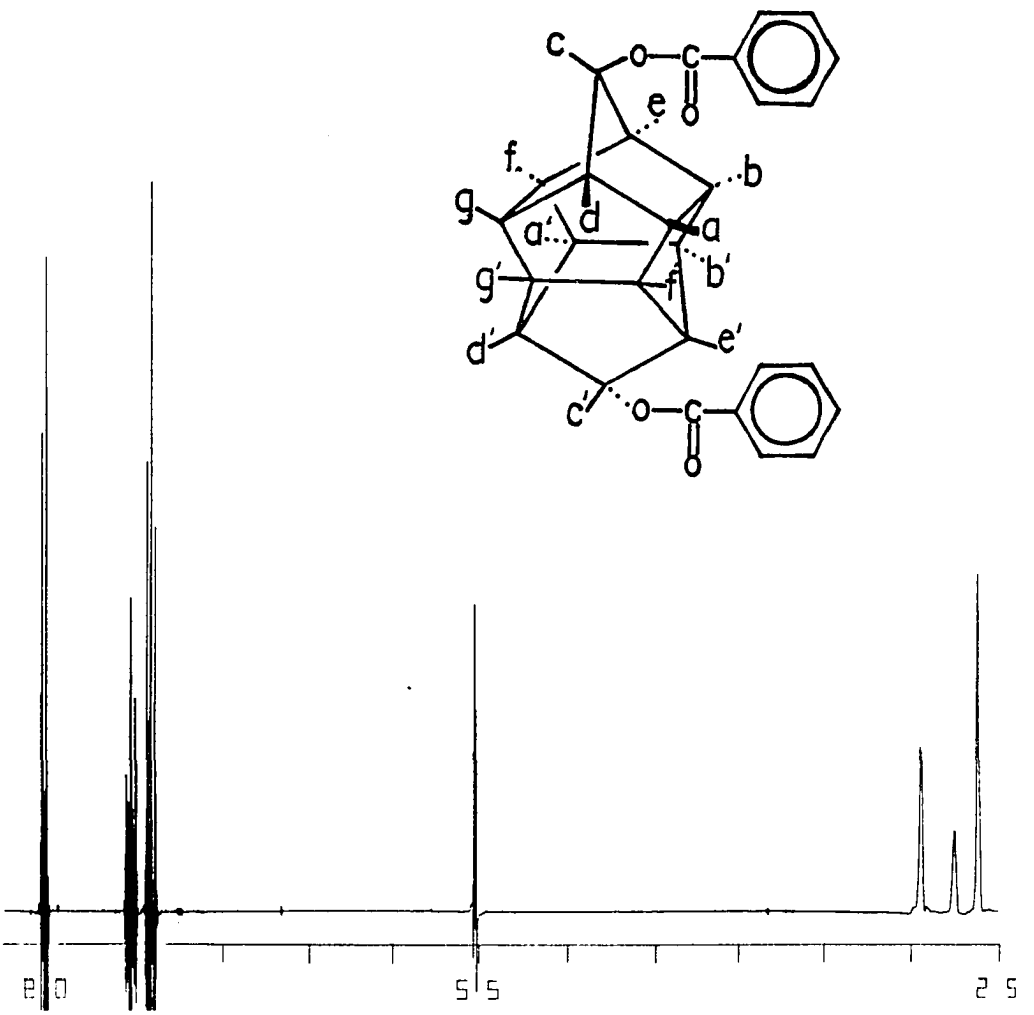

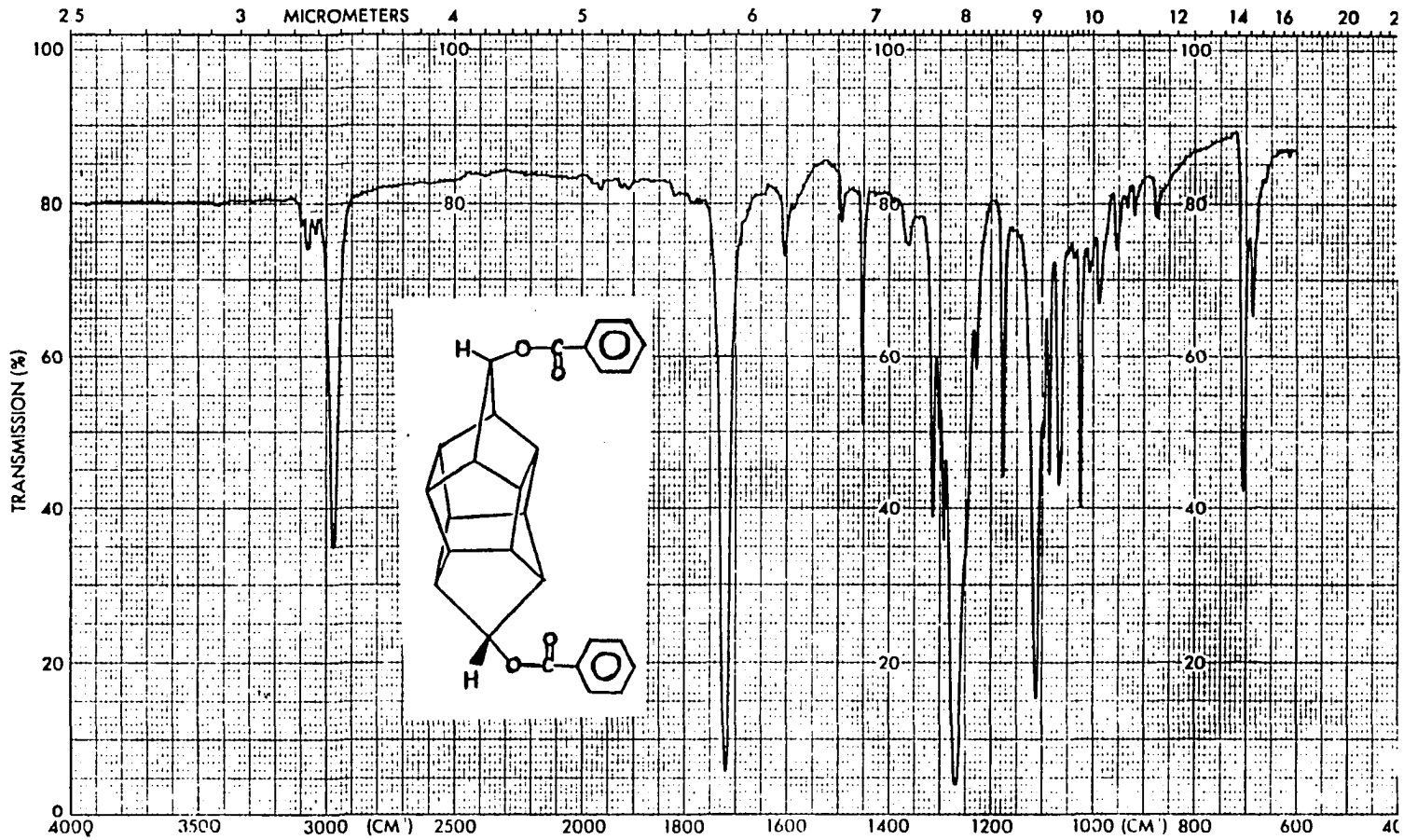

Figure IV-8. IR Spectrum of Benzoyloxy Cage Compound XVI (CCl_4).

FIGURE IV-9

Mass Spectrum of Benzoyloxy Cage Compound XVI.

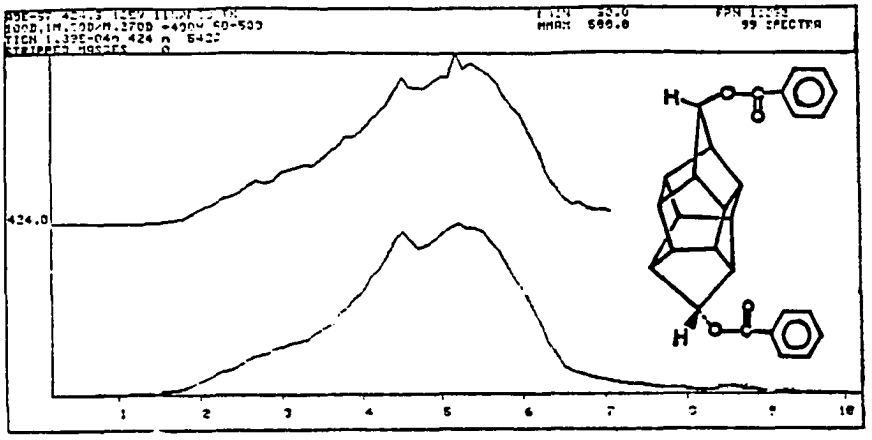

MASS	%	MASS	%	MASS	%	MASS	%	MASS	%
60.1	.7	100.2	.1	156.1	.1	210.9	.1	361.1	.1
61.1	3.6	113.0	.1	157.1	.1	213.1	.2	378.1	.4
62.2	.3	115.1	3.2	165.0	6.8	217.9	.1	379.2	.6
63.1	.2	116.1	1.7	166.1	1.7	219.2	.1	380.0	.2
65.1	.1	117.1	.6	167.1	1.3	222.0	.1	381.1	.1
67.1	.1	118.1	.1	168.1	.5	223.0	.1	406.0	6.9
68.1	.2	119.1	.2	169.1	2.1	224.1	.2	407.2	1.4
69.2	.1	120.1	.2	170.1	.4	225.0	.1	407.9	.4
70.1	.9	121.2	.1	171.1	.1	236.1	.3	408.9	.1
71.1	.3	122.1	.1	176.1	.1	237.1	.5	423.0	3.1
72.1	.1	123.1	.1	178.1	.7	238.1	.1	424.0	18.9
74.2	.3	126.0	.1	179.1	4.0	254.1	.2	425.1	5.3
75.1	.4	127.2	.5	180.1	31.0	256.9	.2	426.0	.8
76.1	1.0	128.2	1.6	181.1	6.0	258.2	.1		
77.1	41.1	129.0	1.4	182.1	.6	260.9	.0		
78.1	3.0	130.0	.3	183.1	.1	269.0	.1		
79.1	1.7	131.0	.4	185.1	.1	270.1	.1		
80.1	.2	132.0	.1	186.0	.1	274.1	.2		
81.0	.3	133.9	.1	187.0	.1	275.0	.1		
89.1	.3	135.0	.1	191.0	.1	284.0	.2		
91.1	3.5	139.0	.2	192.1	.1	294.0	.1		
92.1	.5	141.1	3.0	195.1	.1	297.0	.1		
93.1	.1	142.1	.7	196.1	.1	300.0	.1		
94.1	.1	143.1	.3	196.1	.1	302.0	5.7		
95.2	.1	146.1	.1	197.0	1.2	303.0	1.3		
103.1	.1	149.1	.0	198.0	.3	304.1	.2		
104.1	.6	151.0	.3	199.0	.1	319.0	7.0		
105.1	2.0	152.1	1.5	207.1	.1	320.0	1.6		
105.1	100.0	153.0	2.2	208.1	.1	321.0	.2		
106.1	8.7	154.0	1.5	209.0	.1	330.0	.1		
107.1	.7	155.1	.9	210.1	.1	347.1	.1		

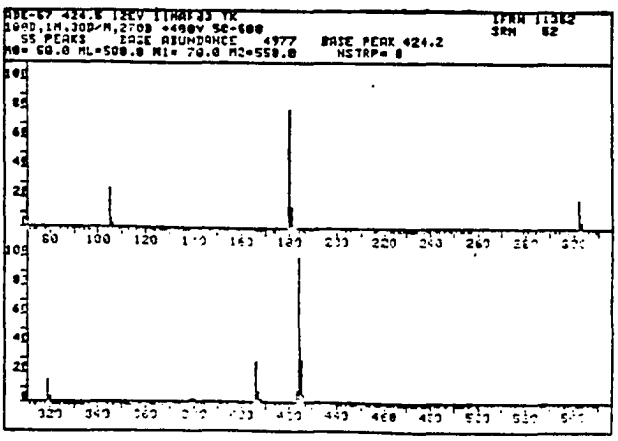

MASS	%	MASS	%
BIG 60		303.2	6.6
77.0	1.1	304.2	.6
103.0	.4	310.2	.6
105.0	25.1	319.2	14.0
106.0	3.2	320.2	3.0
115.2	.5	321.1	.6
116.0	.5	339.1	.3
116.0	.3	347.1	.6
130.1	.6	378.3	1.4
143.0	.7	379.3	1.0
164.2	.3	380.3	1.0
165.1	.7	381.2	.2
167.2	.5	406.2	20.0
169.2	.2	407.3	7.3
180.1	80.5	408.1	1.0
181.1	14.7	423.2	8.3
192.0	.9	424.2	100.0
195.9	.3	425.2	29.1
197.1	.2	426.2	5.0
192.2	.2		
197.3	1.0		
199.2	.6		
214.0	.2		
232.7	.2		
234.1	.5		
236.2	1.1		
237.2	.7		
256.2	.4		
257.1	.3		
258.1	.5		
274.1	.6		
294.1	.2		
301.1	.3		
302.2	19.7		

FIGURE IV-10

20 MHz ^{13}C and Spin Echo NMR Spectra of Benzoyloxy Cage Compound XVI ($CDCl_3$).

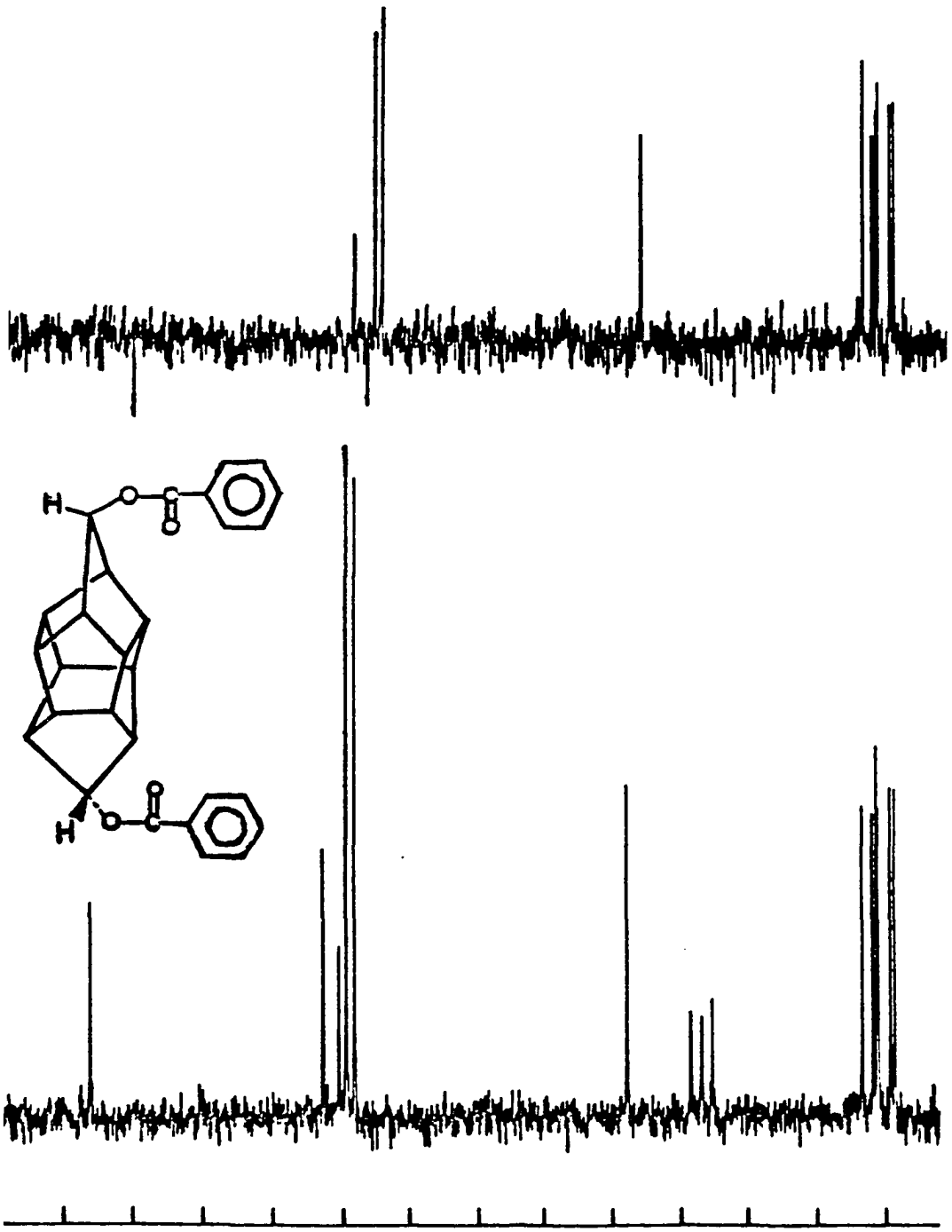

FIGURE IV-11

300 MHz ^{1}H HOMCOR NMR Spectrum of Benzoyloxy Cage Compound XVI ($CDCl_3$).

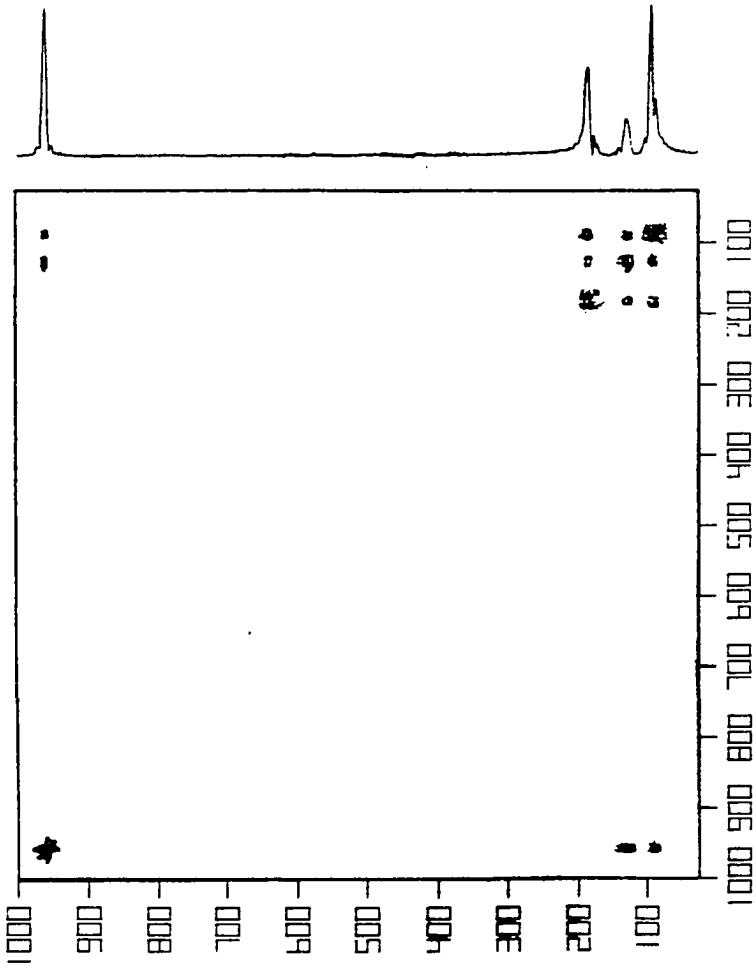

FIGURE IV-12

Expanded Upfield Region of the HOMCOR NMR Spectrum (Fig IV-11) of Benzoyloxy Cage Compound XVI ($CDCl_3$).

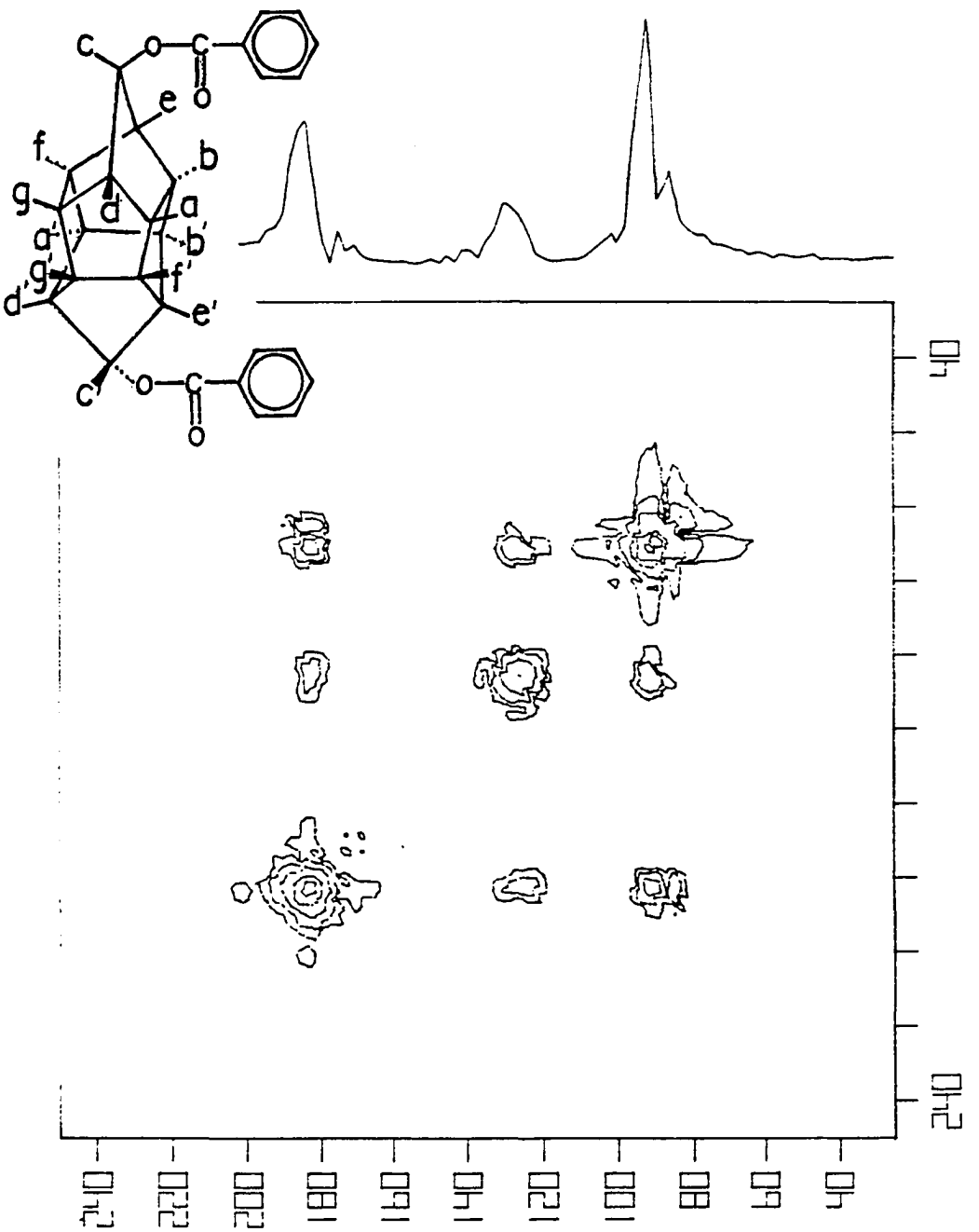

FIGURE IV-13

300 MHz ^{1}H NMR Spectrum of AXTXA Benzoyloxy Dimer Ketone XV ($CDCl_3$/TMS).

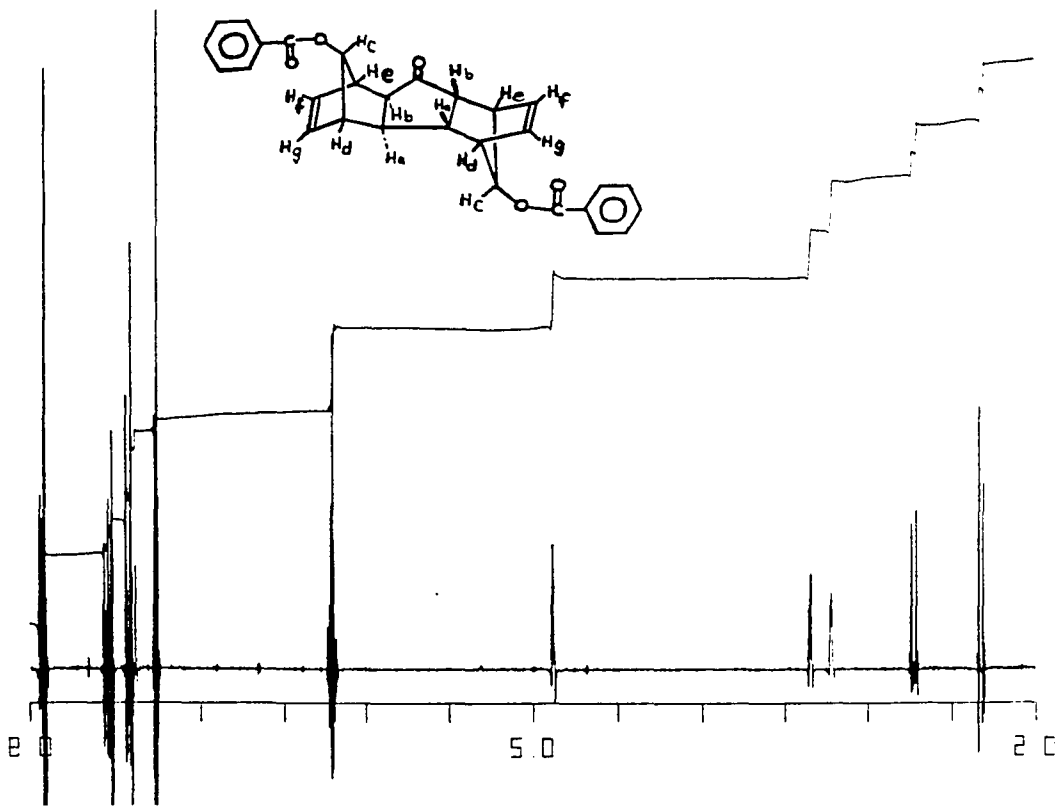

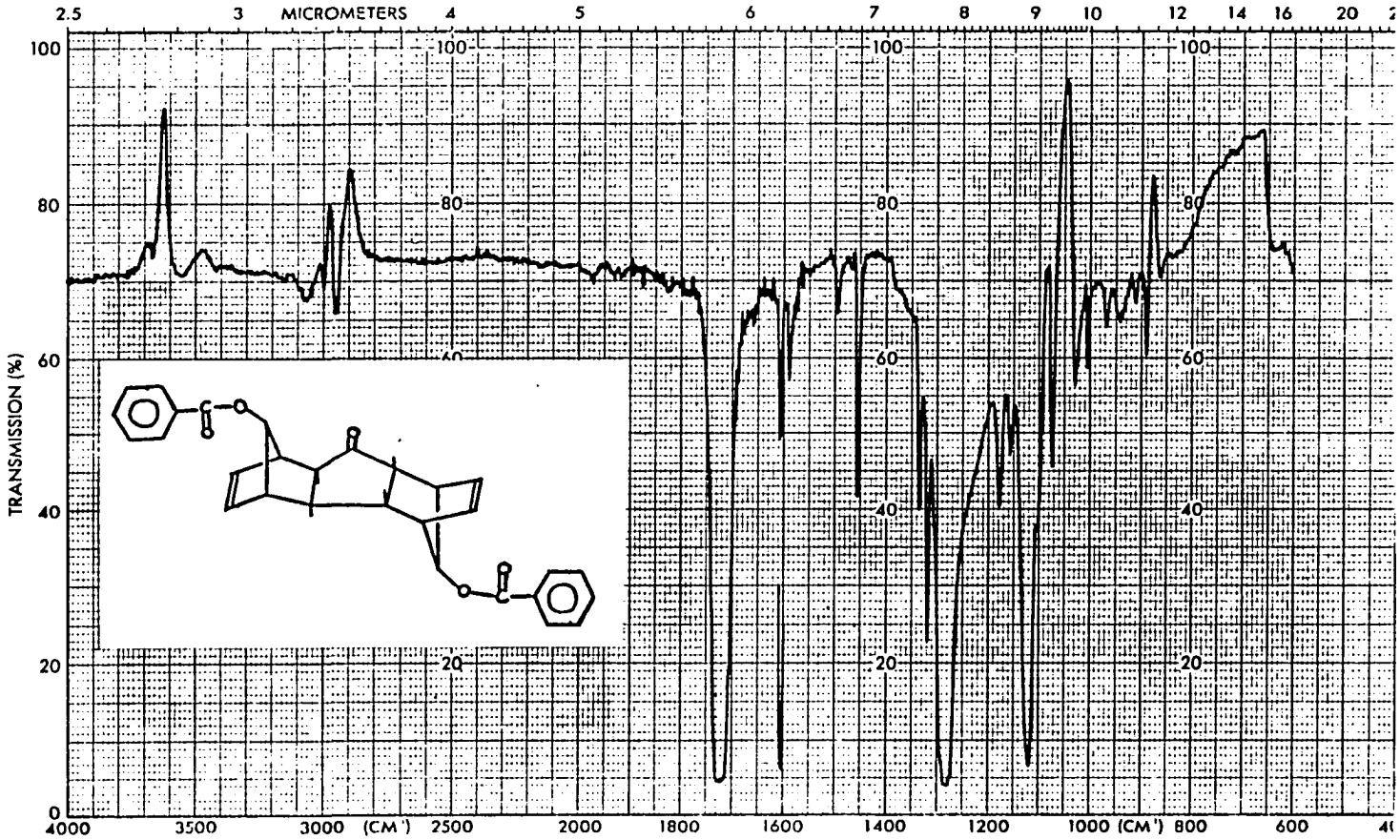

Figure IV-14. IR Spectrum of AXTXA Benzoyloxy Dimer Ketone XV ($CHCl_3$).

FIGURE IV-15

Mass Spectrum of AXTXA Benzoyloxy Dimer Ketone XV.

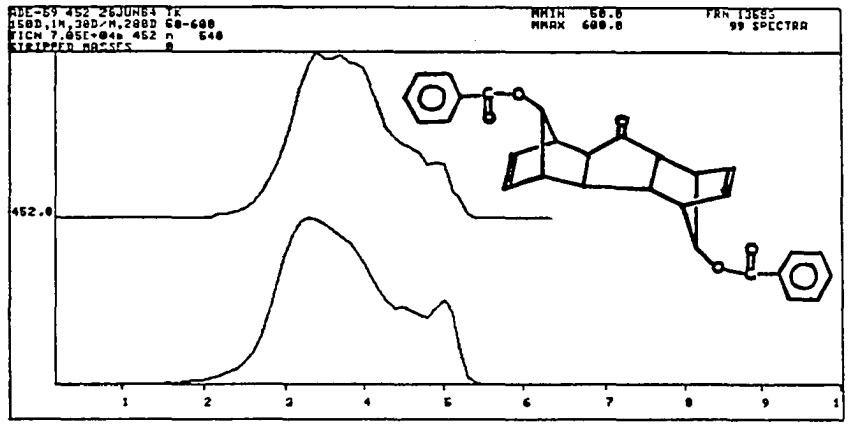

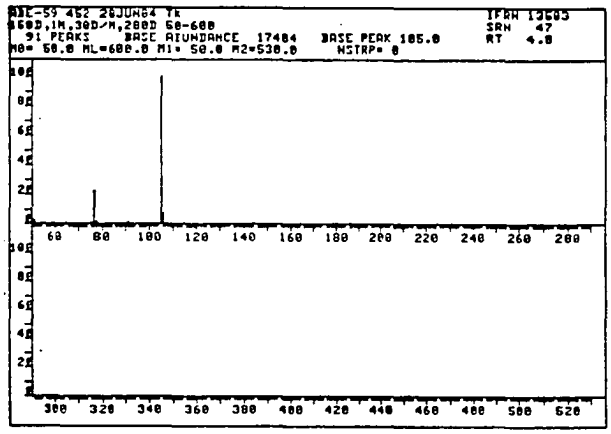

MASS DIG 60	%	MASS	%
		133.0	.2
60.1	.6	140.9	.2
61.1	2.6	144.0	1.0
62.1	.3	144.9	.2
63.1	.3	152.0	.2
55.1	.8	153.0	.3
63.1	.2	161.0	.7
65.0	1.1	165.0	.3
74.1	.1	166.0	.2
75.1	.3	167.0	.2
76.1	.9	179.1	.2
77.0	22.7	180.1	.9
78.0	2.0	181.0	.2
79.0	.8	186.0	1.1
81.0	.3	207.0	.2
83.0	.2	208.0	1.4
85.0	.2	209.0	.2
89.1	.3	225.1	.6
91.1	1.6	226.0	.2
92.1	.3	265.0	.2
103.1	.6	266.0	1.2
105.0	100.0	267.0	.2
106.1	7.0	317.1	.6
107.1	.6	330.0	.6
115.0	1.1	347.1	.2
116.1	.6	452.0	1.0
117.0	.3	453.0	.4
118.0	.2		
119.1	.2		
127.0	.2	LAST 4	
128.1	.3	348.1	.1
128.9	.2	452.0	1.0
131.0	.3	453.0	.4
131.9	.2	454.0	.1

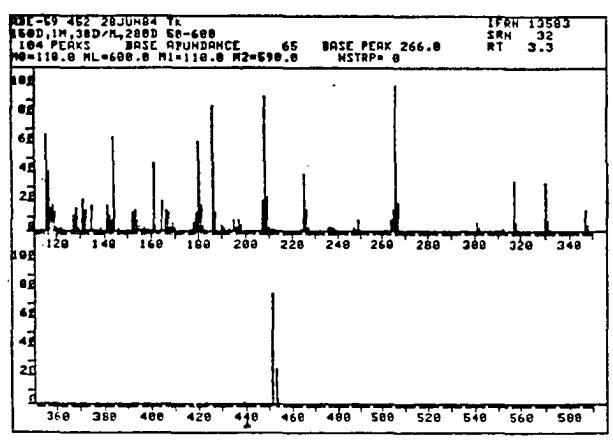

MASS DIG 60	%	MASS	%
		187.1	12.3
115.1	66.2	190.0	4.6
116.1	40.0	191.0	3.1
117.0	15.4	195.0	7.7
118.0	16.9	197.0	7.7
119.0	12.3	198.0	4.6
127.1	10.8	207.0	20.0
128.1	15.4	208.0	92.3
128.9	9.2	209.0	23.1
131.0	21.5	225.0	38.5
131.9	12.3	226.0	13.0
132.9	13.8	247.0	3.1
135.0	16.9	249.0	7.7
141.0	16.9	264.0	7.7
142.0	10.0	265.0	13.8
143.0	7.7	266.0	100.0
144.0	64.6	267.0	18.5
144.9	13.8	301.0	6.2
152.0	12.3	317.0	33.8
153.0	13.8	318.1	6.2
154.0	7.7	330.0	32.3
155.0	4.6	331.0	7.7
161.0	46.2	347.1	13.8
161.9	4.6	348.0	4.6
164.9	20.0	451.9	76.9
166.1	13.8	453.0	24.6
167.1	12.3	453.9	4.6
169.1	6.2		
178.0	6.2		
179.1	12.3	LAST 4	
180.1	61.5	439.0	1.5
181.1	16.9	451.9	76.9
182.1	4.6	453.0	24.6
186.0	86.2	453.9	4.6

FIGURE IV-16

20 MHz ^{13}C and Spin Echo NMR Spectra of AXTXA Benzoyloxy Dimer Ketone XV ($CDCl_3$).

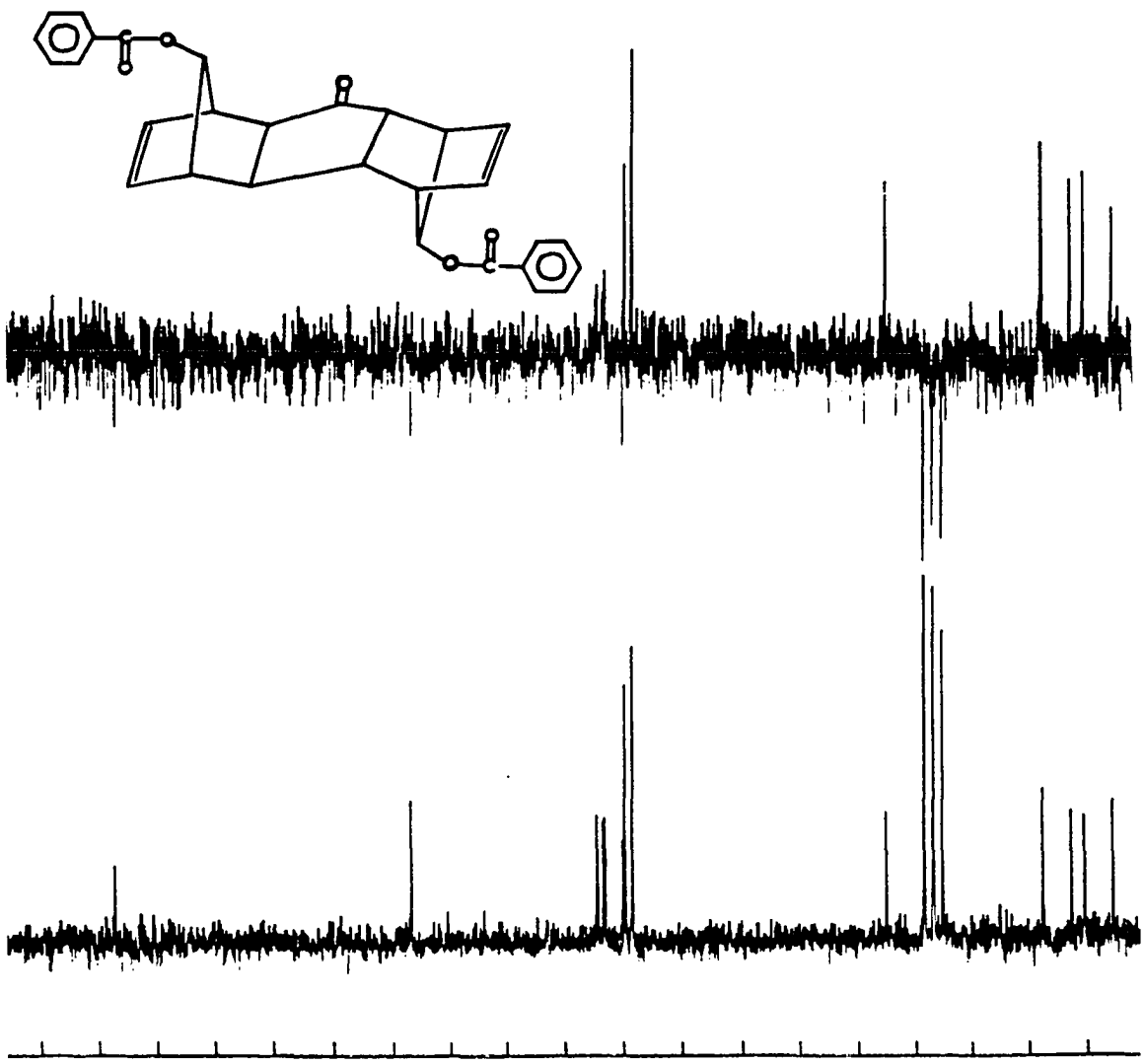

FIGURE IV-17

300 MHz ^{1}H NMR Spectrum of SNTNS Benzoyloxy Dimer Ketone XXXII ($CDCl_3$/TMS).

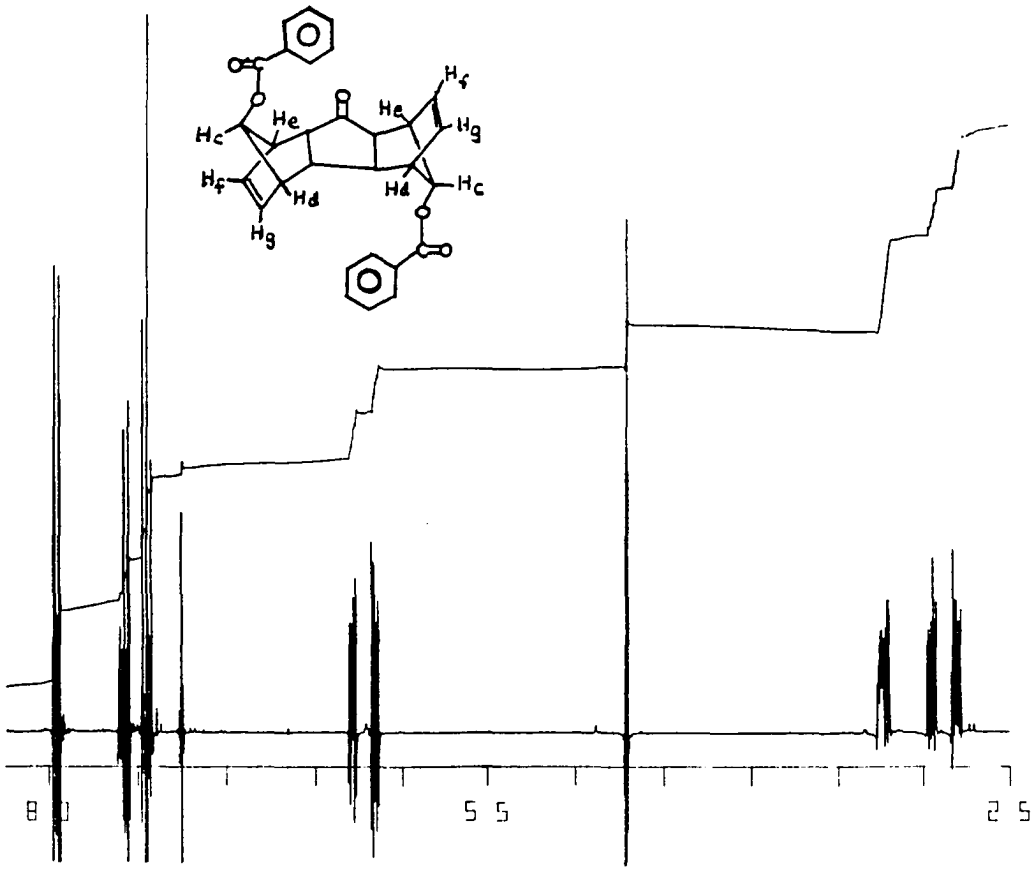

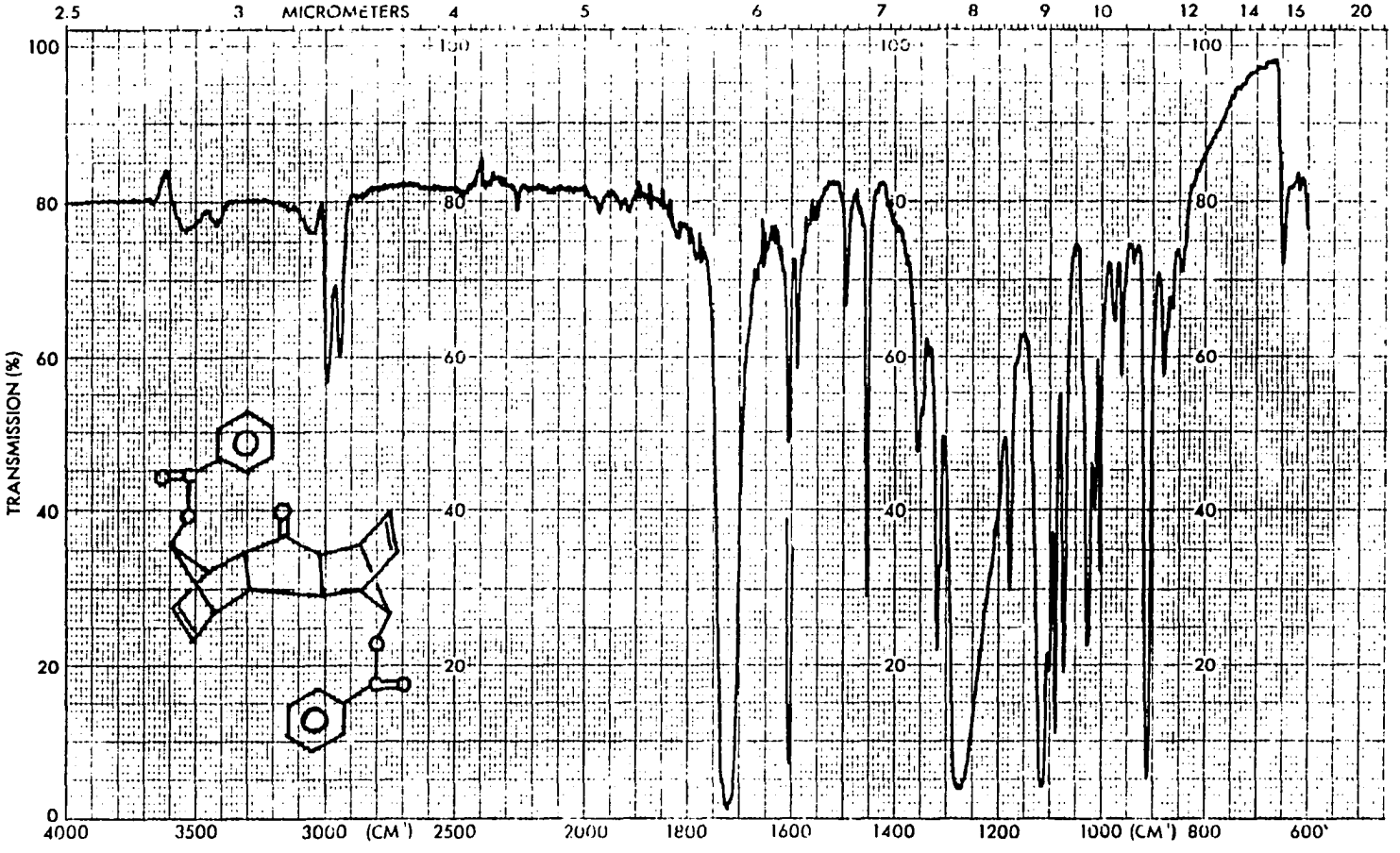

Figure IV-18. IR Spectrum of SNTNS Benzoyloxy Dimer Ketone XXXII ($CHCl_3$).

FIGURE IV-19

Mass Spectrum of SNTNS Benzoyloxy Dimer Ketone XXXII.

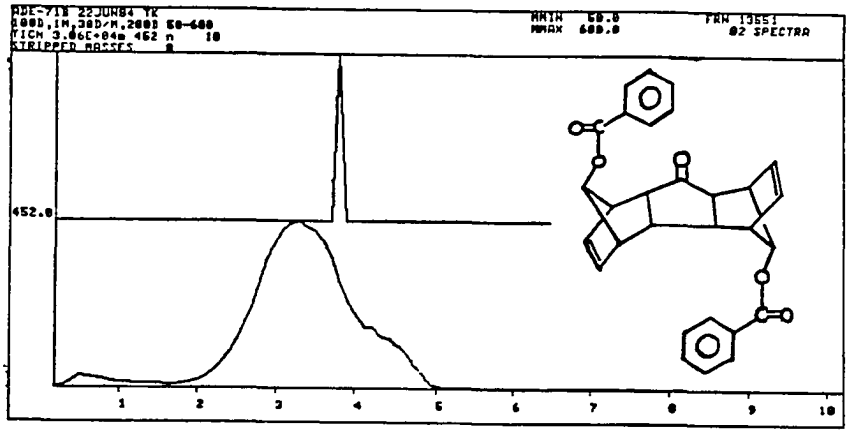

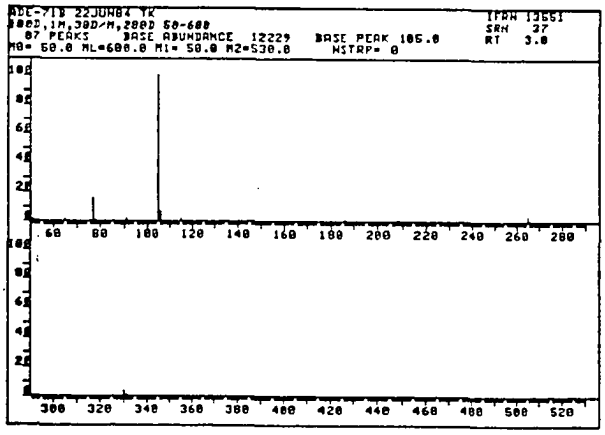

MASS	%	MASS	%
BIG 60		144.0	.6
50.1	.3	145.0	.3
51.1	1.2	152.1	.2
52.1	.2	153.0	.2
55.1	.5	161.0	.6
65.0	.9	165.0	.3
76.1	.6	167.1	.3
77.1	15.5	169.1	.2
78.1	1.3	179.1	.3
79.1	.8	180.1	.7
81.1	.3	181.1	.2
83.0	.6	186.1	1.3
84.9	.5	187.1	.2
89.0	.3	197.0	.3
91.1	2.0	208.1	1.0
92.1	.4	209.0	.3
103.1	.5	226.1	.7
105.0	100.0	236.1	.2
106.0	7.2	265.1	3.0
107.0	.5	266.1	1.0
115.1	2.0	267.1	.2
116.1	.6	301.1	.6
117.1	.7	302.2	.2
119.1	.8	330.1	2.4
120.1	.3	331.1	.9
127.1	.3	347.2	.2
128.2	.3	408.1	.2
129.0	.2		
131.0	.0		
132.0	.3	LAST 4	
133.0	.3	408.1	.2
141.1	.4	423.2	.1
142.0	.7	424.1	.1
143.0	.5	452.1	.1

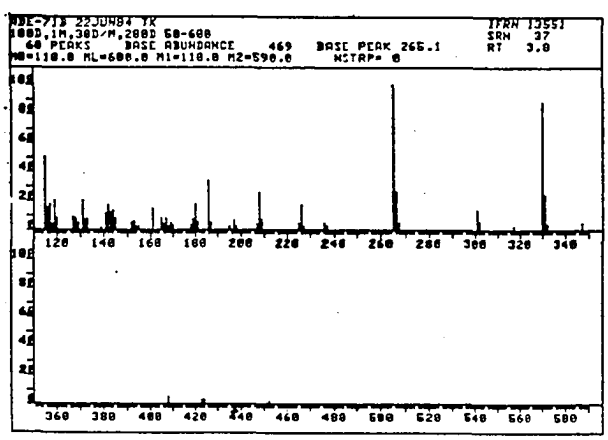

MASS	%	MASS	%
BIG 60		186.1	34.1
115.1	51.0	187.1	5.3
116.1	16.0	195.0	3.0
117.1	17.7	197.0	7.0
118.1	4.1	198.1	3.8
119.1	20.0	207.2	4.5
126.1	8.7	208.1	26.0
127.1	9.0	209.0	7.0
128.2	8.1	225.1	4.5
129.0	4.9	226.1	17.3
131.0	20.5	227.2	3.0
132.0	7.7	236.1	5.5
133.0	8.5	237.1	3.0
139.0	2.1	265.1	100.0
141.1	11.5	266.1	26.9
142.0	17.5	267.1	5.1
143.0	12.4	301.1	13.6
144.0	14.1	302.2	6.0
145.0	8.3	317.2	2.6
152.1	5.3	330.1	88.7
153.0	5.0	331.1	24.3
154.0	3.0	332.1	4.7
155.0	2.6	347.2	5.5
161.0	14.5	408.1	4.9
165.0	8.1	423.2	3.0
166.0	4.1	424.1	3.0
167.1	8.3	462.1	2.1
168.2	2.8		
169.1	5.5		
170.1	3.4	LAST 4	
178.1	3.4	408.1	4.9
179.1	7.2	423.2	3.0
180.1	17.9	424.1	3.0
181.1	6.2	462.1	2.1

FIGURE IV-20

20 MHz ^{13}C and Spin Echo NMR Spectra of SNTNS Benzoyloxy Dimer Ketone XXXII ($CDCl_3$).

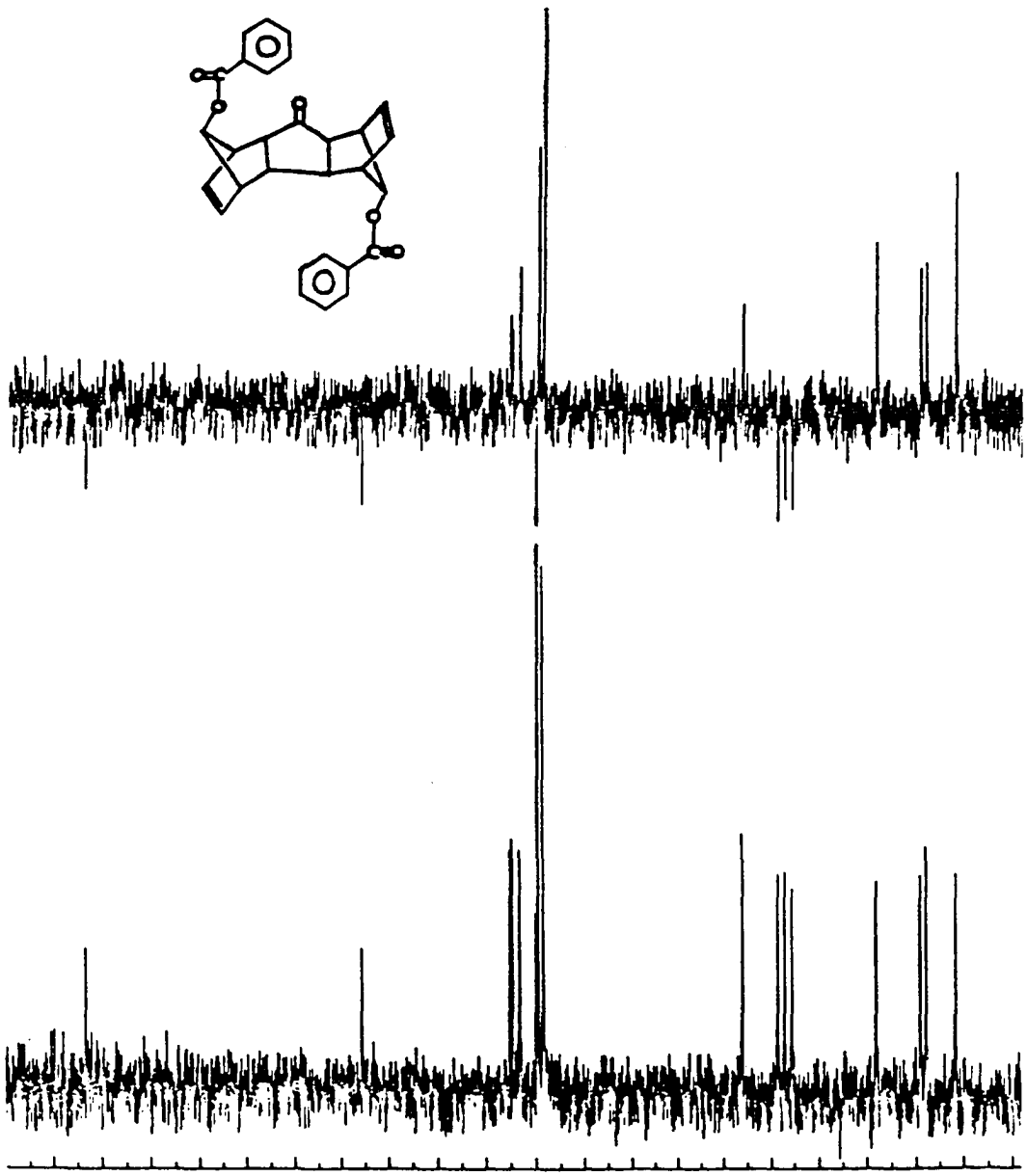

FIGURE IV-21

300 MHz ^{1}H NMR Spectrum of AXTNA Benzoyloxy Dimer Ketone XXXIII ($CDCl_3$/TMS).

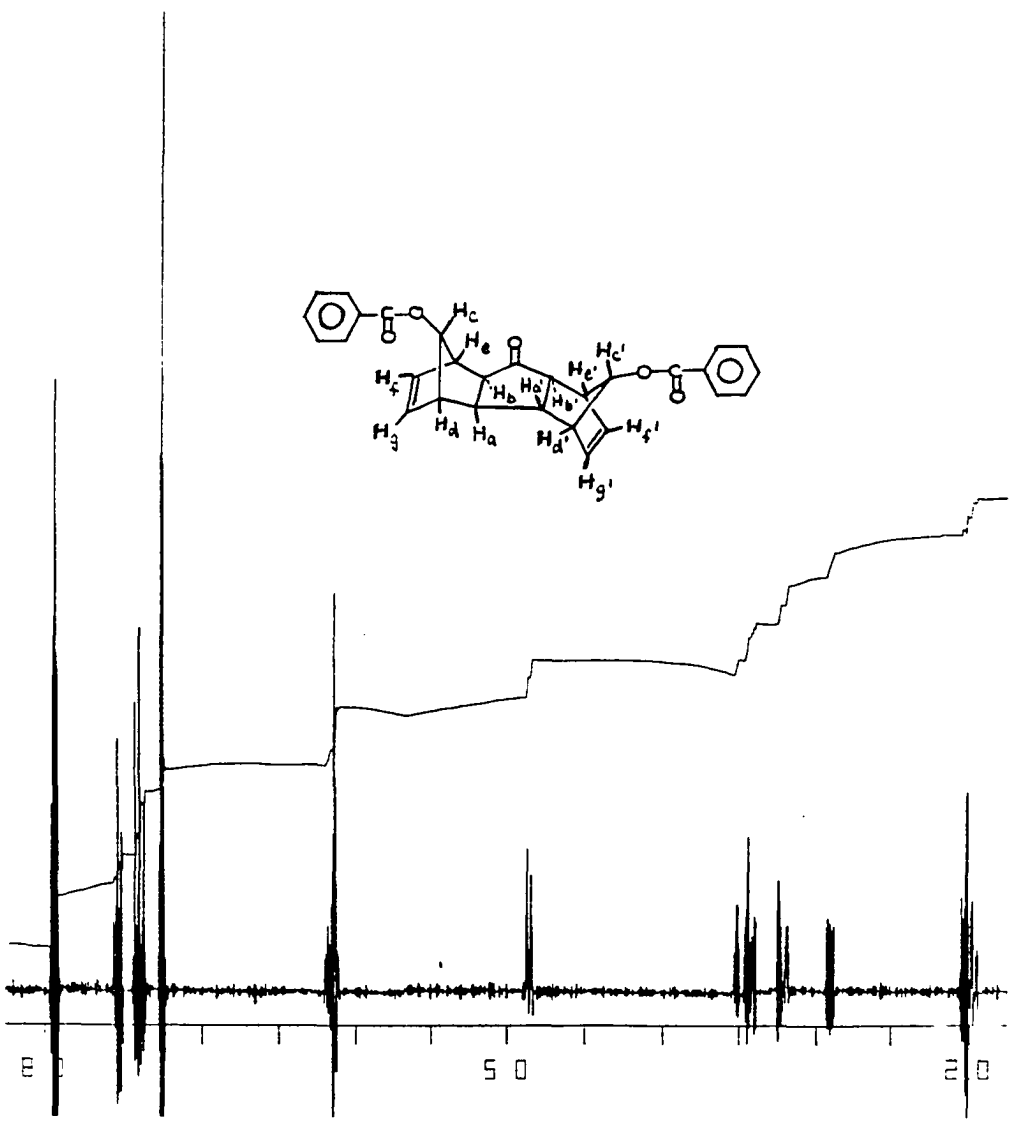

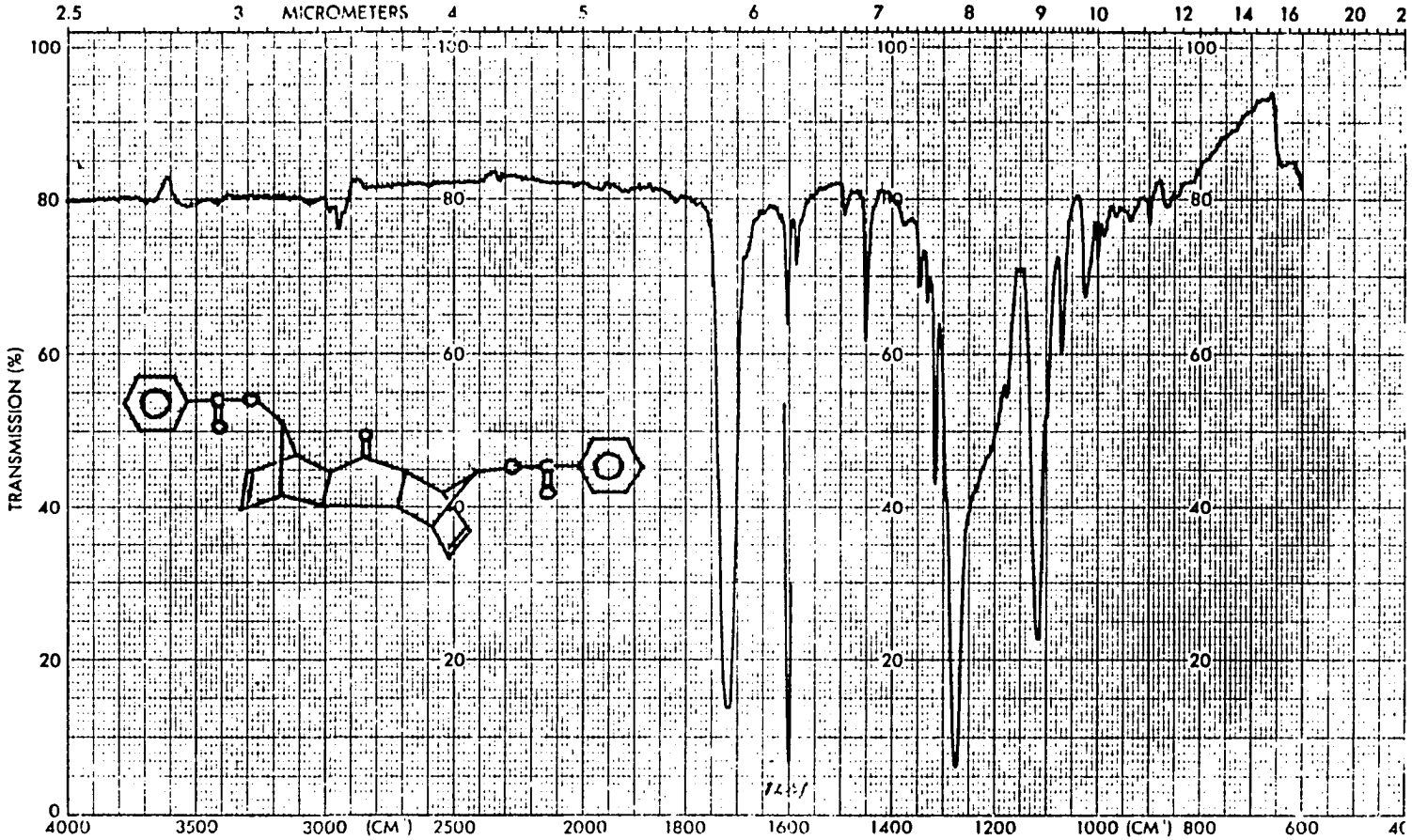

Figure IV-22. IR Spectrum of AXTNA Benzoyloxy Dimer Ketone XXXIII ($CHCl_3$).

FIGURE IV-23

Mass Spectrum of AXTNA Benzoyloxy Dimer Ketone XXXIII.

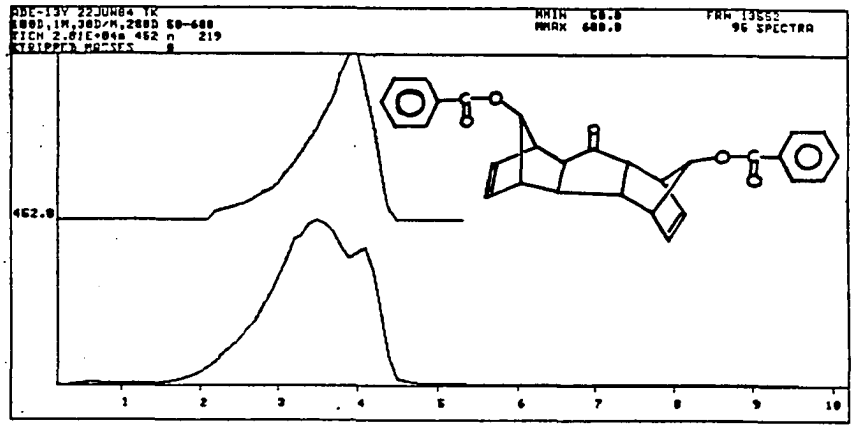

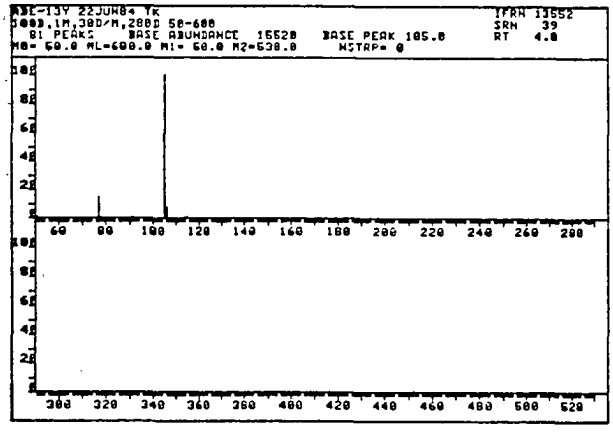

MASS	%	MASS	%
BIC 60		152.0	.1
50.1	.2	153.0	.2
51.1	1.2	161.0	.6
52.1	.1	165.0	.2
53.1	.1	166.0	.2
65.1	.4	167.2	.1
66.0	.7	179.1	.2
75.1	.1	180.1	.8
76.1	.5	181.0	.2
77.1	14.5	186.1	.8
78.1	1.2	187.1	.1
79.1	.6	207.0	.3
81.0	.2	208.1	.0
83.0	.1	209.0	.2
89.0	.2	225.1	.3
91.1	1.1	226.1	.2
92.1	.2	265.1	.4
103.1	.4	266.1	.8
105.0	100.0	267.1	.2
106.0	7.4	301.1	.1
107.1	.5	317.2	.3
115.1	.9	330.1	.4
116.1	.5	331.1	.1
117.1	.2	347.2	.3
118.1	.1	423.2	.1
119.1	.2	452.1	1.4
127.2	.1	453.1	.4
128.2	.2		
129.0	.1		
131.0	.3	LAST 4	
133.0	.2	424.1	.1
141.0	.2	452.1	1.4
144.0	.0	453.1	.4
145.0	.2	454.1	.1

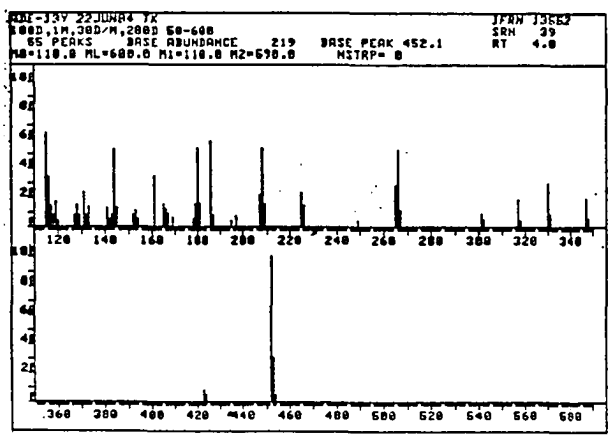

MASS	%	MASS	%
BIC 60		207.0	22.4
115.1	64.4	208.1	64.3
116.1	34.2	209.0	15.5
117.1	15.1	225.1	23.7
118.1	8.2	226.1	14.6
119.1	17.4	249.1	4.6
120.1	4.1	265.1	28.3
127.2	8.7	266.1	53.4
128.2	15.1	267.1	11.4
129.0	8.7	301.1	9.6
131.0	23.3	302.2	5.0
132.0	8.2	317.2	19.2
133.0	14.2	318.2	4.6
141.0	13.2	330.1	38.1
142.0	5.5	331.1	9.1
143.0	8.2	347.2	19.6
144.0	53.4	348.1	6.4
145.0	13.2	423.2	8.7
152.0	8.2	424.1	5.5
153.0	11.0	452.1	100.0
154.1	6.4	453.1	31.1
161.0	34.7	454.1	5.5
165.0	16.0		
166.0	12.3		
167.2	9.6		
169.0	6.0		
178.1	5.5		
179.1	15.5		
180.1	53.9		
181.0	16.4	LAST 4	
186.1	58.4	424.1	5.5
187.1	8.2	452.1	100.0
196.0	4.6	453.1	31.1
197.0	7.0	454.1	5.5

FIGURE IV-24

20 MHz ^{13}C and Spin Echo NMR Spectra of AXTNA Benzoyloxy Dimer Ketone XXXIII ($CDCl_3$).

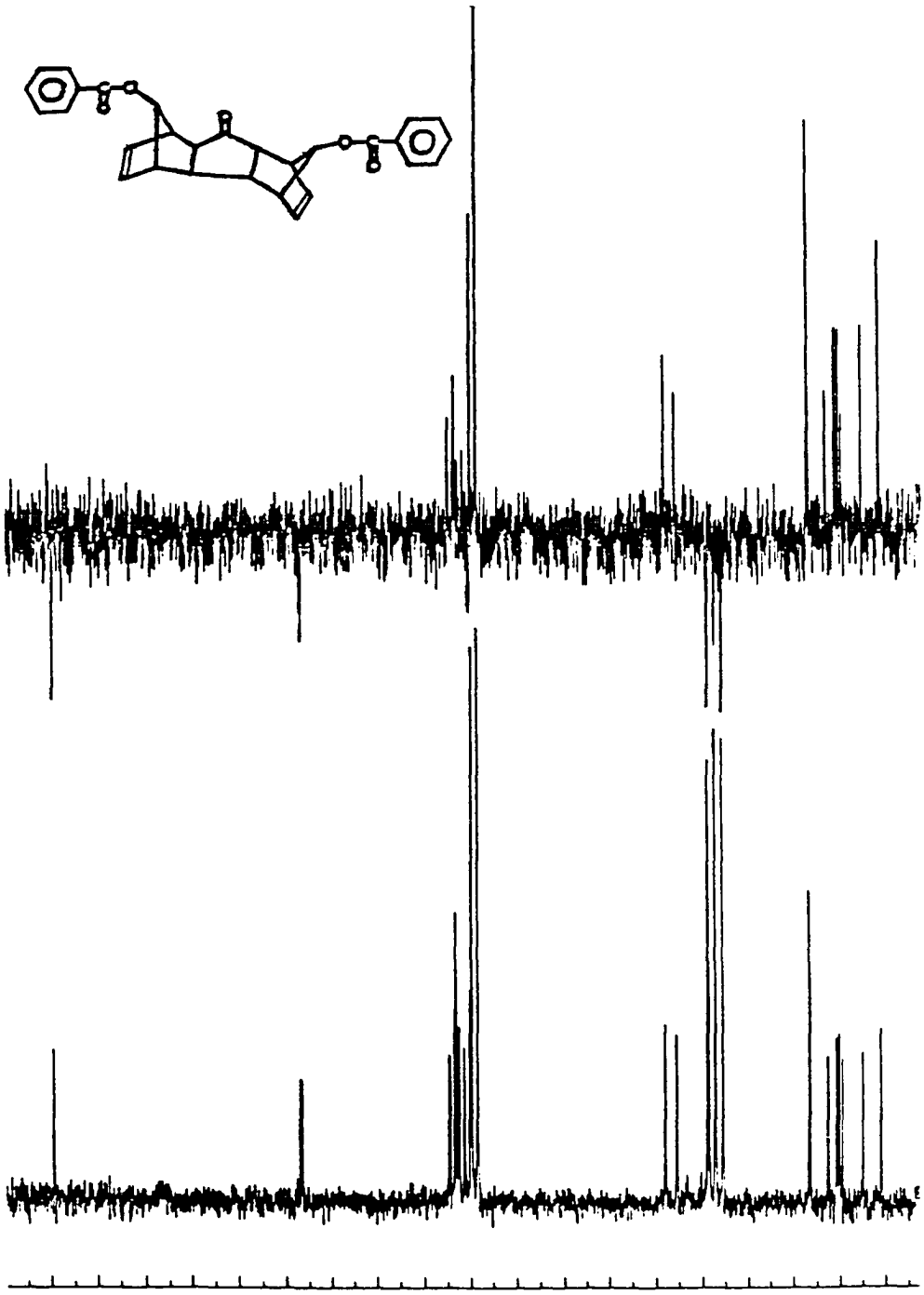

FIGURE IV-25

300 MHz ^{1}H HOMCOR NMR Spectrum of AXTNA Benzoyloxy Dimer Ketone XXXIII ($CDCl_3$).

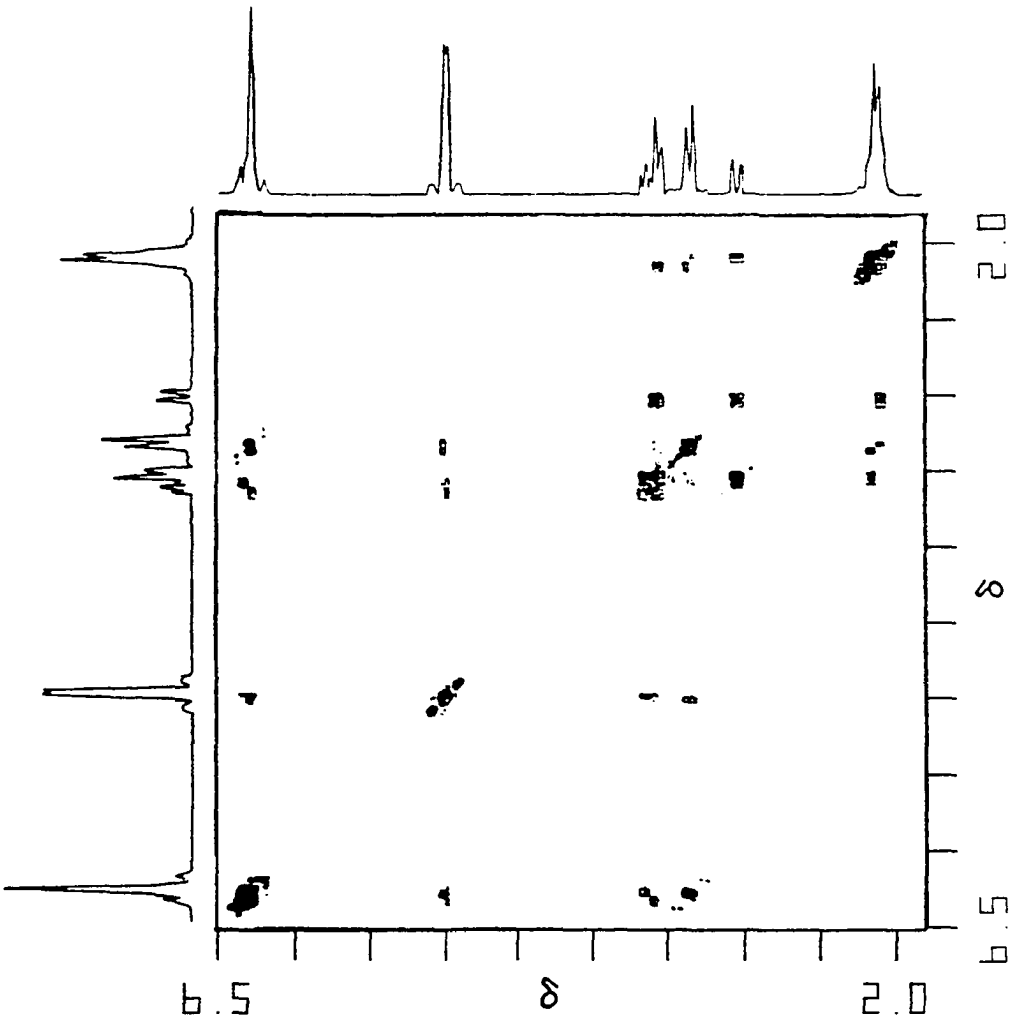

FIGURE IV-26

300 MHz ^{1}H NMR Spectrum of Benzoyloxy Cage Diketone XXXIV ($CDCl_3$/TMS).

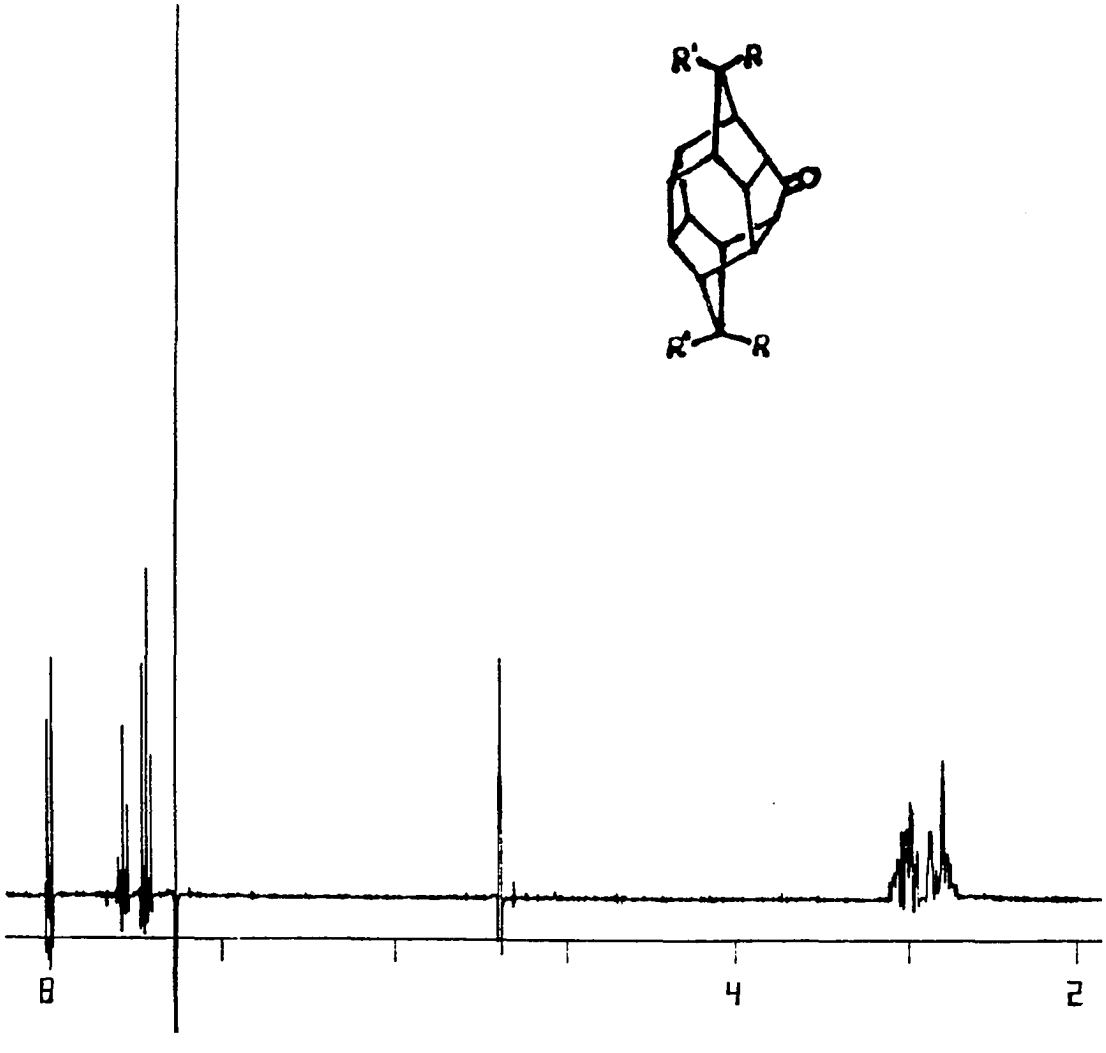

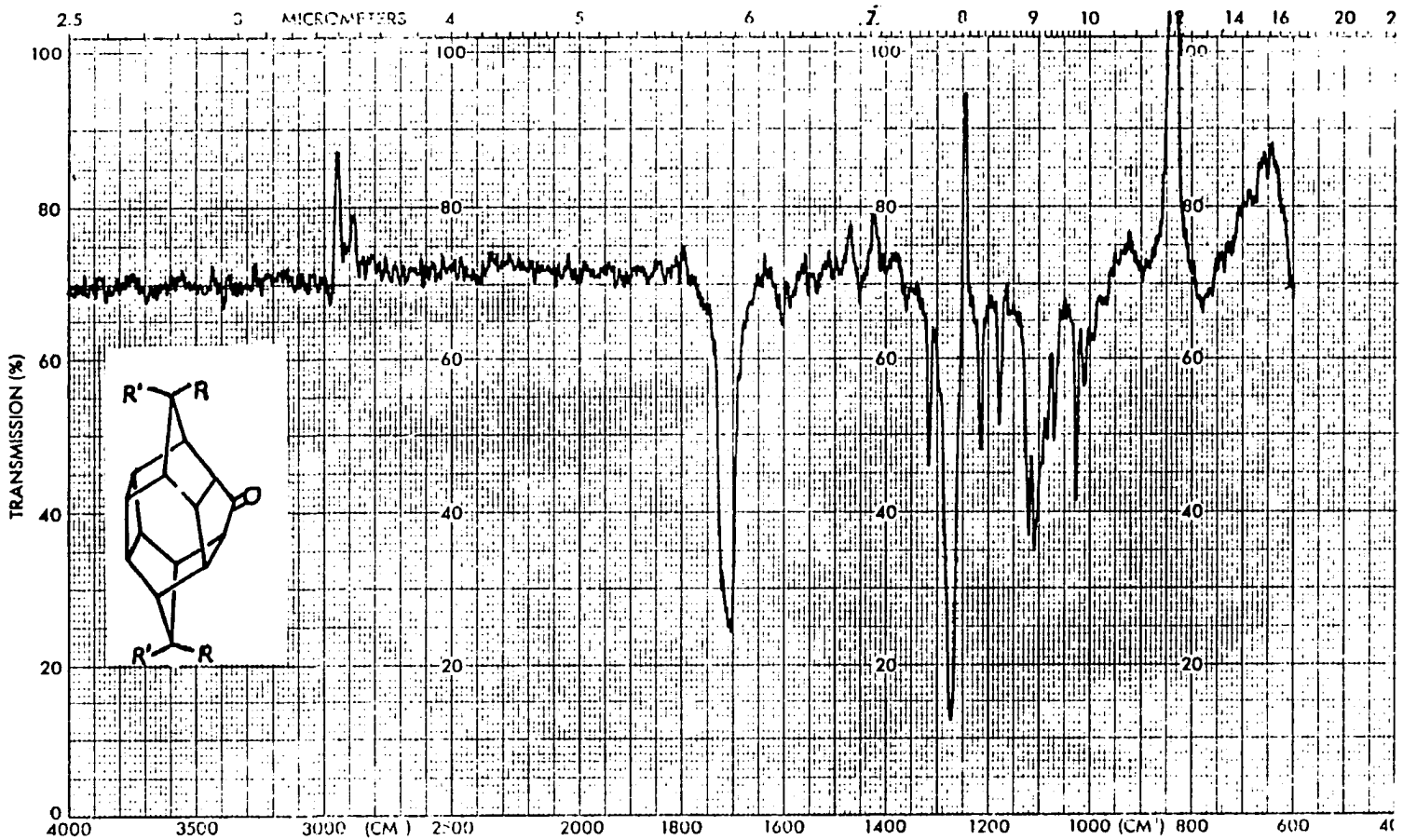

Figure IV-27. IR Spectrum of Benzoyloxy Cage Diketone XXXIV ($CHCl_3$).

FIGURE IV-28

Mass Spectrum of Benzoyloxy Cage Diketone XXXIV.

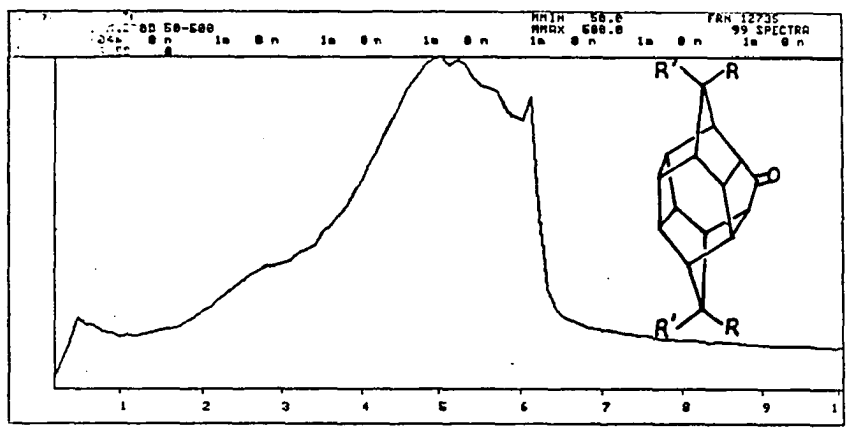

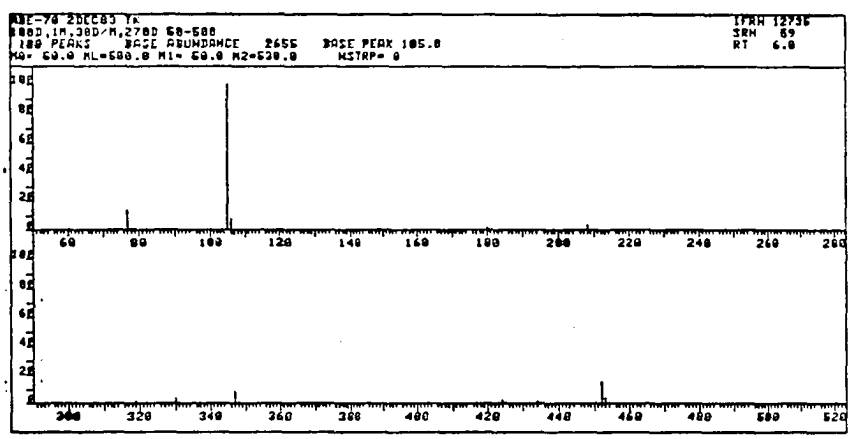

ABE-70 20DEC83 TK
FRN12735, SPECTRUM 69, 188PEAKS, RT 6.03 MIN, BASE PEAK 105.0, 26550.
MOST INTENSE 100 WARNING.....POSSIBLE OVERFLOW

MASS	%	MASS	%	MASS	%	MASS	%	MASS	%	MASS	%
60.1	.1	90.0	.0	127.1	.2	171.0	.0	234.0	.0	348.0	2.2
61.1	.6	91.1	.9	128.1	.5	177.0	.0	236.0	.1	349.1	.3
62.1	.1	92.1	.2	129.0	.2	178.0	.2	237.0	.1	360.1	.0
63.1	.0	93.0	.1	130.0	.3	179.1	.5	241.0	.0	364.9	.0
65.1	.1	94.0	.1	131.0	.6	180.1	2.0	247.1	.0	380.1	.2
66.1	.0	95.1	.1	132.0	.3	181.0	.5	250.0	.1	381.2	.0
67.1	.1	96.1	.0	132.9	.2	182.0	.1	264.9	.0	388.0	.0
68.1	.1	97.1	.1	133.9	.0	183.0	.0	267.0	.0	396.0	.4
68.1	.0	98.1	.0	135.0	.0	185.9	.0	274.0	.0	397.0	.1
63.0	.0	99.1	.1	139.1	.1	190.0	.0	276.2	.1	405.0	.0
65.1	.2	102.1	.1	141.0	.6	191.0	.1	281.0	.1	406.0	.6
66.0	.1	103.1	.5	141.9	.2	192.0	.0	283.1	.0	407.0	.2
67.0	.1	105.0	100.0	143.0	.1	193.0	.2	284.0	.2	408.1	.2
69.0	.1	106.0	7.5	143.9	.1	193.9	.1	285.0	.0	409.0	.0
70.0	.0	107.0	.6	145.1	.0	195.0	.1	301.1	.1	423.1	1.1
71.1	.1	108.0	.1	146.9	.1	196.0	.0	302.1	.9	424.0	2.9
73.0	.1	109.2	.0	148.1	.0	197.0	.3	303.1	.2	425.0	.0
74.1	.1	110.0	.0	149.0	.0	198.0	.6	304.1	.0	426.0	.2
75.0	.2	111.0	.0	151.0	.1	199.0	.1	312.1	.2	434.1	1.0
76.1	.6	112.0	.0	152.0	.3	207.0	.7	313.0	.0	435.1	.7
77.0	13.9	113.1	.0	153.0	.5	208.1	3.7	318.0	.0	436.1	.2
78.1	1.3	115.1	.9	154.0	.3	209.0	.0	319.1	1.6	452.0	15.3
79.1	.0	116.1	.4	155.0	.2	210.0	.1	320.0	.4	453.0	4.7
80.1	.1	117.1	.2	156.1	.0	218.0	.0	321.0	.1	454.1	.0
81.0	.2	118.1	.1	157.0	.0	219.0	.0	328.1	.0	455.0	.1
82.1	.0	119.1	.2	165.0	.7	221.0	.1	329.1	.1		
83.1	.2	120.1	.1	166.0	.2	223.0	.0	330.1	3.2		
84.1	.0	121.1	.0	167.0	.3	224.1	.1	331.1	1.1		
85.0	.2	122.1	.1	168.0	.3	225.0	.2	332.1	.2		
87.0	.0	123.1	.0	169.0	.3	226.1	.1	333.2	.0		
89.0	.2	126.0	.0	170.0	.2	227.0	.0	347.1	0.5		

FIGURE IV-29

75 MHz ^{13}C and Spin Echo NMR Spectra of Benzoyloxy Cage Compound XXXIV ($CDCl_3$).

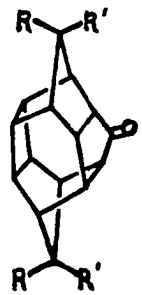

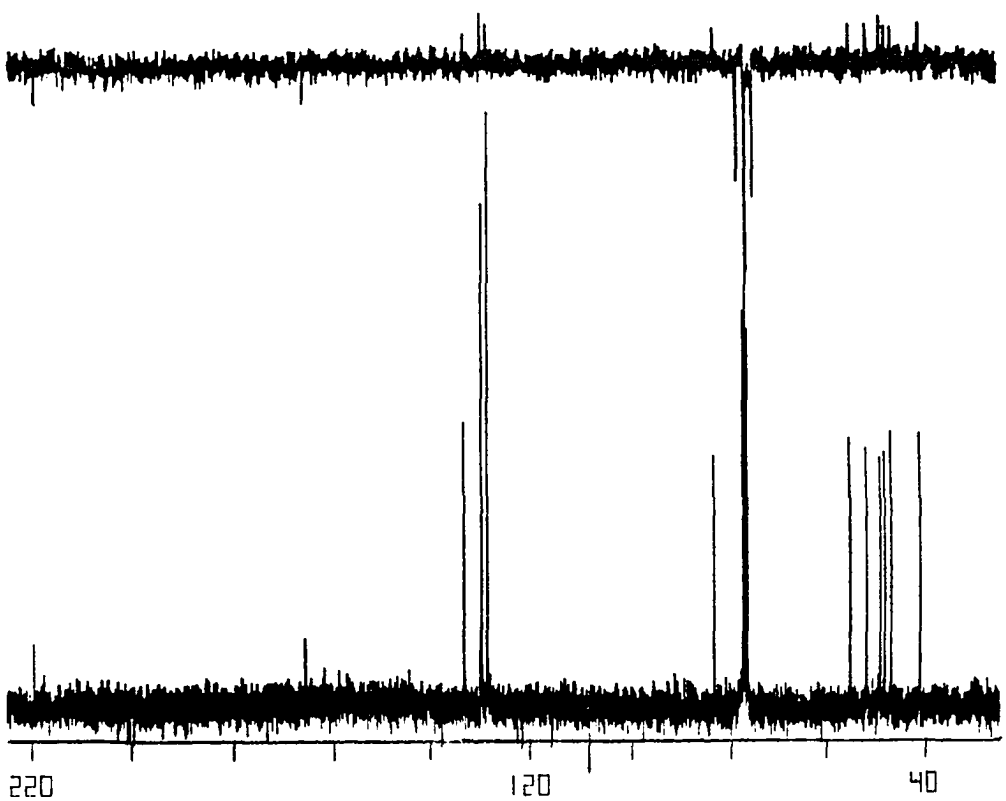

and one non-bridgehead), while the bridgehead at δ 2.62 is coupled to the signals at δ 2.94 and 2.61. It easy to see that the non-bridgehead proton signal at δ 2.61 must be on the opposite side of the molecule relative to the bridgehead proton at δ 2.75. otherwise, coupling between the signals at δ 2.75 and 2.61 would be observed.

Characterization of XV required a more detailed approach. Returning to the NMR of XV (Fig IV-13), a sharp AB pattern centered at δ 2.53 is observed which, as discussed in Part I, is characteristic of a trans cyclopentanone ring junction in dimeric ketones of the type studied in this lab. The two types of aromatic resonances, a two-hydrogen multiplet at δ 7.95 and a three-hydrogen multiplet at δ 7.50, are easily identified. The two syn-bridgehead protons $H_e(H_{e'})$ (δ 3.35) were identified by decoupling the downfield half [$H_b(H_{b'})$, δ 2.72] of the AB pattern and observing the simplification of the δ 3.35 signal. The anti-bridgehead protons [$H_d(H_{d'})$, δ 3.22] were identified by decoupling the upfield half [$H_a(H_{a'})$, δ 2.32] of the AB pattern and observing the simplification of the δ 3.22 signal. Reciprocal decouplings confirmed these observations. However, what is not obvious is the syn or anti nature of the 7-substituent.

In the past, nuclear magnetic resonance proton decoupling experiments have been used as an aid in structural elucidation of dimer ketones whose NMR spectra are similar to that of XV. In particular, two types of long range coupling, 'vinyl' and 'W-letter' (discussed in Part I), have proven useful in this regard.[2,17,18] Since the NMR of XV is very similar to those of the 7-phenyl (VII, PART I, Fig I-22) and 7-o-anisyl (IX, PART I, Fig I-26) dimer ketones, an AXTXA stereochemistry for XV was tentatively assumed. This should be verifiable by one or both of the long range couplings discussed above. Pursuant to this end, a 100 MHz decoupling experiment on compound XV was performed (see Fig IV-30 for normal 100 MHz NMR spectrum and Fig IV-31 for the decoupling experiments). A

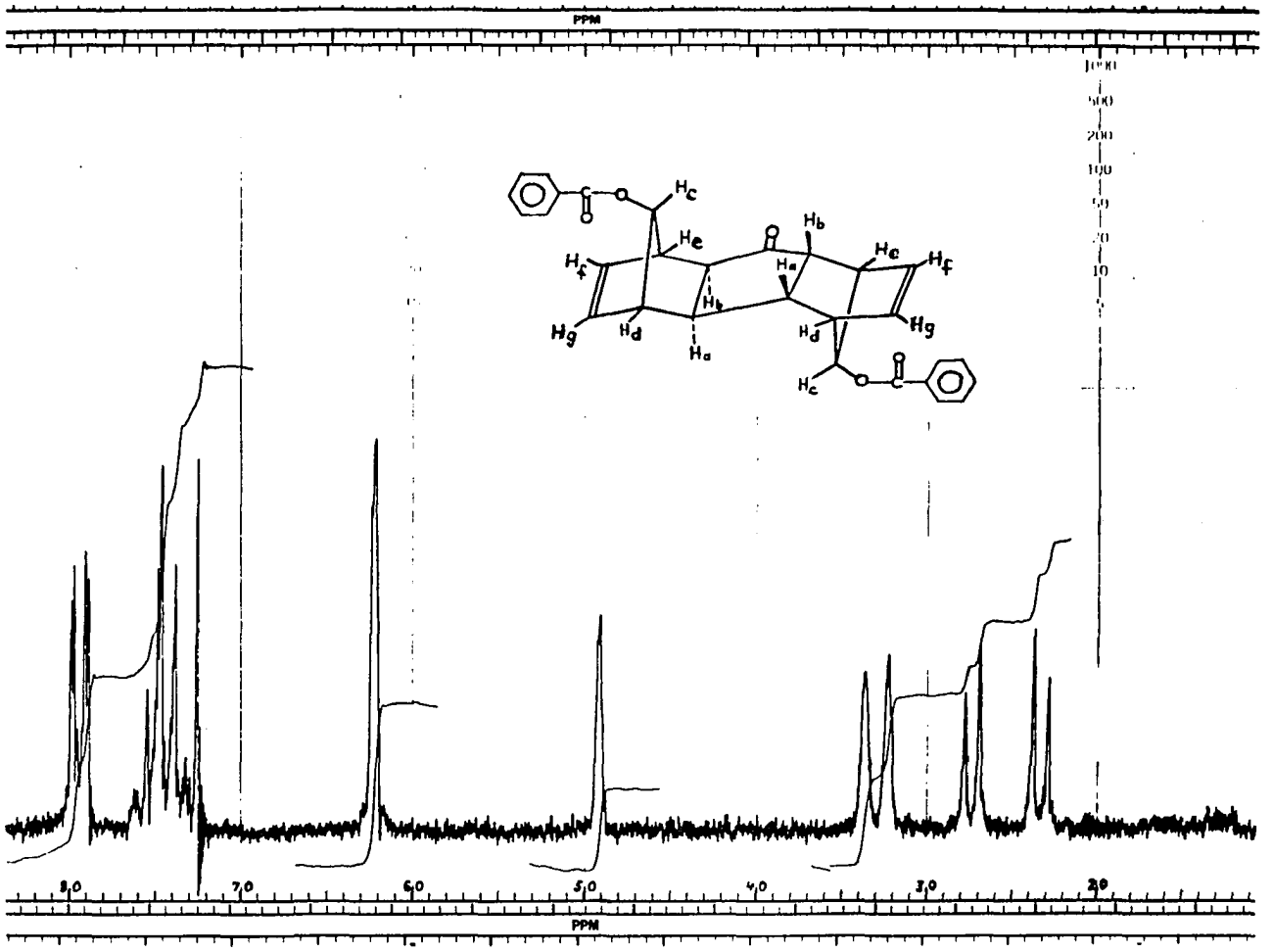

Figure IV-30. 100 MHz ^{1}H NMR Spectrum of AXTXA Benzoyloxy Dimer Ketone XV ($CDCl_3$/TMS).

FIGURE IV-31

100 MHz ^{1}H NMR Decoupling Experiments on AXTXA Benzoyloxy Dimer Ketone XV ($CDCl_3$/TMS).

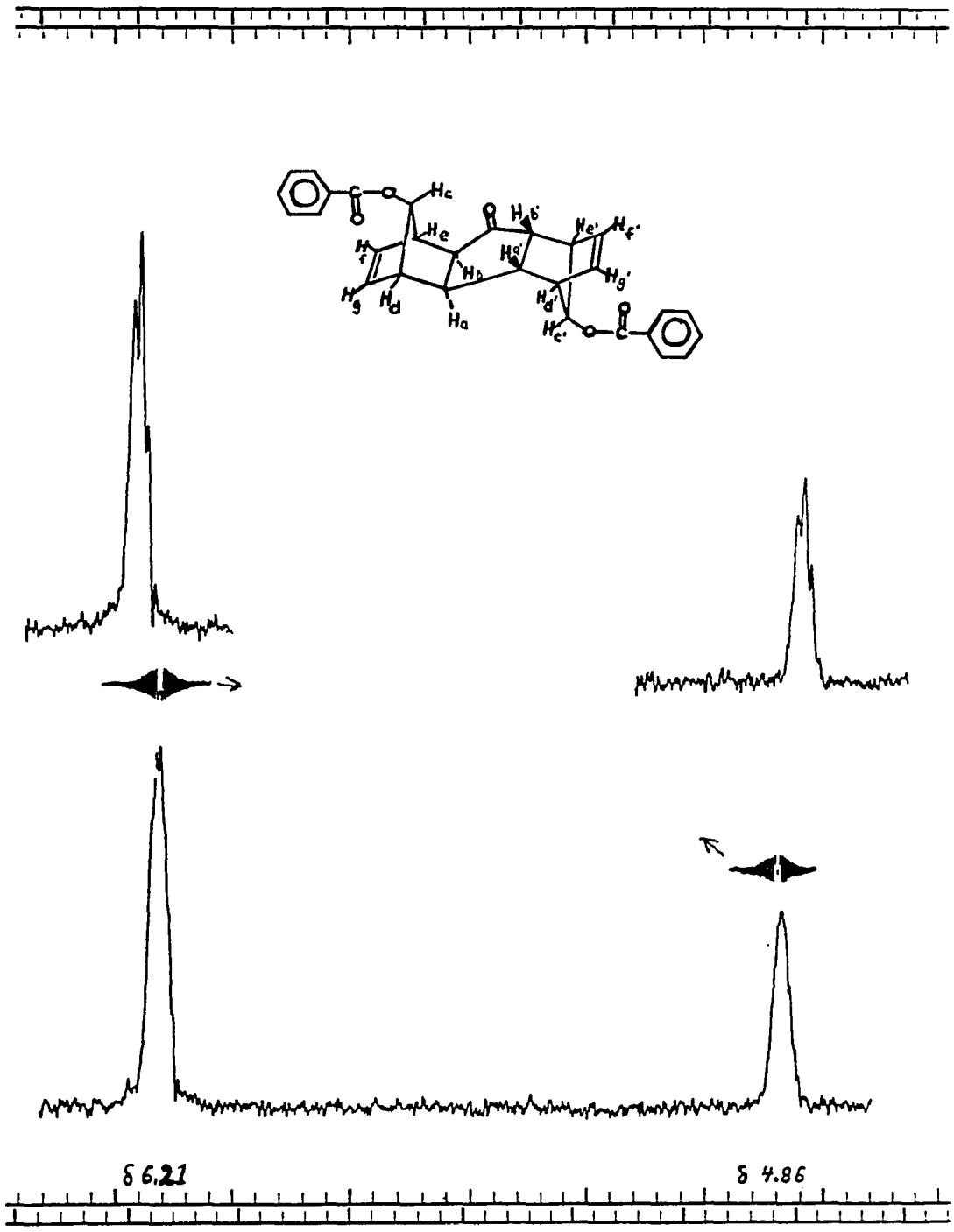

vinyl long range decoupling was first conducted by irradiation of bridge protons $H_c(H_{c'})$ (δ 4.89) while looking for a change in vinyl protons $H_f(H_{f'})$ and $H_g(H_{g'})$ (centered at δ 6.21). Simplification of the $H_f(H_{f'})$ and $H_g(H_{g'})$ proton signals and narrowing of the peak width at half-height was observed. The reciprocal decoupling, irradiation of $H_f(H_{f'})$ and $H_g(H_{g'})$ while observing $H_c(H_{c'})$, produced a similar simplification and narrowing of peak width. This is unequivocal proof that the structure of XV is AXTXA as has been shown earlier for the similar compound XI.[19] Further information regarding the proton assignments of XV in Fig IV-30 was gathered at 300 MHz. Decoupling of syn-bridgehead $H_e(H_{e'})$ resulted in simplification of $H_b(H_{b'})$ and the downfield half [$H_f(H_{f'})$, δ 6.22] of the vinyl signal which is centered at δ 6.21. Decoupling the anti-bridgehead signal [$H_d(H_{d'})$, δ 3.22] simplified the $H_a(H_{a'})$ signal and the upfield half [$H_g(H_{g'})$, δ 6.20] of the vinyl signal.

Identification of the structure of dimer ketone XXXII was attempted using 300 MHz NMR decoupling experiments. A trans ring juncture was believed to be present in XXXII because decoupling the bridgehead centered at δ 3.24 [$H_d(H_{d'})$ and $H_e(H_{e'})$] resulted in an AB pattern for $H_b(H_{b'})$ (δ 2.95) and $H_a(H_{a'})$ (δ 2.81) centered at δ 2.88. The doubled doublets of both $H_b(H_{b'})$ and $H_a(H_{a'})$ which are observed in the undecoupled spectrum are attributed to coupling with a vicinal-bridgehead proton which must be <u>exo</u> in order to exhibit coupling of the magnitude observed (i.e., $^{J}H_{exo}H_{bridgehead}$ = 2.9-4.3 Hz, while $^{J}H_{endo}H_{bridgehead}$ ≈ 0 Hz)].[17] This can occur only when the NTN configuration is present! Further information confirming the proton assignments of XXXII in Fig IV-17 was seen when successive decouplings of $H_a(H_{a'})$ and $H_b(H_{b'})$ resulted in simplification of $H_d(H_{d'})$ (δ 3.25) and $H_e(H_{e'})$ (δ 3.22), respectively. Also, upon successive irradiation of the signals

corresponding to protons $H_f(H_{f'})$ (δ 6.16) and $H_g(H_{g'})$ (δ 6.29), the resonances of $H_e(H_{e'})$ and $H_d(H_{d'})$, respectively, were simplified. Irradiation of the vinyl protons $H_f(H_{f'})$ and $H_g(H_{g'})$ produced no simplification of the $H_c(H_{c'})$ (δ 4.71) signal nor did the reciprocal experiment. This seemed to indicate the the 7-substituent was syn to the cyclopentanone carbonyl because $^{J}H_{vinyl}H_{syn}$ = 0.20-0.35 Hz $\leq$ $^{J}H_{vinyl}H_{anti}$ = 0.30-0.85 Hz.[17] The SNTNS configuration was confirmed by a single crystal X-ray structure which will be discussed in the Experimental section. A computer drawn representation and numbering scheme are shown in Fig IV-32 and a molecular packing diagram is shown in Fig IV-33.

Solution of the structure of unsymmetrical dimer ketone XXXIII via NMR was more complicated due to the overlapped spectrum and marginal resolution (Fig IV-21). Lack of a simple AB pattern at high field rules out an XTX structure since $^{J}H_aH_{a'}$ ≈ 0 Hz due to the lack of molecular symmetry. Bridge proton H_c (δ 4.87), when decoupled, identified bridgeheads H_d (δ 3.19) and H_e (δ 3.24), while decoupling bridge proton $H_{c'}$ (δ 4.84) identified bridgeheads $H_{d'}$ (δ 3.45) and $H_{e'}$ (δ 3.51). Decoupling $H_{a'}$ (δ 2.90) simplified $H_{d'}$, $H_{b'}$ (δ 3.42), and H_a (δ 1.97, with $^{J}H_aH_{a'}$ = 2.12 Hz!). The process of elimination leaves H_b at δ 2.03. The fact that $^{J}H_{endo}H_{bridgehead}$ ≈ 0 (as suggested in the literature[17]) is seen in the HOMCOR spectrum (Fig IV-25), where endo protons H_a and H_b are observed to be coupled to H_d and H_e, respectively. The spectrum also shows evidence that H_b and $H_{b'}$ are coupled! A HOM2DJ[20] (Homonuclear 2-dimensional J-resolved) NMR spectrum (Figs IV-34 through IV-36) was also taken of compound XXXIII. Unequivocal proof of the structure of compound XXXIII was obtained by single crystal X-ray crystallography and will be discussed in the Experimental section. A computer drawn representation and numbering scheme are shown in Fig IV-37 and a unit cell is shown in Fig IV-38.

FIGURE IV-32

Computer Drawn Representation and Numbering Scheme of the SNTNS Benzoyloxy Dimer Ketone XXXII.

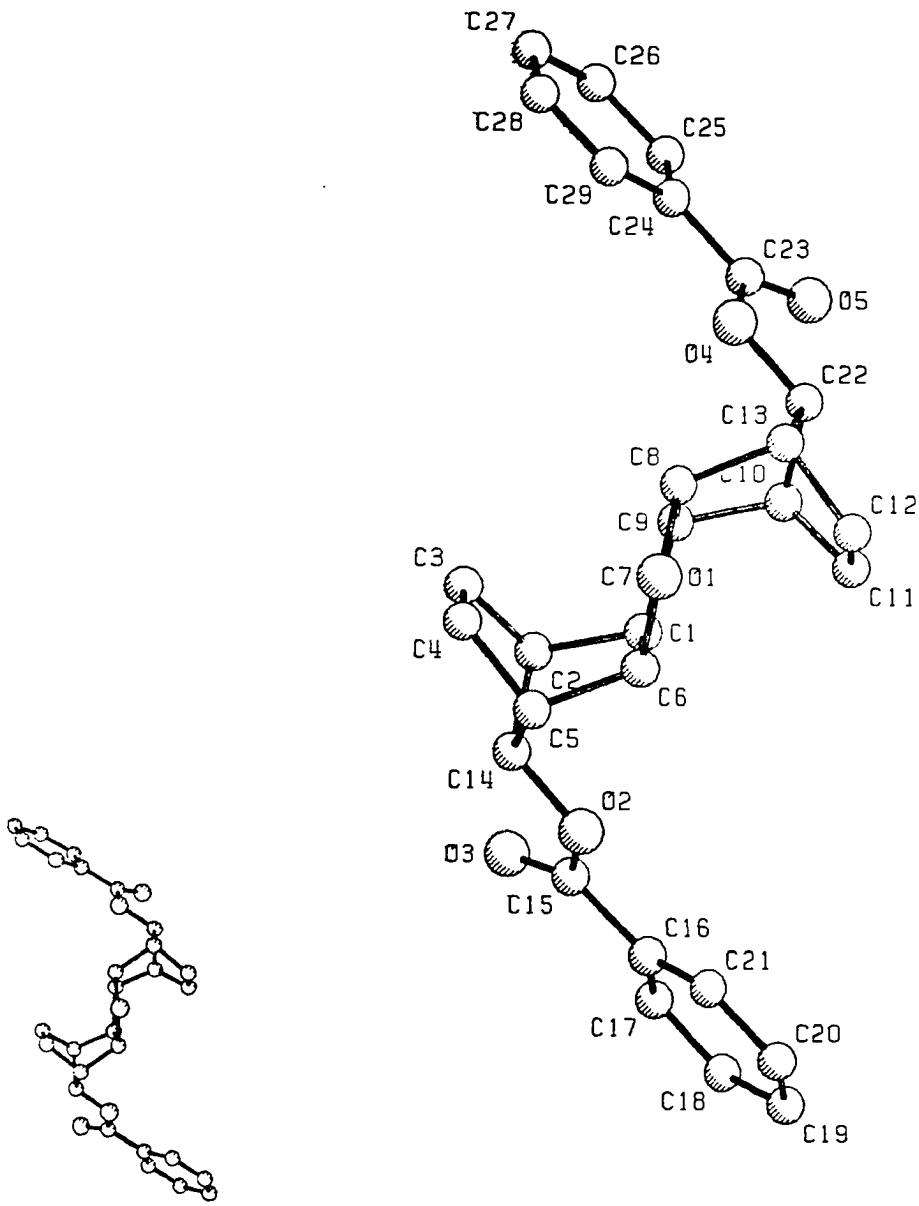

FIGURE IV-33

Computer Drawn Representation of the Molecular Packing Diagram of the SNTNS Benzoyloxy Dimer Ketone XXXII.

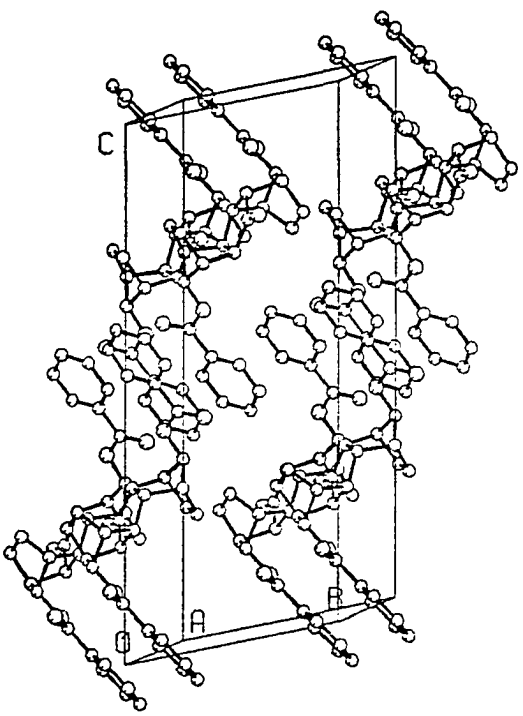

FIGURE IV-34

Contour Plot of the 300 MHz ^1H HOM2DJ NMR Spectrum of AXTNA Benzoyloxy Dimer Ketone XXXIII ($CDCl_3$).

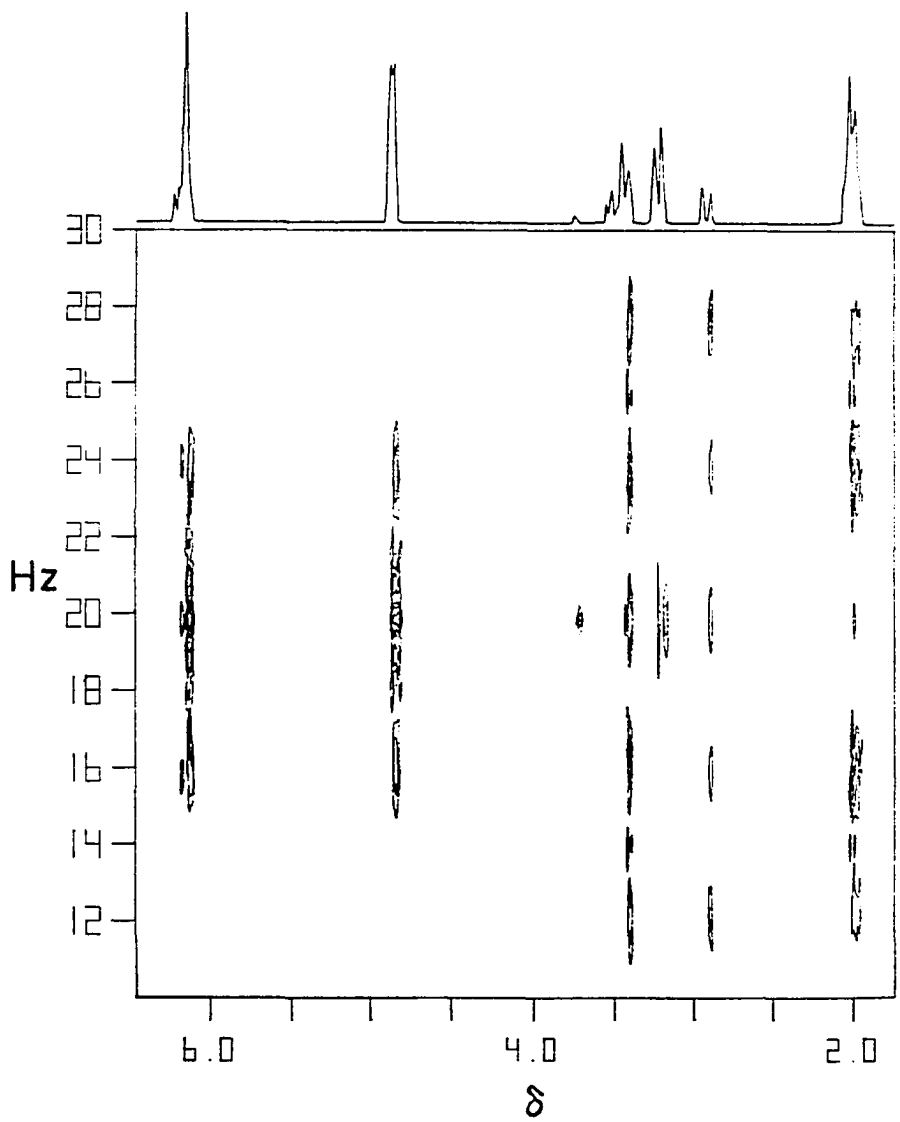

FIGURE IV-35

Expanded contour plot of the 300 MHz ^{1}H HOM2DJ NMR spectrum of AXTNA benzoyloxy dimer ketone XXXIII which includes the 2.88 to 3.68 ppm chemical shift and 13 to 30 Hz spectral region of Fig IV-3 ($CDCl_3$).

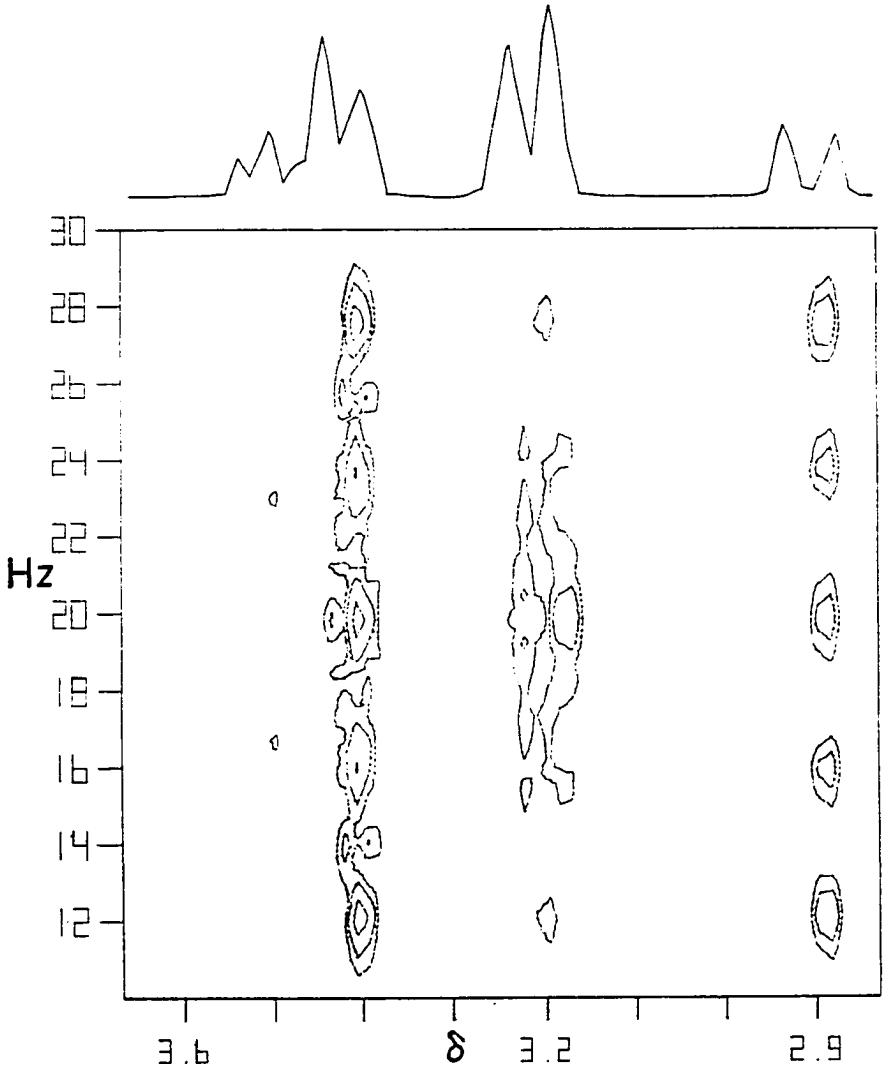

FIGURE IV-36

Stacked Plot of the 300 MHz ^{1}H HOM2DJ NMR Spectrum of AXTNA Benzoyloxy Dimer Ketone XXXIII ($CDCl_3$).

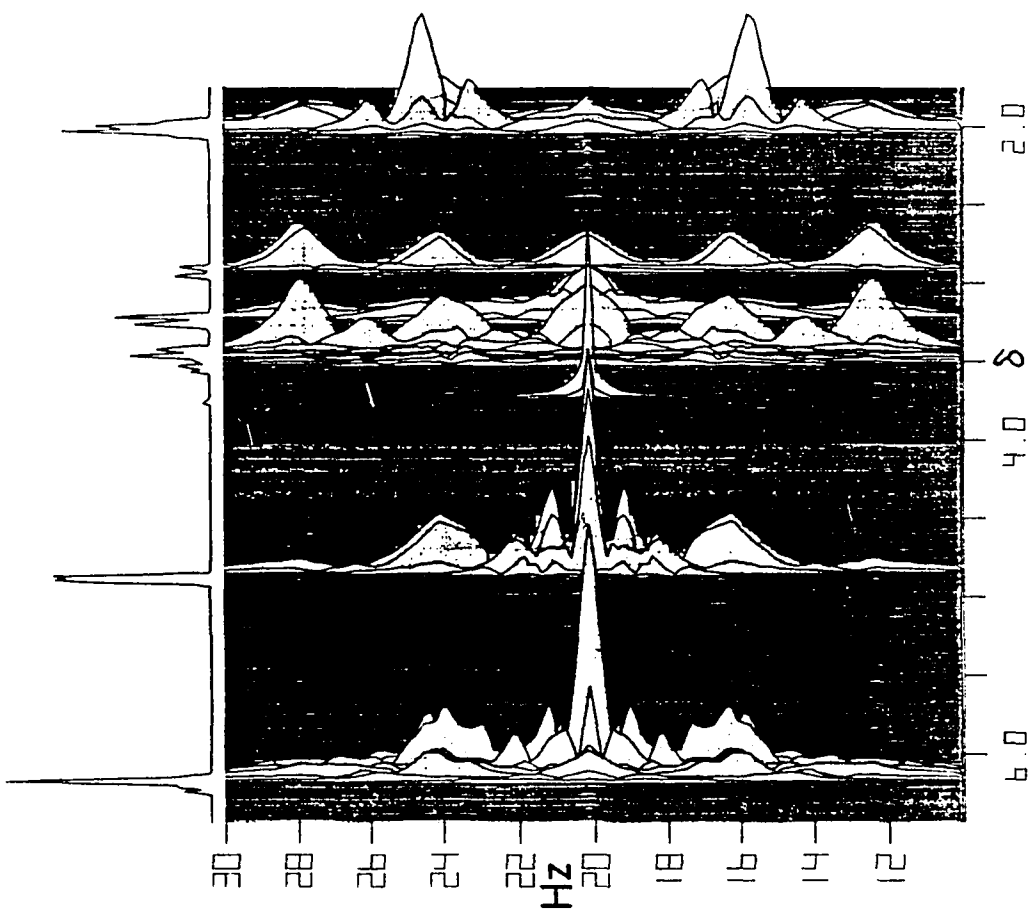

FIGURE IV-37

Computer Drawn Representation and Numbering Scheme of the AXTNA Benzoyloxy Dimer Ketone XXXIII.

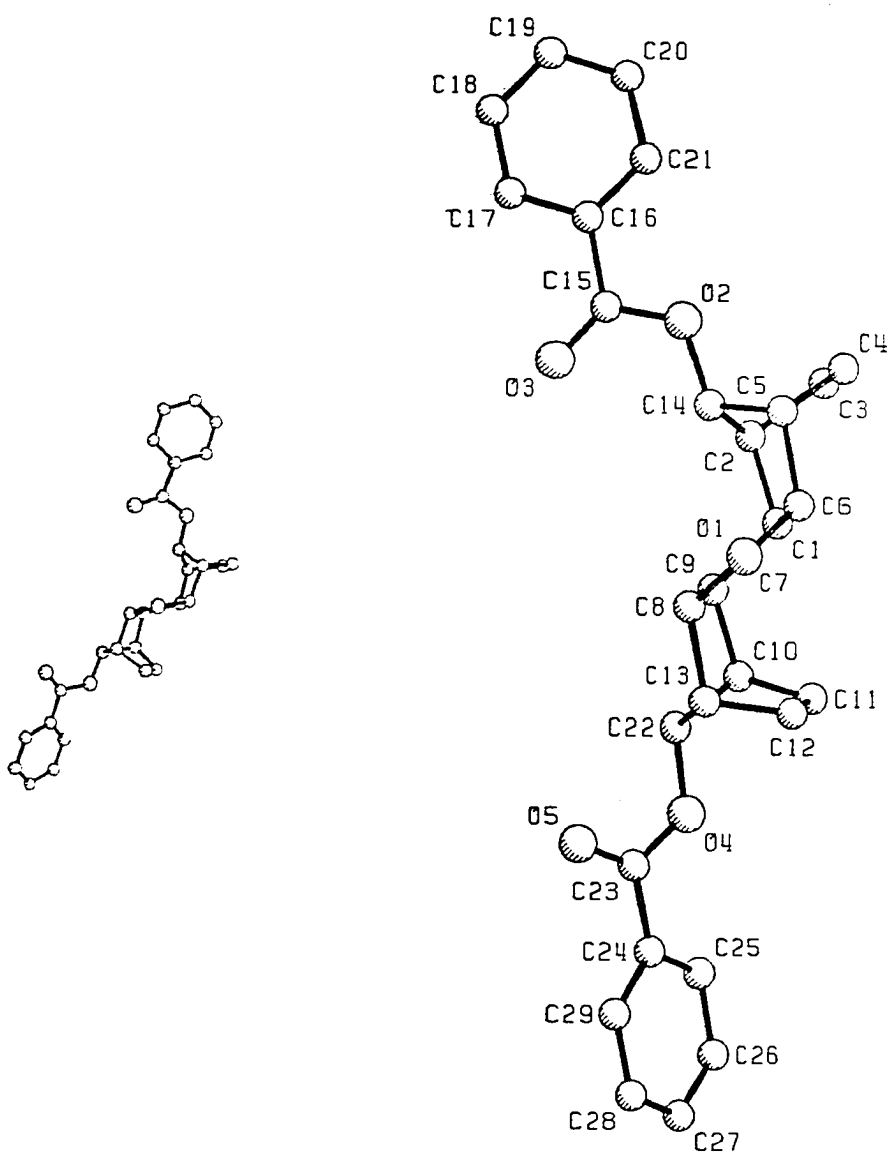

FIGURE IV-38

Computer Drawn Representation of the Molecular Packing Diagram of the AXTNA Benzoyloxy Dimer Ketone XXXIII.

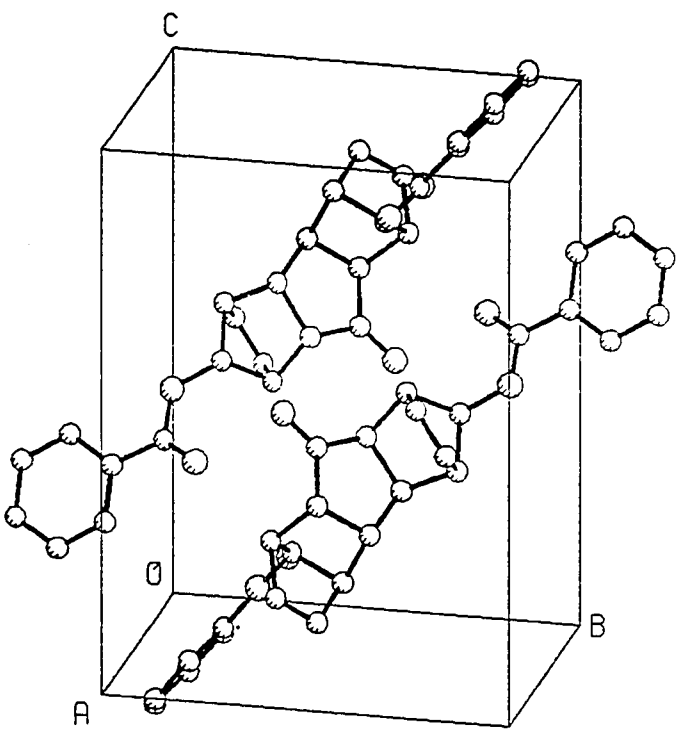

The structure of cage dimer ketone diester XXXIV is suggested by: (i) the absence of olefinic signals in its ^{1}H NMR spectrum (Fig IV-26); (ii) the IR spectrum (Fig IV-27) which showed the presence of ketone carbonyl and absence of olefinic absorptions; (iii) the mass spectrum (Fig IV-28) which contained the correct molecular weight for a dimeric ketone of the type discussed above; (iv) the absence of olefinic carbon resonances in the ^{13}C and spin echo spectra (Fig IV-29). The ^{13}C and spin echo spectra confirm that XXXIV is completely symmetrical because of the limited number of ^{13}C signals [i.e., 12 signals: 11 from precursor olefin 7-benzoyloxynorbornadiene (it is not unusual for the quaternary aromatic carbon to disappear owing to a long T_1) plus 1 from the inserted carbonyl carbon]. It remains to be determined whether the 7-substituents are both syn or both anti to the inserted carbonyl group. Decoupling the C7-bridge protons [$H_C(H_{C'})$, δ 5.39] identifies bridgehead protons at δ 2.88 and 3.01.

Having failed to obtain the anticipated SXTNS stereochemistry, attention was given to increasing the electron density at the ester oxygen by substituting an electron donating methoxy group at the para position on the aromatic ring. It was believed that, by increasing the availability for sharing of the lone pairs on oxygen, the Scheme IV-1 and/or Scheme IV-2 mechanism would predominate over the steric controlled mechanism which was suggested by formation of XV.

7-p-Anisoyloxynorbornadiene (Figs IV-39 through IV-42 for NMR, IR mass, and spin echo spectra, respectively) was reacted with $Fe(CO)_5$ and the crude mixture was separated via careful column chromatography. First eluted was unchanged XVII (the proton assignments of which were determined by decoupling experiments) followed by cage diester XIX (Figs IV-43 through IV-47 for NMR, IR, mass spin echo, and HOMCOR spectra, respectively). Next to be eluted was compound XVIII (AXTXA, Figs IV-48 through IV-51 for NMR, IR, mass, and spin echo spectra, respectively). Last to be eluted were small amounts of gummy residue which have not been thoroughly

FIGURE IV-39

300 MHz ^{1}H NMR Spectrum of 7-p-Anisoyloxynorbornadiene XVII ($CDCl_3$/TMS).

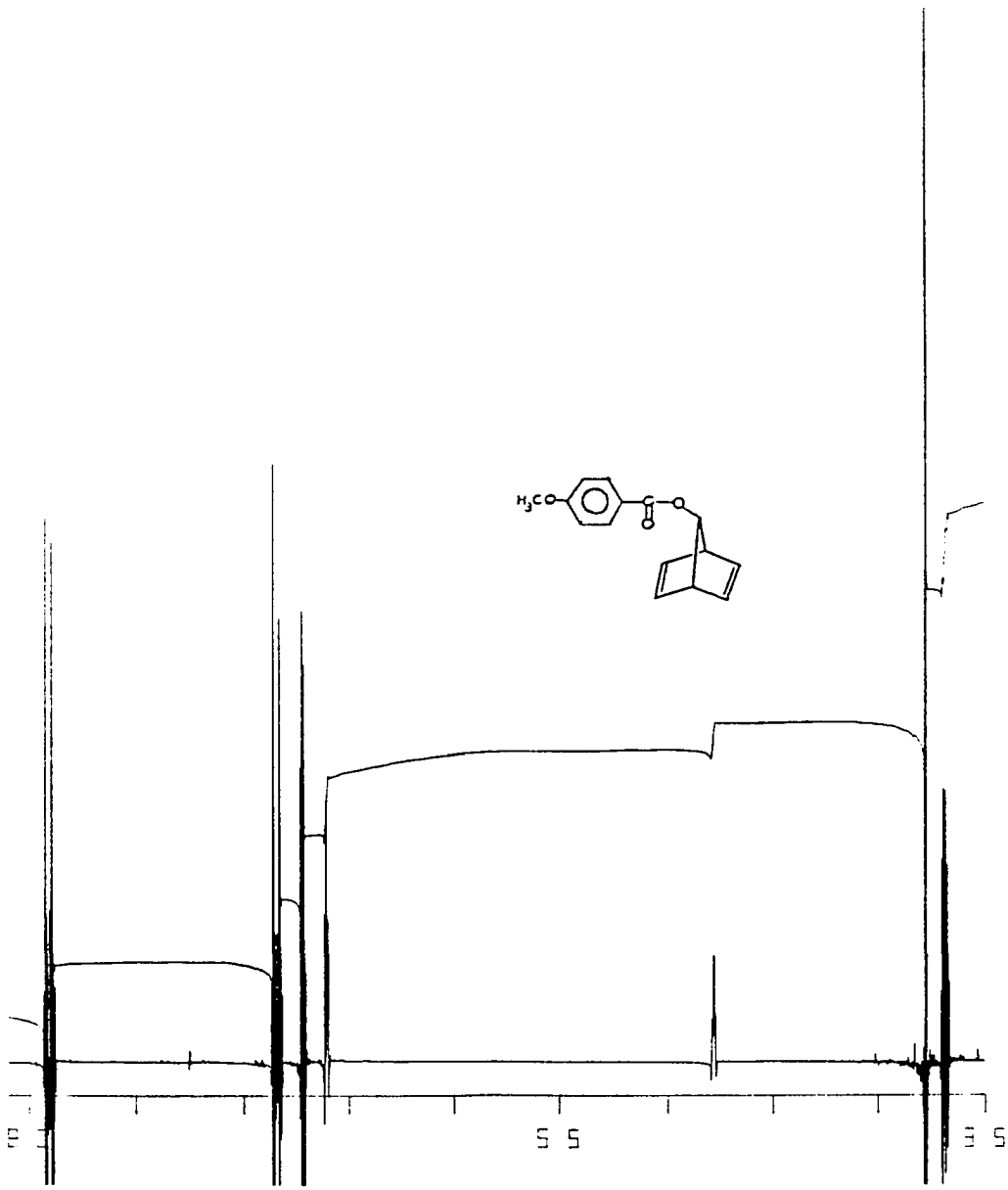

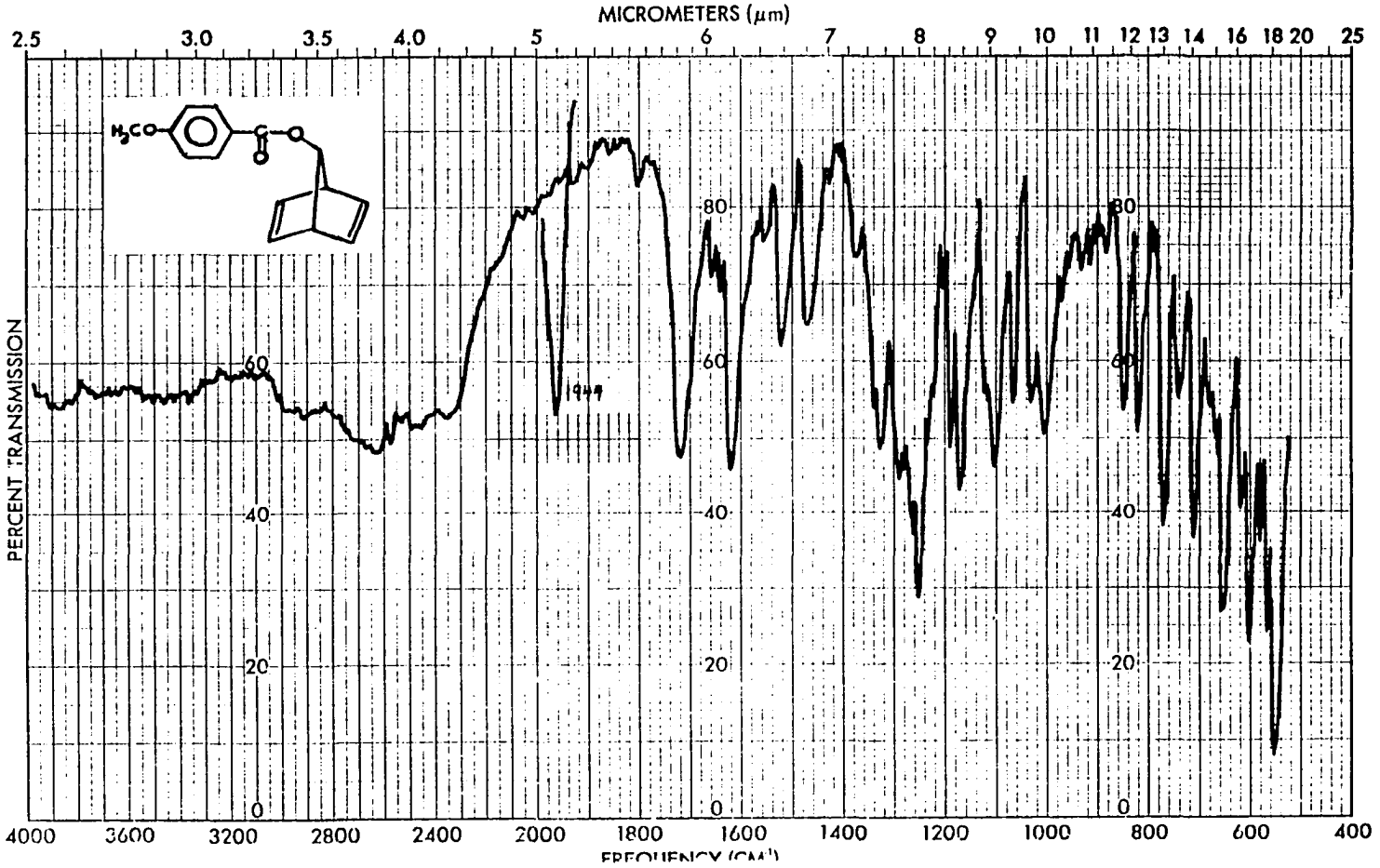

Figure IV-40. IR Spectrum of 7-p-Anisoyloxynorbornadiene XVII (KBr).

FIGURE IV-41

Mass Spectrum of 7-p-Anisoyloxynorbornadiene XVII.

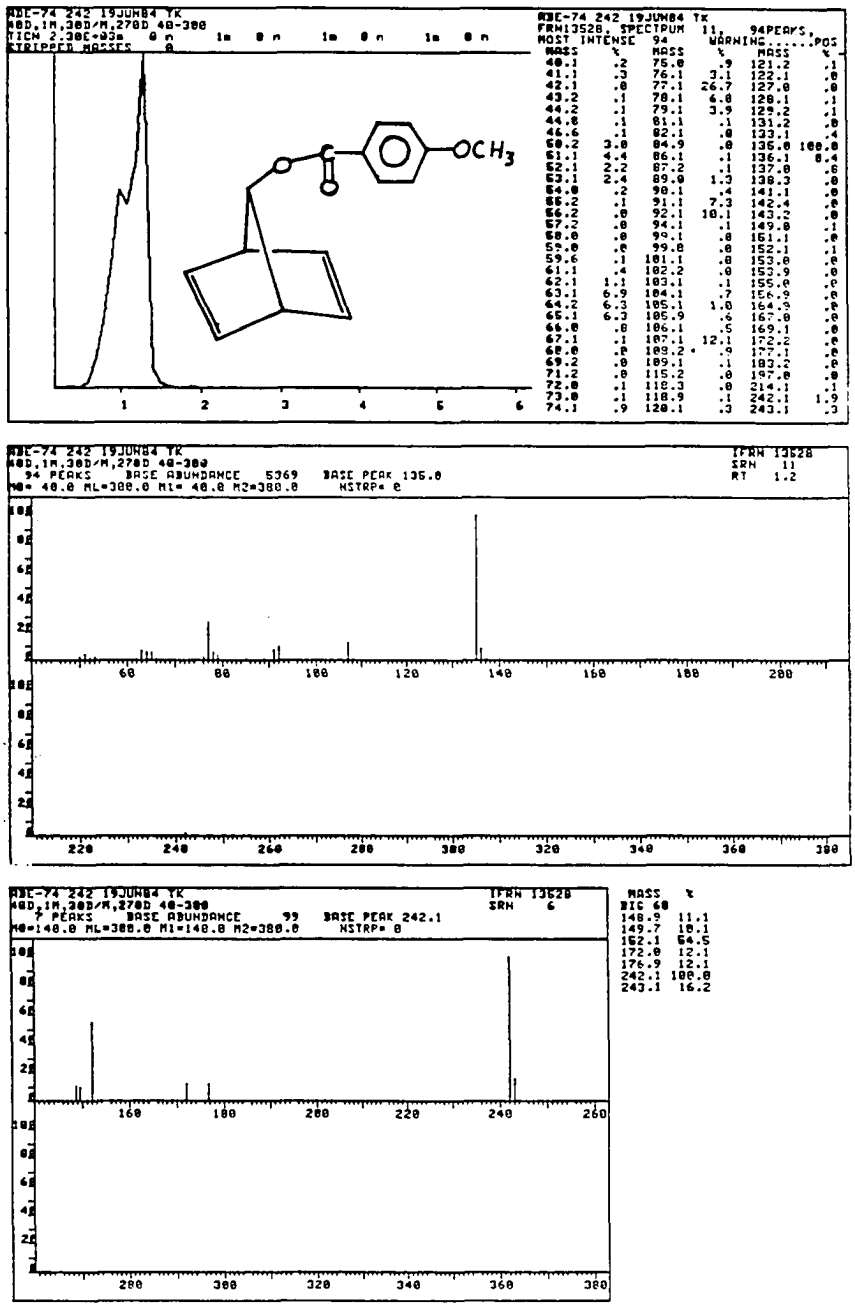

FIGURE IV-42

20 MHz ^{13}C and Spin Echo NMR Spectra of 7-p-Anisoyloxynorbornadiene XVII ($CDCl_3$).

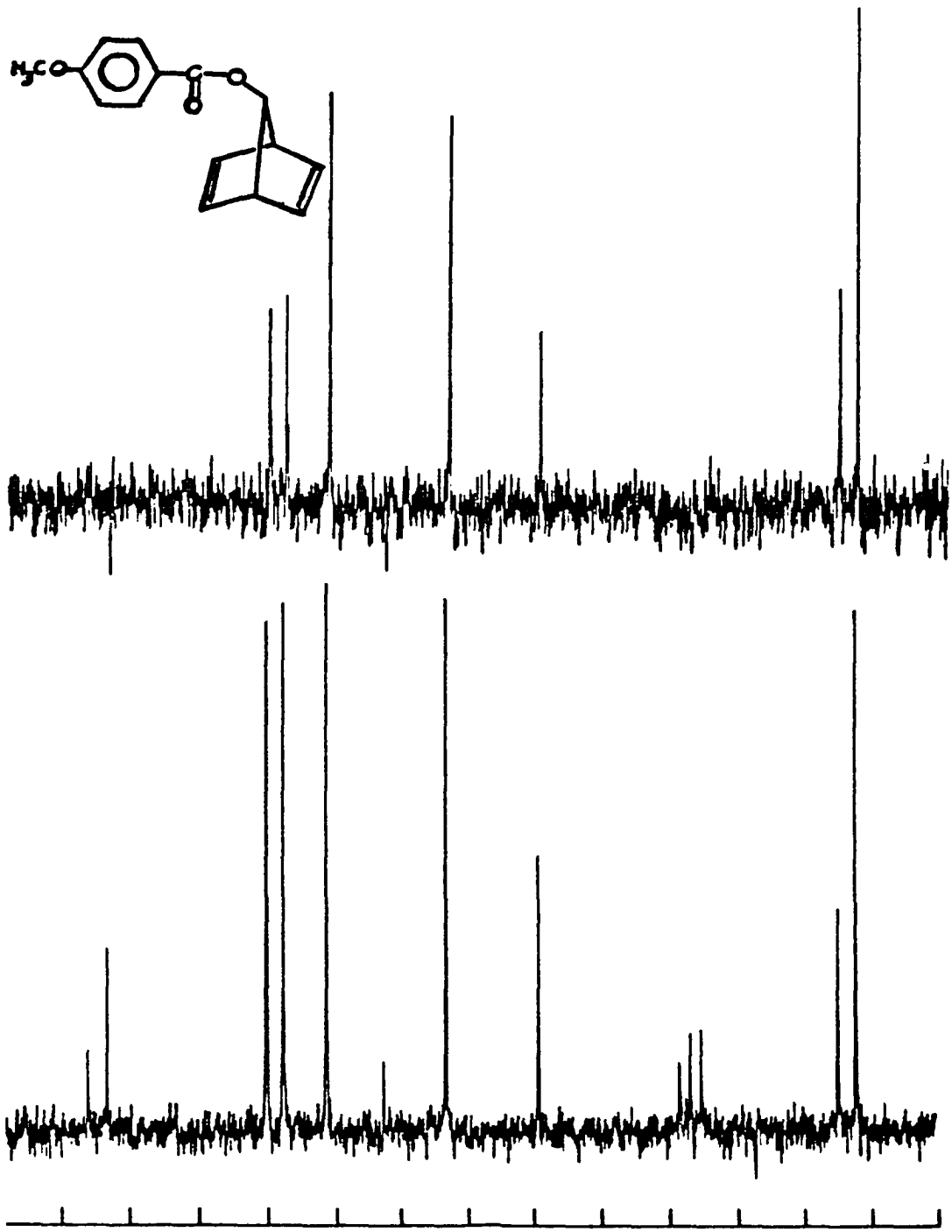

FIGURE IV-43

300 MHz ^{1}H NMR Spectrum of p-Anisoyloxy Cage Compound XIX ($CDCl_3$/TMS).

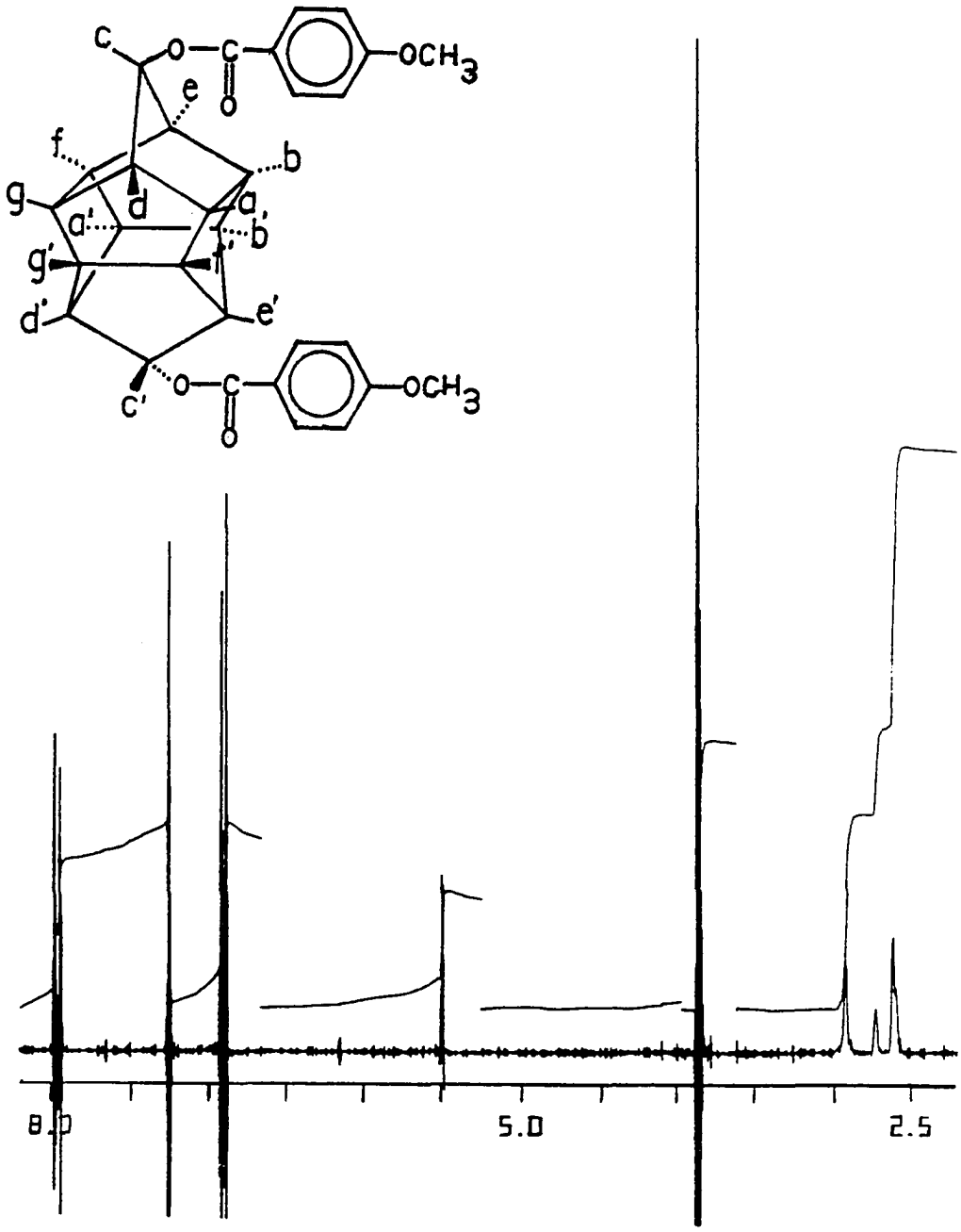

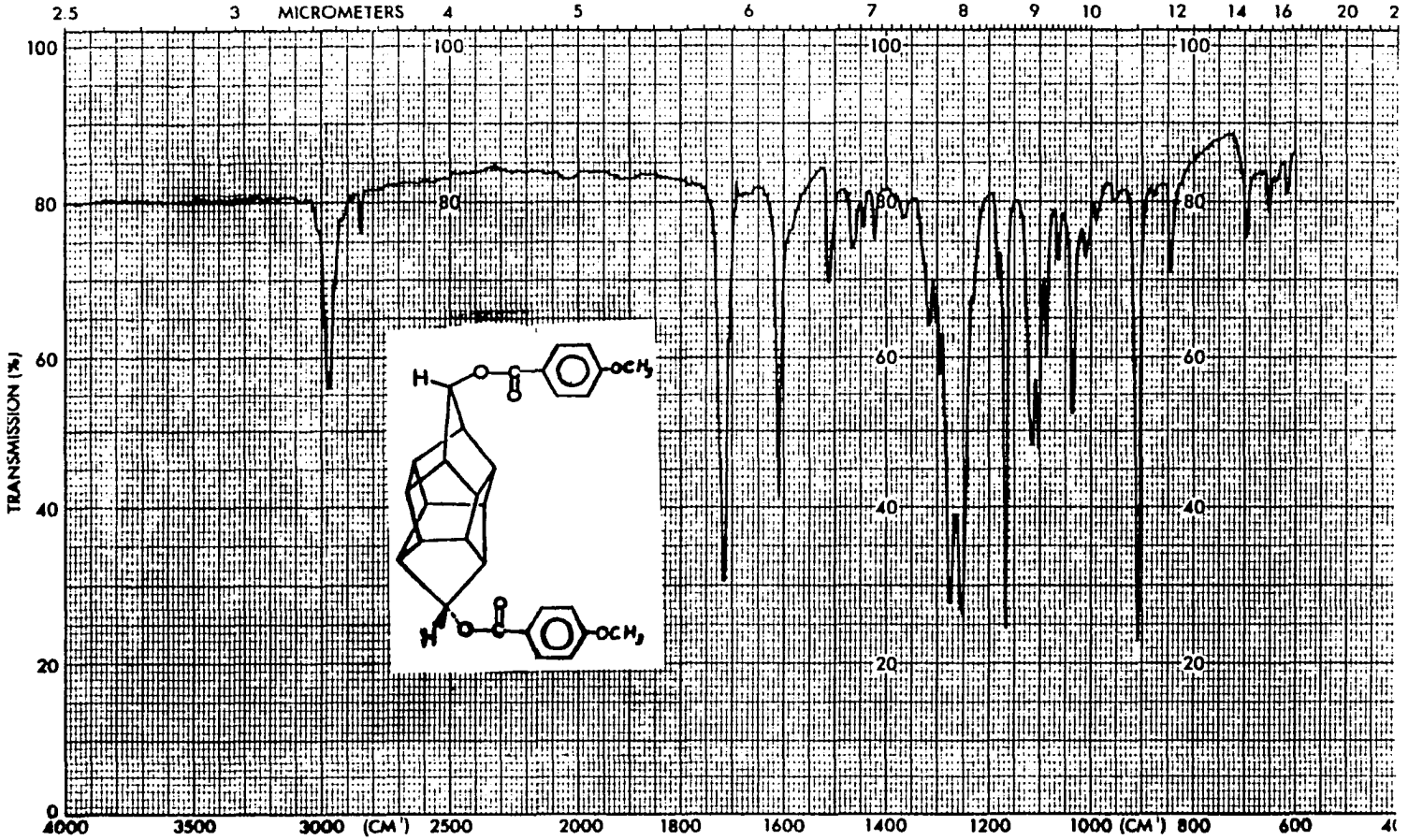

Figure IV-44. IR Spectrum of p-Anisoyloxy Cage Compound XIX.

FIGURE IV-45

Mass Spectrum of p-Anisoyloxy Cage Compound XIX.

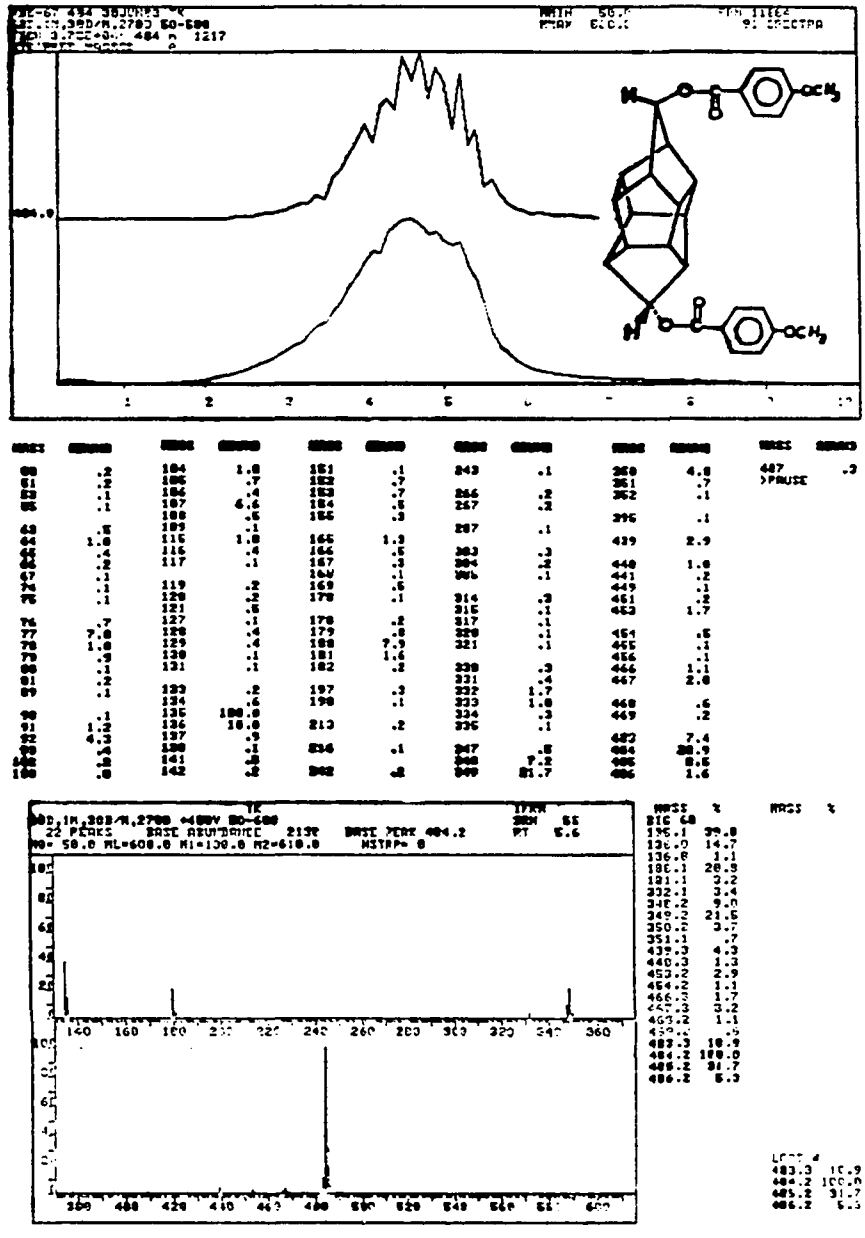

FIGURE IV-46

20 MHz ^{13}C and Spin Echo NMR Spectra of p-Anisoyloxy Cage Compound XIX ($CDCl_3$).

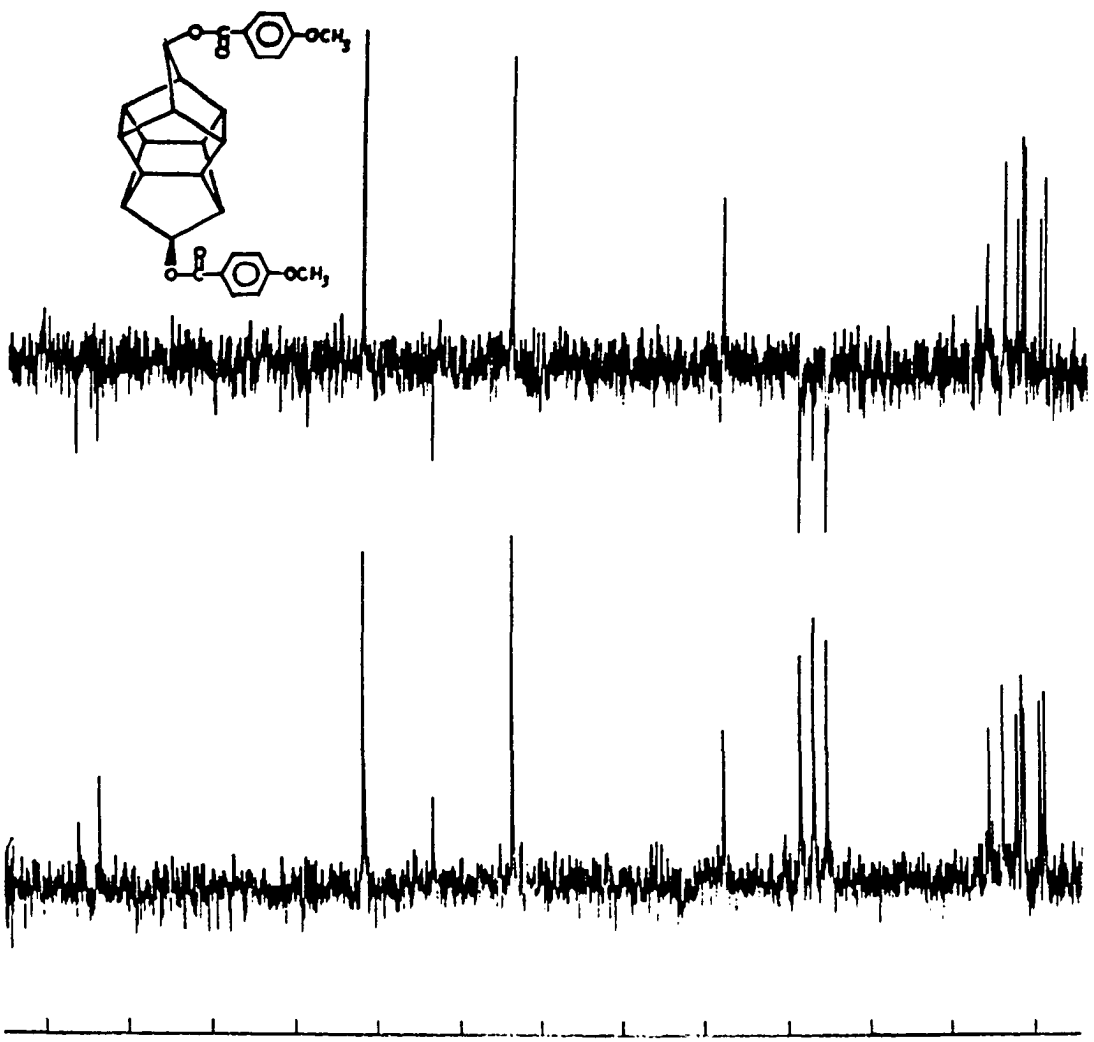

FIGURE IV-47

300 MHz ^{1}H HOMCOR NMR Spectrum of p-Anisoyloxy Cage Compound XIX ($CDCl_3$).

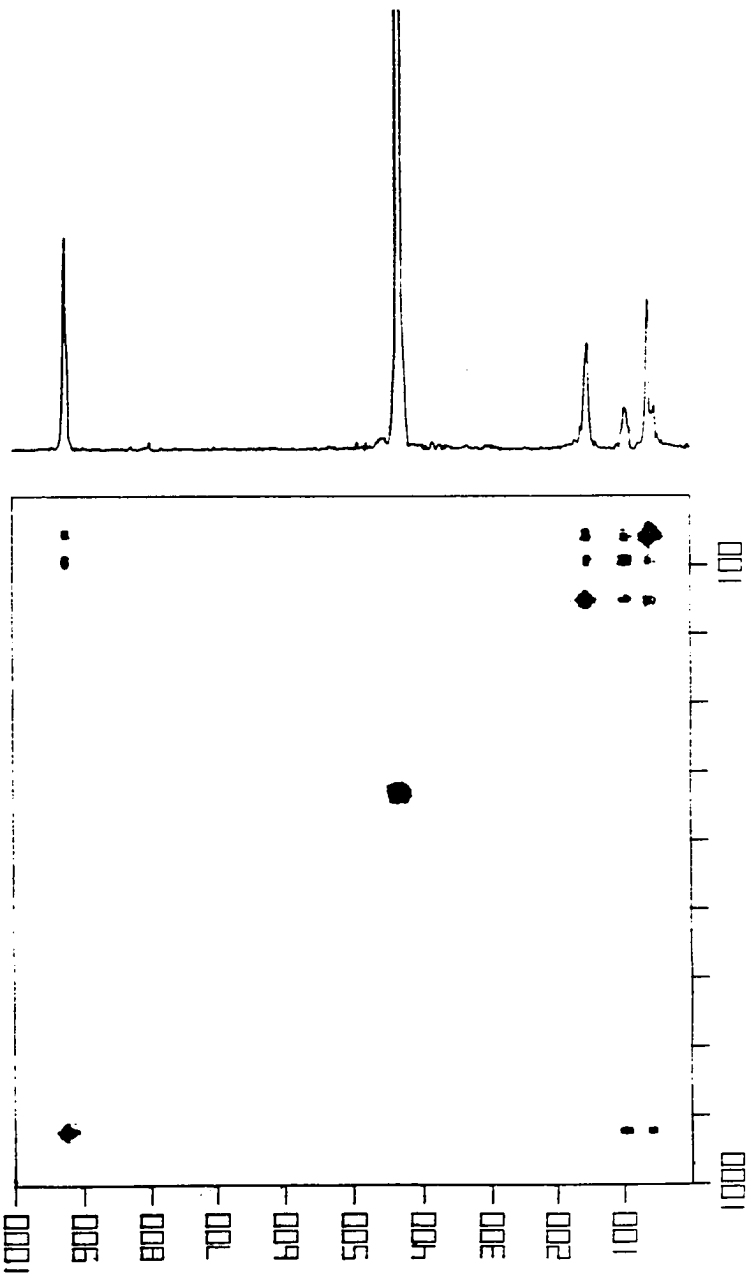

FIGURE IV-48

300 MHz ^{1}H NMR Spectrum of AXTXA p-Anisoyloxy Dimer Ketone XVIII ($CDCl_3$/TMS).

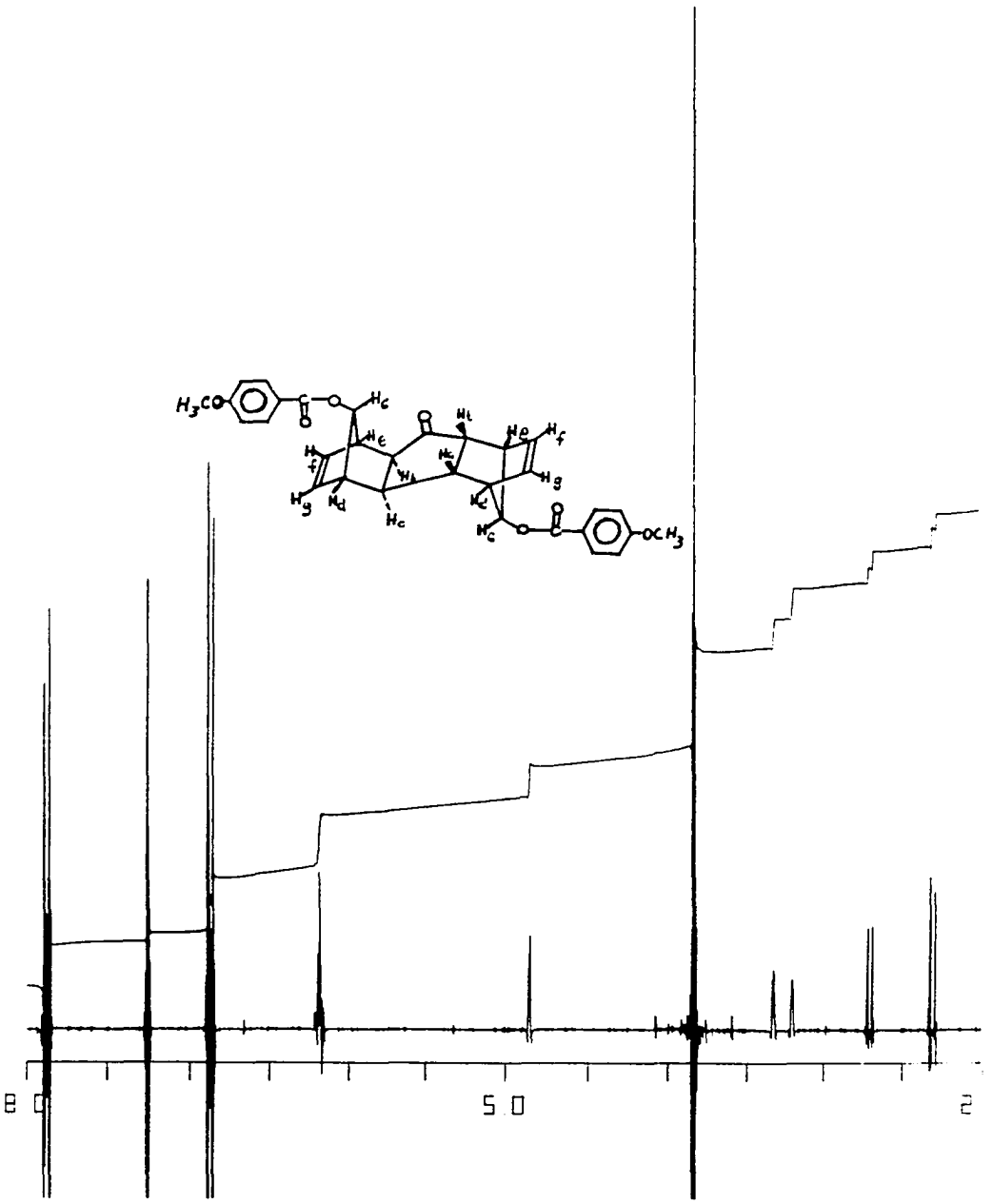

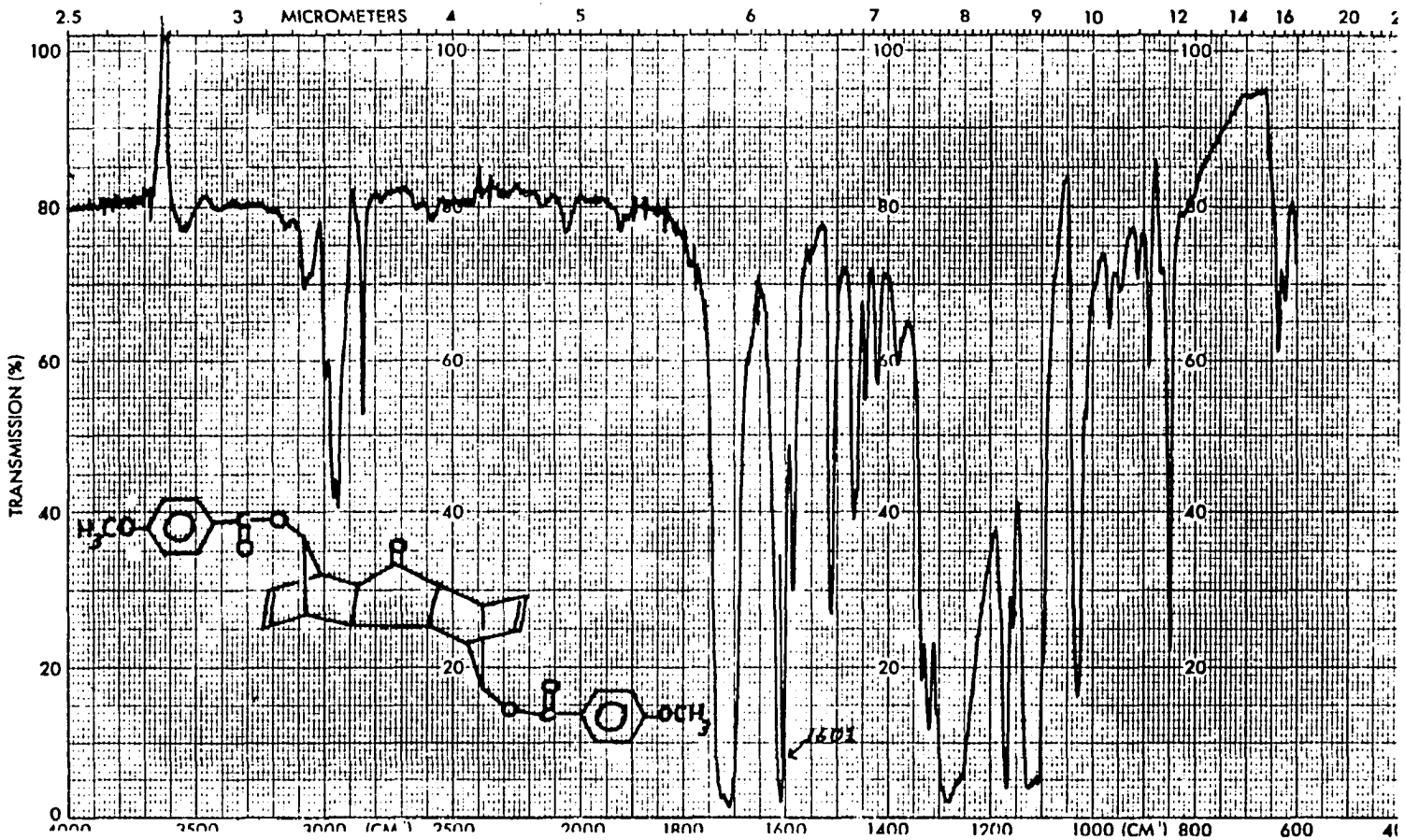

Figure IV-49. IR Spectrum of AXTXA p-Anisoyloxy Dimer Ketone XVIII ($CHCl_3$/TMS).

FIGURE IV-50

Mass Spectrum of AXTXA p-Anisoyloxy Dimer Ketone XVIII.

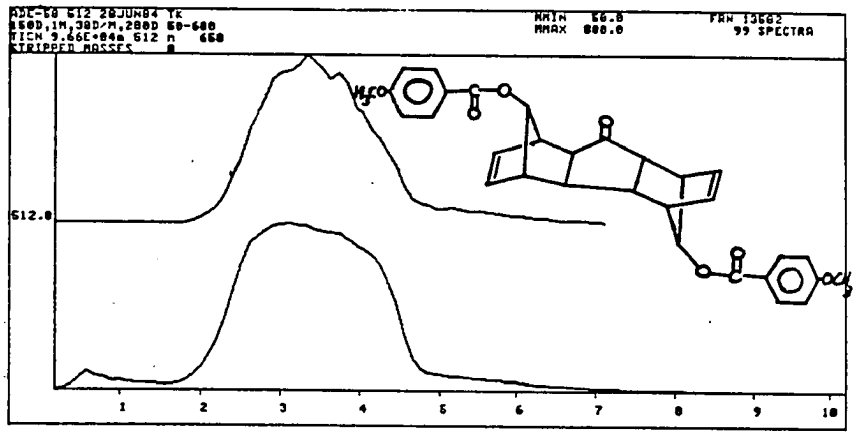

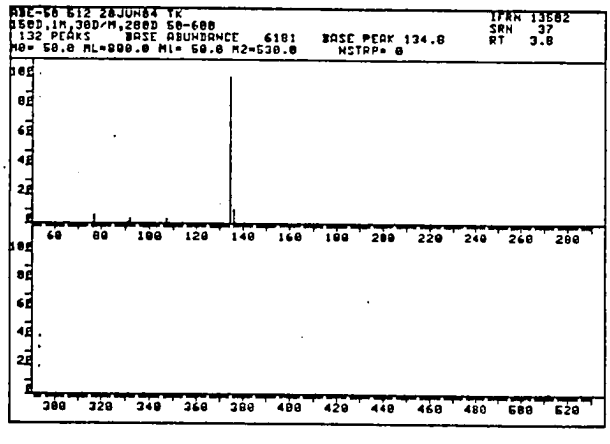

MASS	%	MASS	%
BIG 60		128.9	.1
60.1	.1	130.9	.2
61.1	.2	132.0	.1
63.1	.2	133.0	.2
65.1	.5	134.0	100.0
63.1	.5	136.0	9.7
64.2	.7	136.9	.9
65.0	.7	141.0	.1
66.0	.1	144.0	.4
75.1	.2	144.9	.1
76.1	.5	152.0	.2
77.0	6.1	153.0	.1
78.0	.6	157.0	.2
79.1	.5	164.9	.1
81.0	.2	166.0	.1
83.0	.1	167.1	.1
89.0	.1	172.0	.4
91.1	1.1	207.0	.2
92.1	3.0	208.0	.2
93.0	.3	208.9	.1
103.1	.3	216.0	.4
104.1	.6	217.0	.1
105.0	.4	296.0	.5
106.1	.2	297.0	.1
107.1	3.5	499.0	.1
108.1	.3	612.0	.9
115.0	.7	613.0	.3
116.1	.4		
117.1	.1		
119.0	.2	LAST 4	
120.0	.1	612.0	.9
121.0	.2	613.0	.3
127.1	.1	614.0	.1
129.1	.1	627.9	.0

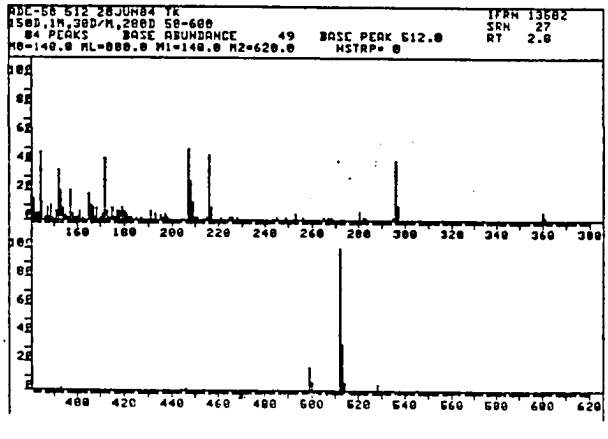

MASS	%	MASS	%
BIG 60		191.0	6.1
141.0	14.3	193.0	4.1
142.0	4.1	196.0	4.1
143.0	4.1	197.0	4.1
144.0	46.9	198.0	2.0
144.9	12.2	207.0	49.0
147.0	0.2	208.0	26.5
148.0	2.0	209.0	12.2
148.9	10.2	210.0	2.0
149.9	2.0	211.0	2.0
151.0	6.1	215.1	2.0
152.0	34.7	216.0	44.9
153.0	20.4	217.0	0.2
154.0	0.2	221.0	2.0
155.0	4.1	225.0	2.0
156.0	2.0	226.0	2.0
157.0	20.4	263.0	4.1
159.0	4.1	280.9	6.1
161.0	6.1	296.0	40.8
165.0	10.4	297.0	10.2
166.0	10.2	368.0	6.1
167.1	0.2	499.0	16.3
169.1	2.0	500.0	6.1
169.9	0.2	612.0	100.0
171.0	4.1	613.0	32.7
172.0	42.9	614.0	6.1
173.0	6.1	620.0	4.1
175.0	0.2		
176.0	2.0		
177.0	6.1	LAST 4	
178.0	6.1	612.0	100.0
179.1	0.2	613.0	32.7
180.1	6.1	614.0	6.1
181.0	4.1	620.0	4.1

FIGURE IV-51

20 MHz ^{13}C and Spin Echo NMR Spectra of AXTXA p-Anisoyloxy Dimer Ketone XVIII ($CDCl_3$).

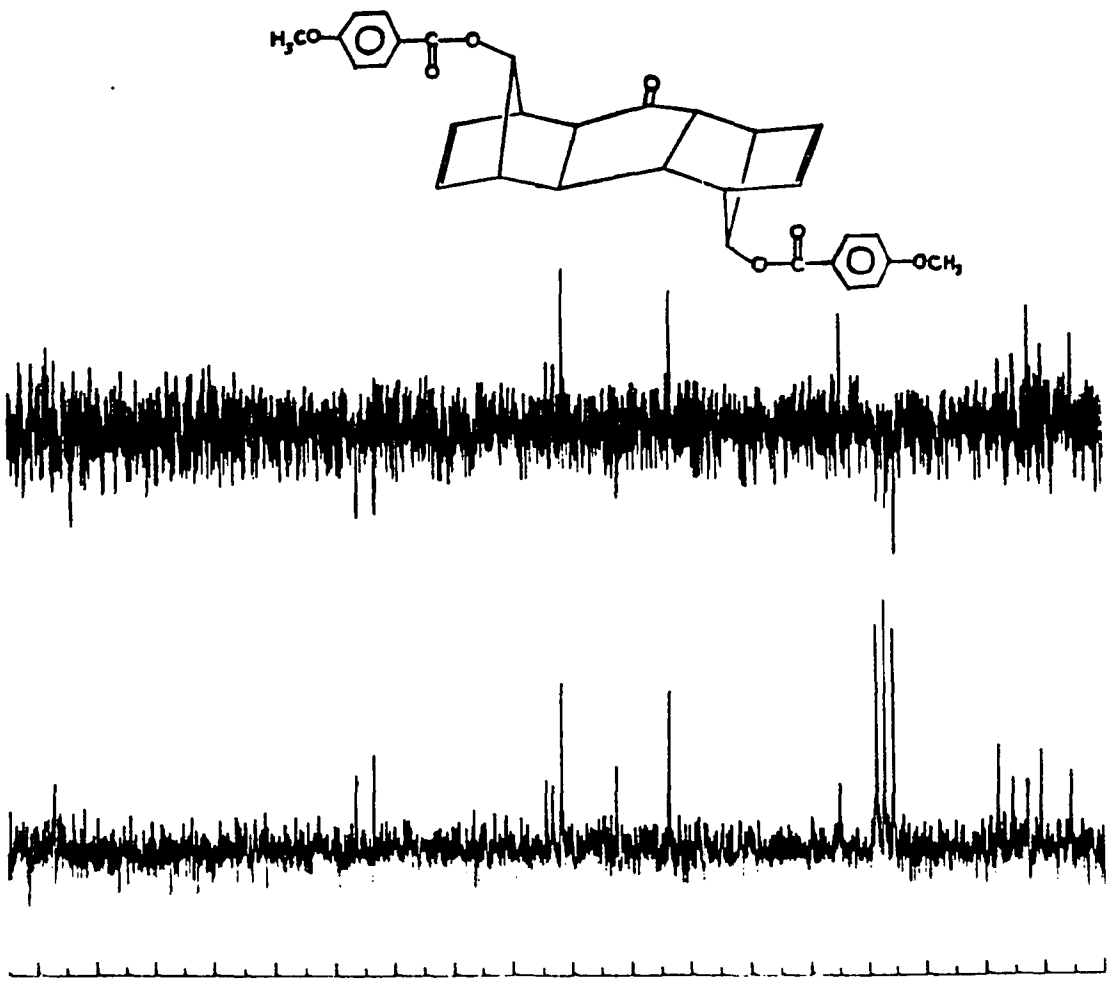

identified. However, partial identification of the residue was based on mass spectral data which show a molecular ion of m/e 514 which might be attributed to the bisnorbornyl ketone shown in Fig IV-52.

FIGURE IV-52

Possible Fragment of Molecular Weight 514.

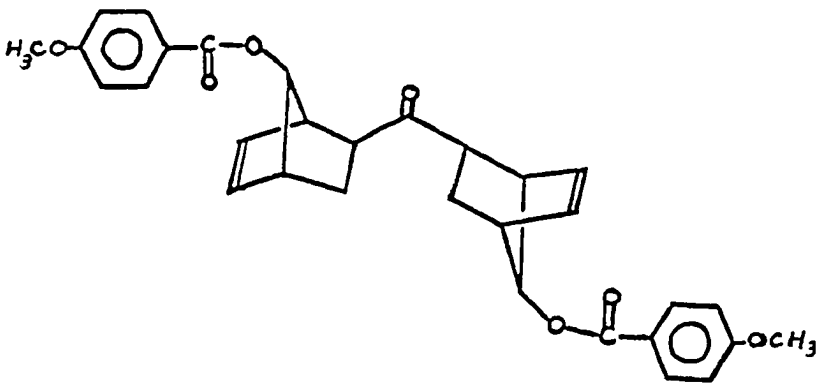

The presence of such a ketone has been demonstrated in $Ni(CO)_4$ promoted coupling of norbornadiene[1,7,21] and has been demonstrated in this lab upon reacting 7-t-butoxynorbornadiene with $Fe(CO)_5$.[22]

Compound XIX (as with XVI) was assigned its structure based on: (i) comparison of its NMR (Fig IV-43) and IR (Fig IV-44) spectra with those of V and also of XVI; (ii) accurate molecular weight determination by mass spectrometry; (iii) elemental analysis of its carbon and hydrogen content; (iv) IR, ^{13}C, spin echo, and HOMCOR spectra which contain the appropriate absorptions. The HOMCOR spectrum (Fig IV-47) identifies the bridgeheads located at δ 2.74 and 2.62 by their coupling to bridge proton $H_c(H_{c'})$ (δ 5.49).

As with AXTXA compound XV, complete configurational determination and proton assignment (Fig IV-48) of AXTXA XVIII was accomplished by a series of ^1H decoupling experiments. The AB pattern centered at δ 2.51 [i.e., $^{\delta}H_a(H_{a'})$ = 2.31, $^{\delta}H_b(H_{b'})$ = 2.70, and $^{J}H_a(H_{a'})$-$H_b(H_{b'})$ = 8.22 Hz] confirmed the trans ring juncture. Minimal simplification of $H_d(H_{d'})$ (δ 3.20) and

$H_e(H_{e'})$ (δ 3.32) upon irradiation of $H_a(H_{a'})$ and $H_b(H_{b'})$, respectively, confirmed the XTX structure (i.e., $^{J}H_{endo}H_{bridgehead}$ ≈ 0.0 Hz).[17] Proton $H_f(H_{f'})$ (δ 6.21) was assigned by decoupling $H_e(H_{e'})$, and $H_g(H_{g'})$ (δ 6.18) was assigned by decoupling $H_d(H_{d'})$. The position of the 7-substituent was determined by decoupling the vinyl protons and observing a sharpening and narrowing of $H_c(H_{c'})$ (δ 4.85) which indicates anti 7-substituent stereochemistry.

Metal-catalyzed dimerizations of norbornadiene (NBD) have been studied quite well.[23] Among the dimers which are produced in these reactions, Binor-S (XXXVI, Fig IV-53a)[24] and the cage compound[25] heptacyclo[6.6.0.0^{2,6}.0^{3,13}.0^{4,11}.0^{5,9}.0^{10,14}]tetradecane (HTCD, XXXV, Fig IV-53b) have been isolated in which endo-cis-endo (N-C-N) coupling has occurred with a high efficiency. Early attempts to verify the structure of XXXV were precluded by crystal twinning.[25] The structure of XXXV was instead inferred by chemical methods.[26a] Dimerization of both compounds has to be initiated by metals capable of holding two norbornadiene ligands facing each other via their endo sides. Intermediates with such a geometry have frequently been proposed.

Recently, Chow reported the characterization and single crystal X-ray structure of bis(norbornadieny)dicarbonylmolybdenum complex XXXVII (Fig IV-53c). This isolable intermediate is produced during the reaction of norbornadiene with $Mo(CO)_6$, and leads directly to the formation of XXXV.[27] The geometry of the complex indicates that the two norbornadiene ligands bind to the metal in a tilted fashion in which one double bond lies closer to the metal than the other. The fact that the two ligands are also oriented 90° with respect to each other, logically explains why the cage molecule XXXV is formed in preference to the still unknown structure heptacyclo-[7.4.1.0^{2,8}0.3,7.0^{4,12}.0^{6,11}.0^{10,13}]tetradecane (XXXVIII, Fig IV-53d).

The synthesis of XXXVII was accomplished by refluxing a solution

FIGURE IV-53

Intermediates in the Metal-Catalyzed Dimerizations of Norbornadiene.

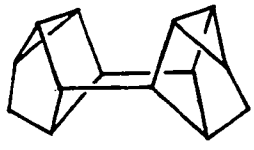

XXXVI

a

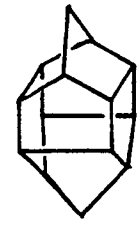

XXXV

b

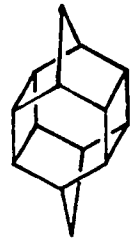

XXXVIII

d

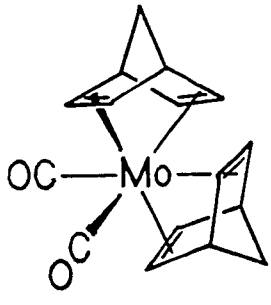

XXXVII

c

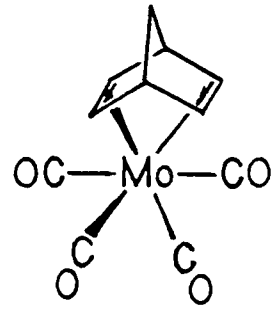

XXXIX

e

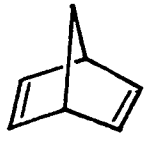

NBD

$\xrightarrow{Mo(CO)_6}$ XXXIX $\longrightarrow$ XXXVII $\longrightarrow$ XXXV Eq IV-6

of molybdenum hexacarbonyl (1 equiv.) and norbornadiene (3 equiv.) in petroleum ether (110-140°C) for 40 hours. It was found that the $Mo(CO)_6$-catalyzed dimerization proceeds through four separate stages. At each stage of the reaction the major product could be isolated. The complete sequence was easily monitored by periodically eluting a silica gel TLC plate with n-hexane. The formation of mono(norbornadiene)tetracarbonylmolybdenum (XXXIX, Fig IV-53e) was observed first, reaching its optimal yield (55%) at ca. 20 hours, and was gradually transformed to XXXVII until it completely disappeared. Continuous refluxing for 110 hours destroyed XXXVII to give XXXV as the only major product in a yield of 26%. This is the highest yield ever reported for XXXV. The well-defined reaction sequence of NBD → XXXIX → XXXVII → XXXV (Eq IV-8) is uniquely different from analogous reactions which generally produce several isomeric dimers simultaneously.

Cage compound XXXV has continued to fascinate organic chemists.[26] Attempts to functionalize XXXV by direct substitution of C-H bonds using electrophilic or free-radical reagents have not been successful.[28] Compounds XVI and XIX discussed above are, to our knowledge, the only known functionalized HCTD's other than the 13,14-di-t-butoxy derivative (V)[1] which was listed in Table IV-1. The ester substituents of XVI and XIX now permit expansion of the meager list of 7-functionalized HCTD's to include cage diol (XXXX) and cage diketone (XXXXI) shown below.[29]

Cage diesters XVI and XIX are most conveniently isolated by precipitation from the crude norbornadiene derivative-iron pentacarbonyl reaction mixture by dilution with an equal volume of absolute ethanol. Hydrolysis of XVI and XIX was effected by refluxing in an excess ethanolic KOH solution; the cage compound heptacyclo[$6.6.0.0^{2,6}.0^{3,13}.0^{4,11}.0^{5,9}.0^{10,14}$]tetradecane-7,12-diol (XXXX, Figs IV-54 through IV-57 for NMR, IR, mass, and ^{13}C spectra, respectively) was obtained thereby in 85% yield. Oxidation of XXXX with pyridinium chlorochromate in methylene chloride-dimethyl

FIGURE IV-54

300 MHz ^{1}H NMR Spectrum of Cage Diol XXXX (Pyr-d_5/TMS).

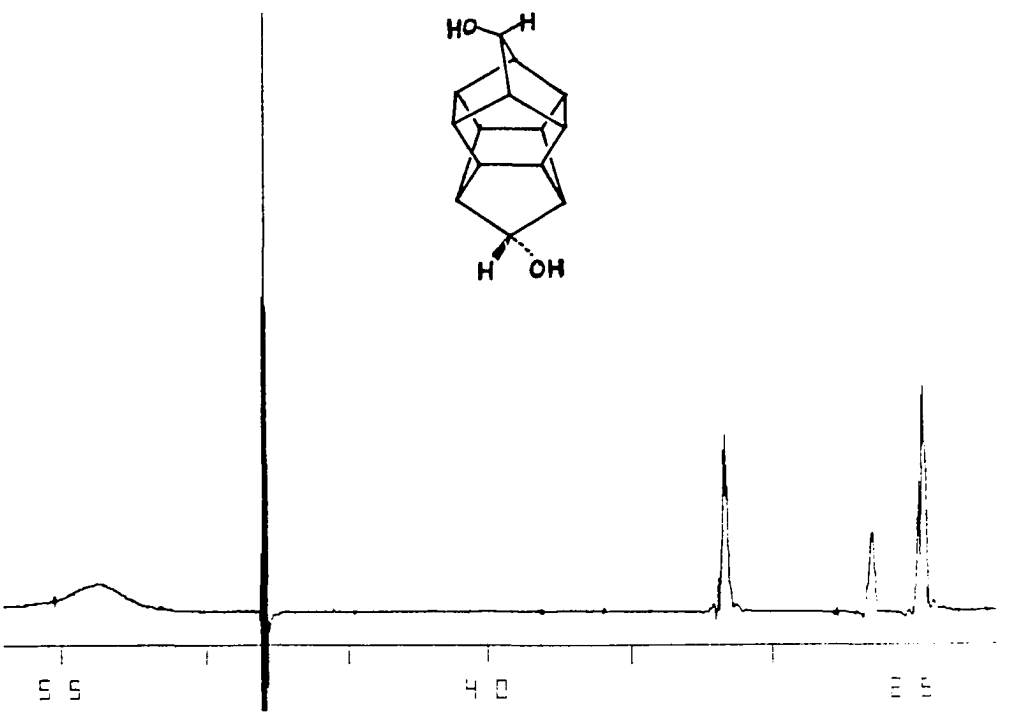

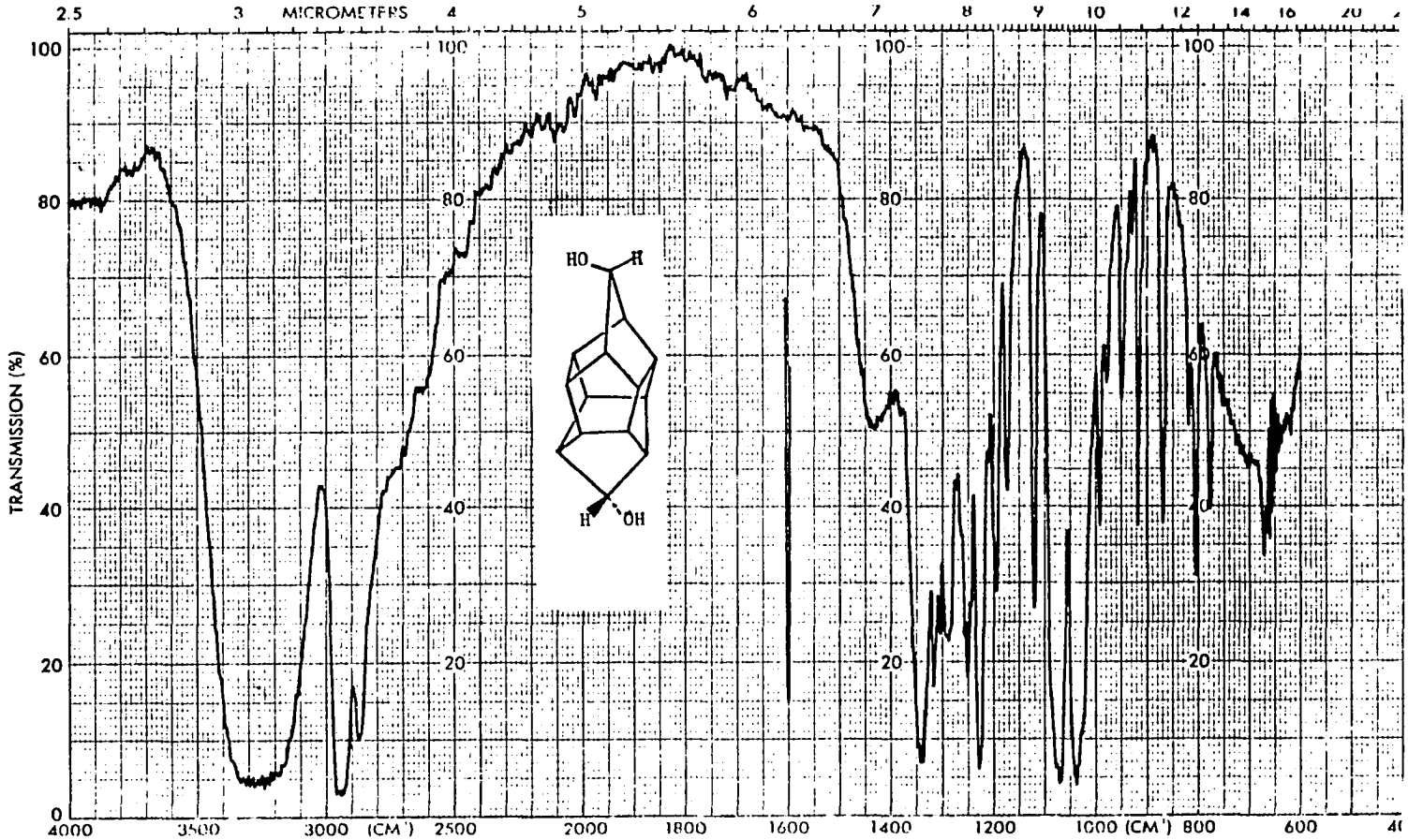

Figure IV-55. IR Spectrum of Cage Diol XXXX (KBr).

FIGURE IV-56

Mass Spectrum of Cage Diol XXXX.

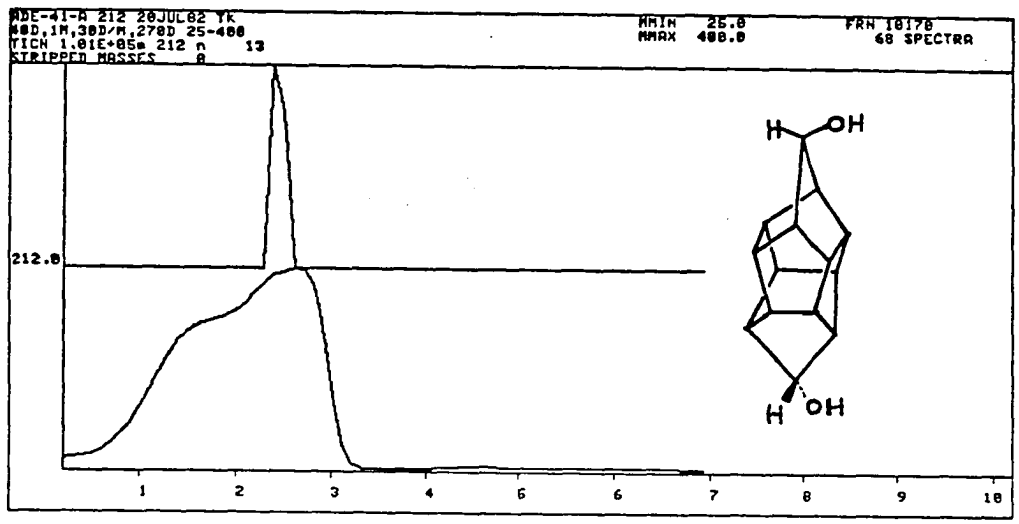

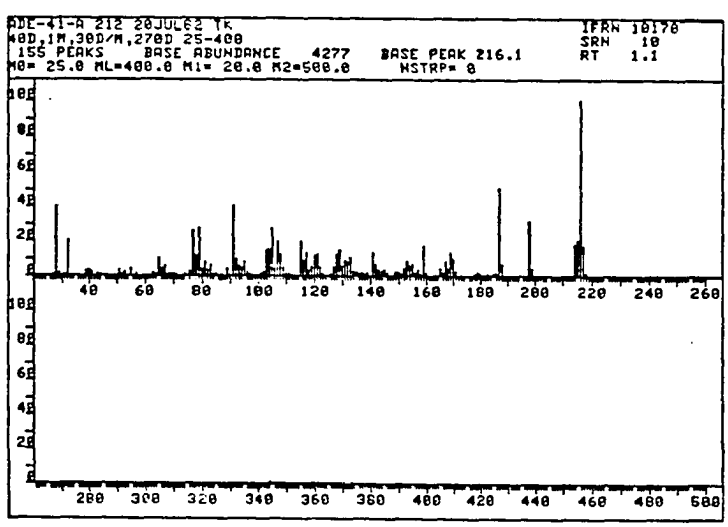

MASS	%	MASS	%
BIG 60		127.2	5.3
28.1	40.3	128.2	12.3
32.1	20.0	129.0	15.2
65.2	4.7	130.0	5.0
65.1	10.1	131.0	8.9
66.1	4.3	132.0	8.5
67.1	6.0	133.0	10.5
77.1	26.1	141.1	13.5
78.1	11.5	142.1	7.1
79.1	27.3	152.2	4.3
80.1	4.7	153.0	8.4
81.1	8.5	154.1	6.2
83.1	7.1	155.2	6.9
89.1	4.3	159.2	17.3
91.1	40.7	165.1	4.5
92.1	9.7	167.1	8.2
93.1	6.0	168.1	4.5
94.1	5.5	169.1	13.0
95.1	8.2	170.1	9.6
103.1	15.2	187.2	50.5
104.2	14.7	188.2	6.9
105.0	27.0	198.1	31.7
106.0	4.1	199.2	4.4
107.1	19.3	214.1	18.1
108.2	12.0	215.1	20.0
109.0	5.4	216.1	100.0
115.1	19.5	217.1	17.5
116.2	9.5		
117.1	12.9		
118.2	3.9	LAST 4	
119.1	5.1	216.1	100.0
120.1	11.5	217.1	17.5
121.1	12.1	218.1	1.6
122.1	4.0	344.2	.9

FIGURE IV-57

20 MHz ^{13}C NMR Spectrum of Cage Diol XXXX (Pyr-d_5/TMS).

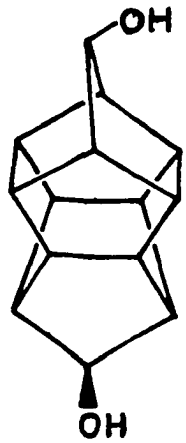

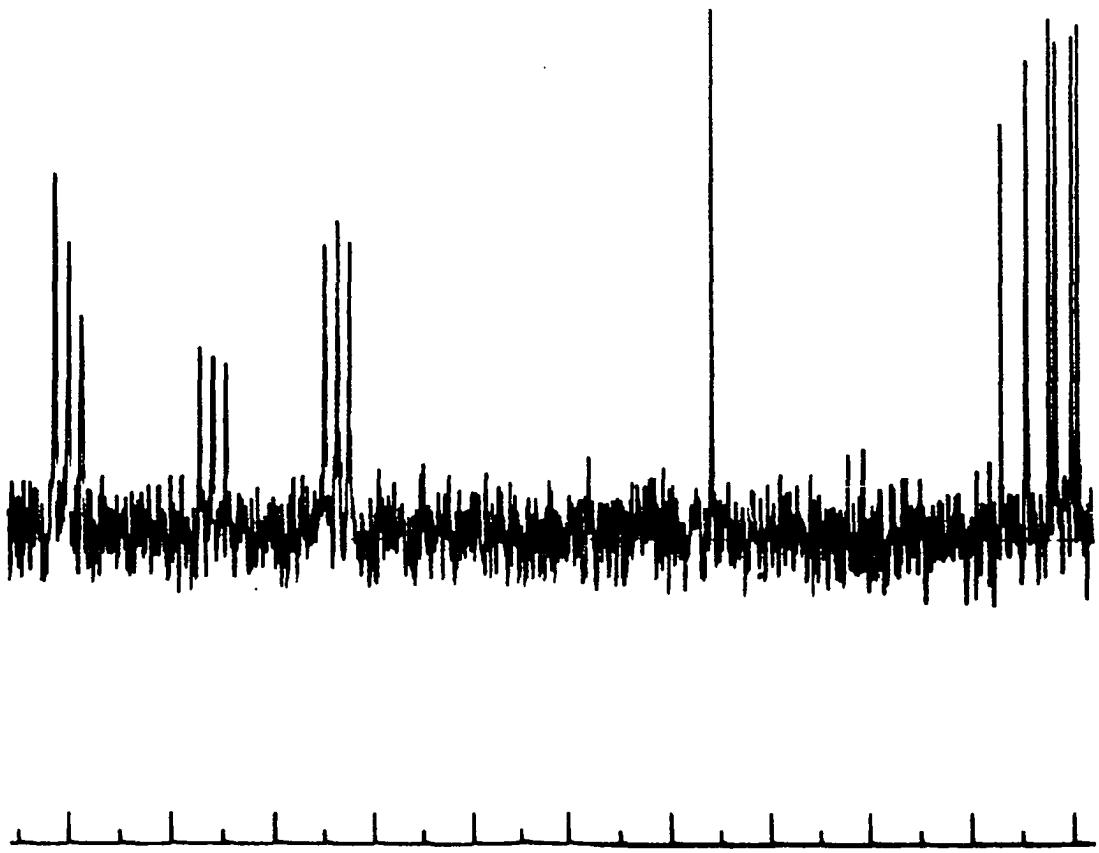

sulfoxide solution[30] afforded cage diketone heptacyclo[6.6.0.-$0^{2,6}.0^{3,13}.0^{4,12}.0^{5,9}.0^{10,14}$]tetradecane-7,12-dione (XXXXI, Figs IV-58 through IV-61 for NMR, IR, mass, and ^{13}C spectra, respectively) in 93% yield.

Compound XXXXI, like the parent hydrocarbon (HCTD, XXXV), possesses unusual symmetry properties. It is one of the rare existing rigid, polycyclic organic molecules that belongs to point group D_{2d}. Compound XXXXI is a dendroasymmetric molecule with a perpendobiplanar structure (i.e., XXXXI possesses fourfold alternating axial symmetry) and, in addition, it contains a C_2 rotation axis that is coincident with its major axis.[31]

Cycloreversion of XXXXI to 2 mol each of benzene and carbon monoxide is expected to be a highly exoergic process. However, this pericyclic reaction is forbidden to occur thermally in a concerted fashion due to the restraints imposed by orbital symmetry considerations.[32] Accordingly, the exothermicity of this process may well be offset by a relatively high activation energy barrier. Indeed, XXXXI is thermally stable; it can be stored for months at ambient temperatures. Also, a cursory high resolution mass spectral study of XXXXI revealed no detectable quantities of carbon monoxide upon electron impact at elevated temperatures.

It is interesting to compare the 300 MHz ^1H NMR spectra of the compounds from this study which are listed in Table IV-4. The non-aromatic protons of each compound are labeled relative to IX (i.e., compound V from PART I) and were assigned chemical shifts based upon extensive proton decoupling experiments. The table indicates that for XTX compounds XV and XVIII, substitution of benzoyloxy and p-anisyloxy for phenyl and o-anisyl reverses the relative chemical shifts of the syn and anti vinyl protons and results in a downfield shift of 1.61-1.70 ppm for the bridge protons of XV and XVIII. Syn-substitution by benzoyloxy and NTN configuration results in only a 1.45-1.54 ppm downfield shift. SNTNS compound XXXII contains syn and anti bridgehead protons whose

FIGURE IV-58

300 MHz ^{1}H NMR Spectrum of Cage Diketone XXXXI ($CDCl_3$/TMS).

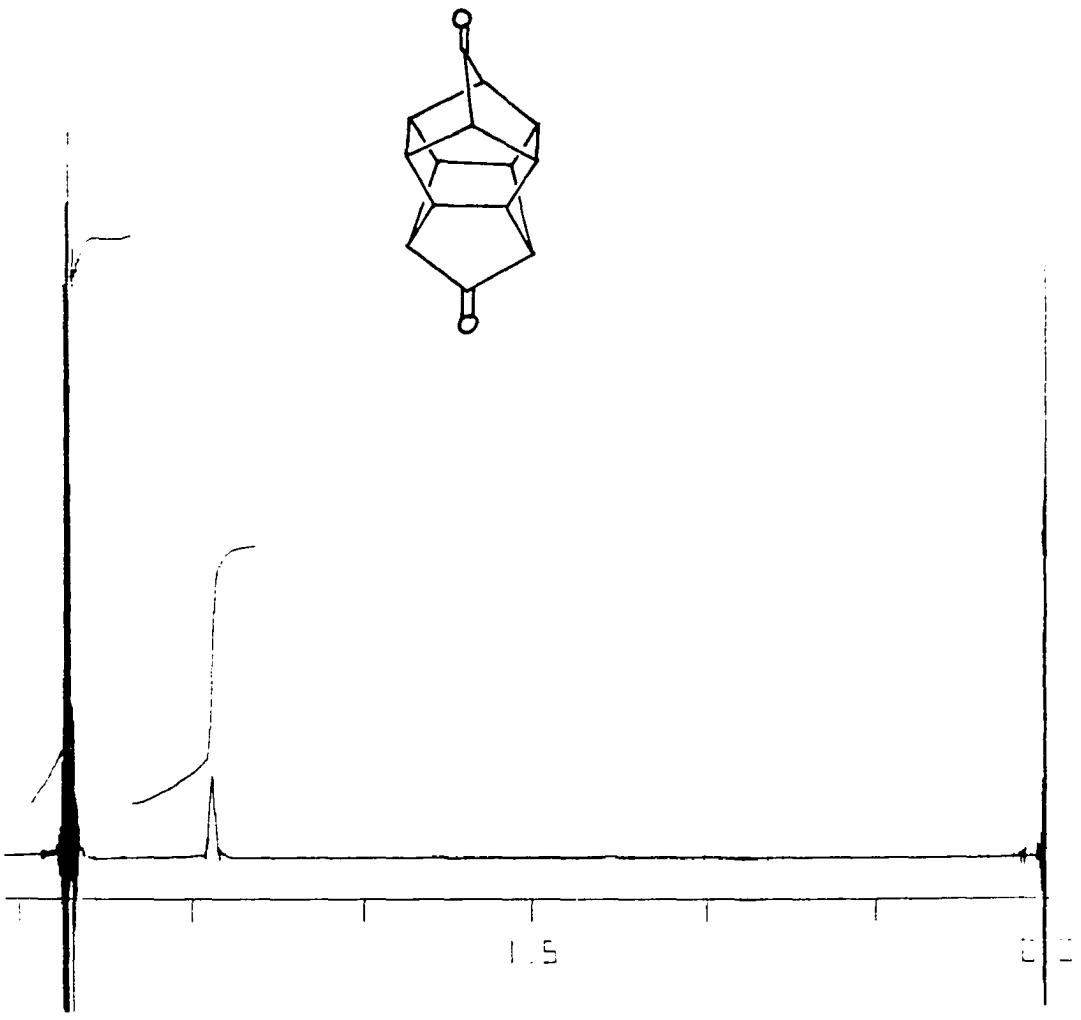

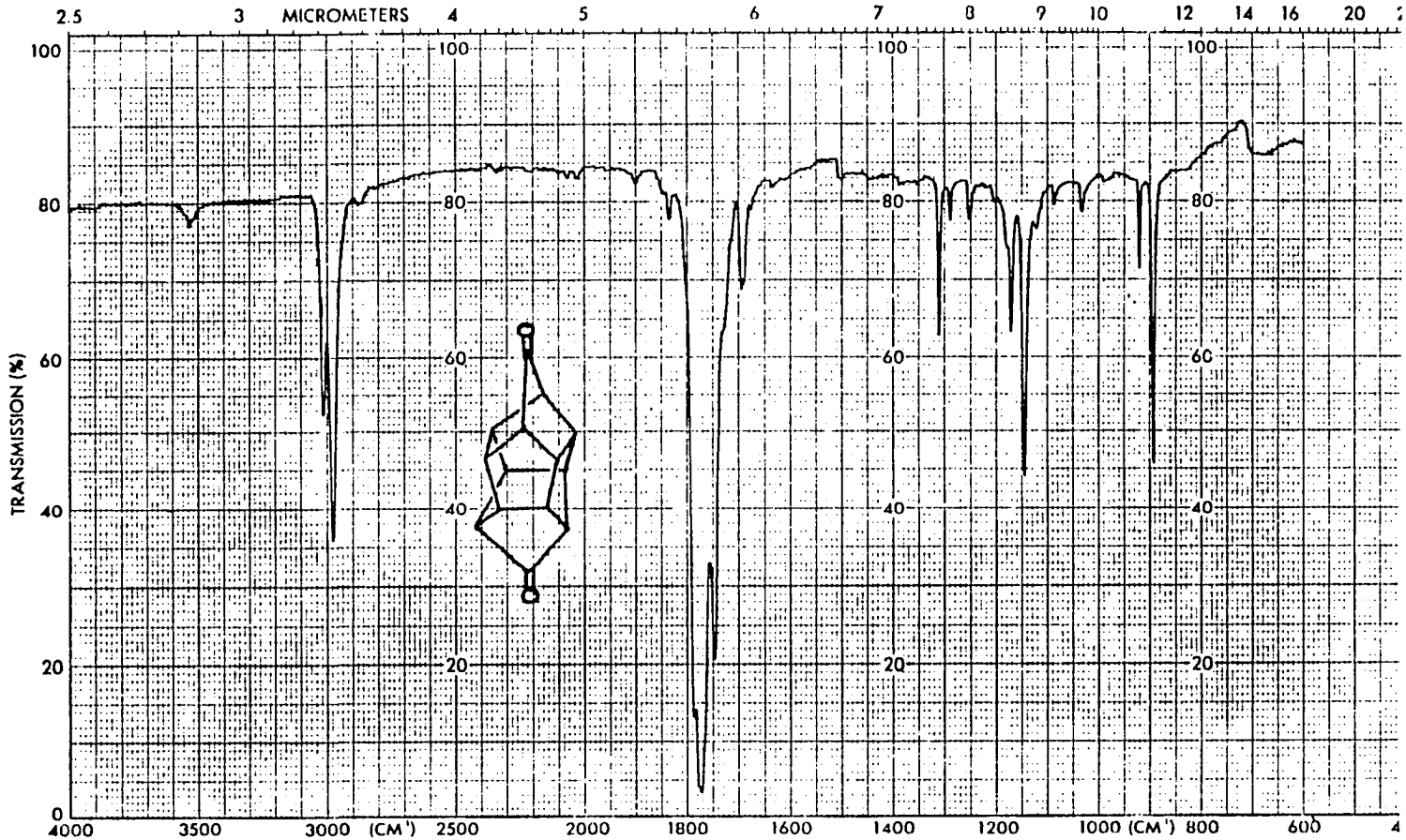

Figure IV-59. IR Spectrum of Cage Diketone XXXXI (CCl_4).

FIGURE IV-60.

Mass Spectrum of Cage Diketone XXXXI.

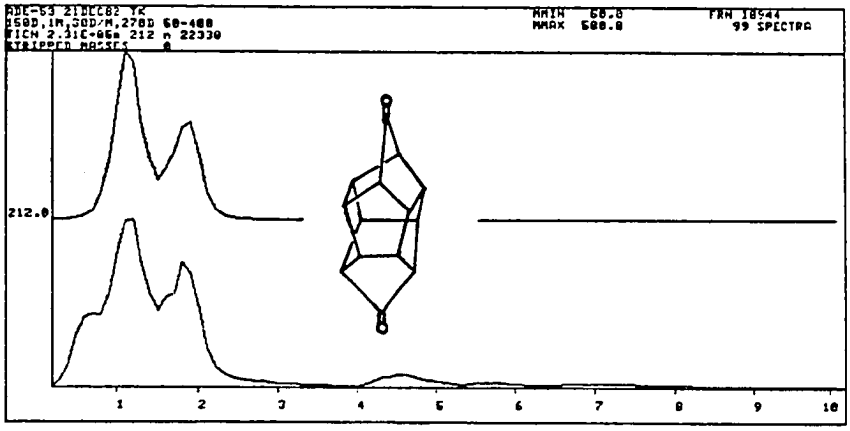

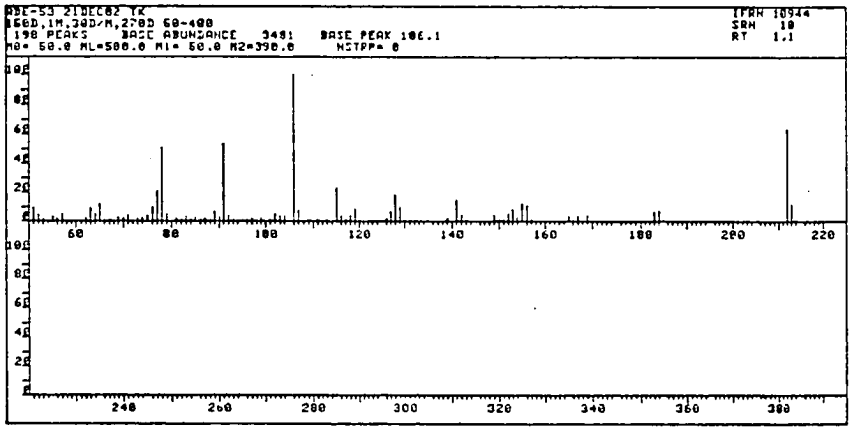

ADE-53 21DEC82 TK
FRN10944, SPECTRUM 10, 198PEAKS, RT 1.10 MIN, BASE PEAK 106.1, 34810.
MOST INTENSE 196 WARNING.....POSSIBLE OVERFLOW

MASS	%	MASS	%	MASS	%	MASS	%	MASS	%	MASS	%
50.1	4.1	81.1	2.0	113.2	1.4	145.0	.3	178.2	.1	210.2	.1
51.1	8.9	82.1	1.1	114.1	.6	146.1	.1	179.2	.2	212.2	64.1
52.1	4.6	83.1	2.5	115.1	22.4	147.1	.4	180.2	.1	213.1	11.2
53.1	2.1	84.2	1.1	116.2	4.0	149.0	4.4	181.2	.3	214.2	1.0
54.1	.4	85.1	2.9	117.2	1.0	150.1	.3	183.2	6.7	215.3	.1
55.1	2.9	86.0	1.0	118.1	3.5	151.1	1.7	184.2	7.6	216.1	.0
56.2	1.7	87.1	1.7	119.1	0.2	152.1	5.1	185.2	1.3	217.2	.1
57.1	5.2	88.1	.9	120.1	.9	153.1	8.1	186.2	.1	218.2	.0
57.9	1.1	89.1	6.9	121.1	.6	154.1	3.5	187.0	.1	218.7	.0
59.1	.5	90.1	3.4	122.2	.4	155.1	12.1	188.1	.0	219.2	.1
60.1	1.1	91.1	52.3	123.1	.5	156.2	10.7	189.1	.1	220.2	.0
61.1	.6	92.1	4.6	124.2	.3	157.1	1.6	190.1	.0	221.2	.1
62.1	1.0	93.1	.9	125.1	.7	158.2	.2	191.2	.2	222.2	.1
63.1	8.9	94.1	.6	126.1	1.0	159.2	.1	192.1	.1	223.3	.1
64.2	5.3	95.1	1.6	127.2	6.7	160.2	.1	193.3	.1	224.3	.0
65.0	11.7	96.1	.9	128.2	17.7	161.2	.1	194.3	.1	225.2	.0
66.1	1.4	97.1	1.8	129.1	9.9	162.1	.1	195.1	.1	227.3	.0
67.1	1.5	98.1	1.0	130.1	1.1	163.1	.3	196.2	.1	228.2	.4
68.2	.5	99.1	1.7	131.0	.7	166.1	3.5	197.2	.1	229.3	.1
69.1	3.2	100.2	.4	132.0	.3	166.1	1.4	198.1	.1	230.2	.1
70.2	1.0	101.1	1.5	133.0	.3	167.1	3.6	199.1	.1	231.3	.0
71.2	4.1	102.1	5.2	134.0	.4	168.1	.7	200.1	.1	232.3	.0
72.1	.6	103.1	3.7	135.0	.5	169.1	4.6	201.2	.1	233.0	.0
73.1	2.0	104.1	3.6	136.1	.2	170.1	.7	202.2	.1	235.3	.0
74.1	2.5	106.1	100.0	137.0	.4	171.1	.1	203.0	.0	236.3	.0
75.1	3.6	107.1	7.9	138.1	.3	172.1	.1	204.2	.0	237.3	.0
76.1	10.1	108.1	.6	139.1	2.3	173.1	.1	205.2	.1	241.1	.0
77.1	21.0	109.0	.9	141.0	15.0	174.2	.1	206.2	.1	245.1	.0
78.1	51.1	110.1	.5	142.1	4.3	175.1	.1	207.1	.5	246.2	.0
79.1	5.0	111.2	1.0	143.1	.9	176.2	.1	208.1	.1	247.4	.0
80.2	.5	112.2	.5	144.1	.2	177.2	.3	209.1	.1	251.2	.1

FIGURE IV-61

20 MHz ^{13}C NMR Spectrum of Cage Diketone XXXXI ($CDCl_3$).

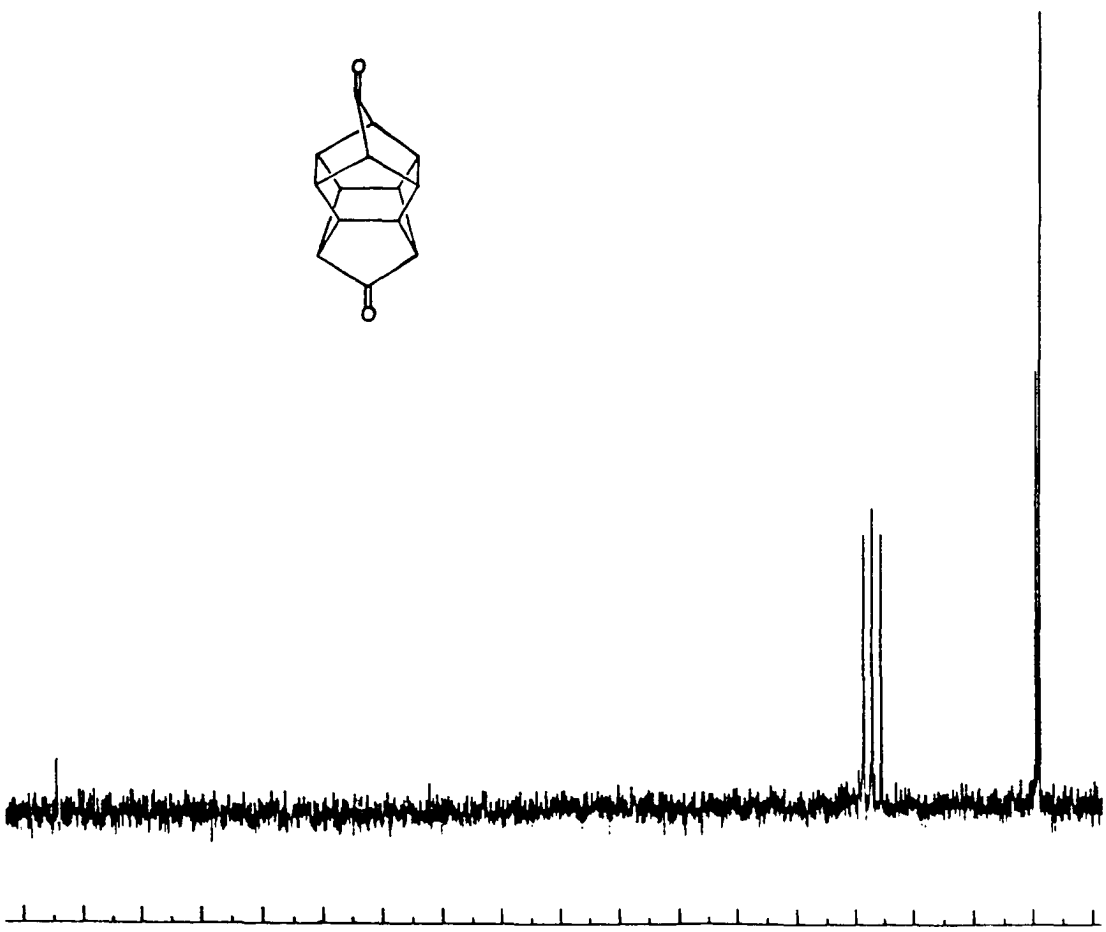

TABLE IV-4

Chemical Shift Comparison of Aliphatic and Vinylic Protons of Some Norbornadiene-Derivative Dimer Ketones Discussed in this Study.

Cmpd.	Fig. #	Vinylic anti	Vinylic syn	Bridge	Bridgehead syn	Bridgehead anti	Cyclopentanone syn	Cyclopentanone anti
IX[a]	I-22	6.11	6.03	3.17	3.45	3.24	2.71	2.25
XI	I-26	6.10	6.06	3.26	3.44	3.24	2.72	2.27
XV	IV-14	6.20	6.22[b]	4.89	3.35	3.22	2.72	2.32
XXXII	IV-18	6.29	6.16	4.71	3.22	3.25[c]	2.95	2.81
XXXIII	IV-22	6.14	6.14[d]	4.87	3.24	3.19	2.03	1.97
		(6.19)	(6.13)	(4.84)	(3.51)	(3.45)	(3.42)	(2.90)
XVIII	IV-49	6.18	6.21[b]	4.85	3.32	3.20	2.70	2.31

(a) Protons are labeled relative to those of IX (i.e., compound VII, PART I, Fig I-22). Chemical shifts were measured at 300 MHz and are recorded in ppm.

(b) Syn [$H_{f(f')}$] and anti [$H_{g(g')}$] vinyl proton chemical shift assignments are reversed relative to IX.

(c) Syn [$H_{e(e')}$] and anti [$H_{d(d')}$] bridgehead chemical shift assignments are reversed relative to IX.

(d) Assignments of the vinylic protons of XXXIII are tentative because of signal overlap, but are believed to be correct. The values in parenthesis correspond to the respective diastereomeric protons on the <u>endo</u>-bound fragment of XXXIII.

chemical shifts are reversed relative to compounds IX, XI, and XVIII. Electron donation by p-methoxy results in an upfield shift of the bridge proton in XVIII relative to that of XV.

Turning attention to reaction 9, 2-carboethoxynorbornadiene (XX)[33] (Figs IV-62 through IV-65, for NMR, IR, mass, and spin echo spectra, respectively) was allowed to react with $Fe(CO)_5$ and the crude reaction product mixture was separated via column chromatography. First eluted was unchanged XX, followed by unknown compounds designated as XXIa and XXIb (cf. NMR spectra of Fig IV-66 and Fig IV-67, respectively). From the NMR spectra it may be seen that the two-hydrogen vinyl signal of XX (δ 6.7) has been eliminated leaving only the vinyl hydrogen adjacent to the carboethoxy group. This is conclusive evidence ruling out the presence of compounds XXV through XXXI listed in Table IV-3 in which one or both carboethoxy groups are substituted on the central cyclopentanone ring. Also apparent is the AB pattern which has been shown to be exclusive to the XTX configuration. The positions of the CH_2 quartet (δ 4.2) and CH_3 triplet (δ 1.3) have not moved significantly from their positions in XX. The bridge hydrogen signal at δ 2.1 in XX has been shifted to higher field (ca. δ 1.5) as a result of the loss of one double bond. A mixture of compounds XXII, XXIII, and XXIV has evidently been isolated as suggested by the number of bridgehead signals (3.1-3.5 ppm) in the figures. All three compounds would be expected to exhibit the AB pattern seen in both figures, but XXII and XXIV would only give rise to two different bridgeheads each. Only compound XXIII can produce more than two bridgehead signals and Fig IV-67 may be indicative of a relatively pure sample in which there is an overlap of two bridgehead proton signals at δ 3.3. Integrations are correct but signal multiplicity is not clear. Other indications that a mixture of diastereomers has been isolated is the lack of resolution (cf. the NMR of XX) of the resonances (particularly in Fig IV-66), the wide melting point range (128-142°C), and the inability to recrystallize

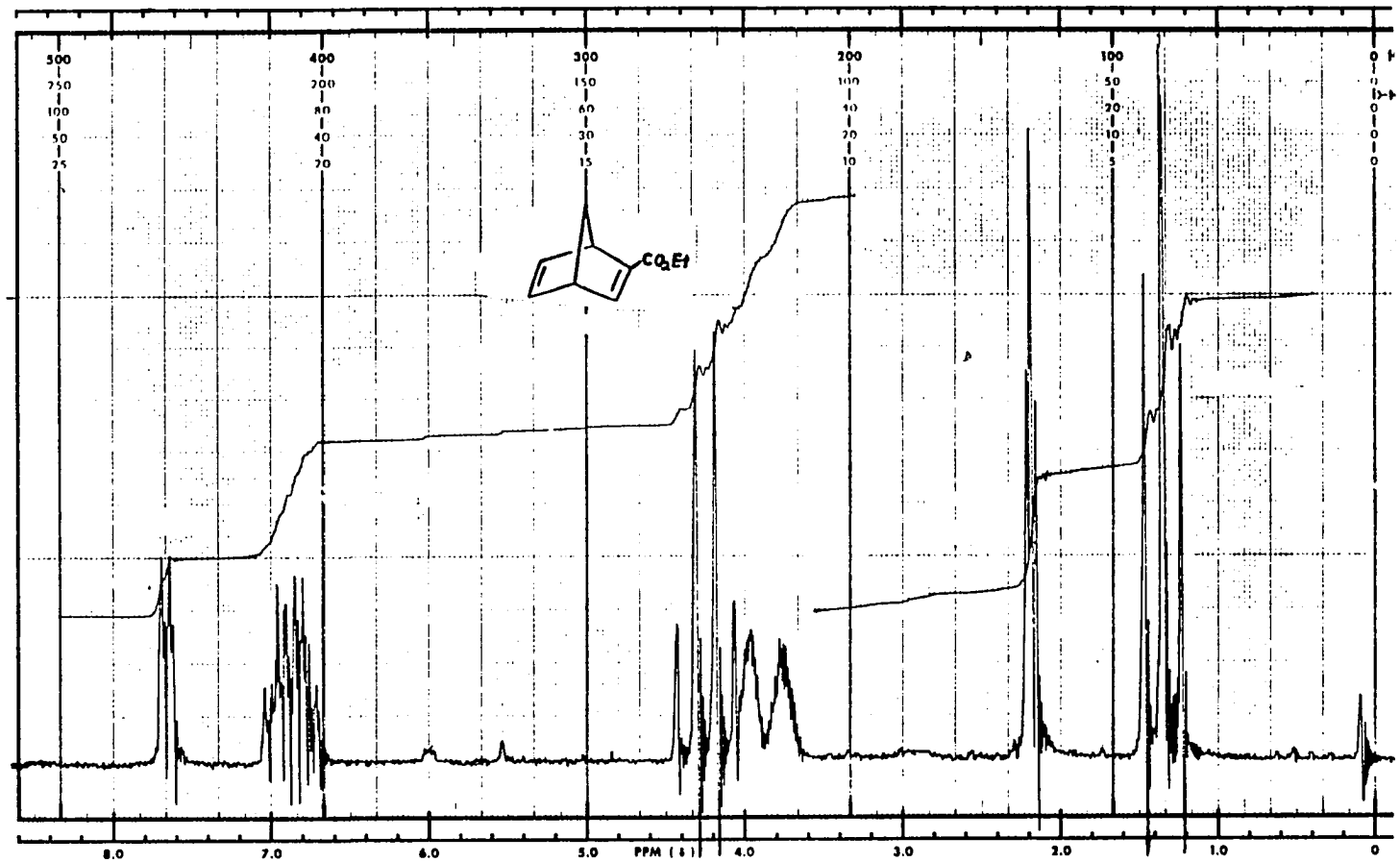

Figure IV-62. 60 MHz ^{1}H NMR Spectrum of 2-Carboethoxynorbornadiene XX ($CDCl_3$/TMS).

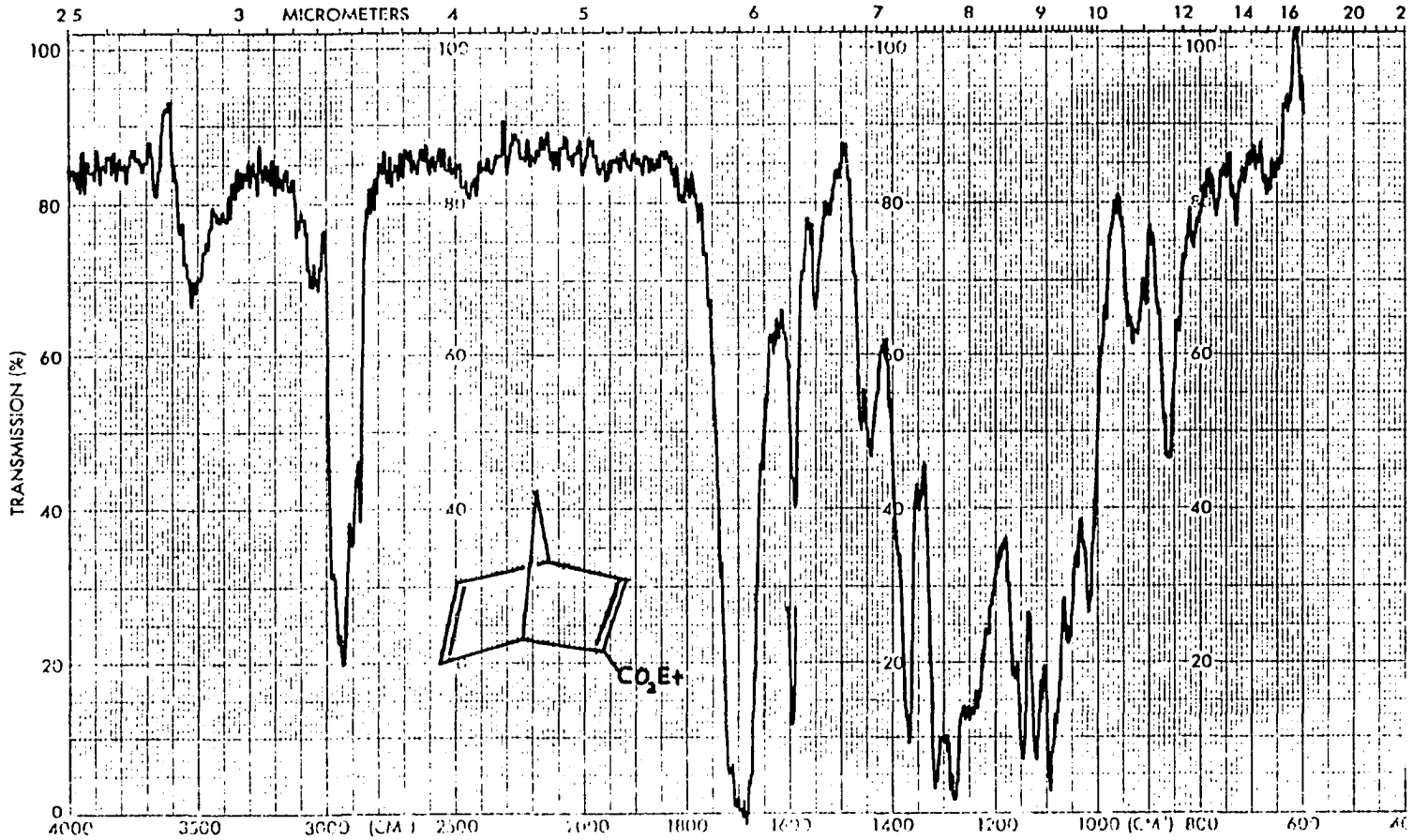

Figure IV-63. IR Spectrum of 2-Carboethoxynorbornadiene XX (film).

FIGURE IV-64

Mass Spectrum of 2-Carboethoxynorbornadiene XX.

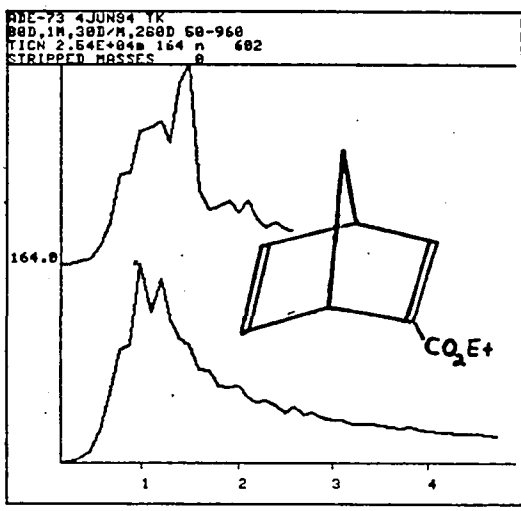

ABE-73 4JUN84 TK
FRN13468, SPECTRUM 14, 103PEAKS, RT 1.60 MIN,
MOST INTENSE 103

MASS	%	MASS	%	MASS	%	MASS	%
50.1	3.2	81.1	6.3	117.1	1.5	163.1	5.1
51.1	7.9	82.0	6.0	118.1	9.9	164.0	34.6
52.2	2.6	83.1	7.0	119.1	52.2	165.0	2.0
53.1	8.3	84.1	78.0	120.1	6.4	166.0	.7
54.1	1.1	85.1	3.7	121.0	6.6	167.1	2.2
55.1	7.6	86.0	52.8	122.1	2.7	169.0	.8
56.1	1.1	87.0	1.6	123.1	15.5	180.1	1.4
57.1	3.0	88.0	8.9	124.2	2.4	181.1	.6
58.1	.7	89.0	7.6	125.1	4.7	197.1	.6
59.1	.6	90.1	8.4	126.1	.8	207.0	1.1
60.1	1.0	91.1	100.0	127.1	1.3		
61.1	.9	92.2	14.7	129.0	.9		
62.1	2.8	93.0	10.4	131.0	.7		
63.1	7.8	94.1	3.9	132.1	.7		
64.2	2.8	95.1	12.1	133.0	2.8		
65.1	29.7	96.1	3.1	134.0	7.1		
66.1	43.9	97.1	4.6	135.0	29.1		
67.1	12.8	98.1	1.1	136.0	7.4		
68.1	3.5	99.1	2.6	137.0	1.7		
69.0	4.2	101.1	.9	138.0	2.9		
70.0	1.9	103.1	1.4	139.0	2.6		
71.1	5.1	105.1	17.1	141.0	8.0		
72.1	.9	106.1	12.2	142.0	.9		
73.0	2.9	107.1	10.1	143.0	.6		
74.0	2.4	108.1	2.5	149.0	3.1		
75.1	1.9	109.1	3.7	150.0	1.5		
76.1	1.2	110.1	4.3	151.0	2.4		
77.1	29.7	111.1	3.5	152.1	1.0		
78.1	10.6	112.1	2.9	153.0	2.5		
79.1	36.9	113.1	1.3	154.1	.7		
80.1	4.1	115.1	1.0	155.0	1.1		

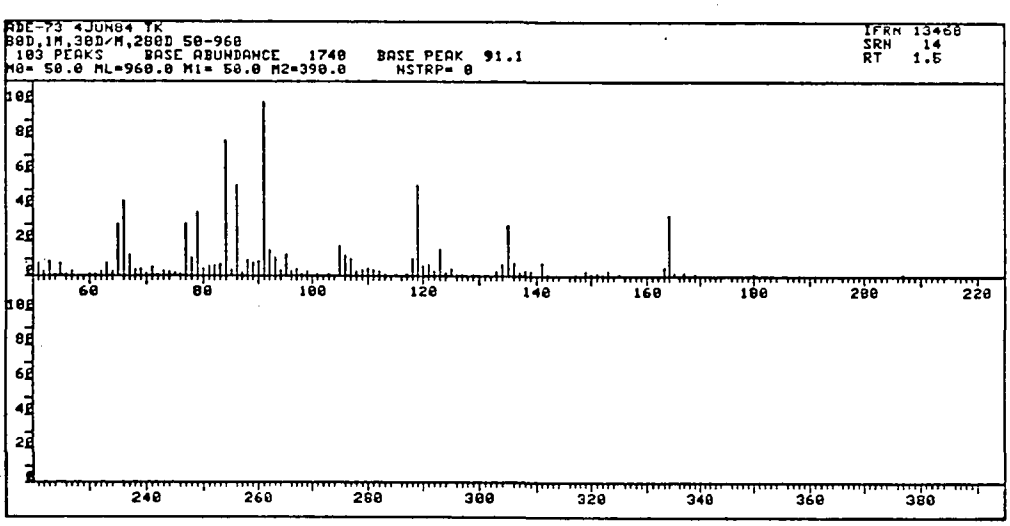

FIGURE IV-65

20 MHz ^{13}C and Spin Echo NMR Spectra of 2-Carboethoxynorbornadiene XX ($CDCl_3$).

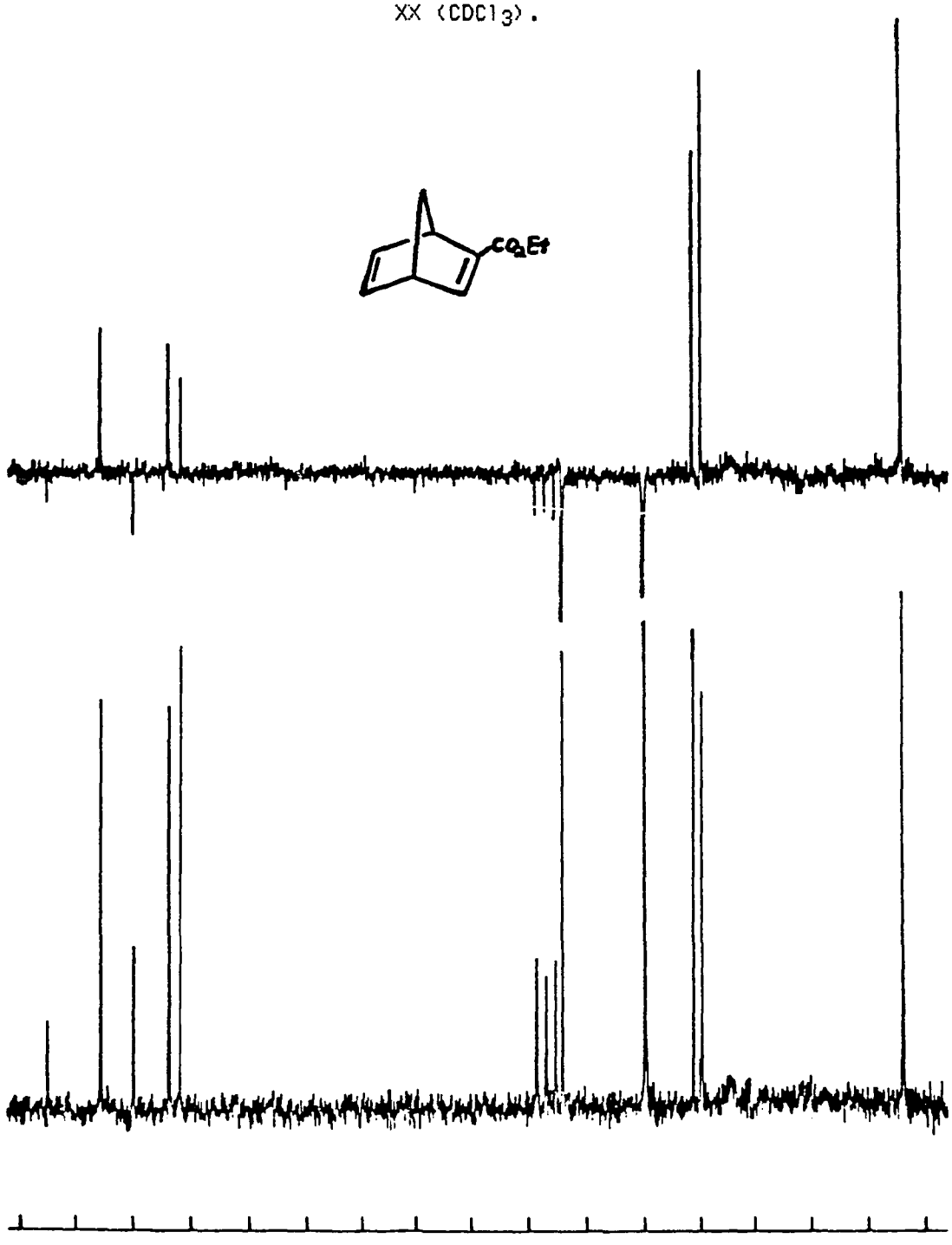

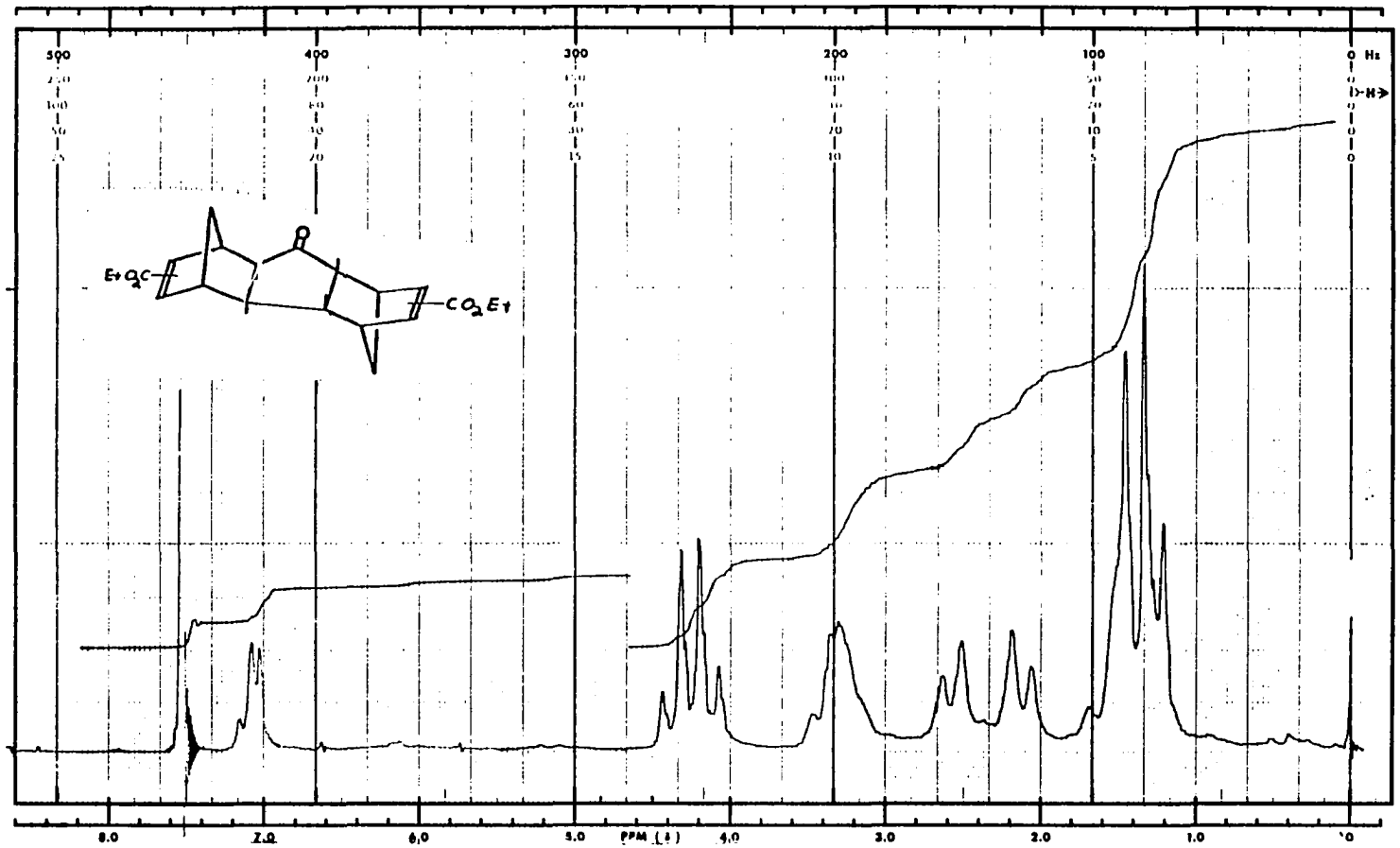

Figure IV-66. 60 MHz ^{1}H NMR Spectrum of Compound XXIa ($CDCl_3$/TMS).

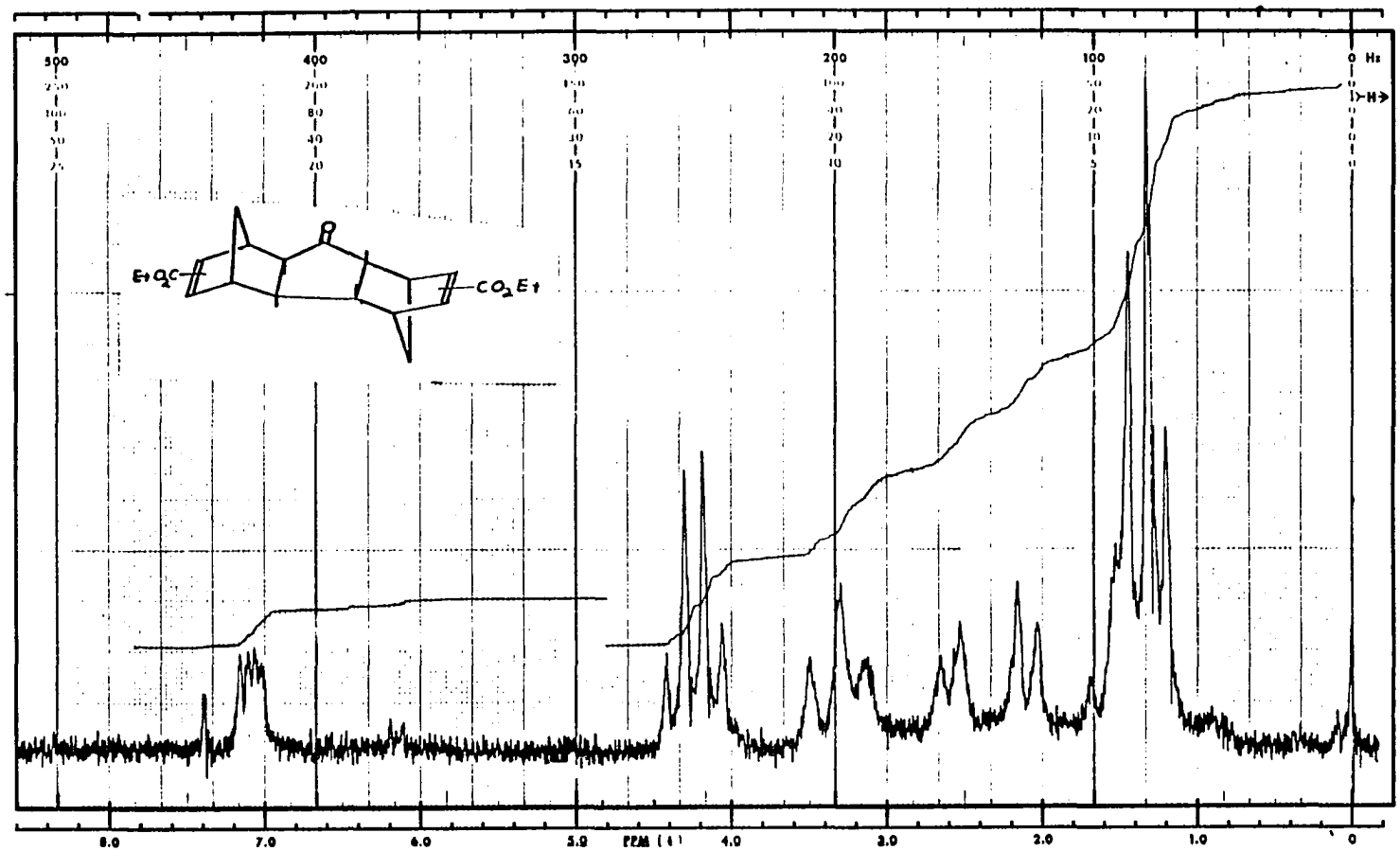

Figure IV-67. 60 MHz 1H NMR Spectrum of Compound XXIb (CDCl3/TMS).

the initial solid products.

Experimental

Infrared spectra were taken on Perkin-Elmer IR-8 and 298 spectrophotometers. Mass spectra were run on a Hewlett-Packard 5985 GC/MS spectrometer. Proton NMR spectra were recorded on IBM/Bruker NR-80, and Varian models T-60, XL-100, and XL-300 spectrometers. All decouplings, unless otherwise specified, were determined at 300 MHz. Melting points were determined on a Thomas-Hoover capillary melting point apparatus and are uncorrected.

7-benzoyloxynorbornadiene (XIV) was commercially obtained from Frinton laboratories, S. Vineland, NJ., and was also made by the method of Tanida and Tsuji.[34] 7-p-anisoyloxynorbornadiene (XVII) was prepared from 7-norbornadienol (itself prepared via the Grignard reaction of phenylmagnesium bromide with 7-benzoyloxynorbornadiene) and p-anisoyl chloride, obtained from Aldrich Chemical Company, Inc., Milwaukee, Wi., by standard methods.[35] Compound XX (2-carboethoxynorbornadiene) was prepared via the Diels-Alder reaction[33] of freshly cracked cyclopentadiene and ethyl propiolate, (the latter also obtained from Aldrich). The solvent di-n-butyl ether was distilled from lithium aluminum hydride at reduced pressure and stored over molecular sieves. Elemental analyses were performed by Chemalytics, Inc., Tempe, Az.

Reaction of 7-Benzoyloxynorbornadiene (XIV) with $Fe(CO)_5$[29]

To 10.0 g (47.1 mmol) of 7-norbornadienyl benzoate (XIV) in 50 mL of freshly distilled di-n-butyl ether under nitrogen was added a solution of 18.5 g (94.4 mmol) of $Fe(CO)_5$ in 10 mL of di-n-butyl ether. The resulting mixture was refluxed under nitrogen for 72 hours and then allowed to cool to room temperature. To the cooled reaction mixture was added a solution of 52 g of $FeCl_3 \cdot 6H_2O$ in 200 mL of acetone, and the resulting mixture was stirred at room

temperature for 1 week to decompose any unreacted iron pentacarbonyl and Fe(0) complexes that might be present.[36] The reaction mixture was then diluted with 300 mL of distilled water and extracted several times with ethyl acetate (7 x 100 mL portions). The combined extracts were washed with water, dried over $MgSO_4$, and filtered , and the filtrate was concentrated in vacuo to afford a viscous, dark brown oil. Dilution of this oil with an equal volume of absolute ethanol followed by refrigeration overnight resulted in precipitation of relatively pure XVI. An analytical sample of XVI was obtained following suction filtration via column chromatography on Florisil (100-200 mesh, 10% ethyl acetate-hexane eluent); recrystallization from ethyl acetate-hexane mixed solvent afforded XVI as a colorless microcrystalline solid (1.5 g, 29%): mp 192.5-193.0°C. Isolation of dimer ketones XV, XXXII, XXXIII, and XXXIV from the filtrate was accomplished via column chromatography on Florisil (100-200 mesh, 15% ethyl acetate-hexane eluent). The first fraction collected contained 4.9 g of unreacted 7-benzoyloxynorbornadiene and the second contained a mixture of XV and XXXII. Partial evaporation of the solvent from this fraction at room temperature and pressure precipitated XV (0.16 g, 3%); recrystallization from $CHCl_3$-hexane afforded pure XV (mp 252-253°C) as a white microcrystalline solid. Evaporation of the mother liquor afforded XXXII (0.11 g, 2%); recrystallization from $CHCl_3$-hexane gave pure microcrystalline XXXII (mp 219-220°C). The third fraction yielded XXXIII (0.05 g, 1%) which was recrystallized from $CHCl_3$-hexane (mp 218.5-219°C). Fraction four contained what is believed to be XXXIV (0.02 g, 0.4%); recrystallization from $CHCl_3$-hexane gave thin colorless flakes of XXXIV (mp 210°C). Repeated attempts to grow crystals of XXXIV which were suitable for X-ray analysis were unsuccessful because of their tendency to form very thin flakes. Subsequent fractions contained 0.67 g of uncharacterized residues.

Characterization of Cage Dimer XVI.[29]

^{1}H NMR spectrum (300 MHz, $CDCL_3$, Fig IV-7): δ 8.05 (m, 4 H, o-phenyl protons), 7.5 (m, 6 H, m- and p-phenyl protons), 5.52 (m, 2 H, C7 protons), 2.94 (m, 4 H), 2.75 (m, 2 H, bridgehead protons), 2.62 (m, 2 H, bridgehead protons), 2.62 (m, 2 H), 2.61 (m, 2 H);

IR spectrum (KBr pellet, Fig IV-8): 3000-2300 (b), 1737 (s), 1660 (w), 1560 (w), 1520 (w), 1464 (w), 1300 (s), 1242 (s), 1200 (w), 1180 (w), 1130 (m), 1090 (w), 1072 (m), 1040 (w), 995 (w), 865 (w), 785 (m), 665 (m), cm^{-1};

Mass spectrum (70 eV, Fig IV-9): m/e (relative intensity) 424 (M^+, 32.9), 406 (8.5), 310 (10.8), 302 (9.8), 180 (28.8), 105 (100), 77 (27.1);

^{13}C and Spin Echo spectra (20 MHz, $CDCl_3$, Fig IV-10): δ 166.08 (s), 132.75 (d), 130.57 (s), 129.47 (d), 128.25 (d), 87.91 (d), 53.36 (d), 51.88 (d), 51.30 (d), 51.05 (d), 49.21 (d), 48.62 (d);

HOMCOR NMR spectra (300 MHz, $CDCl_3$, Figs IV-11 and IV-12).

Anal. Calculated for $C_{28}H_{24}O_4$: C, 79.22; H, 5.70. Found: C, 79.25; H, 5.87.

Characterization of AXTXA Dimer Ketone (XV).[29]

^{1}H NMR spectrum ($CDCl_3$, Fig IV-13): δ 8.0 (m, 4 H, o-phenyl protons), 7.5 (m, 6 H, m- and p-phenyl protons), 6.22 (m, J = 6.0 Hz, J′ = 2.8 Hz, 2 H, syn-vinyl protons), 6.20 (m, J = 6.0 Hz, J′ = 2.4 Hz, 2 H, anti-vinyl protons), 4.89 (t, J = 1.7 Hz, 2 H, bridge protons), 3.35 (m, J = 2.8 Hz, J′ = 1.7 Hz, 2 H, syn-bridgehead protons), 3.22 (m, J = 2.4 Hz, J′ = 1.7 Hz, 2 H, anti-bridgehead protons), AB pattern (J_{AB} = 8.3 Hz), δ_B 2.72 (2 H, syn-cyclopentanone ring protons), δ_A 2.32 (2H, anti-cyclopentanone ring protons);

^{1}H NMR decoupling experiments (100 MHz, $CDCl_3$, Figs IV-30 and IV-31);

IR spectrum ($CHCl_3$ solution cell, Fig IV-14): 1722 (vs), 1609 (m),

1590 (w), 1495 (w), 1455 (m), 1335 (m), 1319 (m), 1282 (vs), 1179 (m), 1158 (m), 1120 (s), 1074 (m), 1029 (w), 1005 (w), 890 (w) cm^{-1};

Mass spectrum (70 eV, Fig IV-15): m/e (relative intensity) 452 (M^+, 1.0), 105 (100.0), 77 (22.7). Results of high resolution mass spectrum for $C_{29}H_{24}O_5$ were: Calculated, 452.16237 g/mol; Found, 452.16493 g/mol;[37]

^{13}C and Spin Echo spectra (20 MHz, $CDCl_3$, Fig IV-16): δ 217.16 (s), 166.76 (s), 134.29 (d), 133.26 (d), 133.11 (d), 129.95 (s), 129.61 (d), 128.37 (d), 85.11 (d), 57.82 (d), 52.79 (d), 50.50 (d), 45.55 (d).

Characterization of SNTNS Dimer Ketone (XXXII).[29]

^1H NMR spectrum (300 MHz, $CDCl_3$, Fig IV-17): δ 7.96 (m, 4 H, o-phenyl protons), 7.60-7.42 (m, 6 H, m- and p-phenyl protons), 6.29 (dd, J = 6.2 Hz, J′ = 3.3 Hz, 2 H, anti vinyl protons), 6.16 (dd, J = 6.2 Hz, J′ = 3.3 Hz, 2 H, syn vinyl protons), 4.71 (t, J = 2.0 Hz, 2 H, bridge protons), 3.25 (m, J = 3.8 Hz, J′ = 3.3 Hz, J′′ = 2.0 Hz, 2 H, anti bridgehead protons), 3.22 (m, J = 4.8 Hz, J′ = 3.3 Hz, J′′ = 2.0 Hz, 2 H, syn bridgehead protons), 2.95 (dd, J = 8.5 Hz, J′ = 4.8 Hz, 2 H, syn cyclopentanone ring protons), 2.81 (dd, J = 8.5 Hz, J′ = 3.8 Hz, 2 H, anti cyclopentanone ring protons);

IR spectrum ($CHCl_3$ solution cell, Fig IV-18): 2975 (w), 1722 (s), 1605 (m), 1588 (w), 1453 (m), 1355 (w), 1318 (s), 1275 (vs), 1177 (m), 1115 (s), 1088 (s), 1072 (s), 1027 (m), 1003 (m), 910 (s), cm^{-1};

Mass spectrum (70 eV, Fig IV-19): m/e (relative intensity) 452 (M^+, 0.1), 105 (100.0), 77 (15.5);

^{13}C and Spin Echo NMR spectra (20 MHz, $CDCl_3$, Fig IV-20): δ 223.07 (s), 165.60 (s), 135.02 (d), 134.75 (d), 133.24 (d), 129.89 (s), 129.48 (d), 128.49 (d), 86.08 (d), 58.07 (d), 49.15 (d), 47.95 (d), 41.77 (d).

Anal. Calculated for $C_{29}H_{24}O_5$: C, 76.96; H, 5.35. Found C,

75.32; F, 5.27.

Single-Crystal X-ray Structural Analysis of SNTNS (XXXII)[38]

Compound XXXII was carefully recrystallized from chloroform-hexane mixed solvent as fibrous, colorless needles. A single crystal of approximate dimensions 0.15 x 0.48 x 0.60 mm was selected and mounted on a Nonius CAD-4 automatic diffractometer equipped with MoK_α radiation and a graphite monochrometer. A total of 4084 reflections were collected at ambient temperature in the sphere $3^o \leq 2\theta \leq 50^o$. After averaging, 3965 unique reflections were obtained including 2165 observed reflections where $I_o \geq 2\sigma(I)$. The unit cell parameters resulting from least squares calculations on 25 high 2θ reflections were a = 6.577 (2), b = 8.751 (2), c = 21.738 (6) Å. α = 78.22 (2), β = 81.26 (3), γ = 67.88 (3) deg., $\underline{V}$ = 1131 (14) $Å^3$. The space group[39] P1 was assumed and gave satisfactory refinement. Other details of data collection were as follows: scan method, $\theta/2\theta$; scan rate, variable up to 45 sec per scan; scan range, calculated by 1.0 + 0.20 tan θ with 25% extension on each side for backgrounds. Three intensity monitors were checked every 2 hours of X-ray time and fluctuated randomly 2% over the entire data collection. Three orientation monitors were centered after every 200 observations. With $\underline{Z}$ = 2, the calculated density was 1.329 g cm^{-3} and $\mu(MoK_\alpha)$ = 0.52 cm^{-1}. Absorption corrections were not applied.

The initial carbon atoms were placed on positions resulting from a direct methods calculation[40]. The complete molecule was located through a series of least squares and Fourier calculations. Hydrogen atoms were placed in calculated positions and held invariant with U(H) approximately equal to 1.5 times the equivalent isotropic thermal parameter of the carbon atom to which it was bound. All atoms lie on general positions. Full matrix least squares on all observed reflections yielded R = 0.067 and R_w = 0.064.[41] The

maximum shift in the last cycle was < 0.02σ, the number of variables was 307, and the number of observations was 2165. In a final difference map the largest peak represented < 0.2 e/Å^3. Neutral atom scattering factors were obtained from reference 42. Figure IV-32 is a computer drawn representation and numbering scheme and Fig IV-33 is a computer drawn representation of the molecular packing diagram. Tables IV-5 and IV-6 list the carbon, oxygen, and hydrogen atomic positional and thermal parameters, respectively. Tables IV-7 and IV-8 list the non-hydrogen atom bond angles and bond lengths, respectively.

Characterization of AXTNA Dimer Ketone (XXXIII).[29]

^{1}H NMR spectrum (300 MHz, $CDCl_3$, Fig IV-21): δ 7.94 (m, 4 H, o-phenyl protons), 7.46 (m, 6,H, m- and p-phenyl protons), 6.19 (dd, J = 5.8 Hz, J′ = 2.9 Hz, 1 H, endo-bound anti vinyl proton), 6.14 (m, 2 H, exo-bound syn and anti vinyl protons), 6.13 (dd, J = 5.8 Hz, J′ = 2.5 Hz, 1 H endo-bound anti vinyl proton), 4.87 (t, J = 1.8 Hz, 1 H, exo-bound bridge proton), 4.84 (t, J = 1.6 Hz, 1 H, endo-bound bridge proton), 3.51 (m, J 5 4.9 Hz, J′ = 2.5 Hz, J′′ = 1.8 Hz, 1 H, endo-bound syn bridgehead proton), 3.45 (m, J = 4.4 Hz, J′ = 2.9 Hz, J′′ = 1.6 Hz, 1 H, endo-bound anti bridgehead proton), 3.42 (dd, J = 8.6 Hz, J′ = 4.9 Hz, 1 H, syn-exo cyclopentanone ring proton), 3.24 (m, J = 1.8 Hz, J′ = 1.0 Hz, 1 H, endo-bound syn bridgehead proton), 3.19 (m, J = 1.8 Hz, J′ = 1.0 Hz, endo-bound anti bridgehead proton), 2.90 (ddd, J = 8.6 Hz, J′ = 4.4 Hz, J′′ = 2.0 Hz, 1 H, anti-exo cyclopentanone ring proton), 2.03 (dd, J = 8.9 Hz, J′ = 1.0 Hz, 1 H, syn-endo cyclopentanone ring proton), 1.97 (ddd, J = 8.9 Hz, J′ = 2.0 Hz, J′′ = 1.0 Hz, 1 H, anti-endo cyclopentanone ring proton);

IR spectrum ($CHCl_3$ solution cell, Fig IV-22): 1719 (s), 1604 (w), 1587 (w), 1452 (w), 1317 (m), 1275 (s), 1115 ′(s), 1070 (w), 1025 (w) cm^{-1};

Mass spectrum (70 eV, Fig IV-23): m/e (relative intensity) 452 (M^+, 1.4), 105 (100.0), 77 (14.5);

TABLE IV-5

Atomic Positional Parameters for Carbon, Oxygen, and Hydrogen.

Atom	x	y	z
C_1	0.8746(5)	0.2175(4)	0.7183(2)
C_2	0.8943(6)	0.0314(4)	0.7210(2)
C_3	1.0480(8)	-0.0780(5)	0.7705(2)
C_4	1.2494(7)	-0.0827(5)	0.7489(2)
C_5	1.2372(6)	0.0243(5)	0.6856(2)
C_6	1.1117(6)	0.2097(4)	0.6965(2)
C_7	1.1941(6)	0.2499(5)	0.7503(2)
C_8	1.0176(6)	0.2907(4)	0.8037(2)
C_9	0.8108(5)	0.2826(4)	0.7817(2)
C_{10}	0.6471(6)	0.4678(5)	0.7789(2)
C_{11}	0.7407(7)	0.5774(5)	0.7290(2)
C_{12}	0.9157(8)	0.5822(5)	0.7507(2)
C_{13}	0.9468(6)	0.4759(5)	0.8146(2)
C_{14}	1.0547(6)	-0.0131(5)	0.6629(2)
C_{15}	0.8265(7)	0.0745(6)	0.5785(2)
C_{16}	0.7635(7)	0.1955(6)	0.5200(2)
C_{17}	0.5827(9)	0.2027(8)	0.4926(3)
C_{18}	0.517(1)	0.314(1)	0.4382(4)
C_{19}	0.631(1)	0.4179(9)	0.4095(3)
C_{20}	0.809(1)	0.4082(8)	0.4376(3)
C_{21}	0.8770(8)	0.2983(7)	0.4918(3)
C_{22}	0.7049(6)	0.5123(5)	0.8369(2)
C_{23}	0.4797(7)	0.4242(6)	0.9218(2)
C_{24}	0.4790(8)	0.3039(6)	0.9806(2)
C_{25}	0.2760(9)	0.2968(8)	1.0079(3)
C_{26}	0.270(1)	0.187(1)	1.0614(4)
C_{27}	0.457(2)	0.0821(9)	1.0897(3)
C_{28}	0.654(1)	0.0919(8)	1.0620(3)
C_{29}	0.6684(9)	0.2015(6)	1.0080(3)
O_1	1.3782(4)	0.2499(5)	0.7502(2)
O_2	0.9833(4)	0.0963(3)	0.6047(1)
O_3	4.7473(5)	-0.0301(4)	0.6009(2)
O_4	0.6848(4)	0.4033(3)	0.8954(1)
O_5	0.3184(5)	0.5300(4)	0.8990(2)
H_1	0.74607	0.30076	0.68884
H_2	0.73575	0.01785	0.72647
H_3	1.00204	-0.14093	0.08460
H_4	1.39713	-0.15219	0.77293
H_5	1.39252	0.00640	0.65770
H_6	1.13096	0.29477	0.65433
H_8	1.07927	0.20596	0.84595
H_9	0.73713	0.19889	0.81132
H_{10}	0.48034	0.48147	0.77336
H_{11}	0.67659	0.64023	0.68406
H_{12}	1.01849	0.65099	0.72643
H_{13}	1.05492	0.49474	0.84271
H_{14}	1.08730	-0.13478	0.65118
H_{17}	0.49315	0.12128	0.51374
H_{18}	0.37370	0.32120	0.41768
H_{19}	0.58175	0.50345	0.36643
H_{20}	0.89958	0.48933	0.41652
H_{21}	1.01970	0.29271	0.51231
H_{22}	0.60291	0.63399	0.84843
H_{25}	0.12590	0.37782	0.98673
H_{26}	0.11229	0.18162	1.08247
H_{27}	0.44943	-0.00482	1.13226
H_{28}	0.80373	0.01030	1.08331
H_{29}	0.82612	0.20717	0.98753

TABLE IV-6

Carbon, Oxygen, and Hydrogen Thermal Parameters.[a]

Atom	U11	U22	U33	U12	U13	U23
C_1	0.027(2)	0.035(2)	0.067(3)	-0.011(2)	0.000(2)	-0.012(2)
C_2	0.048(2)	0.041(2)	0.064(3)	-0.023(2)	0.017(2)	-0.020(2)
C_3	0.087(3)	0.032(2)	0.063(3)	-0.023(2)	0.002(3)	-0.004(2)
C_4	0.058(3)	0.038(2)	0.078(4)	0.005(2)	-0.009(2)	-0.010(2)
C_5	0.033(2)	0.051(3)	0.085(3)	-0.012(2)	0.010(2)	-0.018(2)
C_6	0.036(2)	0.044(2)	0.071(3)	-0.019(2)	0.000(2)	-0.006(2)
C_7	0.036(2)	0.043(2)	0.100(3)	-0.016(2)	-0.008(2)	-0.008(2)
C_8	0.033(2)	0.045(2)	0.066(3)	-0.013(2)	-0.014(2)	-0.008(2)
C_9	0.031(2)	0.033(2)	0.066(3)	-0.010(2)	-0.005(2)	-0.010(2)
C_{10}	0.041(2)	0.047(2)	0.066(3)	-0.006(2)	-0.013(2)	-0.023(2)
C_{11}	0.074(3)	0.034(2)	0.069(3)	-0.002(2)	-0.018(2)	-0.008(2)
C_{12}	0.085(3)	0.040(2)	0.085(4)	-0.031(2)	-0.003(3)	-0.013(2)
C_{13}	0.049(2)	0.051(3)	0.073(3)	-0.023(2)	-0.015(2)	-0.015(2)
C_{14}	0.054(2)	0.041(2)	0.068(3)	-0.019(2)	0.008(2)	-0.012(2)
C_{15}	0.054(3)	0.065(3)	0.075(4)	-0.023(2)	0.010(2)	-0.033(3)
C_{16}	0.058(3)	0.071(3)	0.066(3)	-0.008(2)	0.005(2)	-0.035(3)
C_{17}	0.086(4)	0.139(6)	0.090(5)	-0.036(4)	-0.008(3)	-0.039(4)
C_{18}	0.094(5)	0.199(9)	0.084(6)	-0.008(5)	-0.020(4)	-0.046(6)
C_{19}	0.128(7)	0.110(6)	0.080(5)	0.017(4)	-0.013(4)	-0.029(4)
C_{20}	0.147(6)	0.084(4)	0.098(5)	-0.030(4)	-0.026(4)	0.005(4)
C_{21}	0.096(4)	0.073(4)	0.084(4)	-0.027(3)	-0.014(3)	-0.003(3)
C_{22}	0.054(3)	0.044(2)	0.061(3)	-0.012(2)	-0.013(2)	-0.012(2)
C_{23}	0.054(3)	0.076(3)	0.074(4)	-0.019(2)	-0.008(3)	-0.039(3)
C_{24}	0.085(4)	0.067(3)	0.059(3)	-0.035(3)	0.002(3)	-0.028(3)
C_{25}	0.095(4)	0.148(6)	0.080(4)	-0.063(4)	0.019(3)	-0.039(4)
C_{26}	0.168(8)	0.197(9)	0.076(6)	-0.128(7)	0.030(5)	-0.038(5)
C_{27}	0.203(9)	0.111(6)	0.074(5)	-0.097(6)	0.013(5)	-0.024(4)
C_{28}	0.147(6)	0.088(4)	0.099(5)	-0.038(4)	-0.007(4)	0.002(4)
C_{29}	0.094(4)	0.068(4)	0.089(4)	-0.026(3)	-0.009(3)	0.001(3)
O_1	0.031(2)	0.126(3)	0.176(4)	-0.037(2)	0.006(2)	-0.074(3)
O_2	0.056(2)	0.061(2)	0.065(2)	-0.028(2)	0.005(1)	-0.015(2)
O_3	0.089(2)	0.103(3)	0.099(3)	-0.063(2)	0.011(2)	-0.030(2)
O_4	0.050(2)	0.060(2)	0.062(2)	-0.014(1)	-0.011(1)	-0.013(2)
O_5	0.051(2)	0.105(3)	0.092(3)	-0.010(2)	-0.013(2)	-0.030(2)
H_1	0.05680					
H_2	0.07020					
H_3	0.08460					
H_4	0.09390					
H_5	0.07110					
H_6	0.06900					
H_8	0.06540					
H_9	0.05720					
H_{10}	0.06780					
H_{11}	0.08390					
H_{12}	0.09470					
H_{13}	0.07350					
H_{14}	0.07400					
H_{17}	0.16020					
H_{18}	0.18230					
H_{19}	0.16680					
H_{20}	0.18170					
H_{21}	0.13130					
H_{22}	0.07290					
H_{25}	0.14580					
H_{26}	0.16710					
H_{27}	0.14820					
H_{28}	0.16710					
H_{29}	0.13010					

(a) The values of U(H) for hydrogen are ≈ 1.5 the equivalent isotropic thermal parameter of the carbon atom to which it is bound.

TABLE IV-7

Bond Angles Involving
Carbon and Oxygen Atoms.

Atoms	Angle(deg)
$C_1-C_2-C_3$	108.3(4)
$C_1-C_2-C_{14}$	100.4(4)
$C_1-C_6-C_5$	104.0(4)
$C_1-C_6-C_7$	106.1(4)
$C_1-C_9-C_8$	108.2(3)
$C_1-C_9-C_{10}$	115.3(4)
$C_2-C_1-C_6$	102.2(3)
$C_2-C_1-C_9$	115.6(4)
$C_2-C_3-C_4$	107.6(5)
$C_2-C_{14}-C_5$	94.8(4)
$C_2-C_{14}-O_2$	114.6(3)
$C_3-C_2-C_{14}$	97.7(3)
$C_3-C_4-C_5$	108.3(4)
$C_4-C_5-C_6$	106.9(5)
$C_4-C_5-C_{14}$	97.8(4)
$C_5-C_6-C_7$	112.2(4)
$C_5-C_{14}-O_2$	110.0(4)
$C_6-C_1-C_9$	107.7(4)
$C_6-C_5-C_{14}$	100.8(3)
$C_6-C_7-C_8$	111.4(3)
$C_6-C_7-O_1$	124.2(5)
$C_7-C_8-C_9$	106.0(4)
$C_7-C_8-C_{13}$	112.5(4)
$C_8-C_7-O_1$	124.4(6)
$C_8-C_9-C_{10}$	102.2(4)
$C_8-C_{13}-C_{12}$	106.3(5)
$C_8-C_{13}-C_{22}$	100.4(4)
$C_9-C_8-C_{13}$	104.2(3)
$C_9-C_{10}-C_{11}$	108.3(3)
$C_9-C_{10}-C_{22}$	100.1(4)
$C_{10}-C_{11}-C_{12}$	107.4(5)
$C_{10}-C_{22}-C_{13}$	95.3(4)
$C_{10}-C_{22}-O_4$	114.9(4)
$C_{11}-C_{10}-C_{22}$	97.8(4)
$C_{11}-C_{12}-C_{13}$	108.5(5)
$C_{12}-C_{13}-C_{22}$	97.8(4)
$C_{13}-C_{22}-O_4$	109.9(4)
$C_{14}-O_2-C_{15}$	116.4(4)
$C_{15}-C_{16}-C_{17}$	117.8(6)
$C_{15}-C_{16}-C_{21}$	123.1(5)
$C_{16}-C_{15}-O_2$	111.6(5)
$C_{16}-C_{15}-O_3$	125.2(5)
$C_{16}-C_{17}-C_{18}$	119.8(8)
$C_{16}-C_{21}-C_{20}$	120.2(6)
$C_{17}-C_{16}-C_{21}$	119.2(7)
$C_{17}-C_{18}-C_{19}$	121.2(8)
$C_{18}-C_{19}-C_{20}$	117.7(9)
$C_{19}-C_{20}-C_{21}$	121.9(8)
$C_{22}-O_4-C_{23}$	116.7(4)
$C_{23}-C_{24}-C_{25}$	117.6(5)
$C_{23}-C_{24}-C_{29}$	122.4(5)
$C_{24}-C_{23}-O_4$	111.9(4)
$C_{24}-C_{23}-O_5$	125.6(5)
$C_{24}-C_{25}-C_{26}$	119.1(7)
$C_{24}-C_{29}-C_{28}$	118.9(6)
$C_{25}-C_{24}-C_{29}$	120.0(7)
$C_{25}-C_{26}-C_{27}$	122.1(9)
$C_{26}-C_{27}-C_{28}$	118.1(5)
$C_{27}-C_{28}-C_{29}$	122.3(8)
$O_2-C_{15}-O_3$	123.3(6)
$O_4-C_{23}-O_5$	122.5(6)

TABLE IV-8

Bond Lengths Involving
Carbon and Oxygen Atoms.

Atoms	Bond Length(Å)
C_1-C_2	1.574(7)
C_1-C_6	1.540(5)
C_1-C_9	1.537(7)
C_2-C_3	1.510(7)
C_2-C_{14}	1.531(7)
C_3-C_4	1.325(7)
C_4-C_5	1.492(9)
C_5-C_6	1.567(7)
C_5-C_{14}	1.528(7)
C_6-C_7	1.514(8)
C_7-C_8	1.507(7)
C_7-O_1	1.211(5)
C_8-C_9	1.539(6)
C_8-C_{13}	1.567(7)
C_9-C_{10}	1.567(6)
C_{10}-C_{11}	1.514(8)
C_{10}-C_{22}	1.532(8)
C_{11}-C_{12}	1.326(7)
C_{12}-C_{13}	1.502(9)
C_{13}-C_{22}	1.522(6)
C_{14}-O_2	1.445(7)
C_{15}-C_{16}	1.480(9)
C_{15}-O_2	1.340(7)
C_{15}-O_3	1.202(8)
C_{16}-C_{17}	1.384(9)
C_{16}-C_{21}	1.372(9)
C_{17}-C_{18}	1.38(1)
C_{18}-C_{19}	1.38(2)
C_{19}-C_{20}	1.37(1)
C_{20}-C_{21}	1.37(1)
C_{22}-O_4	1.446(7)
C_{23}-C_{24}	1.48(1)
C_{23}-O_4	1.344(6)
C_{23}-O_5	1.209(7)
C_{24}-C_{25}	1.395(9)
C_{24}-C_{29}	1.370(8)
C_{25}-C_{26}	1.36(2)
C_{26}-C_{27}	1.37(1)
C_{27}-C_{28}	1.37(1)
C_{28}-C_{29}	1.37(1)

Mass spectrum (Chemical Ionization): m/e (relative intensity) 453 (M + H, corresponding to $C_{29}H_{25}O_5$, 9.0), 331 (100.0), 267 (29.0), 105 (22.0);

^{13}C and Spin Echo NMR spectra (20 MHz, $CDCl_3$, Fig IV-24): δ 219.09 (s), 166.66 (s), 166.46 (s), 134.26 (d), 133.18 (d), 133.10 (d), 133.04 (d), 132.38 (d), 131.21 (d), 130.04 (s), 129.99 (s), 129.61 (d) (2 carbons), 128.33 (d) (2 carbons), 87.78 (d), 85.37 (d), 56.32 (d) (2 carbons), 52.64 (d), 50.71 (d), 50.11 (d), 49.37 (d), 44.86 (d), 41.03 (d);

HOMCOR NMR spectrum (300 MHz, $CDCl_3$, Fig IV-25);

HOM2DJ NMR spectra (300 MHz, $CDCl_3$, Fig IV-34 through IV-36).

Anal. Calculated for $C_{29}H_{24}O_5$: C, 76.96; H, 5.35. Found: C, 76.88; H, 5.43.

Single-Crystal X-ray Structural Analysis of AXTNA (XXXIII)[38]

Compound XXXIII was carefully recrystallized from chloroform-hexane mixed solvent. A colorless fragment of approximate dimensions 0.20 x 0.38 x 0.48 mm was mounted on a Nonius CAD-4 automatic diffractometer equipped with CuK_α radiation. A total of 4793 reflections were collected at ambient temperature in the sphere $2^o \leq 2\theta \leq 150^o$. After averaging, 4668 unique reflections were obtained including 3762 observed reflections where $I_o \geq 2\sigma(I)$. The unit cell parameters resulting from least-squares calculations on 25 high 2θ reflections were: a = 9.198 (2), b = 9.968 (2), c = 13.054 (3) Å, α = 94.23 (2), β = 105.35 (2), γ = 99.77 (1) deg., V = 1129 Å^3. The space group[39] P1 was assumed and gave satisfactory refinement. Other details of data collection were: scan method, θ/2θ; scan rate, variable up to 45 sec per scan; scan range, calculated by 0.90 + 0.20 tan θ, with 25% extension on each side for backgrounds. Three intensity monitors were checked every 2 hours of X-ray time and fluctuated randomly 2% over the entire data collection. Three

orientation monitors were centered after every 200 observations. With Z = 2, the calculated density was 1.331 g cm^{-3}, and $\mu(CuK_\alpha)$ = 6.47 cm^{-1}. Absorption corrections were not applied.

The structure was solved by direct methods calculations.[40] Hydrogen atoms were placed with reference to a difference Fourier map and were refined positionally and isotropically. All atoms lie on general positions. Full matrix least squares on all observed reflections yielded R = 0.049 and R_w = 0.067.[41] The maximum shift in the last cycle was 0.5 σ, the number of variables was 403, and the number of observations was 3762. In a final difference map the largest peak represented less than 0.2 e/$Å^3$. Neutral atom scattering factors were obtained from reference 42. Figure IV-37 is a computer drawn representation and numbering scheme, and Fig IV-38 is a computer drawn representation of the unit cell. Tables IV-9 and IV-10 list the atomic positional and thermal parameters, respectively, for carbon, oxygen, and hydrogen. Tables IV-11 and IV-12 list the bond angles and bond lengths, respectively, for non-hydrogen atoms. Table IV-13 lists the bond lengths involving hydrogen.

Characterization of Cage Dimer Ketone (XXXIV).[29]

^{1}H NMR spectrum (300 MHz, $CDCl_3$, Fig IV-26): δ 7.99 (m, 4 H, o-phenyl protons), 7.50 (m, 6,H, m and o-phenyl protons), 5.39 (t, J = 1.73 Hz, 2 H, bridge protons), 3.06-3.02 (m, 4 H, aliphatic non-bridgehead protons), 3.01 (m, 2 H, bridgehead protons), 2.88 (m, 2 H, bridgehead protons), 2.80-2.77 (m, 4 H, aliphatic non-bridgehead protons);

IR spectrum ($CHCl_3$ solution cell, Fig IV-27): 1710 (s), 1317 (m), 1274 (s), 1213 (m), 1177 (w), 1120 (m), 1109 (m), 1085 (m), 1070 (m), 1027 (m), 1010 (w) cm^{-1};

Mass spectrum (70 eV, Fig IV-28): m/e (relative intensity) 452 (M^+, 15.3), 105 (100.0), 77 (13.9);

TABLE IV-9

Atomic Positional Parameters for Carbon, Oxygen, and Hydrogen.

Atom	x	y	z
C_1	0.2613(2)	0.3824(2)	0.7207(1)
C_2	0.3595(2)	0.4640(2)	0.8311(1)
C_3	0.2455(3)	0.5060(2)	0.8857(1)
C_4	0.1852(2)	0.6019(2)	0.8353(2)
C_5	0.2574(2)	0.6278(2)	0.7455(1)
C_6	0.1923(2)	0.4966(2)	0.6615(1)
C_7	0.2521(3)	0.5083(2)	0.5654(1)
C_8	0.3524(2)	0.4060(2)	0.5583(1)
C_9	0.3538(2)	0.3211(2)	0.6529(1)
C_{10}	0.2838(2)	0.1732(2)	0.5947(1)
C_{11}	0.1199(2)	0.1710(2)	0.5371(2)
C_{12}	0.1182(2)	0.2432(2)	0.4564(2)
C_{13}	0.2815(2)	0.2952(2)	0.4575(1)
C_{14}	0.4164(2)	0.5999(2)	0.7941(1)
C_{15}	0.6540(2)	0.7248(2)	0.9087(1)
C_{16}	0.7261(2)	0.8302(2)	1.0036(1)
C_{17}	0.8822(3)	0.8588(3)	1.0428(3)
C_{18}	0.9510(4)	0.9559(4)	1.1320(3)
C_{19}	0.8663(3)	1.0234(3)	1.1797(2)
C_{20}	0.7130(3)	0.9961(3)	1.1412(2)
C_{21}	0.6414(3)	0.8987(2)	1.0525(2)
C_{22}	0.3574(2)	0.1800(2)	0.5028(1)
C_{23}	0.3720(2)	0.0411(2)	0.3523(1)
C_{24}	0.3162(2)	-0.0951(2)	0.2877(1)
C_{25}	0.2445(2)	-0.2079(2)	0.3245(1)
C_{26}	0.1940(2)	-0.3319(2)	0.2606(2)
C_{27}	0.2105(3)	-0.3439(2)	0.1583(2)
C_{28}	0.2802(3)	-0.2330(2)	0.1212(2)
C_{29}	0.3346(3)	-0.1088(2)	0.1852(1)
O_1	0.2224(2)	0.5890(2)	0.5025(2)
O_2	0.5014(1)	0.7054(1)	0.8816(1)
O_3	0.7242(2)	0.6636(2)	0.8627(1)
O_4	0.3103(1)	0.0507(1)	0.4341(1)
O_5	0.4608(2)	0.1321(2)	0.3338(1)
H_1	0.184(2)	0.314(2)	0.733(2)
H_2	0.439(2)	0.416(2)	0.871(2)
H_3	0.207(3)	0.456(9)	0.943(2)
H_4	0.099(2)	0.647(2)	0.844(2)
H_5	0.251(2)	0.711(2)	0.715(2)
H_6	0.081(2)	0.480(2)	0.637(2)
H_8	0.456(2)	0.453(2)	0.560(1)
H_9	0.458(2)	0.322(2)	0.696(1)
H_{10}	0.302(2)	0.104(2)	0.638(2)
H_{11}	0.035(3)	0.125(3)	0.562(2)
H_{12}	0.029(3)	0.266(2)	0.411(2)
H_{13}	0.303(2)	0.323(2)	0.392(2)
H_{14}	0.477(2)	0.596(2)	0.745(1)
H_{17}	0.930(4)	0.807(4)	1.005(3)
H_{18}	1.054(4)	0.976(3)	1.151(2)
H_{19}	0.923(3)	1.095(3)	1.243(2)
H_{20}	0.649(3)	1.039(3)	1.177(2)
H_{21}	0.532(3)	0.881(2)	1.028(2)
H_{22}	0.476(2)	0.208(2)	0.527(1)
H_{25}	0.236(2)	-0.200(2)	0.397(2)
H_{26}	0.147(3)	-0.405(3)	0.289(2)
H_{27}	0.180(3)	-0.433(3)	0.121(2)
H_{28}	0.285(3)	-0.238(2)	0.051(2)
H_{29}	0.388(2)	-0.026(2)	0.163(2)

TABLE IV-10

Carbon, Oxygen, and Hydrogen Thermal Parameters.[a]

Atom	U11	U22	U33	U12	U13	U23
C_1	0.063(1)	0.0453(9)	0.0404(8)	0.0046(7)	0.0165(7)	-0.0011(6)
C_2	0.076(1)	0.054(1)	0.0360(7)	0.0141(9)	0.0120(8)	-0.0009(7)
C_3	0.092(1)	0.057(1)	0.0473(9)	0.005(1)	0.0291(9)	-0.0069(8)
C_4	0.074(1)	0.062(1)	0.060(1)	0.009(1)	0.0198(9)	-0.0152(9)
C_5	0.076(1)	0.0446(9)	0.0485(9)	0.0093(8)	0.0102(8)	-0.0036(7)
C_6	0.061(1)	0.0483(9)	0.0472(9)	0.0072(8)	0.0070(8)	-0.0038(7)
C_7	0.098(1)	0.0456(9)	0.0403(8)	0.0025(9)	0.0089(9)	0.0010(7)
C_8	0.074(1)	0.053(1)	0.0414(8)	-0.0045(8)	0.0213(8)	-0.0020(7)
C_9	0.059(1)	0.055(1)	0.0392(8)	0.0087(8)	0.0136(7)	0.0009(7)
C_{10}	0.083(1)	0.0474(9)	0.0492(9)	0.0151(9)	0.0282(9)	0.0032(7)
C_{11}	0.073(1)	0.055(1)	0.074(1)	-0.0028(9)	0.031(1)	-0.022(1)
C_{12}	0.071(1)	0.063(1)	0.061(1)	0.017(1)	-0.001(1)	-0.024(1)
C_{13}	0.088(1)	0.056(1)	0.0365(8)	0.0088(9)	0.0169(8)	-0.0020(7)
C_{14}	0.066(1)	0.054(1)	0.0418(8)	0.0014(8)	0.0119(8)	-0.0087(7)
C_{15}	0.069(1)	0.0479(9)	0.060(1)	0.0154(8)	0.0057(9)	-0.0024(8)
C_{16}	0.062(1)	0.0444(9)	0.056(1)	0.0080(8)	0.0001(8)	0.0042(7)
C_{17}	0.071(2)	0.099(2)	0.124(2)	0.033(1)	-0.017(1)	-0.037(2)
C_{18}	0.069(2)	0.115(2)	0.143(3)	0.021(2)	-0.035(2)	-0.040(2)
C_{19}	0.097(2)	0.075(2)	0.071(1)	0.003(1)	-0.014(1)	-0.016(1)
C_{20}	0.086(2)	0.092(2)	0.072(1)	0.000(1)	0.013(1)	-0.026(1)
C_{21}	0.065(1)	0.075(1)	0.061(1)	-0.001(1)	0.013(1)	-0.015(1)
C_{22}	0.067(1)	0.062(1)	0.0459(9)	0.0120(9)	0.0200(8)	-0.0020(8)
C_{23}	0.069(1)	0.066(1)	0.0517(9)	0.0192(9)	0.0269(8)	0.0047(8)
C_{24}	0.058(1)	0.063(1)	0.0464(8)	0.0223(8)	0.0201(7)	0.0043(7)
C_{25}	0.070(1)	0.070(1)	0.0497(9)	0.0210(9)	0.0248(9)	0.0056(8)
C_{26}	0.077(1)	0.066(1)	0.070(1)	0.011(1)	0.029(1)	0.001(1)
C_{27}	0.078(1)	0.073(1)	0.066(1)	-0.018(1)	0.022(1)	-0.014(1)
C_{28}	0.091(1)	0.087(2)	0.052(1)	0.026(1)	0.032(1)	-0.006(1)
C_{29}	0.081(1)	0.073(1)	0.054(1)	0.024(1)	0.0344(9)	0.0071(9)
O_1	0.193(2)	0.0624(9)	0.0545(8)	0.031(1)	0.025(1)	0.0171(7)
O_2	0.0647(8)	0.0627(8)	0.0544(7)	-0.0012(6)	0.0089(6)	-0.0168(6)
O_3	0.082(1)	0.091(1)	0.114(1)	0.0322(9)	0.0065(9)	-0.038(1)
O_4	0.0820(9)	0.0591(7)	0.0515(6)	0.0148(6)	0.0307(6)	-0.0030(5)
O_5	0.117(1)	0.077(1)	0.089(1)	-0.0042(9)	0.063(1)	-0.0084(8)
H_1	0.064(5)					
H_2	0.059(5)					
H_3	0.095(8)					
H_4	0.079(6)					
H_5	0.072(6)					
H_6	0.062(5)					
H_8	0.061(5)					
H_9	0.057(5)					
H_{10}	0.076(6)					
H_{11}	0.096(8)					
H_{12}	0.16(1)					
H_{13}	0.303(2)					
H_{14}	0.477(2)					
H_{17}	0.930(4)					
H_{18}	0.13(1)					
H_{19}	0.107(8)					
H_{20}	0.12(1)					
H_{21}	0.089(7)					
H_{22}	0.061(5)					
H_{25}	0.085(7)					
H_{26}	0.087(7)					
H_{27}	0.098(8)					
H_{28}	0.094(7)					
H_{29}	0.079(7)					

(a) Anisotropic thermal parameters for carbon and oxygen are of the form:
$T = \exp[-2\pi^2(U_{11}\underline{h}^2\underline{a}^{*2}+\cdots+U_{23}\underline{k}\underline{l}\underline{b}^*\underline{c}^*]$;
and for hydrogen: $T = \exp(-8\pi^2 U \sin^2\theta/\lambda^2)$.

TABLE IV-11
Bond Angles Involving
Carbon and Oxygen Atoms.

Atoms	Angle(deg)
$C_1-C_2-C_3$	105.8(2)
$C_1-C_2-C_{14}$	99.63(9)
$C_1-C_6-C_5$	103.7(1)
$C_1-C_6-C_7$	106.8(1)
$C_1-C_9-C_8$	107.5(1)
$C_1-C_9-C_{10}$	116.3(1)
$C_2-C_1-C_6$	101.8(1)
$C_2-C_1-C_9$	115.1(1)
$C_2-C_3-C_4$	108.0(1)
$C_2-C_{14}-C_5$	95.1(1)
$C_2-C_{14}-O_2$	113.33(9)
$C_3-C_2-C_{14}$	100.2(1)
$C_3-C_4-C_5$	107.7(2)
$C_4-C_5-C_6$	105.7(1)
$C_4-C_5-C_{14}$	100.8(1)
$C_5-C_6-C_7$	111.9(1)
$C_5-C_{14}-O_2$	110.0(1)
$C_6-C_1-C_9$	107.42(9)
$C_6-C_5-C_{14}$	98.4(1)
$C_6-C_7-C_8$	111.0(1)
$C_6-C_7-O_1$	124.1(2)
$C_7-C_8-C_9$	107.1(1)
$C_7-C_8-C_{13}$	112.6(2)
$C_8-C_7-O_1$	124.9(1)
$C_8-C_9-C_{10}$	102.3(1)
$C_8-C_{13}-C_{12}$	106.2(1)
$C_8-C_{13}-C_{22}$	97.7(1)
$C_9-C_8-C_{13}$	103.2(1)
$C_9-C_{10}-C_{11}$	107.1(1)
$C_9-C_{10}-C_{22}$	98.7(1)
$C_{10}-C_{11}-C_{12}$	107.7(2)
$C_{10}-C_{22}-C_{13}$	94.5(1)
$C_{10}-C_{22}-O_4$	110.3(1)
$C_{11}-C_{10}-C_{22}$	101.2(1)
$C_{11}-C_{12}-C_{13}$	108.1(1)
$C_{12}-C_{13}-C_{22}$	100.9(1)
$C_{13}-C_{22}-O_4$	115.0(1)
$C_{14}-O_2-C_{15}$	117.5(1)
$C_{15}-C_{16}-C_{17}$	118.6(2)
$C_{15}-C_{16}-C_{21}$	122.3(2)
$C_{16}-C_{15}-O_2$	111.7(1)
$C_{16}-C_{15}-O_3$	124.4(2)
$C_{16}-C_{17}-C_{18}$	119.2(2)
$C_{16}-C_{21}-C_{20}$	120.6(2)
$C_{17}-C_{16}-C_{21}$	119.1(2)
$C_{17}-C_{18}-C_{19}$	121.3(3)
$C_{18}-C_{19}-C_{20}$	119.7(2)
$C_{19}-C_{20}-C_{21}$	120.1(2)
$C_{22}-O_4-C_{23}$	116.3(1)
$C_{23}-C_{24}-C_{25}$	122.7(1)
$C_{23}-C_{24}-C_{29}$	118.0(1)
$C_{24}-C_{23}-O_4$	111.6(1)
$C_{24}-C_{23}-O_5$	124.6(1)
$C_{24}-C_{25}-C_{26}$	120.1(1)
$C_{24}-C_{29}-C_{28}$	119.9(2)
$C_{25}-C_{24}-C_{29}$	119.3(1)
$C_{25}-C_{26}-C_{27}$	120.2(2)
$C_{26}-C_{27}-C_{28}$	120.1(2)
$C_{27}-C_{28}-C_{29}$	120.4(1)
$O_2-C_{15}-O_3$	123.9(2)
$O_4-C_{23}-O_5$	123.7(1)

TABLE IV-12

Bond Lengths Involving

Carbon and Oxygen Atoms.

Atoms	Bond Length(Å)
C_1-C_2	1.563(2)
C_1-C_6	1.552(2)
C_1-C_9	1.542(2)
C_2-C_3	1.511(2)
C_2-C_{14}	1.527(2)
C_3-C_4	1.316(2)
C_4-C_5	1.510(2)
C_5-C_6	1.565(2)
C_5-C_{14}	1.513(3)
C_6-C_7	1.502(2)
C_7-C_8	1.500(2)
C_7-O_1	1.204(2)
C_8-C_9	1.546(2)
C_8-C_{13}	1.570(2)
C_9-C_{10}	1.555(2)
$C_{10}-C_{11}$	1.492(3)
$C_{10}-C_{22}$	1.526(2)
$C_{11}-C_{12}$	1.317(2)
$C_{12}-C_{13}$	1.499(3)
$C_{13}-C_{22}$	1.521(2)
$C_{14}-O_2$	1.447(2)
$C_{15}-C_{16}$	1.488(2)
$C_{15}-O_2$	1.330(2)
$C_{15}-O_3$	1.198(2)
$C_{16}-C_{17}$	1.362(3)
$C_{16}-C_{21}$	1.363(2)
$C_{17}-C_{18}$	1.389(4)
$C_{18}-C_{19}$	1.349(4)
$C_{19}-C_{20}$	1.338(4)
$C_{20}-C_{21}$	1.389(3)
$C_{22}-O_4$	1.445(2)
$C_{23}-C_{24}$	1.478(2)
$C_{23}-O_4$	1.340(2)
$C_{23}-O_5$	1.204(2)
$C_{24}-C_{25}$	1.388(2)
$C_{24}-C_{29}$	1.393(2)
$C_{25}-C_{26}$	1.373(2)
$C_{26}-C_{27}$	1.383(2)
$C_{27}-C_{28}$	1.368(3)
$C_{28}-C_{29}$	1.378(3)

Table IV-13

Bond Lengths Involving

Hydrogen Atoms.

Atom	Bond Length(Å)
C_1-H_1	0.96(2)
C_2-H_2	1.00(2)
C_3-H_3	1.04(2)
C_4-H_4	1.00(2)
C_5-H_5	0.95(2)
C_6-H_6	0.97(2)
C_8-H_8	0.98(2)
C_9-H_9	0.97(2)
C_{10}-H_{10}	0.93(2)
C_{11}-H_{11}	0.99(2)
C_{12}-H_{12}	0.95(2)
C_{13}-H_{13}	0.97(2)
C_{14}-H_{14}	0.97(1)
C_{17}-H_{17}	0.92(3)
C_{18}-H_{18}	0.89(3)
C_{19}-H_{19}	1.01(2)
C_{20}-H_{20}	0.97(3)
C_{21}-H_{21}	0.96(2)
C_{22}-H_{22}	1.03(2)
C_{25}-H_{25}	0.97(2)
C_{26}-H_{26}	0.93(2)
C_{27}-H_{27}	0.94(2)
C_{28}-H_{28}	0.96(2)
C_{29}-H_{29}	0.98(2)

Mass spectrum (Chemical ionization): m/e (relative intensity) 453 (M + H, corresponding to $C_{29}H_{25}O_5$, 26.0), 331 (53.0), 267 (100.0), 187 (22.0), 145 (14.0), 123 (12.0), 105 (64.0), 85 (27.0), 83 (26.0), 81 (26.0), 79 (12.0), 71 (32.0), 70 (14.0), 69 (37.0), 67 (25.0);
^{13}C and Spin Echo NMR spectra (75 MHz, $CDCl_3$, Fig IV-29): δ 219.56 (s), 165.69 (s), 133.21 (d), 129.67 (s), 127.60 (d), 128.41 (d), 83.25 (d), 55.08 (d), 51.87 (d), 49.72 (d), 48.00 (d), 46.69 (d), 41.02 (d).

Synthesis of 7-p-Anisoyloxynorbornadiene (XVII)[29]

To 10.5 g (61.6 mmol) of p-anisoyl chloride in 30 mL of dry pyridine was added dropwise with stirring 15.67 g (144.9 mmol) of 7-norbornadienol while the mixture was protected by a $CaCl_2$ drying tube. After refluxing for one hour and cooling to room temperature, 100 mL of a 10% $NaHCO_3$ solution was added to dissolve unreacted acid chloride or acid. The layers were separated and the organic layer was extracted with a 10% HCl solution, dried over $MgSO_4$ and concentrated in vacuo to afford an oily residue which crystallized upon addition of pentane with cooling. Recrystallization from ether-pentane gave 11.22 g (75.24% yield) of white crystals (mp 81.5-82°C).

Characterization of 7-p-Anisoyloxynorbornadiene (XVII).[29]
^1H NMR spectrum (300 MHz, $CDCl_3$, Fig IV-39): AA'BB' pattern (J_{AB} = 8.8 Hz), $\delta_{BB'}$ 7.90 (2 H, o-phenyl protons), $\delta_{AA'}$ 6.85 (2 H, m-phenyl protons), 6.72 (m, J = 4.1 Hz, J' = 2.1 Hz, 2 H, syn-vinyl protons), 6.61 (m, J = 3.8 Hz, J' = 2.1 Hz, 2 H, anti-vinyl protons) 4.79 (t, J = 1.9 Hz, 1 H, bridge proton), 3.80 (s, 3 H, OCH_3), 3.69 (m, J = 4.1 Hz, J' = 3.8 Hz, J'' = 1.9 Hz, 2 H, bridgehead protons);
IR spectrum (KBr pellet, Fig IV-40): 1720 (m), 1620 (m), 1520 (w), 1470 (w), 1330 (m), 1290 (m), 1255 (s), 1190 (m), 1172 (m), 1104 (m),

1069 (w), 1030 (w), 1004 (m), 850 (w), 811 (m), 772 (m), 712 (m), cm^{-1};

Mass spectrum (70 eV, Fig IV-41): m/e (relative intensity) 242 (M^+, 1.9), 135 (100.0), 107 (12.1), 92 (10.1), 77 (26.7);

^{13}C and Spin Echo spectra (20 MHz, $CDCl_3$, Fig IV-42): δ 166.08 (s), 163.27 (s), 140.21 (d), 137.74 (d), 131.50 (d), 122.60 (s), 113.39 (d), 99.31 (d), 55.17 (d), 52.46 (d).

Anal. Calculated for $C_{15}H_{14}O_3$: C, 74.36; H, 5.82. Found: C, 74.26; H, 5.69.

Reaction of 7-p-Anisoyloxynorbornadiene (XVII) with $Fe(CO)_5$[29]

To 12.37 g (51.1 mmol) of 7-p-anisoyloxynorbornadiene (XVII) in 60 mL of freshly distilled di-n-butyl ether under nitrogen was added a solution of 20.42 g (104.3 mmol) of $Fe(CO)_5$ in 15 mL of di-n-butyl ether. The resulting mixture was refluxed under nitrogen for 26 hours and then allowed to cool to room temperature. To the cooled reaction mixture was added a solution of 44.25 g of $FeCl_3 \cdot 6H_2O$ in 170 mL of acetone, and the resulting mixture was stirred at room temperature for 1 week to decompose any unreacted iron pentacarbonyl and Fe(0) complexes that might be present. The reaction mixture was then diluted with 500 mL of distilled water and extracted several times with ethyl acetate (5 x 100 mL portions). The combined extracts were washed with water, dried over $MgSO_4$, and filtered, and the filtrate was concentrated in vacuo to afford a viscous, dark brown oil. Dilution of this oil with an equal volume of absolute ethanol followed by refrigeration overnight resulted in precipitation of relatively pure XIX. An analytical sample of XIX was obtained following suction-filtration via column chromatography on Florisil (100-200 mesh, 10% ethyl acetate-hexane eluent); recrystallization from ethyl acetate-hexane mixed solvent afforded colorless microcrystalline cage dimer XIX (1.1 g, 23%); mp 140-141°C. Isolation of dimer ketone XVIII from the filtrate was

accomplished via column chromatography on Florisil (100-200 mesh, 15% ethyl acetate-hexane eluent). The first fraction collected contained 7.51 g of unreacted 7-p-anisoyloxynorbornadiene. The second fraction contained dimer ketone XVIII (0.19 g, 4%) which was recrystallized from ethyl acetate-hexane mixed solvent affording microcrystalline solid XVIII (mp 241.3-241.7°C). Subsequent fractions contained 1.93 g of uncharacterized residues.

Characterization of Cage Dimer (XIX).[29]

^{1}H NMR spectrum (300 MHz, $CDCl_3$, Fig IV-43): AA'BB' pattern (J_{AB} = 9.1 Hz), $\delta_{BB'}$ 7.97 (4 H, o-phenyl protons), $\delta_{AA'}$ 6.90 (4 H, m-phenyl protons), 5.49 (m, 2 H, C7 protons), 3.86 (s, 6 H, OCH_3), 2.93 (m, 4 H), 2.74 (m, 2 H, bridgehead protons), 2.62 (m, 2 H, bridgehead protons), 2.62 (m, 2 H), 2.61 (m, 2 H);

IR spectrum (KBr pellet, Fig IV-44): 3100-2400 (b), 1730 (s), 1637 (s), 1535 (w), 1485 (w), 1342 (s), 1310 (s), 1290 (s), 1190 (s), 1140 (m), 1122 (m), 1100 (m), 1050 (m,), 1025 (w), 967 (w), 865 (s), 783 (w), cm^{-1};

Mass spectrum (70 eV, Fig IV-45): m/e (relative intensity) 484 (M^+, 28.9), 349 (21.7), 136 (10.0), 135 (100.0):

^{13}C and Spin Echo NMR spectra (20 MHz, $CDCl_3$, Fig IV-46): δ 165.99 (s), 163.40 (s), 131.59 (d), 123.21 (s), 113.61 (d), 87.78 (d), 53.37 (d), 53.54 (d), 52.05 (d), 51.45 (d), 51.24 (d), 49.34 (d), 48.75 (d).

HOMCOR NMR spectrum (300 MHz, $CDCl_3$, Fig IV-47).

Anal. Calculated for $C_{30}H_{28}O_6$: C, 74.36; H, 5.82. Found C, 74.50; H, 5.71.

Characterization of AXTXA Dimer Ketone (XVIII).[29]

^{1}H NMR spectrum (300 MHz, $CDCl_3$, Fig IV-48): AA'BB' pattern (J_{AB} = 8.9 Hz), $\delta_{BB'}$ 7.89 (4 H, o-phenyl protons), $\delta_{AA'}$ 6.87 (4 H, m-phenyl protons), 6.21 (m, J = 6.0 Hz, J' = 3.0 Hz, 2 H, syn vinyl protons), 6.18 (m, J = 6.4 Hz, J' = 2.6 Hz, anti vinyl

protons), 4.85 (t, J = 1.7 Hz, 2 H, bridge protons), 3.32 (m, J = 3.0 Hz, J′ = 1.7 Hz, 2 H, syn bridgehead protons), 3.20 (m, J = 2.6 Hz, J′ = 1.7 Hz, 2 H, anti bridgehead protons), AB pattern (J_{AB} = 8.22 Hz), δ_B 2.70 (2 H, syn cyclopentanone ring protons), δ_A 2.31 (2 H anti cyclopentanone ring protons);

IR spectrum ($CHCl_3$ solution cell, Fig IV-49): 3000-2945 (m), 1718 (vs), 1609 (s), 1585 (m), 1512 (m), 1467 (m), 1445 (w), 1420 (w), 1380 (w), 1335 (m), 1320 (s), 1280 (br s), 1170 (s), 1115 (s), 1030 (s), 968 (w), 890 (w), 848 (m), 638 (w), 622 (w);

Mass spectrum (70 eV, Fig IV-50): m/e (relative intensity) 512 (M^+, 1.0), 136 (9.7), 134 (100.0), 77 (6.1);

^{13}C and Spin Echo NMR spectra (20 MHz, $CDCl_3$, Fig IV-51): δ 216.84 (s), 166.49 (s), 163.53 (s), 134.29 (d), 133.23 (d), 131.66 (d), 122.39 (s), 113.61 (d), 84.90 (d), 57.87 (d), 55.36 (d), 52.84 (d), 50.53 (d), 45.57 (d).

Anal. Calculated for $C_{31}H_{28}O_7$: C, 72.64; H, 5.51. Found; C, 72.35; H, 5.44.

Synthesis of Cage Diol (XXXX)[29]

A mixture of 0.8 g (1.7 mmol) of cage diester XIX (alternatively, cage diester XVI may be used), 0.2 g (3.6 mmol) of potassium hydroxide (finely ground), and 0.2 mL of water was dissolved in 40 mL of absolute ethanol and then refluxed for 3.5 hours. The resulting mixture was cooled and suction-filtered. Chloroform (150 mL) was added to the filtrate, and the resulting mixture was extracted with dilute aqueous sodium bicarbonate solution. The organic layer was washed with water, dried over anhydrous magnesium sulfate, and filtered, and the filtrate was concentrated in vacuo. The waxy residue thereby obtained was recrystallized from chloroform, affording cage diol XXXX as a colorless microcrystalline solid (0.31 g, 85%), mp 207-209°C. An analytical sample, mp 209.5°C, was obtained by chromatography on Florisil (chloroform eluent) followed

by recrystallization from chloroform.

Characterization of Cage Diol (XXXX).[29]

^{1}H NMR spectrum (300 MHz, Pyr-d_5, Fig IV-54): δ 5.36 (br s, 2 H, OH), 4.80 (t, J = 1.8 Hz, 2 H, bridge protons), 3.17 (m, 4 H, non-bridgehead protons), 2.64 (m, 2 H, bridgehead protons), 2.48 (m, 2 H, bridgehead protons), 2.46 (m, 4 H, non-bridgehead protons);

IR spectrum (KBr pellet, Fig IV-55): 3282 (vs), 2950 (s), 2875 (s), 1430 (w), 1342 (s), 1315 (s), 1309 (m), 1290 (m), 1250 (m), 1228 (s), 1197 (m), 1174 (w), 1122 (m), 1072 (s), 1040 (s), 990 (w), 915 (w), 872 (w), 804 (m), 777 (w), 672 (w) cm^{-1};

Mass spectrum (70 eV, Fig IV-56): m/e (relative intensity) 217 (17.5), 216 (M^+, 100.0), 215 (20.8), 214 (18.1), 198 (31.7), 187 (50.5), 169 (13.0), 159 (17.3), 141 (13.5), 133 (10.5), 129 (15.2), 128 (12.3), 121 (12.1), 120 (11.5), 117 (12.9), 115 (19.5), 108 (12.8), 105 (27.0), 104 14.7), 91 (40.7), 79 (27.3), 78 (11.5), 77 (26.1), 65 (10.1), 32 (20.8), 28 (40.3);

^{13}C NMR spectra (20 MHz, Pyr-d_5, Fig IV-57): δ 85.85 (d), 57.07 (d), 54.51 (d), 52.32 (d), 51.70 (d), 50.15 (d), 49.51 (d).

Anal. Calculated for $C_{14}H_{16}O_2$: C, 77.75; H, 7.46. Found, C, 77.98; H, 7.61.

Synthesis of Cage Diketone (XXXXI)[29]

To 0.2 g (0.9 mmol) of cage diol (XXXX) dissolved in a minimum amount of dimethyl sulfoxide was added 3 mL of methylene chloride. The resulting mixture was added rapidly at room temperature to a vigorously stirred mixture of 0.7 g (3.3 solution. The organic layer was washed with water, dried over anhydrous magnesium sulfate, and XXXX, the light orange suspension of PCC rapidly darkened. The mixture was stirred at room temperature overnight, at which time the mixture was extracted several times with ether. The combined ethereal extracts were washed with water, dried over anhydrous

magnesium sulfate, and filtered, and the filtrate was concentrated in vacuo. The solid residue was recrystallized from chloroform-hexane mixed solvent, affording cage diketone XXXXI (0.185 g, 93%) as a colorless microcrystalline solid, mp 309-311° (sealed tube). An analytical sample of XXXXI, mp 313°C, was obtained by careful column chromatography on Florisil (60-100 mesh, 1:1 chloroform-hexane eluent) followed by repeated recrystallization of the eluate from chloroform-hexane mixed solvent.

Characterization of Cage Diketone (XXXXI).[29]

^{1}H NMR spectrum (300 MHz, $CDCl_3$, Fig IV-58): δ 2.85 (br, 8 H, non-bridgehead protons), 2.44 (br, 4 H, bridgehead protons);

IR spectrum (CCl_4 solution cell, Fig IV-59): 3018 (m), 2978 (m), 1787 (m), 1775 (s), 1696 (s), 1321 (w), 1172 (w), 1145 (m), 892 (m) cm^{-1};

Mass spectrum (70 eV, Fig IV-60): m/e (relative intensity) 212 (M^+, 64.1), 156 (10.7), 155 (12.1), 141 (15.0), 115 (22.4), 106 (100.0), 91 (53.3), 78 (51.1), 77 (21.0), 76 (10.0), 65 (11.7);

^{13}C NMR spectra (20 MHz, $CDCl_3$, Fig IV-61): δ 214.58 (s), 49.46 (d), 48.89 (d).

Anal. Calculated for $C_{14}H_{12}O_2$: C, 79.23; H, 5.70. Found C, 79.31; H, 5.52.

Synthesis of 2-Carboethoxynorbornadiene (XX)[33]

To 20.63 g (312 mmol) of freshly distilled cyclopentadiene was added 25 g (254.8 mmol) of ethyl propiolate and 3.13 mg of hydroquinone and the resulting mixture was refluxed for two hours at 110°C. After cooling, the reaction vessel was equipped with a 6-inch vigreux column, fitted with an efficient vacuum distillation head, and vacuum distilled (65°C, 0.3 torr; lit.[33] 84°C, 5.0 torr) to afford 25.42 g (60.75% yield) of 2-carboethoxynorbornadiene.

Characterization of 2-Carboethoxynorbornadiene (XX).

^{1}H NMR spectrum (60 MHz, $CDCl_3$, Fig IV-62): δ 7.62 (d, J = 3.3 Hz, 1 H, syn-cis vinyl proton), 6.90 (dd, J = 5.0 Hz, J′ = 2.9 Hz, 1 H, anti-cis vinyl proton), 6.71 (dd, J = 5.0 Hz, J′ = 2.9 Hz, 1 H, anti-trans vinyl proton), 4.18 (q, J = 7.1 Hz, 2 H, CH_2 carboethoxy protons), 3.89 (m, J = 3.3 Hz, J′ = 2.9 Hz, 1 H, trans bridgehead proton), 3.70 (m, J = 2.9 Hz, 1 H, cis bridgehead proton), 2.14 (ddd, J = 6.4 Hz, J′ = 1.8 Hz, J′′ = 1.8 Hz, 1 H syn bridge proton), 2.10 (ddd, J = 6.4 Hz, J′ = 1.8 Hz, J′′ = 1.8 Hz, 1H anti bridge proton), 1.28 (t, J = 77.1 Hz, 3 H, methyl protons);

IR spectrum (salt plate, Fig IV-63): 2975 (s), 1720 (s), 1601 (m), 1570 (w), 1465 (m), 1390 (s), 1310 (s), 1245 (s), 1175 (s), 1115 (s), 1060 (s), 1030 (s), 935 (w), 875 (m), 828 (m), 765 (s), 730 (w), 700 (m), cm^{-1};

Mass spectrum (70 eV, Fig IV-64): m/e (relative intensity) 164 (M^+, 34.6), 135 (29.1), 123 (15.5), 119 (52.2),, 107 (10.1), 106 (12.2), 105 (17.1), 95 (12.1), 93 (10.4), 92 (14.7), 91 (100.0), 86 (52.8), 84 (78.0), 79 (36.9), 78 (10.6), 77 (29.7), 67 (12.8), 66 (43.9), 65 (29.7);

^{13}C and Spin Echo NMR spectra (20 MHz, $CDCl_3$, Fig IV-65): δ 164.89 (s), 155.37 (d), 149.71 (s), 143.62 (d), 141.67 (d), 74.16 (s), 59.92 (s), 51.34 (d), 49.85 (d), 14.07 (t).

Reaction of 2-Carboethoxynorbornadiene (XX) with Iron Pentacarbonyl

To a stirred solution of 14.25 g (86.3 mmol) of 2-carboethoxynorbornadiene in 150 mL of di-n-butyl ether under nitrogen was added 34.39 g (175 mmol) of $Fe(CO)_5$, and the resulting solution was refluxed for 168 hours. Upon cooling, the rusty brown mixture was added to 131.27 g of $FeCl_3 \cdot 6H_2O$ in 500 mL of acetone and was allowed to stir for one week. At the end of this time 1500 mL of water was added and the mixture was extracted five times with 100 mL portions of ethyl ether. The combined extracts were dried over

$MgSO_4$, condensed in vacuo, and the resulting dark brown oil was put on a Florisil column (100-200 mesh). Elution with hexane gave solvent and unreacted XX (1.74 grams). The second fraction (NMR, Fig IV-66 of crude XXIa) was eluted with 10% ethyl acetate-hexane. The third fraction contained the compound(s) XXIb whose NMR is shown in Fig IV-67. Recrystallization of both crude mixtures from ethyl acetate-hexane resulted in oiling out and all attempts to isolate single pure compounds met with no success.

Characterization of Crude Mixture XXIa.

^{1}H NMR spectrum (60 MHz, $CDCl_3$, Fig IV-66): δ 7.04 (m, 2 H, vinyl protons), 4.2 (q, 4 H, CH_2 carboethoxy protons), 3.3 (m, 4 H, bridgehead protons), 2.55 (d, 2 H, syn-cyclopentanone ring protons), 2.1 (d, 2 H, anti-cyclopentanone ring protons), 1.35 (m, 10 H, four C7 and six CH_3 protons).

Characterization of Crude XXIb.

^{1}H NMR spectrum (60 MHz, $CDCl_3$, Fig IV-67): δ 7.04 (m, 2 H, vinyl protons), 4.2 (q, 4 H, CH_2 carboethoxy protons), 3.5 (m, 1 H, bridgehead proton), 3.3 (m, 2 H, bridgehead protons), 3.1 (m, 1 H, bridgehead proton), 2.55 (d or m, 2H, anti-cyclopentanone ring protons), 1.3 (m, 10 H, four C7 and six CH_3 carboethoxy protons).

Conclusion

Concerning the stereochemistry and mechanism of the iron pentacarbonyl-promoted coupling of strained olefins to carbon monoxide, it has been shown that the presence of a lone pair-bearing substituent at the 7-position is not necessarily sufficient to induce SXTNS dimer ketone formation. The dimeric ketone products which result from the reactions of iron pentacarbonyl with 7-benzoyloxynorbornadiene and with 7-*p*-anisoyloxynorbornadiene suggest that: (i) the electron pairs on the 7-Lewis base oxygen are not sufficiently available to

direct the syn-$Fe(CO)_4$ complexation (Eq IV-4) and aid in expulsion of carbon monoxide, or (ii) the steric bulk of the aromatic ring effectively blocks the syn double bond from cyclization and insertion of CO.

The structure of cage dimer ketone diester compound (XXXIV), which was formed in the reaction of 7-benzoyloxynorbornadiene with $Fe(CO)_5$, was suggested by the spectral evidence of Figs IV-26 through IV-29.

Since the dimeric ketone products resulting from the reaction 7-benzoyloxynorbornadiene are several in number, it is probable that 7-p-anisoyloxynorbornadiene also yields more than just the one AXTXA isomer.

Expansion of the meager list of functionalized HTCD's has been demonstrated by synthesis of cage diesters XVI and XIX, and the subsequent synthesis of cage diol XXXX and unique cage diketone XXXXI.

Separation, purification, and characterization of the products resulting from the reaction of 2-carboethoxynorbornadiene with $Fe(CO)_5$ were found to be difficult. However, based upon the NMR spectra of XXIa (Fig IV-66) and XXIb (Fig IV-67), it is evident that the dimeric ketones separated from the reaction mixture contained no central cyclopentanone ring which was carboethoxy-substituted, and that the configurations of the products were XTX. A complete determination of the stereochemistry of the individual products will shed additional light on the steric and electronic factors which combine to determine the stereochemistry and mechanism of $Fe(CO)_5$-promoted coupling of norbornadienes to carbon monoxide.

BIBLIOGRAPHY

1. Marchand, A. P.; Hayes, B. R. Tetrahedron Lett. 1977, 1027.

2. (a) Marchand, A. P.; Goodin, D. B.; Hossain, M. B.; van der Helm, D. J. Org. Chem. 1984, 49, 2897. (b) Goodin, D. B.; B.S. Thesis, University of Oklahoma, 1977.

3. Speert, A.; Gelan, J.; Anteunis, M.; Marchand, A. P.; Laszlo, P. Tetrahedron Lett. 1973, 2271.

4. (a) King, R. B. "Transition Metal Organic Chemistry"; Academic Press: New York, 1969; pp 143-144. (b) Pettit, R.; Emerson, G. F. Adv. Organometal. Chem. 1964, 1, 1.

5. (a) Green, M.; Lucken, E. A. C. Helv. Chim. Acta 1962, 45, 1870. (b) Cookson, R. C.; Henstock, J.; Hudec, J. J. Am. Chem. Soc. 1966, 88, 1059.

6. Cf. (a) Weissberger, E. W.; Laszlo, P. Acc. Chem. Res. 1976, 9, 209. (b) Weissberger, E.; Page, G. J. Am. Chem. Soc. 1977, 99, 147.

7. Mantzaris, J.; Weissberger, E. J. Am. Chem. Soc. 1974, 96, 1873, 1880.

8. Grandjean, J.; Laszlo, P.; Stockis, A. J. Am. Chem. Soc. 1974, 96, 1622.

9. Laszlo, P.; Stockis, A. J. Organometal. Chem. 1976, 117, C41.

10. Laszlo, P.; Stockis, A. "Abstracts of Papers", 1st Chemical Congress of the North American Continent, Mexico City, Mexico, Nov. 30-Dec. 5, 1975; Paper No. ORGA-59.

11. (a) Astin, K. B.; Mackenzie, K. J. Chem. Soc. Perkin Trans. 2 1975, 1004. (b) Mazzocchi, P. H.; Stahly, B.; Dodd, J.; Rondan, N. G.; Domelsmith, L. N.; Rozeboom, M. D.; Caramella, P.; Houk, K. N. J. Am. Chem. Soc. 1980, 92, 6482.

12. Marchand, A. P. "Abstracts of Papers", 38th Southwest and 6th Rocky Mountain Regional Meeting of the American Chemical Society, El Paso, Tx, December 1-3, 1982; American Chemical Society: Washington, D. C., 1982, Abstr. 235.

13. Marchand, A. P.; Hayes, B. R.; van der Helm. D.; Neely, S. C. "Abstracts of Papers", 1st Chemical Congress of the North American Continent, Mexico City, Mexico, November 30-December 5, 1975; Paper No. ORGA-59.

14. Grevels, F. W.; Schulz, D.; von Gustorf, E. K. Angew. Chem. Int., Ed. Engl. 1974, 13, 534.

15. A. P. Marchand personal communication.

16. Shoolery, J. N. J. Nat. Prod. 1984, 47, 226.

17. Marchand, A. P.; Rose, J. E. J. Am. Chem. Soc. 1968, 90, 3724.

18. Snyder, E. I.; Franzus, B. J. Am. Chem. Soc. 1964, 86, 1166.

19. Baird, W. C.; Surridge, H. J. Org. Chem. 1972, 37, 304.

20. (a) Nagayama, K.; Bachmann, P.; Wurtrich, K.; Ernst, R. R. J. Magn. Reson. 1978, 31, 133. (b) Hall, L. D.; Sukumar, S. Chem. Commun. 1979, 292.

21. (a) Mantzaris, J.; Weisberger, E. Tetrahedron Lett. 1972, 2815. (b) Baird, C. W.; Cookson, R. C.; Hudec, J.; Williams, R. O. J. Chem. Soc. 1963, 410.

22. Hayes, B. R., Ph.D. Dissertation, University of Oklahoma, 1975.

23. (a) Schrauzer, G. N. Adv. Catal. 1968, 18, 373. (b) Arnold, D. R.; Trecker, D. J.; Whipple, E. B. J. Am. Chem. Soc. 1965, 87, 2596.

24. (a) Schrauzer, G. N.; Ho, R. K. Y.; Schlesinger, G. Tetrahedron Lett. 1970, 543. (b) Schrauzer, G. N.; Bastian, B. N.; Fosselius, G. A. J. Am. Chem. Soc. 1966, 88, 4890.

25. (a) Lemal, D. M.; Shim, K. S. Tetrahedron Lett. 1961, 368. (b) Bird, C. W.; Colinese, D. L.; Cookson, R. C.; Hudec, J.; Williams, R. O. Tetrahedron Lett. 1961, 373.

26. (a) Acton, N.; Roth, R. J.; Katz, T. J.; Frank, J. K.; Maier, C. A.; Paul, I. C. J. Am. Chem. Soc. 1972, 94, 5446. (b) Scharf, H. D.; Weisgerber, G.; Hover, H. Tetrahedron Lett. 1967, 4227. (c) Hollowood, M. A.; McKervey, M. A.; Hamilton, R.; Rooney, J. J. J. Org. Chem. 1980, 45, 4954.

27. Chow, T. J.; Wu, M.; Liu, L. J. Organometal. Chem. 1985, 281, C33.

28. Godleski, S., University of Rochester, personal communication.

29. Marchand, A. P.; Earlywine, A. D. J. Org. Chem. 1984, 49, 1660.

30. Corey, E. J.; Suggs, J. W. Tetrahedron Lett. 1975, 2747.

31. McCasland, G. E.; Horvat, R.; Roth, M. R. J. Am. Chem. Soc. 1959, 81, 2399.

32. Woodward, R. B.; Hoffmann, R. "The Conservation of Orbital Symmetry"; Verlag Chemie: Weinheim/Bergstr., West Germany, and Academic Press: New York, 1970; p 169.

33. Graham, P. J.; Buhle, E. L.; Pappas, N. J. Org. Chem. 1961, 26, 4658.

34. Tanida, H.; Tsuji, T. J. Org. Chem. 1964, 29, 849.

35. Cason, J.; Rapoport, H. "Basic Experimental Organic Chemistry"; Prentice-Hall, Inc.: Englewood Cliffs, NJ., 1964; p 249.

36. Shvo, Y.; Hazum, E. J. Chem. Soc., Chem. Commun. 1974, 336.

37. Mass spectral data on dimer ketone XV was provided by C. E. Costello, Massachusetts Institute of Technology, Cambridge, Ma.

38. The assistance of M. J. Heeg in performing the X-ray crystal studies of compounds XXXII and XXXIII is appreciated.

39. "International Tables for X-ray Crystallography", Vol. 1, 3rd ed., Kynoch Press, Birmingham, England (1969).

40. All computations were performed using local modifications of the programs of SHELX-76: Sheldrick, G. M., University Chemical Laboratory, Cambridge, England, 1976.

41. $R_w=[\Sigma w(|F_o|-|F_c|)^2/\Sigma w(F_o)^2]^{1/2}$.

42. "International Tables for X-ray Crystallography", Vol. 4, Kynoch press, Birmingham, England (1974).

PART V

THE ELECTROPHILIC AROMATIC THALLATION OF SELECTED BIOMOLECULES

Introduction

Thallium(III) trifluoroacetate (TTFA) has been shown to be an extremely reactive thallating agent for electrophilic aromatic substitution.[1-3] Acid sensitive substrates may be thallated in the absence of light with a solution of TTFA in acetonitrile, while less sensitive aromatics may be thallated with TTFA in trifluoroacetic acid (TFA). Alternatively, TTFA can be isolated after its preparation (refluxing thallium(III) oxide in TFA) and added to TFA or acetonitrile solutions of the substrate to be thallated. $ArTl(OCOCF_3)_2$ (Arylthallium bistrifluoroacetate) products of thallation are generally stable, colorless, crystalline solids and in general are soluble in solvents such as methanol, ethanol, glyme, acetonitrile, tetrahydrofuran, and DMSO.[3a,b] Identification of these $ArTl(OCOCF_3)_2$ compounds by NMR is facilitated by Tl-H coupling constants which are about 130 times greater than the corresponding H-H coupling constants.[4] This has been qualitatively attributed to Fermi contact interaction resulting from the large effective nuclear charge on the thallium atom (see Fig V-1).[4,5] Also, infrared spectra of $ArTl(OCOCF_3)_2$ compounds normally possess three sets of absorptions at approximately 720, 800, and 835 cm^{-1} which are assignable, respectively, to the $C-CO_2$ in-plane bending, CF_3 symmetric stretching, and C-C stretching modes of the trifluoroacetate group (Fig V-2).[6,7] Another product of thallation, $Ar_2Tl(OCOCF_3)$, possesses sharp singlet absorptions in

FIGURE V-1

NMR Spectrum of Phenylthallium Bis(trifluoroacetate).[86]

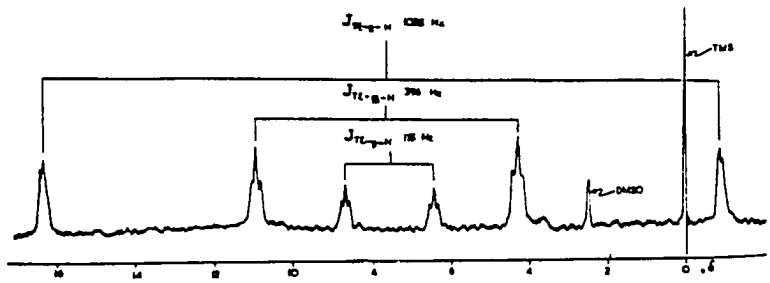

FIGURE V-2

IR Spectrum of Mesitylthallium Bis(trifluoroacetate).[86]

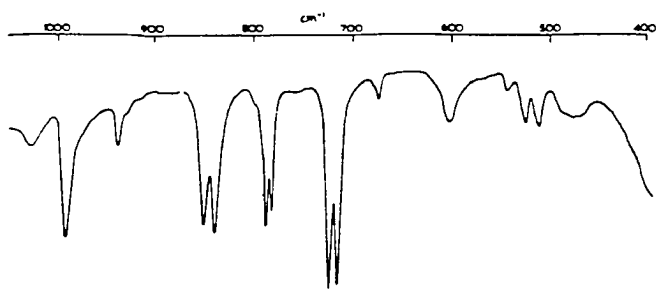

FIGURE V-3

IR Spectrum of Dimesitylthallium Trifluoroacetate.[86]

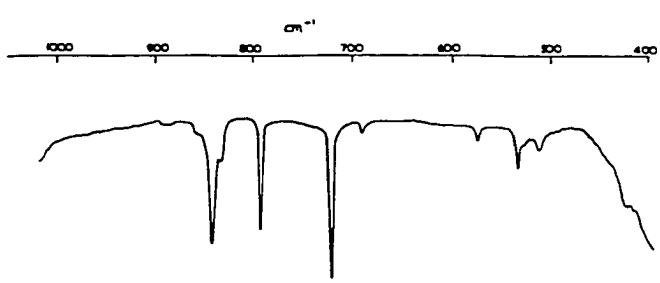

this same region, while $ArTl(OCOCF_3)_2$ compounds always exhibit doublets[4] (cf. Fig V-2 and V-3).

Aromatic thallation is a reversible reaction. The large steric bulk of TTFA results in predominant para substitution (kinetic control) for many monosubstituted benzenoid compounds containing simple ortho-para directing substituents (Eq V-1). Under the

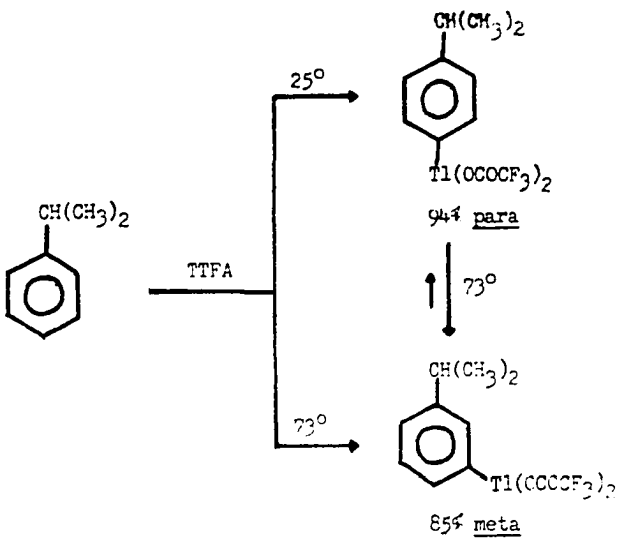

Rate-controlled

Eq V-1

Equilibrium-controlled

conditions of refluxing TFA (73°C), meta substitution (thermodynamic control) is favored. When the substrate is benzoic acid, methyl benzoate, or benzyl methyl ether, ortho substitution predominates following initial complexation of the thallium electrophile with the substituent (via intramolecular delivery to the nearby ortho position, Eq V-2). Thus, choice of substrate and/or reaction conditions provides a tremendous amount of control over

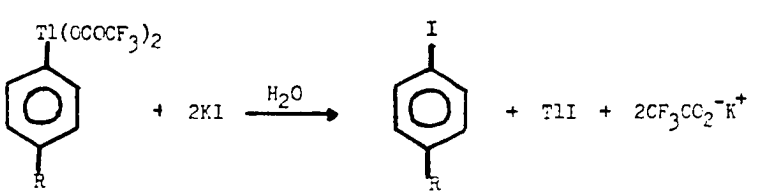

Eq V-2

orientation in these electrophilic aromatic substitution reactions.[1]

Another feature of interest in organothallium chemistry is the ease with which $Tl(OCOCF_3)_2$ can be replaced by iodide, chloride, and fluoride to yield stable $ArTlX_2$(X = I, Cl, F) compounds.[8] A simple in situ one-step synthesis of aromatic iodides may be effected by addition of an aqueous potassium or sodium iodide solution to a solution of the aromatic in TFA (Eq V-3).[9]

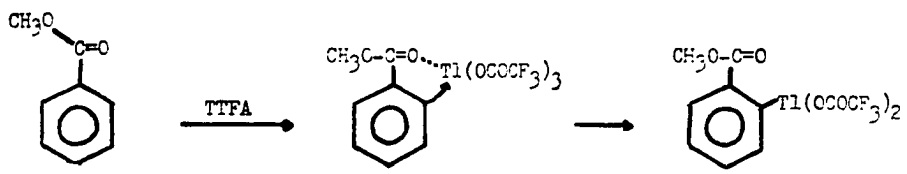

Eq V-3

Results and Discussion

The preparation and utilization of these synthetically useful $ArTl(OCOCF_3)_2$ intermediates is the subject this chapter with emphasis placed on thallation of certain biomolecules. These reactions may then be used to introduce radioactive iodine (^{123}I, ^{131}I) into molecules such as those in Table V-1 which are suitable for in vivo labeling and subsequent in vitro tracer studies.

Identification of TTFA (I) from reaction 1 (Table V-2) is based on the IR spectrum (Fig V-4). The three singlets at ca. 729, 812, and 848 cm^{-1} correspond to the $C-CO_2$ in-plane bending, CF_3 symmetric stretching, and C-C stretching of the trifluoroacetate group as discussed earlier. Subsequent reactions of this product also confirmed its identity.

Compound II, formed upon reaction of benzoic acid with TTFA, has a melting point of 240-246°C (decomp). Although the observed melting point is close to the literature value (mp 247-248°C), the melting points of $ArTl(OCOCF_3)_2$ compounds cannot be used as reliable criteria of purity since they vary erratically according to

TABLE V-1

Suggested Syntheses of Arylthallium Biomolecular Intermediates Suitable for In-Vivo Radioiodination and Tracer Studies.

Estradiol $\xrightarrow{\text{TTFA/TFA}}$ 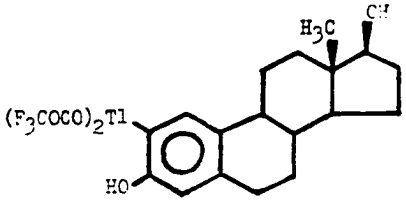

Eq V-4

Diethylstilbestrol $\xrightarrow{\text{TTFA/TFA}}$ 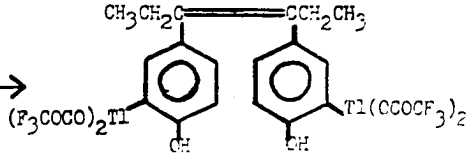

Eq V-5

'trans' aryl groups

L-tyrosine $\xrightarrow{\text{TTFA/TFA}}$ 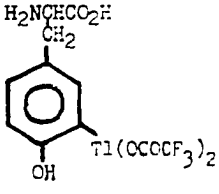

Eq V-6

L-tryptophan $\xrightarrow{\text{TTFA/TFA}}$ 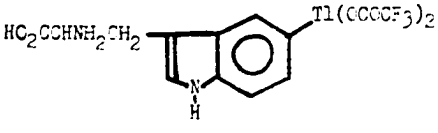

Eq V-7

Tyramine $\xrightarrow{\text{TTFA/TFA}}$ 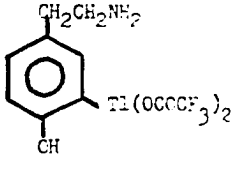

Eq V-8

TABLE V-1 (cntd.)

Epinephrine $\xrightarrow{\text{TTFA/TFA}}$ 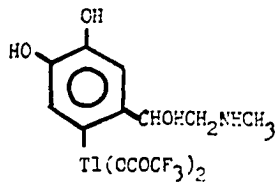

Eq V-9

Norepinephrine $\xrightarrow{\text{TTFA/TFA}}$ 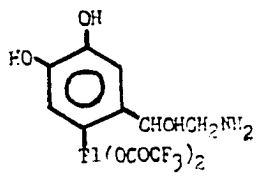

Eq V-10

Mescaline $\xrightarrow{\text{TTFA/TFA}}$ 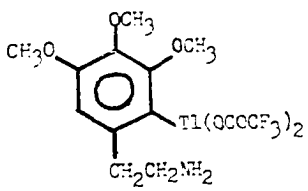

Eq V-11

Phenylephrine $\xrightarrow{\text{TTFA/TFA}}$ 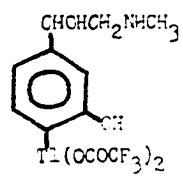

Eq V-12

Dopamine $\xrightarrow{\text{TTFA/TFA}}$ 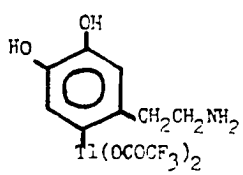

Eq V-13

TABLE V-2

Preliminary Reactions Conducted in Order to Produce Thallium(III) Trifluoroacetate and Several Simple Arylthallium Intermediates.

Reaction		Reference
1. $Tl_2O_3 + 6CF_3CO_2H \xrightarrow{heat} 2\ Tl(OCOCF_3)_3$	I	84[b]
2a. Benzoic Acid $\xrightarrow{TTFA}$	o-Carboxyphenylthallium bis(trifluoroacetate) II	84[a]
2b. Benzoic Acid $\xrightarrow[(2)\ KI/H_2O]{(1)\ TTFA}$	o-Iodobenzoic Acid	71[c]
3a. $PhCONH_2 \xrightarrow{TTFA}$	o-Carboxamidophenylthallium bis(trifluoroacetate) III	82[e]
3b. $PhCONH_2 \xrightarrow{TTFA}$	di(o-Carboxamidophenyl)thallium trifluoroacetate IV	
4. p-Xylene $\xrightarrow{TTFA}$	2,5-Xylylthallium bis(trifluoroacetate) V	84,91
5. Anisole $\xrightarrow{TTFA}$	p-Anisylthallium bis(trifluoroacetate) VI	84b,86

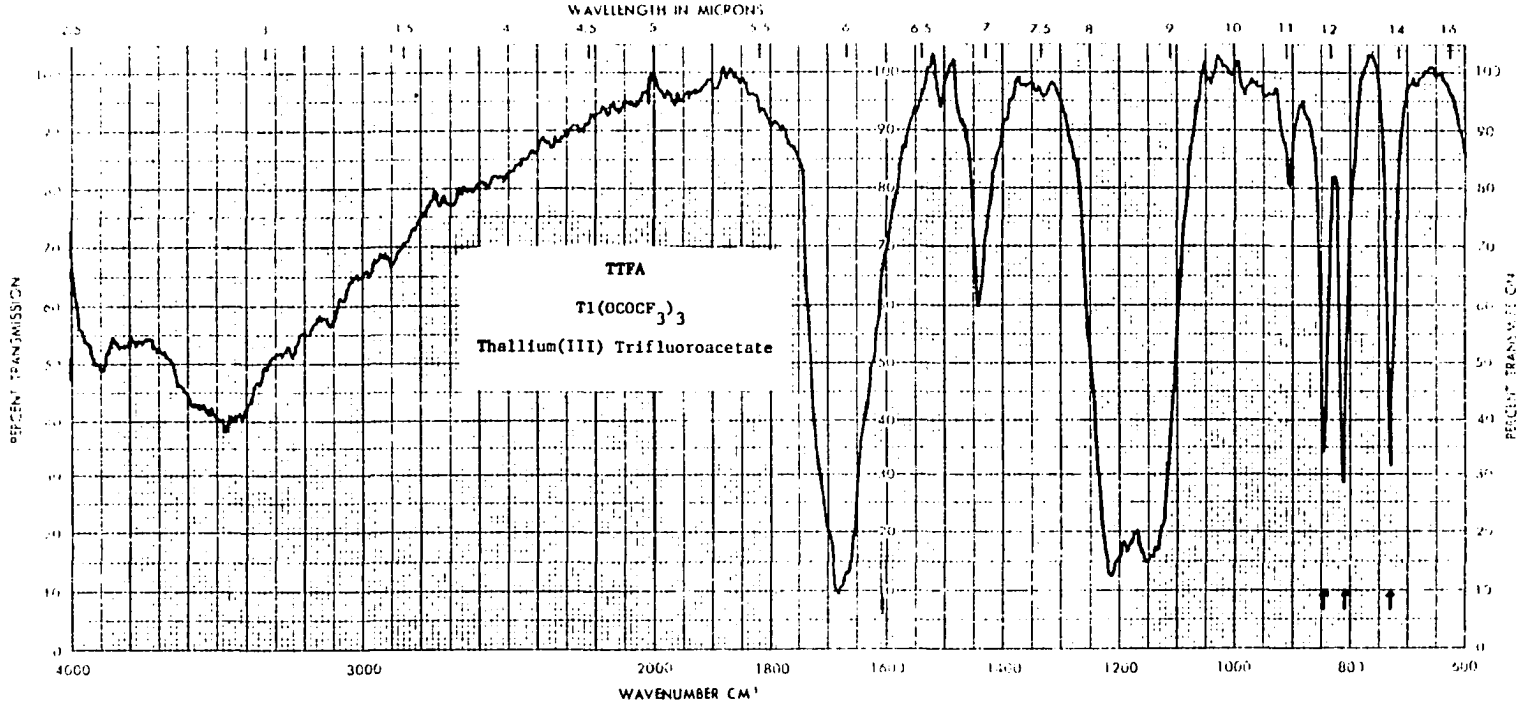

Figure V-4. IR Spectrum of Thallium(III) Trifluoroacetate (KBr).

the rate of heating, amount of sample, degree of compactness, and crystal size.[3b] The IR spectrum of thallated benzoic acid (Fig V-5) shows three doublets at 740, 800, and 863 cm^{-1} corresponding to the literature values.[4] The NMR spectrum possesses Tl-H coupling constants which also agree with the literature values (Fig V-6). The second step of reaction 2 was also performed affording o-iodobenzoic acid (NMR and mass spectrum, Figs V-7 and V-8, respectively). In addition to this, thallated benzoic acid was allowed to react with radioactive $Na^{131}I$ forming ^{131}I-o-iodobenzoic acid.[3c]

Compound III and/or IV (reaction 3) was produced in good yield[1e] and its IR is seen in Fig V-9. Absorptions at 732, 808, and 841 cm^{-1} are sharp singlets and may indicate the product to be $(H_2NCOC_6H_4)_2Tl(OCOCF_3)$ (IV). To date it has not been possible to obtain mass spectra of any of the arylthallium compounds, because of their low volatility, with the result that identification of the product(s) of reaction 3 has not been completed. The NMR (Fig V-10) is consistent with both III and IV and the Tl-H coupling constants compare well with those of thallated benzoic acid.

The IR (Fig V-11) of the product (V) of reaction 4 has values of 735, 790, and 815 cm^{-1} for the three critical doublets. Literature values of the Tl-H coupling constants are shown on the NMR spectrum (Fig V-12).[8]

Characterization of compound VI was not immediately possible since isolation proved very difficult. However, an NMR of the crude product (Fig V-13) indicates thallation has occurred. No literature references concerning isolation of thallated anisole could be located. Other workers have synthesized iodinated anisole in situ by addition of aqueous KI to a solution of the supposed thallated anisole (cf. Eq V-3) for proof that thallation had indeed occurred.[2] This procedure was duplicated (Fig V-14) since methoxy-substituted compounds play an important role in subsequent investigations of the thallation of certain biomolecules.

Table V-3 lists the earliest attempts to produce thallated

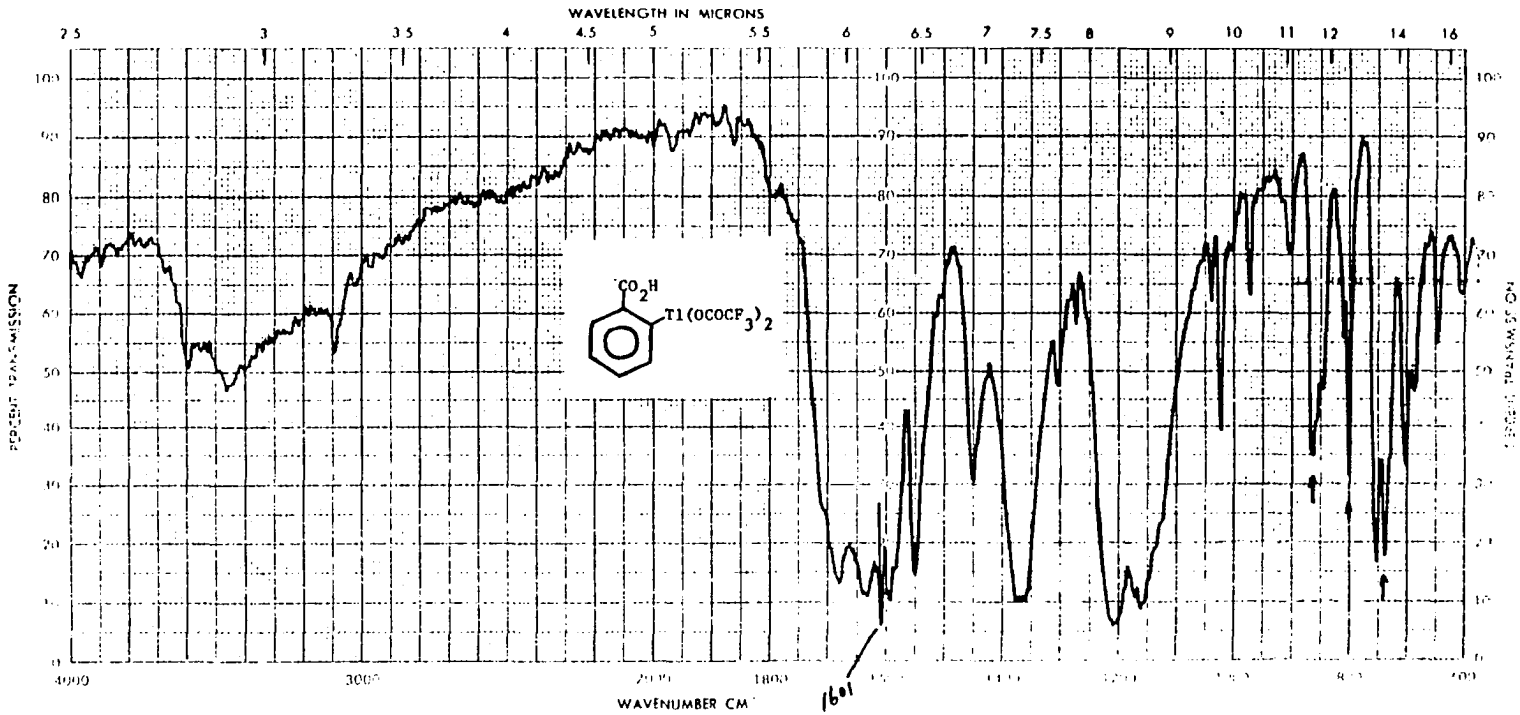

Figure V-5. IR Spectrum of o-Carboxyphenylthallium Ditrifluoroacetate II (KBr).

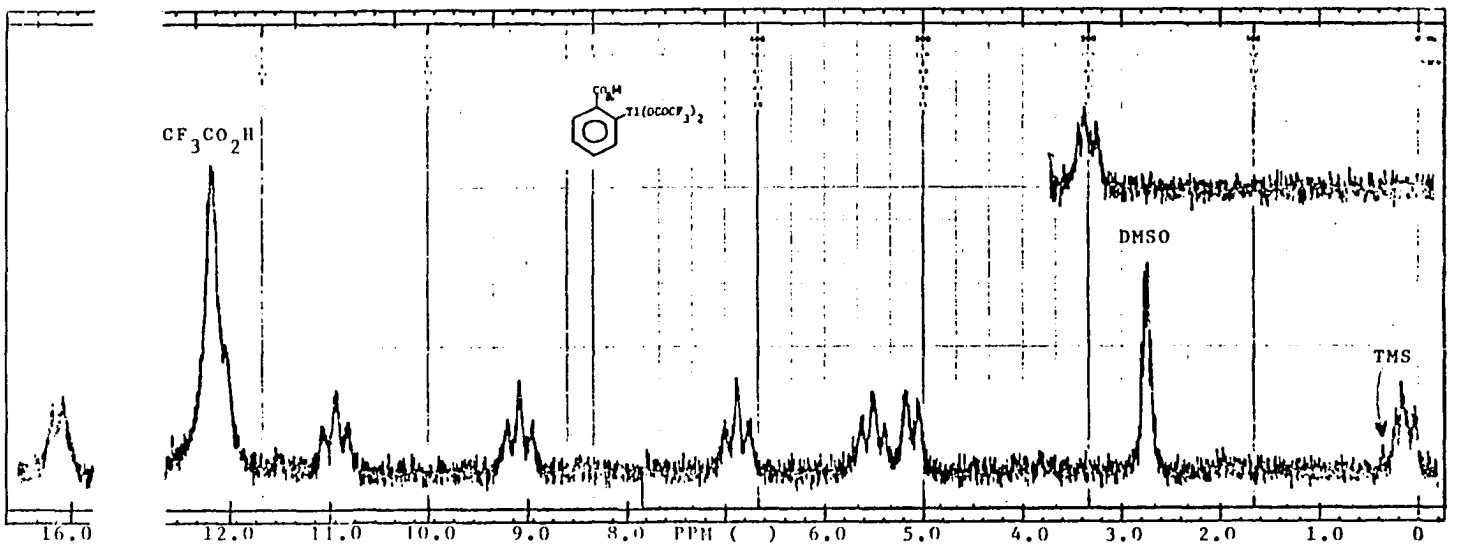

Figure V-6. 60 MHz ^{1}H NMR Spectrum of o-Carboxyphenylthallium Ditrifluoroacetate II (DMSO-d_6/TMS).

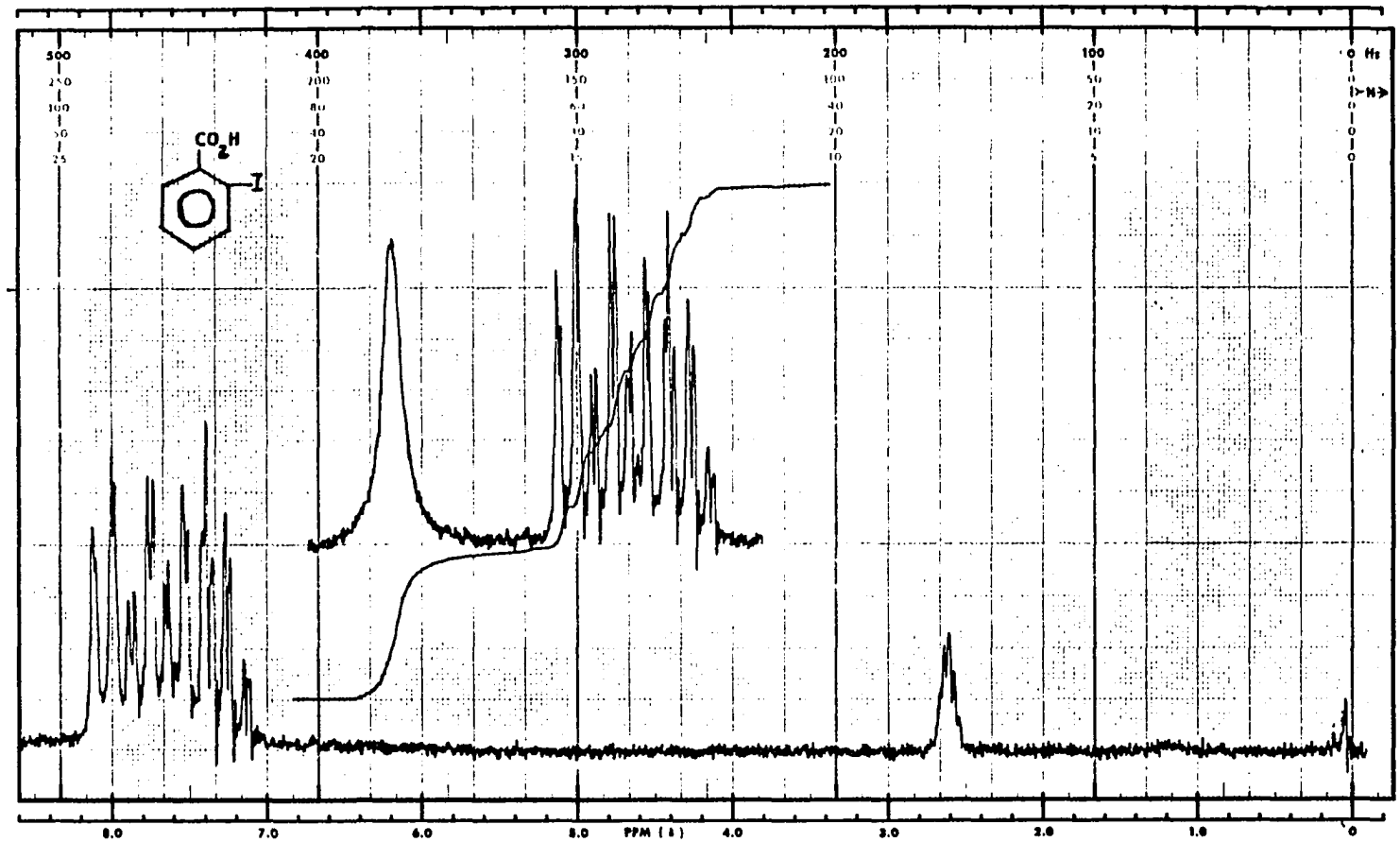

Figure V-7. 60 MHz ^{1}H NMR Spectrum of o-Iodobenzoic Acid ($CDCl_3$/TMS).

FIGURE V-8

Mass Spectrum of o-Iodobenzoic Acid.

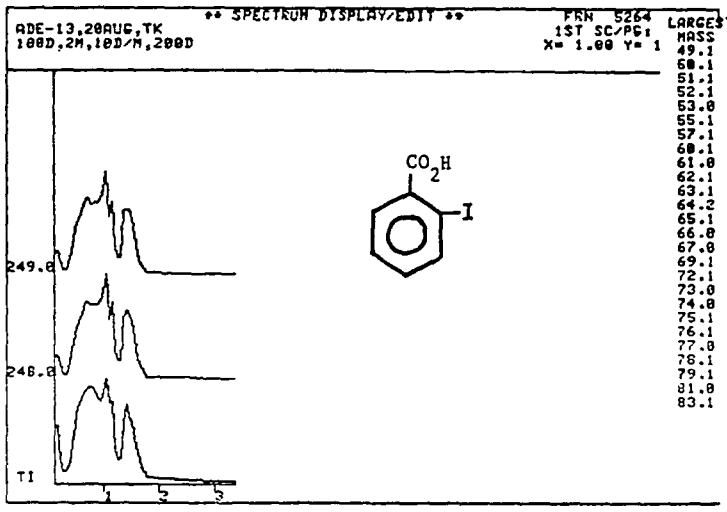

LARGEST 69

MASS	%	MASS	%	MASS	%
49.1	2.0	84.1	.2	151.9	.4
60.1	14.3	85.0	.3	152.9	.3
51.1	4.1	90.0	.1	163.9	.3
52.1	.3	91.1	.4	164.9	.2
53.0	1.3	92.0	2.3	175.9	.7
55.1	.2	93.0	5.6	177.0	.4
57.1	.2	94.1	.5	191.0	.1
60.1	.4	95.1	.2	202.9	17.7
61.0	1.1	101.2	.2	203.9	1.1
62.1	1.1	103.0	.3	219.9	.3
63.1	1.7	104.1	2.2	231.0	55.6
64.2	1.4	105.1	1.9	231.9	4.7
65.1	14.4	106.1	.2	232.9	.3
66.0	1.3	115.5	.7	247.9	100.0
67.0	.5	119.1	.3	249.0	7.5
69.1	.7	121.0	4.2	250.0	.7
72.1	.4	122.1	1.7		
73.0	5.3	123.1	.2		
74.0	19.4	124.0	.5		
75.1	10.2	127.0	27.6		
76.1	16.1	127.9	1.6		
77.0	5.2	128.9	.2		
78.1	.4	138.9	.3		
79.1	.2	142.9	.4		
81.0	.3	143.9	1.0		
83.1	.2	150.9	.2		

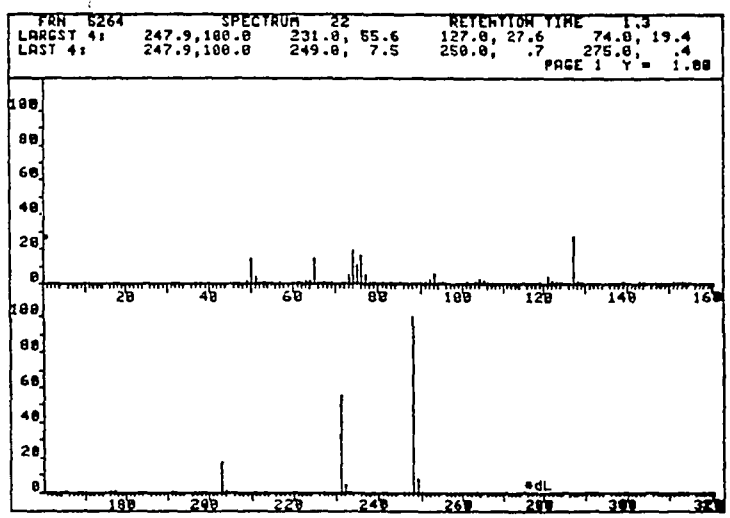

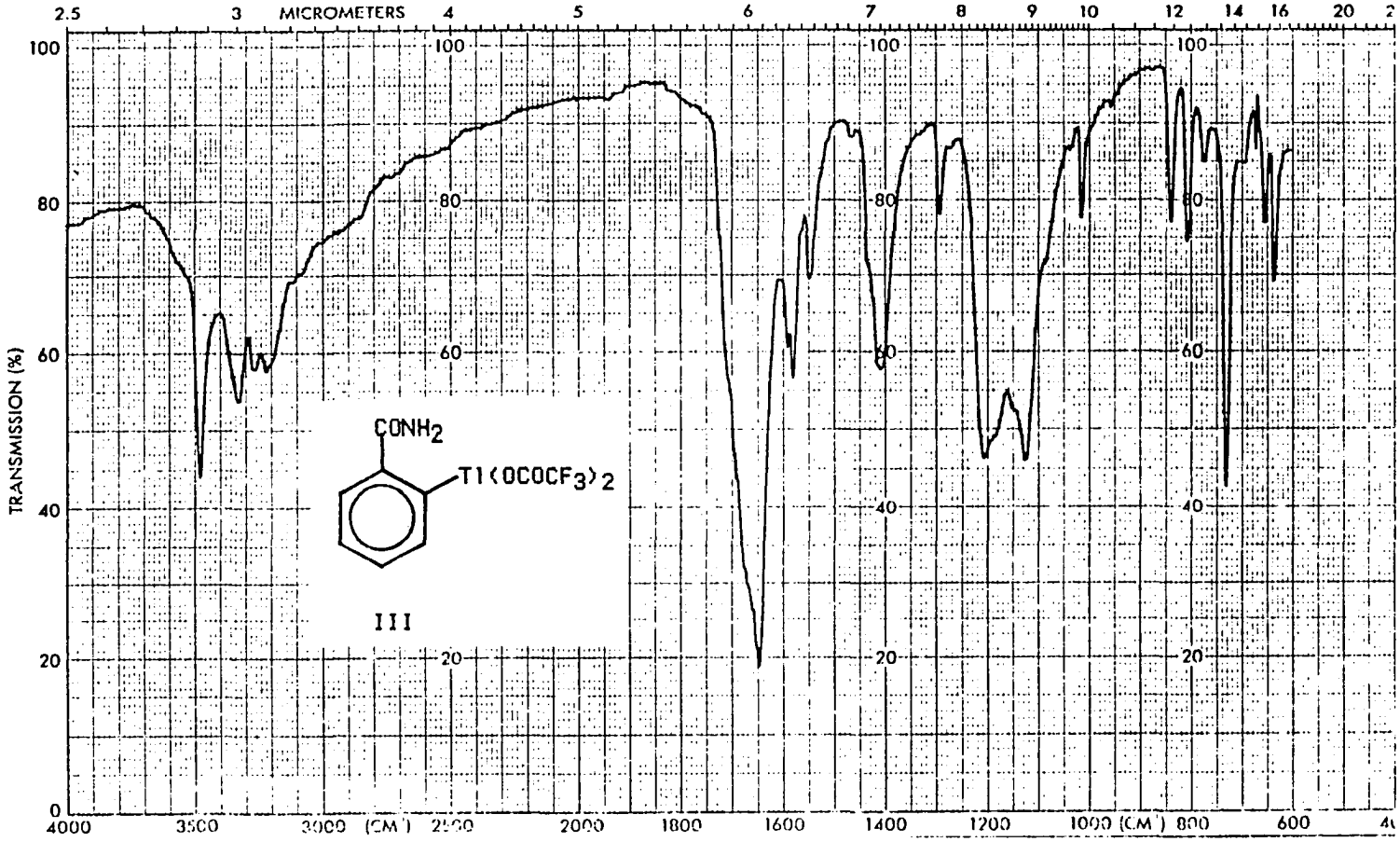

Figure V-9. IR Spectrum of o-Carboxamidophenylthallium Ditrifluoroacetate III (KBr).

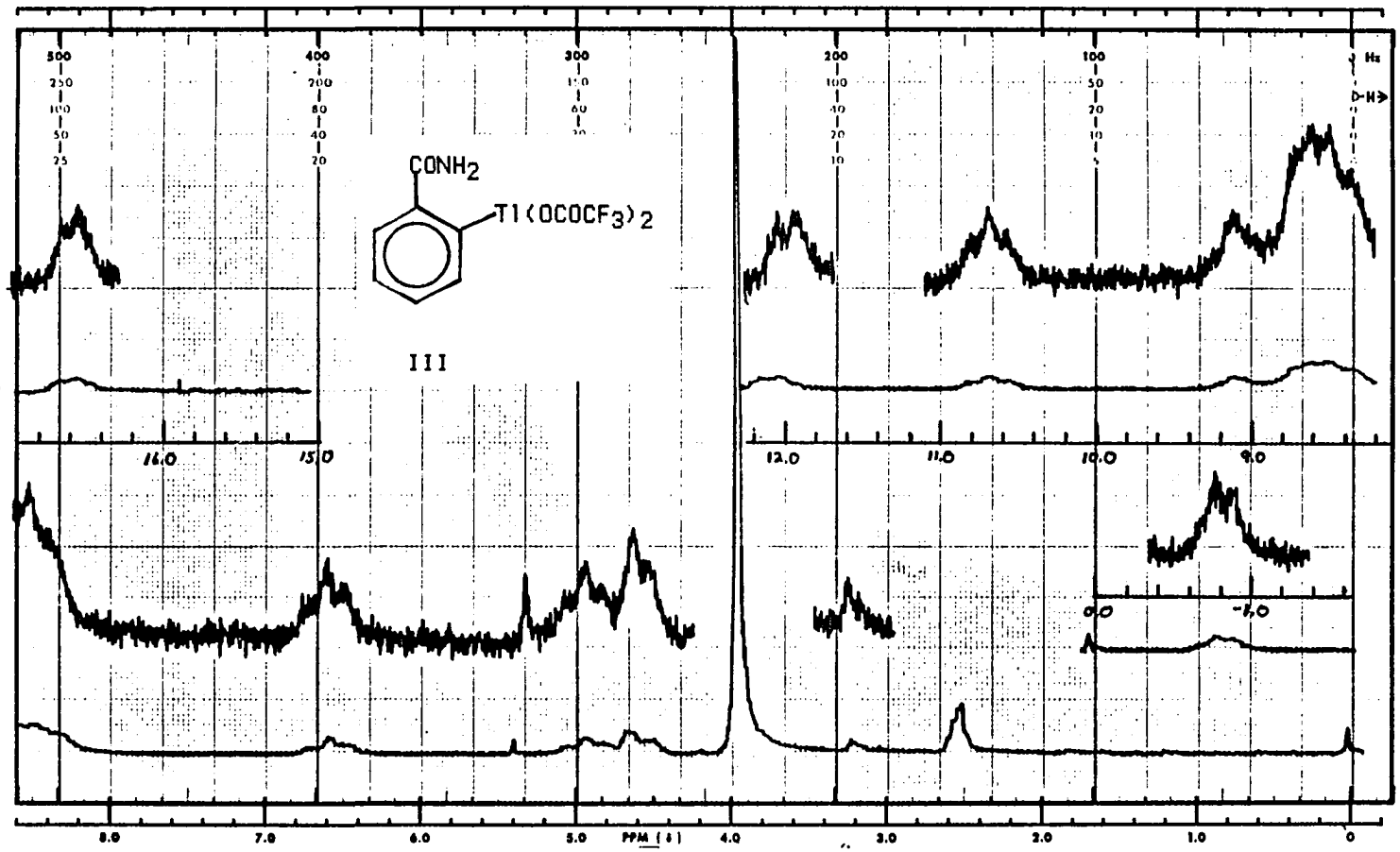

Figure V-10. 60 MHz ^{1}H NMR Spectrum of o-Carboxamidophenylthallium Ditrifluoroacetate III (DMSO-d_6/TMS).

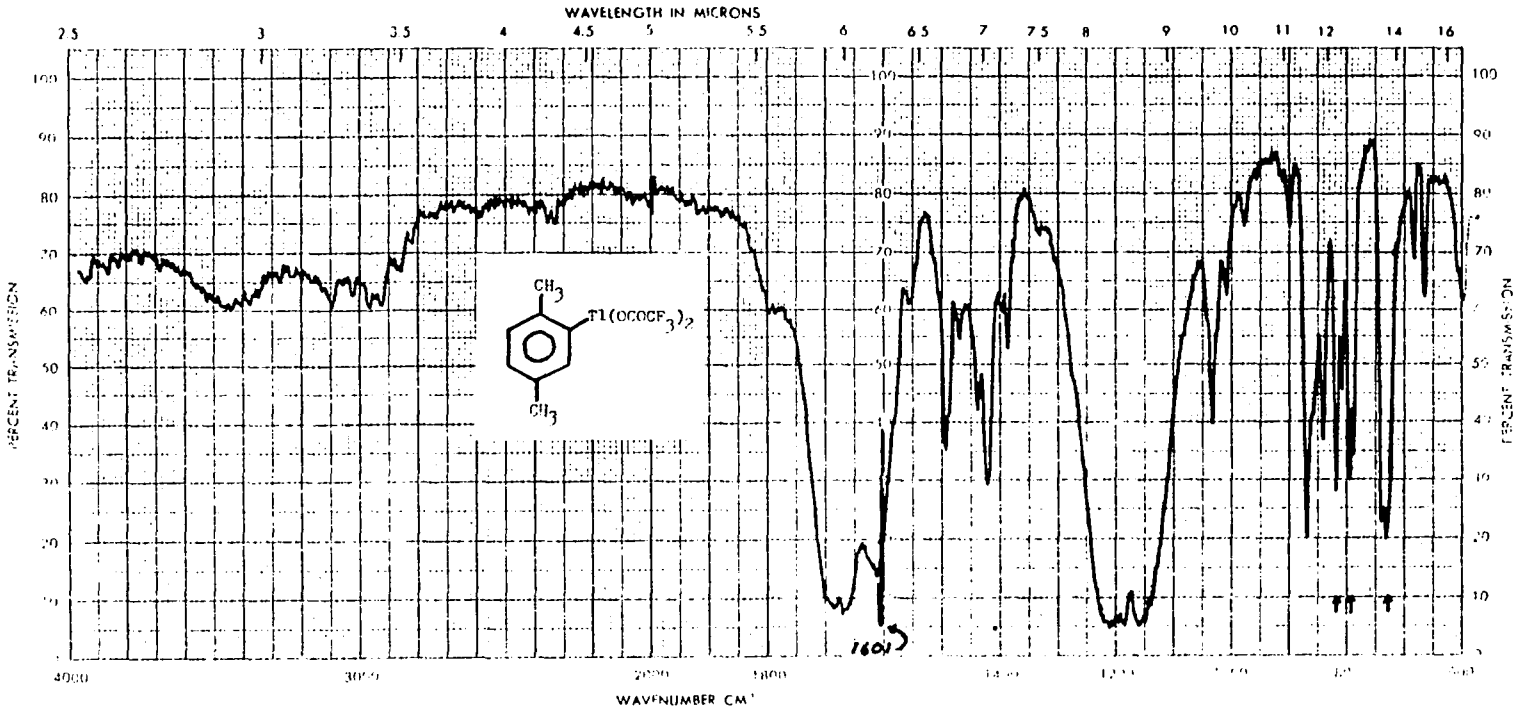

Figure V-11. IR Spectrum of p-Xylylthallium Ditrifluoroacetate V (KBr).

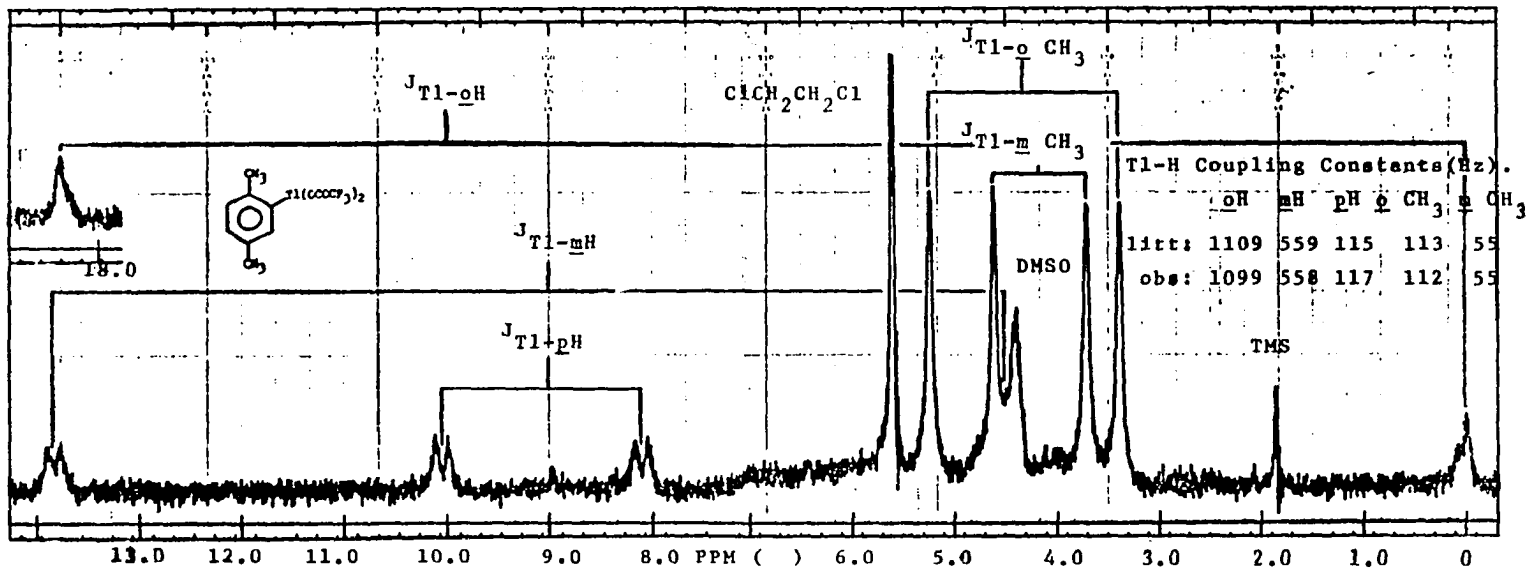

Figure V-12. 60 MHz ^1H NMR Spectrum of p-Xylylthallium Ditrifluoroacetate V ($DMSO-d_6$/TMS).

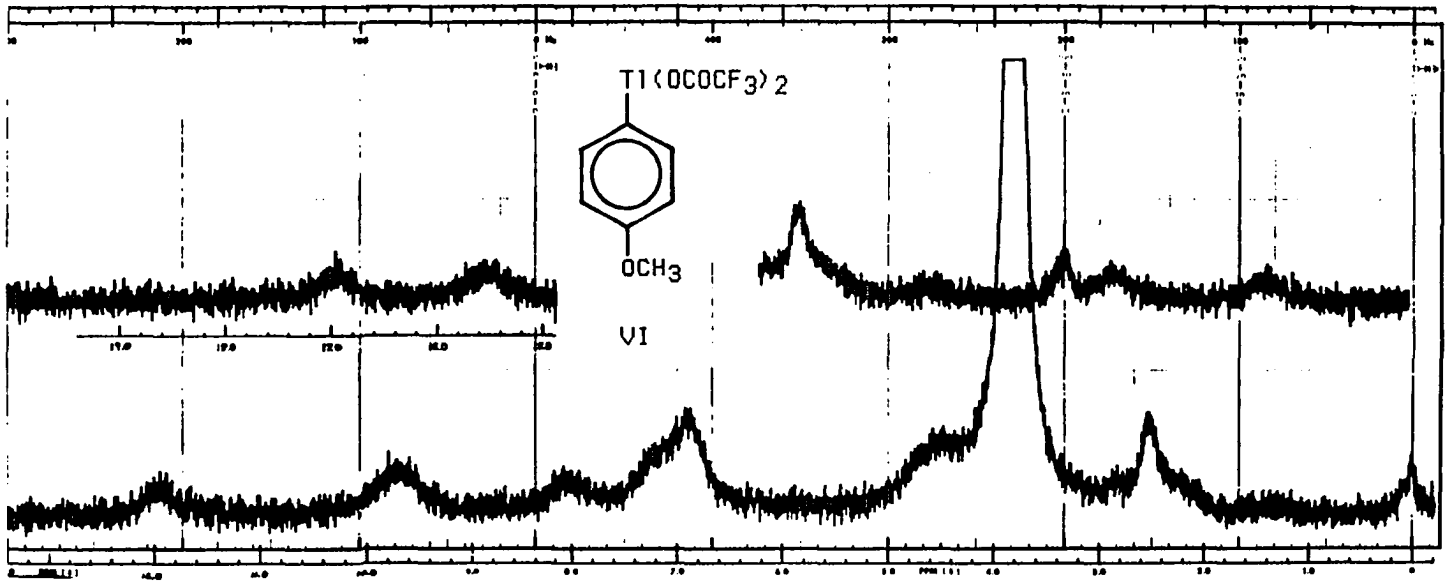

Figure V-13. 60 MHz ^{1}H NMR Spectrum of p-Anisylthallium Ditrifluoroacetate VI (DMSO-d_6/TMS).

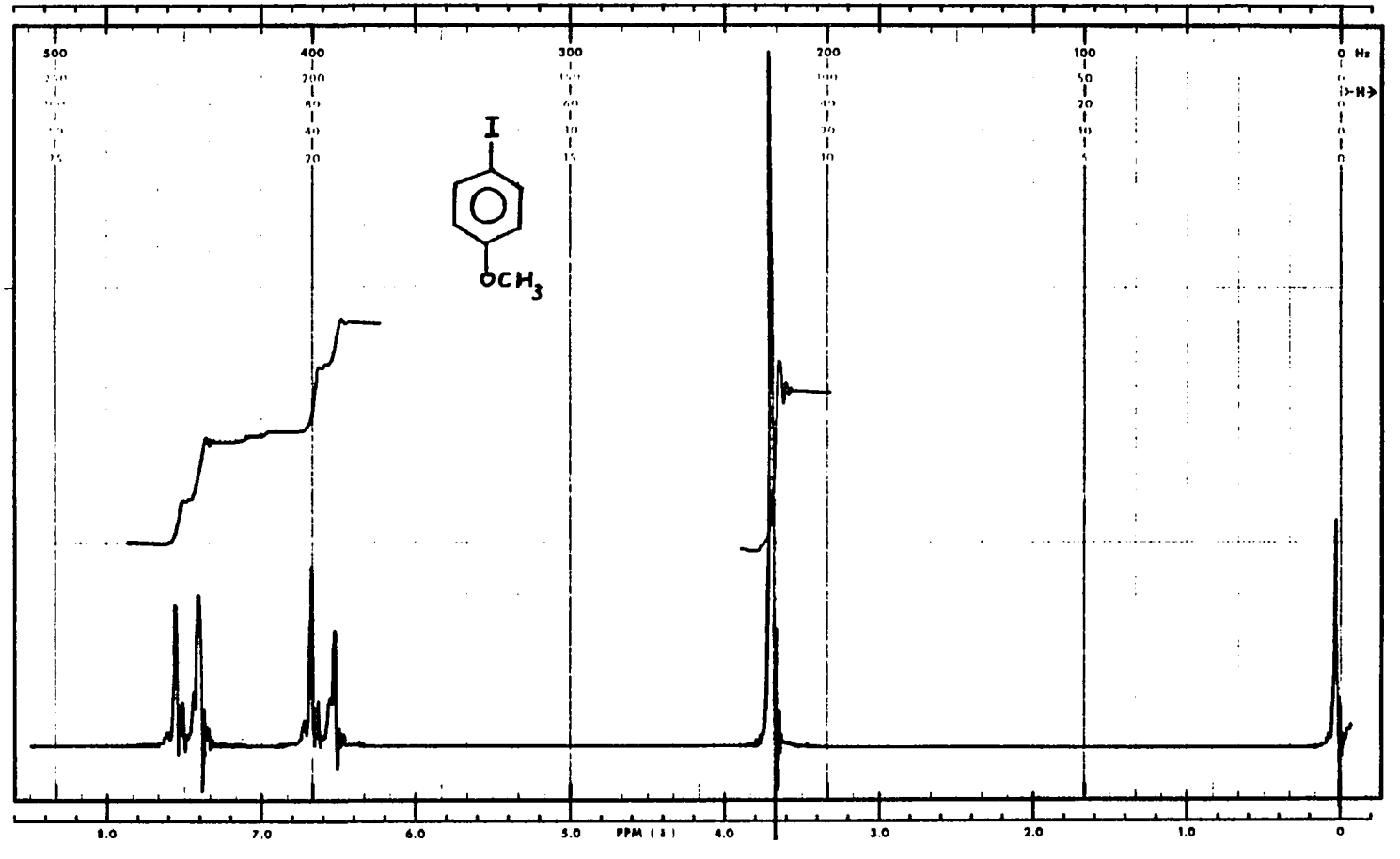

Figure V-14. 60 MHz ^{1}H NMR Spectrum of p-Iodoanisole ($CDCl_3$/TMS).

TABLE V-3

Early Attempts to Produce Thallated Hippuric Acid.

Reaction	Substrate	Reagent	Solvent	Reaction Conditions	Time (hrs)
6.(a)	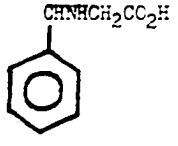	TTFA	TFA	R.T.	144
7.(b)	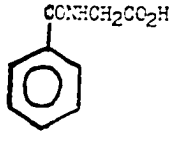	TTFA	TFA CF_3CO_2H	73°	12
8.(c)	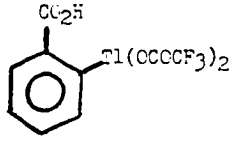	$SOCl_2$	$SOCl_2$	reflux	1.5
9.(d)	solid from reaction 8	$NH_2CH_2CO_2H$	H_2O/OH	R.T.	.17

(a) Red glassy oil obtained; IR and NMR indicated no thallation.

(b) $CF_3COOCOF_3$ added to remove H_2O; CF_3SO_3H added to increase strength of TTFA.[10]

(c) $SOCl_2$ used in attempt to make acid chloride of II, for use in reaction 9. White solid obtained.

(d) Schotten-Bauman technique; solid from reaction 8 added with shaking to 100 mg of $H_2NCH_2CO_2H$ in aqueous NaOH resulting in a clear solution. No IR evidence of thallium was in clear product oil.

hippuric acid with no success. The resulting products were uncharacterized viscous oils whose NMR and IR spectra show no evidence of thallation. Variation of reaction conditions and reaction times did not give the desired products. It may be that the Lewis acid character of thallium(III) reagents is such that they complex with amides and deactivate the aromatic ring toward electrophilic substitution. Another explanation may be that the thallium(III) reagent complexes with the carboxylic acid carbonyl more readily than with the amide carbonyl. In the case of hippuric acid, such complexation would hold the thallium reagent too far from the aromatic ring for effective electrophilic attack. Salts formed from such reactions either precipitate out or form oils upon attempted recrystallization.

N,N′-Dicyclohexylcarbodiimide (DCC, non water soluble),[11] 1-ethyl-3-(3-dimethylaminopropyl)carbodiimide hydrochloride (EDCI, water soluble),[12] and 1-cyclohexyl-3-(2-morpholinoethyl)-carbodiimide metho-p-toluene sulfonate (water soluble)[13] are examples of diimides used to facilitate peptide bond formation.

Equation V-14 illustrates the mechanism of the proposed use of

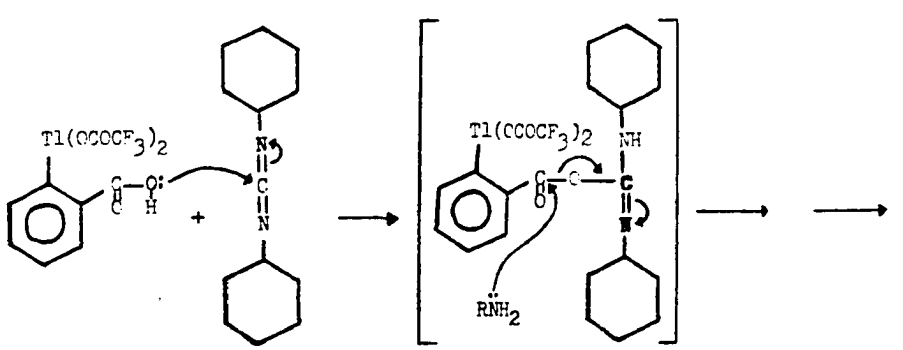

Eq V-14

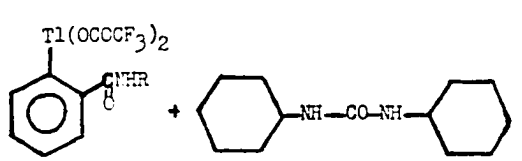

R = $-CH_2CO_2H$

R = $-CH_2CO_2Et$

R = $-CH_2CO_2(CH_3)_3$

DCC to form the peptide bond in thallated hippuric acid and several of its derivatives. Reactions 10, 11, and 12 of Table V-4 were conducted to test the feasibility of using DCC with aromatic compounds containing thallium. Compound II was allowed to react first with DCC in THF and then with $H_2NCH_2CO_2H$. The product, which precipitated as a white solid from the reaction mixture, was

TABLE V-4

Proposed Use of Dicyclohexylcarbodiimide (DCC) to Form the Peptide Bond in Thallated Hippuric Acid and its Ethyl and t-Butyl Esters.

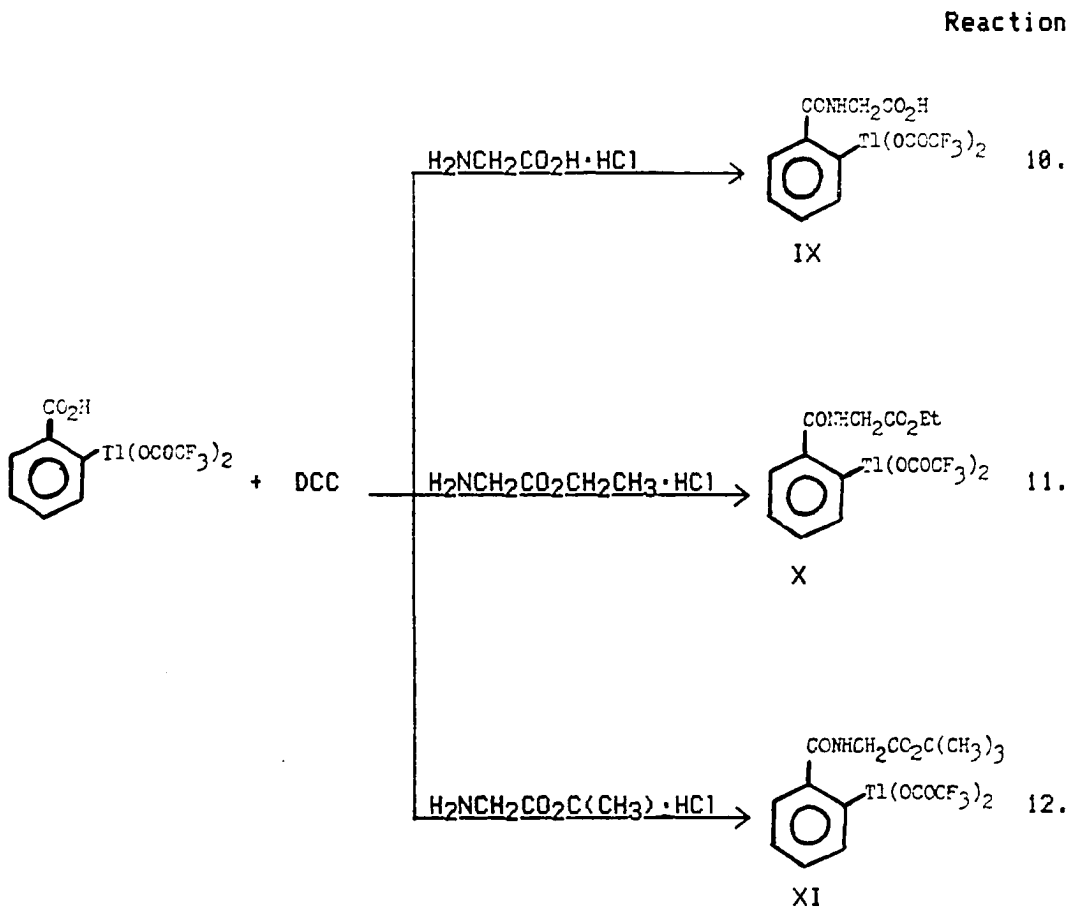

identified by comparison with Sadtler IR spectrum #895 of a known sample of dicyclohexyl urea. Workup of the remaining solution gave a white solid (IX) whose NMR in DMSO-d_6/TMS is shown in Fig V-15. Although the resolution of the figure is poor, evidence that thallation has occurred may be inferred from the chemical shifts of the signals at δ 12.0, 9.8, and 9.0. Upon consideration of the fact that the non-protected carboxyl group of glycine may compete with the amino group of glycine for attack at the ester carbonyl of the intermediate isourea (VII) (step 2 of Eq V-14), it was felt that protection of the C-terminal end of the amino acid would insure only mono-peptide formation between the C-terminal end of II and the N-terminal end of glycine.

In accordance with the above, the C-terminal-protected ethyl glycinate hydrochloride ($H_2NCH_2CO_2Et \cdot HCl$) was used in place of glycine for the reaction shown in Eq V-14. The first product isolated from the reaction was the white solid dicyclohexyl urea which precipitated from the reaction mixture at room temperature. The compound whose NMR is shown in Fig V-16 was then recovered. The IR spectrum (Fig V-17) possesses the characteristic three doublets at 722, 798, and 850 cm^{-1}. Comparison of the coupling constants of X with the literature values for II supports the belief that coupling has occurred to form the desired 2-bis(trifluoroacetato)thallio-ethyl hippurate.

Reaction 12 was run using the C-terminal-protected salt tert-butyl glycinate hydrochloride, with the easily hydrolized tert-butyl group protecting the C-terminus of the amino acid. Again, dicyclohexyl urea was initially isolated. Precipitation of compound XI (NMR, Fig V-18 and IR, Fig V-19) followed after addition of 1 mL of CF_3CO_2H to decompose unreacted DCC, and addition of 1,2-dichloroethane. Following isolation of XI, the mother liquor was condensed to afford a compound with a much smaller tert-butyl signal (NMR, Fig V-20) but with other resonances intact. This reduction of the tert-butyl signal was attributed to partial hydrolysis by

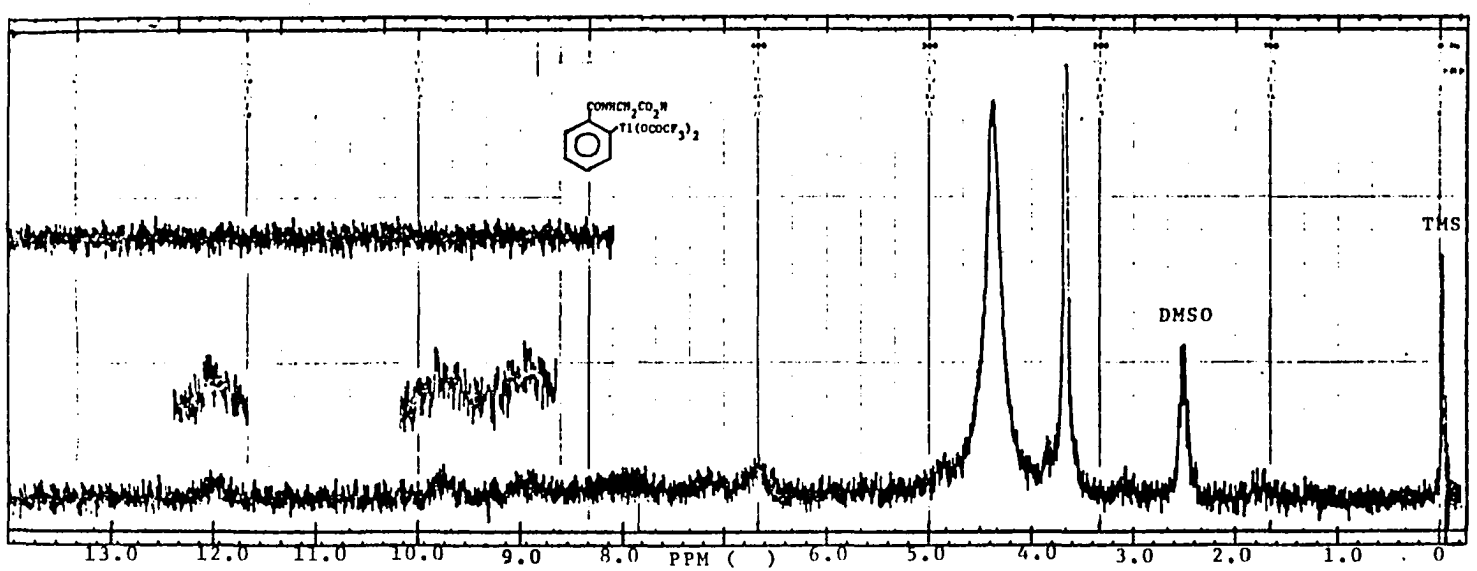

Figure V-15. 60 MHz ^{1}H NMR Spectrum of 2-Bis(trifluoroacetato)thallio-hippuric Acid IX (DMSO-d_6/TMS).

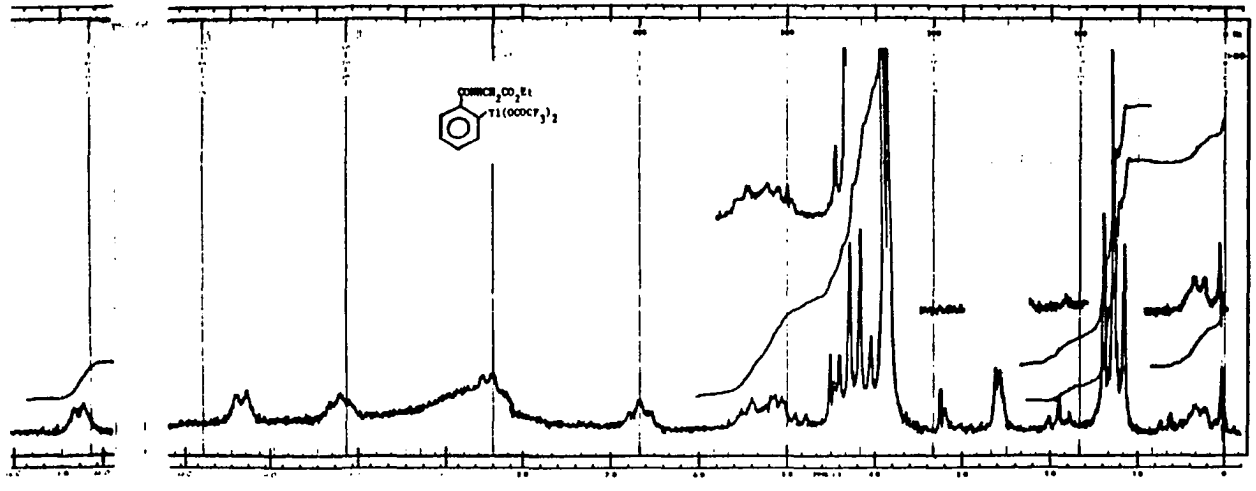

Figure V-16. 60 MHz ^{1}H NMR Spectrum of 2-Bis(trifluoroacetato)thallio-ethyl Hippurate X (DMSO-d_6/TMS).

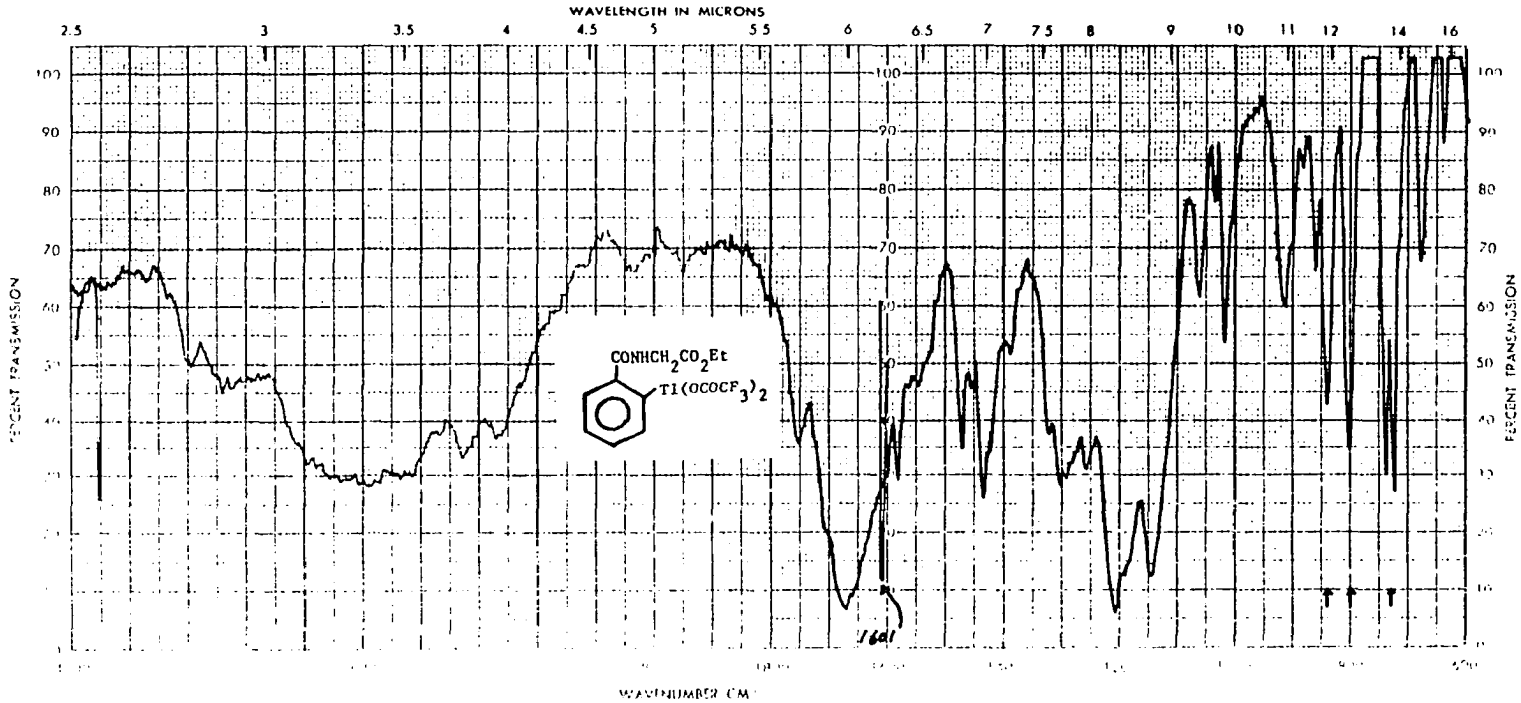

Figure V-17. IR Spectrum of 2-Bis(trifluoroacetato)thallio-ethyl Hippurate X (KBr).

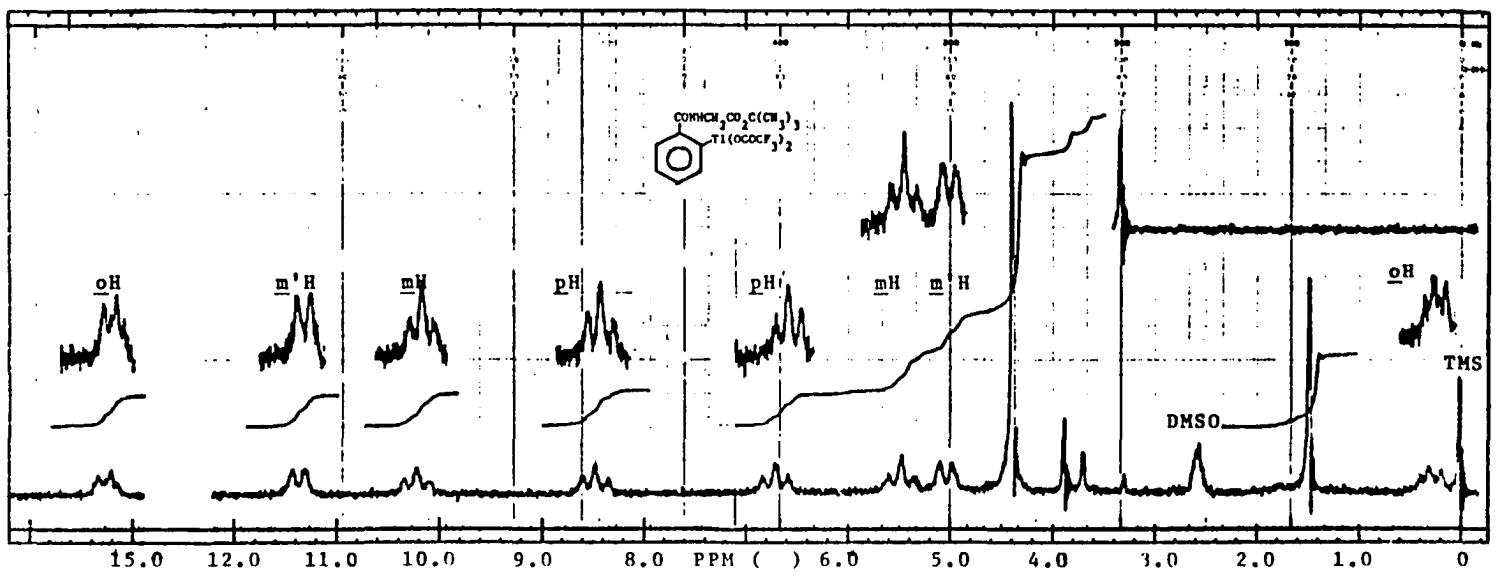

Figure V-18. 60 MHz ^{1}H NMR Spectrum of 2-Bis(trifluoroacetato)thallio-tertiarybutyl Hippurate XI (DMSO-d_6/TMS).

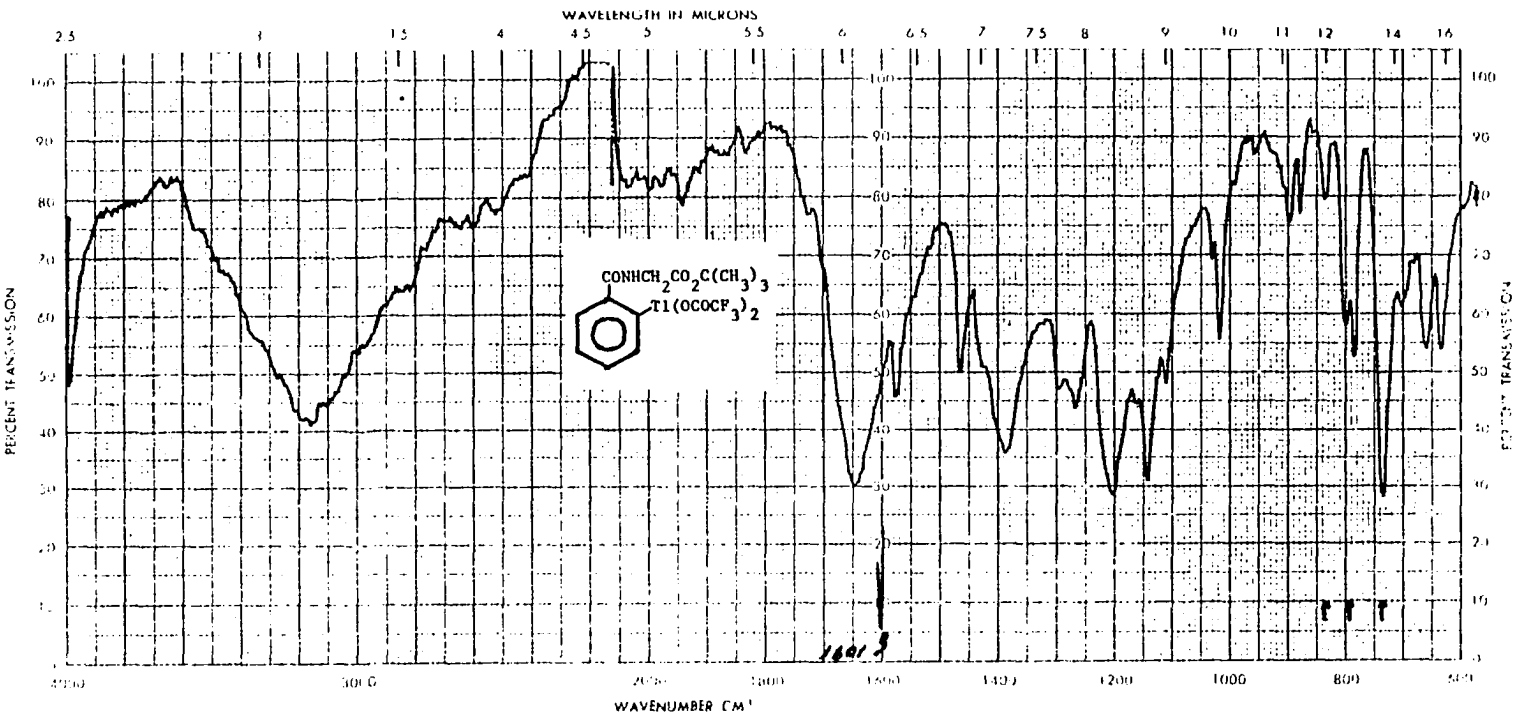

Figure V-19. IR Spectrum of 2-Bis(trifluoroacetato)thallio-tertiarybutyl Hippurate XI (KBr).

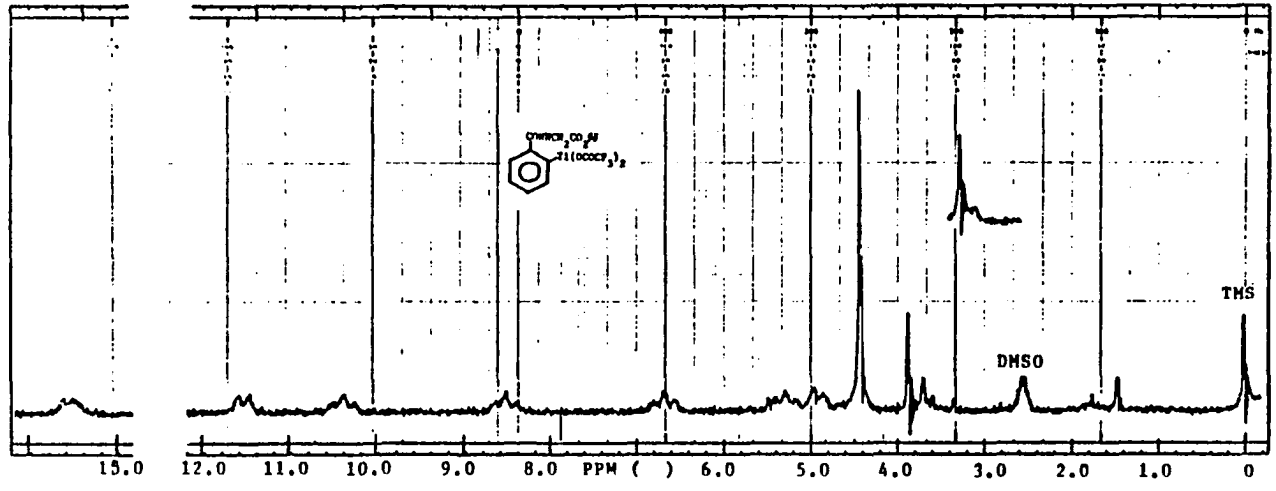

Figure V-20. 60 MHz ^{1}H NMR Spectrum of Product IX Resulting from the Condensation of 2-Bis(trifluoroacetato)thallio-tertiarybutyl Hippurate XI (DMSO-d_6/TMS).

CF_3CO_2H upon condensation of the mother liquor.[14] The IR spectrum of the hydrolysis product (Fig V-21) compares well with that of Fig V-19, except in the carboxylic acid hydroxyl region (3405 cm^{-1}), and supports the belief that hydrolysis has occurred to form IX.

DCC, then, can provide a route to thallated ethyl hippurate and also to thallated hippuric acid via the tert-butyl ester intermediate without loss of thallium during hydrolysis. These findings are significant since direct thallation of hippuric acid has not been positively demonstrated by other methods. A problem arises, however, because iodination of the isolated ethyl and tert-butyl thallated intermediates, X and XI, respectively, has been unsuccessful.

Finally, in situ iodination of methyl hippurate (XII) was attempted (reaction 13). The NMR (Fig V-22) and IR (Fig V-23)

Reaction 13

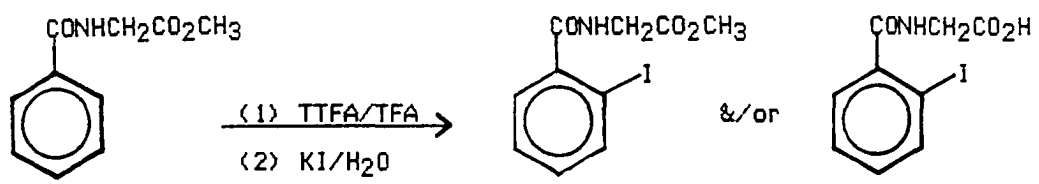

XII XIII XIV

spectra are not consistent with expectations based on assumed formation of the desired o-iodo-methyl hippurate XIII. However, the mass spectrum (Fig V-24) indicates that XIII has indeed been formed. The bulk of the reaction product was identified as o-iodohippuric acid (XIV) based upon NMR, IR, and mass spectral evidence (Fig V-25, V-26, and V-27, respectively). Use of $Na^{131}I$ gave preliminary yields of up to 90%.[3c] Failure to directly iodinate hippuric acid suggests that hydrolysis occurs after the thallation-iodination sequence of reaction 13.

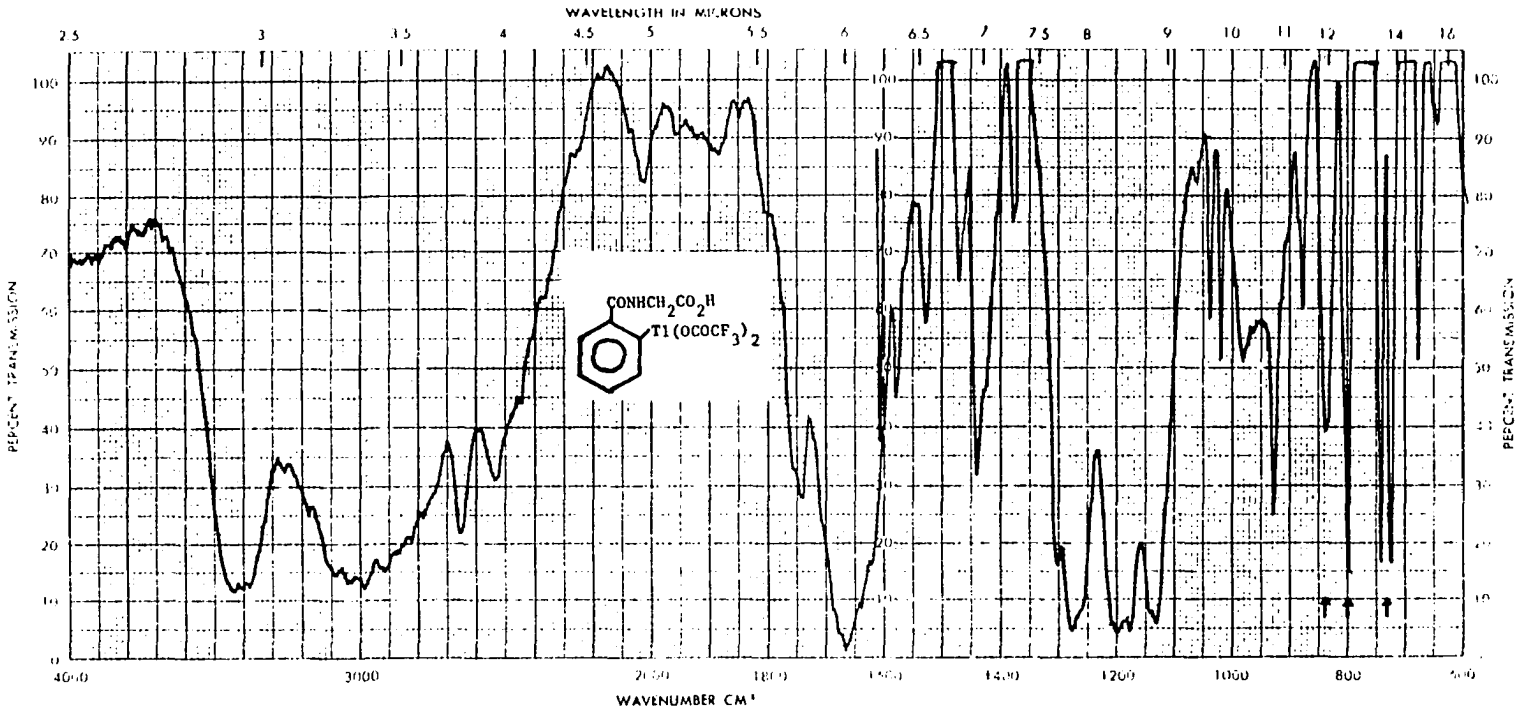

Figure V-21. IR Spectrum of 2-Bis(trifluoroacetato)thallio-hippuric Acid IX (KBr).

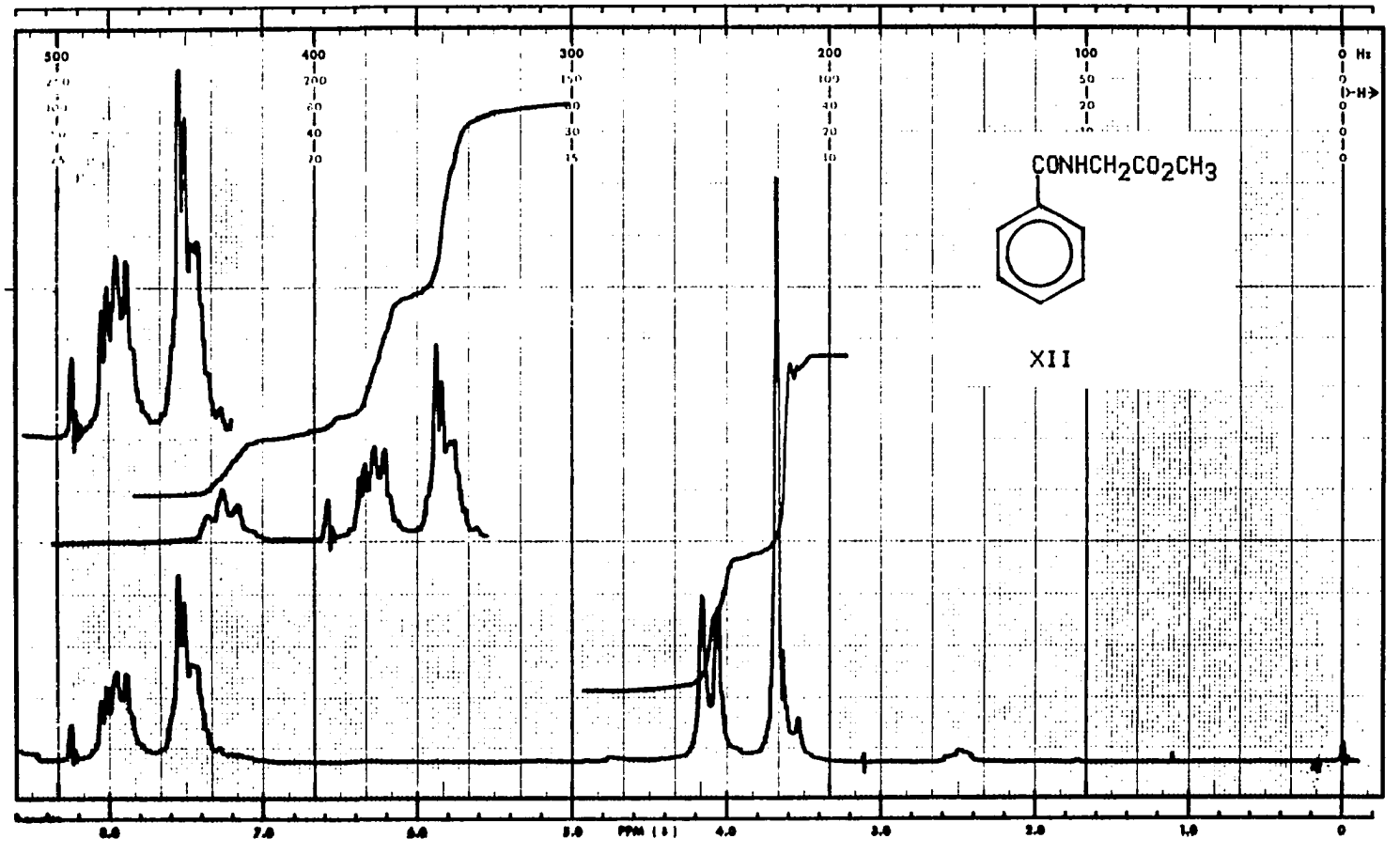

Figure V-22. 60 MHz ^{1}H NMR Spectrum Methyl Hippurate XII (DMSO-d_6/TMS).

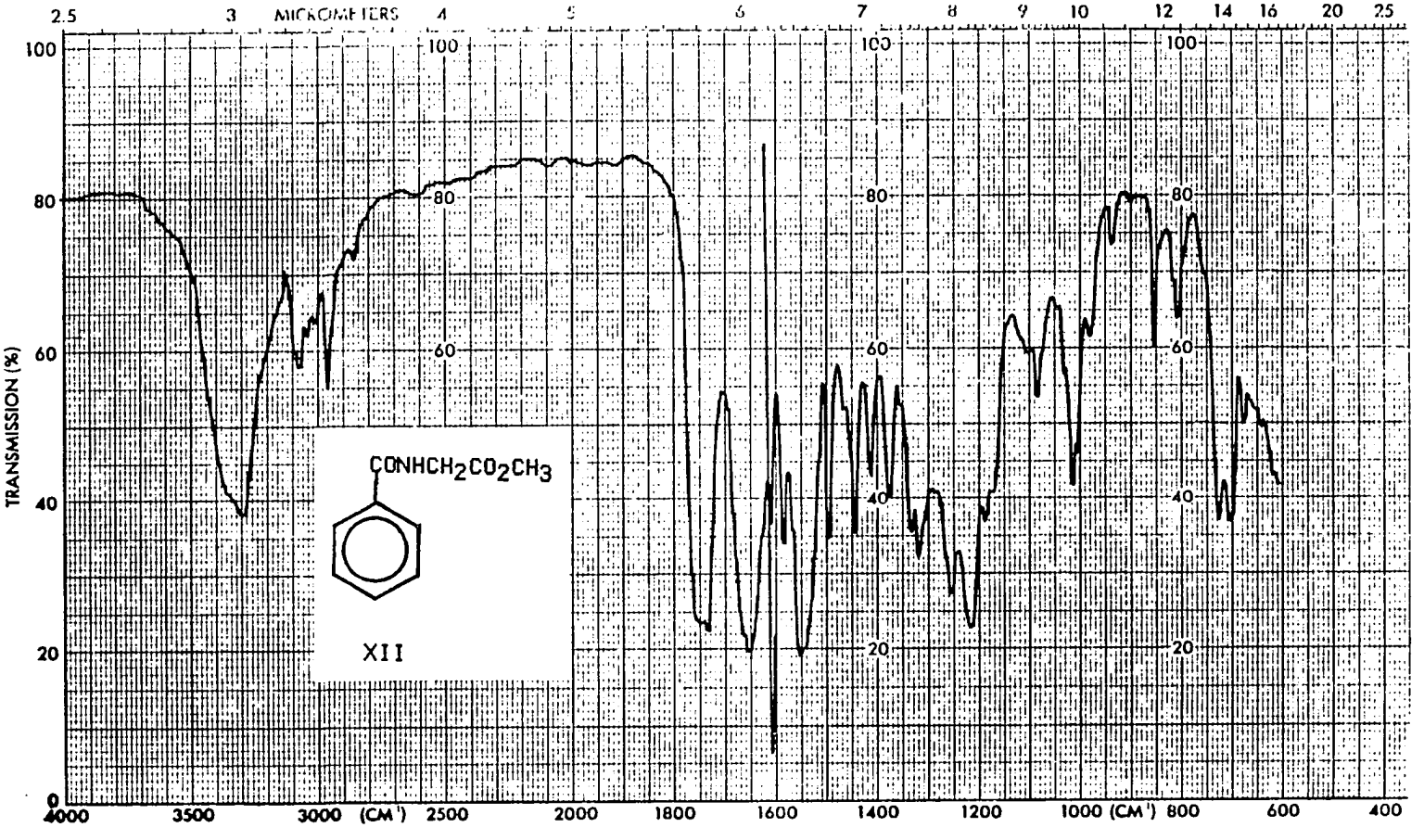

Figure V-23. IR Spectrum of Methyl Hippurate XII (KBr).

FIGURE V-24

Mass Spectrum containing the parent ion (m/e 319) of the anticipated o-Iodo-methyl Hippurate XII.

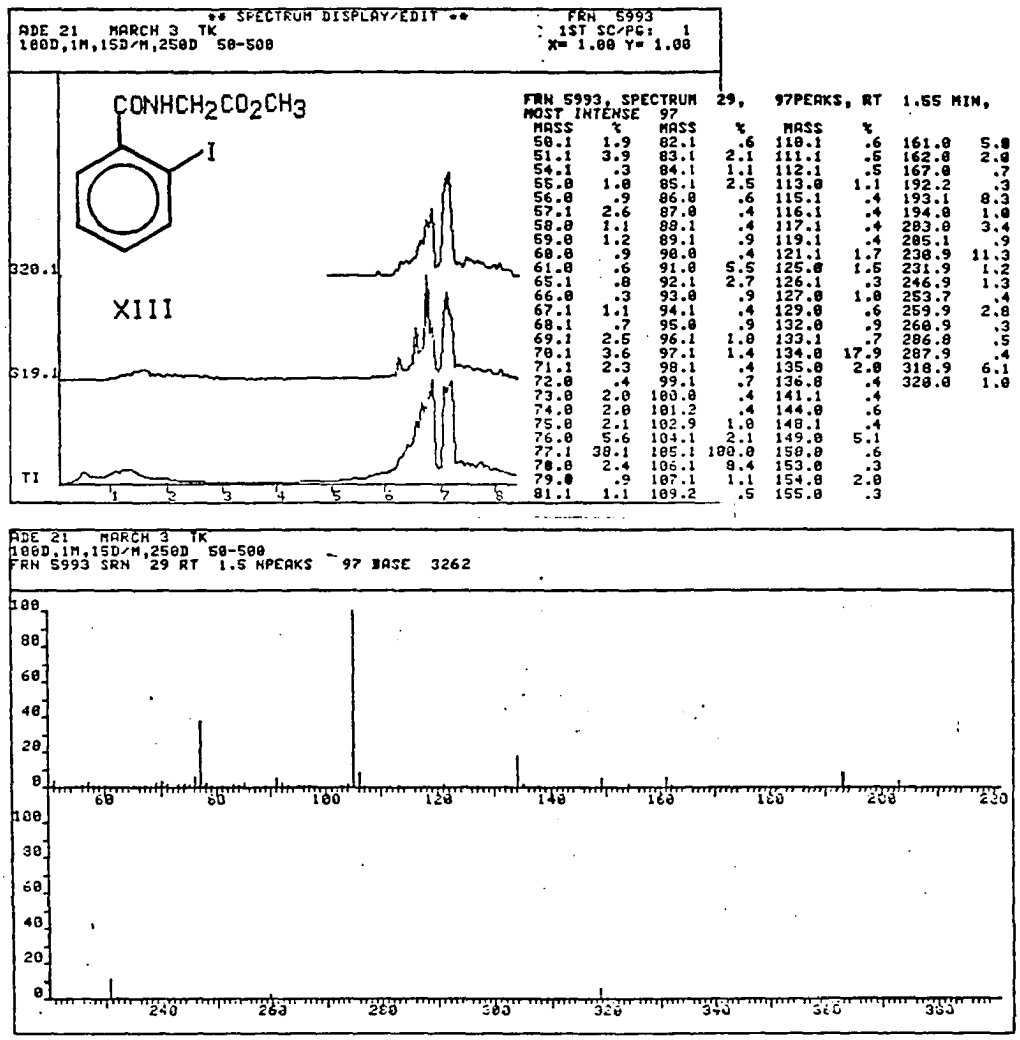

FIGURE V-25

300 MHz ^{1}H NMR Spectrum of o-Iodohippuric Acid XIV (DMSO-d_6/TMS).

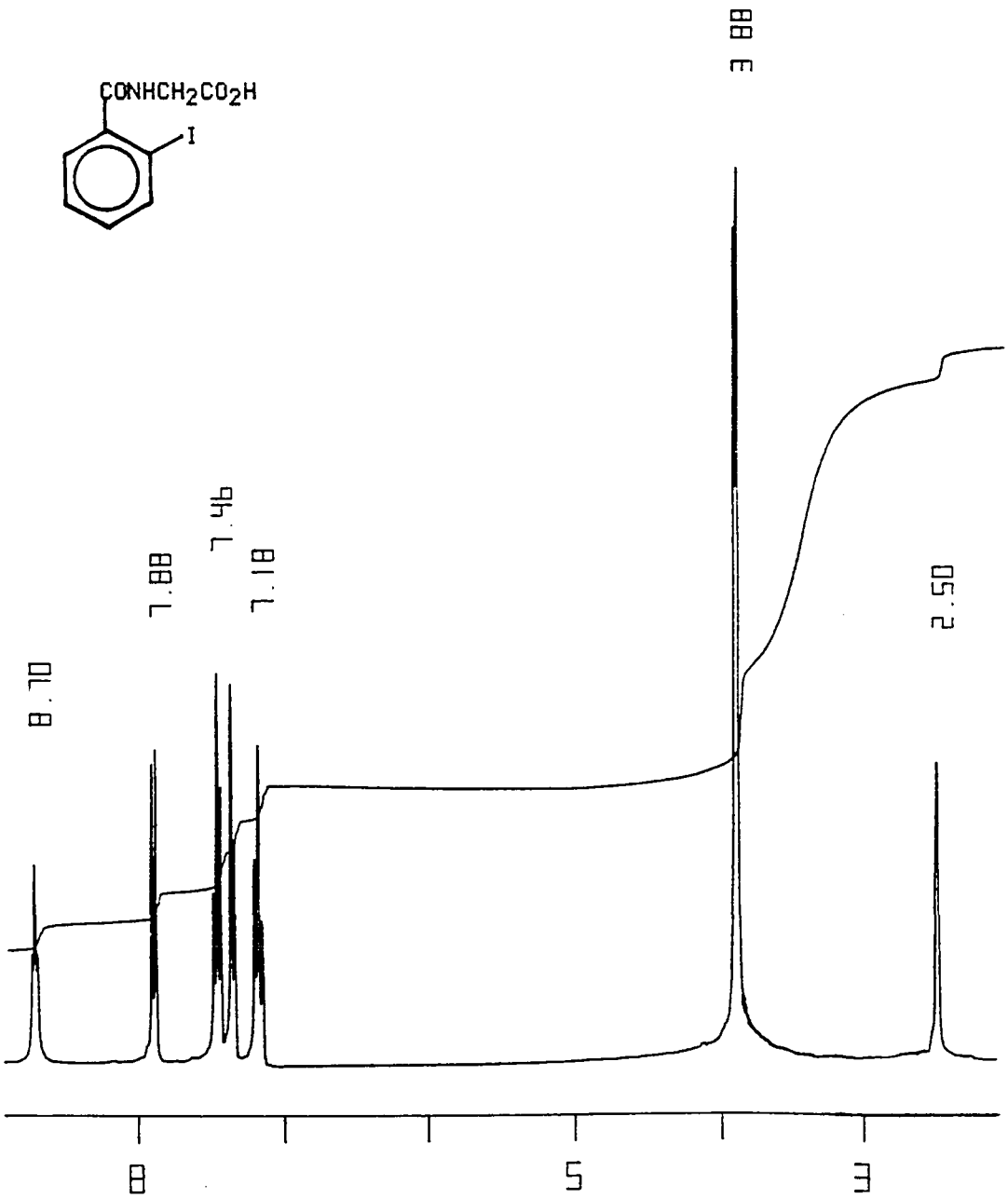

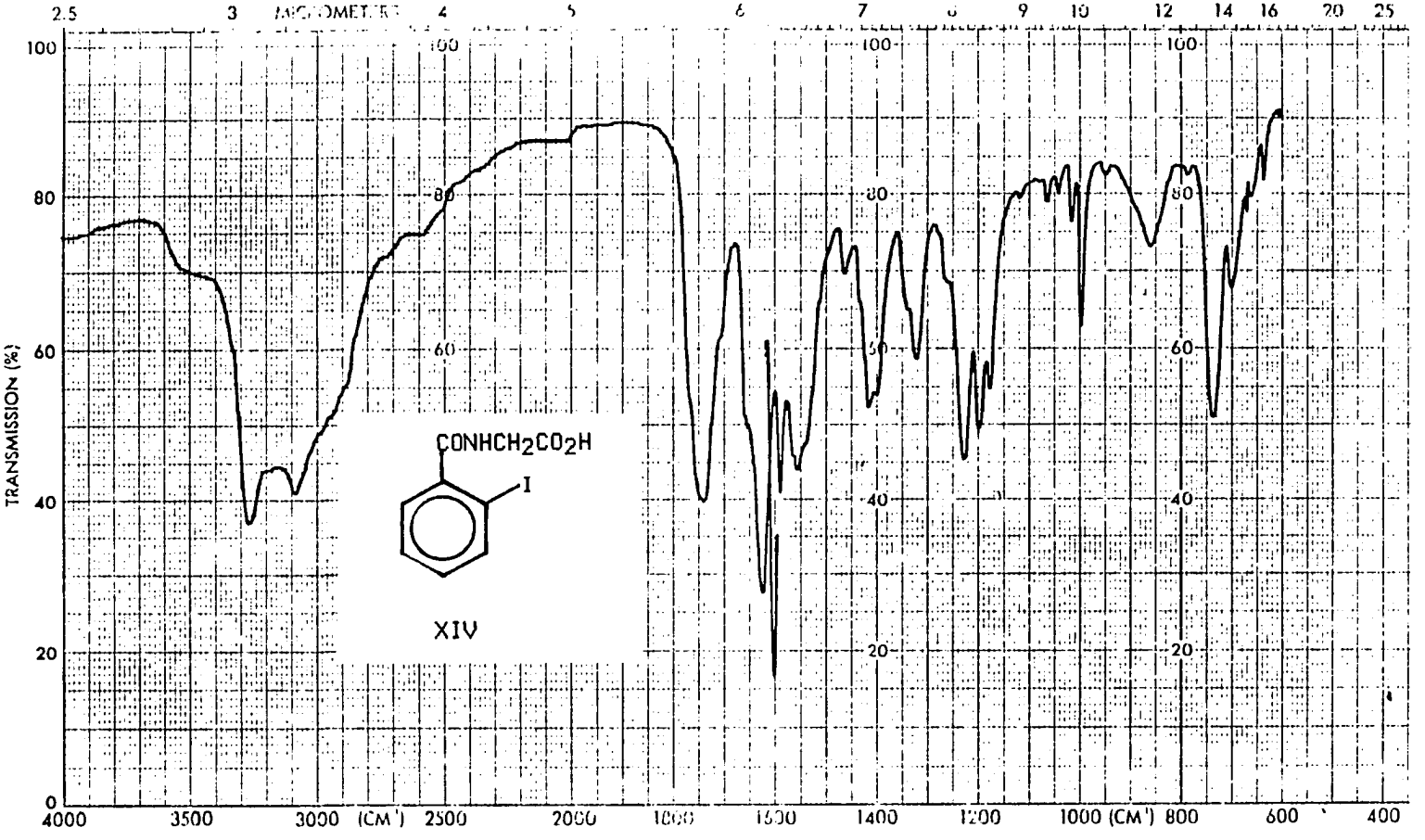

Figure V-26. IR Spectrum of o-Iodohippuric Acid XIV.

FIGURE V-27

Mass Spectrum of o-Iodohippuric Acid XIV.

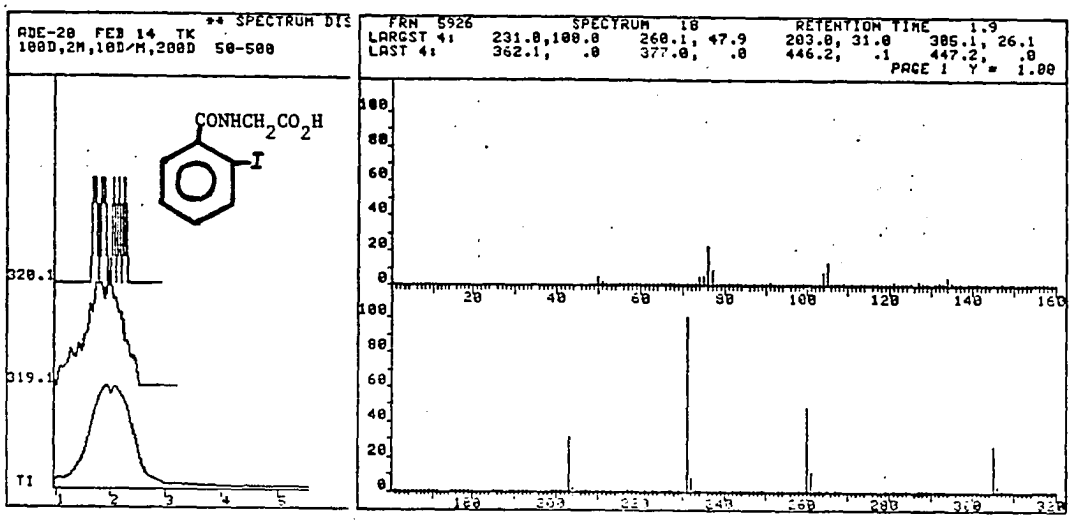

FILE 5926 SPECTRUM 18 RT= 1.92 MIN

MASS	%	MASS	%	MASS	%	MASS	%	MASS	%	MASS	%
51.1	2.0	71.1	.2	90.1	.4	111.1	.1	139.0	.2	229.0	.2
52.1	.2	72.1	.1	91.1	1.3	116.1	.7	141.0	.1	231.0	100.0
53.0	.2	73.1	1.2	92.1	.8	117.1	.2	143.5	.1	232.1	7.8
55.1	.2	74.1	4.9	93.1	.3	118.1	.2	149.1	.5	233.0	.5
56.1	.9	75.1	4.8	95.1	.1	119.1	.3	152.0	.1	248.0	.2
57.1	.3	76.1	22.7	97.2	.2	120.1	1.1	153.0	.1	260.1	47.9
59.1	.1	77.1	8.9	98.1	.1	121.1	2.0	160.1	.2	261.1	11.1
60.0	.2	78.0	1.0	99.1	.1	122.1	.2	161.1	.1	262.1	.9
61.0	.1	79.1	.2	100.2	.2	126.9	2.5	176.0	.2	287.0	.5
62.0	.2	81.1	.1	101.2	.2	128.0	1.7	177.0	.2	288.0	.1
63.0	.4	83.2	.2	102.1	.5	129.4	.4	179.1	.2	305.1	26.1
64.1	.3	84.1	.2	103.1	.8	132.1	1.9	201.1	.1	306.1	2.7
65.1	.4	85.1	.2	104.1	7.3	133.1	1.0	203.0	31.0	307.1	.3
67.0	.1	87.1	.2	105.0	12.9	134.0	5.4	204.1	2.1		
69.1	.2	88.1	.1	106.1	1.0	135.0	1.5	205.1	.1		
70.1	.1	89.1	.2	107.1	.1	136.0	.1	206.1	.2		

LAST

MASS	%	MASS	%	MASS	%	MASS	%	MASS	%	MASS	%
284.5	.0	287.0	.5	288.0	.1	289.0	.0	305.1	26.1	306.1	2.7
307.1	.3	308.1	.0	319.1	.1	320.1	.0	332.1	.1		
334.1	.1	335.1	.0	362.1	.0	377.0	.0	446.2	.1		

Compound XV, used in reaction 14, was made by standard methylation procedures.[15] Reaction 14 was conducted to produce

Reaction 14

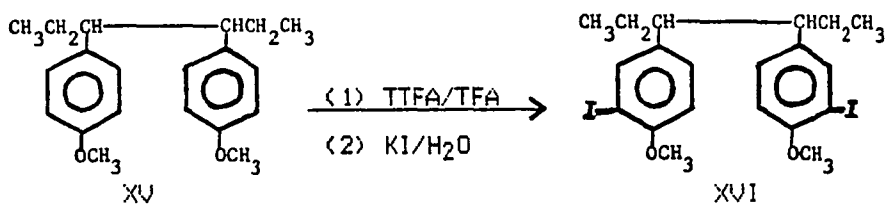

3,4-bis(3-iodo-p-anisyl)hexane (XVI), whose NMR, IR, and mass spectra are shown in Fig V-28, V-29, and V-30, respectively. The in situ iodination technique was used since isolation of the di-thallated intermediate was not successful (cf. isolation of thallated anisole). This process has been used to produce ^{131}I-3,4-bis(3-iodo-p-anisyl)-hexane.[3c]

Thallation of aromatic amines and aromatic compounds containing primary aliphatic amine substituents is not reported in the literature, but thallation of aromatic amides, aromatic compounds containing tertiary amide substituents, and aromatic compounds containing tertiary amine substituents has been reported.[16] Thallation-iodination of XVIII failed, so it was felt that successful synthesis of the products of Eqs V-6 through V-13 of Table V-1 could best be accomplished by protecting nitrogen with the easily removed trifluoroacetyl group.

The sequence of reactions utilized for the synthesis of 2-iodo-4,5-dimethoxyphenethylamine (XXIII) was suggested as shown in Scheme V-1. Synthesis of XVII, XVIII, and XIX was as in the literature[17] and trifluoroacetylation[18] gave XX (see Fig V-31, V-32, and V-33 for NMR, IR, and mass spectra, respectively).

In situ thallation-iodination of XX followed after the manner

FIGURE V-28

300 MHz ^{1}H NMR Spectrum of 3,4-bis(3-Iodo-p-anisyl)hexane XVI ($CDCl_3$/TMS).

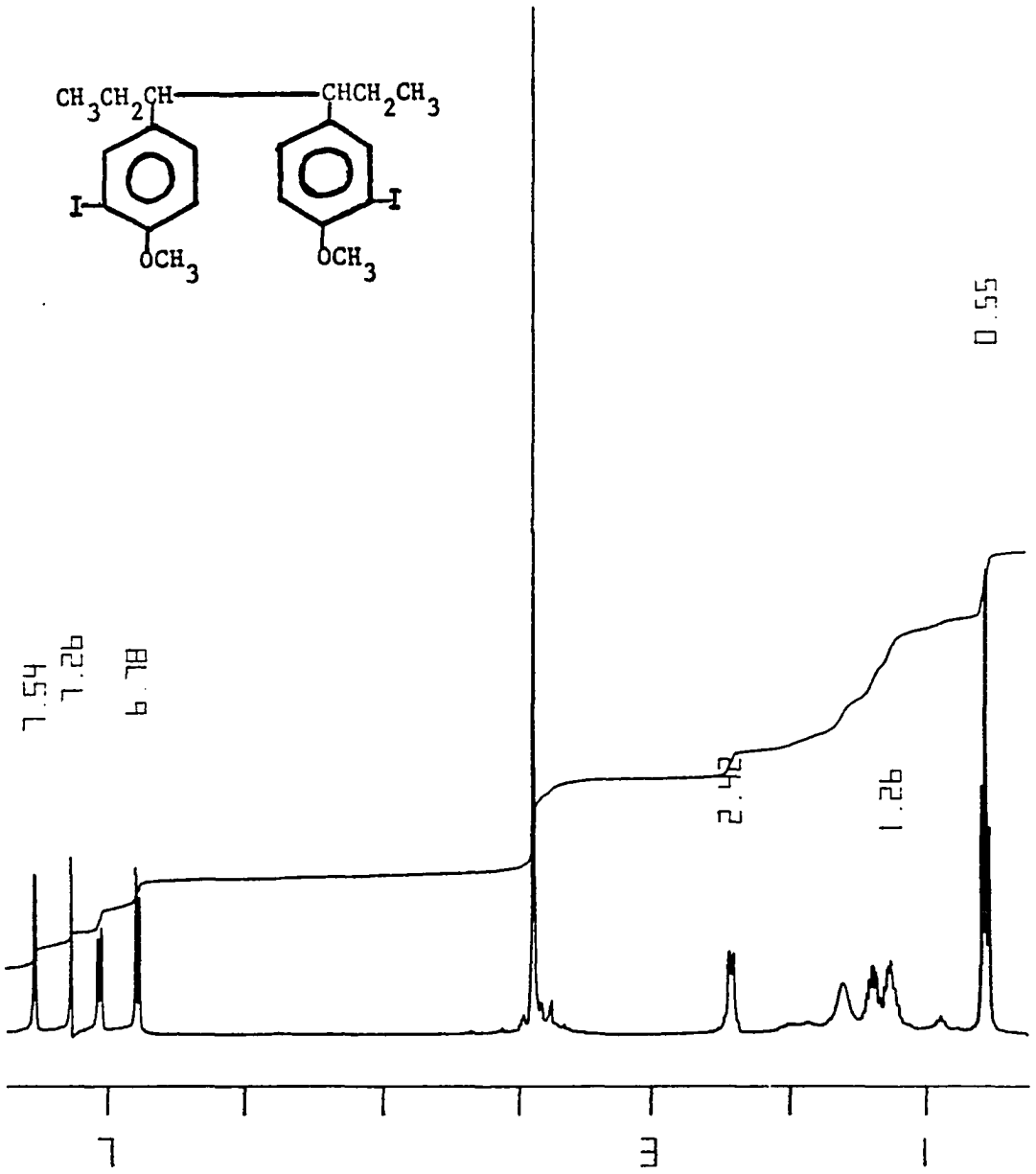

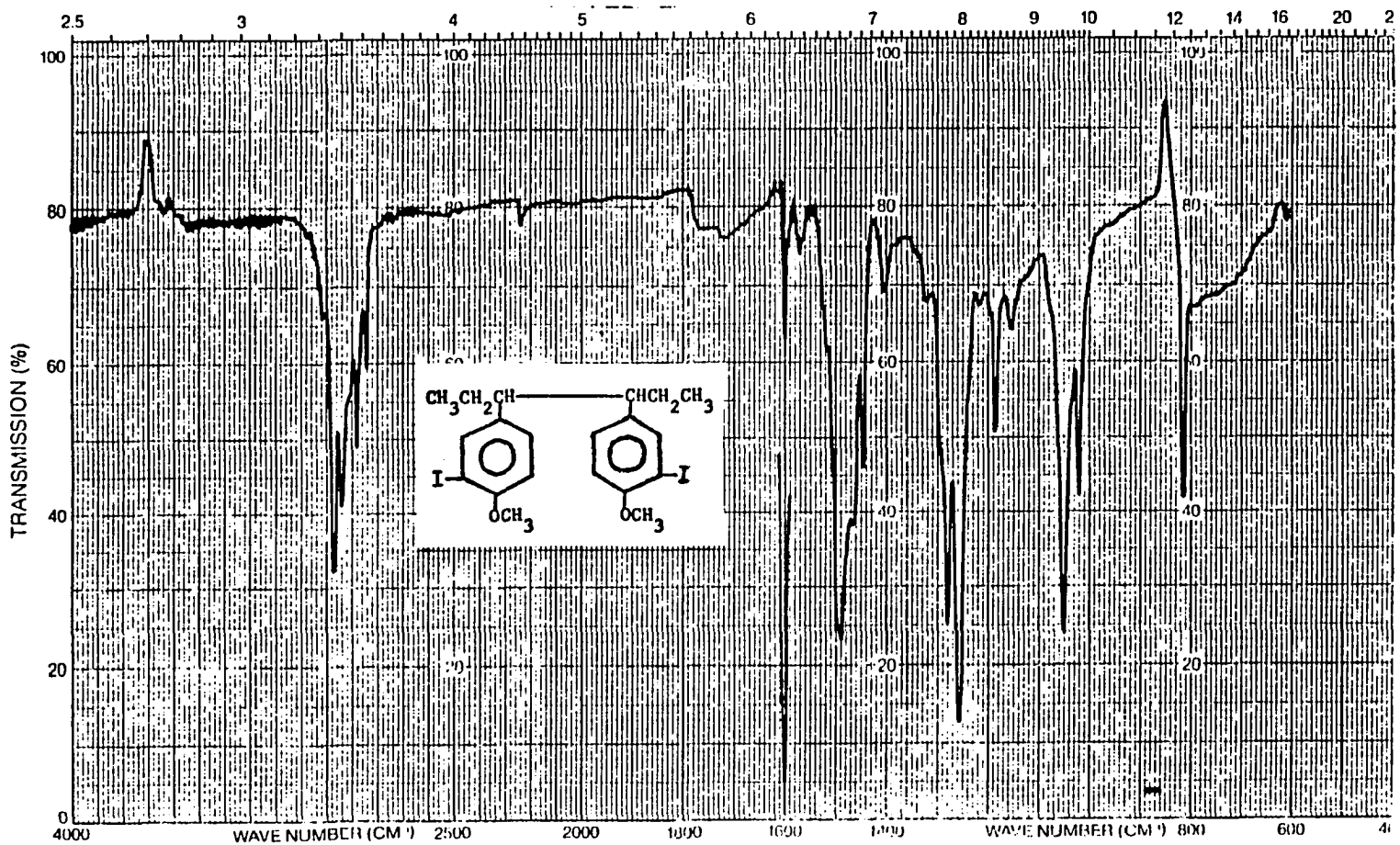

Figure V-29. IR Spectrum of 3,4-Bis(3-iodo-p-anisyl)hexane XVI ($CHCl_3$).

FIGURE V-30

Mass Spectrum of 3,4-bis(3-Iodo-p-anisyl)hexane XVI ($CHCl_3$).

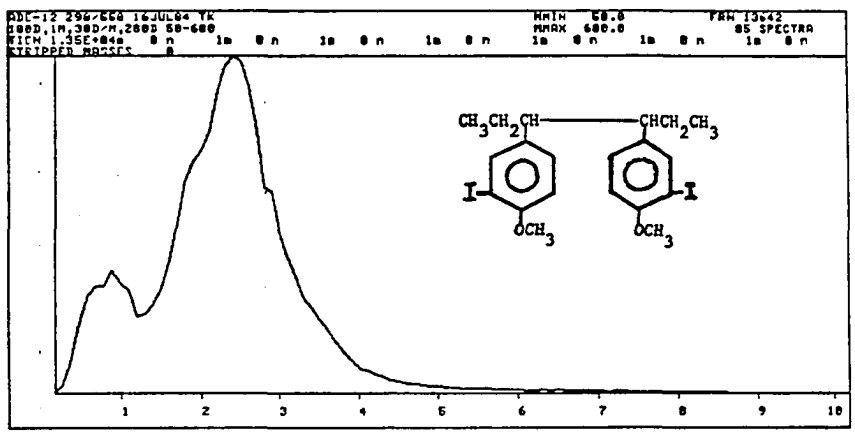

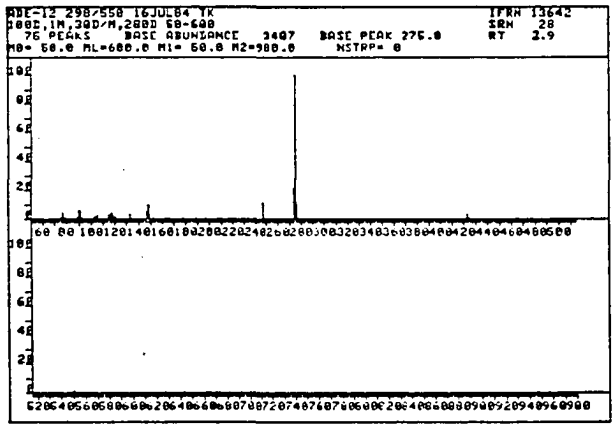

MASS	%	MASS	%
BIG 60		136.0	.5
61.2	.6	147.1	5.5
63.1	.5	148.1	10.0
65.2	.5	149.1	3.1
69.1	.8	150.0	.6
66.1	.7	151.0	.6
71.2	.4	152.0	.9
73.1	.4	163.1	.5
75.1	.4	165.0	.9
76.1	1.0	179.1	.4
77.1	4.1	189.2	.4
78.1	1.4	195.1	.4
79.1	1.1	207.1	.4
89.0	2.2	245.0	.6
90.1	6.1	247.0	11.2
91.1	5.5	248.0	1.0
92.1	.9	259.0	.4
102.1	.0	260.0	.4
103.1	2.3	261.0	.6
104.1	1.0	274.0	21.5
105.1	3.0	275.0	100.0
106.1	.4	276.0	10.3
115.1	2.7	277.0	.9
116.2	1.0	423.1	3.3
117.1	4.7	424.1	.9
118.1	2.7	550.1	2.3
119.1	2.0	551.1	.6
121.1	1.0		
127.0	.6		
128.1	.6	LAST 4	
131.0	.7	423.1	3.3
132.1	.4	424.1	.9
133.0	3.3	550.1	2.3
134.0	.7	551.1	.6

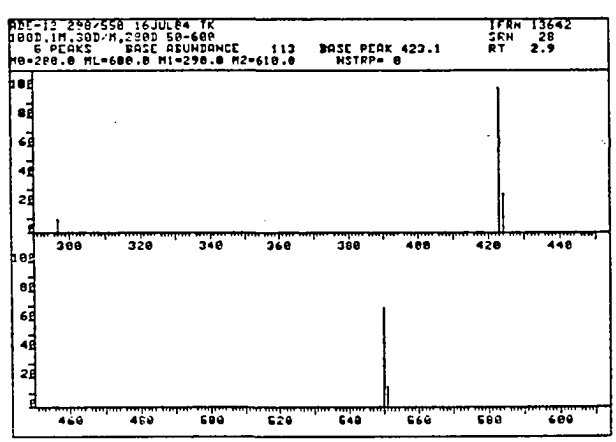

MASS	%	MASS	%
BIG 60			
297.2	8.8		
423.1	100.0		
424.1	26.5		
550.1	68.1		
551.1	14.2		
		LAST 4	
		423.1	100.0
		424.1	26.5
		550.1	68.1
		551.1	14.2

SCHEME V-1

Proposed Synthesis of 2-Iodo-4,5-dimethoxyphenethylamine (XXIII).

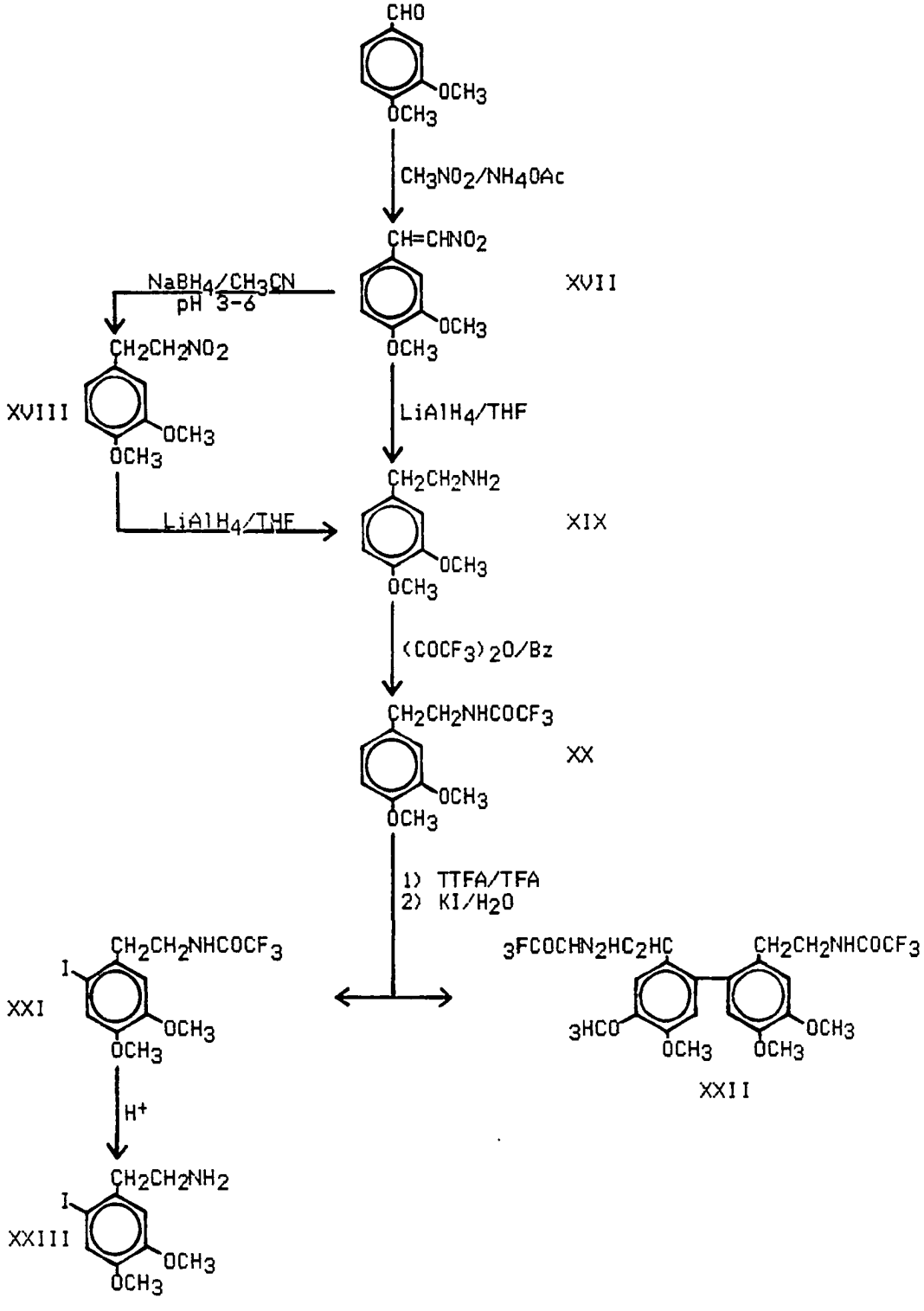

FIGURE V-31

300 MHz ^1H NMR Spectrum of

N-Trifluoroacetyl-3,4-dimethoxyphenethylamine XX ($CDCl_3$/TMS).

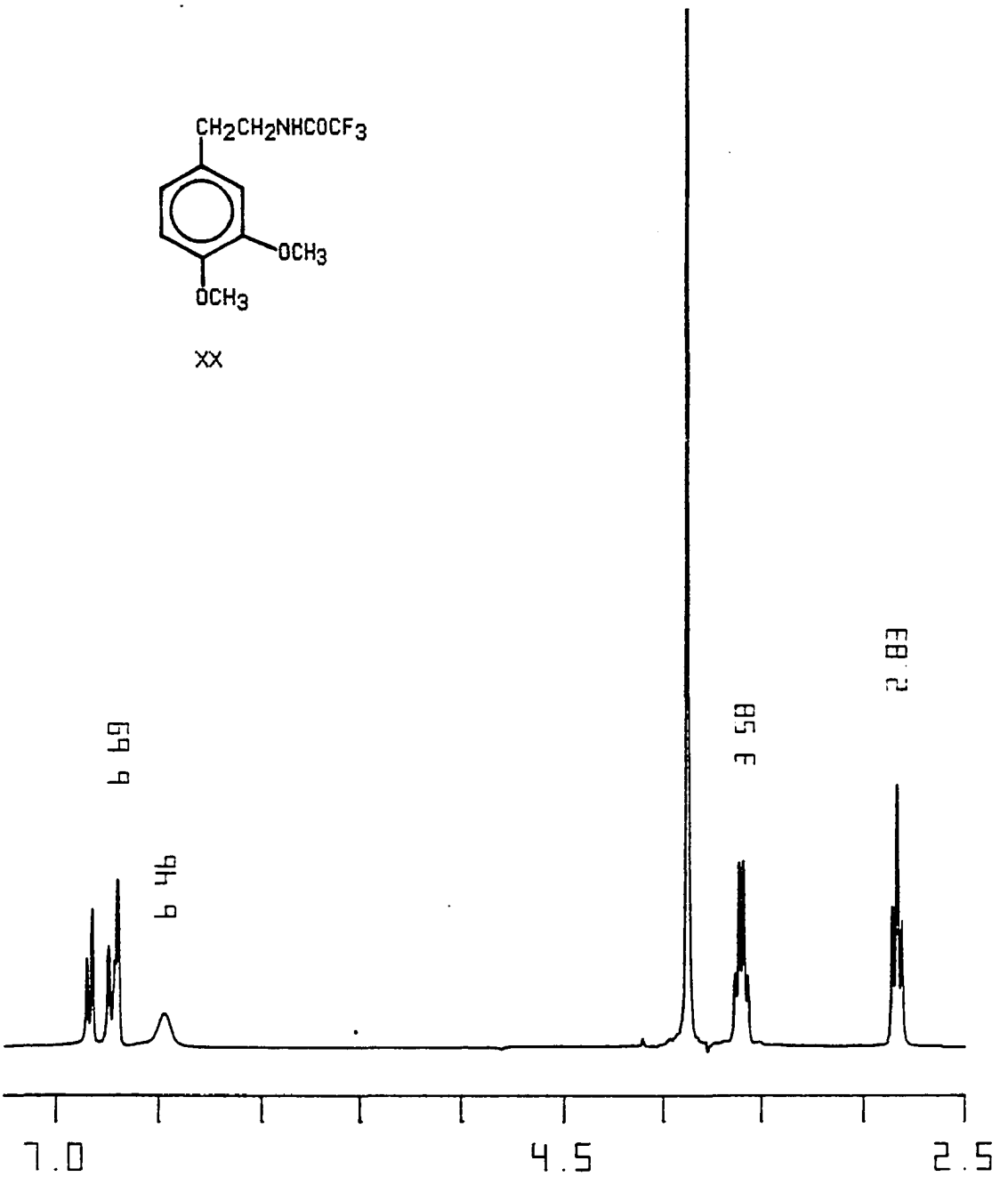

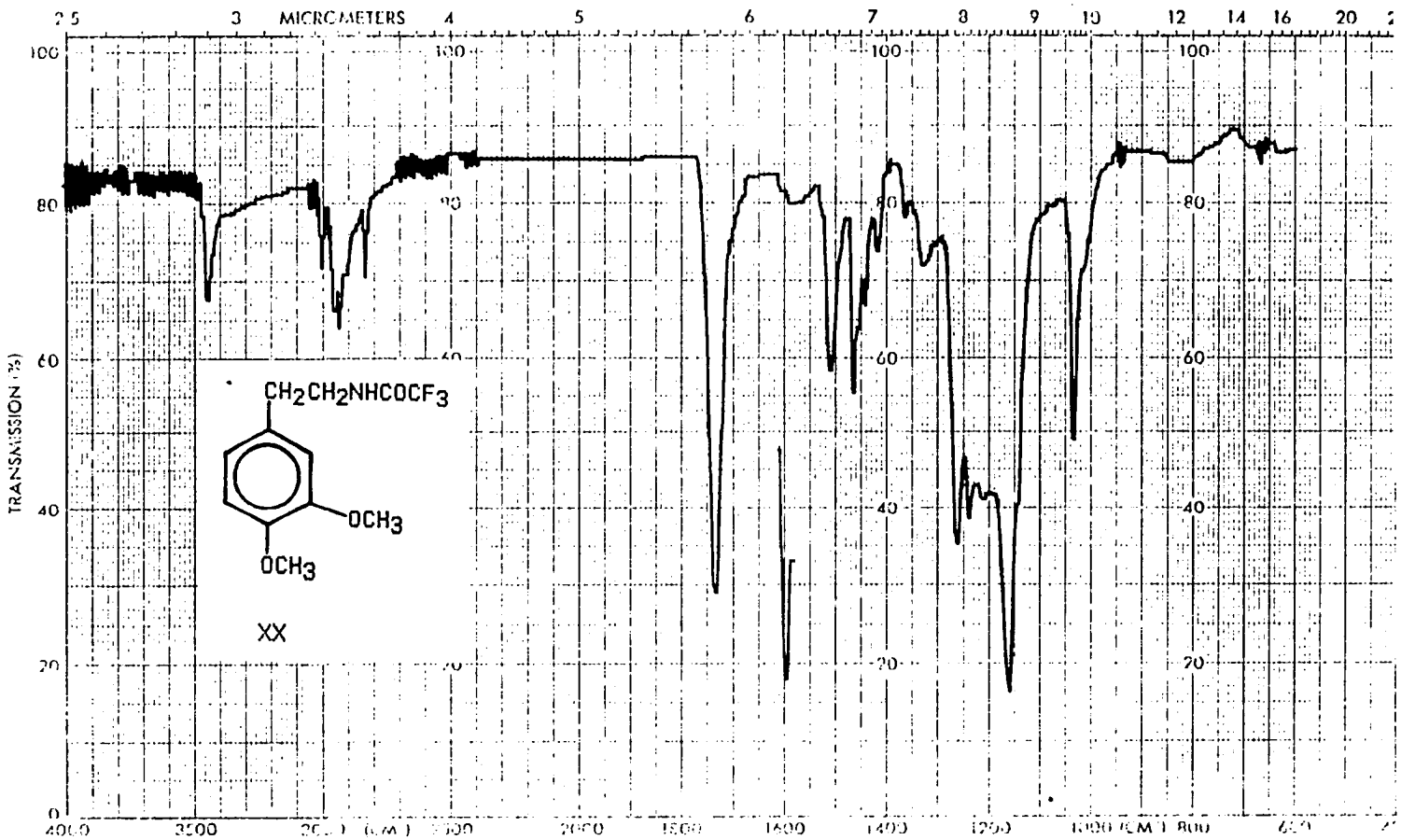

Figure V-32. IR Spectrum of N-Trifluoroacetyl-3,4-dimethoxyphenethylamine XX (CCl_4).

FIGURE V-33

Mass Spectrum of

N-Trifluoroacetyl-3,4-dimethoxyphenethylamine XX (CCl_4).

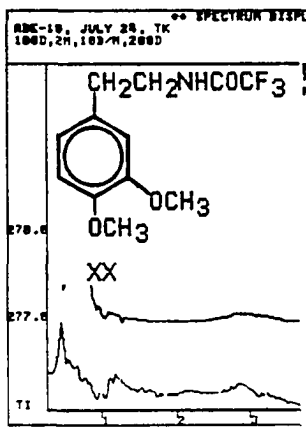

** SPECTRUM DISPLAY/EDIT **

ADE-10, JULY 28, TK
100D,2M,103/M,200D

FRM 6200
1ST SC/PG: 1
X= 1.00 Y= 1.00

FRM 6200 SPECTRUM 16 RET. TIME = .7
SPHUSE

MASS	ABUND	MASS	ABUND	MASS	ABUND	MASS	ABUND
50.1	.3	76.1	.4	102.1	.4	127.2	.5
51.1	1.0	77.0	4.0	103.1	1.0	128.1	.2
52.2	.4	78.0	4.5			129.0	.0
53.1	.5	79.1	2.3	104.1	.7	130.1	.2
54.1	.2	80.1	.0	105.1	4.3	131.1	.4
55.1	1.9	81.1	1.9	106.1	4.4		
56.1	.7	82.2	1.2	107.1	7.6	132.1	.4
57.1	1.9	83.1	2.2	108.1	2.4	133.0	.9
58.2	.2	84.1	.9	109.1	1.3	134.1	.6
59.1	.2	85.1	1.2	110.2	.7	135.1	2.8
60.1	.5	86.1	.2	111.2	1.2	136.1	1.5
61.1	.2	87.1	.0	112.2	.4	137.1	2.0
		88.1	.2	113.1	.5	138.1	.7
62.1	.2	89.1	1.6	114.1	.2	139.1	.5
63.1	.6			115.1	.5	140.1	.2
64.2	.4	90.1	2.1	116.1	.3	141.1	.4
65.1	2.5	91.1	4.2	117.1	.3	142.1	.1
66.1	.5	92.1	.8			143.1	.4
67.1	1.1	93.1	1.7	118.1	1.5	144.0	.1
68.1	.6	94.1	.9	119.1	1.3	145.0	.3
69.1	6.2	95.1	1.0	120.1	.7		
70.1	.0	96.1	1.0	121.1	2.9	146.2	.2
71.1	1.4	97.1	2.8	122.1	1.0	147.1	.6
72.1	.1	98.1	1.0	123.2	1.0	148.1	1.1
73.0	1.1	99.1	.5	124.2	.5	149.0	9.8
74.0	.7	100.1	2.3	125.2	.6	150.0	1.7
75.1	.3	101.1	.6	126.1	2.6	151.1	100.0

FRM 6200 SPECTRUM 16 RET. TIME = .7
SPHUSE

MASS	ABUND	MASS	ABUND	MASS	ABUND	MASS	ABUND
152.1	9.5	177.1	.2	202.0	.3	228.2	.2
153.0	1.2	178.1	.3	203.1	.2	229.2	.3
154.1	.2	179.1	.5	204.1	.1		
155.1	.2	180.1	.3	205.1	.3	230.1	.1
156.1	.1	181.2	.2	206.2	.2	231.2	.2
157.1	.3	182.2	.1	207.2	.5	232.2	.1
158.2	.1	183.2	.2	208.1	.8	233.1	.2
159.2	.2	184.1	.1	209.2	.3	234.2	.2
		185.2	.4	210.1	1.0	235.2	.2
160.1	.1	186.1	.1	211.2	.4	236.2	.0
161.1	.3	187.2	.1	212.2	.1	237.2	.3
162.1	.2			213.2	.4	238.2	.4
163.1	.6	188.1	.0	214.2	.1	239.3	.3
164.1	42.9	189.1	.2	215.1	.2	240.1	.1
165.1	6.1	190.2	.3			241.2	.2
166.2	.8	191.2	.3	216.1	.2	242.3	.2
167.1	.5	192.1	.3	217.1	.2	243.3	.3
168.1	.2	193.1	.3	218.1	.2		
169.0	.4	194.2	.3	219.2	.3	244.1	.2
170.1	.1	195.1	.2	220.2	.2	245.1	.3
171.2	.3	196.1	.2	221.2	.3	246.1	.2
172.2	.1	197.1	.2	222.2	.3	247.2	.2
173.2	.2	198.1	.1	223.1	.4	248.2	.1
		199.2	.3	224.1	.2	249.3	.2
174.1	.1	200.1	.2	225.2	.2	250.2	.3
175.1	.2	201.0	.2	226.2	.1	251.2	.2
176.1	.3			227.2	.3	252.2	.2

FRM 6200 SPECTRUM 16 RET. T

MASS	ABUND	MASS	ABUND
253.2	.2	279.2	1.3
254.3	.2	280.2	.3
255.3	.5		
256.2	.7		
257.2	.6		
258.1	.3		
259.2	.2		
260.1	.3		
261.1	.3		
262.2	.2		
263.2	.1		
264.3	.4		
265.2	.4		
266.3	.2		
267.2	.2		
268.1	.1		
269.2	.2		
270.3	.2		
271.3	.2		
272.2	.1		
273.1	.1		
274.2	.1		
275.2	.2		
277.1	51.4		
278.1	7.0		

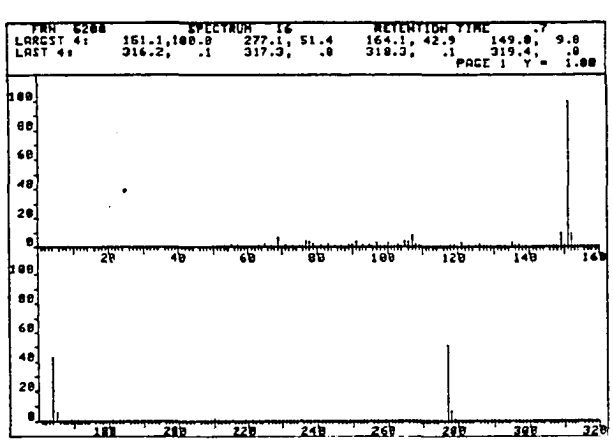

discussed earlier.[9] However, the only evidence for formation of the desired N-trifluoroacetyl-2-iodo-4,5-dimethoxyphenethylamine (XXI) is the presence of a very small molecular ion at m/e 403 (2.5%) (Fig V-34). Instead, the predominant product of the sequence was biaryl compound XXII which results from Tl(III)-promoted oxidative coupling of the substrate (see Figs V-35, V-36, and V-37, for NMR, IR, and mass spectra, respectively).[19] That the compound is a 2,2′ symmetrically coupled biphenyl is indicated by the simplicity of the NMR. In an attempt to prevent this dimerization reaction, the nitrogen and catacholic hydroxyl groups were protected with trifluoroacetyl groups and the labeling of this tristrifluoroacetylated dopamine derivative with ^{131}I was attempted. Chromatography of the product indicated the presence of two separate radioactive compounds in the same relative abundance. It could not be determined whether iodination was occurring via the $ArTl(OCOCF_3)_2$ intermediate or via direct iodination of the substrate with I_2 (formed in situ via oxidation of NaI by TTFA).[3c]

Conclusion

Synthesis, thallation, iodination, and in situ thallation-iodination of a variety of aromatic compounds have been demonstrated. Techniques developed here have been used to synthesize the biologically active radioiodinated compounds ^{131}I-o-iodobenzoic acid, ^{131}I-o-iodohippuric acid, and ^{131}I-3,4-bis(3-iodo-p-anisyl) hexane.[3c] Importantly, in situ thallation-radioiodination is adaptable to short lived radioiodine ^{123}I.

Experimental

NMR spectra were run on IBM Model NR-80, Varian Models EM360A, T-60, and XL 300 spectrometers. IR spectra were taken on Perkin-Elmer Models IR-8 and 298 infrared spectrometers and mass spectra were recorded on a Hewlett-Packard Model 5985 GC/MS

FIGURE V-34

Mass Spectrum of the Compound with the Expected Molecular Weight of 403 which is Believed to be the Desired N-Trifluoroacetyl-2-iodo-4,5-dimethoxyphenethylamine XXI.

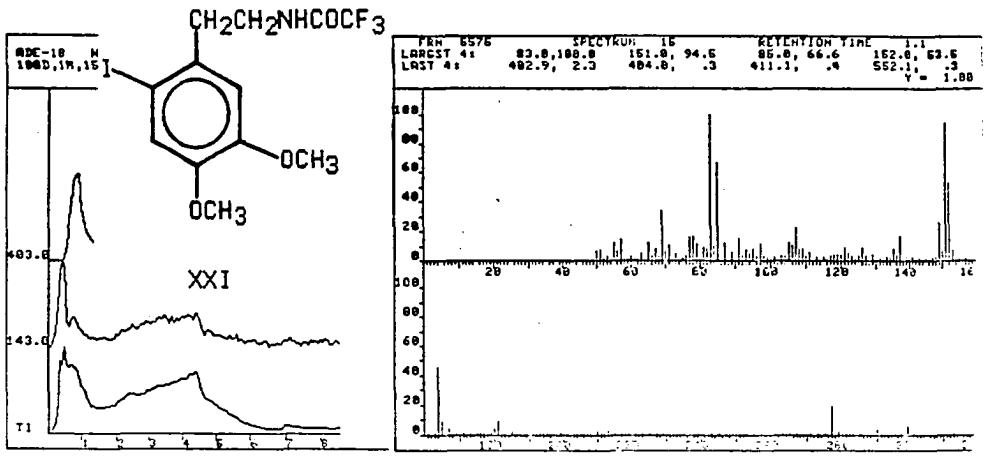

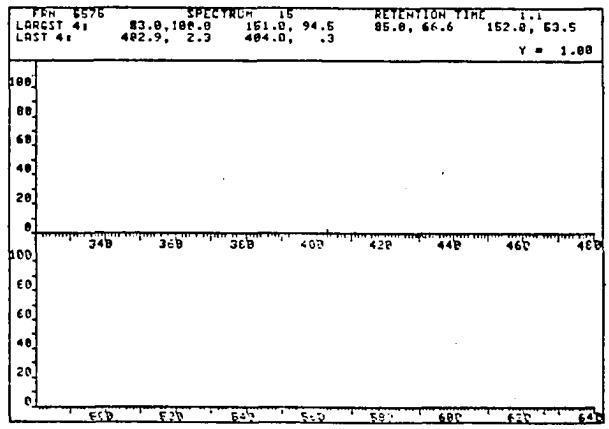

FILE 6576 SPECTRUM 21 263 PEAKS RT= 1.40 MIN BASE PEAK= 3932
LARGEST 182

MASS	%	MASS	%	MASS	%	MASS	%	MASS	%	MASS	%	MASS	%
49.1	1.2	76.0	3.0	103.1	2.9	129.0	6.0	159.2	1.1	196.0	1.3	244.1	1.6
50.0	7.0	77.0	21.4	104.1	2.4	131.0	1.6	161.0	1.3	197.2	1.4	254.1	.8
51.1	10.1	78.0	20.7	105.0	13.7	132.1	1.4	162.2	.8	199.2	2.0	255.2	.9
52.2	1.7	79.1	15.7	106.1	15.0	133.1	2.9	163.1	1.0	207.1	1.4	256.2	1.9
53.0	3.1	80.1	5.7	107.1	27.9	134.0	3.2	164.1	47.2	208.0	2.1	257.1	1.1
54.1	2.1	81.1	11.7	108.1	10.7	135.1	10.3	165.1	9.0	209.1	2.0	261.1	.8
55.1	15.2	82.0	9.4	109.1	12.3	136.0	5.0	166.1	2.0	210.1	2.7	263.0	1.1
56.1	6.4	83.0	88.3	110.1	4.0	137.0	29.1	167.1	4.1	211.2	1.3	264.2	.9
57.1	19.6	84.1	8.5	111.2	7.2	138.0	5.1	168.0	1.7	212.0	2.0	268.1	1.3
59.1	1.7	85.0	50.5	112.1	3.0	139.1	5.1	169.1	1.0	213.1	1.0	269.1	1.3
60.1	4.3	86.1	4.7	113.2	5.1	140.0	2.4	171.1	1.0	222.1	1.3	270.1	1.3
61.1	1.0	87.0	10.0	114.0	2.7	141.1	4.2	175.2	.9	224.2	.8	271.0	1.6
62.1	1.3	89.0	7.6	115.1	4.0	142.0	.9	176.1	1.0	225.1	1.0	277.0	23.0
63.1	4.6	90.0	9.9	116.2	1.0	143.0	2.8	177.1	1.7	227.3	.9	278.0	6.8
64.1	2.6	91.1	19.7	117.1	2.5	144.9	1.5	178.0	.9	228.1	.9	282.2	2.5
65.0	17.7	92.1	6.5	118.0	5.5	147.0	2.4	179.3	1.4	229.2	1.1	285.1	1.3
66.1	4.0	93.1	7.7	119.1	5.3	148.1	2.2	180.1	10.9	231.1	.8	286.1	3.0
67.0	8.5	94.1	6.6	120.0	5.1	149.0	19.6	181.1	14.9	232.0	.8	290.0	4.4
68.2	3.3	95.1	14.3	121.1	11.8	150.0	7.8	182.1	2.6	233.1	.8	279.2	1.4
69.0	50.4	96.1	6.4	122.0	5.6	151.1	100.0	183.2	2.0	236.2	2.6	289.2	9.5
70.1	6.7	97.1	10.4	123.2	6.2	152.1	86.9	185.1	2.6	237.2	1.3	300.1	2.3
71.2	12.7	98.1	5.7	124.1	3.0	153.0	10.0	191.1	.6	238.1	1.0	301.3	.9
72.0	2.2	99.1	4.7	125.1	4.5	154.0	1.6	192.0	1.2	239.3	1.0	312.2	1.3
73.0	6.8	100.1	1.4	126.0	7.0	155.2	2.6	193.2	1.5	241.1	1.1	402.9	2.5
74.0	2.3	101.0	0.3	127.2	4.1	156.0	1.1	194.1	1.6	242.2	1.0		
75.1	1.2	102.1	1.5	128.1	1.8	157.1	2.5	195.1	1.1	243.2	3.7		

FIGURE V-35

300 MHz ^{1}H NMR Spectrum of Biaryl Compound
2,2′-di-(N-Trifluoroacetylaminoethyl)-4,4′,5,5′-tetramethoxybiphenyl
XXII ($CDCl_3$/TMS).

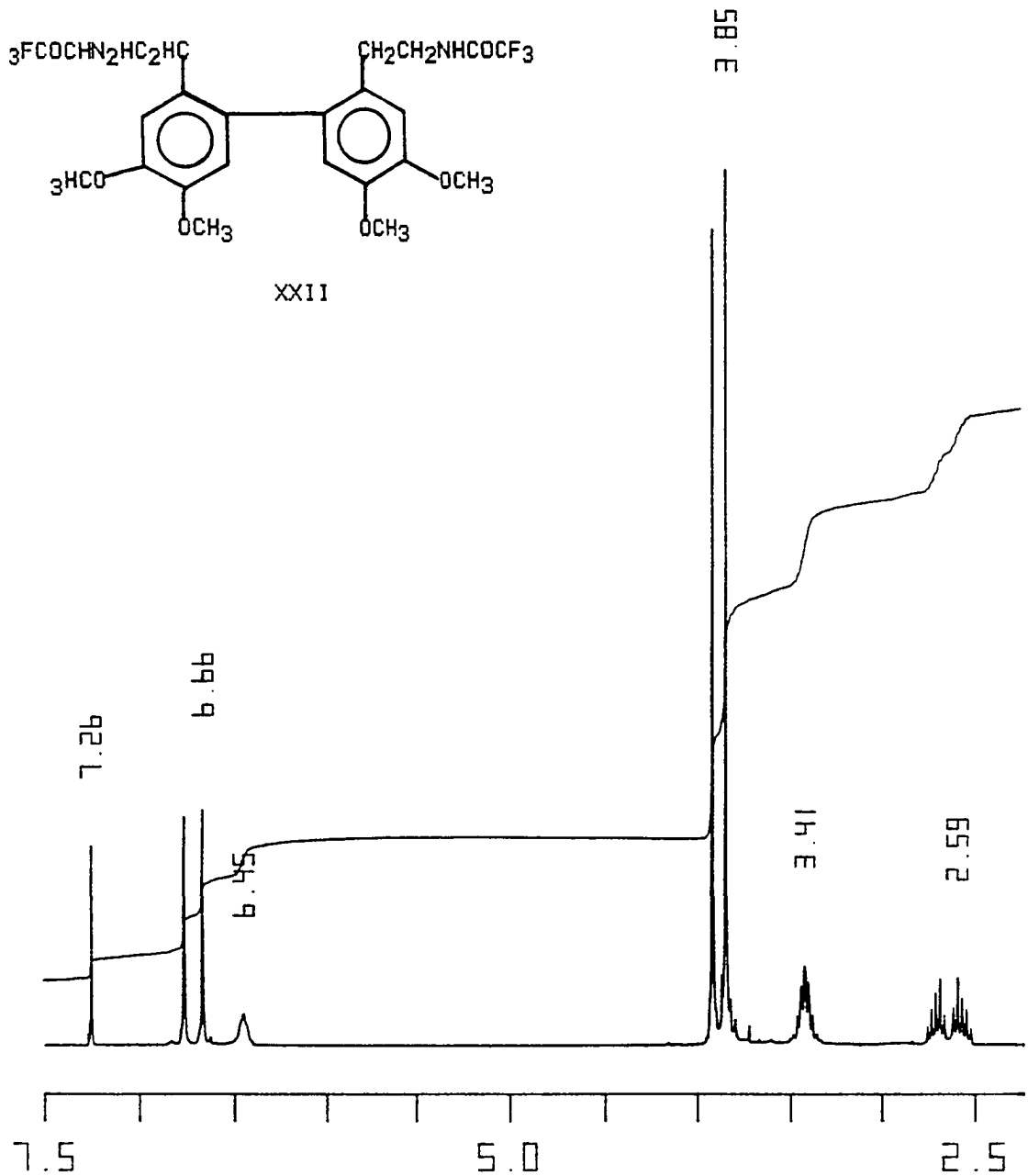

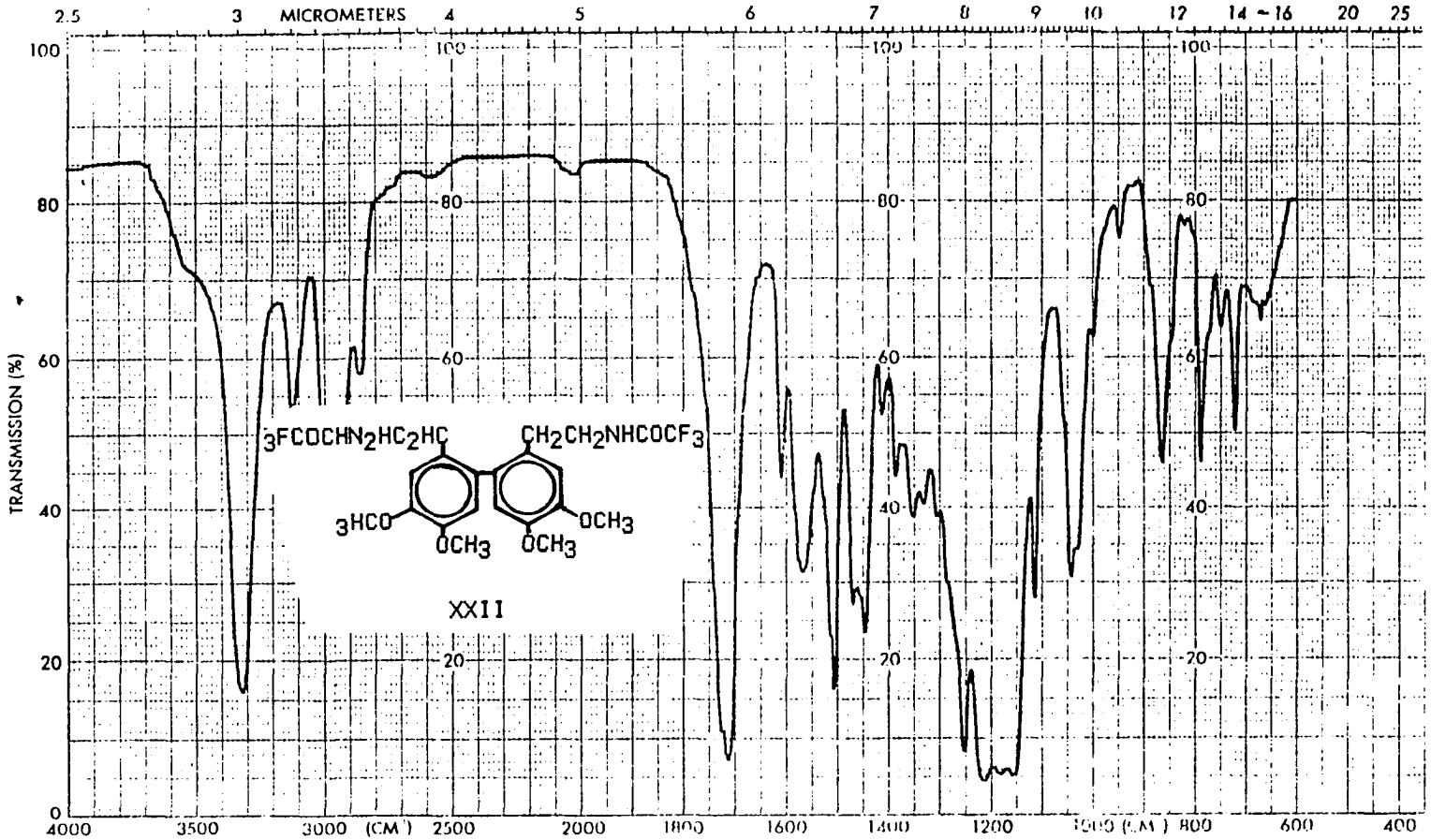

Figure V-36. IR Spectrum of
2,2′-Di-(N-trifluoroacetylaminoethyl)-4,4′,5,5′-tetramethoxybiphenyl XXII (KBr).

FIGURE V-37

Mass Spectrum of

2,2′-di-(N-Trifluoroacetylaminoethyl)-4,4′,5,5′-tetramethoxybiphenyl

XXII.

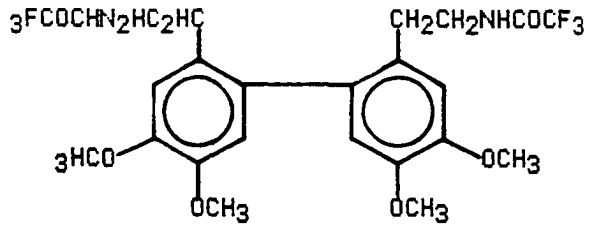

XXII

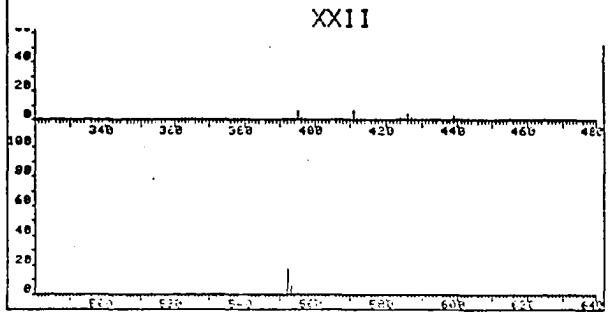

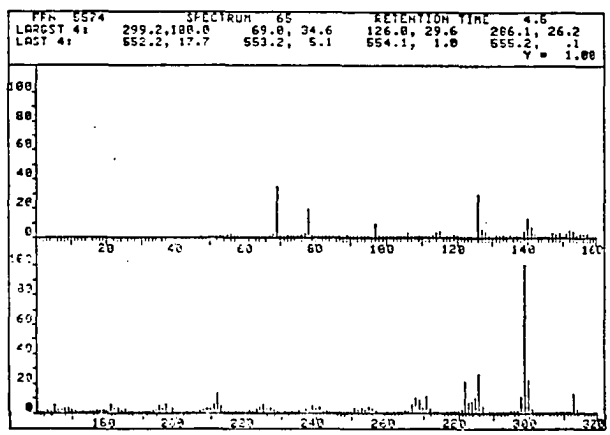

FILE 5574 SPECTRUM 65 325 PEAKS RT= 4.47 MIN BASE PEAK= 14943
LARGEST 102

MASS	%	MASS	%	MASS	%	MASS	%	MASS	%	MASS	%	MASS	%
50.1	.7	96.0	1.0	131.0	1.8	168.0	2.7	210.1	2.8	252.1	2.3	296.1	1.4
51.0	1.3	97.0	0.9	132.0	1.7	169.0	3.3	211.1	5.4	253.1	2.7	297.1	1.2
53.0	.8	98.1	1.9	133.1	1.7	170.1	1.7	212.1	13.3	254.1	2.2	298.2	11.1
55.1	1.8	102.0	1.1	133.0	2.0	171.1	1.1	213.1	4.7	255.1	4.0	299.2	100.0
56.1	2.3	103.1	.8	135.1	1.8	176.1	.6	214.0	1.0	256.1	2.7	300.1	22.4
57.1	.8	104.1	.8	139.1	3.9	177.1	1.1	220.1	.8	257.1	1.7	301.2	3.0
58.1	1.6	105.0	.9	140.0	12.7	178.1	1.4	221.1	1.4	264.0	.7	311.2	.9
59.2	.9	106.0	3.6	141.1	7.4	179.1	1.2	222.1	1.3	265.1	1.0	312.1	.6
63.1	.8	107.1	1.1	141.9	2.1	180.0	1.6	223.1	2.2	266.1	1.1	313.2	12.1
65.1	.7	111.1	.6	143.0	1.2	181.1	5.0	224.1	3.5	267.1	5.6	314.2	2.8
66.0	.7	112.2	1.1	147.1	3.0	182.1	2.9	225.1	5.2	268.0	10.5	380.2	.7
67.1	1.1	112.9	1.9	147.0	2.1	183.1	2.7	226.1	3.4	269.1	9.0	394.2	1.1
68.1	2.2	114.1	2.9	149.0	3.7	184.0	1.5	227.1	3.3	270.1	4.1	395.1	5.7
69.0	34.6	115.1	4.1	149.9	1.1	185.1	1.7	228.1	2.2	271.1	10.7	396.1	1.7
70.0	1.6	116.1	.8	151.0	2.4	191.1	.7	229.1	.6	272.1	3.0	406.2	1.1
72.1	1.6	117.1	1.1	152.0	5.3	193.1	1.3	235.2	1.1	279.2	.8	411.1	6.7
75.0	1.2	119.2	1.1	153.0	4.6	194.2	2.0	236.1	1.3	280.1	1.2	412.1	1.6
76.0	1.4	119.2	1.6	154.0	1.6	195.1	4.3	237.1	1.7	281.1	2.0	424.2	1.6
77.0	2.3	120.1	1.5	155.2	2.6	196.0	3.4	238.2	2.0	282.2	21.4	425.2	4.5
78.0	19.7	121.1	.9	156.0	2.7	197.0	5.4	239.1	4.3	283.1	7.1	427.2	1.6
79.0	1.5	124.2	.9	166.9	2.1	198.0	2.0	240.1	2.6	284.1	8.2	439.2	2.3
80.1	1.7	125.0	26.6	182.1	1.3	199.0	2.4	241.1	5.9	285.1	10.5	440.2	.9
93.0	.7	127.1	5.5	184.1	1.2	203.1	.9	242.1	1.7	286.1	26.2	488.1	.9
94.2	1.1	128.0	4.5	186.1	5.5	207.1	1.3	243.1	1.3	287.1	4.7	552.2	17.7
92.0	1.4	129.0	1.5	187.1	1.8	208.0	2.3	250.1	.7	289.1	.8	553.2	5.1
93.1	.8	130.0	.7	187.1	2.0	209.0	2.8	251.2	2.7	295.1	1.5	554.1	1.0

spectrometer.

N,N′-dicyclohexylcarbodiimide, glycine, ethyl glycinate hydrochloride, nitromethane, and 3,4-dimethoxybenzaldehyde were obtained from Aldrich Chemical Company, Inc., Milwaukee, Wi. Tl_2O_3 was obtained from Alpha, Danvers, Ma. Glycine tert-butyl ester hydrochloride was obtained from Vega Biochemicals, Tucson, Az. Hexestrol was obtained from Sigma Chemical Company, St. Louis, Mo.

Syntheses of o-carboxyphenylthallium ditrifluoroacetate (II),[3] o-iodobenzoic acid, ^{131}I-o-iodobenzoic acid,[3c] o-carboxamidophenylthallium ditrifluoroacetate (IV),[1e] 2,5-xylylthallium ditrifluoroacetate (V),[8] and p-iodoanisole[2] were performed as described in the literature.

Preparation of Thallium(III) Trifluoroacetate (TTFA)[3b]

Tl_2O_3 (50 g, 110 mmol) was refluxed for 46 hours in 200 mL of trifluoroacetic acid and 25 mL of H_2O, with stirring and in the absence of light. After filtration to remove unreacted Tl_2O_3 (13.0 g), the clear solution was concentrated in vacuo to a white semisolid mass, placed on a high vacuum line, and dried to afford 80.57 g (91.5% yield) of white powdery TTFA.

IR spectrum (KBr, Fig V-5) 3450 (m), 1682 (s), 1443 (m), 1213-1132 (s), 904 (w), 848 (m), 812 (m), 729 (m) cm^{-1}.

Synthesis of 2-Bis(trifluoroacetato)thallio-hippuric Acid (IX)

o-Carboxyphenylthallium ditrifluoroacetate (II) (3.67 g, 6.6 mmol) (prepared according to the procedure given by McKillop, et al.)[3] and 1.51 g (7.3 mmol) of N,N′-dicyclohexylcarbodiimide (DCC)[11] in 25 mL of THF were stirred for 30 minutes, while protected from light and air. Then, 0.5 g (6.6 mmol) of glycine in 10 mL of THF was added, and the resulting mixture was stirred for 18 hours. Trifluoroacetic acid (2 mL) was added to decompose any unreacted DCC, and the resulting cold milky suspension was filtered

to remove dicyclohexyl urea. The filtrate was concentrated in vacuo to a semisolid white mass which was again filtered after standing overnight in the refrigerator. The melting point of the crude white solid was 190-205°C.

^{1}H NMR spectrum (60 MHz, DMSO-d_6, Figs V-20 and V-15): δ 15.6 (d, 1 H, o-H), 11.4 (d, 1 H, m′-H), 10.4 (t, 1 H, m-H), 8.6 (t, 1 H, p-H), 6.7 (t, 1 H, p-H), 5.3 (t, 2 H, m-H), 4.9 (d, 1 H, m′-H), 3.6 (s, 2 H, CH_2), -0.1 (d, 1H, o-H);

IR spectrum (KBr, Fig V-21): 3405 (s), 3000 (b), 2650 (m), 2530 (m), 1740 (m), 1665 (s), 1580 (m), 1530 (w), 1470 (w), 1440 (m), 1377 (w), 1278 (s), 1200 (s), 1133 (s), 1038 (w), 1018 (w), 980 (m), 927 (m), 877 (w), 837 (m), 799 (s), 741 (s), 723 (s) cm^{-1}.

Synthesis of 2-Bis(trifluoroacetato)thallio-ethyl Hippurate (X)

o-Carboxyphenylthallium ditrifluoroacetate (II) (1.0 g, 1.8 mmol) and 0.42 g (2.0 mmol) of DCC in 25 mL of THF were stirred for 30 minutes in a flask protected from light. Ethyl glycinate hydrochloride (0.25 g, 1.8 mmol), dissolved in a minimum amount of water, was then added, the milky suspension was stirred 4 hours, quenched with 1 mL of CF_3CO_2H, and the insoluble urea was filtered. In vacuo concentration of the clear solution followed by cooling and filtration gave 0.37 g of crude (X).

^{1}H NMR spectrum (60 MHz, DMSO-d_6, Fig V-16): δ 15.4 (d, 1 H, o-H), 11.3 (d, 1 H, m′-H), 10.3 (t, 1 H, m-H), 8.9 (m, 1 H, NH), 8.4 (t, 1 H, p-H), 6.7 (t, 1 H, p-H), 5.4 (t, 1 H, m-H), 5.1 (d, 1 H, m′-H), 4.2 (q, 2 H, ethyl CH_2), 3.8 (d, 2 H, CH_2), 1.3 (t, 3 H, CH_3), 0.3 (d, 1 H, o-H);

IR spectrum (KBr, Fig V-17): 3000 (b), 2657 (w), 2530 (w), 1752 (w), 1671 (s), 1581 (w), 1470 (w), 1434 (m), 1300 (m), 1257 (w), 1209 (s), 1145 (s), 1062 (w), 1018 (w), 913 (w), 839 (m), 801 (m), 730 (m) cm^{-1}.

Synthesis of 2-Bis(trifluoroacetato)thallio-t-butyl Hippurate (XI)

o-Carboxyphenylthallium ditrifluoroacetate (II) (3.29 g, 6.0 mmol) and 1.23 g (6.0 mmol) of DCC were dissolved in 50 mL of THF and allowed to stir for 30 minutes. To the stirred solution, protected from light, was added 1 g (6.0 mmol) of glycine tert-butyl glycinate hydrochloride dissolved in a minimum amount of water, and the resulting solution was stirred for 4 hours. The suspension was filtered, and the clear solution was concentrated in vacuo to afford a crude mixture of XI.

^{1}H NMR spectrum (60 MHz, DMSO-d_6, Fig V-18): δ 15.3 (d, 1 H, o-H), i1.4 (d, 1 H, m′-H), 10.2 (t, 1 H, m-H), 8.5 (t, 1 H, p-H), 6.7 (t, 1 H, p-H), 5.5 (t, 1 H, m-H), 5.0 (t, 1 H, m′-H), 4.4 (s, 2 H, CH_2), 1.5 (s, 3 H, t-butyl H), 0.3 (d, 1 H, o-H);

IR spectrum (KBr, Fig V-19): 3153 (b), 1650 (s), 1575 (m), 1464 (m), 1377 (s), 1275 (m), 1203 (s), 1143 (s), 1111 (w), 1028 (m), 878 (w), 835 (w), 793 (m), 735 (s), 660 (m), 645 (m) cm^{-1}.

Attempted In Situ Thallation-iodination of Methyl Hippurate (XII)

Methyl hippurate (XII) (3.56 g, 18.4 mmol) was added to 35 mL of dry CH_3CN containing 10 g (18.4 mmol) of TTFA (note: upon mixing CH_3CN and TTFA, the solution became black-brown in color) and the resulting mixture was stirred at reflux for 61 hours. After 36 hours the solution became clear yellow. A solution of potassium iodide (7.03 g, 424 mmol) in 20 mL of water was added to the cool solution which became bright yellow. $Na_2S_2O_5$ (2.0 g) was added after 20 minutes and the mixture stirred was for several hours. The suspension was rendered basic with 4N NaOH, chloroform was added, the suspension was vacuum filtered, and the filtrate was rotary evaporated to afford a sweet smelling oil. The NMR and IR (Figs V-22 and V-23, respectively) indicated unreacted methyl hippurate, but the mass spectrum (Fig V-24) shows the expected 319 m/e molecular ion of o-iodomethyl hippurate (XIII).

^{1}H NMR spectrum ($CDCl_3$, Fig V-22): δ 8.9 (t, J = 6 Hz, 1 H,

N-H), 7.95 (m, 2 H, Ar-H), 7.5 (m, 3 H, Ar-H), 4.1 (d, J = 6 Hz, 2H, CH_2), 3.65 (s, 3 H, CH_3);

IR spectrum (NaCl plates, Fig V-23): 3340 (m), 1750 (s), 1650 (s), 1550 (s), 1495 (m), 1445 (m), 1330 (m), 1240 (s), 1013 (m), 715 (m) cm^{-1};

Mass spectrum (70 eV, Fig V-24): m/e (relative intensity) 319 (M^+, 6.1), 231 (11.3), 134 (17.9), 105 (100.0), 77 (38.1).

Synthesis of o-Iodohippuric Acid (XIV)

To 3.94 g (20.4 mmol) of methyl hippurate was added 35 mL of TFA containing 11.07 g (20.0 mmol) of TTFA, and the stirred mixture was refluxed under N_2 for 22 hours. To the hot solution was added 7.79 g of potassium iodide in 15 mL of water, causing the solution to become purple-black. After 15 minutes, 0.1 g of $Na_2S_2O_5$ was added to the stirred solution. Fifteen minutes later the dark solution was rendered basic with 4N NaOH, suction filtered, and the filtrate extracted with $CHCl_3$. Neutralization of the aqueous layer produced a white precipitate which was collected by suction filtration. The crude precipitate was dissolved in 10% $NaHCO_3$ and upon acidification deposited white needles of o-iodohippuric acid XIV: mp 172-173°C (lit.[20] 170°C).

^{1}H NMR spectrum (300 MHz, DMSO-d_6/TMS, Fig V-25): δ 8.70 (t, J = 5.78 Hz, 1 H, N-H), 7.89 (d, J = 7.57 Hz, 1 H, Ar-H), 7.46 (t, J = 7.53 Hz, 1 H, Ar-H), 7.36 (d, J = 7.32, 1 H, Ar-H), 7.18 (t, J = 7.04 Hz, 1 H, Ar-H), 3.89 (d, J = 5.62 Hz, 2 H, CH_2), 2.50 (DMSO-d_6);

IR spectrum (KBr, Fig V-26): 3265 (m), 3083 (m), 1740 (m), 1625 (s), 1590 (m), 1555 (m), 1410 (m), 1320 (w), 1228 (m), 1199 (w), 1178 (w), 996 (w), 737 (m) cm^{-1};

Mass spectrum (70 eV, Fig V-27): m/e (relative intensity) 305 (M^+, 26.1), 261 (11.1), 260 (47.9), 231 (100.0), 203 (31.0), 105 (12.9), 76 (22.7).

Synthesis of 3,4-bis(p-Anisyl)hexane (XV)[20]

Hexestrol (10 g, 38 mmol) was dissolved in 10 mL of water and 75 mL of n-propanol. NaOH (5.14 g, 125 mg) was then added, and the mixture was brought to reflux. Then, 14.4 g (114 mmol) of dimethyl sulfate was cautiously added dropwise, and reflux was continued for 3½ hours. The milky solution became pale yellow, and precipitation of white solid followed shortly. After cooling, filtration of the cold solution gave 9.16 g (83% yield) of dimethylated product XV: mp 142-143°C (lit.[15] mp 143-144°C).

Synthesis of 3,4-bis(3-Iodo-p-anisyl)hexane (XVI)

3,4-bis(p-Anisyl)hexane (XV, 3.0 g, 10.1 mmol) in 10 mL of TFA was added to 10.92 g (20.1 mmol) of TTFA in 20 mL of TFA at -25°C and was stirred for 15 minutes (a black solution formed immediately upon mixing). A solution of 7.67 g of potassium iodide in 15 mL of water was added all at once, and the resulting mixture was stirred for an additional 15 minutes. $Na_2S_2O_5$ (3.0 g) was added to destroy free iodine and the solution was rendered basic with 4N NaOH. Yellow thallium iodide was removed via suction filtration and the mixture was rotary evaporated, thereby affording an orange oil which partially solidified upon standing at room temperature. This was dissolved in $CHCl_3$ and filtered through a short silica gel column. Evaporation of the eluant followed by recrystallization from hexane afforded a white, crystalline compound: mp 199.5°C (cf. reference 3c, mp 199-200°C).

^{1}H NMR spectrum (300 MHz, $CDCl_3$, Fig V-28): δ 7.54 (d, J = 2.2 Hz, 1 H, Ar-H), 7.26 ($CDCl_3$), 7.05 (dd, J = 8.4 Hz, J′ = 2.2 Hz, 1 H, Ar-H), 6.17 (d, J = 8.4 Hz, 1 H, Ar-H), 2.41 (dd, J = 5.3 Hz, J′ = 3.0 Hz, 1 H, benzylic-H), 1.39 (dqd, J = 13 Hz, J′ = 7.3 Hz, J′′ = 3 Hz, 1 H, CH (ethyl CH_2), 1.26 (dqd, J = 13 Hz, J′ = 7.3 Hz, J′′ = 5.3 Hz, 1 H, CH (ethyl CH_2), 0.55 (dd, J = 7 Hz, J′ = 6.7 Hz, 3 H, CH_3);

IR spectrum ($CDCl_3$ solution cell, Fig V-29): 2950 (m), 1602 (w), 1490 (s), 1445 (m), 1405 (w), 1280 (s), 1257 (s), 1187 (m), 1050 (s), 1021 (m), 814 (m) cm^{-1};

Mass spectrum (70 eV, Fig V-30): m/e (relative intensity) 550 (M^+, 0.5), 276 (10.3), 275 (100.0), 274 (21.5), 148 (10.0).

Anal. Calculated for $C_{20}H_{24}I_2O_2$: C, 44.66; H, 4.40. Found: C, 43.69; H, 4.38.[3c]

Synthesis of α-(3,4-Dimethoxyphenyl)-β-nitroethene (XVII)

3,4-Dimethoxybenzaldehyde (10 g, 60.2 mmol), ammonium acetate (4.0 g, 51.9 mmol), 5 mL (81.9 mmol) of nitromethane, and 40 mL of glacial acetic acid were gently refluxed for 1½ hours. Upon cooling to room temperature, precipitation of yellow crystals ensued. Recrystallization from ethanol gave 10.23 g (81% yield) of yellow crystalline XVII: mp 141-142°C (lit.[17b] mp 140-142°C).

Synthesis of α-(3,4-Dimethoxyphenyl)-β-nitroethane (XVIII)

To 12 g (57.4 mmol) of α-(3,4-dimethoxyphenyl)-β-nitroethene (XVII) in 300 mL of vigorously stirred acetonitrile at 0°C was added dropwise a solution of 10.92 g (288.6 mmol) of sodium borohydride in 225 mL of H_2O containing 1½ mL of a 40% sodium hydroxide solution.[17c] The pH was kept between 3 and 6 by addition of 3N HCl. After an additional 2 hours at 0°C, the mixture was diluted with 200 mL of H_2O and extracted thoroughly with dichloromethane. The organic layers were combined, dried over $MgSO_4$, and partially evaporated. Upon cooling, 3.61 g of unreacted XVII precipitated from the mixture and was separated by suction filtration. Further evaporation afforded an orange semisolid oil which was vacuum distilled (99°C, 0.6 torr; lit.[16e] 139-140°C, 0.1 torr) producing a yellow semisolid mass which was recrystallized from Et_2O/pentane: mp 50-52°C (lit.[17e] mp 51-52°C).

Synthesis of 3,4-Dimethoxyphenethylamine (XIX)

To a 1 liter round bottom flask equipped with a $CaCl_2$ drying tube and containing 13.7 g (361 mmol) of LAH in 300 mL of dry THF was added 25 g (120 mmol) of α-(3,4-dimethoxyphenyl)-β-nitroethene (XVII) in 200 mL of dry THF dropwise. The resulting mixture was refluxed for 2 hours, cooled to room temperature, and 41 g of water was added dropwise. The solution was filtered and the organic layer was separated, dried over $MgSO_4$, and concentrated in vacuo to an orange oil. Vacuum distillation of the oil afforded 17.57 g (81% yield) of pale yellow liquid: 99°C, 0.6 torr (lit.[17f] 140°C, 2.0 torr).

Synthesis of N-trifluoroacetyl-3,4-dimethoxyphenethylamine (XX)

Using standard procedures,[18] trifluoroacetic anhydride (11.07 g, 52.7 mmol) and 250 mL of benzene were placed in a dry 500 mL 3-neck round bottom flask equipped with a $CaCl_2$ drying tube. After addition of 9.63 g (53.1 mmol) of 3,4-dimethoxyphenethylamine (XIX) in 25 mL of benzene, the mixture was refluxed for 1 hour and was allowed to stir overnight. The resulting dark orange mixture was extracted several times with 10% bicarbonate (causing the solution to become yellow), washed with water, dried over $MgSO_4$, and rotary evaporated to a dark brown liquid which formed 9.23 g (63% yield) of soft glassy crystals from pentane: mp 83-84.5°C.

^{1}H NMR spectrum (300 MHz, $CDCl_3$, Fig V-31): δ 6.83 (d, J = 8.1 Hz, 1 H, o-H), 6.72 (dd, J = 8.0 Hz, J′ = 2.1 Hz, 1 H, m-H), 6.69 (d, J = 2.2 Hz, 1 H, o-H), 6.47 (br, 1 H, N-H), 3.86 (s, 6 H, OCH_3), 3.59 (dt, J = 13.2 Hz, J′ = 6.9 Hz, 2 H, CH_2N), 2.83 (t, J = 6.9 Hz, 2 H, CH_2Ar);

IR spectrum (CCl_4 solution cell, Fig V-32): 3347 (w), 2940 (w), 1733 (s), 1510 (m), 1464 (m), 1262 (s), 1240 (s), 1211 (s), 1159 (vs), 1033 (m) cm^{-1};

Mass spectrum (70 eV, Fig V-33): m/e (relative intensity) 278 (M +

7.8), 277 (M^+, 57.1), 164 (42.9), 151 (100.0).

An elemental analysis of this new compound has not been performed.

In Situ Thallation-iodination of

N-trifluoroacetyl-3,4-dimethoxyphenethylamine (XX)

To 3.92 g (7.2 mmol) of TTFA in 2 mL of TFA at -25°C was added dropwise with stirring 2.0 g (7.2 mmol) of N-trifluoroacetyl-3,4-dimethoxyphenethylamine (XX) in 10 mL of THF and the resulting black mixture was stirred for 25 minutes. Potassium iodide (2.75 g, 16.6 mmol) in 7 mL of water was added all at once, and the stirring was continued for an additional 15 minutes after the reaction had reached room temperature. $Na_2S_2O_5$ (1.0 g) was added and the stirring was continued for 15 minutes. The solution was rendered basic with 4N NaOH, diluted with chloroform, and suction filtered. The chloroform layer was dried over anhydrous $MgSO_4$, filtered, and rotary evaporated to afford a white solid which, on the basis of NMR, IR, and mass spectra, is believed to be 2,2′-di-(N-trifluoroacetylaminoethyl)-4,4′,5,5′-tetramethoxybiphenyl (XXII): mp 204-206°C.

^{1}H NMR spectrum (300 MHz, $CDCl_3$, Fig V-35): δ 7.26 ($CDCl_3$), 6.76 (s, 2 H, Ar-H), 6.67 (s, 2 H, Ar-H), 6.45 (bt, J = 6.4 Hz, 2 H, N-H), 3.92 (s, 6 H, OCH_3), 3.85 (s, 6 H, OCH_3), 3.41 (ddd, J = 12.05 Hz, J′ = 6.5 Hz, J′′ = 6.3 Hz, 4 H, NCH_2), 2.68 (dt, J = 13.5 Hz, J′ = 6.0 Hz, 2 H, ArC-H), 2.59 (dt, J = 13.5 Hz, J′ = 6.0 Hz, 2 H, ArC-H);

IR spectrum (KBr, Fig V-36): 3320 (s), 3121 (w), 2950 (m), 1717 (s), 1610 (m), 1567 (m), 1507 (s), 1460 (m), 1253 (s), 1180 (bs), 1113 (m), 1040 (m), 863 (m), 789 (m), 722 (m) cm^{-1};

Mass spectrum (70 eV, Fig V-37): m/e (relative intensity) 552 (17.7), 313 (12.1), 300 (22.4), 299 (100.0), 298 (11.1), 286 (26.2), 285 (10.5), 282 (21.4), 271 (10.7), 268 (10.6), 212 (13.3), 140 (12.7), 126 (29.6), 78 (19.7), 69 (34.6).

As stated in the discussion (*vide supra*), GC/MS of the product resulting from the in situ thallation-iodination of XX revealed a minor component of molecular weight 403 which is the same as that of the anticipated iodo compound XXI.

Mass spectrum of XXI (70 eV, Fig V-34): m/e (relative intensity) 403 (M^+, 2.8), 277 (23.0), 181 (14.9), 180 (10.9), 164 (47.2), 153 (10.8), 152 (85.9), 151 (100.0), 137 (29.1), 135 (10.3), 121 (11.8), 109 (12.3), 108 (10.7), 107 (27.9), 106 (15.8), 105 (13.7), 97 (18.4), 95 (14.3), 91 (19.7), 87 (10.0), 85 (58.5), 83 (88.2), 81 (11.7), 79 (15.7), 78 (20.7), 77 (21.4), 71 (12.7), 69 (50.4), 65 (17.7), 57 (19.6), 55 (15.2), 51 (10.1).

BIBLIOGRAPHY

1. (a) McKillop, A.; Taylor, E. C. Adv. Organometal. Chem. 1973, 11, 147. (b) Taylor, E. C.; McKillop, A. Acc. Chem. Res. 1970, 3, 338. (c) McKillop, A.; Taylor, E. C. Chemistry in Britain 1973, 9, 4. (d) McKillop, A.; Taylor, E. C. Endeavor 1976, 35, 88. (e) Larock, R. C.; Fellows, C. J. Org. Chem. 1980, 45, 363.

2. Deacon, G. B.; Tunaley, D.; Smith, R. N. M. J. Organometal. Chem. 1978, 144, 111.

3. (a) McKillop, A.; Fowler, J. S.; Zelesko, M. J.; Hunt, J. D.; Taylor. E. C. Tetrahedron Lett. 1969, 2423. (b) McKillop, A..; Fowler, J. S.; Zelesko, M. J.; Hunt, J. D.; Taylor, E. C.; Kienzle, F.; McGillivary, G. J. Am. Chem. Soc. 1971, 93, 4841, 4845. (c) Gilliland, D. L.; Basmadjian, G. P.; Marchand, A. P.; Hinkley, G. H.; Earlywine, A. D.; Ice, R. D. J. Radioanal. Chem. 1981, 65, 107.

4. McKillop, A.; Hunt, J. D.; Taylor, E. C. J. Organometal. Chem. 1970, 24, 77.

5. (a) Maher, J. P.; Evans, D. F. J. Chem. Soc. 1965, 637. (b) Hinton, J. F.; Briggs, R. W. J. Magn. Reson. 1976, 22, 447.

6. Kagarise, R. E. J. Chem. Phys. 1957, 27, 519.

7. Baillie, M. J.; Brown, D. H.; Moss, K. C.; Sharpe, D. W. A. J. Chem. Soc. 1968, 3110.

8. Taylor, E. C.; Kienzle, F.; McKillop, A. Org. Syn. 1976, 55, 70.

9. McKillop, A.;; Fowler, J. S.; Zelesko, M. J.; Hunt, J. D.; Taylor, E. C.; McGillivary, G. Tetrahedron Lett. 1969, 2427.

10. Deacon, G. B.; Tunaley, D. J. Fluorine Chem. 1977, 10, 177.

11. Sheehan, J. C. J. Am. Chem. Soc. 1955, 77, 1067.

12. (a) Sheehan, J. C.; et al. J. Org. Chem. 1961, 26, 2525. (b) Sheehan, J. C.; Preston, J. J. Am. Chem. Soc. 1965, 87, 2492.

13. (a) Ondetti, M. A.; Thomas, P. L. J. Am. Chem. Soc. 1965, 87, 4373. (b) Hoare, D. G.; Koshland Jr., D. E. J. Bio. Chem. 1967, 242, 2447. (c) Sheehan, J. C.; Hlavka, J. J. J. Org. Chem. 1956, 21, 439

14. "Basic Principles of Organic Chemistry"; 2nd. ed., Roberts, J. D., Caserio, M. C., Eds.; W. A. Benjamin, Inc.: Menlo Park, Ca., 1977; p 1239.

15. Pratt, R. J.; Jensen, E. V. J. Am. Chem. Soc. 1956, 78, 4430.

16. Taylor, E. C.; Andrade, J. G.; Rall, G. J. H.; McKillop, A.

J. Am. Chem. Soc. 1980, 102, 6513.

17. (a) Worrall, D. E. Org. Syn. 1929, 9, 66. (b) Raiford, L. C.; Fox, D. E. J. Org. Chem. 1944, 9, 170. (c) Meyers, A. I.; Sircar, J. C. J. Org. Chem. 1967, 32, 4134. (d) Cann, P. F.; Stirling, C. J. M. J. Chem. Soc. Perkin Trans. 1974, 2, 817. (e) Seebach, D.; Henning, R.; Gonnerman, J. Chem. Ber. 1979, 112, 234. (f) Paul, B.; Anand, N. J. Sci. Ind. Research 1958, 17B, 219.

18. Vogel, A. I. "Practical Organic Chemistry"; 3rd ed., Vogel, A. I., Ed., 1956; p 540.

19. McKillop, A.; Turrell, A. G.; Taylor, E. C. J. Org. Chem. 1977, 42, 764.

20. Novello, N. J.; Miriam, S. R.; Sherwin, C. P. J. Biol. Chem. 1926, 67, 563.

PART VI

SYNTHESIS AND NUCLEAR MAGNETIC RESONANCE STUDY OF A SERIES OF 1,4,4A,8A-TETRAHYDRO-ENDO-1,4-METHANONAPHTHALENE-5,8-DIONES AND OF PENTACYCLO[5.4.0.0^{2,6}.0^{3,10}.0^{5,9}]UNDECANE-8,11-DIONES[1]

Introduction

Diels-Alder cycloaddition of an appropriately substituted cyclopentadiene (Ia-c) to an appropriately substituted p-benzoquinone (IIa-c) followed by photocyclization of the resulting endo cycloadduct (IIIa-d) was employed to synthesize the following series of pentacyclo[5.4.0.0^{2,6}.0^{3,10}.0^{5,9}]undecane-8,11-diones: unsubstituted (IVa), and substituted compounds 1-methyl (IVb), 2-methyl (IVc), and 3-methyl (IVd). In addition, a high resolution NMR study of these compounds was completed.

Results and Discussion

As part of a continuing study of the synthesis[2] (Scheme VI-1) and chemistry[3-7] of substituted pentacyclo[5.4.0.0^{2,6}.0^{3,10}.0^{5,9}]undecanes, the synthesis and characterization of unsubstituted, 1-methyl, 2-methyl, and 3-methyl pentacyclo[5.4.0.0^{2,6}.0^{3,10}.0^{5,9}]undecane-8,11-diones (compounds IVa-IVd) was undertaken. In all cases the basic synthetic approach involves Diels-Alder cycloaddition of the appropriately substituted cyclopentadiene (Ia-c) to an appropriately substituted p-benzoquinone (IIa and IIb) followed by intramolecular [2 + 2] photocyclization of the resulting endo cycloadduct (IVa-d).[7]

The unsubstituted isomer IIIa was obtained previously[8] by

SCHEME VI-1

Synthesis of the series of Pentacyclo[5.4.0.0^{2,6}.0^{3,10}.0^{5,9}]undecane-8,11-diones IVa-IVd.

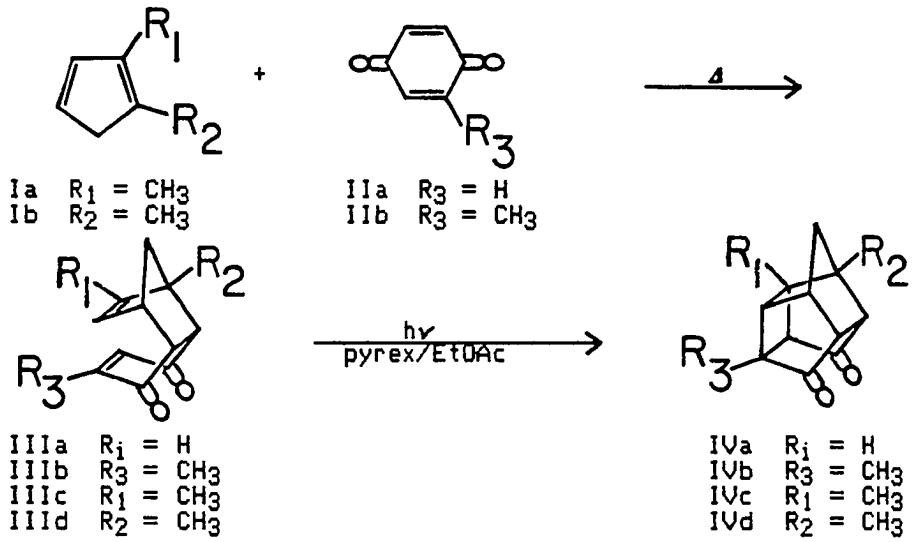

Diels-Alder addition of cyclopentadiene to p-benzoquinone (IIa). The fact that this Diels-Alder reaction proceeds with endo regiospecificity has been verified by the facile intramolecular photocyclization of IIIa to IVa.[9]

The 6-methyl isomer (IIIb) obtained via Diels-Alder addition of cyclopentadiene to toluquinone (IIb)[10] is a single, isomerically pure substance. The endo regiospecificity of this reaction was also verified by the facile intramolecular photocyclization of IIIb to IVb. Interestingly, compound IIIb could not be induced to undergo further Diels-Alder addition to cyclopentadiene even when IIIb was refluxed overnight with excess cyclopentadiene in benzene solution.

The remaining two monomethylpentacyclo[5.4.0.0^{2,6}.0^{3,10}.-0^{5,9}]undecane-8,11-diones (IVc and IVd) were prepared via a similar sequence starting with the Diels-Alder cycloaddition of methylcyclopentadiene to p-benzoquinone. Thermal cracking of the methylcyclopentadiene dimer[11] affords a mixture of 1-methyl- and 2-methylcyclopentadienes.[12] Diels-Alder cycloaddition of the diene mixture to IIa affords a mixture of adducts IIIc and IIId (product ratio ca. 45:55). The mixture of isomeric adducts IIIc and IIId could be

separated conveniently via fractional recrystallization from methanol. That each of these isomeric adducts possesses the endo configuration was shown by their respective facile intramolecular photocyclizations to IVc and IVd.

As part of this study, a single-crystal X-ray structural analysis on IVd was performed. A perspective view of IVd is shown in Fig VI-1.[13] Much of the strain inherent in this ring system is accommodated by a lenghtening of the C_2-C_7 and C_4-C_5 bonds, [both 1.589 (2) Å]. The corresponding carbon-carbon bonds in a closely related polycyclic system studied by Mehta and co-workers[14] have an average length of 1.59 Å.

With the exception of the exocyclic atoms on C_1 and C_8, the compound would have a mirror plane bisecting the C_2-C_7, C_4-C_5, and C_9-C_{10} bonds. This mirror is approximately present in the solid state. Bonds equivalent by mirror symmetry show a maximum variation in bond length of 4σ for bonds involving C_1 or C_8. However, mirror equivalent bonds between atoms not bonded to C_1 or C_8 have differences less than σ. Bond angles show a similar mirror equivalence, with angles between atoms furthest from C_1 and C_8 having the smallest differences.

The two five-membered rings that contain C_1, have a nearly ideal envelope conformation as shown by the values of the asymmetry parameters[15] $\Delta C_{s(2-7)}$ = 0.90°, $\Delta_{s(9-10)}$ = 0.96°. In contrast, the conformation of the five-membered rings with carbonyl groups is highly distorted [$\Delta C_{s(4-10)}$ = 11.2°, $\Delta C_{2(2-3)}$ = 18.9°, and $\Delta C_{s(5-9)}$ = 12.9°, $\Delta C_{2(6-7)}$ = 28.0°]. The four-membered ring is planar with a maximum atomic displacement of 0.0011 (12) Å.

The C_1-C_{12} bond [1.519 (2) Å] is considerably shorter than the normal 1.54 Å. This shortening can be explained in terms of a hybridization effect at C_1. The strained ring system increases the C_{12}-C_1-C_i bond angles beyond the normal 109.5° [i = 2, 114.06 (11)°; i = 10, 115.58 (10)°; i = 11, 118.34 (11)°].

FIGURE VI-1

Perspective View of IVd. Carbon and oxygen atoms are shown as 50% Probability ellipsoids (oxygens are shaded). Hydrogens are displayed as arbitrary spheres.[13] Estimated standard deviations of bond lengths are ±0.002 Å.

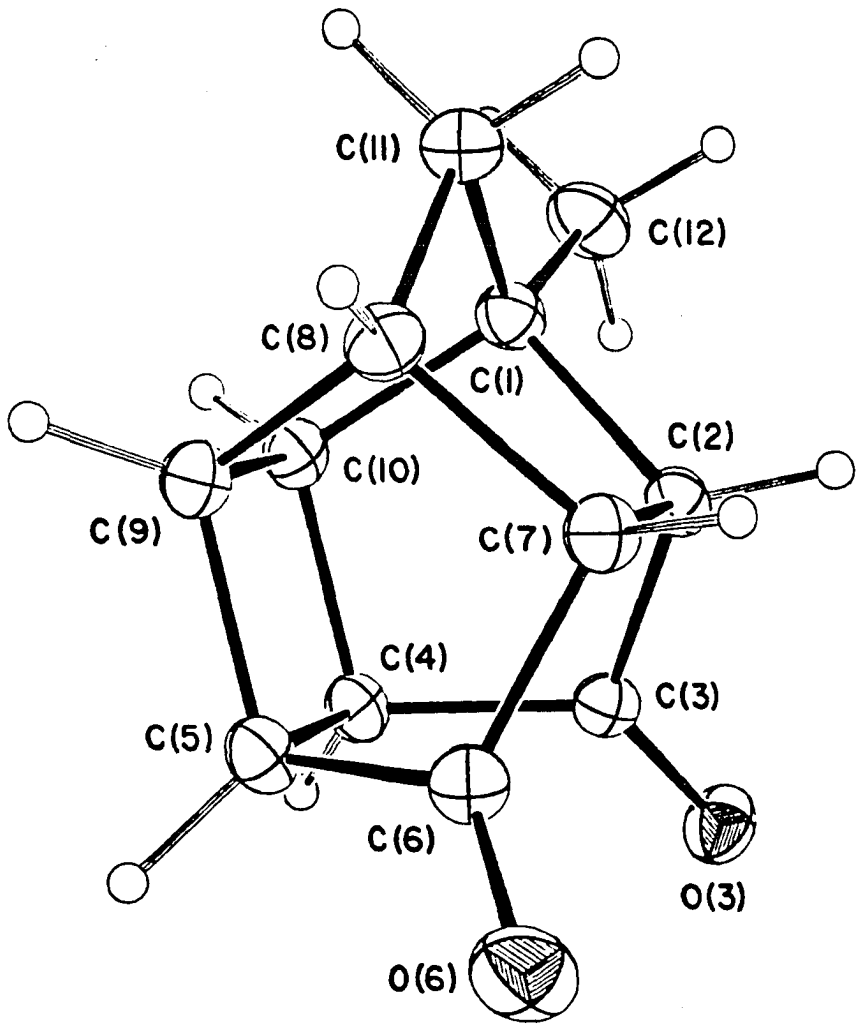

This suggests an increase in the p character of the molecular orbitals directed toward the ring system and an increase in the s character of the orbital directed toward C_{12}.

There are three short intermolecular contacts: $O_3 \cdots H_{10}$ (½ + x, ½ - y, z - ½) 2.48 (2) Å, $O_3 \cdots H_5$ (-x, -y, -z) 2.55 (2) Å, and $O_3 \cdots H_4$ (-x, -y, -z) 2.59 (2) Å.

Experimental

Melting points are uncorrected. All high resolution NMR spectra were recorded on a Varian XL-300 spectrometer. Proton, HOMCOR, and HOM2DJ spectra were record at 300 MHz, and HETCOR spectra were recorded at 300 MHz (in the proton domain) and at 75 MHz (in the ^{13}C domain). Stacked plots of spin echo and ^{13}C spectra were recorded on an IBM/Bruker NR80 spectrometer at 20 MHz. The signals in all proton spectra are reported in parts per million (δ) downfield from internal tetramethylsilane. Signals in all ^{13}C and spin echo spectra are reported in parts per million (δ) relative to the central line of the deuteriochloroform triplet. Assignments of the carbonyl ^{13}C chemical shifts of compounds 'b' through 'd' in both series are tentative. Infrared spectra were obtained on Perkin-Elmer Model 1330 and Beckman Model 4250 infrared spectrophotometers. Mass spectra were obtained on a Hewlett-Packard Model 5985B mass spectrometer (70 eV). Elemental microanalyses were performed by Galbraith Laboratories, Inc., Knoxville, Tn.

Scheme VI-2 illustrates the numbering schemes used in all NMR spectra discussed in the Experimental section and in Tables VI-6 through VI-13. These schemes differ from that which was illustrated earlier in Fig VI-1 during the discussion of the X-ray crystal structure of cage photolysis product IVd.

Chemical shift assignments of syn and anti H_9 protons of the Diels Alder adduct series of compounds (IIIa-IIId) were primarily determined by the long range vinyl coupling between H_{9s} and vinyl

SCHEME VI-2

Numbering Schemes Used in the Discussion of all NMR Spectra in the Experimental Section and in Tables VI-6 through VI-13.

(a) Diels Alder adducts IIIa through IIId.

IIIa: R_1-R_3 = H
IIIb: R_2 & R_3 = H, R_1 = CH_3.
IIIc: R_1 & R_3 = H, R_2 = CH_3.
IIId: R_1 & R_2 = H, R_3 = CH_3.

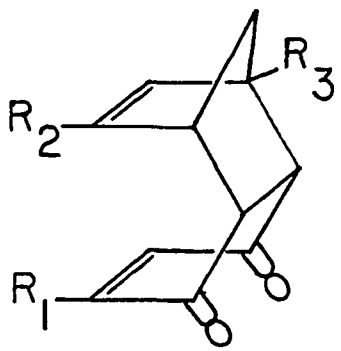

(b) Photolysis products IVa through IVd.

IVa: R_1-R_3 = H.
IVb: R_2 & R_3 = H, R_1 = CH_3.
IVc: R_1 & R_3 = H, R_2 = CH_3.
IVd. R_1 & R_2 = H, R_3 = CH_3.

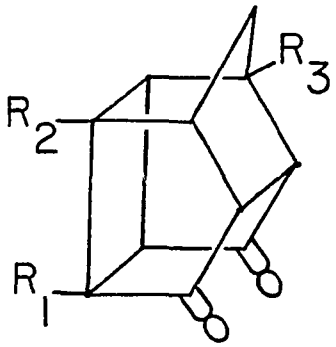

protons H_2 and H_3 (see Scheme VI-2a).[16] The AB pattern of H_{9s} and H_{9a} is easily identified and far upfield. The general sequence of proton assignment was as follows: (1) decoupling of H_{9s} and H_{9a} readily identifies bridgehead protons H_3 and H_5 and confirmation is provided upon decoupling vinylic H_2 and H_3; (2) decoupling of H_3 and H_5 confirms the position of H_{4a} and

H_{8a}; (3) process of elimination leaves H_6 and H_7. Identification of the protons of IIIb-IIId follows a similar sequence with modifications for each compound which are necessary because of the loss of molecular symmetry due to methyl substitution. The 2-dimensional NMR spectra were also used as an aid in signal identification.

The general sequence of steps used to assign individual resonances for compounds IVb-IVd was as follows: (1) the AB pattern of protons H_{4s} and H_{4a} is easily identified and far upfield; (2) decoupling of H_{4s} and H_{4a} results in major changes in protons H_3 and H_5; (3) decoupling of H_3 and H_5 identifies the group of protons which includes H_2, H_6, H_9, and H_{10} but does not identify individual resonances; (4) decoupling of any one of the latter four protons results in a change in H_1 and H_7, but decoupling of H_2 and H_6 produces the greatest change in H_1 and H_7 because of a large vicinal coupling and two 4-bond coupling pathways (e.g., $^{J}H_1$-H_6 via C_2 and via C_7); (5) identification of H_{4s} was accomplished by the decoupling of H_1 and H_7 [a similar rare 5-bond coupling has been observed in cage compounds of comparable structure (cf. Fig VI-2)][17]; (6) 2-Dimensional NMR was also extensively used in making these proton assignments.

FIGURE VI-2

Examples of 5-Bond Long-Range ^1H-^1H Coupling.(17)

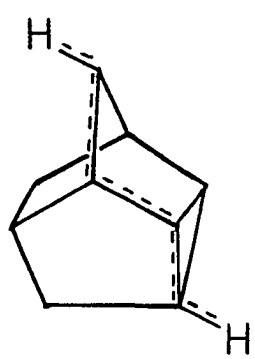

V (J = 2 Hz)

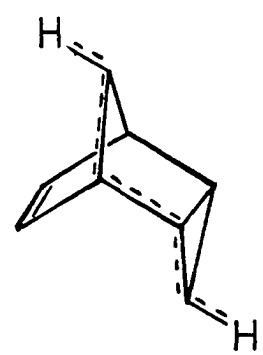

VI (J = 2.3 Hz)

1,4,4a,8a-Tetrahydro-endo-1,4-methanonaphthalene-5,8-dione (IIIa). Synthesis of IIIa was accomplished by using the method previously reported in the literature.[8]

^{1}H NMR spectrum (300 MHz, $CDCl_3$, Fig VI-3): δ 6.58 (s, 2 H, $H_{6,7}$), 6.06 (dd, $J_{2[3]-1[4]}$ = 1.9, $J_{2[3]-4[1]}$ = 1.9 Hz, 2 H, $H_{2,3}$), 3.54 (m, $J_{1[4]-8a[4a]}$ = 4.0, $J_{1[4]-2[3]}$ = 1.9, $J_{1[4]-3[2]}$ = 1.9, $J_{1[4]-9a}$ = 1.9, $J_{1[4]-9s}$ = 1.8 Hz, 2 H, $H_{1,4}$), 3.24 (d, $J_{4a[8a]-4[1]}$ = 4.0 Hz, 2 H, $H_{4a,8a}$), 1.55 (ddd, J_{9a-9s} = 8.7, J_{9a-1} = 1.9, J_{9a-4} = 1.9 Hz, 1 H, H_{9a}), 1.45 (ddd, J_{9s-9a} = 8.7, J_{9s-1} = 1.8, J_{9s-4} = 1.8 Hz, 1 H, H_{9s});

IR spectrum (KBr, Fig VI-4): 3325 (w), 3070 (m), 3040 (m), 2992 (s), 2960 (m), 2938 (m), 2882 (w), 1667 (vs), 1607 (s), 1390 (m), 1338 (m), 1300 (s), 1282 (s), 1235 (s), 1142 (m), 1067 (m), 1000 (w), 970 (m), 917 (m), 872 (m), 853 (m), 728 (m), 710 (w), 698 (w) cm^{-1};

Mass spectrum (70 eV, Fig VI-5): m/e (relative intensity) 175 (M + 1, 5.3), 174 (M^+, 43.9), 91 (17.7), 66 (100.0), 39 (10.7);

^{13}C and Spin Echo spectra (20 MHz, $CDCl_3$, Fig VI-62: δ 198.70 ($C_{5,8}$), 141.35 ($C_{6,7}$), 136.64 ($C_{2,3}$), 47.91 ($C_{1,4}$), 47.83 (C_9), 47.53 ($C_{4a,8a}$);

HOMCOR NMR spectrum (300 MHz, $CDCl_3$, Fig VI-7);

HETCOR NMR spectrum (300 and 75 MHz, $CDCl_3$, Fig VI-8).

Pentacyclo[5.4.0.0^{2,6}.0^{3,10}.0^{5,9}]undecane-8,11-dione (IVa). Synthesis of IVa was performed by using the method previously reported in the literature.[9]

^{1}H NMR spectrum (300 MHz, $CDCl_3$, Fig VI-9): δ 3.19 (dddd, $J_{2[6]-1[7]}$ = 7.0, $J_{2[6]-3[5]}$ = 5.9, $J_{2[6]-7[1]}$ = 1.6, $J_{2[6]-10[9]}$ = 1.5 Hz, 2 H, $H_{2,6}$), 2.95 (dddd, $J_{3[5]-2[6]}$ = 5.9, $J_{3[5]-10[9]}$ = 4.1, $J_{3[5]-4s}$ = 1.7, $J_{3[5]-4a}$ = 1.6 Hz, 2 H, $H_{3,5}$), 2.80 (ddd, $J_{1[7]-2[6]}$ = 7.0, $J_{1[7]-10[9]}$ = 2.7, $J_{1[7]-6[2]}$ = 1.6 Hz, 2 H, $H_{1,7}$), 2.70 (ddd, $J_{9[10]-5[3]}$ = 4.1, $J_{9[10]-7[1]}$ = 2.7, $J_{9[10]-6[2]}$ = 1.5 Hz, 2 H, $H_{9,10}$), 2.06 (dt, J_{4s-4a} = 11.3, $J_{4s-3,5}$ = 1.7 Hz, 1 H, H_{4s}), 1.90 (dt, J_{4a-4s}

FIGURE VI-3

300 MHz ^{1}H NMR Spectrum of
1,4,4a,8a-Tetrahydro-<u>endo</u>-1,4-methanonaphthalene-5,8-dione
IIIa ($CDCl_3$/TMS).

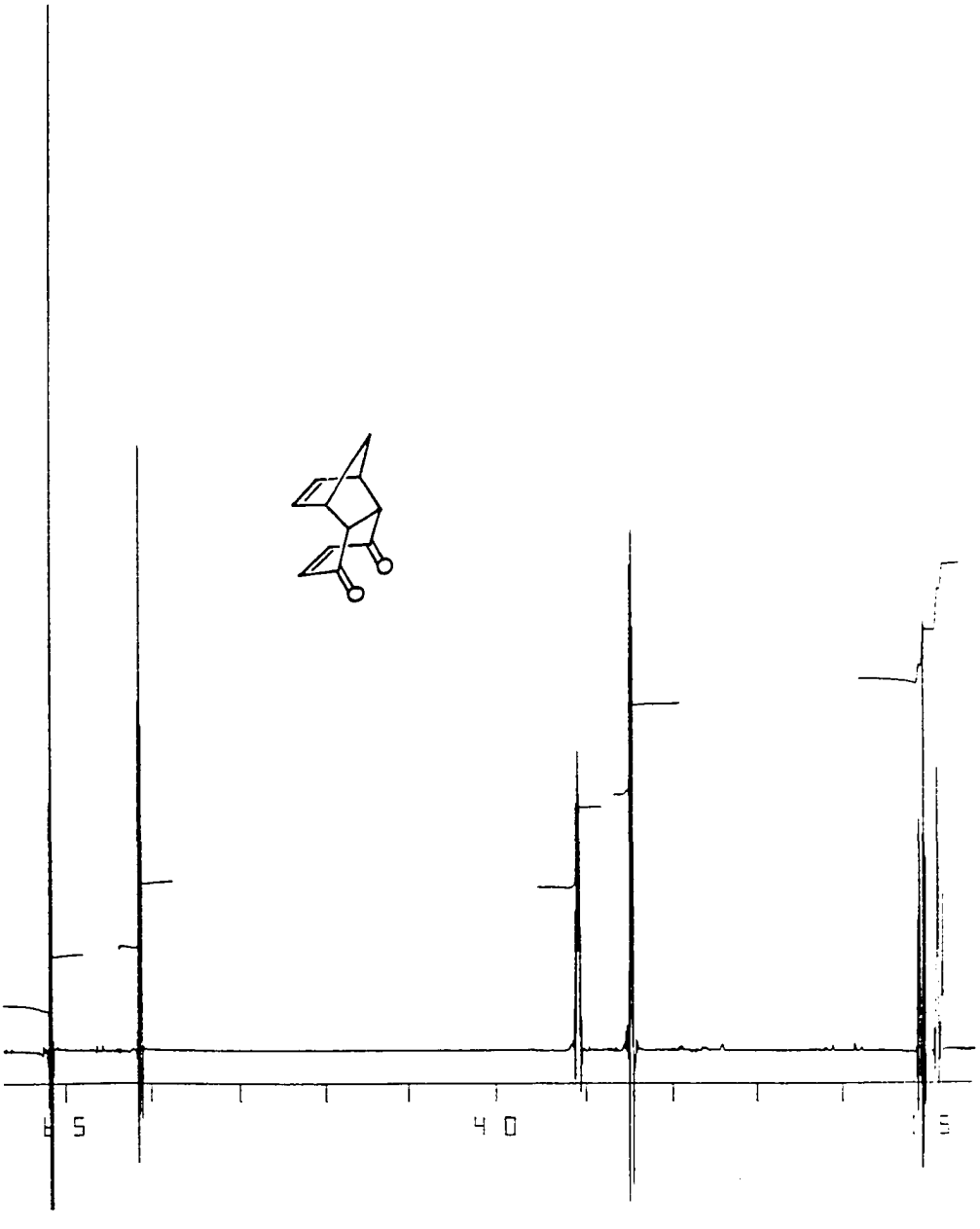

Figure VI-4. IR Spectrum of 1,4,4a,8a-Tetrahydro-<u>endo</u>-1,4-methanonaphthalene-5,8-dione IIIa (KBr).

FIGURE VI-5

Mass Spectrum of

1,4,4a,8a-Tetrahydro-<u>endo</u>-1,4-methanonaphthalene-5,8-dione IIIa.

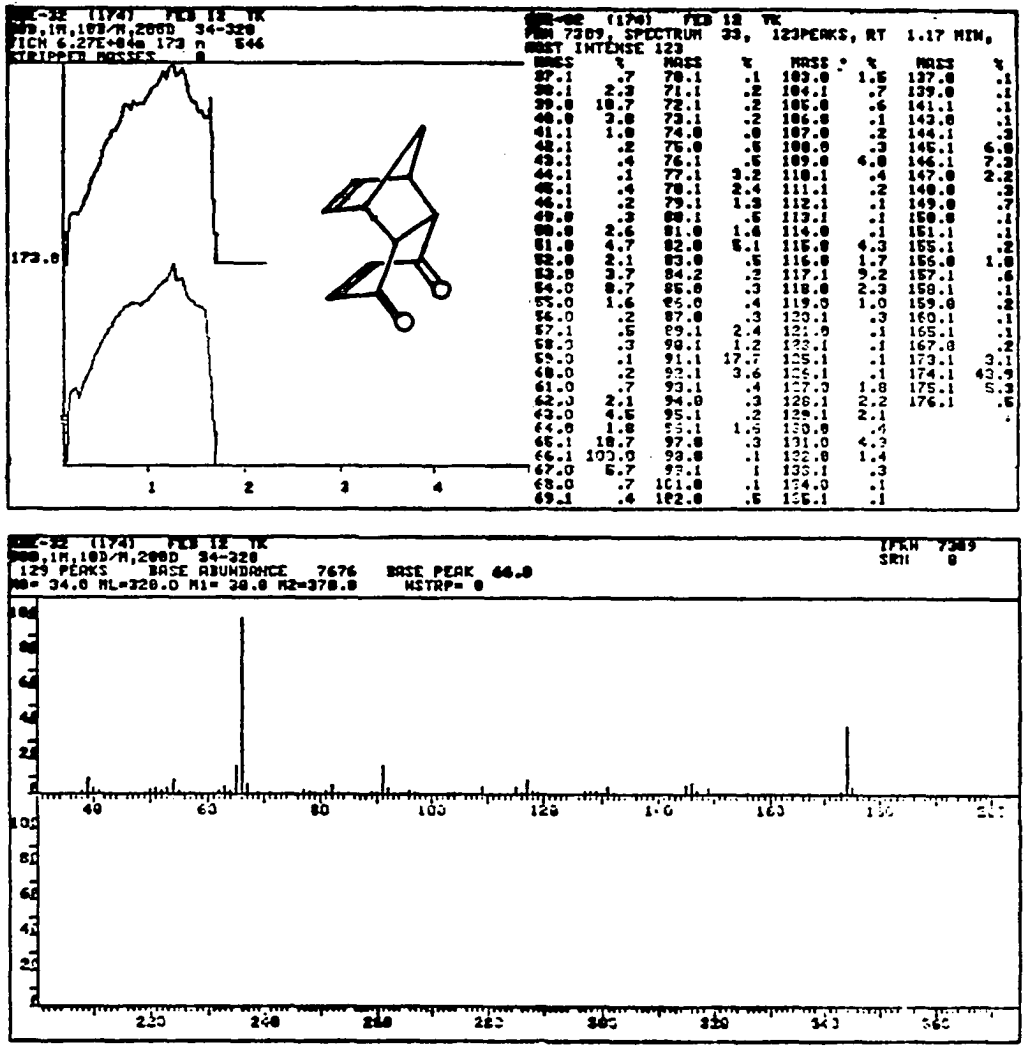

FIGURE VI-6

20 MHz ^{13}C and Spin Echo NMR Spectra of

1,4,4a,8a-Tetrahydro-<u>endo</u>-1,4-methanonaphthalene-5,8-dione IIIa

($CDCl_3$).

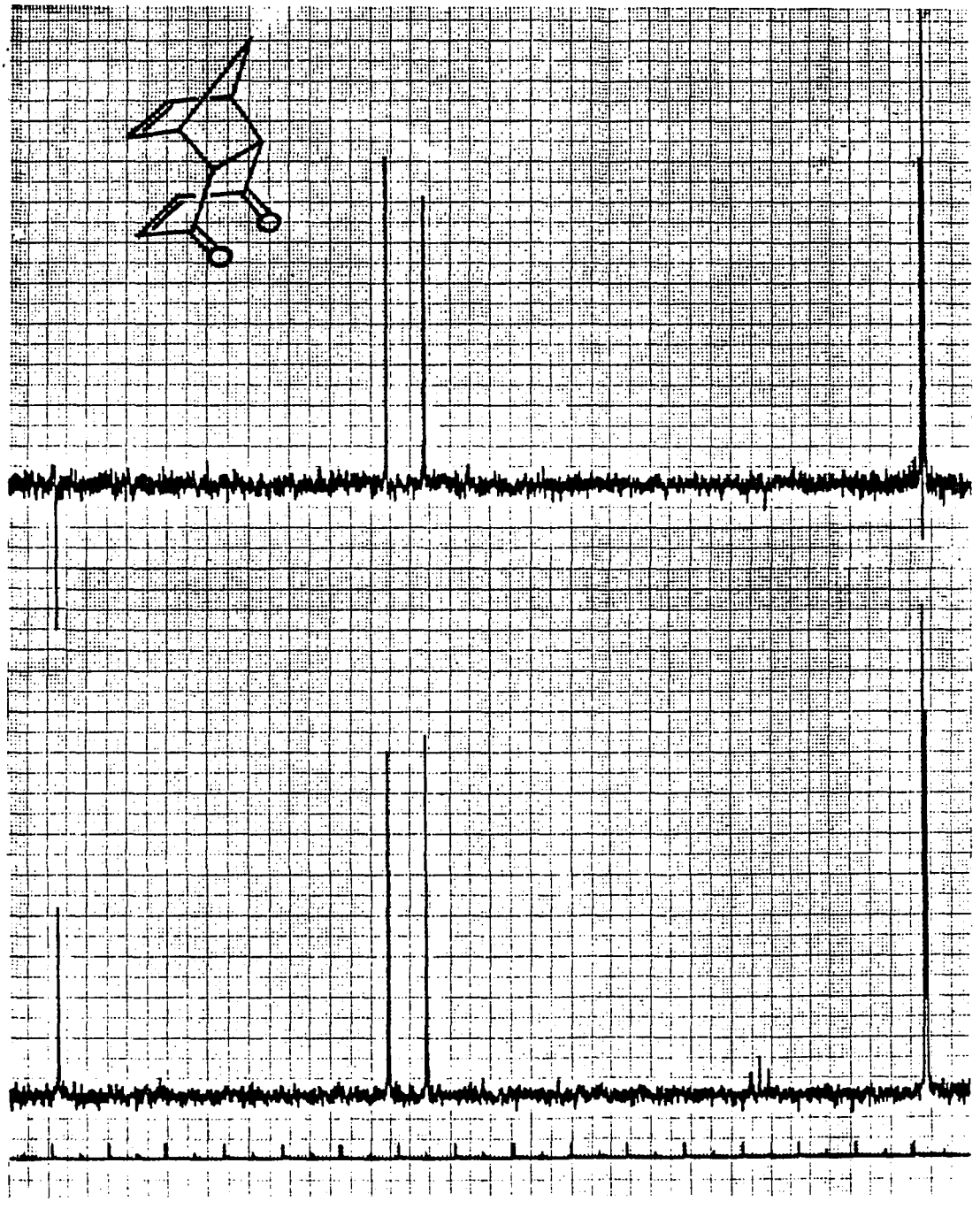

FIGURE VI-7

300 MHz ^{1}H HOMCOR NMR Spectrum of
1,4,4a,8a-Tetrahydro-endo-1,4-methanonaphthalene-5,8-dione IIIa
($CDCl_3$).

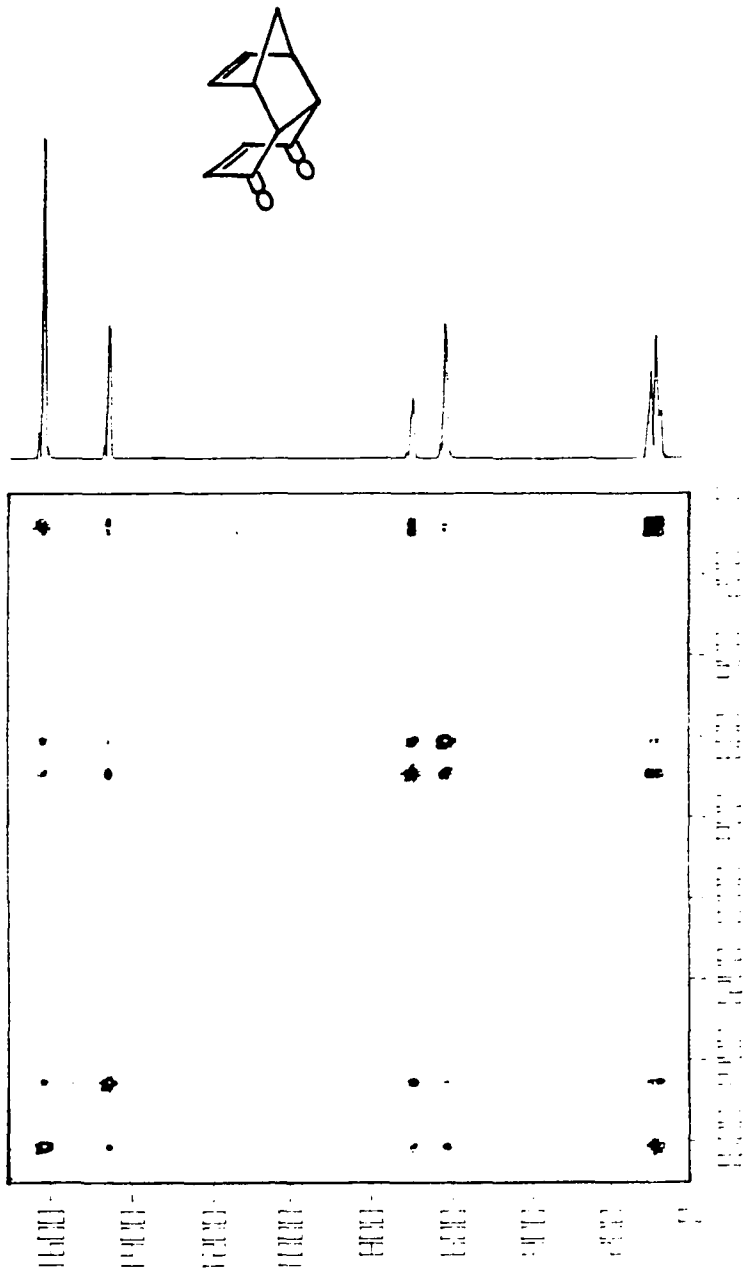

FIGURE VI-8

300 MHz ^{1}H and 75 MHz ^{13}C HETCOR NMR Spectrum of 1,4,4a,8a-Tetrahydro-<u>endo</u>-1,4-methanonaphthalene-5,8-dione IIIa ($CDCl_3$).

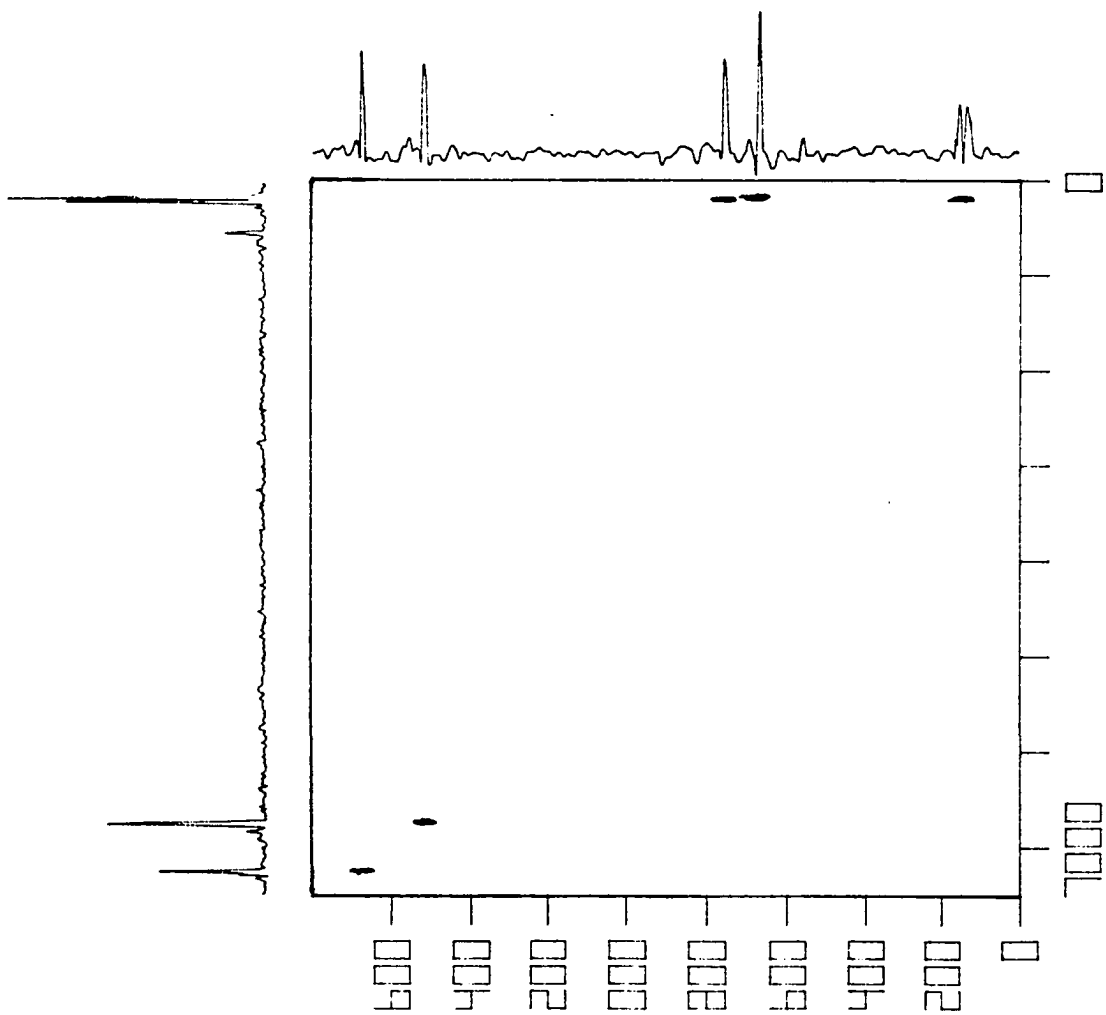

FIGURE VI-9

300 MHz ^{1}H NMR Spectrum of
Pentacyclo[5.4.0.0^{2,6}.0^{3,10}.0^{5,9}]undecane-8,11-dione IVa
($CDCl_3$/TMS).

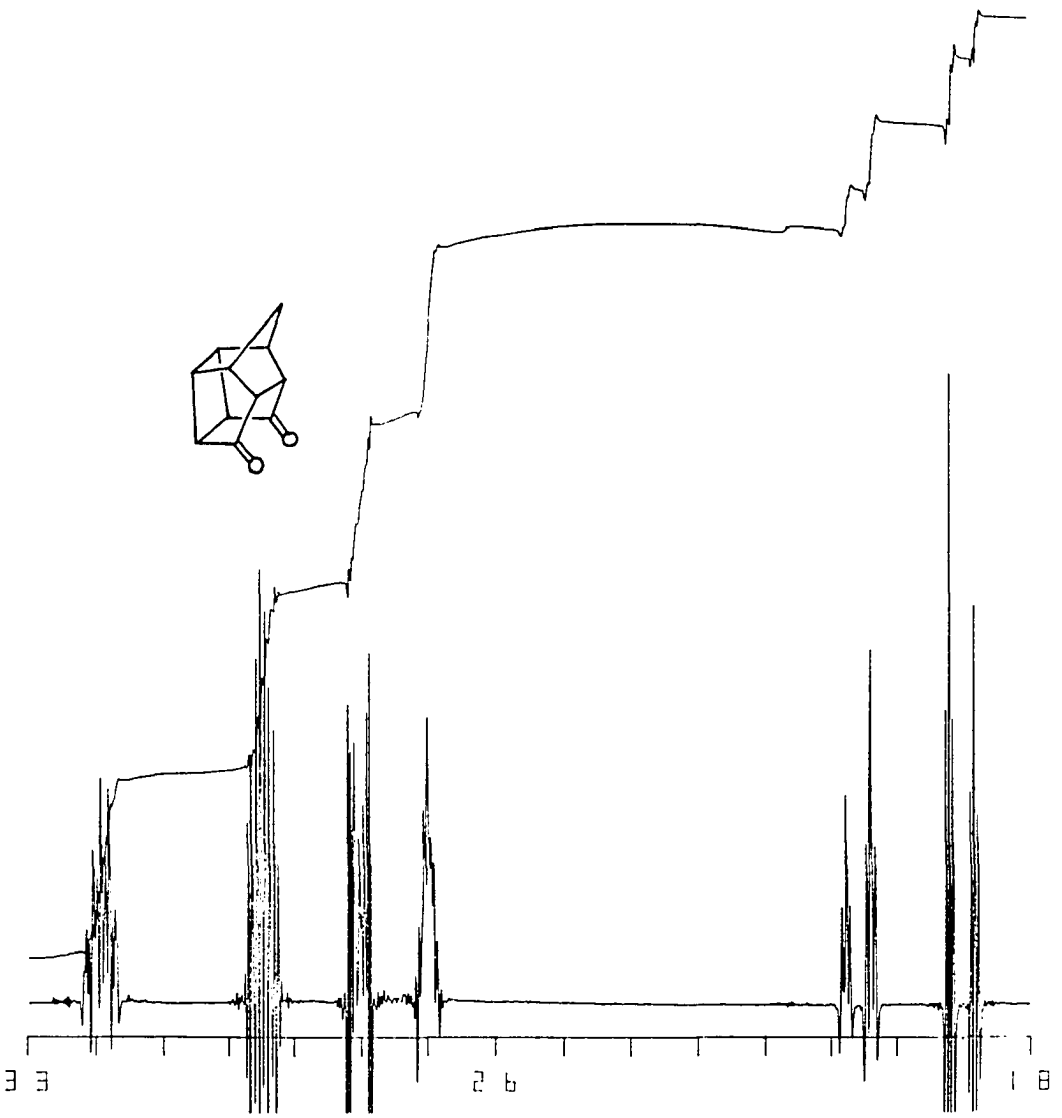

= 11.3, $J_{4a-3,5}$ = 1.6 Hz, 1 H, H_{4a});

IR spectrum (KBr, Fig VI-10): 3455 (w), 2995 (s), 2930 (m), 2870 (m), 1755 (vs), 1724 (vs), 1455 (w), 1300 (w), 1280 (m), 1265 (m), 1220 (m), 1190 (m), 1125 (m), 1070 (m), 1057 (s), 1040 (s), 963 (m), 947 (m), 913 (m), 860 (m), 822 (w), 780 (w), 753 (m) cm^{-1};

Mass spectrum (70 eV, Fig VI-11): m/e (relative intensity) 175 (M + 1, 7.6), (M^+, 64.1), 146 (18.5), 145 (24.5), 131 (17.9), 118 (30.4), 117 (100.0), 116 (11.3), 115 (22.9), 91 (36.9), 77 (10.1), 66 (35.0), 65 (16.4), 51 (11.8), 39 (16.4);

^{13}C and Spin Echo spectra (20 MHz, $CDCl_3$, Fig VI-12): δ 212.03 ($C_{8,11}$), 54.38 ($C_{9,10}$), 44.25 $C_{3,5}$), 43.42 ($C_{1,7}$), 40.04 (C_4), 38.32 ($C_{2,6}$);

HOMCOR NMR spectrum (300 MHz, $CDCl_3$, Fig VI-13);

HOM2DJ NMR spectrum (300 MHz, $CDCl_3$, Fig VI-14 and VI-15);

HETCOR NMR spectrum (300 and 75 MHz, $CDCl_3$, Fig VI-16).

6-Methyl-1,4,4a,8a-tetrahydro-endo-1,4-methanonaphthalene-5,8-dione (IIIb). Synthesis of IIIb was performed by using the method previously reported in the literature.[10]

^1H NMR spectrum (300 MHz, $CDCl_3$, Fig VI-17): δ 6.5 (q, $J_{7\text{-methyl}}$ = 1.4 Hz, 1 H, H_7), 6.07 (ddd, J_{2-3} = 5.8, J_{2-1} = 2.9, J_{2-4} = 1.1 Hz, 1 H, H_2), 6.03 (ddd, J_{3-2} = 5.8, J_{3-4} = 2.8, J_{3-1} = 1.1 Hz, 1 H, H_3), 3.53 (m, J_{4-4a} = 4.1, J_{4-3} = 2.8, J_{4-9a} = 1.7, J_{4-9s} = 1.5, J_{4-2} = 1.1 Hz, 1 H, H_4), 3.53 (m, J_{1-8a} = 4.1, J_{1-2} = 2.9, J_{1-9a} = 1.7, J_{1-9s} = 1.5, J_{1-3} = 1.1 Hz, 1 H, H_1), 3.24 (m, J_{8a-4a} = 8.0, J_{8a-1} = 4.1 Hz, 1 H, H_{8a}), 3.24 (m, J_{4a-8a} = 8.0, J_{4a-4} = 4.1 Hz, 1 H, H_{4a}), 1.94 (d, $J_{\text{methyl-7}}$ = 1.4 Hz, 3 H, CH_3), 1.54 (ddd, J_{9a-9s} = 8.7, J_{9a-1} = 1.7, J_{9a-4} = 1.7 Hz, 1 H, H_{9a}), 1.46 (ddd, J_{9s-9a} = 8.7, J_{9s-1} = 1.5, J_{9s-4} = 1.5 Hz, 1 H, H_{9s});

IR spectrum (CCl_4, Fig VI-18): 3000 (m), 2980 (m), 2940 (m), 2912 (w), 2870 (w), 1713 (vs), 1625 (m), 1440 (w), 1380 (m), 1350 (w), 1332 (m), 1320 (m), 1292 (w), 1260 (s), 1210 (m), 1128 (m), 1058 (m),

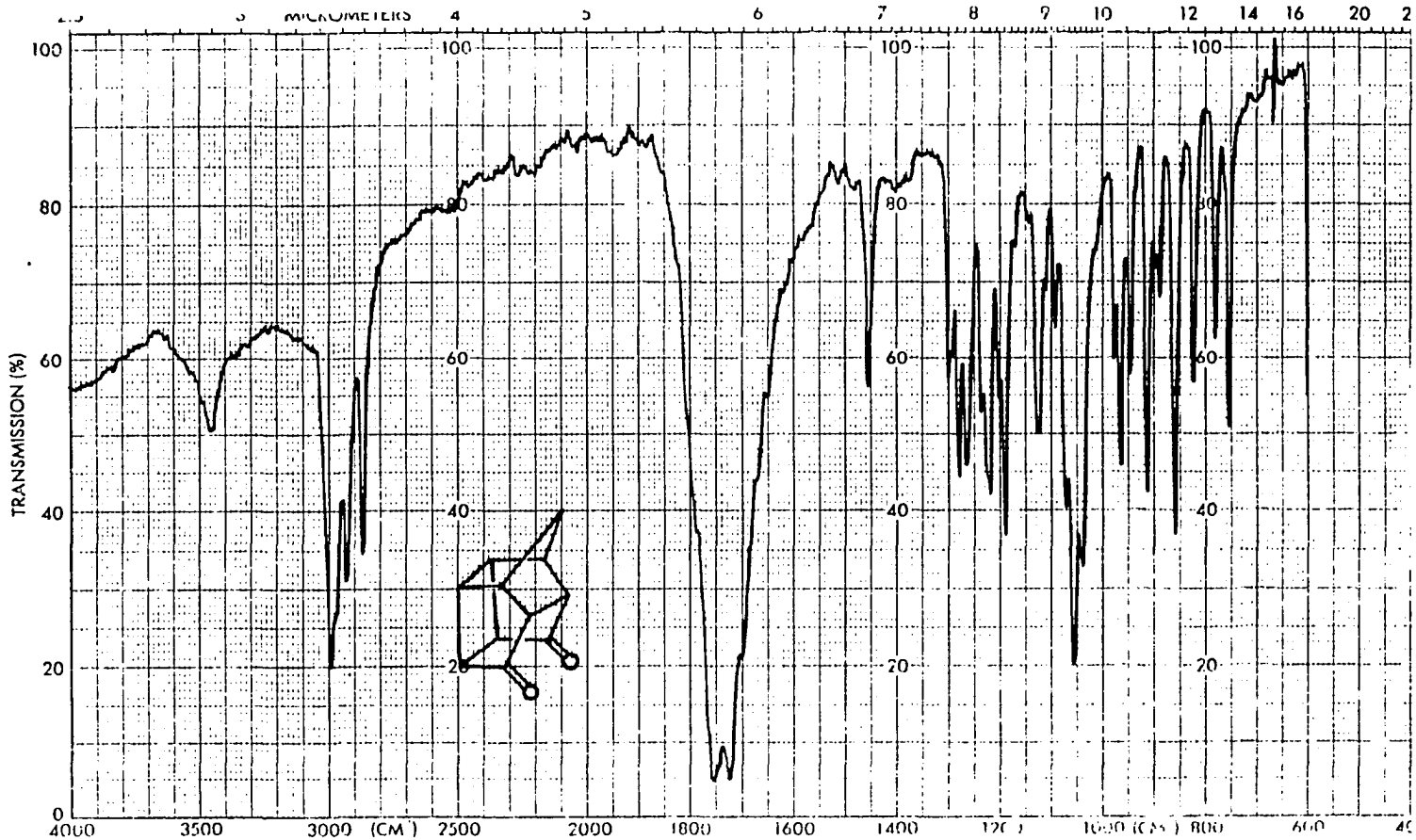

Figure VI-10. IR Spectrum of Pentacyclo[5.4.0.0^{2,6}.0^{3,10}.0^{5,9}]undecane-8,11-dione IVa (KBr).

FIGURE VI-11

Mass Spectrum of

Pentacyclo[5.4.0.0^{2,6}.0^{3,10}.0^{5,9}]undecane-8,11-dione IVa.

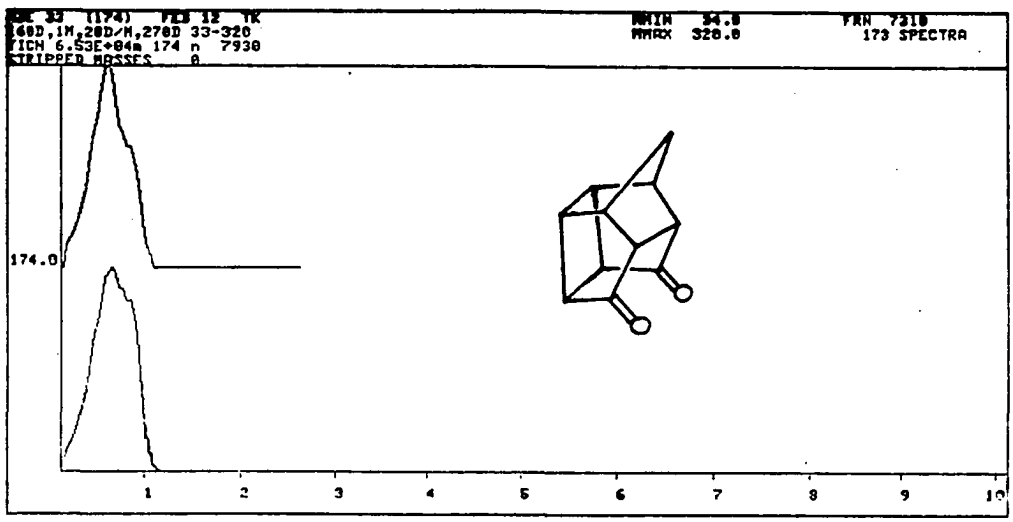

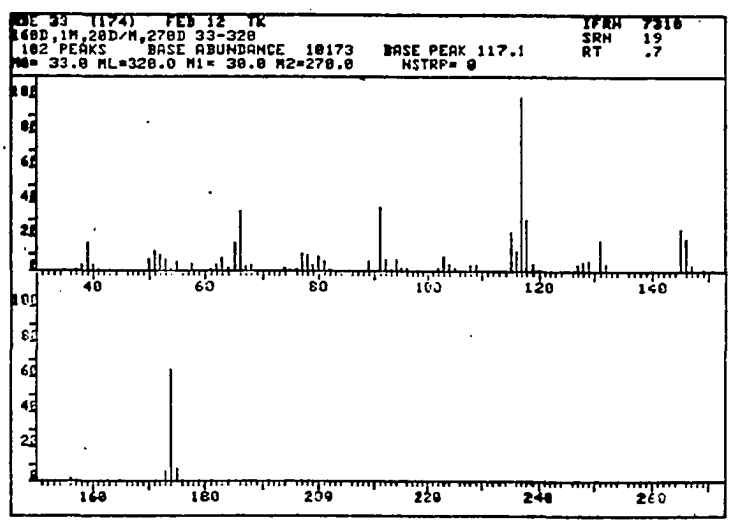

MASS	%	MASS	%
BIG 60		95.1	2.0
38.1	3.6	96.0	2.1
39.0	16.4	102.1	2.1
40.0	3.3	103.0	8.6
41.1	1.6	104.1	4.6
50.0	6.6	105.1	2.3
51.0	11.8	108.0	3.7
52.0	9.2	109.0	3.2
53.0	6.5	115.0	22.9
54.0	2.3	116.1	11.3
55.0	5.2	117.1	100.0
57.9	4.5	118.0	30.4
61.0	1.2	119.0	4.1
62.0	3.3	120.1	1.2
63.0	7.6	127.0	3.5
64.0	2.3	128.1	5.2
65.1	16.4	129.1	5.7
66.0	35.0	131.0	17.9
67.0	2.5	132.0	4.3
68.0	3.7	145.1	24.5
74.1	1.7	146.1	13.5
75.0	1.3	147.0	3.3
76.1	1.6	156.1	1.5
77.1	10.1	157.1	1.3
78.1	8.0	173.1	5.9
79.1	3.3	174.1	64.1
80.0	8.6	175.1	7.6
81.0	6.2		
82.0	1.6		
89.1	5.7		
91.1	36.9		
92.1	7.0		
93.1	1.5		
94.1	7.0		

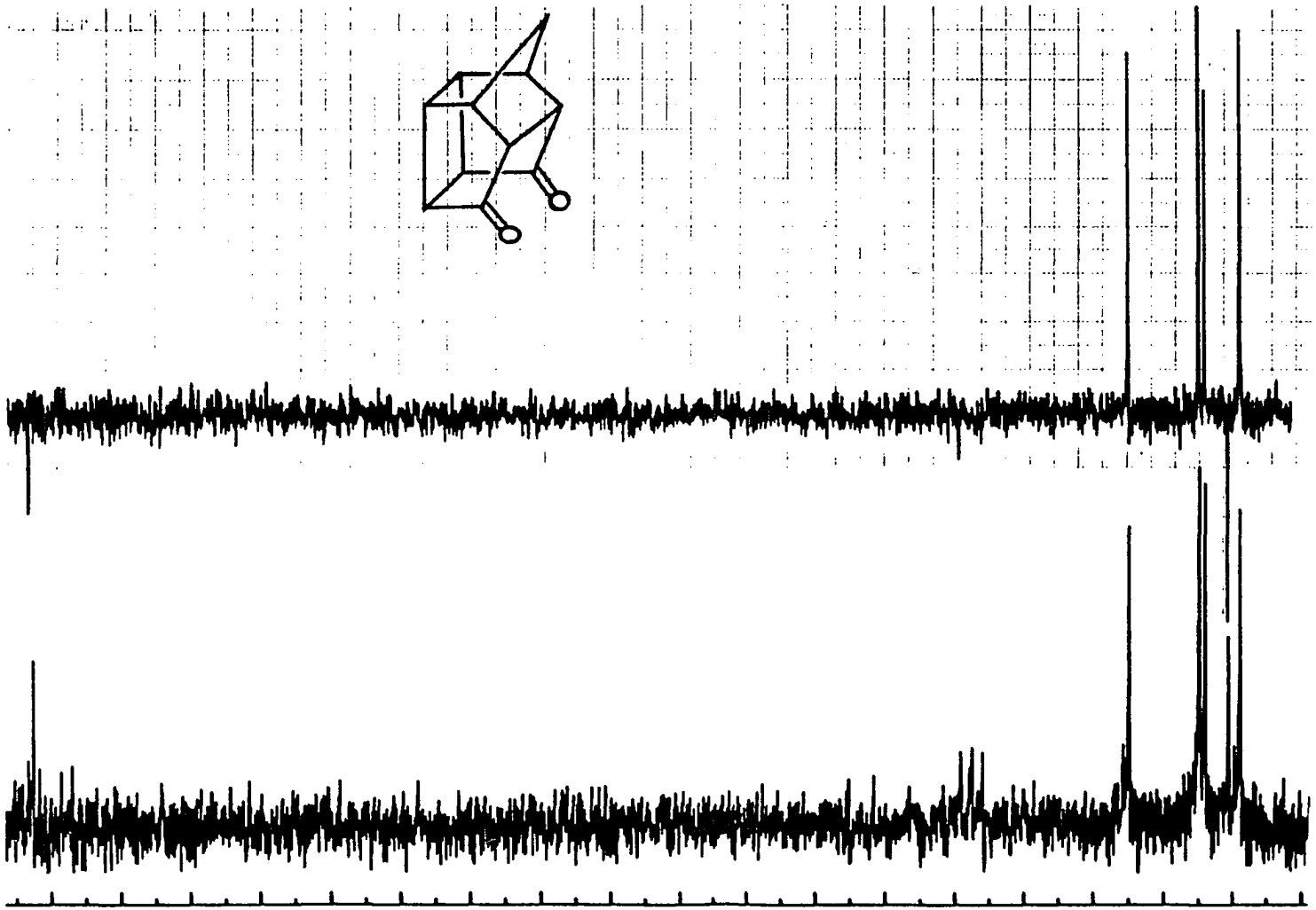

Figure VI-12. 20 MHz ^{13}C and Spin Echo NMR Spectra of Pentacyclo[5.4.0.0^{2,6}.0^{3,10}.0^{5,9}]undecane-8,11-dione IVa ($CDCl_3$).

FIGURE VI-13

300 MHz ^{1}H HOMCOR NMR Spectrum of
Pentacyclo[5.4.0.0^{2,6}.0^{3,10}.0^{5,9}]undecane-8,11-dione IVa
($CDCl_3$).

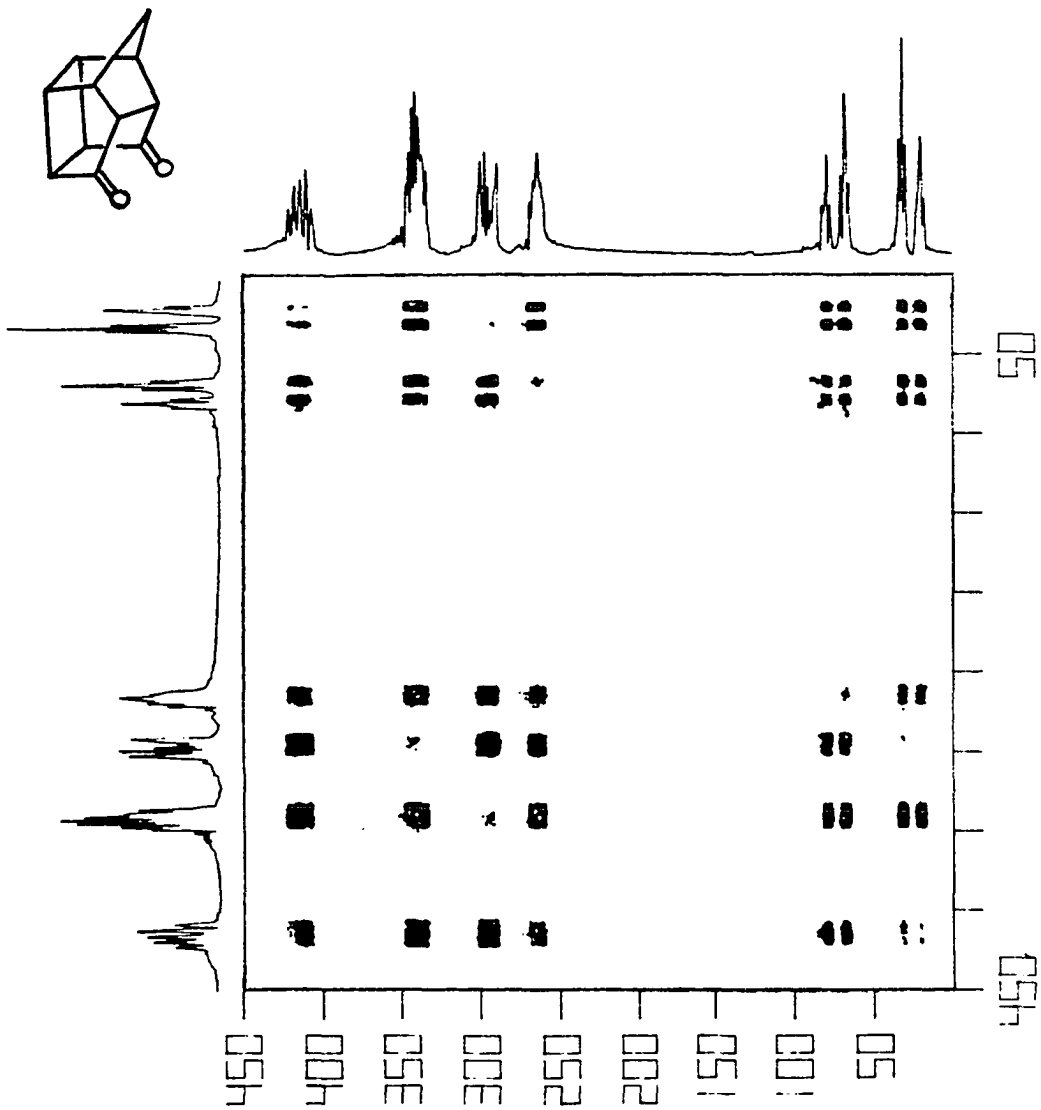

FIGURE VI-14

300 MHz ^{1}H HOM2DJ NMR Spectrum of Pentacyclo[5.4.0.0^{2,6}.0^{3,10}.0^{5,9}]undecane-8,11-dione IVa ($CDCl_3$).

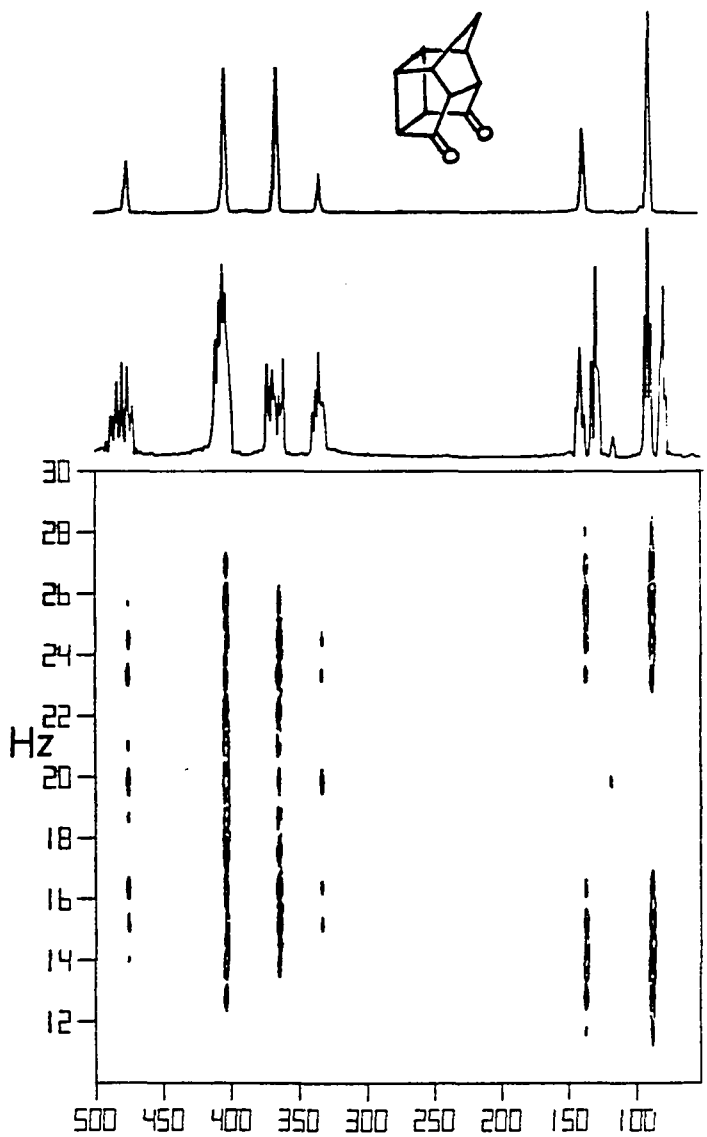

FIGURE VI-15

Stacked Plot of the 300 MHz ^{1}H HOM2DJ NMR Spectrum of Pentacyclo[5.4.0.0^{2,6}.0^{3,10}.0^{5,9}]undecane-8,11-dione IVa ($CDCl_3$).

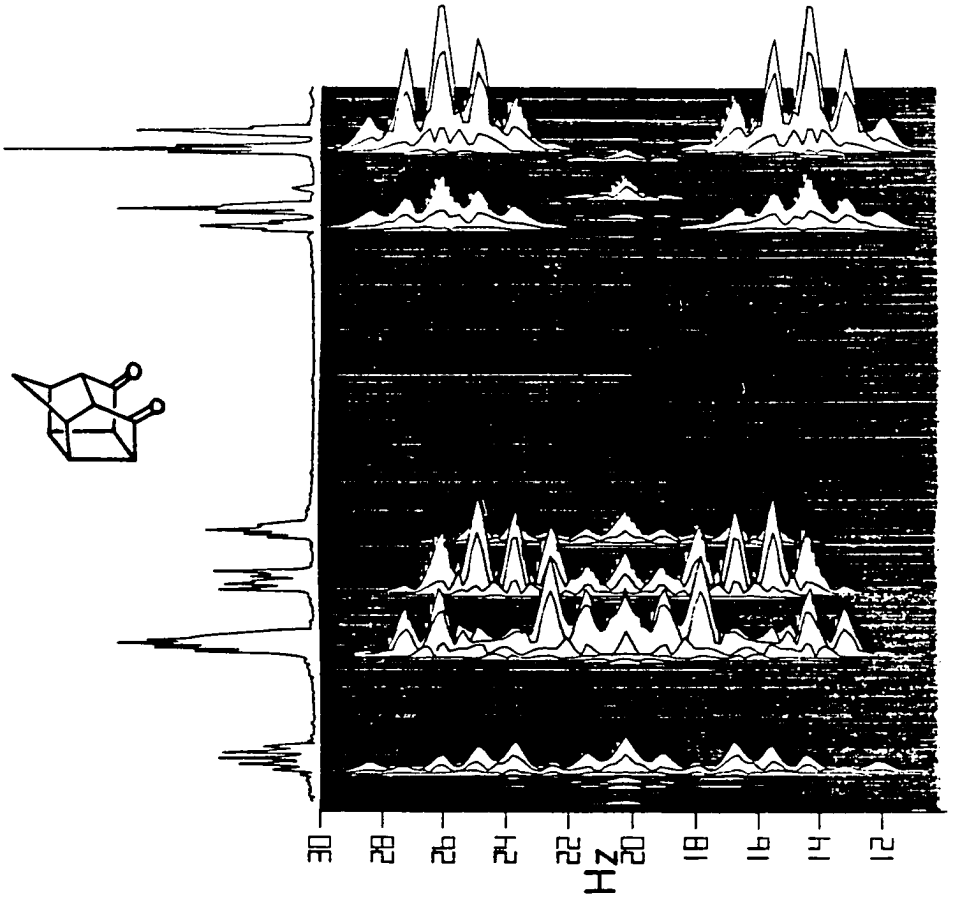

FIGURE VI-16

300 MHz ^{1}H and 75 MHz ^{13}C HETCOR NMR Spectrum of Pentacyclo[5.4.0.0^{2,6}.0^{3,10}.0^{5,9}]undecane-8,11-dione IV ($CDCl_3$).

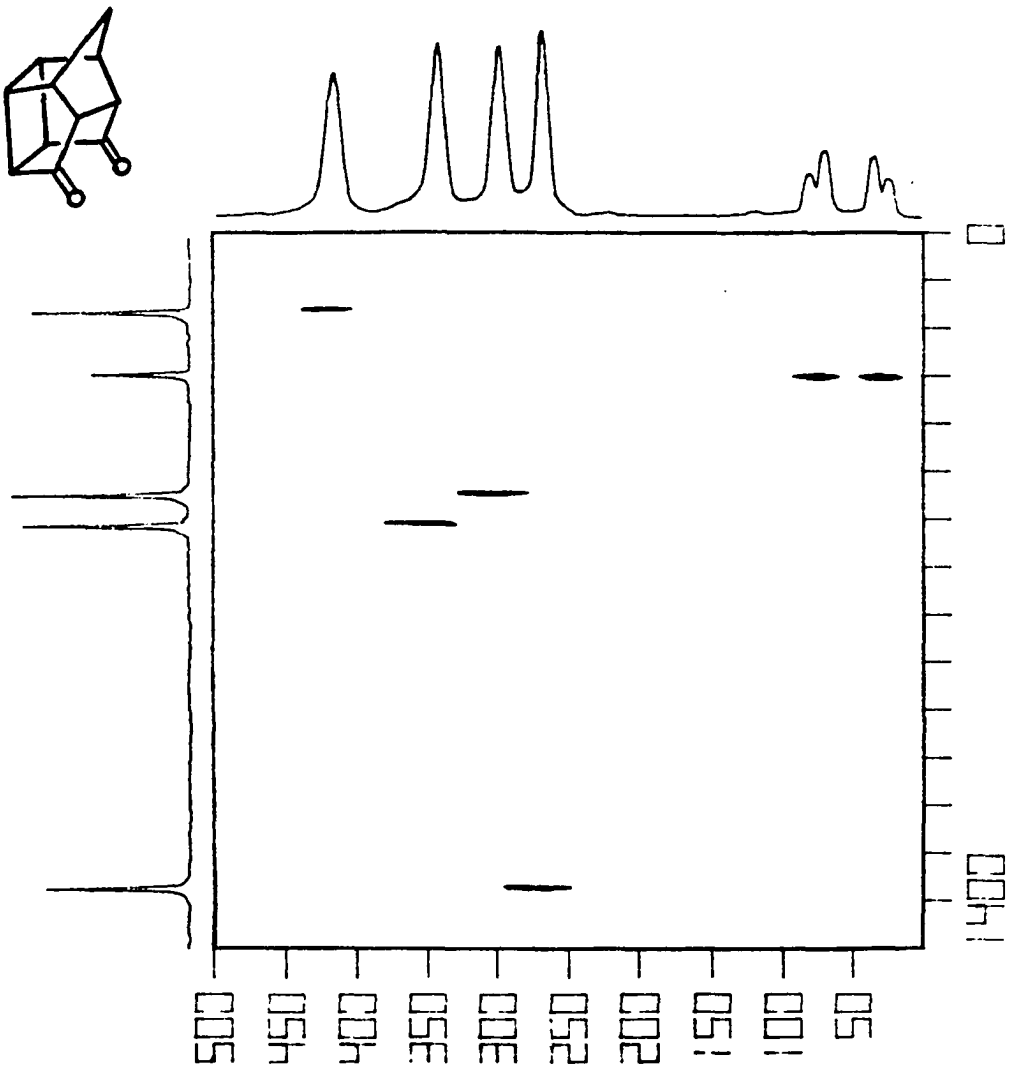

FIGURE VI-17

300 MHz ^{1}H NMR Spectrum of
6-Methyl-1,4,4a,8a-tetrahydro-<u>endo</u>-1,4-methanonaphthalene-5,8-dione
IIIb ($CDCl_3$/TMS).

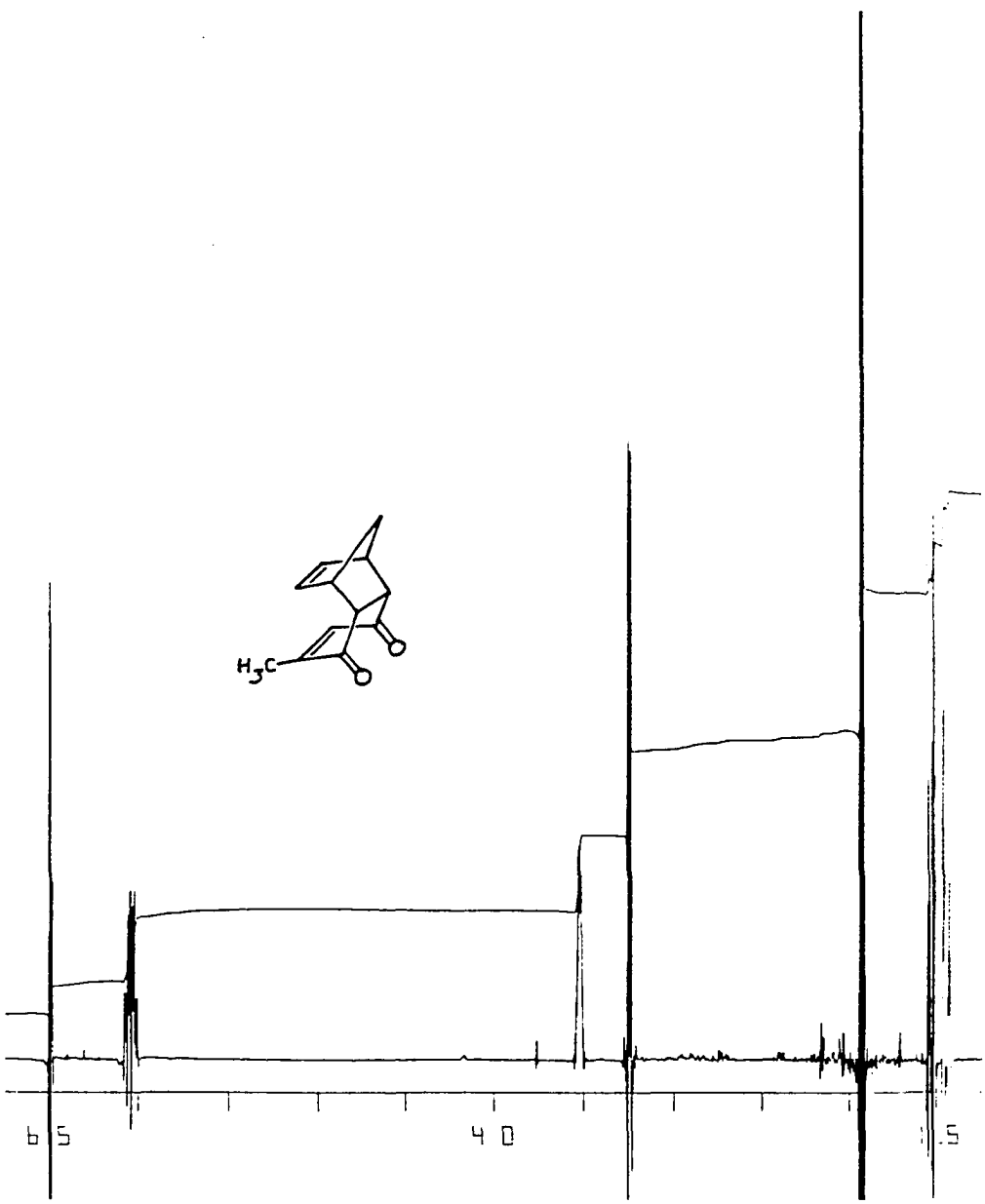

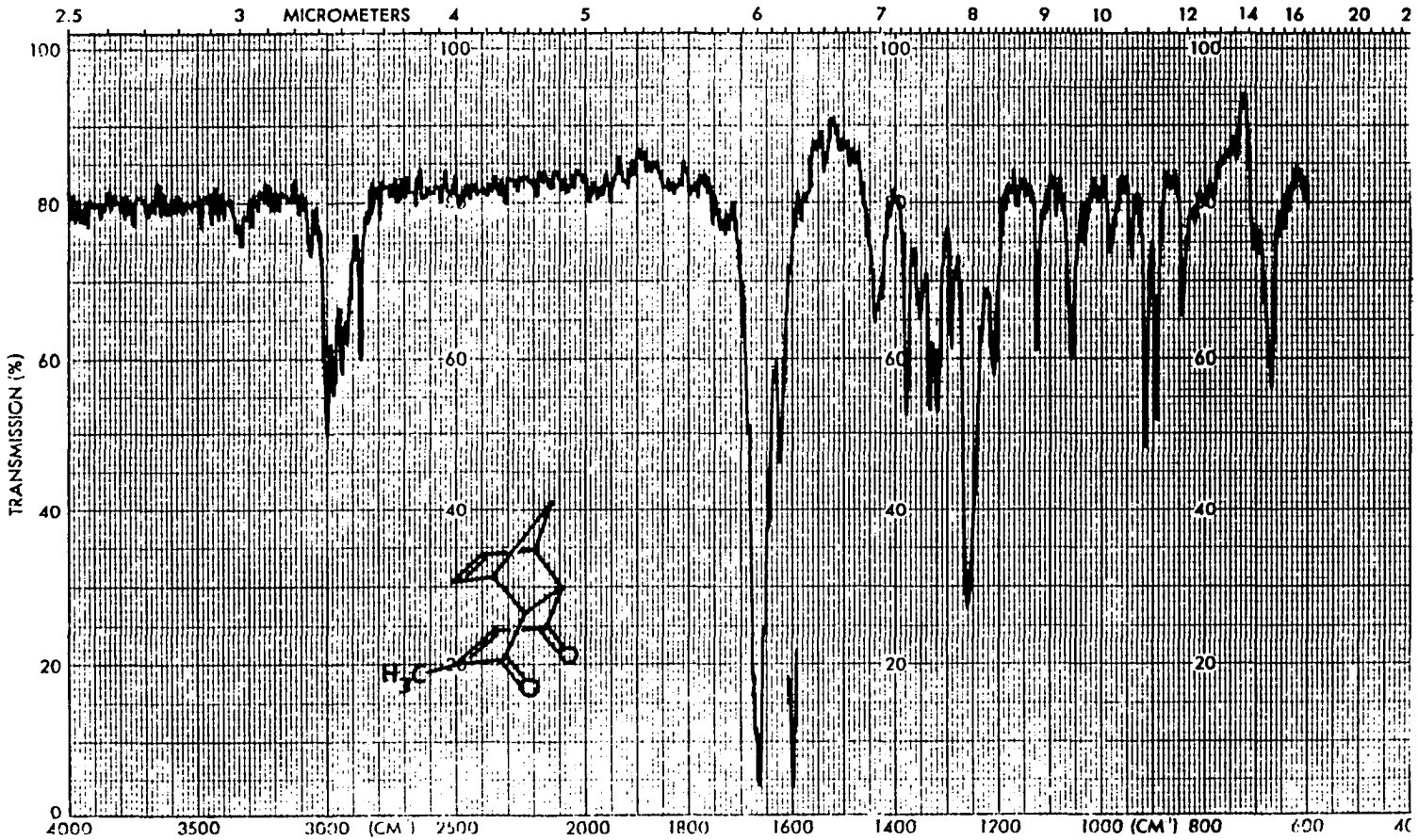

Figure VI-18. IR Spectrum of
6-Methyl-1,4,4a,8a-tetrahydro-<u>endo</u>-1,4-methanonaphthalene-5,8-dione IIIb (CCl_4).

915 (m), 893 (m), 844 (m), 670 (m) cm^{-1};

Mass spectrum (70 eV, Fig VI-19): m/e (relative intensity) 189 (M + 1, 2.5), 188 (16.0), 91 (13.3), 66 (100.0), 65 (14.4);

^{13}C and Spin Echo spectra (20 MHz, $CDCl_3$, Fig VI-20): δ 198.88 (C_8 or C_5), 198.37 (C_5 or C_8), 150.94 (C_6), 139.02 (C_7), 134.90 (C_2), 134.34 (C_3), 48.35 (C_{4a}), 48.19 (C_4), 48.12 (C_9), 47.89 (C_1), 47.51 (C_{8a}), 15.63 (C_{methyl});

HOMCOR NMR spectrum (300 MHz, CDCl3, Fig VI-21);

HETCOR NMR spectrum (300 and 75 MHz, $CDCl_3$, Fig VI-22 through VI-25).

1-Methylpentacyclo[5.4.0.0^{2,6}.0^{3,10}.0^{5,9}]undecane-8,11-dione IVb). A 500 mL ethyl acetate solution containing 7.5 g (40 mmol) of 6-methyl-1,4,4a,8a-tetrahydro-endo-1,4-methanonaphthalene-5,8-dione (IIIb)[18] was irradiated for 16 hours under nitrogen with a Hanovia medium-pressure Hg lamp (Pyrex filter). The solution was concentrated, whereupon IVb crystallized as a colorless, microcrystalline solid: 6.3 g, 84%; mp 64-64°C;

^1H NMR spectrum (300 MHz, $CDCl_3$, Fig VI-26): δ 3.17 (dddd, J_{6-2} = 8.4, J_{6-7} = 6.0, J_{6-5} = 5.8, J_{6-9} = 1.8 Hz, 1 H, H_6), 2.94 (dddd, J_{5-6} = 5.8, J_{5-9} = 4.8, J_{5-4s} = 1.6, J5-4a = 1.5 Hz, 1 H, H_5), 2.88 (dddd, J_{3-2} = 5.4, J_{3-10} = 4.6, J_{3-4s} = 1.6, J_{3-4a} = 1.5 Hz, 1 H, H_3), 2.83 (dddd, J_{2-6} = 8.4, J_{2-3} = 5.4, J_{2-10} = 1.9, J_{2-7} = 1.3 Hz, 1 H, H_2], 2.72 (ddd, J_{10-9} = 11.2, J_{10-3} = 4.6, J_{10-2} = 1.9 Hz, 1 H,, H_{10}), 2.66 (dddd, J_{9-10} = 10.5, J_{9-5} = 4.8, J_{9-7} = 2.8, J_{9-6} = 1.8 Hz, 1 H, H_9), 2.36 (ddd, J_{7-6} = 6.0, J_{7-9} = 2.8, J_{7-2} = 1.3 Hz, 1 H, H_7), 2.05 (dt, J_{4s-4a} = 11.2, $J_{4s-3,5}$ = 1.6 Hz, 1 H, H_{4s}), 1.91 (dt, J_{4a-4s} = 11.2, $J_{4a-3,5}$ = 1.5 Hz, 1 H, H_{4a}), 1.16 (s, 3 H, CH_3);

IR spectrum (KBr, Fig VI-27): 2980 (s), 2970 (s), 2936 (s), 2872 (m), 1746 (vs), 1730 (sh, vs), 1443 (m), 1286 (m), 1227 (m), 1195 (m), 1181 (m), 1111 (m), 1081 (s), 1060 (s), 912 (m), 876 (m) cm^{-1};

FIGURE VI-19

Mass Spectrum of

6-Methyl-1,4,4a,8a-tetrahydro-<u>endo</u>-1,4-methanonaphthalene-5,8-dione

IIIb.

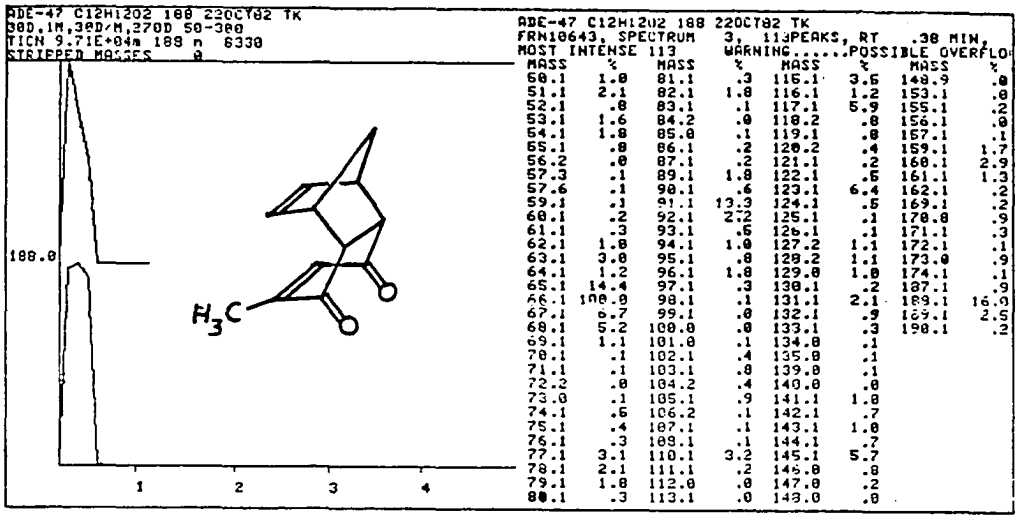

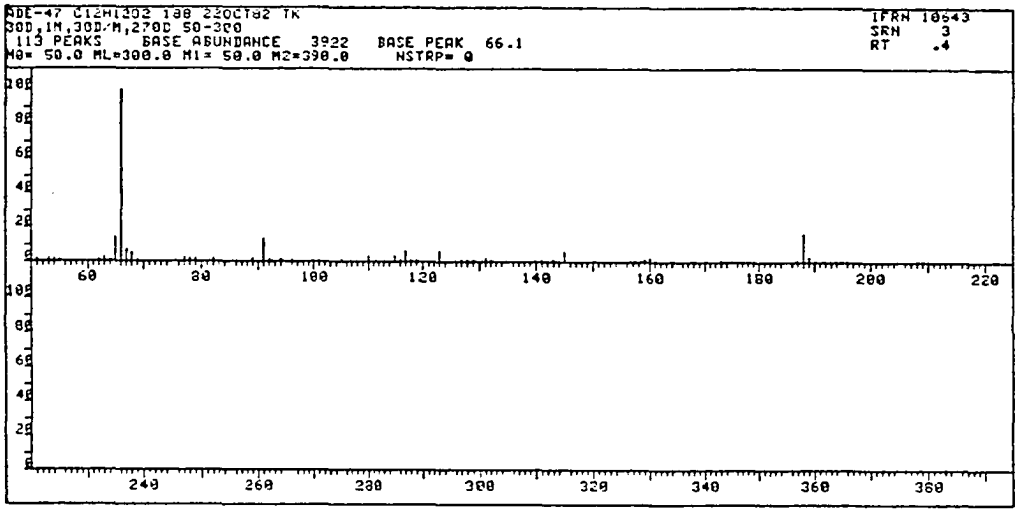

FIGURE VI-20

20 MHz ^{13}C and Spin Echo NMR Spectra of

6-Methyl-1,4,4a,8a-tetrahydro-<u>endo</u>-1,4-methanonaphthalene-5,8-dione

IIIb ($CDCl_3$).

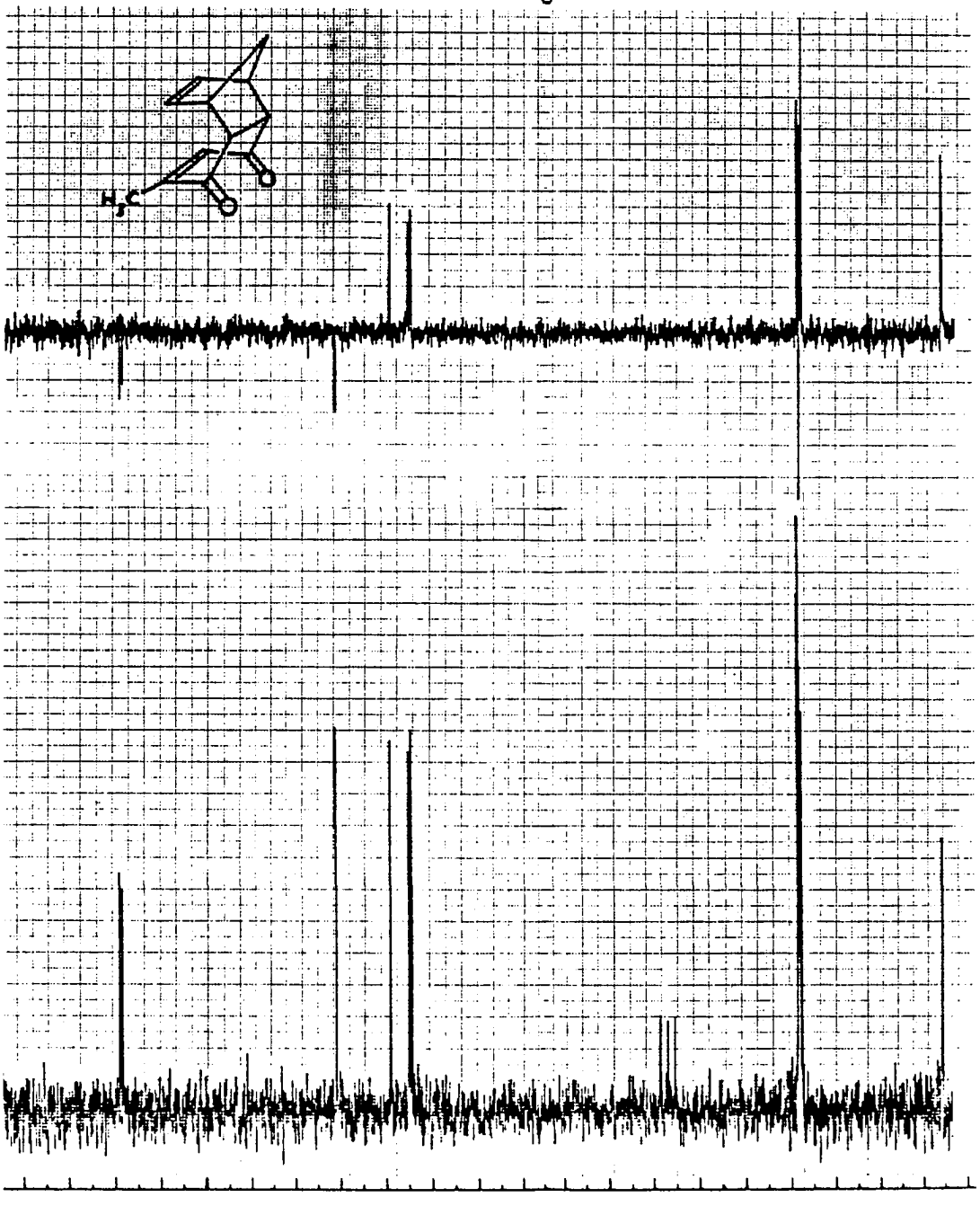

FIGURE VI-21

300 MHz ^{1}H HOMCOR NMR Spectrum of
6-methyl-1,4,4a,8a-tetrahydro-endo-1,4-methanonaphthalene-5,8-dione
IIIb ($CDCl_3$).

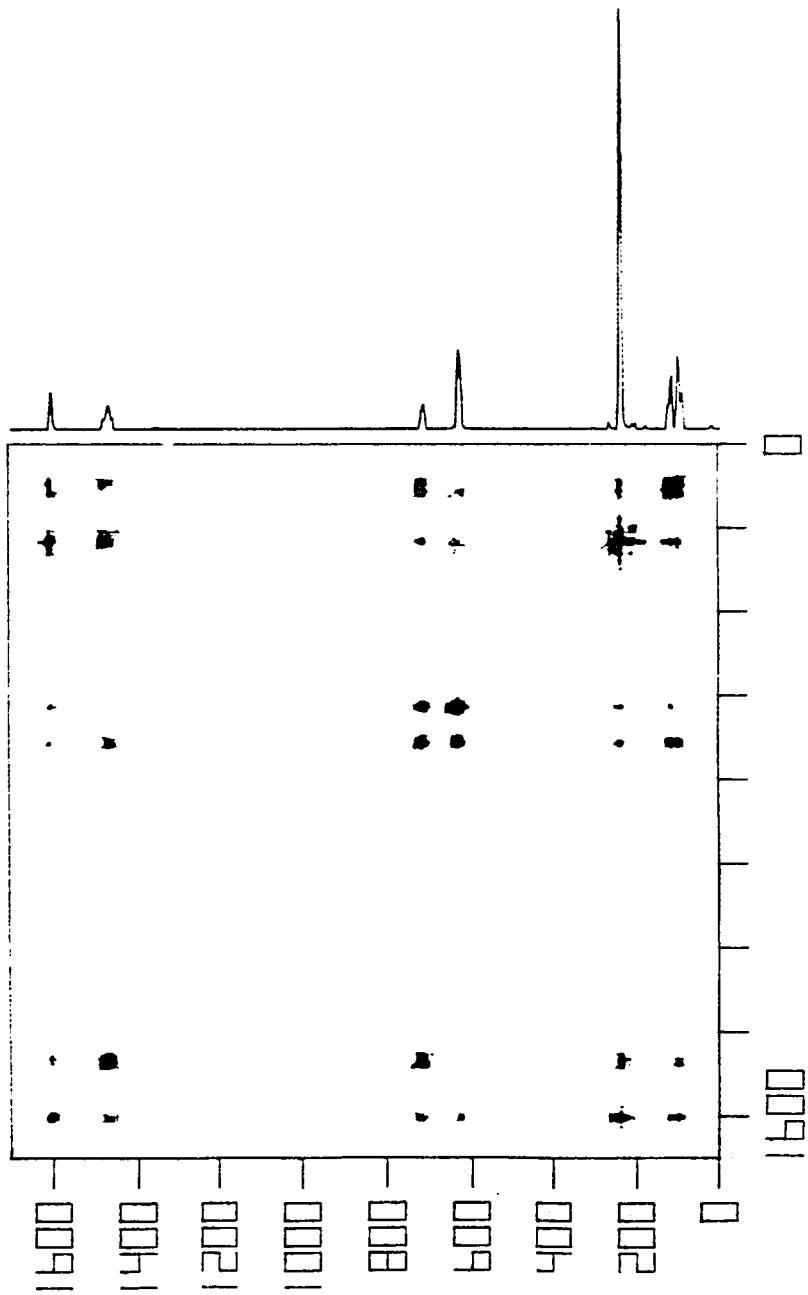

FIGURE VI-22

300 MHz ^{1}H and 75 MHz ^{13}C HETCOR NMR Spectrum of 6-Methyl-1,4,4a,8a-tetrahydro-endo-1,4-methanonaphthalene-5,8-dione IIIb ($CDCl_3$).

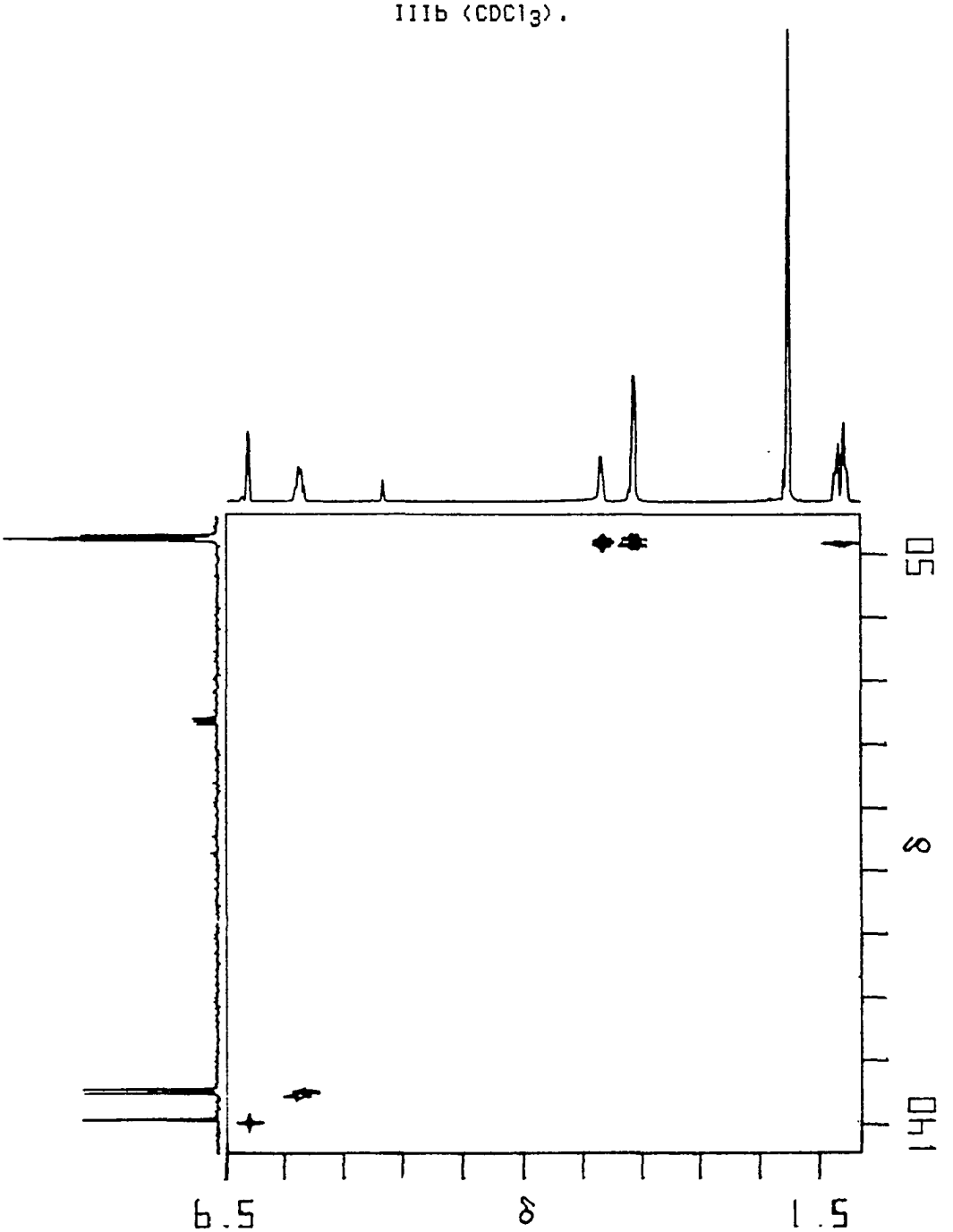

FIGURE VI-23

Expanded Contour Plot of the HETCOR Spectrum of Fig VI-22 which Includes the 1.2-3.6 ppm ^{1}H and 47-50 ppm ^{13}C Spectral Region of 6-Methyl-1,4,4a,8a-tetrahydro-<u>endo</u>-1,4-methanonaphthalene-5,8-dione IIIb ($CDCl_3$).

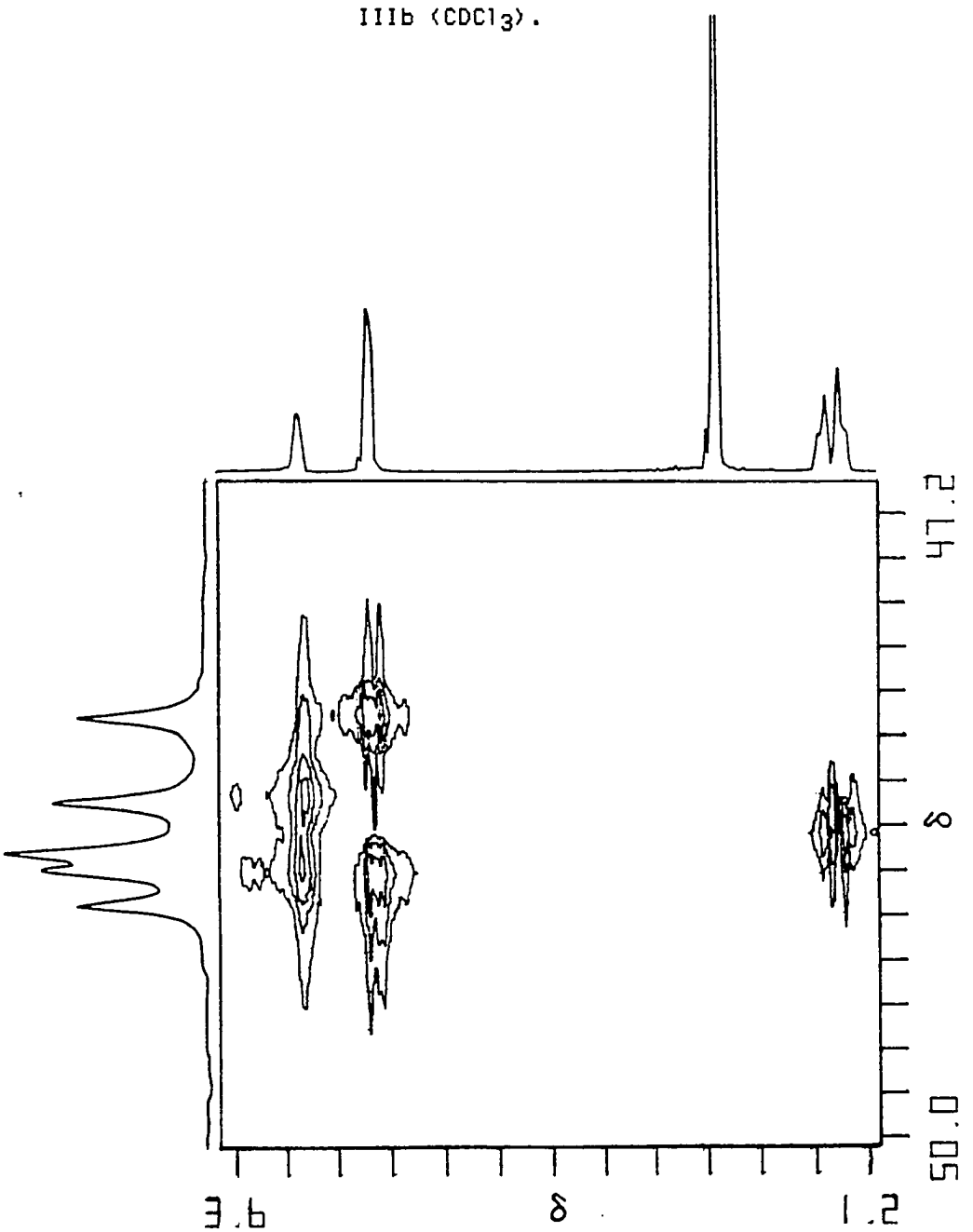

FIGURE VI-24

Expanded Contour Plot of the HETCOR Spectrum of Fig VI-22 which Includes the 5.6-6.5 ^{1}H and 133-141 ppm ^{13}C Spectral Region of 6-Methyl-1,4,4a,8a-tetrahydro-<u>endo</u>-1,4-methanonaphthalene-5,8-dione IIIb ($CDCl_3$).

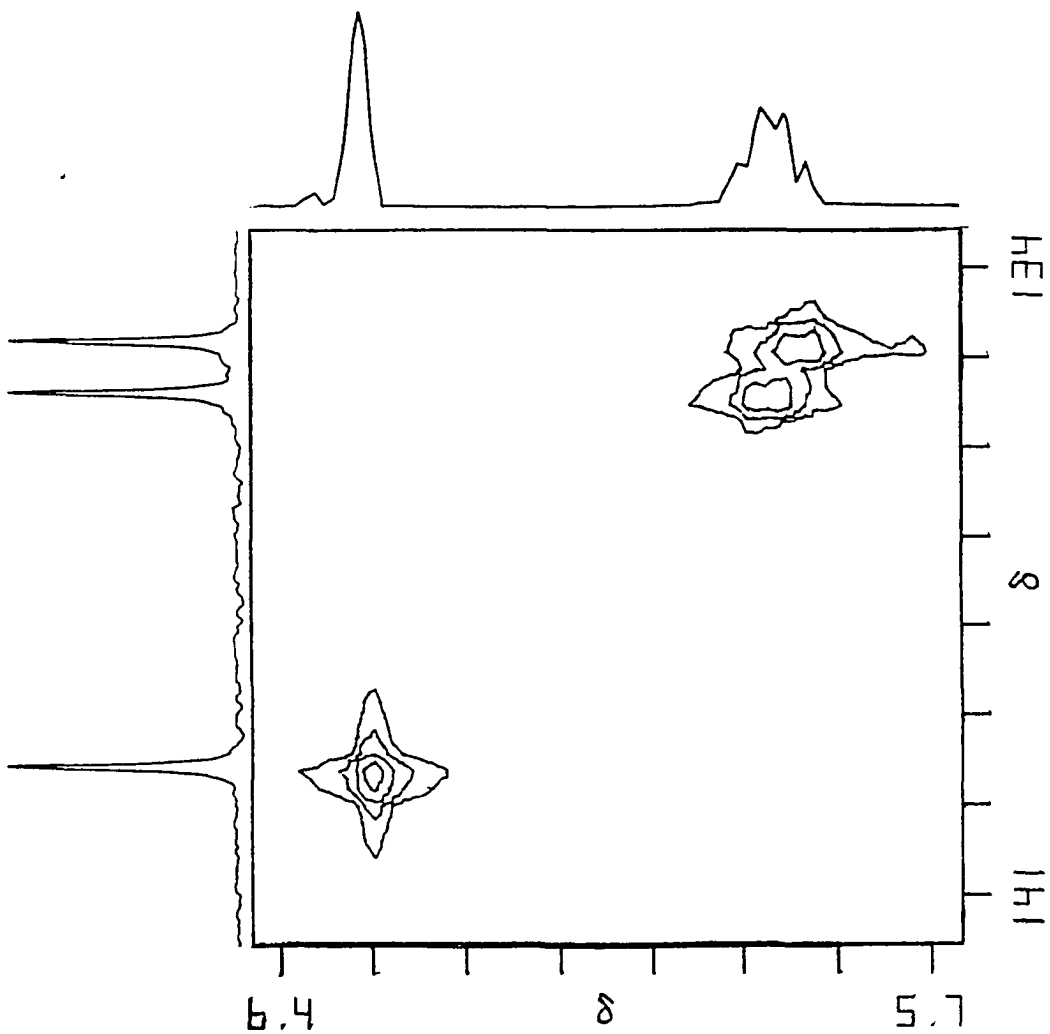

FIGURE VI-25

Stacked Plot of the HETCOR Spectrum of Fig VI-22 of 6-Methyl-1,4,4a,8a-tetrahyd;o-endo-1,4-methanonaphthalene-5,8-dione IIIb ($CDCl_3$).

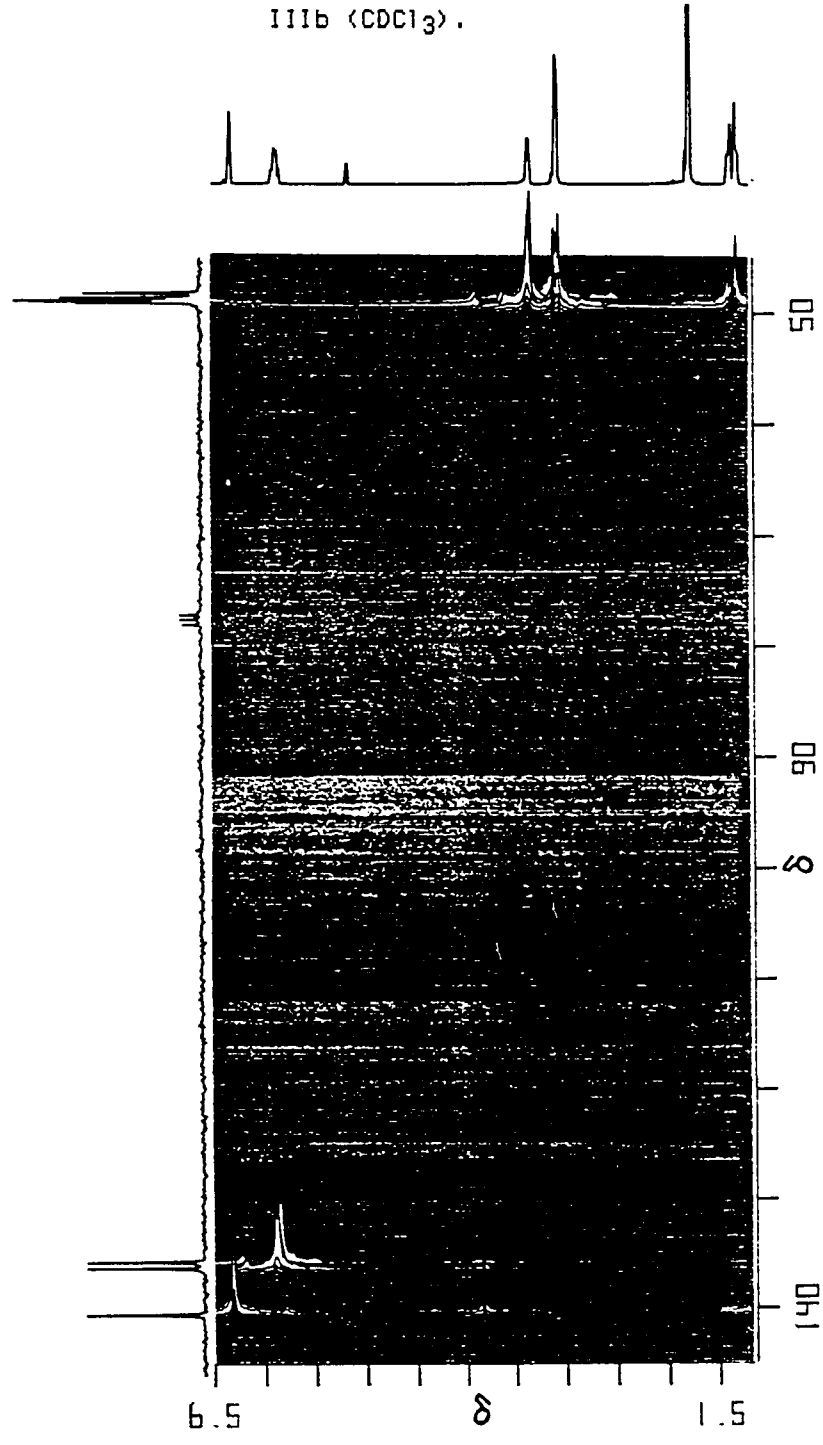

FIGURE VI-26

300 MHz ^{1}H NMR Spectrum of
1-Methylpentacyclo[5.4.0.0^{2,6}.0^{3,10}.0^{5,9}]undecane-8,11-dione
IVb ($CDCl_3$/TMS).

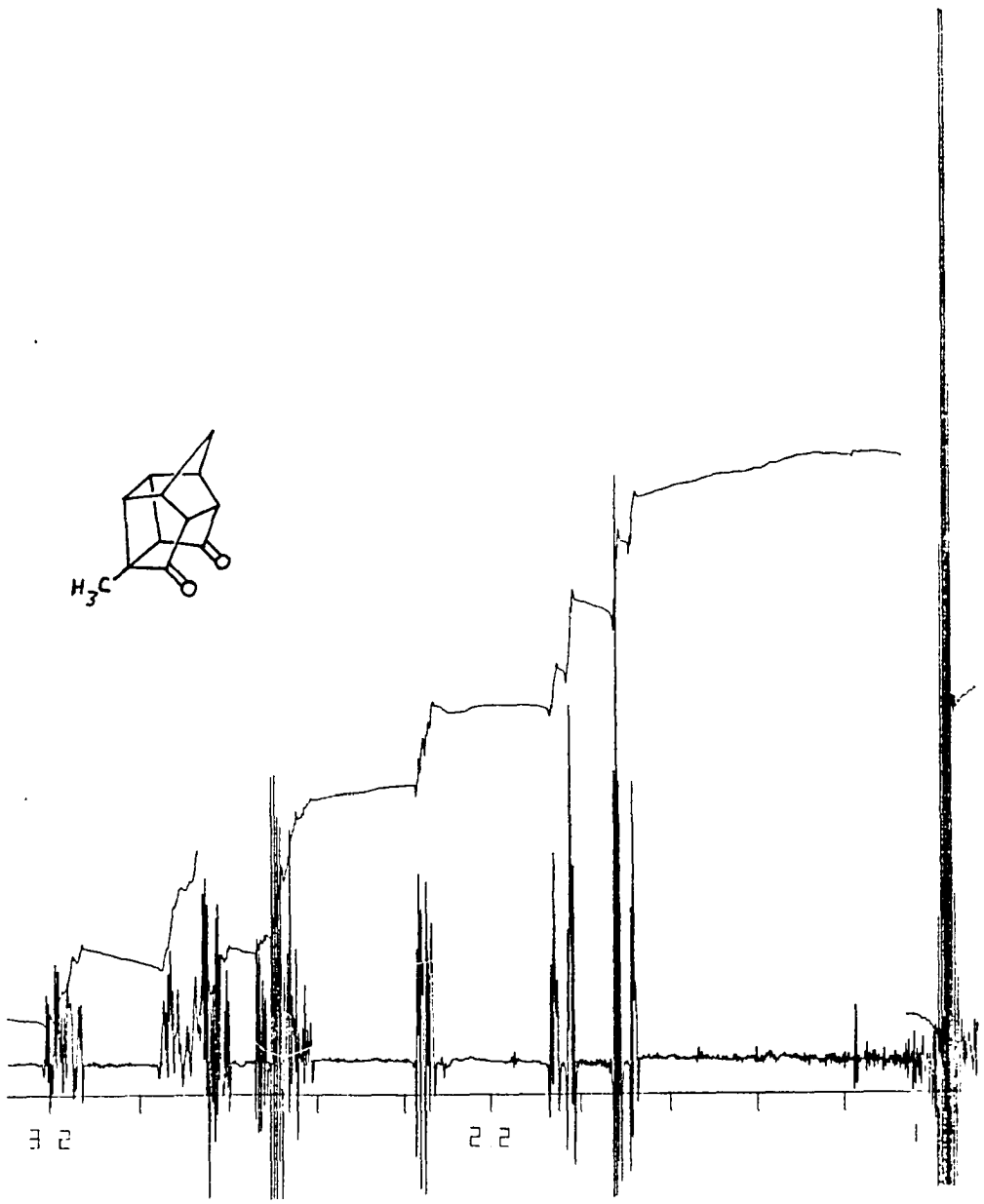

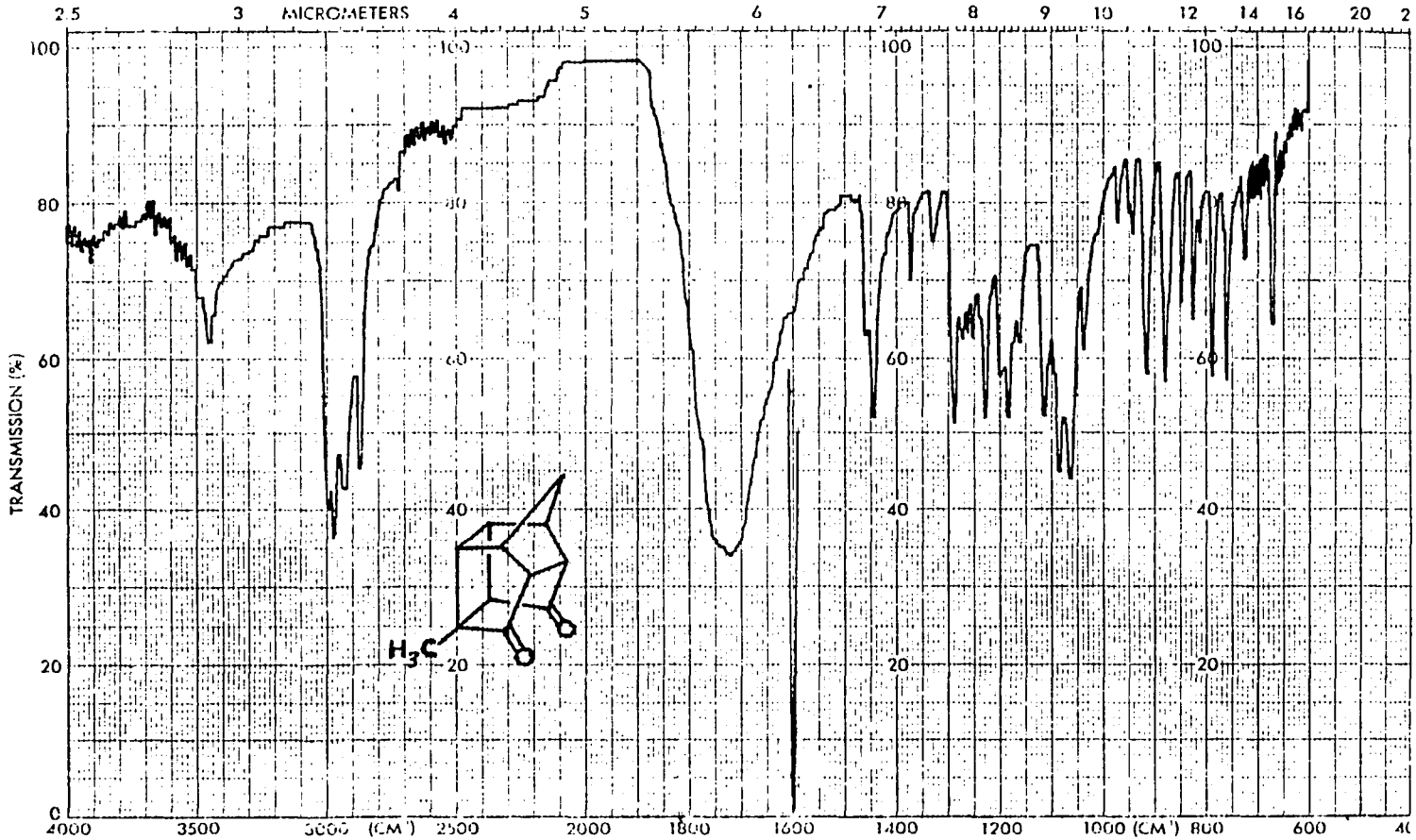

Figure VI-27. IR Spectrum of
1-Methylpentacyclo[5.4.0.0^{2,6}.0^{3,10}.0^{5,9}]undecane-8,11-dione IVb (KBr).

Mass spectrum (70 eV, Fig VI-28): m/e (relative intensity) 189 (M + 1, 14.7), 188 (M^+, 100.0), 160 (39.4), 159 (17.5), 145 (44.4), 132 (34.2), 131 (25.8), 118 (10.6), 117 (81.4), 116 (10.5), 115 (27.9), 105 (10.5), 94 (22.2), 91 (36.9), 80 (2.6), 79 (7.8), 77 (15.5), 66 (34.6), 65 (18.5);

^{13}C and Spin Echo NMR spectra (20 MHz, $CDCl_3$, Fig VI-29): δ 212.46 (C_{11} or C_8), 211.78 (C_8 or C_{11}), 54.41 (C_{10}), 54.24 (C_9), 50.11 (C_7), 48.10 (C_1), 44.75 (C_2), 43.95 (C_5), 43.32 1C_3), 40.46 (C_4), 35.89 (C_6), 15.36 (C_{methyl});

HOMCOR NMR spectrum (300 MHz, $CDCl_3$, Fig VI-30);

HOM2DJ NMR spectra (300 MHz, $CDCl_3$, Fig VI-31 and VI-32);

HETCOR NMR spectrum (300 and 75 MHz, $CDCl_3$, Fig VI-33).

Anal. Calculated for $C_{12}H_{12}O_2$: C, 76.57; H, 6.43. Found: C, 76.68; H, 6.38.

Diels Alder Addition of Methylcyclopentadienes to p-Benzoquinone

To a solution of p-benzoquinone (116 g, 1.07 mmol) in methanol (200 mL) was added a solution of freshly cracked methylcyclopentadiene (mixture of 1-methyl- and 2-methylcyclopentadienes,[12] 86.5 g, 1.08 mmol) in cold methanol (50 mL). The solution was allowed to warm slowly to room temperature, and the product was collected by suction filtration. Yellow brown crystals (IIIc and IIId, 176.9 g, 94%) were obtained. Integration of the proton NMR spectrum of the crude product mixture revealed that IIIc and IIId were formed in the ratio of ca. 45:55. This mixture of isomeric adducts was separated by careful fractional recrystallization from absolute methanol. The isomer that was less soluble in methanol was isolated by this procedure. After several recrystallizations, an analytical sample of 1-methyl-1,4,4a,8a-tetrahydro-endo-1,4-methanonaphthalene-5,8-dione (IIId) was isolated as a pale yellow microcrystalline solid: mp 116-117°C. Continued fractional recrystallization of the mother liquor from the above reaction (using a 1:1

FIGURE VI-28

Mass Spectrum of

1-Methyl-1,4,4a,8a-tetrahydro-<u>endo</u>-1,4-methanonaphthalene-5,8-dione

IVb.

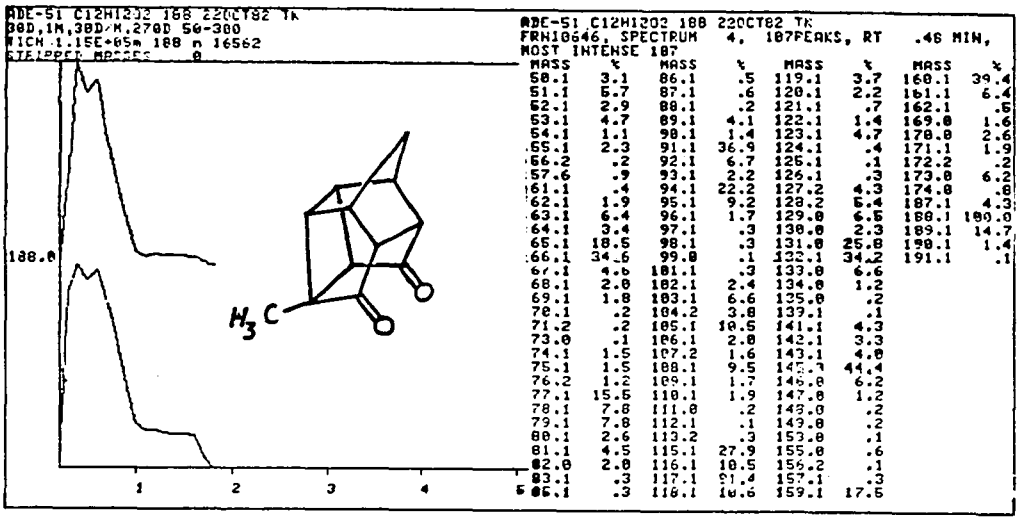

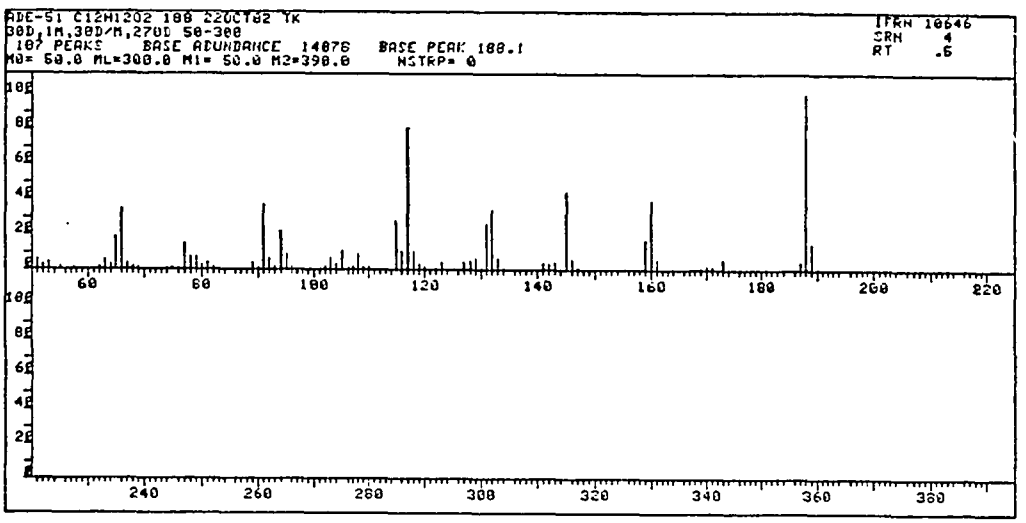

FIGURE VI-29

20 MHz ^{13}C and Spin Echo NMR Spectra of
1-Methylpentacyclo[5.4.0.0^{2,6}.0^{3,10}.0^{5,9}]undecane-8,11-dione
IVb ($CDCl_3$).

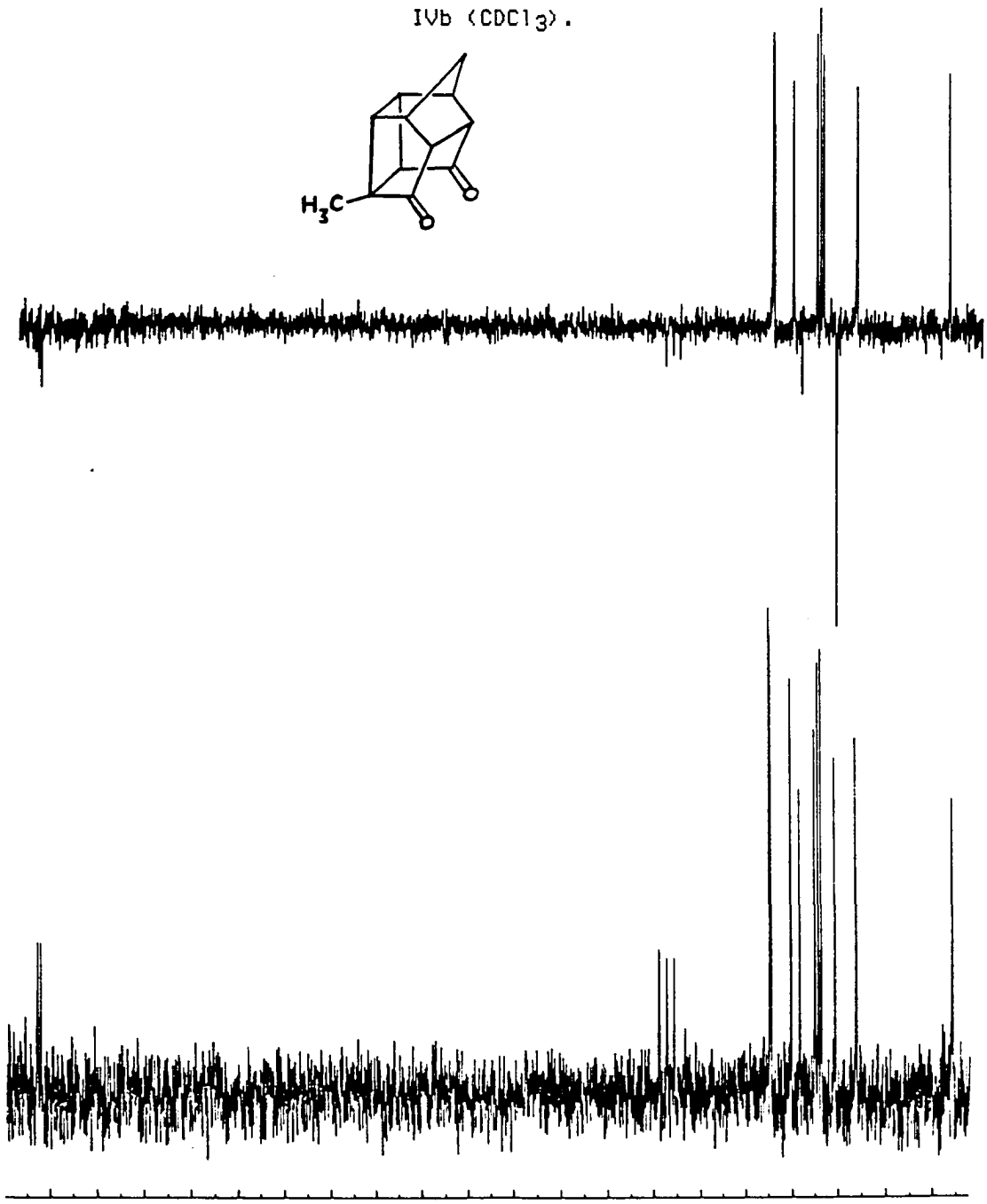

FIGURE VI-30

300 MHz ^{1}H HOMCOR NMR Spectrum of
1-Methylpentacyclo[5.4.0.0^{2,6}.0^{3,10}.0^{5,9}]undecane-8,11-dione
IVb ($CDCl_3$).

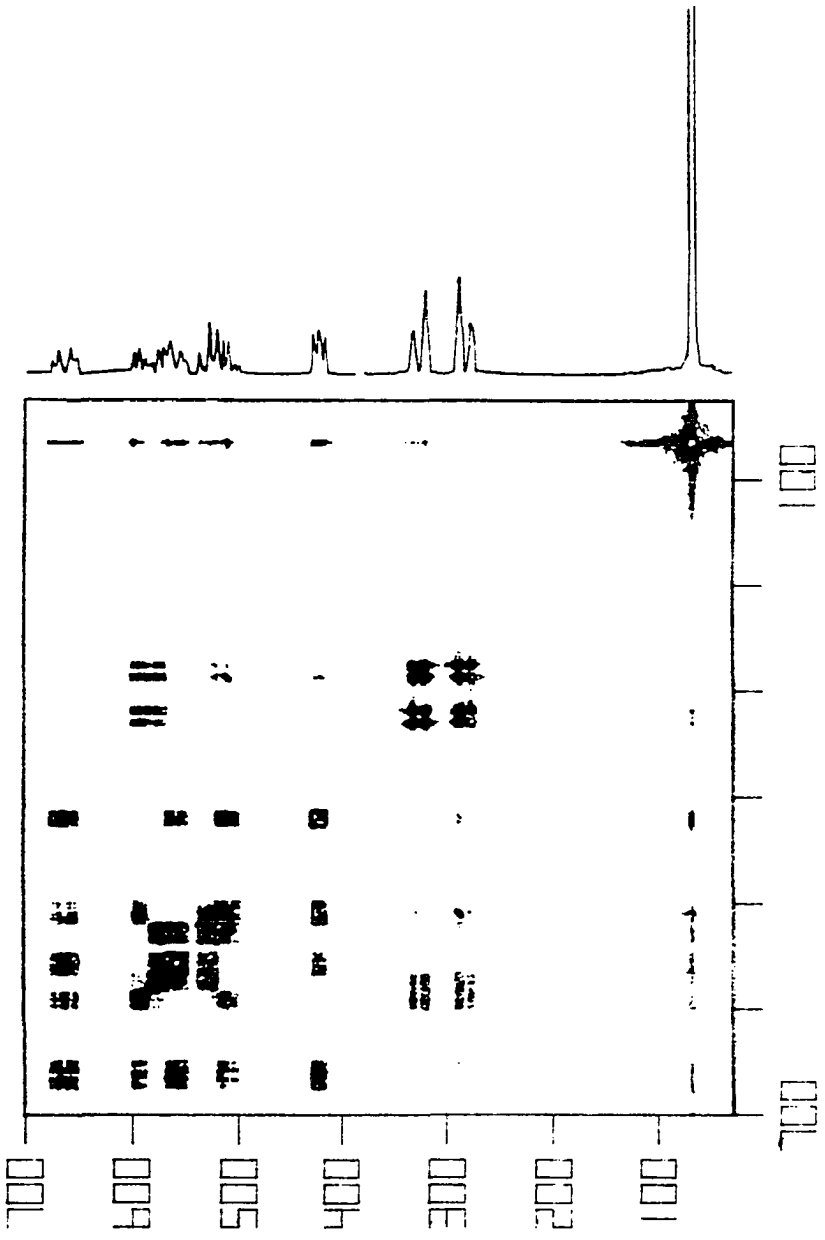

FIGURE VI-31

300 MHz ^{1}H HOM2DJ NMR Spectrum of
1-Methylpentacyclo[5.4.0.0^{2,6}.0^{3,10}.0^{5,9}]undecane-8,11-dione
IVb ($CDCl_3$).

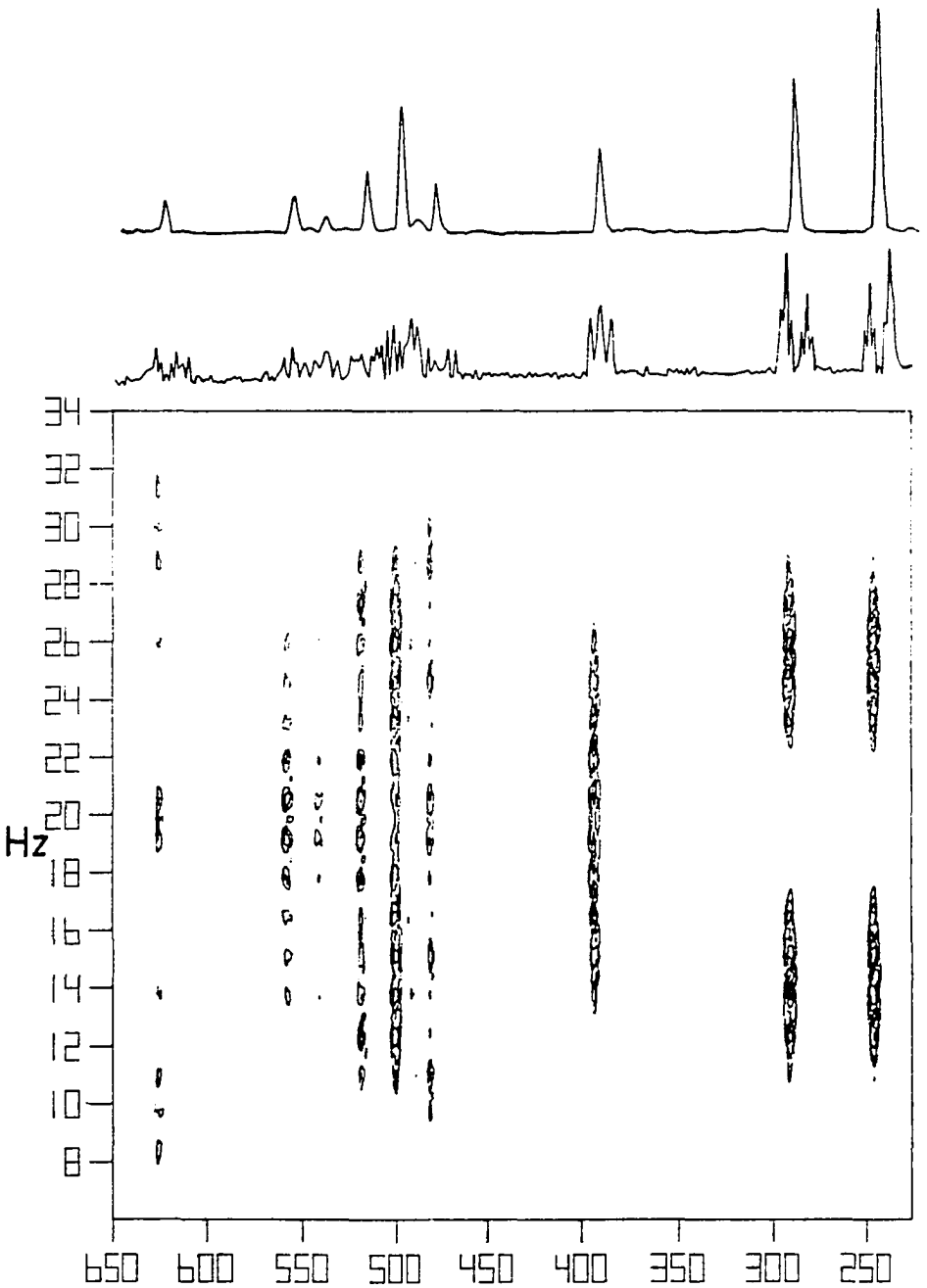

FIGURE VI-32

Stacked Plot of the HOM2DJ NMR Spectrum of Fig IV-31 of 1-Methylpentacyclo[5.4.0.0^{2,6}.0^{3,10}.0^{5,9}]undecane-8,11-dione IVb ($CDCl_3$).

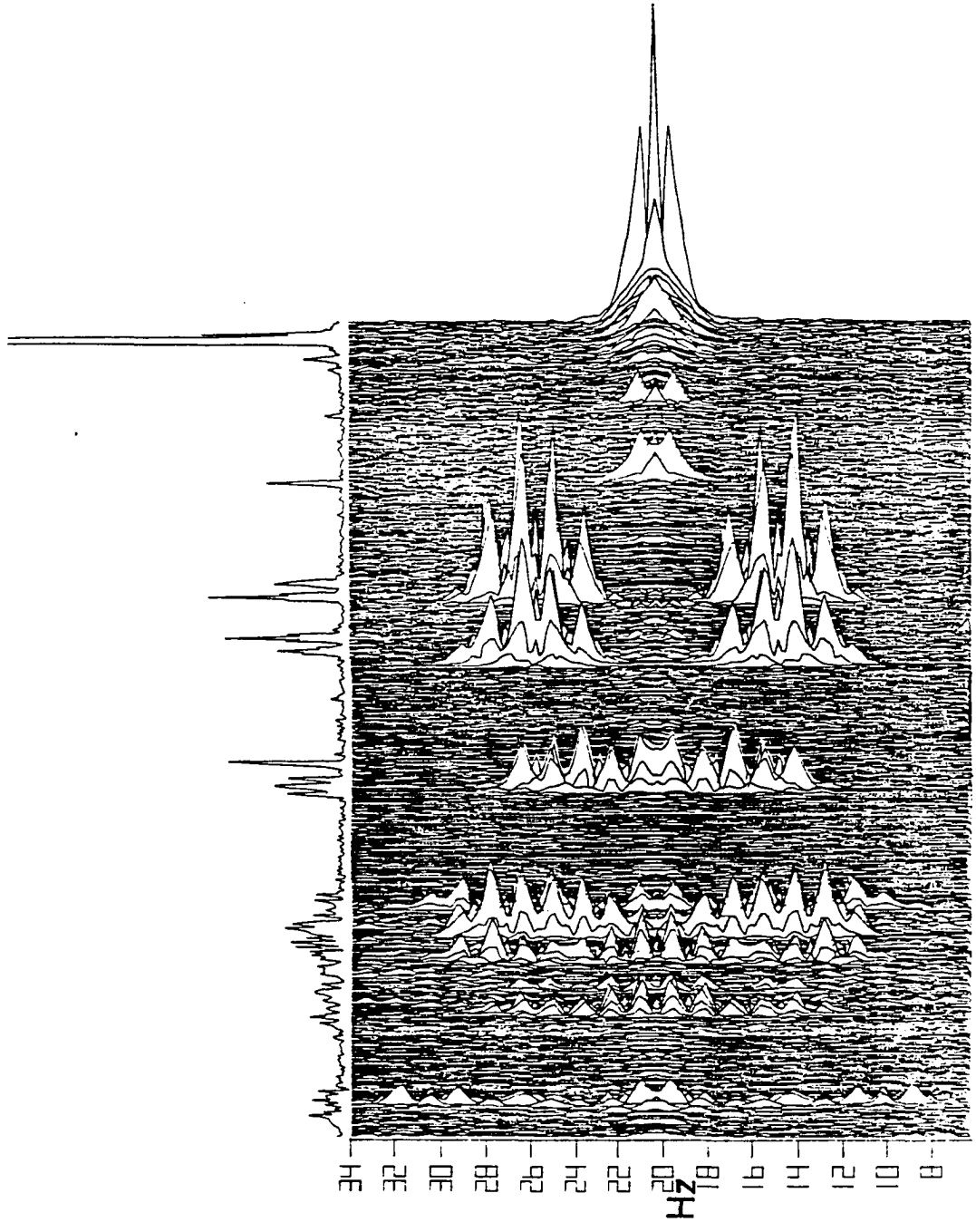

FIGURE VI-33

300 MHz ^{1}H and 75 MHz ^{13}C HETCOR NMR Spectrum of 1-Methylpentacyclo[5.4.0.0^{2,6}.0^{3,10}.0^{5,9}]undecane-8,11-dione IVb ($CDCl_3$).

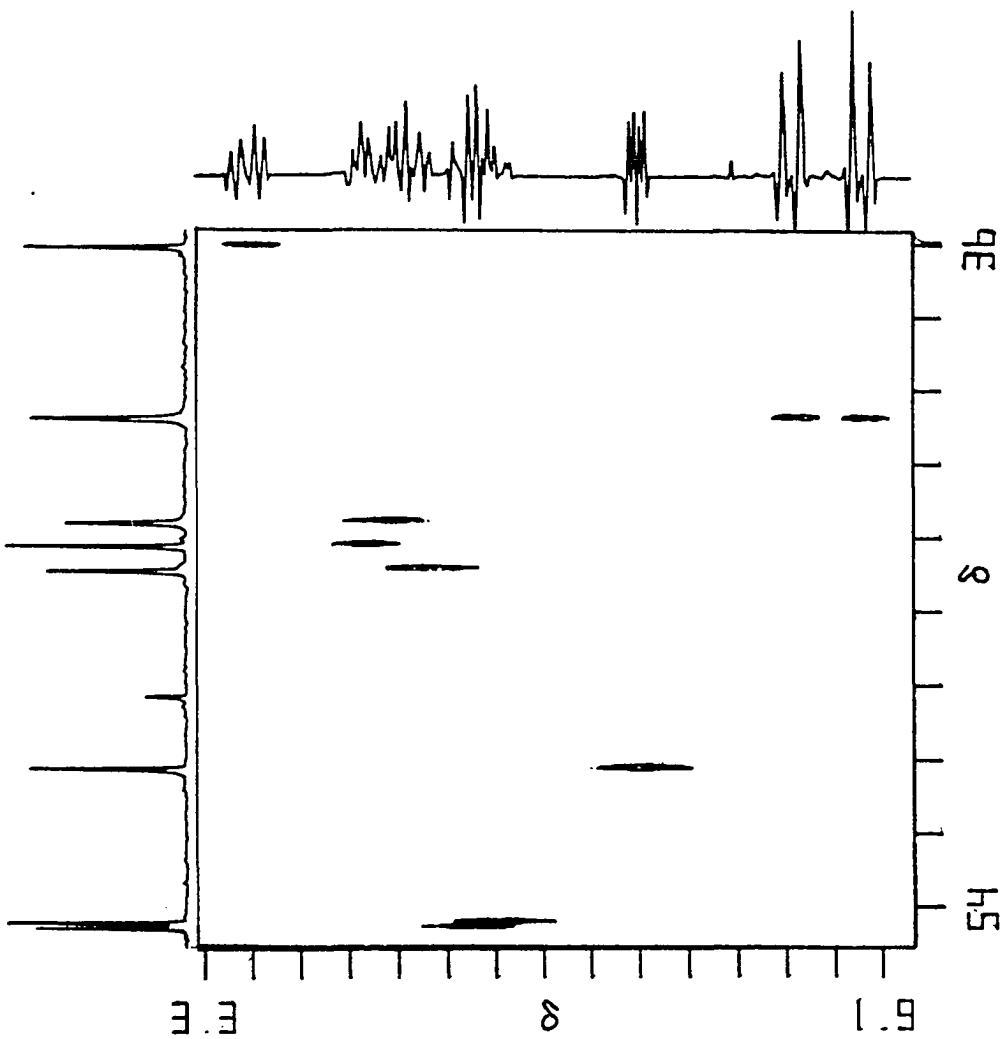

mixture of methanol-hexane) afforded 2-methyl-1,4,4a,8a-tetrahydro-endo-1,4-methanonaphthalene (IIIc) as a pale yellow microcrystalline solid: mp 101.0-101.5°C.

2-Methyl-1,4,4a,8a-tetrahydro-endo-1,4-methanonaphthalene-5,8-dione (IIIc).

^{1}H NMR spectrum (300 MHz, $CDCl_3$, Fig VI-34): δ AB pattern (J_{AB} = 10.4 Hz) δ_B 6.63 (1 H, H_7), δ_A 6.58 (1 H, H_6), 5.62 (dq, J_{3-4} = 3.0, $J_{3\text{-methyl}}$ = 1.6 Hz, 3 H, H_3), 3.41 (m, J_{4-4a} = 4.2, J_{4-3} = 3.0, J_{4-9a} = 1.6, J_{4-9s} = 1.4 Hz, 1 H, H_4), 3.30 (m, J_{1-8a} = 3.9, J_{1-9a} = 1.6, J_{1-9s} = 1.4 Hz, 1 H, H_1), 3.29 (dd, J_{8a-4a} = 8.7, J_{8a-1} = 3.9 Hz, 1 H, H_{8a}), 3.24 (dd, J_{4a-8a} = 8.7, J_{4a-4} = 4.2 Hz, 1 H, H_{4a}), 1.62 (d, $J_{\text{methyl}-3}$ = 1.6 Hz, 3 H, CH_3), 1.57 (ddd, J_{9a-9s} = 8.6, J_{9a-1} = 1.6, J_{9a-4} = 1.6 Hz, 1 H, H_{9a}), 1.43 (ddd, J_{9s-9a} = 8.6, J_{9s-1} = 1.4, J_{9s-4} = 1.4 Hz, 1 H, H_{9s});

IR spectrum (CCl_4 solution cell, Fig VI-35): 3058 (w), 2990 (m), 2970 (m), 2940 (m), 2915 (m), 2870 (m), 1678 (vs), 1605 (m), 1442 (m), 1375 (m), 1321 (w), 1296 (s), 1274 (s), 1135 (m), 1115 (m), 899 (w), 858 (s) cm^{-1};

Mass spectrum (70 eV, Fig VI-36): m/e (relative intensity) 189 (M + 1, 5.6), 188 (M^+, 39.4), 91 (14.4), 80 (100.0), 79 (52.8), 77 (20.1), 66 (3.4), 65 (7.8);

^{13}C and Spin Echo spectra (20 MHz, $CDCl_3$, Fig VI-37): δ 199.49 (C_8 or C_5), 199.13 (C_5 or C_8), 145.42 (C_2), 141.75 (C_7), 141.35 (C_6), 127.45 (C_3), 53.44 (C_1), 49.26 (C_{4a}), 49.02 (C_4), 48.63 (C_9), 48.06 (C_{8a}), 16.21 (C_{methyl});

HOMCOR NMR spectrum (300 MHz, $CDCl_3$, Fig VI-38);

HOM2DJ NMR spectrum (300 MHz, $CDCl_3$, Fig VI-39 through VI-41);

HETCOR NMR spectrum (300 and 75 MHz, $CDCl_3$, Fig VI-42 through VI-44).

Anal. Calculated for $C_{12}H_{12}O_2$: C, 76.57; H, 6.43. Found: C, 76.35; H, 6.41.

FIGURE VI-34

300 MHz ^{1}H NMR Spectrum of
2-Methyl-1,4,4a,8a-tetrahydro-endo-1,4-methanonaphthalene-5,8-dione
IIIc ($CDCl_3$/TMS).

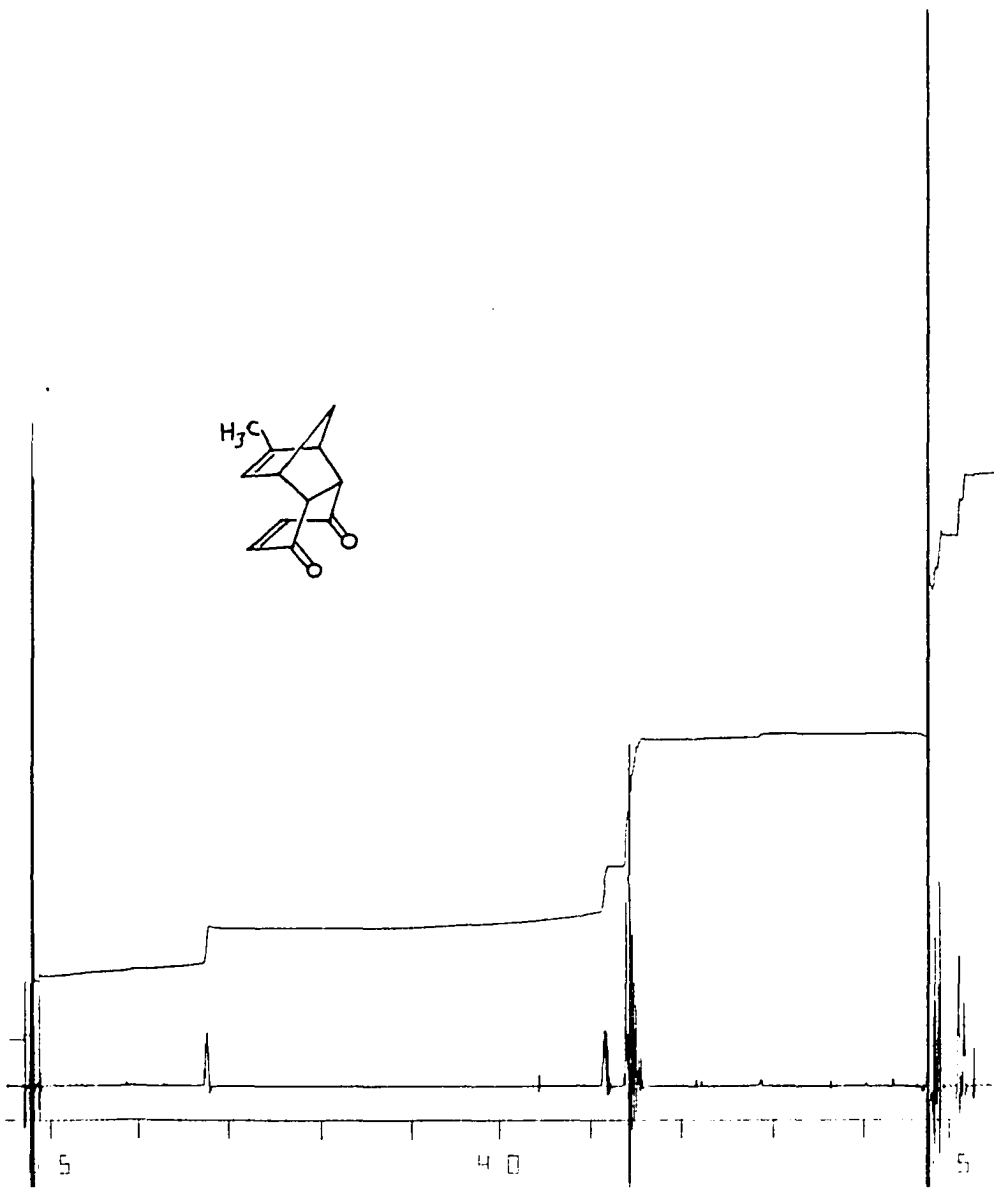

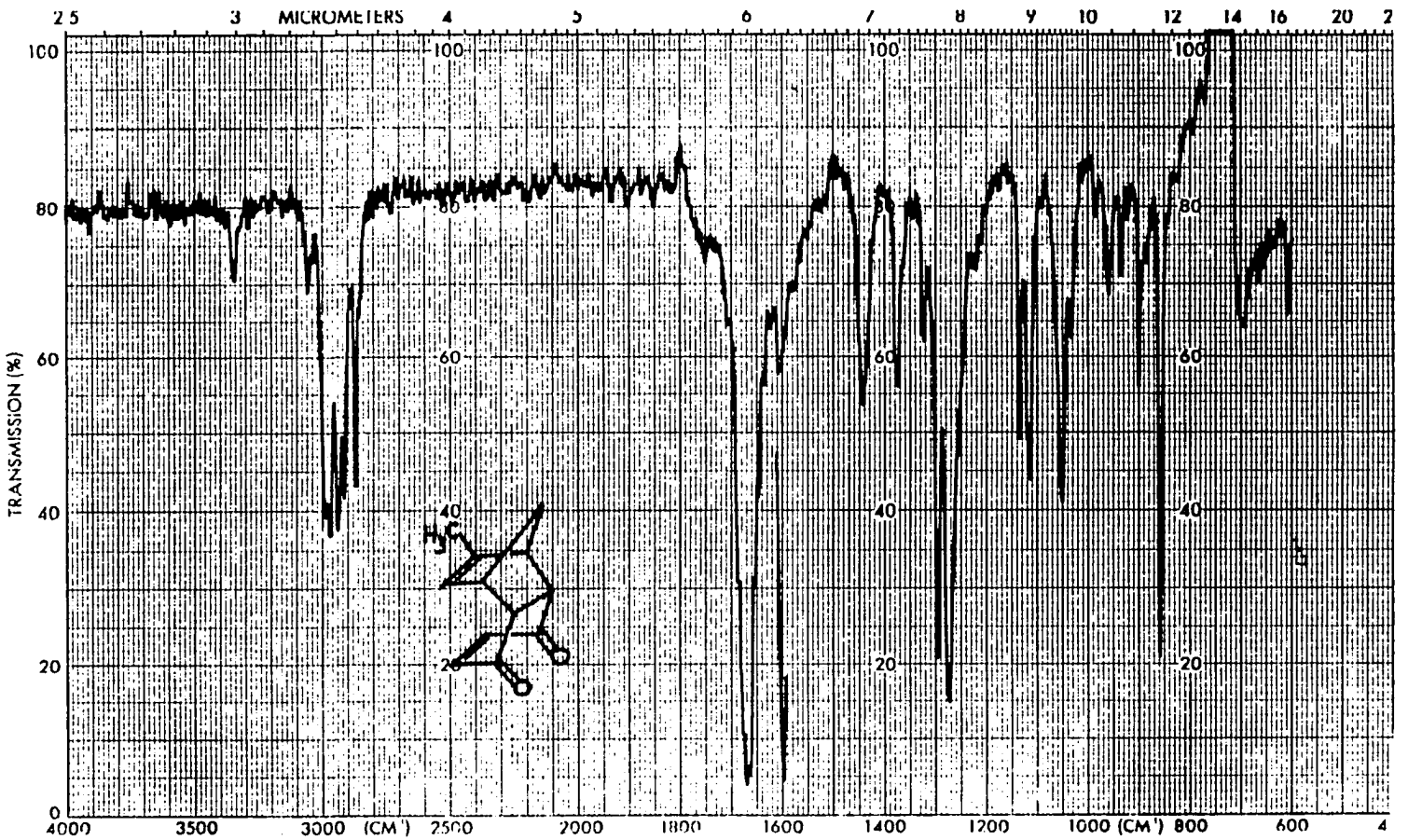

Figure VI-35. IR Spectrum of
2-Methyl-1,4,4a,8a-tetrahydro-<u>endo</u>-1,4-methanonaphthalene-5,8-dione IIIc (CCl_4).

FIGURE VI-36

Mass Spectrum of

2-Methyl-1,4,4a,8a-tetrahydro-<u>endo</u>-1,4-methanonaphthalene-5,8-dione

IIIc

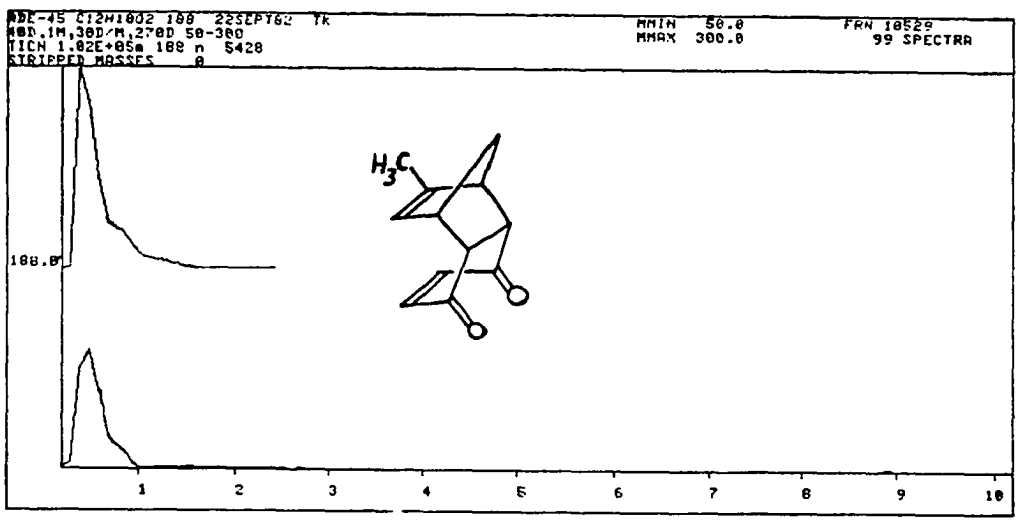

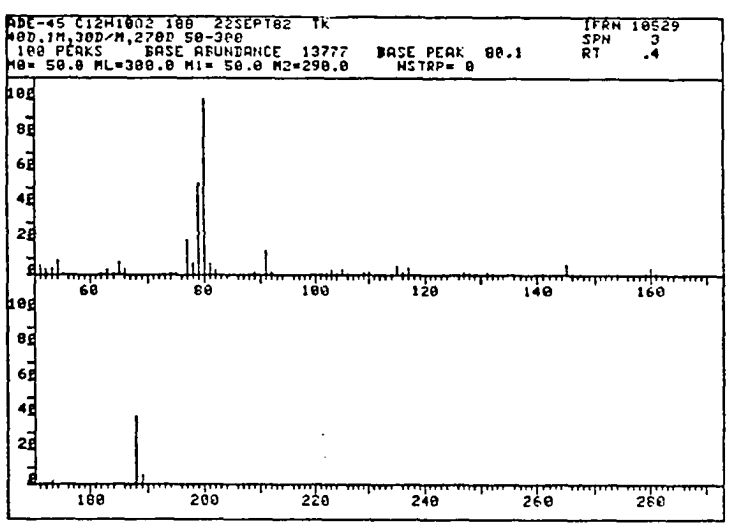

MASS	%	MASS	%
BIG 60		110.1	2.3
50.0	2.6	115.1	5.4
51.2	6.2	116.2	1.9
52.2	3.4	117.1	4.7
53.1	4.8	118.1	.8
54.1	8.5	119.1	.8
55.1	1.6	127.1	1.7
57.2	.4	128.1	1.4
62.1	1.2	129.1	1.2
63.1	3.5	131.1	2.4
64.2	.9	132.1	1.0
65.1	7.8	133.1	.5
66.1	3.4	141.1	1.1
67.1	.7	142.1	.7
74.1	1.1	143.1	.8
75.1	.9	145.0	5.3
77.1	20.1	146.1	1.1
78.1	7.2	147.0	.6
79.1	52.8	159.1	1.5
80.1	100.0	160.1	4.8
81.1	[illegible]	161.0	.9
82.1	4.0	171.0	.4
86.0	.4	173.0	2.4
89.1	1.9	174.1	.5
91.1	14.4	188.1	39.4
92.2	2.2	189.0	5.6
93.2	.7	190.2	.6
102.2	1.0		
103.1	3.4		
104.2	.5	LAST 4	
105.1	3.5	174.1	.5
106.1	1.1	188.1	39.4
107.1	.6	189.0	5.6
109.1	1.9	190.2	.6

FIGURE VI-37

20 MHz ^{13}C and Spin Echo NMR Spectra of
2-Methyl-1,4,4a,8a-tetrahydro-endo-1,4-methanonaphthalene-5,8-dione
IIIc ($CDCl_3$).

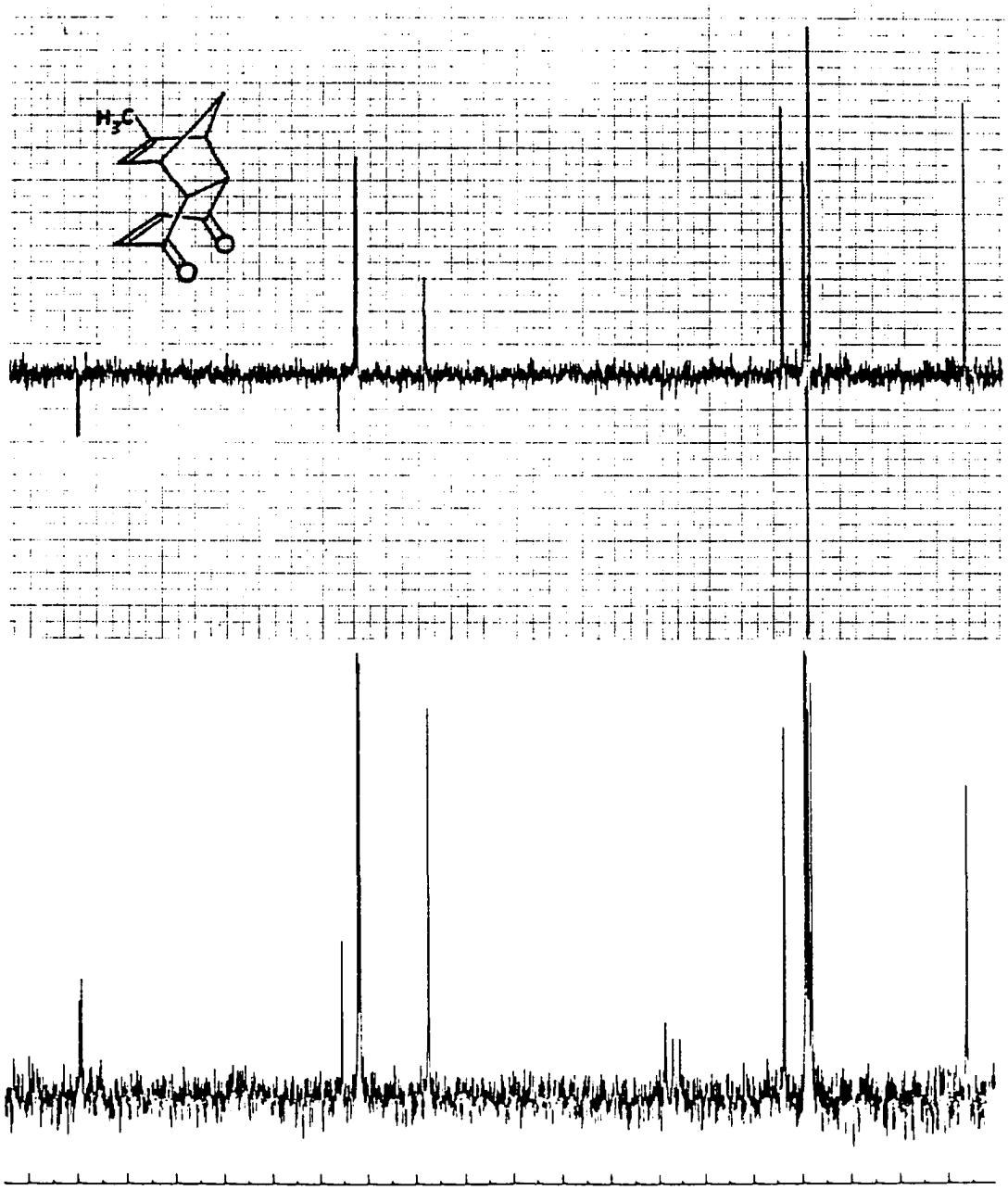

FIGURE VI-38

300 MHz ^{1}H HOMCOR NMR Spectrum of
2-Methyl-1,4,4a,8a-tetrahydro-endo-1,4-methanonaphthalene-5,8-dione
IIIc ($CDCl_3$).

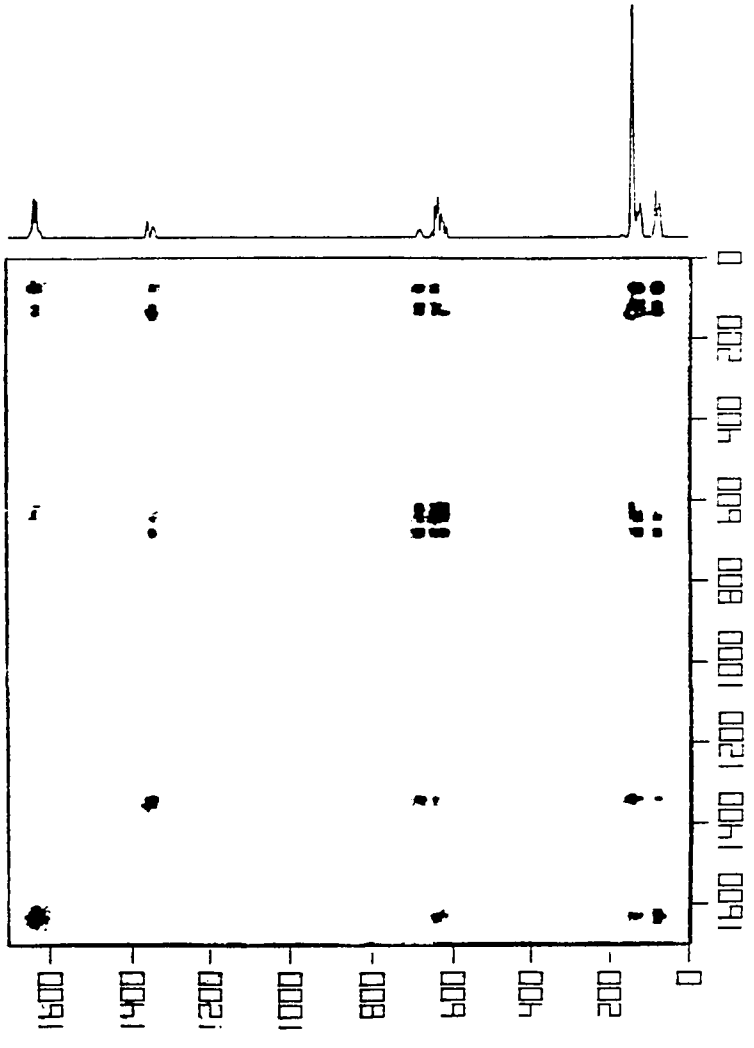

FIGURE VI-39

300 MHz ^{1}H HOM2DJ NMR Spectrum of

2-Methyl-1,4,4a,8a-tetrahydro-<u>endo</u>-1,4-methanonaphthalene-5,8-dione

IIIc ($CDCl_3$).

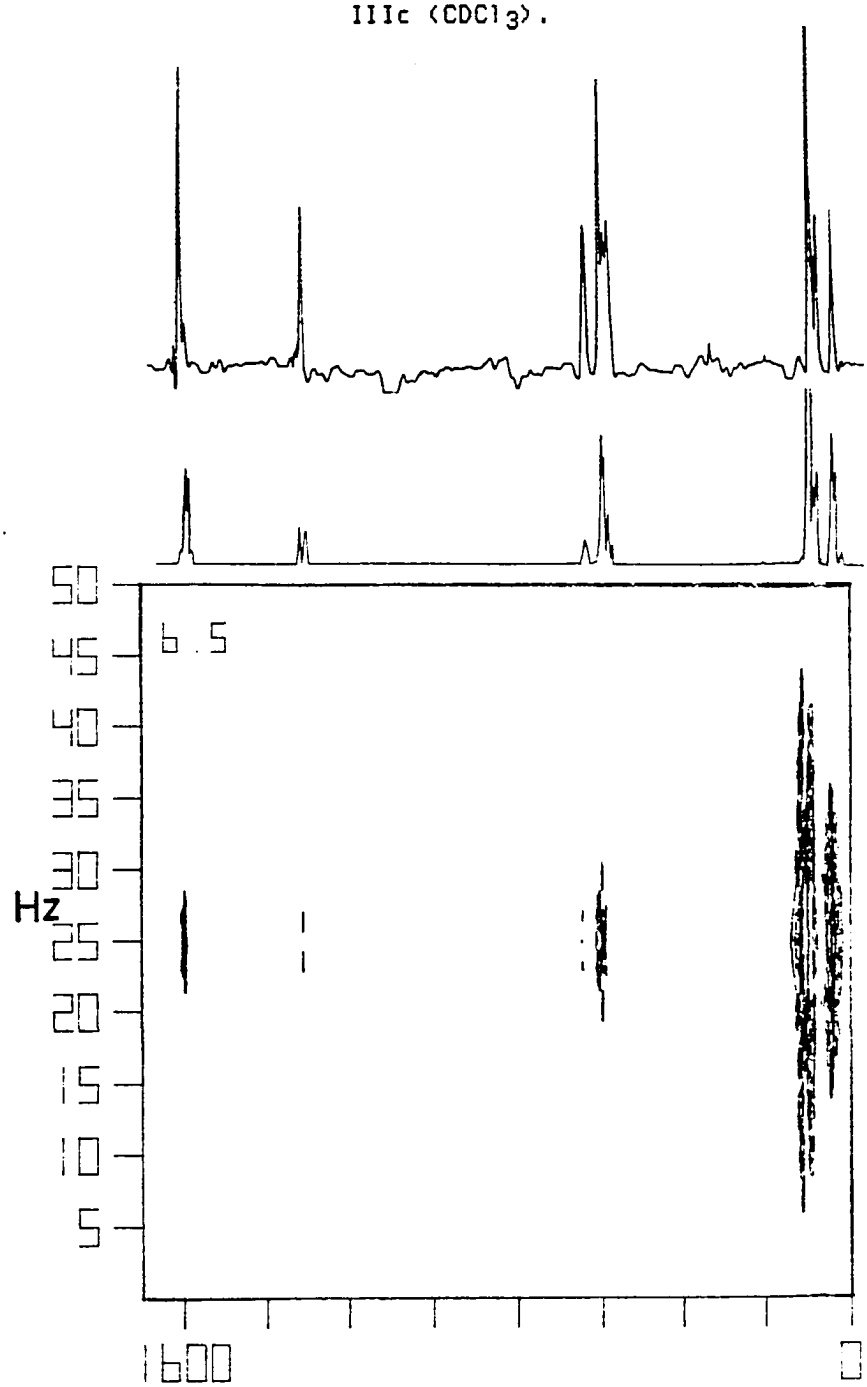

FIGURE VI-40

Expanded Contour Plot of the HOM2DJ Spectrum of Fig VI-39 which Includes the 3.3-3.5 ppm ^{1}H and 15-35 Hz Spectral Region of 2-Methyl-1,4,4a,8a-tetrahydro-<u>endo</u>-1,4-methanonaphthalene-5,8-dione IIIc ($CDCl_3$).

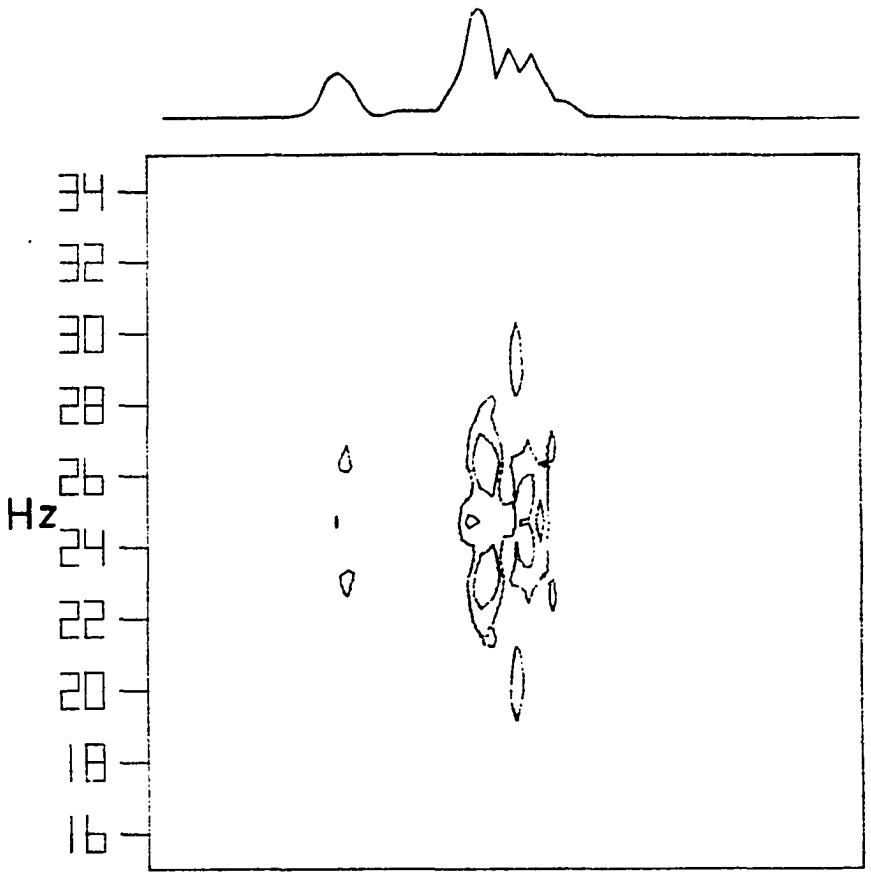

FIGURE VI-41

Stacked Plot of the HOM2DJ Spectrum of Fig VI-39 of 2-Methyl-1,4,4a,8a-tetrahydro-<u>endo</u>-1,4-methanonaphthalene-5,8-dione IIIc ($CDCl_3$).

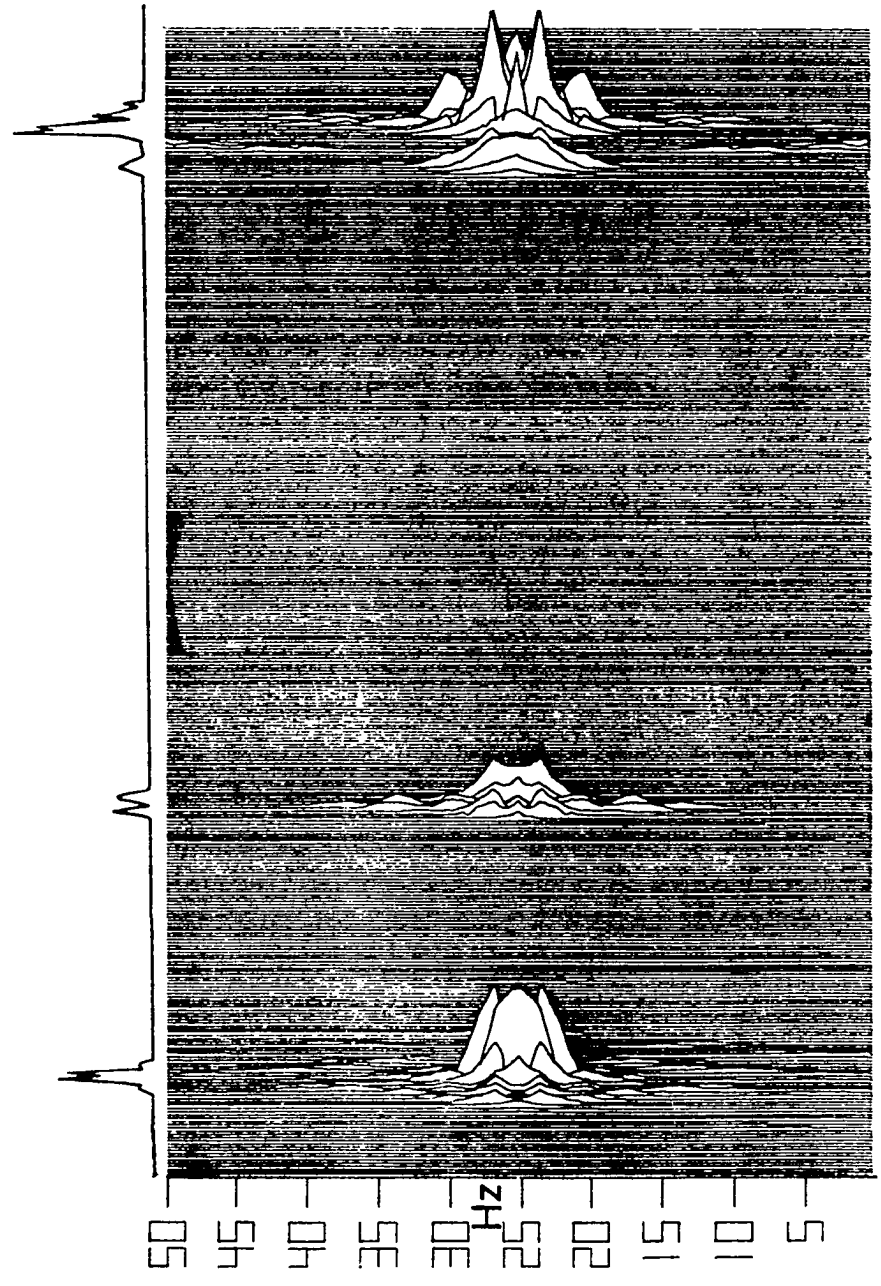

FIGURE VI-42

300 MHz ^{1}H and 75 MHz ^{13}C HETCOR NMR Spectrum of 2-Methyl-1,4,4a,8a-tetrahydro-<u>endo</u>-1,4-methanonaphthalene-5,8-dione IIIc ($CDCl_3$).

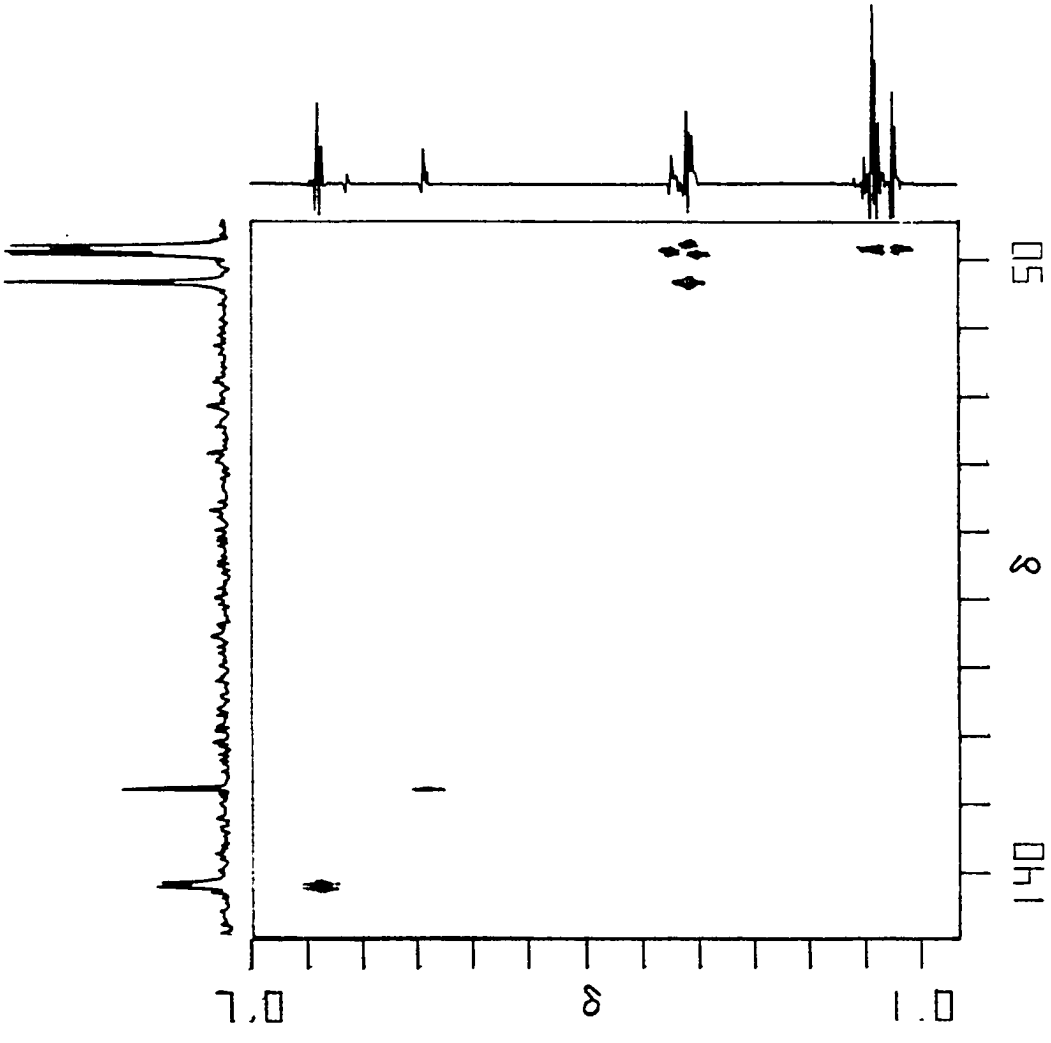

FIGURE VI-43

Expanded Contour Plot of the HETCOR NMR Spectrum of Fig VI-22 which Includes the 2.8-3.4 ^{1}H and 47-55 ppm ^{13}C Spectral Regions of 2-Methyl-1,4,4a,8a-tetrahydro-<u>endo</u>-1,4-methanonaphthalene-5,8-dione IIIc ($CDCl_3$).

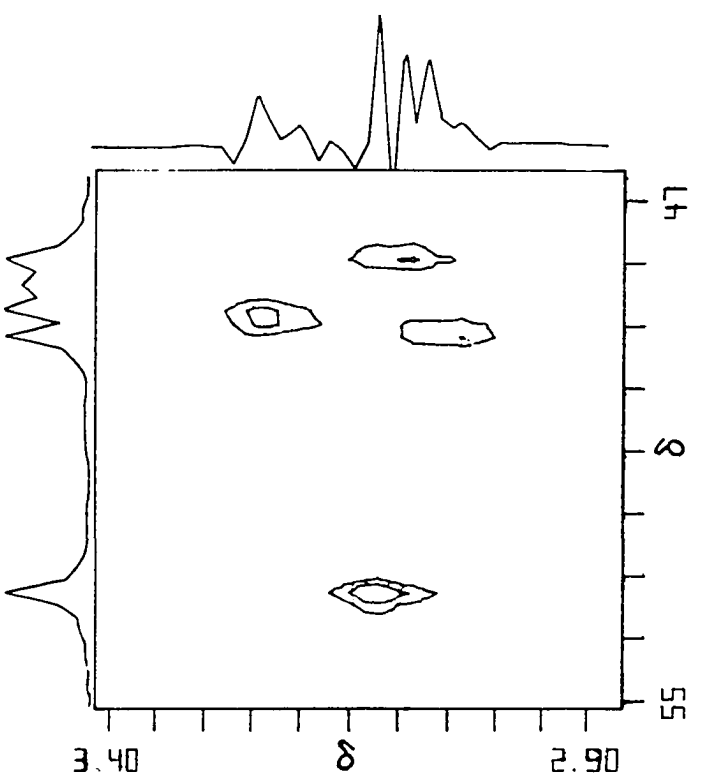

FIGURE VI-44

Stacked Plot of the HETCOR Spectrum of Fig VI-42 of 2-Methyl-1,4,4a,8a-tetrahydro-endo-1,4-methanonaphthalene-5,8-dione IIIc ($CDCl_3$).

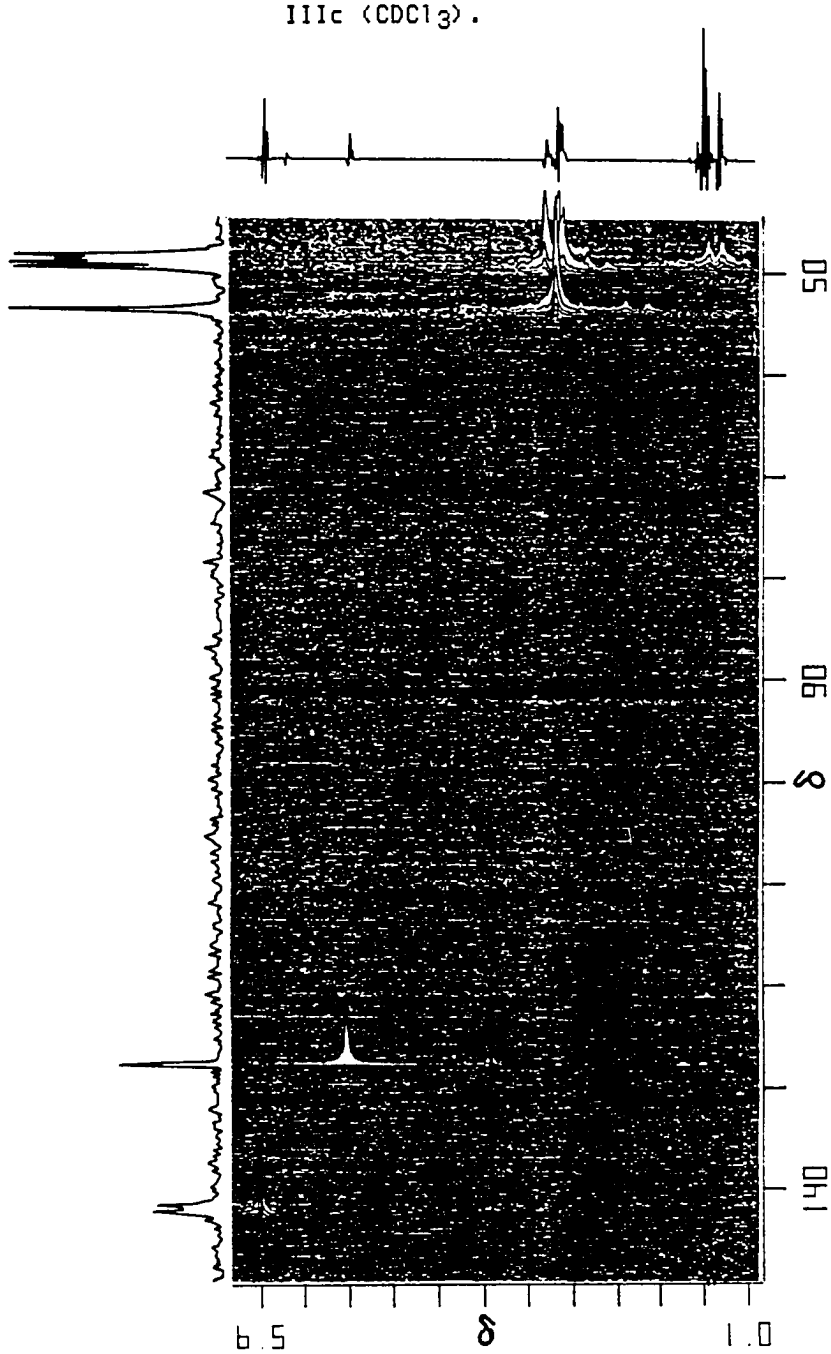

1-Methyl-1,4,4a,8a-tetrahydro-endo-1,4-methanonaphthalene-5,8-dione (IIId).

^{1}H NMR spectrum (300 MHz, $CDCl_3$, Fig VI-45): δ AB pattern (J_{AB} = 10.3 HZ) δ_B 6.57 (1 H, H_6), δ_A 6.53 (1 H, H_7), 6.04 (dd, J_{3-2} = 5.6, J_{3-4} = 2.8 Hz, 1 H, H_3), 5.86 (d, J_{2-3} = 5.6 Hz, 1 H, H_2), 3.44 (m, J_{4-4a} = 4.2, J_{4-3} = 2.8, J_{4-9a} = 2.0, J_{4-9s} = 1.4 Hz, 1 H, H_4), 3.37 (dd, J_{4a-8a} = 8.2, J_{4a-4} = 4.2, 1 H, H_{4a}), 2.88 (d, J_{8a-4a} = 8.2 Hz, 1 H, H_{8a}), 1.57 (s, 3 H, CH_3), 1.44 (dd, J_{9a-9s} = 8.7, J_{9a-4} = 2.0 Hz, 1 H, H_{9a}), 1.39 (dd, J_{9s-9a} = 8.7, J_{9s-4} = 1.4 Hz, 1 H, H_{9s});

IR spectrum (CCl_4 solution cell, Fig VI-46): 3062 (w), 3000 (w), 2970 (m), 2936 (m), 2872 (w), 1678 (vs), 1450 (w), 1381 (w), 1342 (w), 1297 (m), 1274 (m), 1143 (w), 1117 (w), 1079 (m), 1036 (w), 858 (w) cm^{-1};

Mass spectrum (70 eV, Fig VI-47): m/e (relative intensity) 189 (M + 1, 6.6), 188 (M^+, 44.4), 91 (12.8), 80 (100.0), 79 (51.6), 77 (18.6), 66 (1.3), 65 (4.7);

^{13}C and Spin Echo spectra (20 MHz, $CDCl_3$, Fig VI-48): δ 199.26 (C_8 or C_5), 198.60 (C_5 or C_8), 141.90 (C_7), 141.40 (C_6), 138.76 (C_2), 134.70 (C_3), 57.39 (C_1), 54.97 (C_9), 52.29 (C_{8a}), 50.50 (C_{4a}), 48.80 (C_4), 17.08 (C_{methyl});

HOMCOR NMR spectrum (300 MHz, $CDCl_3$, Fig VI-49);

HETCOR NMR spectrum (300 and 75 MHz, $CDCl_3$, Fig VI-50 and VI-51).

Anal. Calculated for $C_{12}H_{12}O_2$: C, 76.57; H, 6.43. Found: C, 76.87; H, 6.67.

2-Methylpentacyclo[5.4.0.0^{2,6}.0^{3,10}.0^{5,9}]undecane-8,11-dione (IVc). Intramolecular photochemical cyclization of IIIc to IVc was performed by using the method described above for the photolytic conversion of IIIb to IVb. Compound IVc prepared via this procedure was obtained as a colorless microcrystalline solid (88%): mp 181-182°C.

^{1}H NMR spectrum (300 MHz, $CDCl_3$, Fig VI-52): δ 2.95 (ddtd,

FIGURE VI-45

300 MHz ^{1}H NMR Spectrum of
1-Methyl-1,4,4a,8a-tetrahydro-<u>endo</u>-1,4-methanonaphthalene-5,8-dione
IVd ($CDCl_3$/TMS).

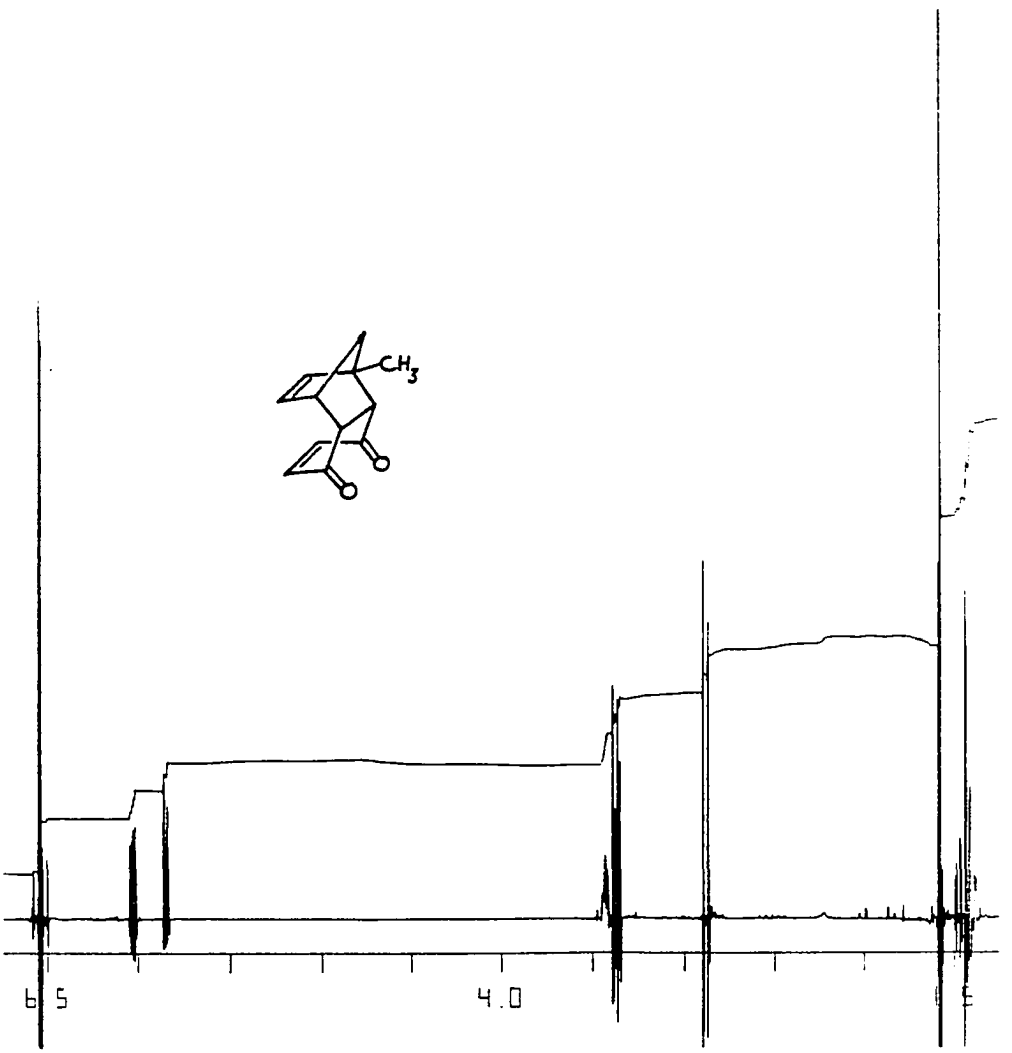

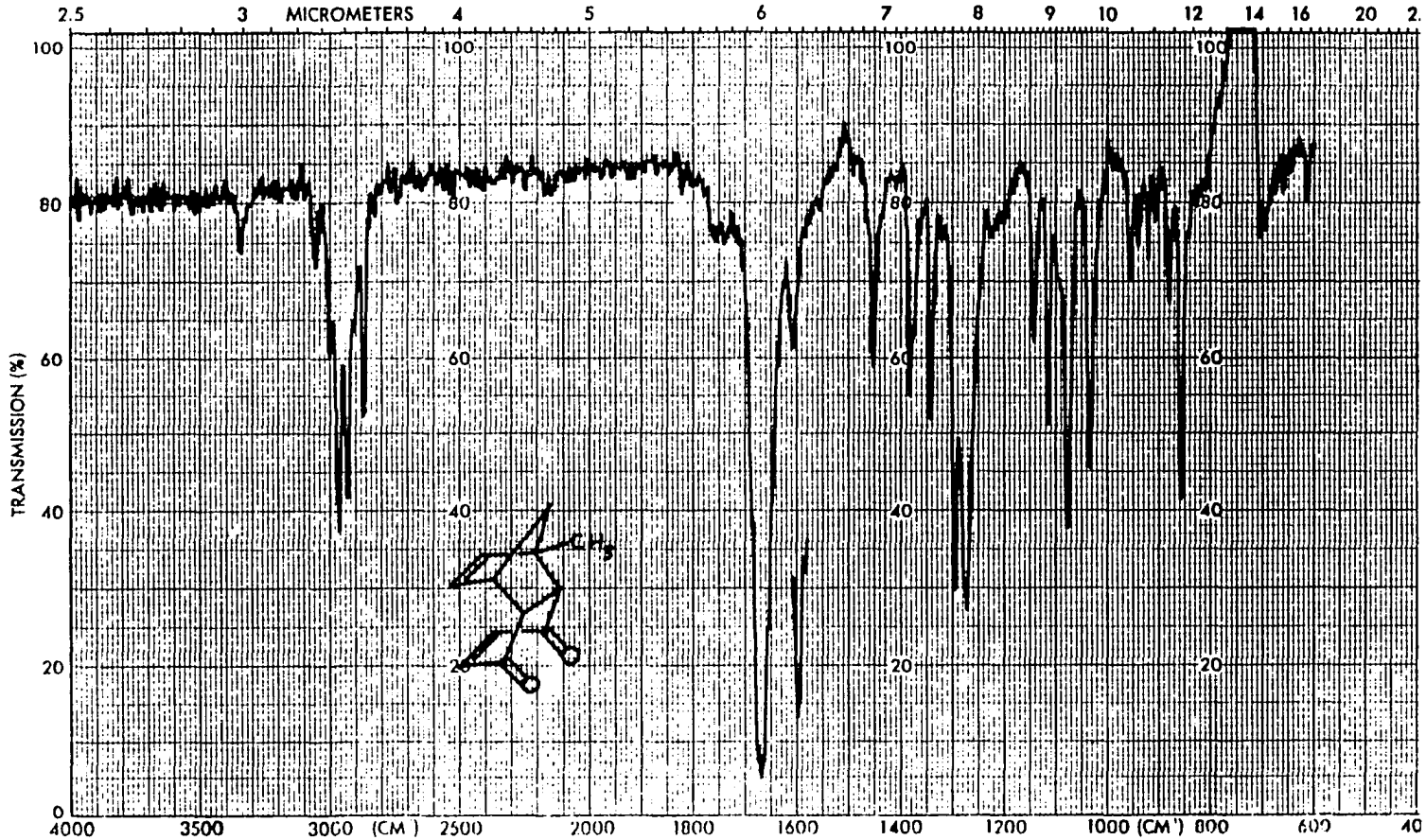

Figure VI-46. IR Spectrum of
1-Methyl-1,4,4a,8a-tetrahydro-<u>endo</u>-1,4-methanonaphthalene-5,8-dione IIId (CCl_4).

FIGURE VI-47

Mass Spectrum of

1-Methyl-1,4,4a,8a-tetrahydro-<u>endo</u>-1,4-methanonaphthalene-5,8-dione

IIId ($CDCl_3$/TMS).

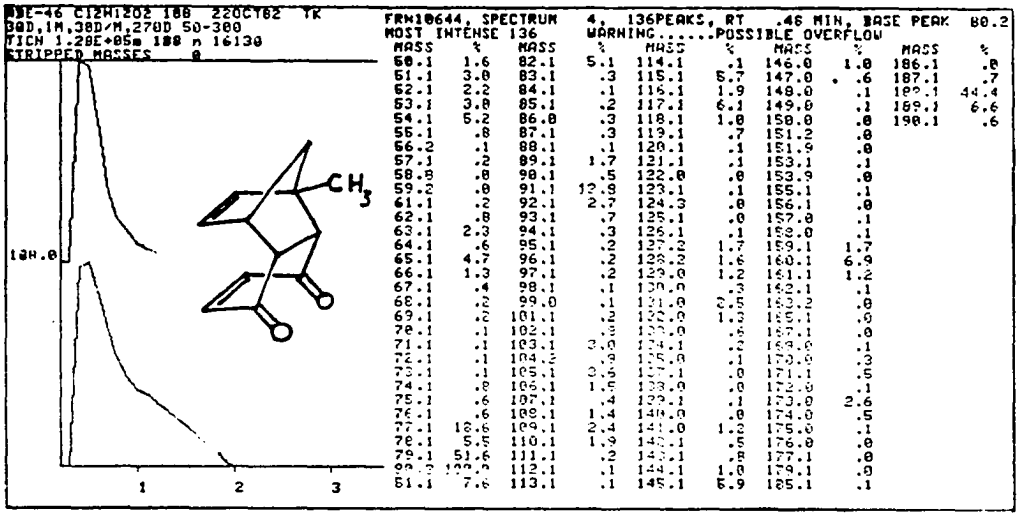

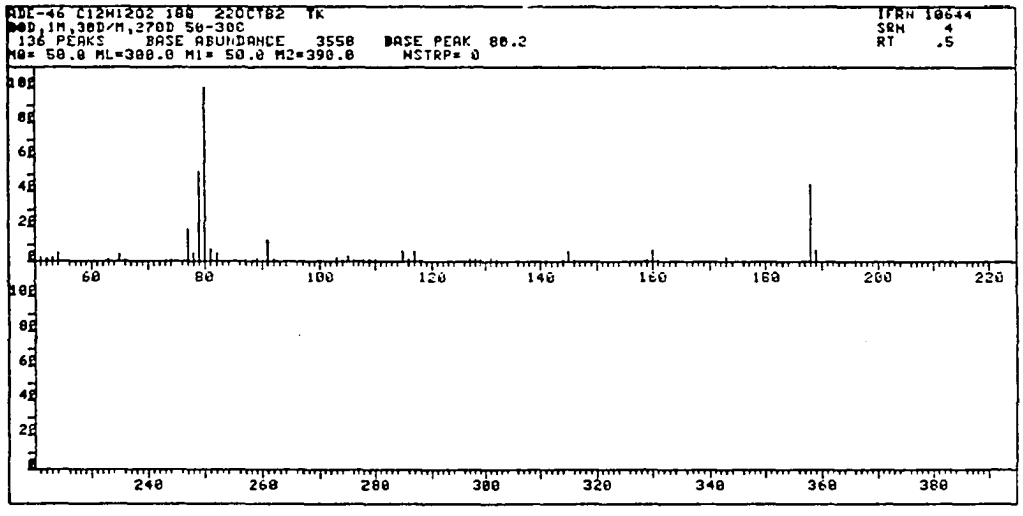

FIGURE VI-48

20 MHz ^{13}C and Spin Echo NMR Spectra of
1-Methyl-1,4,4a,8a-tetrahydro-endo-1,4-methanonaphthalene-5,8-dione
IIId ($CDCl_3$).

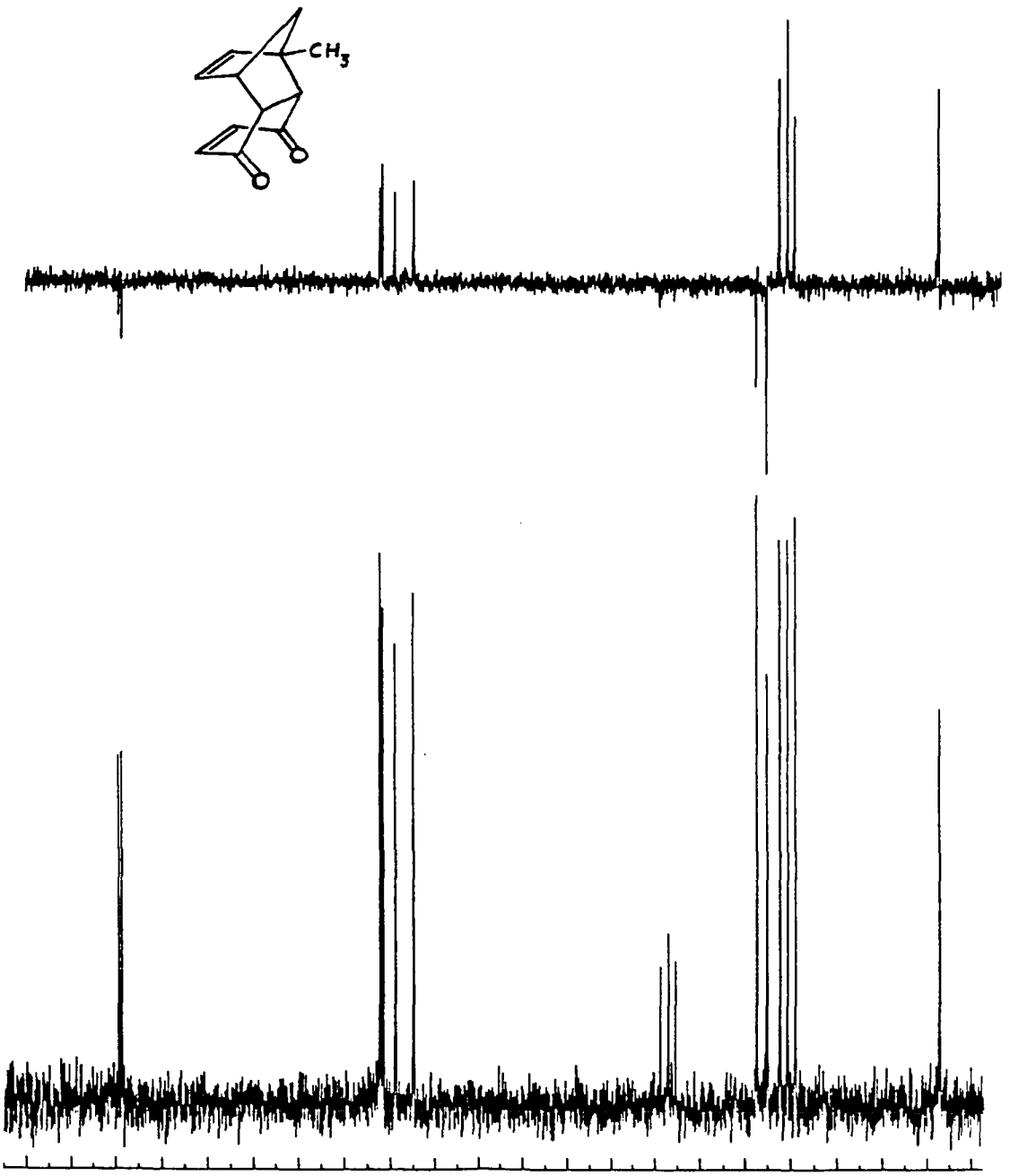

FIGURE VI-49

300 MHz ^{1}H HOMCOR NMR Spectrum of
1-Methyl-1,4,4a,8a-tetrahydro-endo-1,4-methanonaphthalene-5,8-dione
IIId ($CDCl_3$).

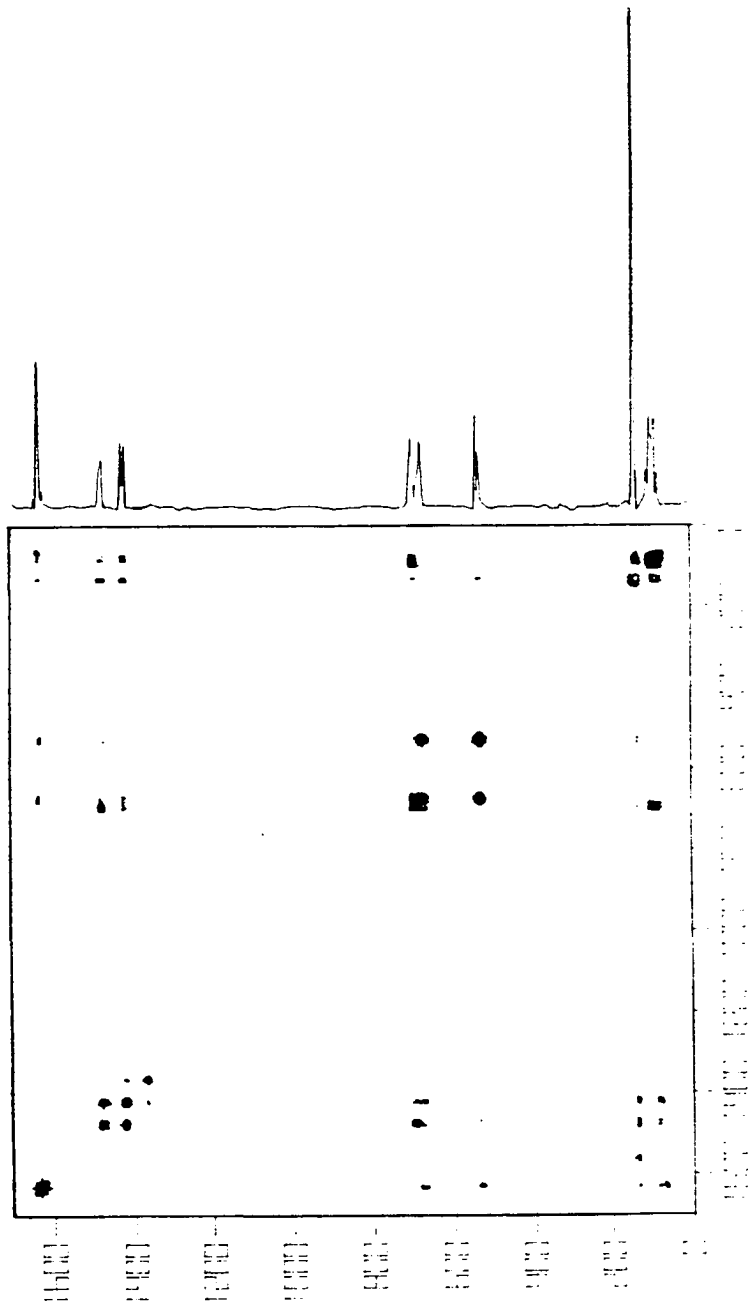

FIGURE VI-50

300 MHz ^{1}H and 75 MHz ^{13}C HETCOR NMR Spectrum of 1-Methyl-1,4,4a,8a-tetrahydro-endo-1,4-methanonaphthalene-5,8-dione IIId ($CDCl_3$).

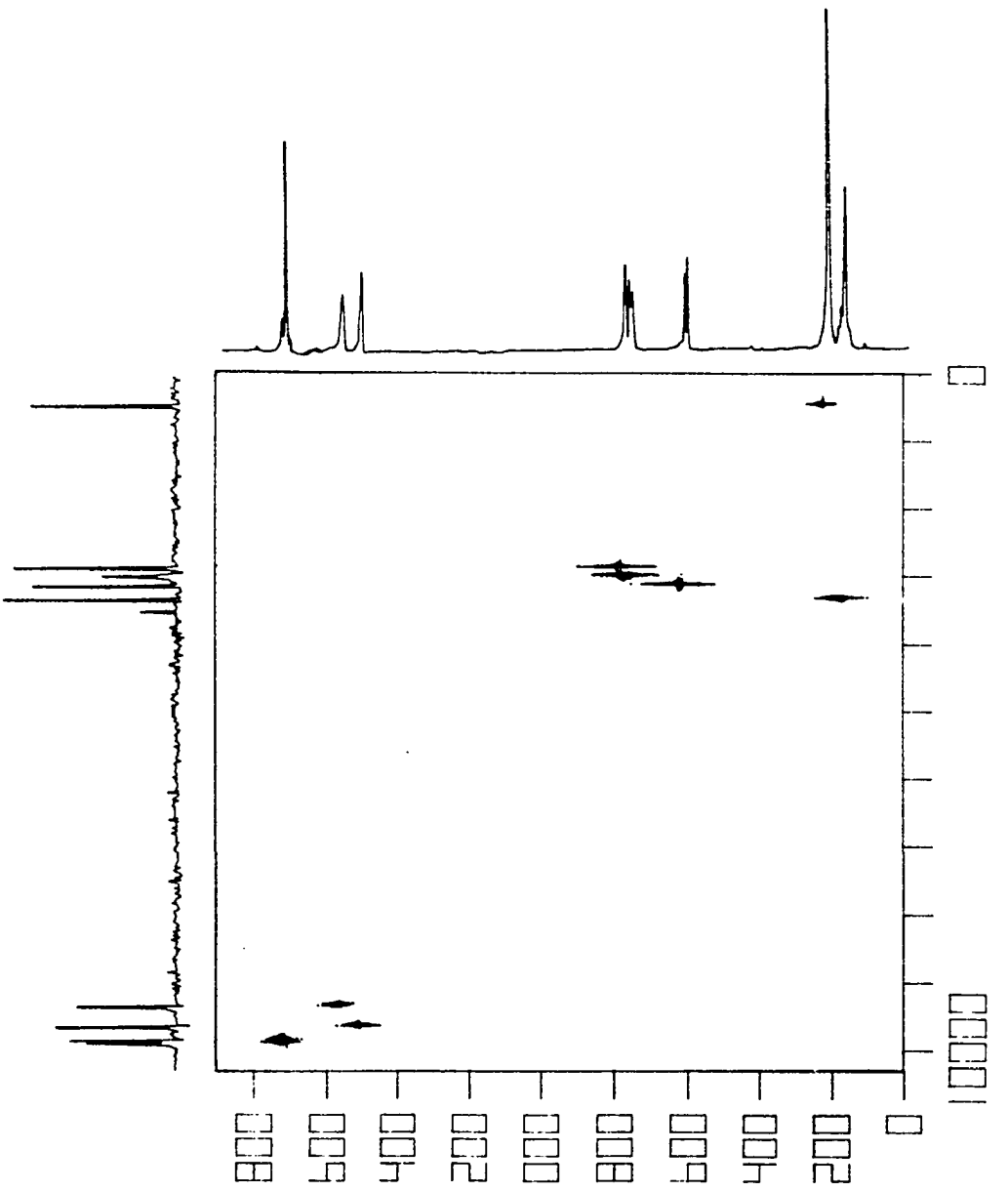

FIGURE VI-51

Expanded Contour Plot of the HETCOR Spectrum of Fig VI-50 which Includes the 5.8-6.1 ^{1}H and 130-145 ppm ^{13}C Spectral Regions of 1-Methyl-1,4,4a,8a-tetrahydro-<u>endo</u>-1,4-methanonaphthalene-5,8-dione IIId ($CDCl_3$).

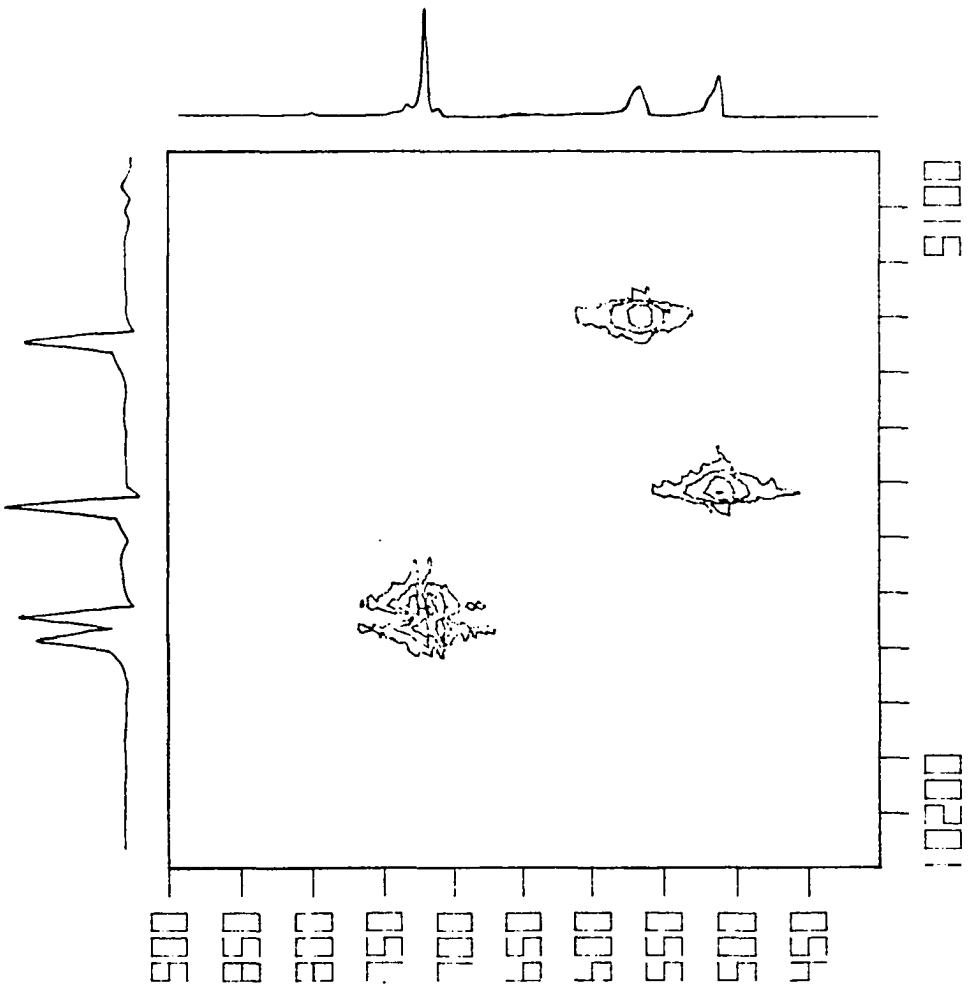

FIGURE VI-52

300 MHz ^{1}H NMR Spectrum of
2-Methylpentacyclo[5.4.0.0^{2,6}.0^{3,10}.0^{5,9}]undecane-8,11-dione
IVc ($CDCl_3$/TMS).

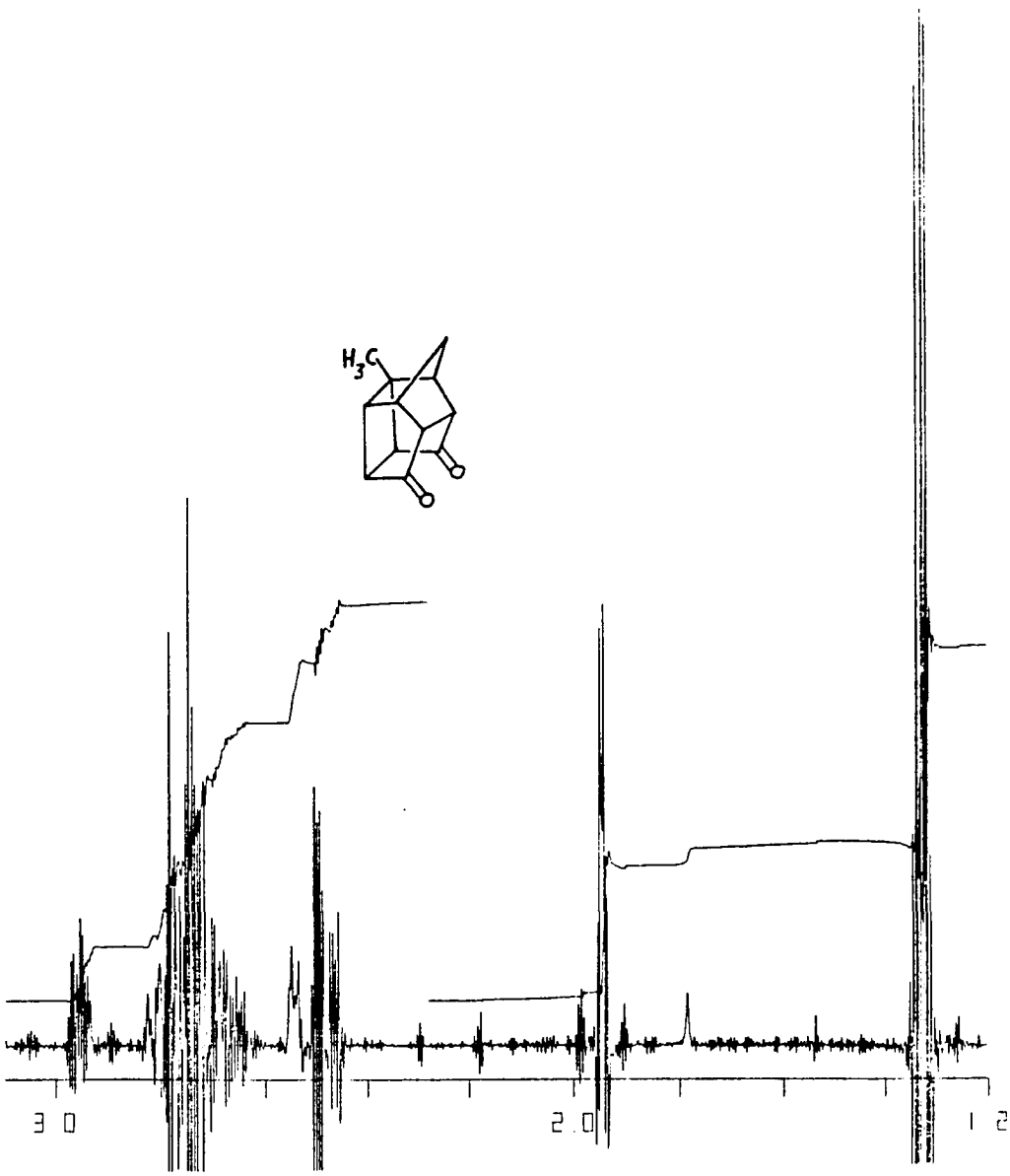

J_{5-6} = 5.3, J_{5-9} = 4.0, J_{5-4s} = 1.6, J_{5-4a} = 1.6, J_{5-3} = 1.2 Hz, 1 H, H_5), 2.80 (dddd, J_{6-7} = 6.6, J_{6-5} = 5.3, J_{6-1} = 1.6, J_{6-9} = 1.5 Hz, 1 H, H_6), 2.77 (ddd, J_{7-1} = 8.4, J_{7-6} = 6.6, J_{7-9} = 2.6 Hz, 1 H, H_7), 2.73 (ddd, J_{10-9} = 10.1, J_{10-3} = 3.9, J_{10-1} = 2.9 Hz, 1 H, H_{10}), 2.67 (dddd, J_{9-10} = 10.1, J_{9-5} = 4.0, J_{9-7} = 2.6, J_{9-6} = 1.5 Hz, 1 H, H_9), 2.54 (dtd, J_{3-10} = 3.9, J_{3-4s} = 1.6, J_{3-4a} = 1.6, J_{3-5} = 1.2 Hz, 1 H, H_3), 2.48 (ddd, J_{1-7} = 8.1, J_{1-10} = 2.9, J_{1-6} = 1.6 Hz, 1 H, H_1), 1.97 (dt, J_{4a-4s} = 11.4, J_{4a-3} = 1.6, J_{4a-5} = 1.6 Hz, 1 H, H_{4a}), 1.93 (dt, J_{4s-4a} = 11.4, J_{4s-3} = 1.6, J_{4s-5} = 1.6 Hz, 1 H, H_{4s}), 1.28 (s, 3 H, CH_3);

<u>IR spectrum</u> (KBr, Fig VI-53): 2978 (sh, s), 2961 (s), 2950 (sh, vs), 2918 (m), 2870 (sh, vs), 2860 (m), 1750 (vs), 1730 (sh, vs), 1710 (sh, vs), 1451 (m), 1368 (w), 1320 (m), 1284 (m), 1272 (m), 1239 (m), 1217 (m), 1191 (m), 1180 (m), 1137 (m), 1121 (m), 1058 (sh, m), 1040 (s), 969 (m), 949 (m), 893 (m), 855 (w), 842 (w), 835 (sh, w), 776 (w), 762 (w), 751 (w) cm^{-1};

<u>Mass spectrum</u> (70 eV, Fig VI-54): m/e (relative intensity) 189 (M + 1, 14.1), 188 (M^+, 100.0), 160 (14.5), 159 (11.8), 145 (29.1), 132 (11.3), 131 (14.1), 118 (5.8), 117 (42.5), 116 (6.5), 115 (20.1), 105 (10.5), 94 (7.1), 91 (20.8), 80 (70.7), 79 (13.2), 77 (8.7), 66 (6.4), 65 (8.2);

^{13}<u>C and Spin Echo spectra</u> (20 MHz, $CDCl_3$, Fig VI-55): δ 211.67 (C_8), 210.46 (C_{11}), 55.64 (C_{10}), 53.04 (C_9), 50.21 (C_3), 48.38 (C_1), 45.99 (C_2), 44.61 (C_5), 44.06 (C_6), 40.30 (C_7), 37.77 (C_4), 20.69 (C_{methyl});

<u>HOMCOR NMR spectrum</u> (300 MHz, $CDCl_3$, Fig VI-56);

<u>HOM2DJ NMR spectrum</u> (300 MHz, $CDCl_3$, Fig VI-57 and VI-58);

<u>HETCOR NMR spectrum</u> (300 and 75 MHz, $CDCl_3$, Fig VI-59 and VI-60).

<u>Anal</u>. Calculated for $C_{12}H_{12}O_2$: C, 76.57; H, 6.43. Found: C, 76.42; H, 6.47.

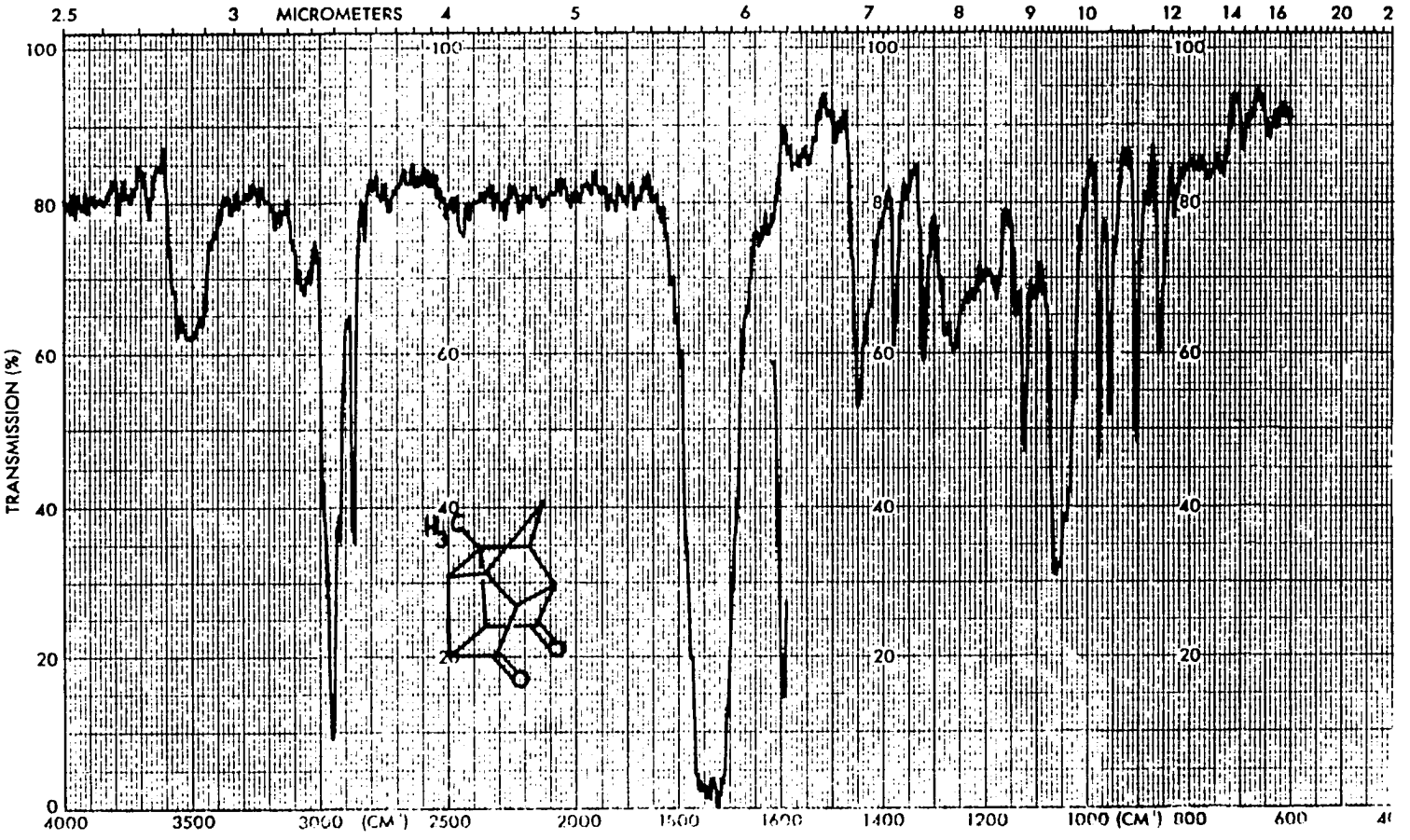

Figure VI-53. IR Spectrum of
2-Methylpentacyclo[5.4.0.0^{2,6}.0^{3,10}.0^{5,9}]undecane-8,11-dione IVc (KBr).

FIGURE VI-54

Mass Spectrum of

2-Methylpentacyclo[5.4.0.0^{2,6}.0^{3,10}.0^{5,9}]undecane-8,11-dione

IVc.

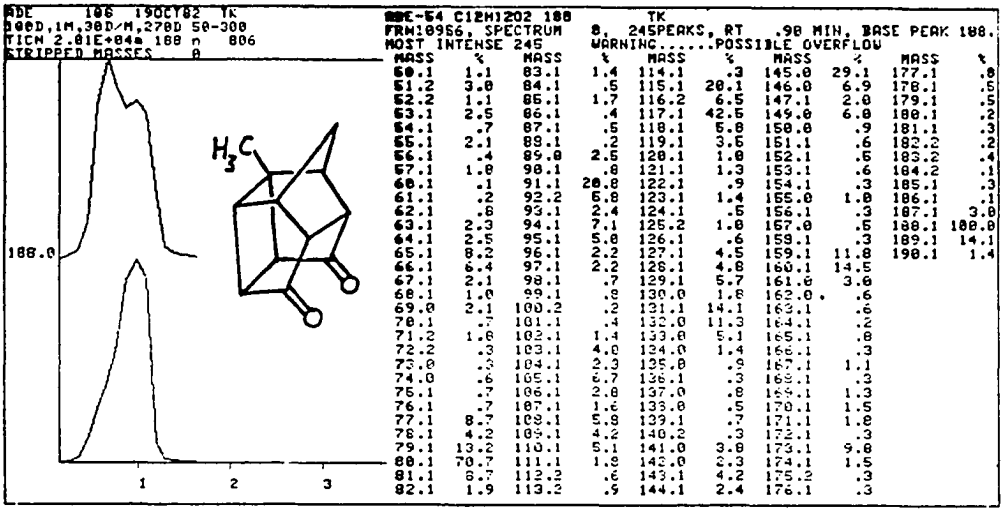

FIGURE VI-55

20 MHz ^{13}C and Spin Echo NMR Spectra of
2-Methylpentacyclo[5.4.0.0^{2,6}.0^{3,10}.0^{5,9}]undecane-8,11-dione
IVc ($CDCl_3$).

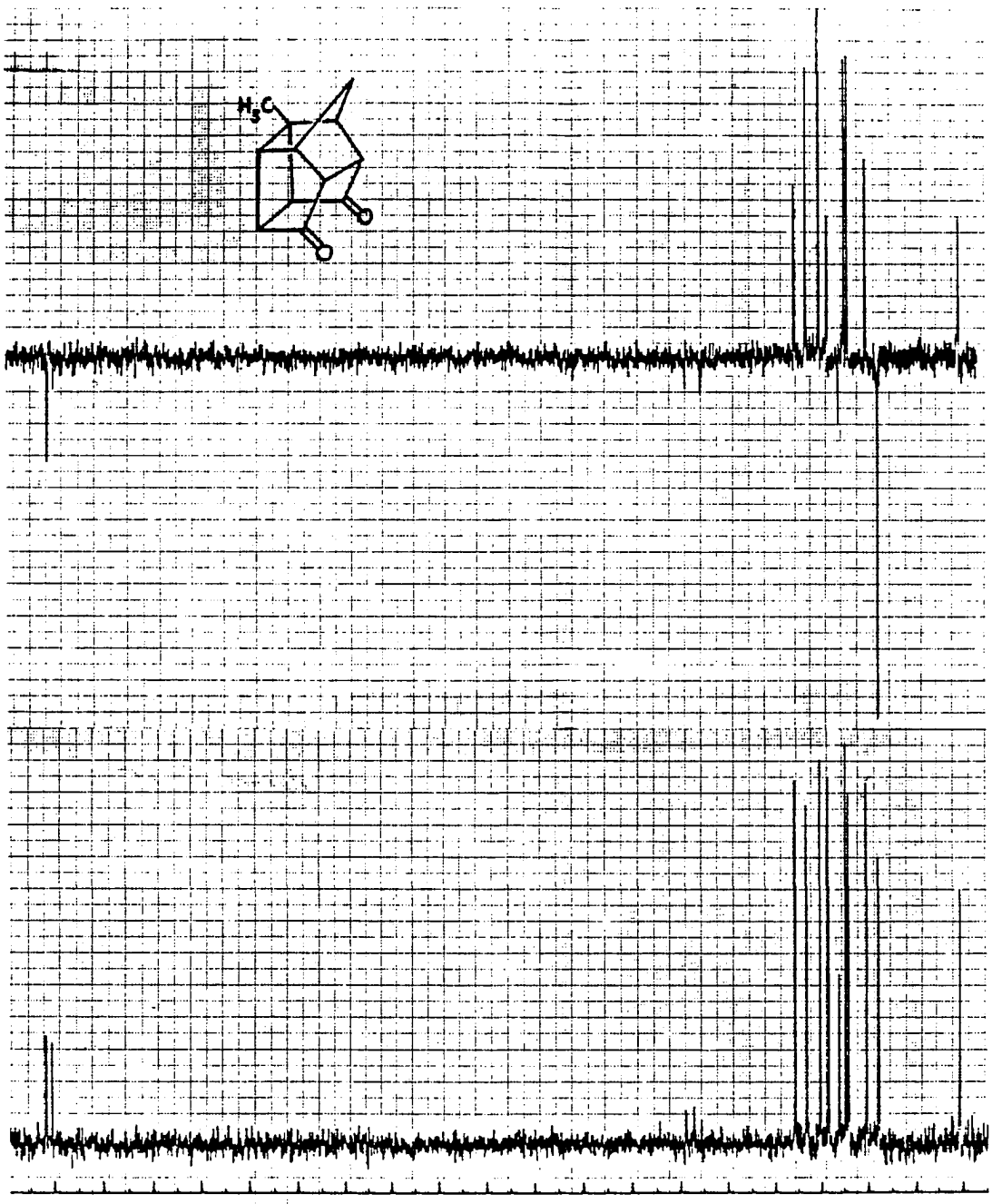

FIGURE VI-56

300 MHz ^{1}H HOMCOR NMR Spectrum of
2-Methylpentacyclo[5.4.0.0^{2,6}.0^{3,10}.0^{5,9}]undecane-8,11-dione
IVc ($CDCl_3$).

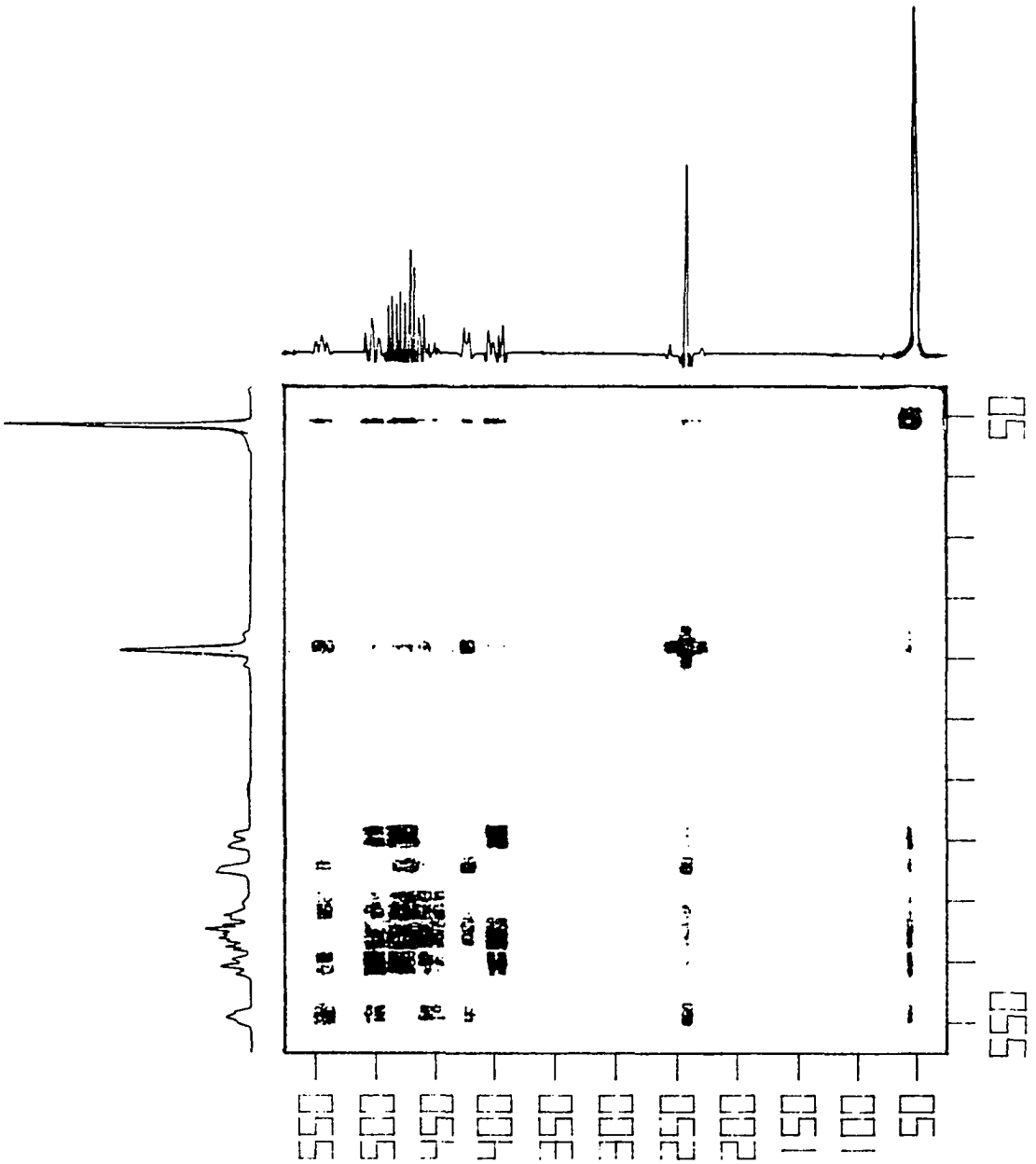

FIGURE VI-57

300 MHz ^{1}H HOM2DJ NMR Spectrum of
2-Methylpentacyclo[5.4.0.0^{2,6}.0^{3,10}.0^{5,9}]undecane-8,11-dione
IVc ($CDCl_3$).

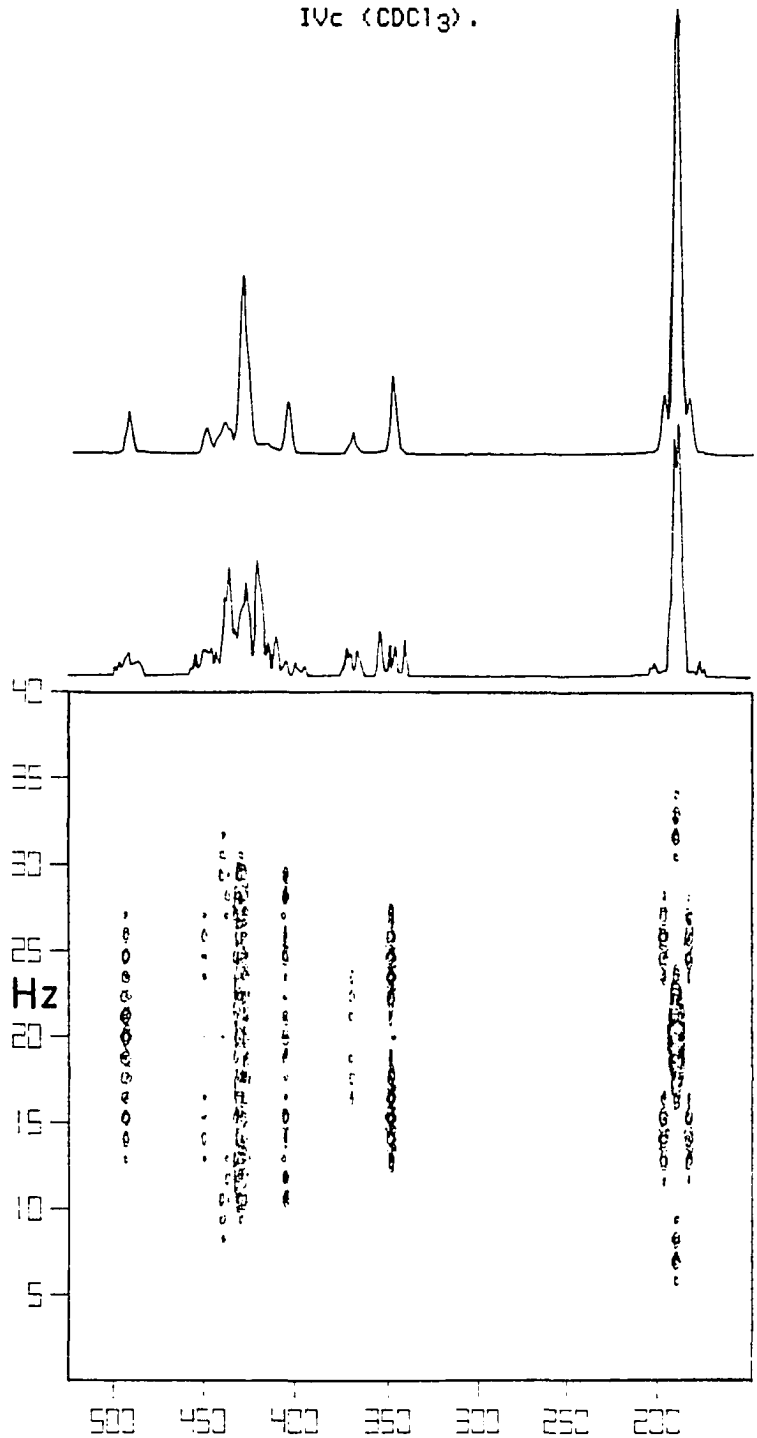

FIGURE VI-58

Stacked Plot of the HOM2DJ NMR Spectrum of Fig VI-57 of 2-Methylpentacyclo[5.4.0.0^{2,6}.0^{3,10}.0^{5,9}]undecane-8,11-dione IVc ($CDCl_3$).

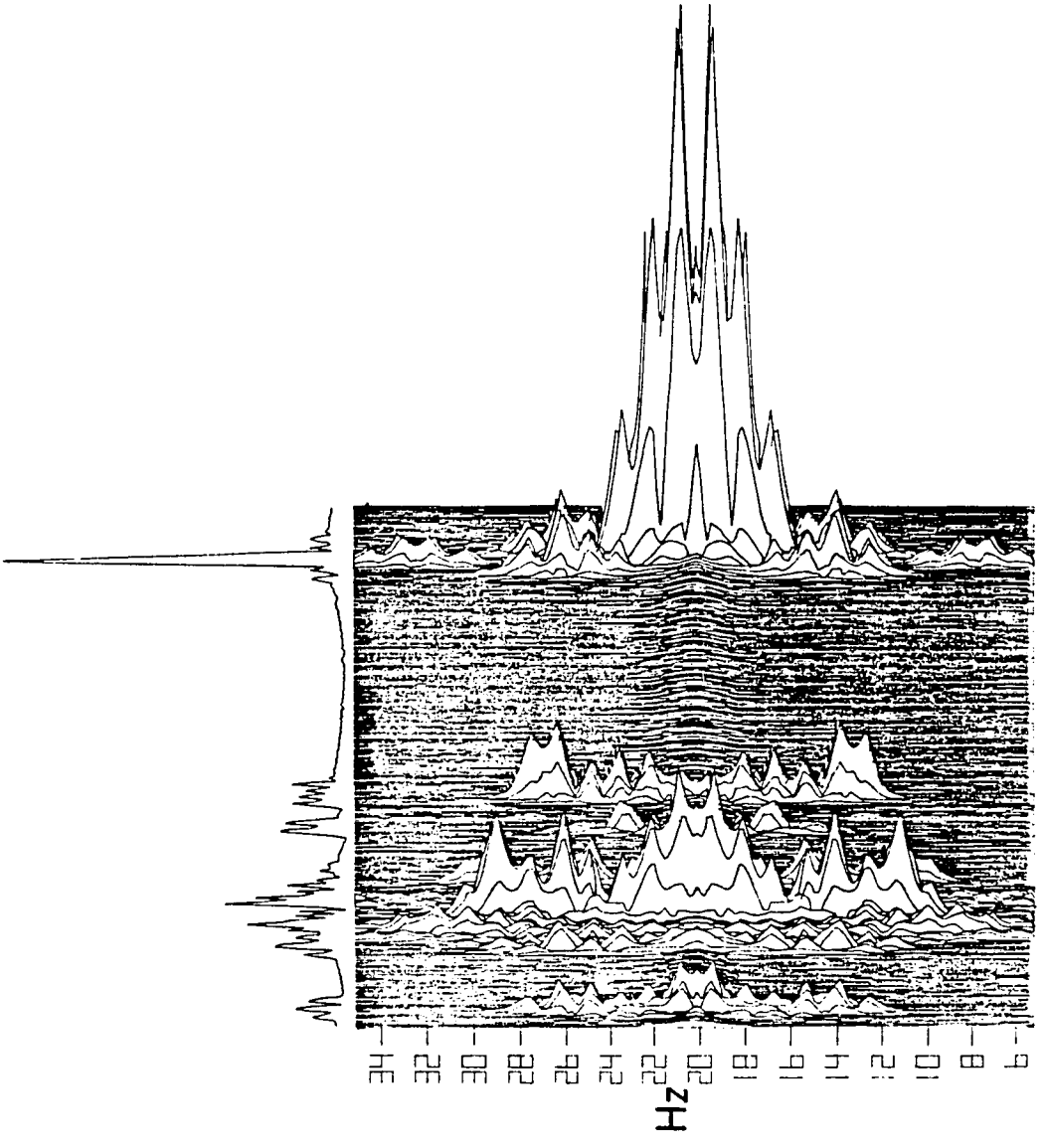

FIGURE VI-59

300 MHz ^{1}H and 75 MHz ^{13}C HETCOR NMR Spectrum of 2-Methylpentacyclo[5.4.0.0^{2,6}.0^{3,10}.0^{5,9}]undecane-8,11-dione IVc ($CDCl_3$).

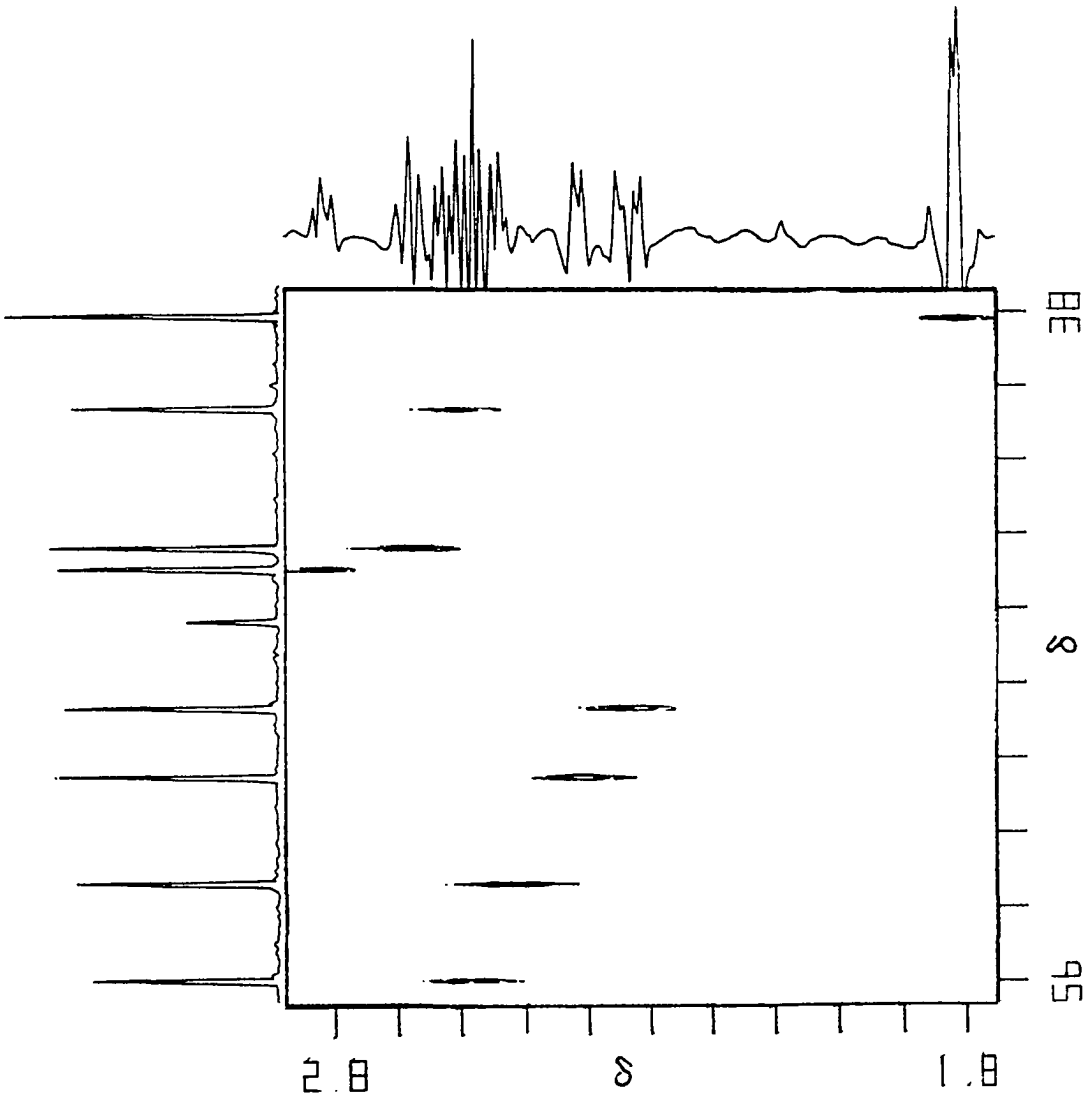

FIGURE VI-60

Stacked Plot of the HETCOR NMR Spectrum of Fig VI-59 of 2-Methylpentacyclo[5.4.0.0^{2,6}.0^{3,10}.0^{5,9}]undecane-8,11-dione IVc ($CDCl_3$).

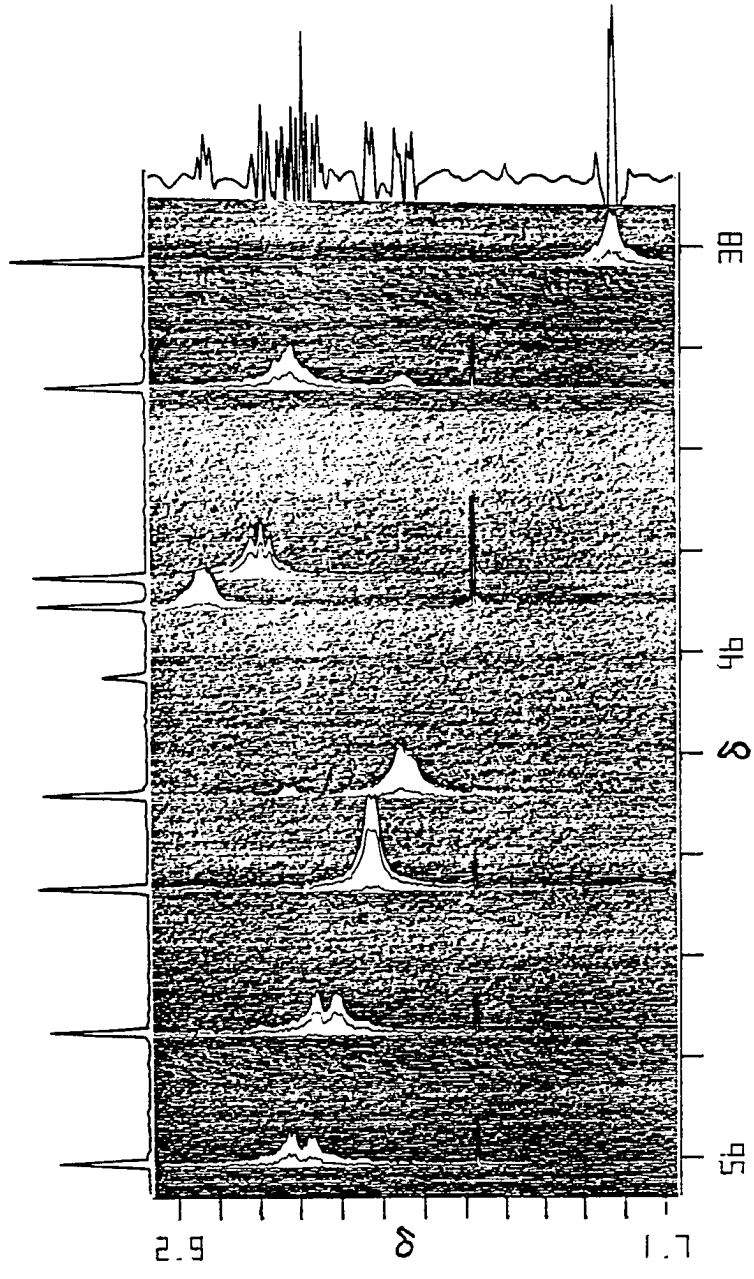

3-Methylpentacyclo[5.4.0.0^{2,6}.0^{3,10}.0^{5,9}]undecane-8,11-dione (IVd). Intramolecular photochemical cyclization of IIId to IVd was performed by using the method described above for the photolytic conversion of IIIb to IVb. Compound IVd prepared via this procedure was obtained as a colorless microcrystalline solid (85%): mp 175°C.

^{1}H NMR spectrum (300 MHz, $CDCl_3$, Fig VI-61): δ 3.28 (dddt, J_{6-2} = 10.8, J_{6-7} = 6.0, J_{6-5} = 5.2, J_{6-1} = 1.8, J_{6-9} = 1.8 Hz, 1 H, H_6), 2.87 (m, J_{7-6} = 6.0, J_{7-9} = 2.4 Hz, 1 H, H_7), 2.87 (m, J_{2-6} = 10.8, J_{2-10} = 2.0 Hz, 1 H, H_2), 2.85 (m, J_{5-6} = 5.2, J_{5-9} = 4.0, J_{5-4a} = 1.5, J_{5-4s} = 1.4 Hz, 1 H, H_5), 2.8 (m, J_{1-10} = 2.5, J_{1-6} = 1.8 Hz, 1 H, H_1), 2.78 (dddd, J_{9-10} = 9.7, J_{9-5} = 4.0, J_{9-7} = 2.4, J_{9-6} = 1.8 Hz, 1 H, H_9), 2.45 (ddd, J_{10-9} = 9.7, J_{10-1} = 2.5, J_{10-2} = 2.0 Hz, 1 H, H_{10}), 1.99 (dd, J_{4s-4a} = 11.2, J_{4s-5} = 1.4 Hz, 1 H, H_{4s}), 1.84 (dd, J_{4a-4s} = 11.2, J_{4a-5} = 1.5 Hz, 1 H, H_{4a}) 1.22 (s, 3 H, CH_3);

IR spectrum (KBr pellet, Fig VI-62): 2982 (s), 2962 (s), 2940 (s), 2918 (s), 2860 (s), 2820 (w), 1750 (vs), 1720 (vs), 1700 (sh, vs), 1447 (s), 1373 (m), 1313 (m), 1273 (s), 1240 (s), 1181 (s), 1118 (m), 1092 (m), 1057 (vs), 971 (m), 912 (m), 860 (m), 814 (w), 774 (w), 750 (w) cm^{-1};

Mass spectrum (70 eV, Fig VI-63): m/e (relative intensity) 189 (M + 1, 13.5), 188 (M^+, 100.0), 173 (8.6), 160 (15.5), 159 (11.2), 145 (32.8), 132 (27.9), 131 (25.3), 117 (91.7), 115 (29.4), 91 (26.1), 81 (6.5), 80 (36.1), 79 (14.4), 77 (15.9), 65 (7.8);

^{13}C and Spin Echo NMR spectra (20 MHz, $CDCl_3$, Fig VI-64): δ 211.92 (C_8 or C_{11}), 211.27 (C_{11} or C_8), 59.91 (C_{10}), 55.39 (C_9), 52.33 (C_3), 45.79 (C_4), 44.31 (C_5), 44.08 (C_7), 44.00 (C_2), 42.86 (C_9), 39.50 (C_6), 15.58 (C_{methyl}): assignments for carbon atoms C_7 and C_2 are tentative;

HOMCOR NMR spectrum (300 MHz, $CDCl_3$, Fig VI-65);

HOM2DJ NMR spectrum (300 MHz, $CDCl_3$, Fig VI-66 and VI-67);

HETCOR NMR spectrum (300 and 75 MHz, $CDCl_3$, Fig VI-68 through

FIGURE VI-61

300 MHz ^{1}H NMR Spectrum of
3-Methylpentacyclo[5.4.0.0^{2,6}.0^{3,10}.0^{5,9}]undecane-8,11-dione
IVd ($CDCl_3$/TMS).

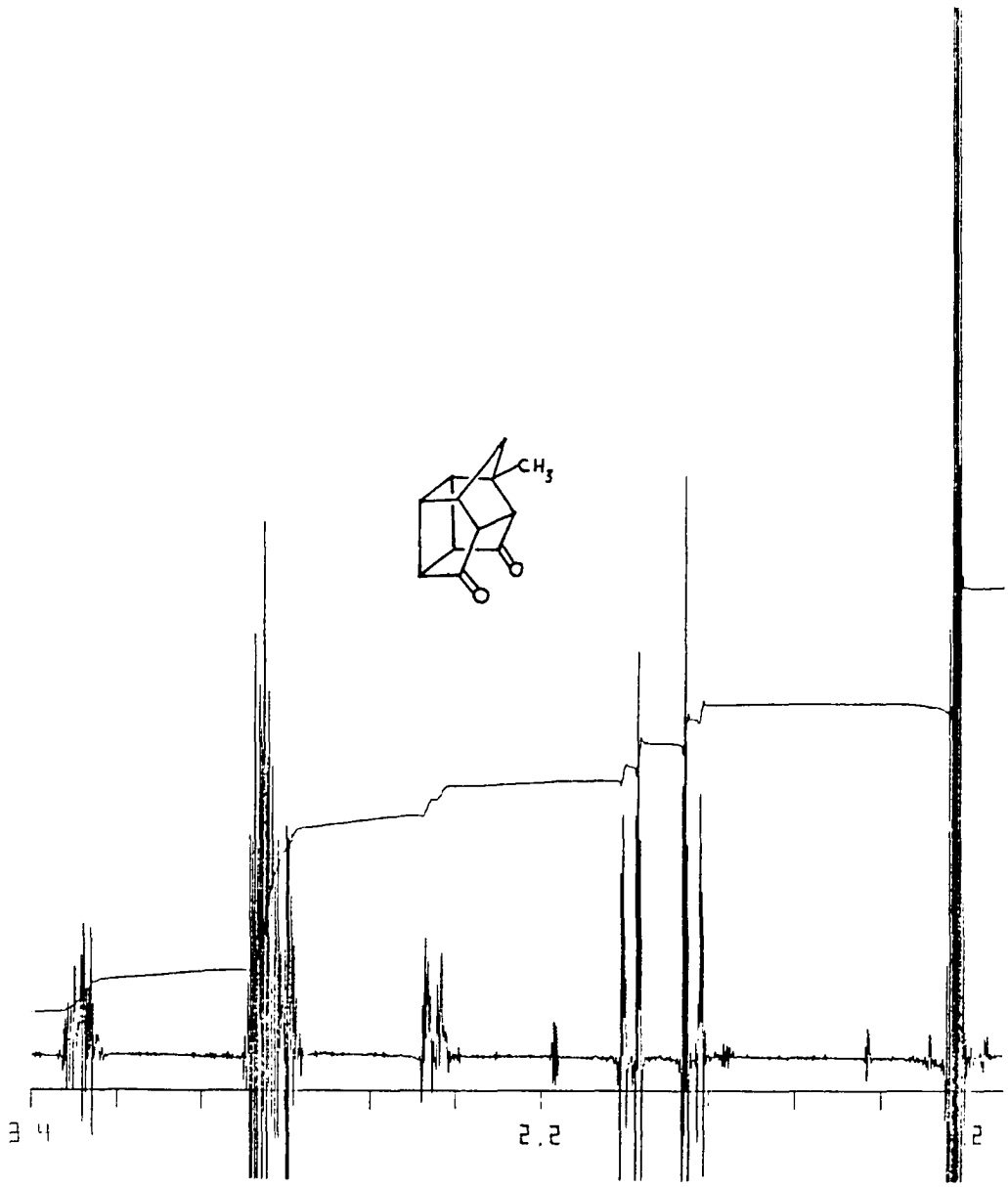

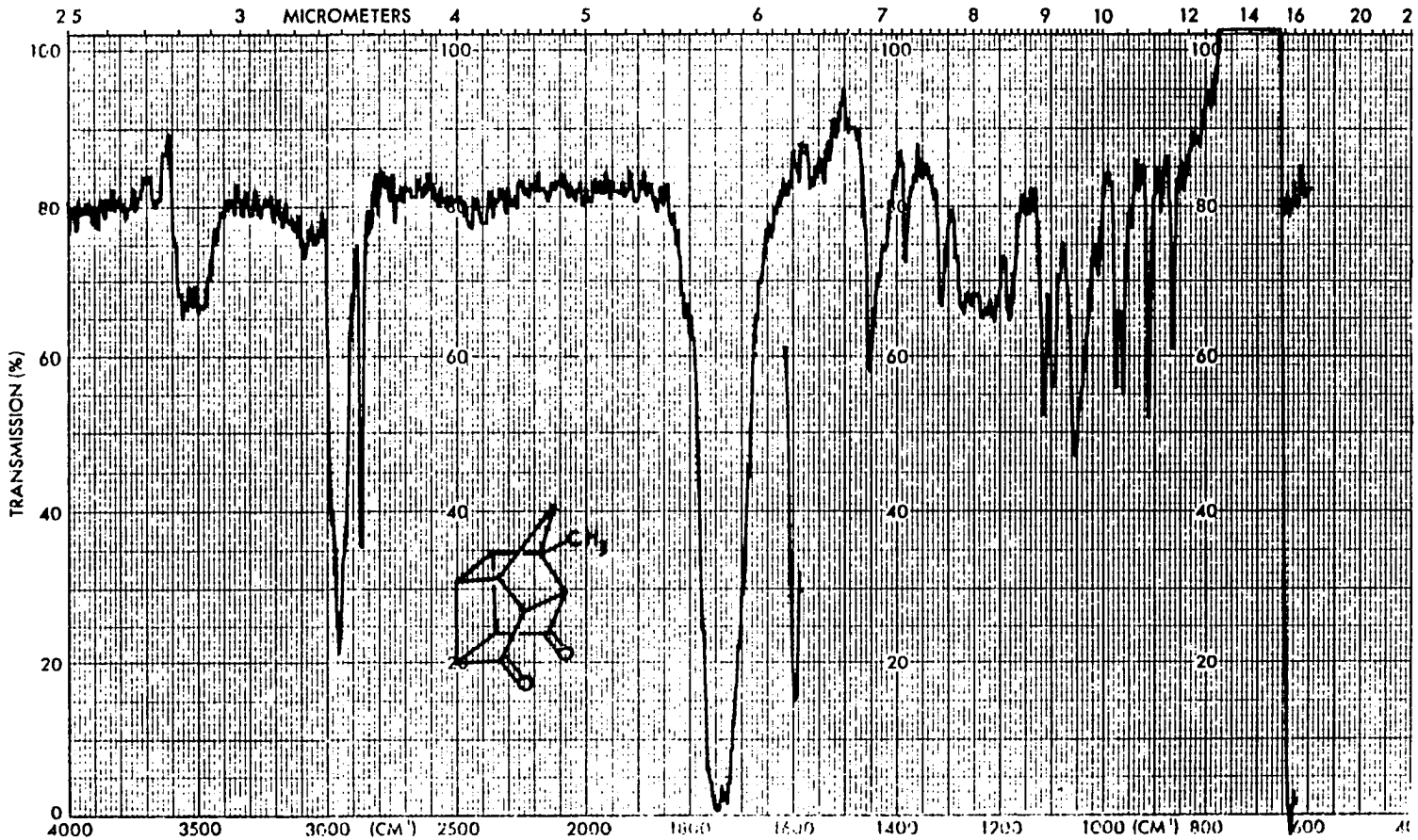

Figure VI-62. IR Spectrum of
3-Methylpentacyclo[5.4.0.0^{2,6}.0^{3,10}.0^{5,9}]undecane-8,11-dione IVd (KBr).

FIGURE VI-63

Mass Spectrum of

3-Methylpentacyclo[5.4.0.0^{2,6}.0^{3,10}.0^{5,9}]undecane-8,11-dione

IVd.

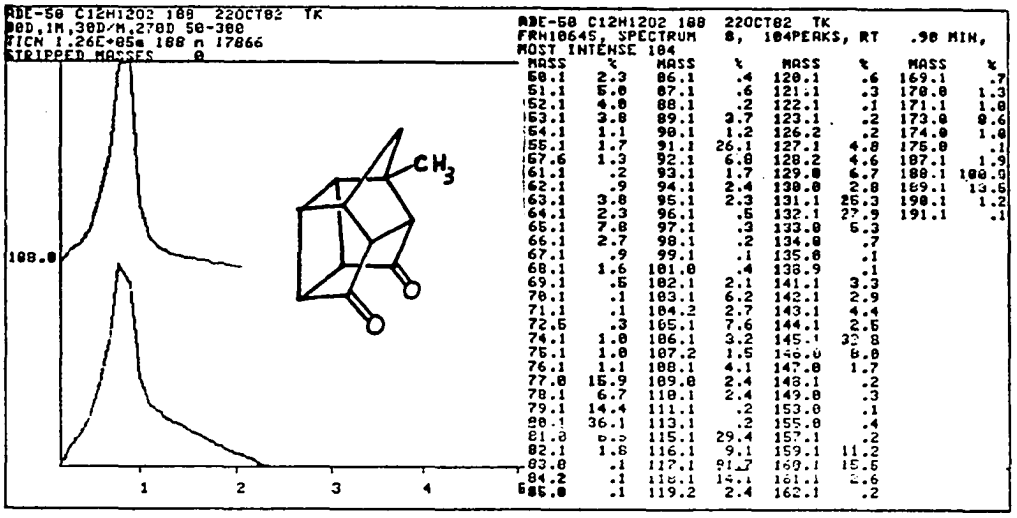

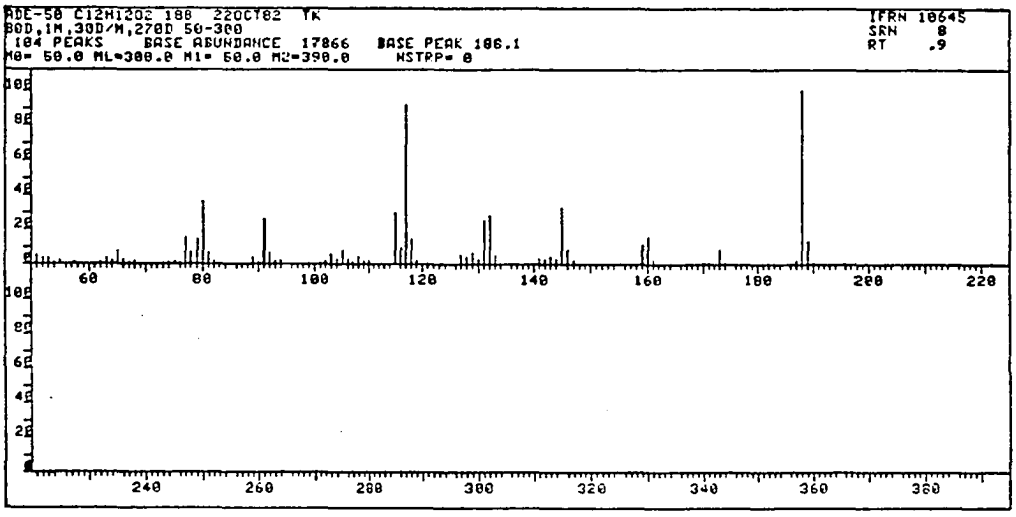

FIGURE VI-64

20 MHz ^{13}C and Spin Echo NMR Spectra of
3-Methylpentacyclo[5.4.0.0^{2,6}.0^{3,10}.0^{5,9}]undecane-8,11-dione
IVd ($CDCl_3$).

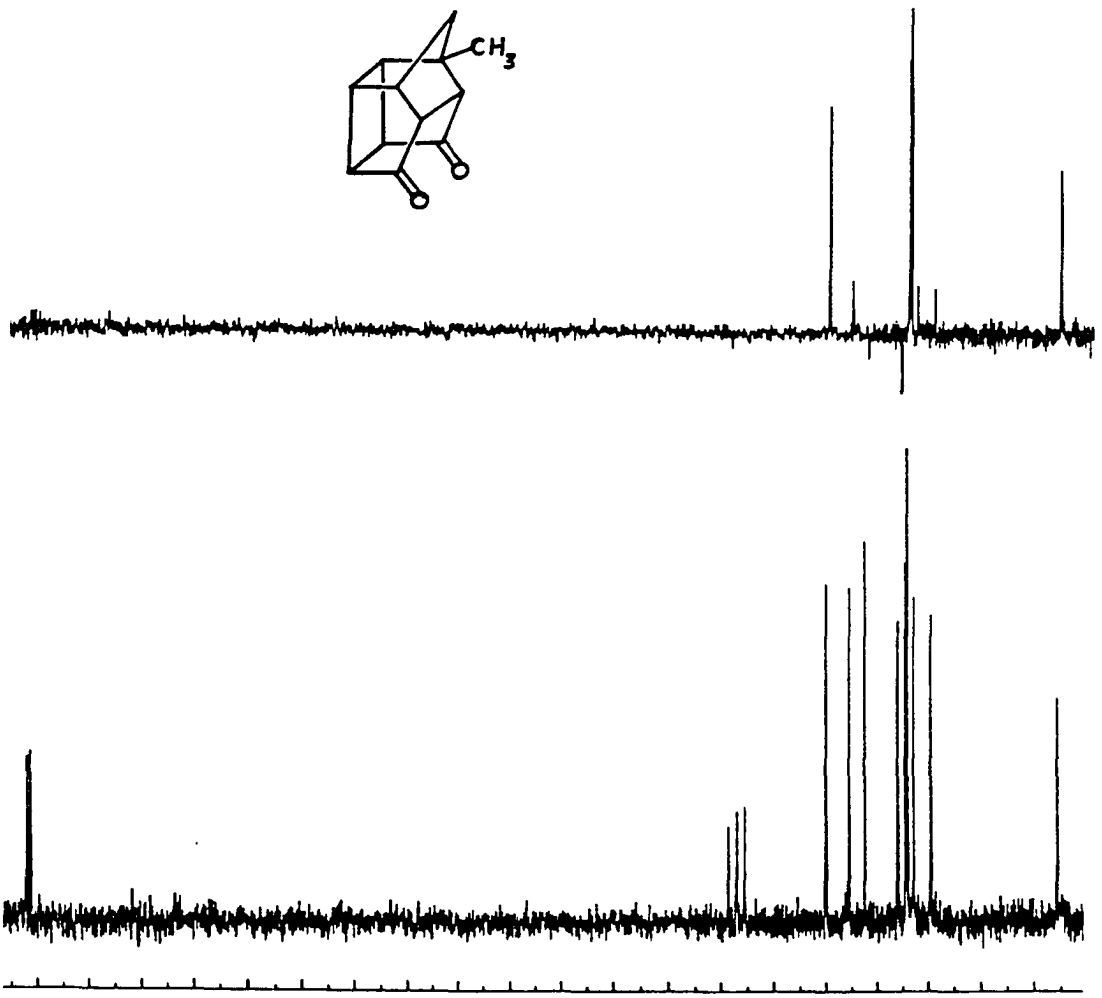

FIGURE VI-65

300 MHz ^{1}H HOMCOR NMR Spectrum of
3-Methylpentacyclo[5.4.0.0^{2,6}.0^{3,10}.0^{5,9}]undecane-8,11-dione
IVd ($CDCl_3$).

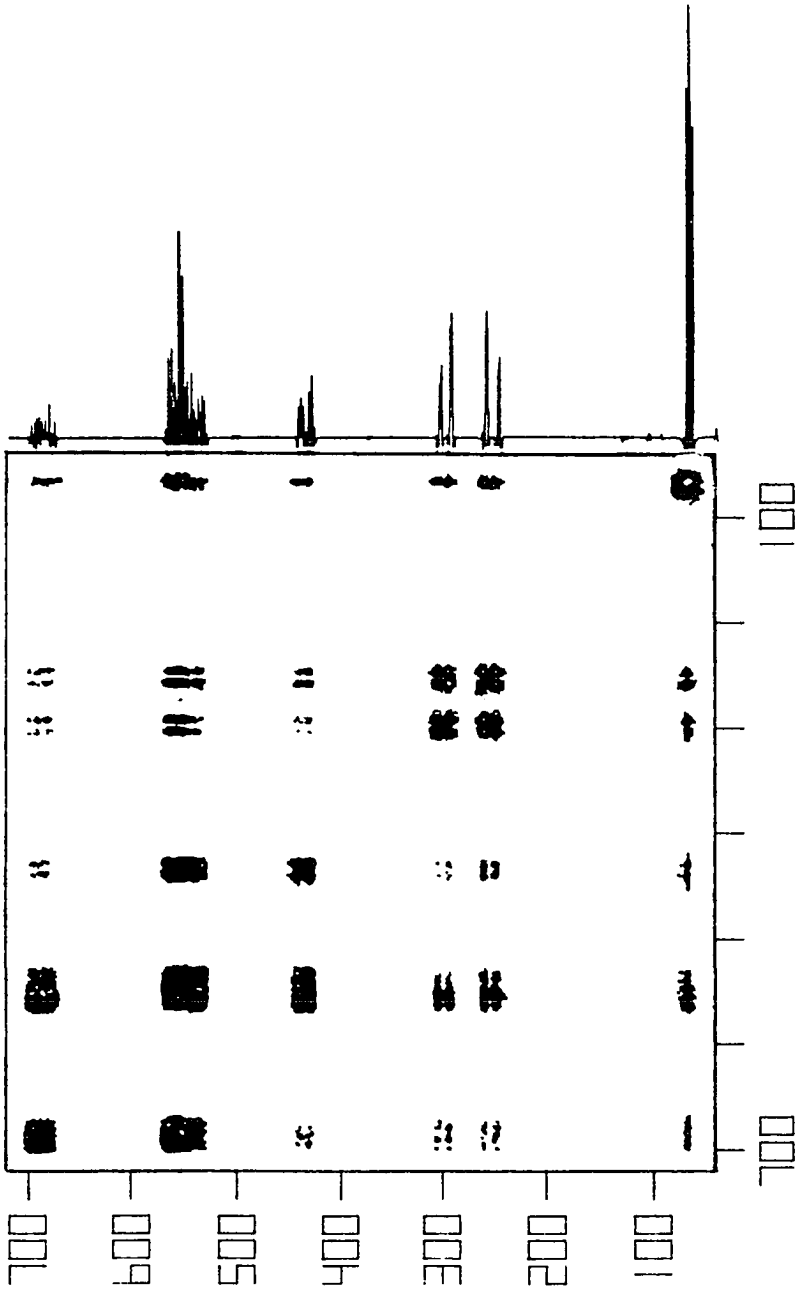

FIGURE VI-66

300 MHz ^{1}H HOM2DJ NMR Spectrum of
3-Methylpentacyclo[5.4.0.0^{2,6}.0^{3,10}.0^{5,9}]undecane-8,11-dione
IVd ($CDCl_3$).

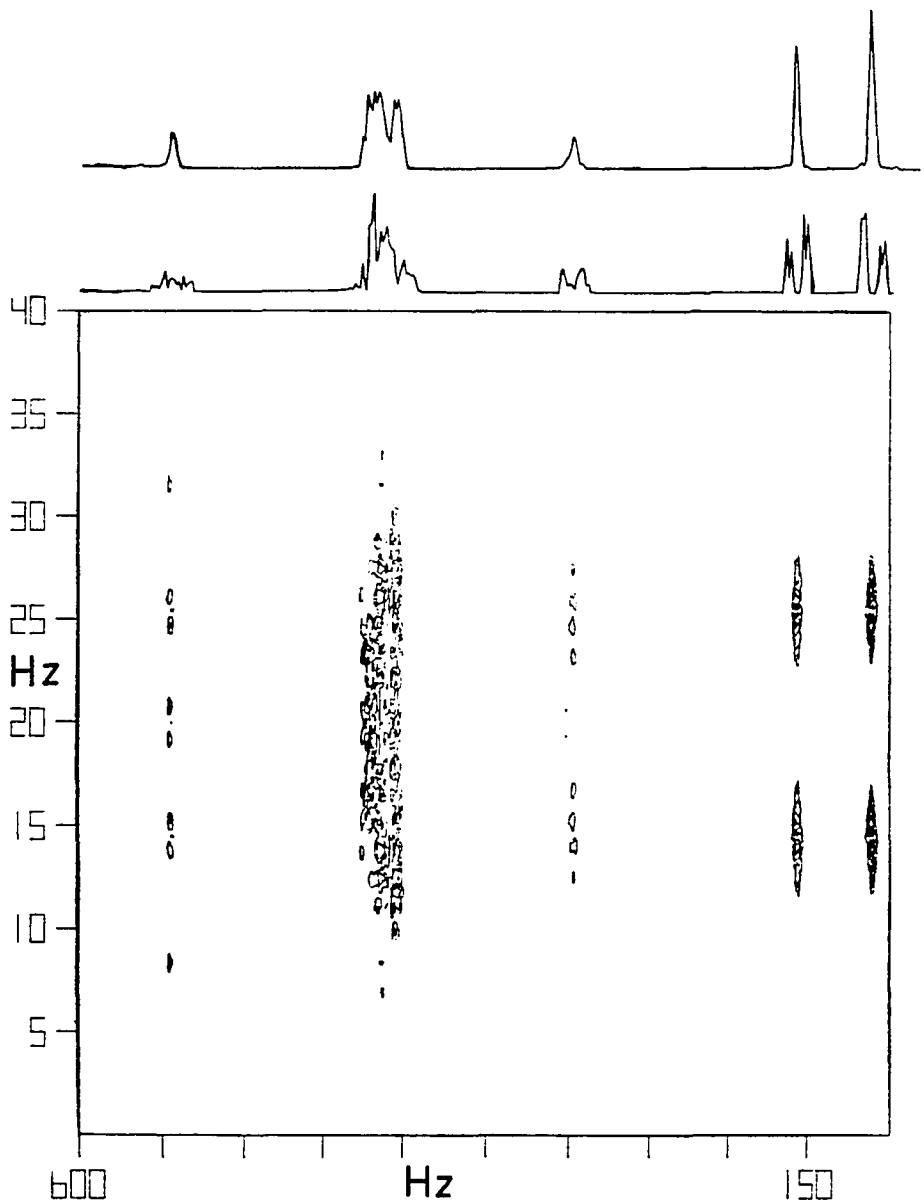

FIGURE VI-67

Stacked Plot of the HOM2DJ NMR Spectrum of Fig VI-66 of 3-Methylpentacyclo[5.4.0.0^{2,6}.0^{3,10}.0^{5,9}]undecane-8,11-dione IVd ($CDCl_3$).

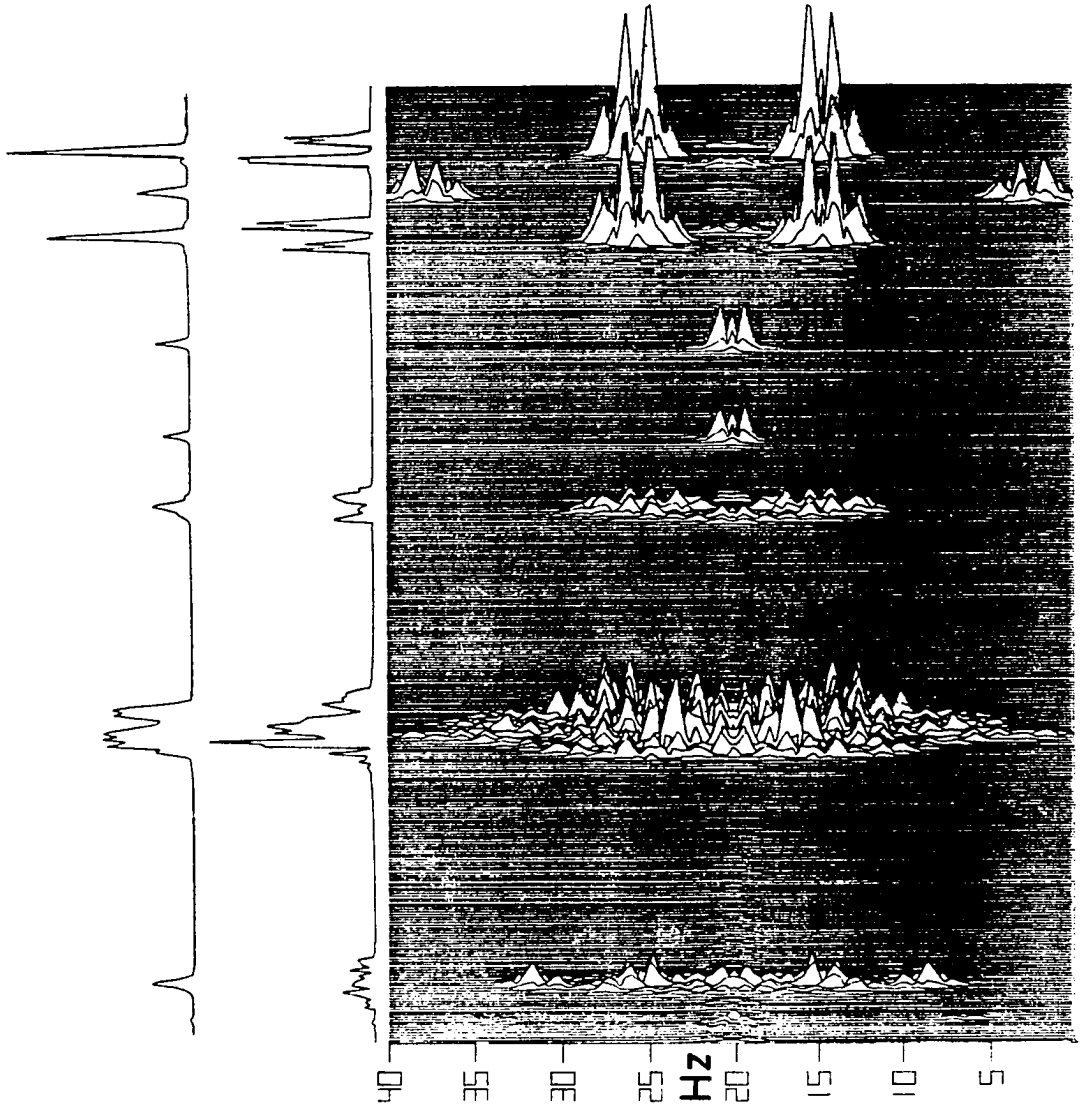

FIGURE VI-68

300 MHz ^{1}H and 75 MHz ^{13}C HETCOR NMR Spectrum of 3-Methylpentacyclo[5.4.0.0^{2,6}.0^{3,10}.0^{5,9}]undecane-8,11-dione IVd ($CDCl_3$).

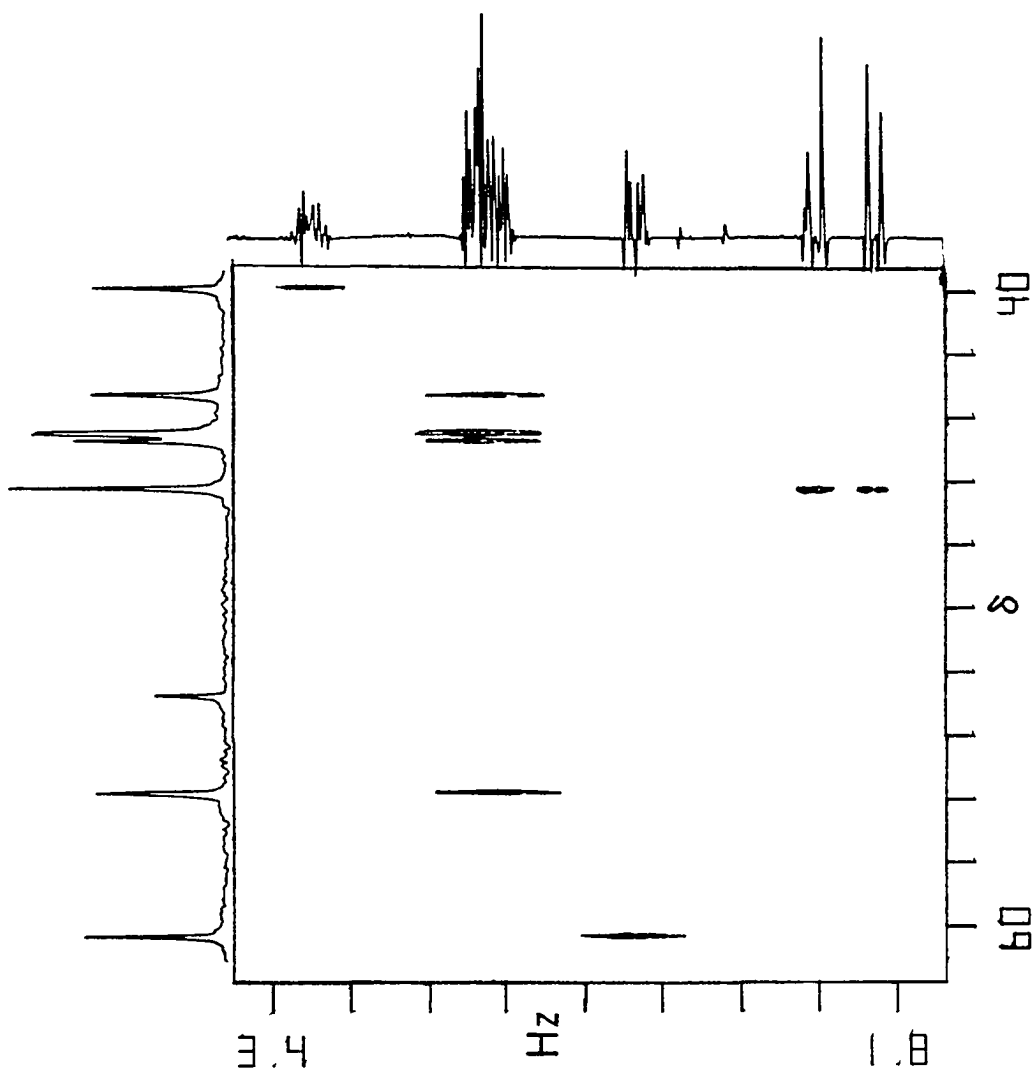

FIGURE VI-69

Expanded Contour Plot of the HETCOR NMR Spectrum of Fig VI-68 which Includes the 1.8-3.4 ^{1}H and 38-62 ppm ^{13}C Spectral Region of 3-Methylpentacyclo[5.4.0.0^{2,6}.0^{3,10}.0^{5,9}]undecane-8,11-dione IVd ($CDCl_3$).

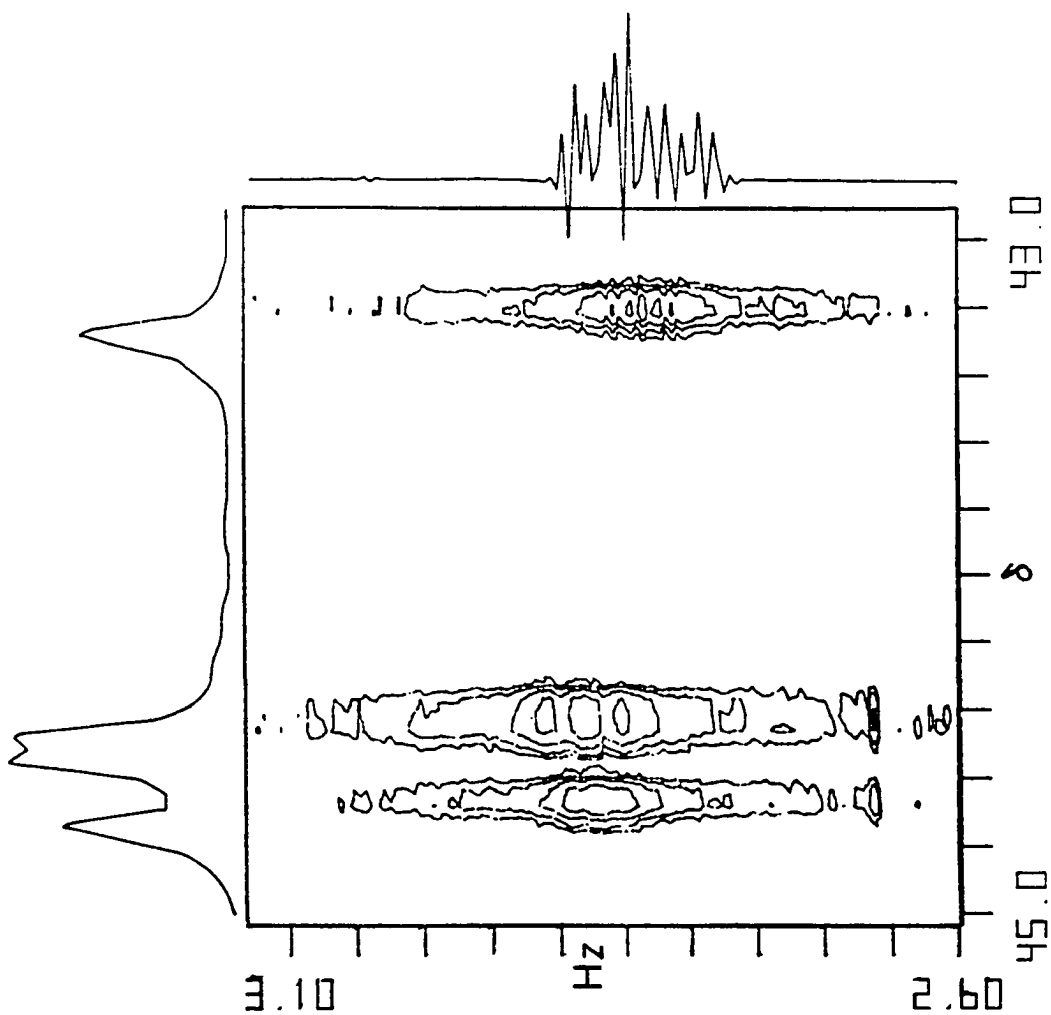

FIGURE VI-70

Stacked Plot of the HETCOR NMR Spectrum of Fig VI-68 of 3-Methylpentacyclo[5.4.0.0^{2,6}.0^{3,10}.0^{5,9}]undecane-8,11-dione IVd ($CDCl_3$).

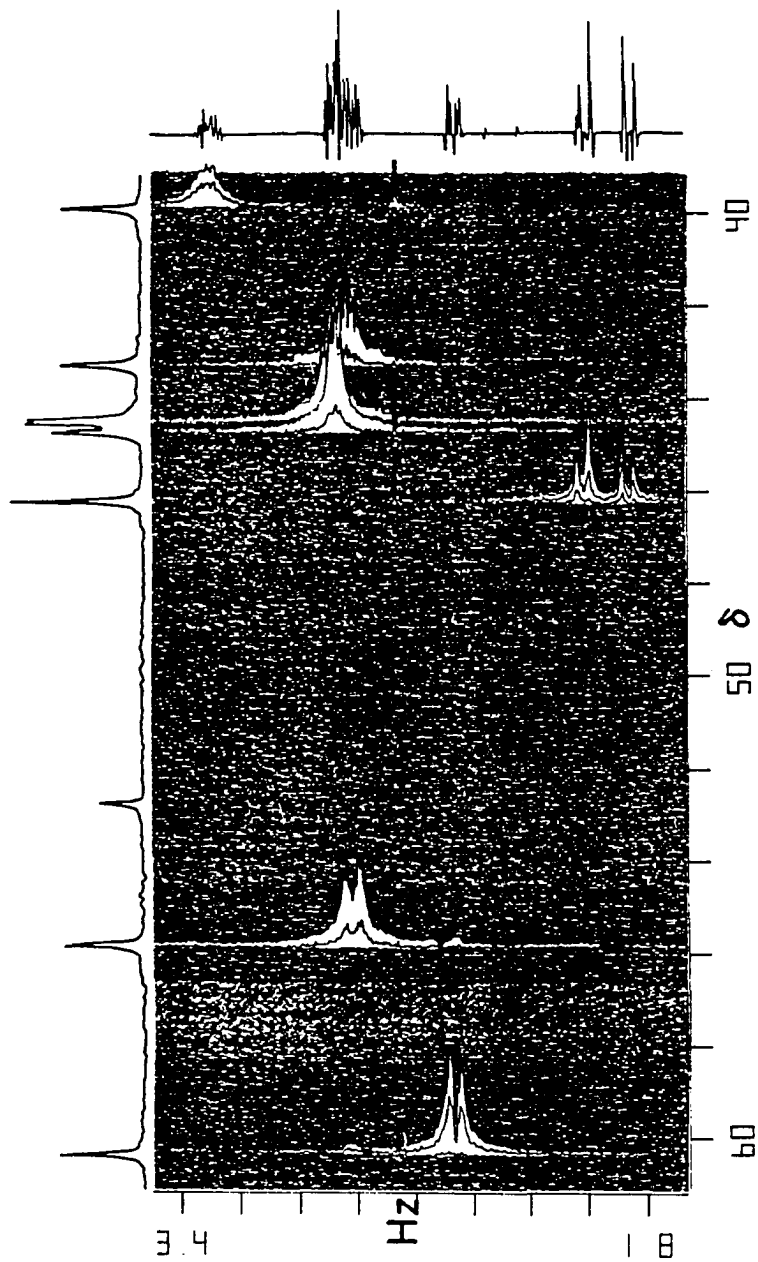

VI-70).

Anal. Calculated for $C_{12}H_{12}O_2$: C, 76.57; H, 6.43. Found: C, 76.84; H, 6.48.

Single-Crystal X-ray Structural Analysis of IVd

A perspective view of IVd is shown in Fig VI-1. A summary of the crystallographic data is listed in Table VI-1. The unit cell parameters were determined from a least squares fit of the ±2θ values of 40 reflections distributed throughout reciprocal space. The measurement of the density by flotation in aqueous KI was hampered by the apparent reaction of the material with water. Lattice constants and intensity data were measured on a Enraf-Nonius CAD-4 diffractometer. Three intensity monitors, remeasured after every 2 hours of X-ray exposure, showed an overall change of 4.8%. Of the 1813 unique data, 147 had measured intensities with $I < 2\sigma(I)$. These weak data were assigned $I = \sigma(I)$.

All non-hydrogen atoms were located on an E map based upon 256 data with the largest E values.[19] The structure was refined by using SHELX[20] with weights of $w = \sigma^{-2}(F)$. Hydrogen atoms were located on a difference electron density map. An analysis of the variance after refinement of the data revealed no systematic variation of $\Sigma w(|F_o|-|F_c|)$[14] with either sin θ or F. The scattering factors for C and O were from Cromer and Mann[21] and the scattering factors for H were from Stewart, Davidson, and Simpson.[22] Atomic positional and thermal parameters are listed in Tables VI-3 and VI-4, respectively. Bond lengths and bond angles for non-hydrogen atoms are listed in Tables VI-5 and VI-6, respectively.

Discussion: Analysis of NMR Spectra of Systems III and IV.

Table VI-7 lists the ^1H chemical shifts and coupling constants of the 1,4,4a,8a-tetrahydro-endo-1,4-methanonaphthalene-5,8-diones IIIa-IIId, while Table VI-8 lists the ^1H chemical shifts of

Table VI-1

Table of Crystallographic Data for
3-Methylpentacyclo[5.4.0.0^{2,6}.0^{3,10}.0^{5,9}]undecane-8,11-dione
(IVd).

(a) Preliminary Information

Formula, F.W.	$C_{12}H_{12}O_2$, 188.23	
Space group, Z	$P2_1/n$, 4	
Cell constants	294(2)K	138(2)K
a(Å)	9.933(2)	9.854(7)
b	11.576(2)	11.4664(9)
c	7.865(2)	7.8100(6)
β	90.00(2)	90.231(7)
V(Å^3)	904.4	882.5
Radiation	MoKα_1	CuKα_1
ρ_c (g cm^{-3})	1.382	
ρ_m	1.37	

Intensity Data and Results

Radiation	CuKα (λ = 1.5418)	
Data limit	2(θ)<150°	
Scan method		(ω)/2θ
Temperature		138(2)K
Unique Data		1813
R		0.044
R_w	0.062	
Maximum on final difference electron density map	0.20	

TABLE VI-2

Atomic Positional Parameters for Carbon, Oxygen, and Hydrogen.[a]

Atom	x	y	z
C_1	-4773(12)	33765(11)	26910(16)
C_2	7689(12)	29952(11)	16082(16)
C_3	1168(12)	22499(11)	2303(16)
C_4	-8552(12)	14595(11)	11676(16)
C_5	-296(12)	6469(11)	24481(17)
C_6	14656(13)	9221(11)	23325(16)
C_7	15981(12)	21853(11)	28890(17)
C_8	7062(13)	22149(11)	45207(17)
C_9	-5071(13)	14272(11)	39718(17)
C_{10}	-13132(12)	22197(11)	27167(16)
C_{11}	931(14)	34348(12)	45168(17)
C_{12}	-12177(15)	44365(12)	19895(21)
O_3	2922(10)	23110(9)	-13018(12)
O_6	23772(1)	2583(9)	19637(14)
H_2	1312(16)	3626(15)	1116(21)
H_4	-1519(18)	1111(17)	444(23)
H_5	-297(17)	-222(15)	2433(21)
H_7	2548(2)	2404(17)	3044(24)
H_8	1223(17)	1974(16)	5546(24)
H_9	-997(16)	1103(15)	4938(21)
H_{10}	-2310(20)	2375(17)	2869(23)
H_{11a}	752(20)	4023(17)	4667(24)
H_{11b}	-620(19)	3557(16)	5370(24)
H_{12a}	-1507(19)	4314(18)	777(26)
H_{12b}	-1984(20)	4616(18)	2670(24)
H_{12c}	-610(22)	5094(19)	2023(28)

(a) Carbon and oxygen values are multiplied by 10^5, and hydrogen values are multiplied by 10^4. Errors for the last digits are in parenthesis.

TABLE VI-3

Carbon, Oxygen, and Hydrogen Thermal Parameters.[a]

Atom	U11	U22	U33	U23	U13	U12
C_1	170(6)	160(6)	189(7)	-16(5)	2(5)	8(4)
C_2	154(6)	156(6)	180(6)	-3(5)	-8(5)	-23(4)
C_3	149(6)	160(6)	170(6)	-10(4)	-12(4)	17(4)
C_4	154(6)	175(6)	182(6)	-6(5)	-29(4)	-24(4)
C_5	177(6)	154(6)	221(7)	11(5)	-15(5)	-3(5)
C_6	179(6)	184(6)	184(6)	-2(5)	-20(5)	30(4)
C_7	133(6)	196(6)	196(6)	-30(5)	-30(5)	-1(4)
C_8	191(6)	216(6)	160(6)	-15(5)	-31(5)	19(5)
C_9	192(6)	188(6)	176(6)	28(5)	10(5)	-5(5)
C_{10}	138(6)	183(6)	193(7)	3(5)	3(5)	3(4)
C_{11}	221(7)	204(7)	192(7)	-47(5)	-9(5)	14(5)
C_{12}	262(7)	180(7)	316(8)	-7(5)	-32(6)	56(5)
O_3	257(5)	289(5)	173(5)	-3(4)	18(4)	-28(4)
O_6	223(5)	242(5)	401(7)	-64(4)	-8(4)	82(4)
H_2	21(4)					
H_4	29(4)					
H_5	23(4)					
H_7	32(5)					
H_8	29(5)					
H_9	22(4)					
H_{10}	28(5)					
H_{11a}	31(4)					
H_{11b}	30(4)					
H_{12a}	38(5)					
H_{12b}	34(5)					
H_{12c}	45(6)					

(a) Anisotropic thermal parameters for carbon and oxygen have been multiplied by 10^4 Å^2 and are of the form:

$T = \exp[-2\pi(h^2U_{11}a^{*2} + k^2U_{22}b^{*2} + l^2U_{33}c^{*2} + klU_{23}b^*\cdot c^* + hlU_{13}a^*\cdot c^* + hkU_{12}a^*\cdot b^*)]$.

The values for U(H) have been multiplied by 10^3 Å^2 and are of the form: $T = \exp(-8\pi^2U\sin^2\theta/\lambda^2)$.

TABLE VI-4

Bond Lengths Involving
Carbon and Oxygen atoms.

Atoms	Bond Length(Å)
C_1-C_2	1.557(2)
C_1-C_{10}	1.562(2)
C_1-C_{11}	1.532(2)
C_1-C_{12}	1.519(2)
C_2-C_3	1.515(2)
C_2-C_7	1.589(2)
C_3-O_3	1.212(2)
C_3-C_4	1.510(2)
C_4-C_5	1.589(2)
C_4-C_{10}	1.559(2)
C_5-C_6	1.510(2)
C_5-C_9	1.563(2)
C_6-O_6	1.213(2)
C_6-C_7	1.518(2)
C_7-C_8	1.551(2)
C_8-C_9	1.557(2)
C_8-C_{11}	1.524(2)
C_9-C_{10}	1.553(2)

TABLE VI-5

Bond Angles Involving

Carbon and Oxygen Atoms.

Atoms	Angle(deg)
$C_1-C_2-C_3$	102.18(9)
$C_1-C_2-C_7$	103.12(10)
$C_1-C_{10}-C_4$	108.09(10)
$C_1-C_{10}-C_9$	103.69(10)
$C_1-C_{11}-C_8$	96.07(10)
$C_2-C_1-C_{10}$	100.71(0)
$C_2-C_1-C_{11}$	103.33(1)
$C_2-C_1-C_{12}$	114.06(11)
$C_2-C_3-O_3$	127.37(12)
$C_2-C_3-C_4$	105.20(10)
$C_2-C_7-C_6$	109.52(10)
$C_2-C_7-C_8$	102.28(9)
$C_3-C_2-C_7$	109.46(10)
$C_3-C_4-C_5$	109.45(10)
$C_3-C_4-C_{10}$	103.11(10)
$C_4-C_3-O_3$	127.35(12)
$C_4-C_5-C_6$	109.71(10)
$C_4-C_5-C_9$	89.34(9)
$C_4-C_{10}-C_9$	90.79(9)
$C_5-C_4-C_{10}$	89.34(9)
$C_5-C_6-C_7$	105.38(10)
$C_5-C_6-O_6$	127.37(12)
$C_5-C_9-C_8$	107.97(10)
$C_5-C_9-C_{10}$	90.53(10)
$C_6-C_5-C_9$	102.87(10)
$C_6-C_7-C_8$	101.99(10)
$C_7-C_6-O_6$	127.15(12)
$C_7-C_8-C_9$	101.43(10)
$C_7-C_8-C_{11}$	104.15(10)
$C_8-C_9-C_{10}$	102.98(10)
$C_9-C_8-C_{11}$	103.17(10)
$C_{10}-C_1-C_{11}$	102.51(10)
$C_{10}-C_1-C_{12}$	115.58(10)
$C_{11}-C_1-C_{12}$	118.34(11)

TABLE VI-6

Chemical Shifts (δ) and Coupling Constants (Hz) for the Series of 1,4,4a,8a-Tetrahydro-endo-1,4-methanonaphthalene-5,8-diones IIIa-IIId.

Proton (J, Hz)	IIIa	IIIb	IIIc	IIId	litt[16]
H_1	3.544(m)	3.528(m)	3.296(m)	-	
J_{1-8a}	4.0	4.1	3.9	-	2.9-3.9
J_{1-2}	1.9	2.9	-	-	2.0-3.2
J_{1-3}	1.9	1.1	?	-	0.5-.95
J_{1-9a}	1.9	1.7	1.6	-	2.0-2.2
J_{1-9s}	1.8	1.5	1.4	-	1.5-1.6
H_4	3.544(m)	3.529(m)	3.411(m)	3.442(m)	
J_{4-4a}	4.0	4.1	4.2	4.2	2.0-3.9
J_{4-3}	1.9	2.8	3.0	2.8	2.0-3.2
J_{4-2}	1.9	1.1	-	?	0.5-.95
J_{4-9a}	1.9	1.7	1.6	2.0	2.0-2.2
J_{4-9s}	1.8	1.5	1.4	1.4	1.5-1.6
H_2	6.063(dd)	6.071(ddd)	-	5.858(d)	
J_{2-3}	-	5.8	-	5.6	5.6-6.1
J_{2-1}	1.9	2.9	-	-	2.0-3.2
J_{2-4}	1.9	1.1	-	?	0.5-.95
H_3	6.063(dd)	6.028(ddd)	5.623(dq)	6.042(dd)	
J_{3-2}	-	5.8	-	5.6	5.6-6.1
J_{3-4}	1.9	2.8	3.0	2.8	2.0-3.2
J_{3-1}	1.9	1.1	?	-	0.5-.95
$J_{3-methyl}$	-	?	1.6	?	?
H_{4a}	3.238(d)	3.241(m)	3.241(dd)	3.365(dd)	
J_{4a-8a}	-	8.0	8.7	8.2	7.4-9.2
J_{4a-4}	4.0	4.1	4.2	4.2	2.9-3.9
H_{8a}	3.238(d)	3.243(m)	3.285(dd)	2.879(d)	
J_{8a-4a}	-	8.0	8.7	8.2	7.4-9.2
J_{8a-1}	4.0	4.1	3.9	-	2.9-3.9
H_6	6.577(s)	-	6.582(d)	6.570(d)	
J_{6-7}	-	-	10.4	10.3	5.6-6.0
H_7	6.577(s)	6.500(q)	6.628(d)	6.529(d)	
J_{7-6}	-	-	10.4	10.3	5.6-6.0
$J_{7-methyl}$	-	1.4	-	-	?
H_{9a}	1.548(ddd)	1.537(ddd)	1.571(ddd)	1.444(dd)	
J_{9a-9s}	8.7	8.7	8.6	8.7	7.7-9.7
J_{9a-1}	1.9	1.7	1.6	-	2.0-2.2
J_{9a-4}	1.9	1.7	1.6	2.0	2.0-2.2
H_{9s}	1.450(ddd)	1.458(ddd)	1.433(ddd)	1.386(dd)	
J_{9s-9a}	8.7	8.7	8.6	8.7	7.7-9.7
J_{9s-1}	1.8	1.5	1.4	-	1.5-1.6
J_{9s-4}	1.8	1.5	1.4	1.4	1.5-1.6
CH_3	-	1.936(d)	1.619(d)	1.570(s)	
$J_{methyl-3}$	-	-	1.6	?	?
$J_{methyl-7}$	-	1.4	-	-	?

TABLE VI-7

Downfield (+) or Upfield (-) ^1H Chemical Shifts (δ) of the 1,4,4a,8a-Tetrahydro-endo-1,4-methanonaphthalene-5,8-diones IIIb-IIId Relative to Those of Unsubstituted Parent Compound IIIa.

Proton	IIIa	IIIb	IIIc	IIId
H_1	3.544	-0.016	-0.248	-
H_4	3.544	-0.015	-0.133	-0.102
H_2	6.063	0.008	-	-0.205
H_3	6.063	-0.035	-0.440	-0.021
H_{4a}	3.238	0.003	0.003	0.127
H_{8a}	3.238	0.005	0.047	-0.359
H_6	6.577	-	0.005	-0.007
H_7	6.577	-0.077	0.051	-0.048
H_{9a}	1.548	-0.011	0.023	-0.104
H_{9s}	1.450	0.008	-0.017	-0.064

IIIb-IIId relative to those of IIIa. Table VI-9 lists the ^{13}C chemical shifts of IIIa-IIId, while Table VI-10 lists the ^{13}C chemical shifts of IIIb-IIId relative to those of IIIa. The distinction between H_{9s} and H_{9a} was made by decoupling H_2 and/or H_3 which resulted in simplification of only H_{9s}. Substitution of methyl results in a downfield shift of 8.78 to 9.59 ppm for the substituted carbon and a 4.76 to 7.14 ppm downfield shift for α aliphatic carbon atoms. An upfield shift for α vinylic carbons of 2.33 to 9.19 ppm was observed (Table VI-9) for these adducts.

Table VI-10 lists the ^{1}H chemical shifts and coupling constants of the pentacyclo[5.4.0.0^{2,6}.0^{3,10}.0^{5,9}]undecane-8,11-diones IVa-IVd, while Table VI-11 lists the ^{1}H chemical shifts of IVb-IVd relative to those of IVa. Table VI-12 lists the ^{13}C chemical shifts of IVa-IVd, while Table VI-13 lists the ^{13}C chemical shifts of IVb-IVd relative to those of IVa. Distinction between H_{4s} and H_{4a} was made by decoupling H_1 and/or H_7 which resulted in simplification of only H_{4s} (cf. Fig VI-2). 'W-letter' long range coupling was present between H_3 and H_5 in compound IVc, and was also observed between H_2 and H_{10} and between H_6 and H_9 in all compounds.[16] Cross-ring 4-bond propanic coupling between diagonally opposed cyclobutane protons (i.e. $^{J}H_1$-H_6 and $^{J}H_2$-H_7) was also generally observed. Another unique 4-bond long range coupling between H_1 and H_{10} and between H_7 and H_9 was always observed in these cage compounds. The interesting observation was made that the relative chemical shifts of the H_{4s} and H_{4a} protons were constant until methyl substitution at C_2 was encountered (cf. compound VIc). This qualitative example of 'steric deshielding' of proton H_{4a} results from a sterically compressed environment created by the proximity and bulk of the methyl group on C_2.[23] Substitution of methyl results in a downfield shift of 4.68 to 8.08 ppm for the substituted carbon and a downfield shift of 4.96 to 6.69 ppm for the α aliphatic carbons (cf. Table VI-13) in

TABLE VI-8

^{13}C Chemical Shifts (δ) for the Series of 1,4,4a,8a-Tetrahydro-endo-1,4-methanonaphthalene-5,8-diones IIIa-IIId.

Carbon	IIIa	IIIb	IIIc	IIId
C_5	198.70(s)	198.37(s)	199.13(s)	198.60(s)
C_8	198.70(s)	198.88(s)	199.49(s)	199.26(s)
C_6	141.35(d)	150.94(s)	141.35(d)	141.40(d)
C_7	141.35(d)	139.02(d)	141.75(d)	141.90(d)
C_2	136.64(d)	134.90(d)	145.42(s)	138.76(d)
C_3	136.64(d)	134.34(d)	127.45(d)	134.70(d)
C_1	47.91(d)	47.89(d)	53.44(d)	57.39(s)
C_4	47.91(d)	48.19(d)	49.02(d)	48.80(d)
C_9	47.83(t)	48.12(t)	48.63(t)	54.97(t)
C_{4a}	47.53(d)	48.35(d)	49.26(d)	50.50(d)
C_{8a}	47.53(d)	47.51(d)	48.06(d)	52.29(d)
C_{methyl}	-	15.63(q)	16.21(q)	17.08(q)

TABLE VI-9

Downfield (+) or Upfield (-) ^{13}C Chemical Shifts (δ) of the 1,4,4a,8a-Tetrahydro-endo-1,4-methanonaphthalene-5,8-diones IIIb-IIId Relative to Those of Unsubstituted Parent Compound IIIa.

Carbon	IIIa	IIIb	IIIc	IIId
C_5	198.70	-0.33	0.43	-0.10
C_8	198.70	0.18	0.79	0.56
C_6	141.35	9.59	0.00	0.05
C_7	141.35	-2.33	0.40	0.55
C_2	136.64	-1.74	8.78	2.12
C_3	136.64	-2.30	-9.19	-1.94
C_1	47.91	-0.02	5.53	9.48
C_4	47.91	0.28	1.11	0.89
C_9	47.83	0.29	0.80	7.14
C_{4a}	47.53	0.82	1.73	2.97
C_{8a}	47.53	-0.02	0.53	4.76

TABLE VI-10

Chemical Shifts (δ) and Coupling Constants (Hz) for the Series of Pentacyclo[5.4.0.0^{2,6}.0^{3,10}.0^{5,9}]undecane-8,11-diones IVa-IVd.

Proton (J, Hz)	IVa	IVb	IVc	IVd
H_2	3.193(dddd)	2.830(dddd)	-	2.870(m)
J_{2-6}	-	8.4	-	10.8
J_{2-1}	7.0	-	-	?
J_{2-3}	5.9	5.4	-	-
J_{2-7}	1.6	1.3	-	?
J_{2-10}	1.5	1.9	-	2.0
H_6	3.193(dddd)	3.176(dddd)	2.802(dddd)	3.278(m)
J_{6-2}	-	8.4	-	10.8
J_{6-7}	7.0	6.0	6.6	6.0
J_{6-5}	5.9	5.8	5.3	5.2
J_{6-1}	1.6	-	1.6	1.8
J_{6-9}	1.5	1.8	1.5	1.8
H_3	2.948(dddd)	2.882(dddd)	2.543(dddd)	-
J_{3-2}	5.9	5.4	-	-
J_{3-10}	4.1	4.6	3.9	-
J_{3-4s}	1.7	1.6	1.6	-
J_{3-4a}	1.6	1.5	1.6	-
J_{3-5}	-	?	1.2	-
H_5	2.948(dddd)	2.938(dddd)	2.950(ddddd)	2.846(m)
J_{5-6}	5.9	5.8	5.3	5.2
J_{5-9}	4.1	4.8	4.0	4.0
J_{5-4s}	1.7	1.6	1.6	1.4
J_{5-4a}	1.6	1.5	1.6	1.5
J_{5-3}	-	?	1.2	-
H_1	2.801(ddd)	-	2.480(ddd)	2.799(m)
J_{1-7}	-	-	8.4	?
J_{1-2}	7.0	-	-	?
J_{1-10}	2.7	-	2.9	2.5
J_{1-6}	1.6	-	1.6	1.8
H_7	2.801(ddd)	2.361(ddd)	2.773(ddd)	2.870(m)
J_{7-1}	-	-	8.4	?
J_{7-6}	7.0	6.0	6.6	6.0
J_{7-9}	2.7	2.8	2.6	2.4
J_{7-2}	1.6	1.3	-	?
H_9	2.699(ddd)	2.656(dddd)	2.672(dddd)	2.780(dddd)
J_{9-10}	-	10.5	10.1	9.7
J_{9-5}	4.1	4.8	4.0	4.0
J_{9-7}	2.7	2.8	2.6	2.4
J_{9-6}	1.5	1.8	1.5	1.8
H_{10}	2.699(ddd)	2.722(ddd)	2.729(ddd)	2.446(ddd)
J_{10-9}	-	10.5	10.1	9.7
J_{10-3}	4.1	4.6	3.9	-
J_{10-1}	2.7	-	2.9	2.5
J_{10-2}	1.5	1.9	-	2.0
H_{4s}	2.058(dt)	2.048(dt)	1.925(ddd)	1.988(dd)
J_{4s-4a}	11.3	11.2	11.4	11.2
J_{4s-3}	1.7	1.6	1.6	-
J_{4s-5}	1.7	1.6	1.6	1.4
H_{4a}	1.898(dt)	1.906(dt)	1.965(ddd)	1.837(dd)
J_{14a-4s}	11.3	11.2	11.4	11.2
J_{4a-3}	1.6	1.5	1.6	-
J_{4a-5}	1.6	1.5	1.6	1.5
H_{methyl}	-	1.164(s)	1.284(s)	1.220(s)

TABLE VI-11

Downfield (+) or Upfield (-) ^{1}H Chemical Shifts (δ) of the Pentacyclo[5.4.0.0^{2,6}.0^{3,10}.0^{5,9}]undecane-8,11-diones IVb-IVd Relative to Those of the Unsubstituted Parent Compound IVa.

Proton	IVa	IVb	IVc	IVd
H_2	3.193	-0.363	-	-0.323
H_6	3.193	-0.017	-0.391	0.085
H_3	2.948	-0.066	-0.405	-
H_5	2.948	-0.010	0.002	-0.102
H_1	2.801	-	0.321	-0.002
H_7	2.801	-0.440	-0.028	0.069
H_9	2.699	-0.043	-0.027	0.081
H_{10}	2.699	0.023	0.030	-0.253
H_{4s}	2.058	-0.010	-0.133	-0.070
H_{4a}	1.898	0.008	-0.067	-0.061

TABLE VI-12

^{13}C Chemical Shifts (δ) and Multiplicities for the Series of Pentacyclo[5.4.0.0^{2,6}.0^{3,10}.0^{5,9}]undecane-8,11-diones IVa-IVd.

Carbon	IVa	IVb	IVc	IVd
C_8	212.03(s)	211.78(s)	211.67(s)	211.27(s)
C_{11}	212.03(s)	212.46(s)	210.46(s)	211.92(s)
C_9	54.38(d)	54.24(d)	53.04(d)	55.39(d)
C_{10}	54.38(d)	54.41(d)	55.64(d)	59.91(d)
C_3	44.25(d)	43.32(d)	50.21(d)	52.33(s)
C_5	44.25(d)	43.95(d)	44.61(d)	44.31(d)
C_1	43.42(d)	48.10(s)	48.38(d)	42.86(d)
C_7	43.42(d)	50.11(d)	40.30(d)	44.08(d)
C_4	40.04(t)	40.46(t)	37.77(q)	45.79(q)
C_2	38.32(d)	44.75(d)	45.99(s)	44.00(d)
C_6	38.32(d)	35.89(d)	44.06(d)	39.50(d)
C_{methyl}	-	15.36(q)	20.69(q)	15.58(q)

TABLE VI-13

Downfield (+) or Upfield (-) ^{13}C Chemical Shifts (δ) of the Pentacyclo[5.4.0.0^{2,6}.0^{3,10}.0^{5,9}]undecane-8,11-diones IVb-IVd Relative to Those of the Unsubstituted Parent Compound IVa.

Carbon	IVa	IVb	IVc	IVd
C_8	212.03	-0.25	-0.36	-0.76
C_{11}	212.03	0.43	-1.57	-0.11
C_9	54.38	-0.14	-1.34	1.01
C_{10}	54.38	0.03	1.26	5.53
C_3	44.25	-0.93	5.96	8.08
C_5	44.25	-0.30	0.36	0.06
C_1	43.42	4.68	4.96	-0.56
C_7	43.42	6.69	-3.12	0.66
C_4	40.04	0.42	-2.27	5.75
C_2	38.32	6.43	7.67	5.68
C_6	38.32	-2.43	5.74	1.18

these cage compounds.

Mass Spectra of Compounds III(a-d) and IV(a-d).

Tables VI-14 and VI-15 list the molecular fragments and their abundances for the Diels Alder adducts (IIIa-IIId) and the subsequent cage diketone photolysis products (IVa-IVd), respectively, as determined via mass spectrometry of the individual compounds.

The base peaks for Diels Alder adducts IIIa-IIId [i.e. m/e 66, 66, 80, and 80, respectively] corresponding to the diene component of each compound, are conveniently accounted for by a 'formal' retro Diels Alder fragmentation pathway (Scheme VI-3). The fact that so

SCHEME VI-3

'Formal' Retro Diels Alder Fragmentation Pathway for Adducts IIIa-d.

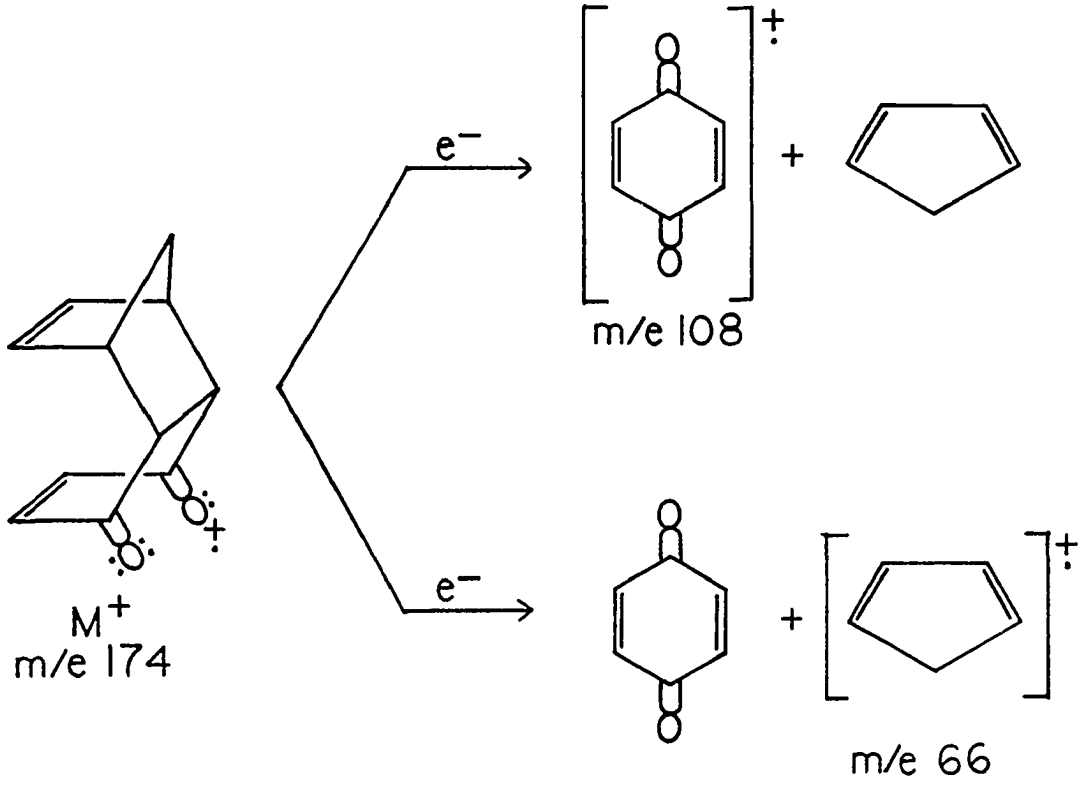

TABLE VI-14

Mass Spectral Molecular Fragments and Abundances[a] for

Diels Alder Adducts IIIa-IIId.

Compound			
IIIa	IIIb	IIIc	IIId
174(M+, 43.9) $C_{11}H_{10}O_2$	188(M+, 16.0) $C_{12}H_{12}O_2$	188(M+, 39.4) $C_{12}H_{12}O_2$	188(M+, 44.4) $C_{12}H_{12}O_2$
91(17.7) C_7H_7	91(13.3) C_7H_7	91(14.4) C_7H_7	91(12.8) C_7H_7
	91(13.3)[b] C_7H_7	91(14.4) C_7H_7	91(12.8) C_7H_7
77(3.1) C_6H_5	77(3.1) C_6H_5	77(20.1) C_6H_5	77(18.6) C_6H_5
	80(0.3) C_6H_8	80(100) C_6H_8	80(100) C_6H_8
66(100) C_5H_6	66(100) C_5H_6	66(3.4) C_5H_6	66(1.3) C_5H_6
	79(1.8) C_6H_7	79(52.8) C_6H_7	79(51.6) C_6H_7
65(18.7) C_5H_5	65(14.4) C_5H_5	65(7.8) C_5H_5	65(4.7) C_5H_5

(a) Abundances are listed in parenthesis.

(b) For paired listings the first fragment in the pair corresponds to the fragment containing the methyl substituent.

TABLE VI-15

Mass Spectral Molecular Fragments and Abundances[a] for Cage Diketone Photolysis Products IVa-IVd.

Compound			
IVa	IVb	IVc	IVd
174(M+, 64.1) $C_{11}H_{10}O_2$	188(M+, 100) $C_{12}H_{12}O_2$	188(M+, 100) $C_{12}H_{12}O_2$	188(M+, 100) $C_{12}H_{12}O_2$
146(18.5) $C_{10}H_{10}O$	160(39.4) $C_{11}H_{12}O$	160(14.5) $C_{11}H_{12}O$	160(15.5) $C_{11}H_{12}O$
145(24.5) $C_{10}H_9O$	145(44.4) $C_{11}H_{11}O$	145(29.1) $C_{11}H_{11}O$	145(32.8) $C_{11}H_{11}O$
118(30.4) C_9H_{10}	132(34.2) $C_{10}H_{12}$	132(11.3) $C_{10}H_{12}$	132(27.9) $C_{10}H_{12}$
	131(25.8)[b] $C_{10}H_{11}$	131(14.1) $C_{10}H_{11}$	131(25.3) $C_{10}H_{11}$
117(100)[c] C_9H_9	117(81.4) C_9H_9	117(42.5) C_9H_9	117(91.7) C_9H_9
	105(10.5) C_8H_9	105(6.7) C_8H_9	105(7.6) C_8H_9
91(36.9) C_7H_7	91(36.9) C_7H_7	91(20.8) C_7H_7	91(26.1) C_7H_7
	91(36.9) C_7H_7	91(20.8) C_7H_7	91(26.1) C_7H_7
77(10.1) C_6H_5	77(15.5) C_6H_5	77(8.7) C_6H_5	77(15.0) C_6H_5
	80(2.6) C_6H_8	80(70.7) C_6H_8	80(36.1) C_6H_8
66(35.0) C_5H_6	66(34.6) C_5H_6	66(6.4) C_5H_6	66(2.7) C_5H_6
	79(7.8) C_6H_7	79(13.2) C_6H_7	79(14.0) C_6H_7
65(16.0) C_5H_5	65(18.5) C_5H_5	65(8.2) C_5H_5	65(7.8) C_5H_5

(a) Abundances are listed in parenthesis.

(b) First fragment of paired listing contains the methyl substituent.

little of the dienophilic 1,4-benzoquinone fragments [i.e., m/e 108 (0.3%), 122 (0.5%), 108 (0.0%), and 108 (1.4%), for IIIa-IIId, respectively] are observed for each compound (Table VI-14) argues against this conclusion. However, should the 108 and 122 fragments for IIIa and IIIb quickly decarbonylate, cyclopentadienone [m/e 80 (0.5%)] and methylcyclopentadienone [m/e 94 (1.0%)] would be formed, respectively, but would disappear very quickly since both are very unstable. Similar consideration of IIIc and IIId is not possible because methylcyclopentadiene, which is formed upon initial fragmentation, also has an m/e of 80 and is the base peak for both compounds. Perhaps a stepwise fragmentation occurs but the 'formal' retro Diels Alder products predominate.

The fragmentation mechanism for the cage diketone series IVa-IVd is not straightforward.

BIBLIOGRAPHY

1. Marchand, A. P.; Suri, S. C.; Earlywine, A. D.,; Powell, D. R.; van der Helm, D. J. Org. Chem. 1984, 49, 670.

2. Marchand, A. P.; Allen, R. W. J. Org. Chem. 1974, 39, 1596.

3. Marchand, A. P.; Chou, T. -C. J. Chem. Soc. Perkin Trans. 1, 1973, 1948.

4. Marchand, A. P.; Chou, T. -C. Tetrahedron 1975, 31, 2655.

5. Marchand, A. P.; Chou, T. -C. Tetrahedron Lett. 1975, 3359.

6. Marchand, A. P.; Chou, T. -C.; Ekstrand, J. D.; van der Helm, D. J. Org. Chem. 1976, 41, 1438.

7. Marchand, A. P.; Kaya, R. J. Org. Chem. 1983, 48, 5392.

8. Cookson, R. C.; Crundwell, E.; Hudec, J. Chem. Ind. (London) 1958, 1003.

9. Cookson, R. C.; Crundwell, E.; Hill, R. R., Hudec, J. J. Chem. Soc. 1964, 3062.

10. Alder, K.; Flock, F. H.; Beumling, H. Chem. Ber. 1960, 93, 1896.

11. Available from Exxon Corporation; the gift of a generous sample of methylcyclopentadiene dimer is gratefully acknowledged.

12. Csicsery, S. M. J. Org. Chem. 1960, 25, 518.

13. Johnson, C. K. "ORTEP"; Report ORNL-3794 revised; Oak Ridge National Laboratory: Oak Ridge, Tn, 1971.

14. Mehta, G.; Singh, V.; Srikrishna, A.; Cameron, T. S.; Chan, C. Tetrahedron Lett. 1979, 4595.

15. Duax, W. L.; Norton, D. A. "Atlas of Steroid Structure"; Plenum: New York, 1975; Vol. 1, pp 16-22.

16. Marchand, A. P.; Rose, R. E. J. Am. Chem. Soc. 1968, 90, 3724.

17. (a) Coates,R. M.; Kirkpatrick, J. L.; J. Am. Chem. Soc. 1968, 90, 4162. (b) Jefford, C. W.; Hill, D. T.; Ghosez, L.; Toppet, S.; Ramey, K. C. J. Am. Chem. Soc. 1969, 91, 1532.

18. Compound IIIb was synthesized via Diels-Alder addition of cyclopentadiene to toluquinone.[10] The material thereby synthesized was recrystallized from methanol to afford a pale yellow microcrystalline solid, mp 61-63°C (lit.[10] mp 62°C).

19. Main, P.; Fiske, S. J.; Hull, S. E.; Lessinger, L.; Germain, G.; Declercq, J. -P.; Woolfson, M. M. "MULTAN 80, A System of Computer Programs for the Automatic Solution of Crystal Structures from X-ray Diffraction Data"; Universities of York,

England, and Louvain-la-Neuve, Belgium, 1980.

20. Sheldrick, G. M. "SHELX-76. Program for Crystal Structure Determination"; University Chemical Laboratory: Cambridge, England, 1976.

21. Cromer, D. T.; Mann, J. B. Acta Crystallogr., Sec. A 1968, A24, 321-324.

22. Stewart, R. F.; Davidson, E. R.; Simpson, W. T. J. Chem. Phys. 1965, 42, 3175-3187.

23. Marchand, A. P. "Stereochemical Applications of NMR Studies in Rigid Bicyclic Systems"; Marchand, A. P., Ed.; Verlag Chemie International: Deerfield Beach, Fla., 1982; pp 14-19.